MONASH University

**NON-DESTRUCTIVE CHARACTERISATION of PIGMENTS
from
DAKHLEH OASIS, AND THE NILE VALLEY, EGYPT
from the
New Kingdom, Ptolemaic and Roman periods**

William Harold Jay ASTC, BSc, PhD

**A thesis submitted for the degree of *Doctor of Philosophy*
at
Monash University**

2017

**Centre for Ancient Cultures
Faculty of Arts**

Copyright notice

SUMMARY

This thesis is directed towards obtaining fundamental knowledge primarily in respect of pigments using modern, non-destructive, state-of-the-art analytical equipment, including Raman spectroscopy, synchrotron XFM beamline radiation, electron microscopy under low or high vacuum, and supplemented by Mössbauer spectroscopy. The pigments studied were those developed by, or used by Egyptian workers from the 18th Dynasty to the end of the Roman period. The pigments investigated are the naturally occurring oxide-based and sulphide-based pigments or the high temperature synthetically prepared Egyptian blue and green pigments and cobalt blue pigments. As stated by Nicholson and Shaw in the introduction to their excellent and comprehensive text in respect of Ancient Egyptian Materials and Technology, over the last several decades the nature of Egyptology has changed with a new emphasis being placed upon technological and sociological questions. This thesis addresses some of these technological questions. This work has been conducted non-destructively, so that the sherds themselves can continue to be investigated by other researchers.
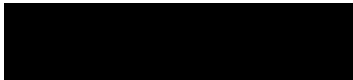
The data developed in this thesis has provided support for some of the earlier theories in respect of Egyptian pigments and their method of application. However, the data has brought into question other theories, in particular, clarification of the order of pigment application by pre- or post-firing. The use of, and type of organic binders selected to apply the pigments to pottery surfaces has been identified. Again, this has brought into question some of the earlier understanding in respect of pigment application. Lichen attack, resulting in pigment modification has also been identified. Similarly, by the positive identification of slips under the pigment, this has created an improved understanding of the decorative processes adopted in Egypt.

A particular emphasis has been placed upon production from the workshops in the Dakhleh Oasis and by way of contrast, in the Nile valley. The Dakhleh Oasis was rich in oxide raw minerals and has been the only exploitable source of cobalt mineralisation discovered in Egypt. By investigating this cobalt blue pigment, this thesis has developed data suggesting a new production hypothesis for its production and its subsequent application in glass technology. Importantly, this thesis now proposes that the cobalt pigments were made in the Oasis and shipped to the Nile valley for their subsequent use as a decorative medium. Similarly, the investigation into the high temperature prepared Egyptian blue and Egyptian green has provided new data in respect of phosphates. A significant body of evidence has been garnered to show that the supposed plant ash sites may have been kiln ash, or ash from cooking ovens as a ready source of the alkali flux in the production of cobalt blue pigments. Egyptian blue and green pigment production probably relied upon trona from the Wadi Natrun as demonstrated by the presence of thénardite on the surface of two Egyptian blue samples with a probable change to plant ash in or just prior to the 2nd century CE.

This thesis has demonstrated the benefits which can be derived from the application of Raman spectroscopy for on-site museum studies.

Declaration

This thesis contains no material which has been accepted for the award of any other degree or diploma at any university or equivalent institution and that, to the best of my knowledge and belief, this thesis contains no material previously published or written by another person, except where due reference is made in the text of the thesis.

William H. Jay
27 April 2016

Publications during enrolment

Jay, W.H., Cashion, J.D., (2013), "Raman spectroscopy of Limehouse porcelain sherds supported by Mössbauer spectroscopy and electron microscopy", *J. Raman Spectrosc.* **44**, 1718-1732.

Jay, W.H., Cashion, J.D., Blenkinship, B. (2015), "Lancaster delftware: a Raman spectroscopy, electron microscopy and Mössbauer spectroscopy compositional study", *J. Raman Spectrosc.*, **46**, 1265-1282.

Cashion, J.D., Hope, C.A., Jay, W.H., (2015)"Complementary Raman and Mössbauer Archaeological Studies", *Proc. 39th Annual Condensed Matter and Materials Meeting*, 3-6 Feb. Wagga Wagga, NSW.

Jay, W.H., Hope, C.A., Cashion, J.D., Howard, D.L., Spiers, K.M., "Blue-Painted Pottery of the New Kingdom: A New Study of Pigment Sourcing and Production", *Cahiers de la Céramique Égyptienne* (forthcoming).

Acknowledgements

CONTENTS

APPENDICES

All data applicable to Appendices and to the subject area are provided at:
https://drive.google.com/drive/folders/0B1MXnIeNTO4icGV6dTFSaXhOQU0?usp=sharing

APPENDIX A2

All Raman spectral database assignments are provided herein.

APPENDIX A3 PIGMENTS on POTTERY, WALLS AND CARTONNAGE
PART I

AMARNA
DEIR al-MEDINEH
DENDERA
KARNAK
MALKATA
SINAI

APPENDIX A3 PIGMENTS on POTTERY, WALLS AND CARTONNAGE
PART II

MUT al-KHARAB
DAKHLEH OASIS

APPENDIX A3 PIGMENTS on POTTERY, WALLS AND PLASTER
PART III

Wall decoration, including plaster substrate, Kellis
Wall decoration, forensic sampling, Kellis
Cartonnage, Kellis
Lithic tool scraping.
Trench samples, forensic sampling , Mut al-Kharab

APPENDIX A4
EGYPTIAN BLUE AND EGYPTIAN GREEN PIGMENTS

AMARNA
Bolton Museum
Petrie Museum, University College London
KARNAK NORTH, LUXOR
TELL ESH-SHARIYA, GAZA STRIP
ANUBIEION, SAQQARA
MUT AL-KHARAB
MALKATA
EGYPTIAN BLUE ON CARTTONNAGE
EGYPTIAN BLUE ON WALL DECORATION
EGYPTIAN BLUE MICRO-SAMPLING 'FORENSIC' TRENCH SAMPLES.

EGYPTIAN GREEN PIGMENTS
> **Egyptian green pigment ("Green frit")**
> **Pottery Sherd**
> **Wall decoration**
> **Cartonnage, Kellis**

APPENDIX A5 Cobalt pigments

AMARNA
DEIR al-MEDINEH
DENDERA
KARNAK
MALKATA
MEMPHIS
MUT al-KHARAB
SINAI

RESEARCH AIMS

This thesis has applied modern analytical instrumentation methods into the non-destructive characterisation of pigments applied to a range of surfaces in Egypt during the new Kingdom to Roman periods. The research aim is to either confirm existing theories, or to elucidate new, fundamental and, therefore previously unknown information in respect of these pigments. This new information is intended to provide an improved understanding into the mineralogy and applications of these various pigments. The principles developed therefore have direct application in other pigment applications.

The research has examined a number of pigment samples from the Dakhleh Oasis, together with additional samples from various sites throughout the Nile valley, Egypt. The samples examined are detailed below in Section 1.1. The greater availability of samples from the Nile valley and the restriction of removal of samples from the Dakhleh Oasis may, simplistically, be seen to bias the outcome of the research conducted. This is accepted. However, more importantly, is the significant and detailed technology developed from the samples examined and which is provided in the thesis and in the accompanying Appendices. Future researchers are thereby provided with a significantly improved platform from which to conduct their research. Thus, Chapter 3 contains significant mineralogical data in respect of the sulphide, oxide and oxyhydroxide ores used as pigments throughout Egypt during this period.

A primary aim of this thesis is to obtain new and more detailed information with respect to the complexity of the high temperature technologies used by the ancient Egyptians to produce synthetic pigments. Egyptian blue and Egyptian green (Chapter 4) were probably the first chemical syntheses to be conducted and precede glass production. Cobalt blue (Chapter 5) production commenced soon after. This research is intended to either confirm existing hypotheses, or enable a reinterpretation of the present understanding and propose alternative hypotheses.

Another aspect of the research is to develop an improved understanding of the specific long-term stability of the mineral complexes, both natural and synthetic, under a variety of conditions, or changes due to its degradation during burial or weathering conditions. An explanation into the excellent adhesion of some pigments to their substrate or, in other instances, to the adhesion failure of the applied decoration will be investigated.

CHAPTER 1. INTRODUCTION

The Egyptians are known to have used pigments for painting on pottery vessels and walls from Predynastic times; examples of the former survive on numerous White Cross Line and D-Ware and the latter from Tomb 100 at Hierakonpolis. They understood the necessity to apply mordants to natural fibres to ensure that the pigments in dyed cloth were fixed and used alums for this purpose (Kuehni 1980; Vogelsang-Eastwood 2000: 278-281). Egyptians were amongst the first peoples to develop metallurgy: to extract copper and lead from ores (Garland and Bannister 1927; Loyson 2011); they were experienced in chemical technologies and this enabled them to modify inorganic pigments, or to produce synthetic pigments (Brill 1970: 105-128; Barkoudah and Henderson 2006). Egyptian pigments before the Roman period are normally inorganic compounds , thus explaining their extraordinarily good preservation of colour, many of which remain as vibrant today as when they were produced Lee and Quirke (2000: 104).

As stated, the focus of this thesis is the study of a range of ancient Egyptian pigments applied to a variety of surfaces by adopting modern analytical instrumentation methods. The research aims are threefold: to obtain new and more detailed information with respect to the complexity of the high temperature technologies used by the ancient Egyptians to produce synthetic pigments; to develop an improved understanding of the specific long-term stability of the mineral complexes, both natural and synthetic, under a variety of conditions, or changes due to its degradation; and to either confirm existing theories, or to elucidate new, fundamental and, therefore previously unknown information in respect of these pigments. This new information is intended to provide an improved understanding of the mineralogy and applications of these various pigments. The principal focus, therefore, is to address some of the unanswered questions or hypotheses arising from a number of the earlier experimental studies; to confirm existing understanding by employing alternative instrumental techniques; and to produce data to enable new hypotheses to be advanced into certain aspects of pigment production or pigment usage. Thus, a particular emphasis is directed towards the mineralogy and chemical composition of those pigments, whether they were directly sought from mineral deposits or were synthetically produced.

In order to determine the chemistry and morphology of the pigments and of the high temperature processes used in Dakhleh Oasis and at various valley sites, and to ensure that the samples retain their integrity, a non-destructive instrumental approach has been adopted. Generally speaking, other than optical examination and electron microscopy, only a limited application of other instrumental technologies has previously been applied to Egyptian artefacts and reported in the published literature. Advances emanating from new or improved analytical instruments and methods enable questions relating to raw materials, production methods and provenance to be re-examined. Thus, it is the application of these advanced instrumental techniques which form the focus of this thesis to determine whether they can provide information not obtainable by the instrument selection proposed by Lee and Quirke (2000: 106). The analytical equipment employed includes Raman spectroscopy, synchrotron XFM beamline radiation, electron microscopy under high and low vacuum, and Mössbauer spectroscopy. Raman spectroscopy is able to examine individual samples at the micron level, and even retrieve data on surfaces where most of the pigment has been lost. XRD is not a suitable instrument for studying silica polymorphs or microscopic or highly

contaminated residual materials, whereas Raman can provide significant information in respect of all such materials. Inorganic pigments and organic compounds such as waxes, egg protein, casein, animal glue, gum Arabic, sugars and a range of oils may all be present within a wall plaster, cartonnage, or pottery decoration, or have been used to fix (bind) a pigment to a substrate, and all are able to be identified in a single spectrum by Raman spectroscopy. The cobalt blue pigment found on several of these sherds has previously been considered by other researchers to be incapable of examination by XRD; it is re-examined in this thesis. This Raman instrumental approach can be directly applied using portable equipment to enable the specimen to be examined *in situ*.

Clark and Gibbs (1997) reported on faience sherds from Amarna using Raman spectroscopy and Coupry *et al*. (1994) discussed this application to blue pigments from the New Kingdom. As described by David *et al*. (2001), Raman spectroscopy has been successfully applied to the study of pigments in historical ancient manuscripts, polychrome statuary and wall paintings. She employed this methodology to investigate pigments from Amarna. Egyptian funerary artefacts from the New Kingdom to the Graeco-Roman period were studied by Edwards *et al*. (2004: 2004a). The application of Raman spectroscopy as a non-destructive method for the characterisation of 18th century Italian ceramics, glazes and glass was discussed in some detail by Ricciardi in her 2006-2007 thesis. The earliest use of Raman that she reported was from the late 1990s for glass and year 2000 for ceramics and pigments. Ambers (2004) has discussed pigments applied to four Egyptian artefacts held by the British Museum, two being limestone figures and two of fragments from the same 4th Dynasty tomb wall paintings.   The use of Raman spectroscopy was investigated by this researcher using the pigment decoration on English porcelain dated to the 1750s and from this work a new study into the pigments developed and used within the Western Desert, Egypt commenced. This thesis is the first reporting of Raman spectroscopy being used to investigate Western Desert, Egypt, pigments.   For comparative purposes, the research was extended to include sherds recovered from the Nile valley at Amarna, Malkata, Karnak and elsewhere.

The recent development of electron microscopes capable of directly inserting larger specimens into the sample chamber and examining them under low vacuum without the requirement for pre-coating with a conducting film has been used for much of the present research. And, as demonstrated in this thesis, the ability to mill samples if required in 1μm steps using a Ga+ ion beam in a FIB and then analyse the milled surface has provided new and relevant data. Such instruments formed part of the instrument selection used.

The combination of two or more instrumental techniques should provide a much greater in-depth chemical and mineralogical analysis and consequently an improved compositional understanding significantly greater than that which can be obtained from the application of a single analytical technique. This multi-instrument research has the potential to bring into question the conclusions reached in a number of published documents by either supporting their tentative hypothesis or, providing an alternative hypothesis.   All instruments used are described in detail in Chapter 2 as is a comprehensive Raman database; this database is supplemented within each chapter as required to support the data generated. The published knowledge, in the form of a literature review appertaining to each pigment, is summarised within the specific chapter, together with the published theoretical data and the present understanding which is applicable to the particular pigment category.   Where necessary,

supporting data tables developed from published information are provided either within the specific chapter or in the respective Appendix. A link is provided:

https://drive.google.com/drive/folders/0B1MXnIeNTO4icGV6dTFSaXhOQU0?usp=sharing

The pigment samples examined derive from Dakhleh Oasis in Egypt's Western Desert, and various sites in the Nile valley and date from the New Kingdom to the Roman period. Restrictions on the removal of cultural materials which are over 100 years of age, recently imposed by the Supreme Council of Antiquities, has resulted in limiting the range of samples available for examination, all of which were obtained before the restrictions were imposed and were kindly made available; the sample size is sufficient to enable a comprehensive body of information to be developed. Whilst the period of investigation spans about 2000 years, insufficient samples from any single Dynastic period or site were available to provide a comprehensive and comparative overall investigation to be conducted into each dynasty or period. There is a greater number originating from the valley, which may be seen to bias the outcome of the research conducted; it has not, however, impacted upon the development of significant and detailed technology.

Because pigments, pottery and plasters, are heterogeneous in nature and the pigment decoration is often discontinuous, areas of the substrate (plaster or pottery slip or fabric) can be exposed within the decorated surface. It is vital that the substrate and the pigment itself be quantified to ensure correct identification of the pigment and of the substrate.   Of necessity, the slip coating or the pottery surface and the plaster on to which wall decorations are applied need to be quantified. Whilst all of these results are provided within the Appendices, only those required for pigment characterisation are tabulated and discussed in any detail within the body of the thesis. Therefore, pigments on pottery, plaster and cartonnage are collectively discussed as individual colours in Chapter 3 together with the mineralogy of the oxide and sulphide pigments and, the pottery fabrics and wall plaster chemistry is discussed in Appendix A3. Subsequent mineralogical or biological changes which may occur upon burial or long-term aerial exposure are also discussed in Chapter 3. And, the identification of key Raman spectral biomarkers of lichen, algal or cyanobacterial biodegradation attack on exposed decorated surfaces can be achieved non-destructively. Lichen attack in wall decoration pigments is discussed in Chapter 4 and Appendix A4.

Shortland *et al*. (2006a) stated that throughout the Dynastic period (c. 3000 – 332 BCE) most Egyptian pottery was predominately undecorated. The first significant change took place during the New Kingdom, 18th to 20th Dynasties (c. 1550 – 1069 BCE) when a wide range of objects were decorated (Aston 2003; Hope 1989, 1991). Colour was then used to decorate walls of buildings, tombs, coffins, pottery and a diverse range of other objects (El Goresy 1997; Baines 1985; Kuehni 1980).   Wall paintings are attested as early as the Predynastic period with reds, yellows, white and black being the colours of choice up until the 5th Dynasty when they were supplemented by copper-based Egyptian blue and Egyptian green ("Green frit") which became available with the advent of high temperature technological processes. By the 18th Dynasty, all of these pigments were being employed in such decorative processes. Thus, during the New Kingdom, a significant expansion in colour decoration occurred and continued into Ptolemaic and Roman periods as different pigments evolved.

It must be noted that the precise shade of painted colours can vary as they are not necessarily completely stable, particularly in wet, oxidising, acidic, or sulphur-containing atmospheres or, in the case of orpiment yellow, it is not lightfast. This thesis will address the present limited understanding of oxide, sulphide and "green earth" pigment chemistry used in Egypt. This information is supported by the development of new data in respect of the various precipitation and high temperature processes involved in the synthesis of cobalt blue, or in the production of Egyptian blue and of green pigments.

Specific chapters have been allocated to the high temperature processes for the manufacture of different types of blue pigment, namely Egyptian blue and green (Chapter 4 the comprehensive supporting technical data Appendix A4) and cobalt blue (Chapter 5 and Appendix A5). This thesis therefore generally follows the reporting principles applied by Lucas and Harris (1989: v) and Nicholson and Shaw (2000: 1). This does introduce certain shortcomings as noted by Lee and Quirke (2000: 108) who considered that this colour-by-colour approach creates a foreign and anachronistic focus on English language colour terms, few if any of which can be considered to correspond to Egyptian perception of colour. Thus, the historical periods of time in which a pigment was used or manufactured are located in the respective chapter for that colour and also discussed under production examples such as walls or pottery. This methodology of grouping all of the generated data in a specific chapter and in its respective Appendix has the advantage of retaining and presenting the data in a comprehensive and readily accessible format. This approach has been adopted in an attempt to allow technological developments observed over time, whether in the Nile valley or in the oases to potentially become more evident.

Copper-based blue pigments were generally reserved for tombs, walls, cartonnage and faience applications. Other naturally occurring blue pigments, including lapis lazuli (the mineral lazulite), azurite and turquoise were used in minor, but important, applications. Lee and Quirke (2000: 111) would disagree with Lucas' (1962: 340) assertion that azurite was used as a pigment, reporting that the Max-Planck project had failed to discover evidence in support of the use of azurite. Although David *et al.* (2001: 470) identified azurite in a fragment in the Manchester Museum (No. 1964) using Raman spectroscopy, thereby confirming the Lucas' assertion; however, it is uncertain whether this pigment emanated from a subsequent restorative addition to the cartonnage.

Visual observations of chemical reactions by early Egyptian artisans provided the basic understanding upon which various high temperature technologies were developed and flourished. Their understanding of high temperature reactions and their ability to continuously replicate these reactions enabled Egyptian workers to synthesise Egyptian blue and Egyptian green from copper minerals such as malachite and later, from metallic copper or copper-tin alloy, often in the form of scrap; during the Roman period. Evidence is now advanced to indicate that a copper-zinc alloy was also employed in Egyptian blue production.

It has been proposed that the technology for using cobalt colourants in glass, glaze and ceramics (blue painted pottery) was discovered during the reign of Thutmose III (c. 1479 – 1425 BCE) and came into common usage during the reigns of his son Amenhotep II (1427-

1400 BCE) and grandson Thutmose IV (1400- 1390 BCE) reaching its zenith during the reigns of Amenhotep III and Akhenaten (1390 -1336 BCE). Hope (2011: 507) reported that it is not impossible that blue painted pottery was made in the reign of Thutmose (III) and that cobalt was certainly utilised in the manufacture of glass and faience at that time (Shortland *et al*. 2006: 91). The first significant usage of blue painted pottery was dated by Hope *et al*. (1980), Kozloff *et al*. (1992) and Hope (2011: 502) to be from the reign of Amenhotep III; quantities of blue painted pottery were recovered from excavations at the palace of Amenhotep III at Luxor, which he only occupied in the last decade of his reign (Hope 1989: 3, 7; Hope *et al*. 2009: 166). The production of cobalt blue pigment appears to have ceased during, or at the end of the reign of Ramesses IV in the 20th Dynasty (1153-1147 BCE) (Hope 1989: 56; 1991: 17-92; 2011; Arnold and Bourriau 1993: 100; Aston 1998: 56; 2004: 191; Shortland *et al*. 2006; Rose 2007: 18; Abe *et al.* 2009; 2012). Shortland *et al*. (2006a) hypothesised that perhaps there was a problem with the supply of the cobaltiferous alum which was used to manufacture the pigment.

The source of the cobalt used in Egypt in the 18th and 19th Dynasties has been the subject of debate. However, the present hypothesis is that it originated from the Dakhleh and Kharga Oases in Egypt (Jay *et al.* forthcoming). Presuming that these oases provided the source for the cobalt, the chemistry used to concentrate the cobalt into a pigment suitable for application to vessels is still a matter of some conjecture. Investigation of samples obtained from Dakhleh Oasis and from the Nile valley may assist in elucidating this question. This subject, together with cobalt extraction chemistry from alum by its dissolution and precipitation as a Mixed Hydroxide Precipitate (MHP) and its subsequent conversion into a cobalt pigment is discussed in detail in Chapter 5 and the supporting analytical data is provided in Appendix A5.

The method of pigment fixation on to various prepared surfaces or potentially by directly firing the pigment on to the pottery surface as part of the pottery production are investigated and discussed in Chapters 3 to 5. This includes the use of fixatives such as wax, including beeswax or egg protein, gum Arabic or other possible ambient temperature fixative (cold decoration).

There is no evidence to date that cobalt was used to colour glass in Egypt prior to the 18th Dynasty. Stern and Schlick-Nolte (1994) suggested that the very earliest blue glass came from Iran or Asia Minor. And, Kaczmarczyk (1986: 373-4) suggested that the Egyptian cobalt source was only in use from the 16th until the 11th century BCE. The use of cobalt for the coloration of glass commenced prior to the reign of Akhenaten as indicated by the presence of ingot moulds and the circular glass ingots recovered from the late 14th century BCE Ulu Burun shipwreck (Nicholson and Henderson 2000: 200; Bass 1986; Bass *et al*. 1989). According to Lilyquist and Brill (1993) and supported by Shortland and Tite (2000), Shortland and Eremin (2006: 582, 593) and Shortland *et al*. (2006), the discovery of dark blue glass apparently occurred during the reign of Thutmose III and became common during the reign of his son, Amenhotep II and grandson Thutmose IV, and abundant during the reigns of his successors, Amenhotep III and Akhenaten.

A very brief investigation of 4th century CE glass sherds from Kellis and 5th century CE sherds from Dayr Abu Matta, Dakhleh Oasis, is provided in Chapter 5 and the supporting data in Appendix A5 to indicate whether a change in cobalt source occurred within Dakhleh Oasis during the Late Roman period.

1.1   SHERDS and MICRO-SAMPLES ANALYSED and their CONTEXT

1.1.1 Western Desert Region and Dakhleh Oasis

A significant number of samples derive from sites within Dakhleh Oasis and therefore it is essential to provide a brief summary of the geographical context. The Western Desert region of Egypt covers two-thirds of the land area of Egypt and occupies one of the driest regions of the Sahara. Seven depressions within the desert, Siwa Qattara, Fayum, Bahariya, Farfra, Dakhleh and Kharga and may represent parts of old drainage systems. The oases are located around and within the southern and western borders of the Libyan Plateau (Kleindienst *et al*. 1999). Dakhleh Oasis is located 800 km south-south-west of Cairo and about 250 km west of modern Luxor (Figures 1.1 and 1.2). It lies about 180 km west from Kharga Oasis and about 380 km south of Farafra Oasis. Dakhleh Oasis occupies an area of about 410 km^2 and is approximately 60 km east-west and between 20 and 30 km north-south. In antiquity, access to the Nile valley was either along the well-travelled desert route Darb Ayn Amur via Kharga Oasis to Abydos or bypassing Kharga and travelling directly from Balat at the eastern entrance to Dakhleh along the desert track of Darb el-Tawil to Assuit (Giddy 1987; Wagner 1987); Bagnall 2001).
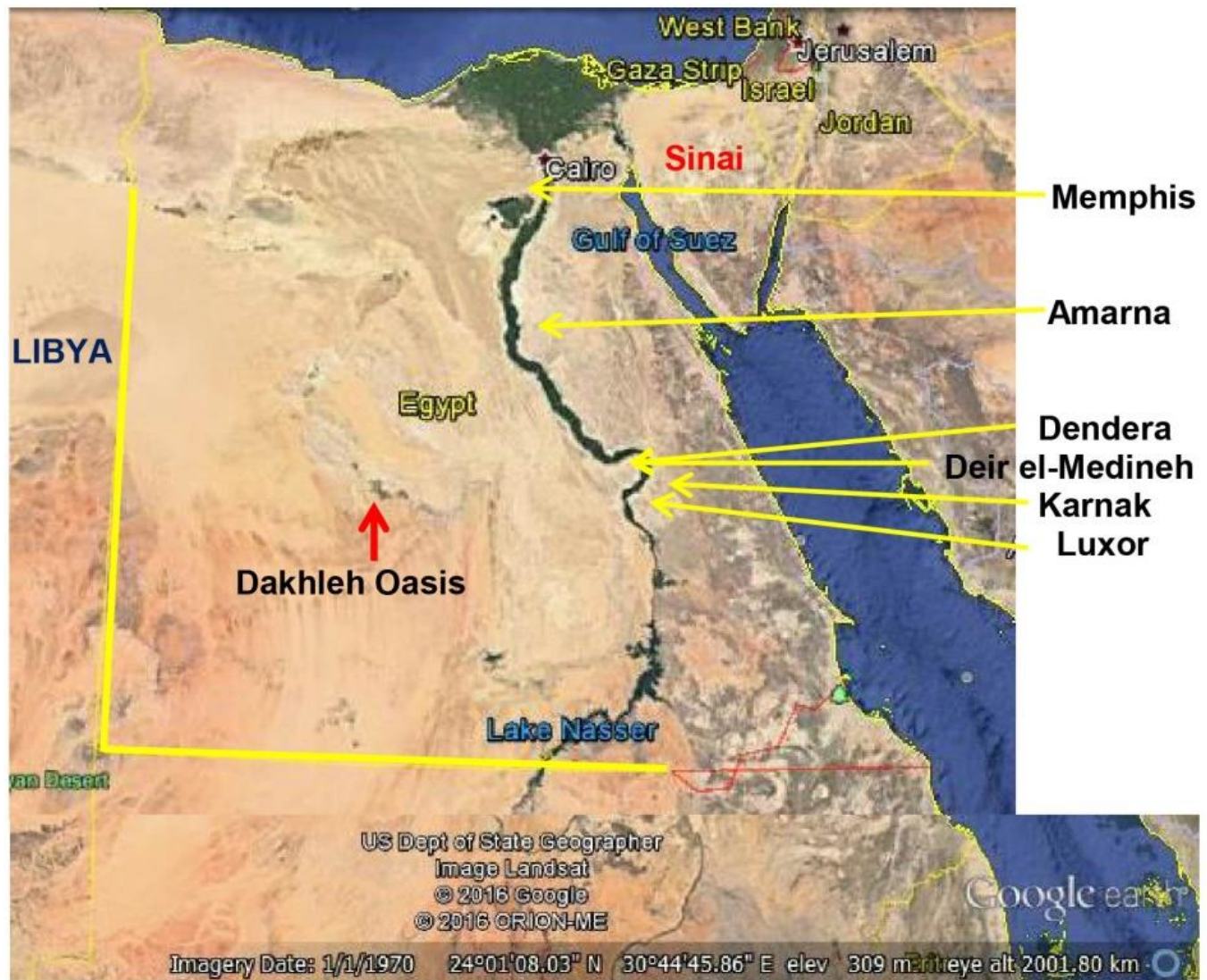
Figure 1.1 Air photo location map of Egypt showing the position for the source of the various samples analysed US Department of State Geographer Image Landsat$^{©}$, Google 2016$^{©}$.

The first Egyptian connection with the Dakhleh Oasis was in the Early Dynastic Period (2920-2650 BCE) as attested in the ceramic assemblage from Mut al-Kharab (Hope and Pettman 2012), which indicates that Egyptians were in contact with the oasis at that time. Egyptian expansion into the region occurred during the Old Kingdom culminating in its annexation and incorporation into the Egyptian administration by Dynasty VI (2345-2181 BCE); (Hope 2001). Whether this was to protect its western border and thereby expand the State, or to create an alternative overland route to the upper reaches of the Nile circumventing the Nubian tribes remains open to conjecture.
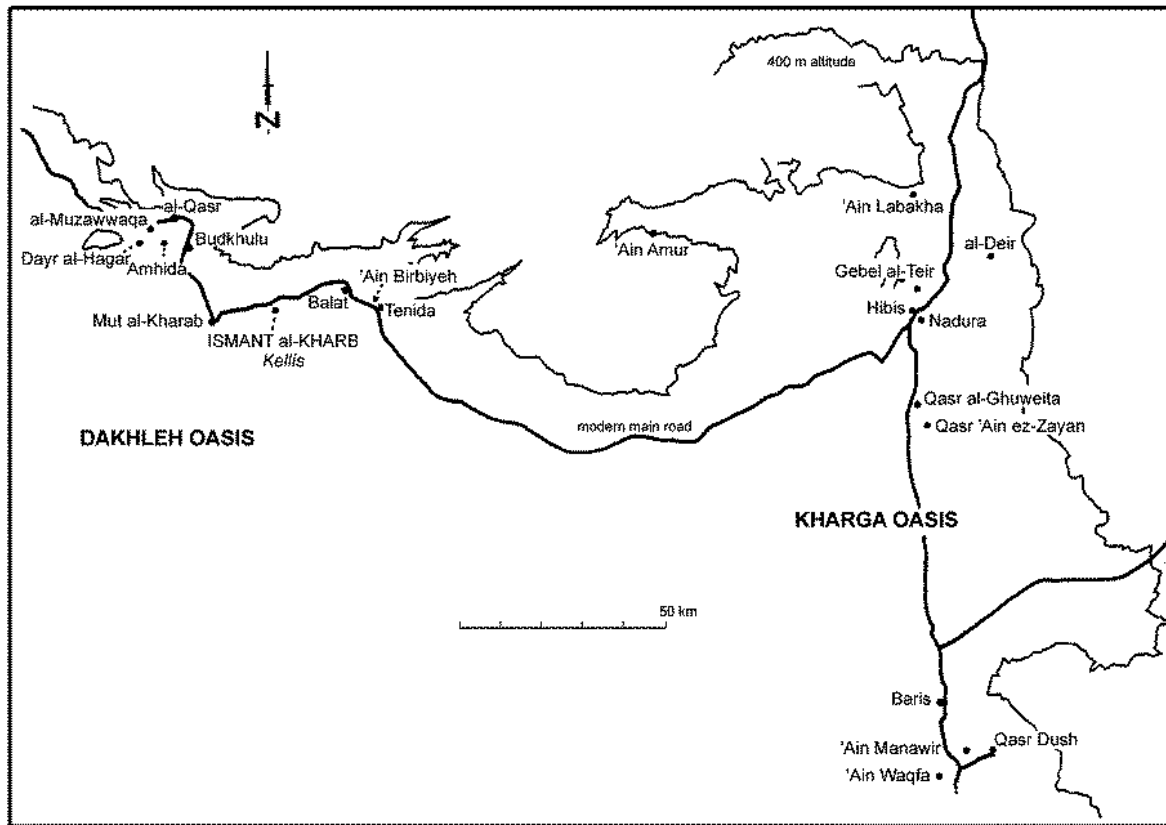
Figure 1.2 The location of the main sites in Dakhleh Oasis (drawing O.E. Kaper)

Dakhleh Oasis was governed from 'Ayn Asil from possibly as early as late Dynasty V and throughout the remainder of the Old Kingdom (Giddy 1987; Hope 2001). It may have remained the capital until the New Kingdom, when Mut al-Kharab took over this role and was probably continuously occupied into the Islamic period (Hope 2015).

The geography and geology is important in understanding the semi-arid environment of the western desert region. To the north, the lowland is overlooked by a 300 m high escarpment which marks the southern edge of the Libyan Plateau at between 420 and 560 m above sea level. And, to the south, it is bounded by a rocky ridge and a rough, sand and gravel-covered desert plain (Kleindienst *et al.* 1999). The geology of Egypt, and thus its relationship to the raw materials available to early Egyptian workers is discussed in Appendix A3.

1.1.1.2 Dakhleh Oasis Project (DOP)

The Dakhleh Oasis Project (DOP) was established in 1977 under the directorship of Anthony Mills to study the human adaptation to a semi-arid environment and to the physical environment (Mills 1999: ix). A survey of the oasis commenced in 1978 and some four hundred and ten archaeological sites, ranging from the Palaeolithic to the Islamic periods were indexed with the majority belonging to historical periods of the last five millennia (Mills 1999: x). Following this survey, sites that had the potential to provide significant information relating to the Project's aims were chosen for intensive examination, Ismant al-Kharab, ancient Kellis being one such site. Associate Professor Colin Hope, Monash University, Australia, has directed excavations on behalf of the DOP at Ismant al-Kharab

and Mut al-Kharab. Dr Gillian Bowen, Monash University, was granted a concession to excavate the Christian site of Dayr Abu Matta and Professor F. Leemhuis, Groningen University, Netherlands holds the concession for Qasr al-Dakhleh.

1.1.1.2.1 Kellis (Ismant al-Kharab)

The ruined village of Kellis is located south east of the modern village of Ismant, approximately 15km to the east of the capital of Mut and is designated as Site 31/420-D6-1 in the Dakhleh Oasis Project's archaeological sites index. Current evidence indicates that the village was occupied from the late Ptolemaic period and abandoned at the end of the 4th century CE (Hope 2001a) for reasons that are not yet understood. Following its abandonment, the site was quickly engulfed in sand and consequently it is extremely well-preserved. Some of the mudbrick structures stand to a height in excess of eight metres, whilst others are preserved to roof height beneath windblown sand (Knudstad and Frey 1999). The dry environment has facilitated the preservation of organic material including the numerous wall paintings that decorate some of the structures.

Excavations commenced in 1986 and are ongoing. The site itself, occupies an area of about 0.75 km^2 in size. For excavation purposes, Hope divided the site into four discrete areas designated A-D; the site also includes the large mausolea of the North and South Tombs and two cemeteries, Kellis 1 and 2 (Figure 1.3). Excavation has been undertaken in each of these areas. They are summarised below.

Area A

Area A, located in the centre of the site, is primarily a 4th century CE residential area containing many streets and lanes, domestic structures and the Large and Small East Churches (Knudstad and Frey 1999). On the north-west, directly south of North Tomb 1 is a nymphaeum (A/11) (Bowen 2007: 29-33). Three mud brick houses, Houses 1 – 3 (A/1, A/2, A/5) have been excavated in full and two others, Houses 4 (A/6) and 5 (A/9) have been excavated in part (Hope 2015). The houses are all of mudbrick with the three contiguous structures, Houses 1 – 3, located on the northern periphery; House 4, roughly central in the area and House 5, on the south-east near the Large East Church, are both double story (Hope 2015).

Two 4th century churches, the Large East Church (A/7) and the Small East Church (A/8) located on the south-east periphery of the site have also been excavated (Bowen 2002; 2003). The Large East Church, which has been tentatively dated to the reign of Constantine I, is a purpose-built basilica constructed of mud brick, with the inner walls, columns and main features being gypsum plastered. The apse, the wall above its entrance and the ceiling were decorated, but little survives *in situ*. Painted plaster, in a variety of colours, was found in the debris in front of the apse (Bowen 2002: 71 fig 4). Two of the samples derive from this structure.

The Small East Church was a pre-existing building modified for ecclesiastical use (Bowen 2003). It is constructed from mudbrick and was gypsum plastered throughout. The apse and the east wall facing the congregation were painted with geometric designs and imitation

columns and cupboards (Knudstad and Frey 1999: 207; Bowen 2003: 158-161, plates 6 – 7). The apse paintings are well preserved; the pigment colours included dark red, deep yellow with some red, the frames have a light red or pink field and doors in white with a dark red filling.
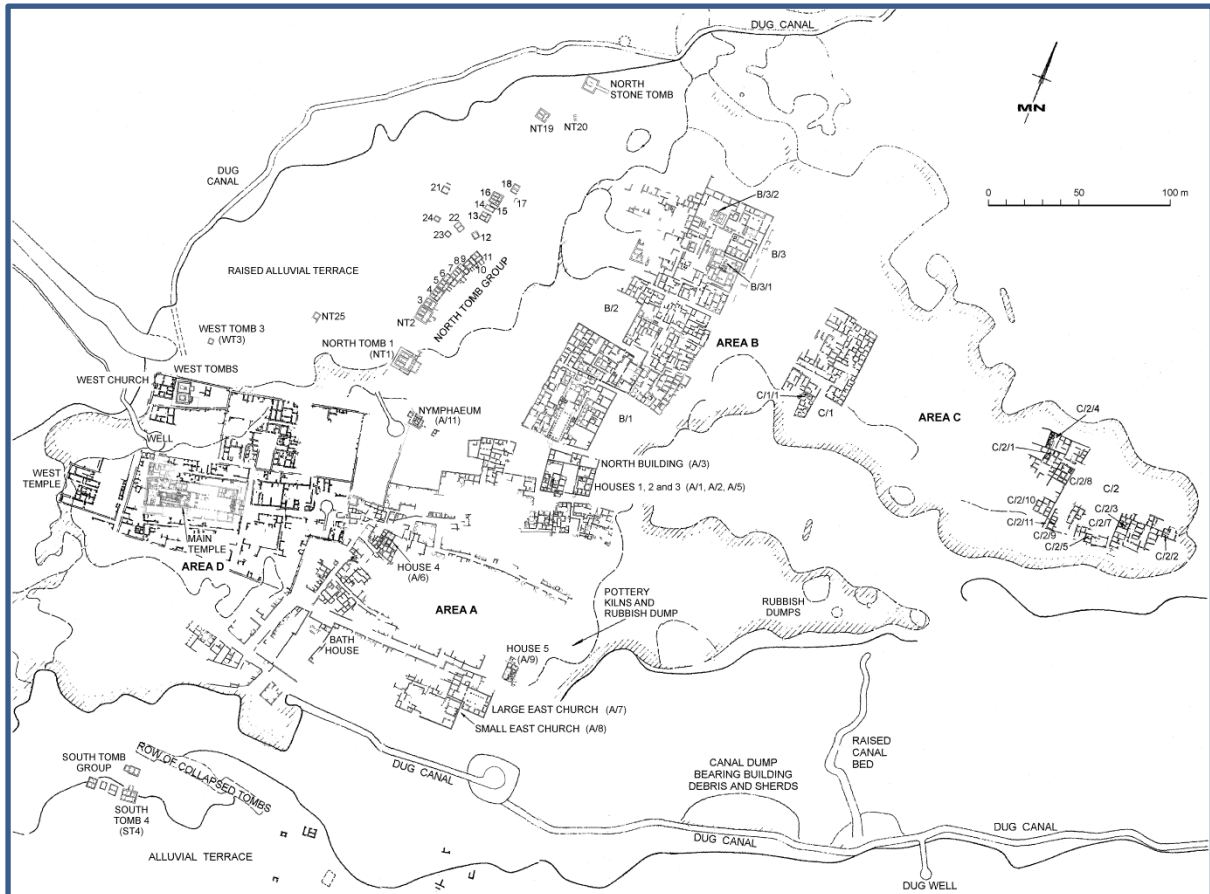
Figure 1.3. Plan of Kellis showing the position of the excavations and which has provided some of the samples analysed (drawing adapted by B. Parr from originals) © A/Prof. C.A. Hope.

Area B

Area B is located to the north of Area A and east of the North Tomb Group. Structure B/1/1 in the south contains more than 216 rooms, courts and corridors (Hope *et al*. 2010; Hope 2015). A test excavation in the south-west corner of a large colonnaded hall revealed elaborate wall and ceiling paintings (Hope 1988: 173-175, figs 12 and 13) and another in the north of the same room also exposed painted wall decoration (Hope (2002: 173). Other decorated rooms are visible at surface level.

Painted residence, B/3/1

The northern part of Area B contains a number of large residences. An elaborate residence B/3/1, constructed probably during the second century CE, witnessed various modification and reuse until the fourth century. It resembles that of a Roman atrium house (Hope *et al*. 2010; Hope 2015: 207; Bowen *et al*. 2007: 21-27) and comprises 22 rooms, several of which are elaborately decorated with varying designs and motifs in polychrome, using various

pigment types (Hope *et al*. 2010: 38; Hope 2015: 207-209). The structure is still in the process of excavation. Forensic, or micro-samples were obtained from fragments located within the rubble on the floor of the structures. As such, there is the potential for sample to become microscopically surface-contaminated from the surrounding rubble.

The only other structure that has been excavated in Area B is a columbarium (B/3/2) located just to the north-west of the abovementioned residence. As with the painted residence, the columbarium was occupied in the 2nd and 3rd centuries (Hope *et al*. 2010).

Area C

Area C is located to the east of Area B and north-east of Area A. It extends to the eastern perimeter of the site. Ten structures, or parts thereof, have been excavated in this region, (C/1/1) and (C/2/1-9). They comprise contiguous mudbrick structures, although some discrete units have been identified (Hope 2015: 211). The buildings are domestic in nature and there is evidence that light industrial activity was carried out in some units: potters' and blacksmiths' workshops (Hickson 2002; Eccleston 2002; Hope 2015: 211-213). Textural evidence indicates that Area C was occupied during the 2nd and 3rd centuries. Some wall paintings have been found here also.

Area D

Area D is on the west of the site; it includes the Main Temple complex, the West Temple, domestic structures (D/8), the West Church (D/6) and the West Tombs. The Main Temple is dedicated to the worship of the god Tutu, his consort Tapshay and mother Neith. Tutu is represented as either a sphinx or in human form and who warded off evil. It was constructed in the late first and second centuries C.E.

The Main Temple complex occupies an area of approximately 40 m X 80 m, the inner temenos measuring approximately 27 m X 70 m and which was subsequently increased in area on all sides. The complex includes the stone temple (D/1) with an extensive colonnaded courtyard to the east, four shrines (D/2 – 5) and a court to the west of the Contra Temple. All of these structures were surrounded by an outer enclosure wall. The colonnaded courtyard and the shrines, all built of mudbrick, were decorated. Shrine 1 (D/2), the *mammisi* (birthhouse) displays a combination of decorative elements including classical-style rectangular panels with grapevine motifs shown around the borders. Above these panels are hieroglyphic inscriptions, figures of Egyptian deities and scenes with human figures garbed in traditional dress. Based upon papyrological evidence, Hope (2001a) proposed that the temple ceased to serve a religious function from around the middle of the 4th century CE and subsequently served various secular functions. A number of pigmented samples from collapsed walls have been obtained from Shrine 1, situated in the southwest corner of the Main Temple.

A series of mudbrick domestic structures (D/8) located to the north of the western section of the temple have also been excavated (Hope 2015: 223-224). Textural evidence indicates that these were occupied throughout the 4th century.

Other excavated structures in Area D include West Tombs 1 and 2 (D/7), the West Church complex D/6) and its associated cemetery (D/7). These are located within Enclosure 4, north of D/8 and on the western periphery of the site. The tombs are Classical in their design and are unique in Egypt (Hope and McKenzie 1999).   Their date of construction is uncertain but they predate the 4th century. The West Church, which comprises a church and a seven-room structure to its south, was built directly behind the West Tombs sometime in the second half of the 4th century (Bowen 2002) and a small cemetery was established to the east of the church with two burials were also located within the church itself (Bowen 2003a; Hope 2003: 244-252).

North and South Tomb Group

The North Tombs are located in the northwestern edge of the settlement and consists at least twenty mud-brick mausolea (Kundstad and Frey 1999: 189-214; Hope 2001b; 2003: 252-282). These tombs are roughly aligned in a single row which extends towards the northernmost area of the site. Six tombs have been excavated: NT1, NT2, NT 5-7 and NT16 (Hope 2004a: 19-26).   North Tomb 1, the largest of the group, was decorated; the walls of Room 4 are painted in monochrome red and the ceiling was once painted in polychrome with geometric and floral motifs, as indicated by the fragments that had fallen in the north-west corner of the room (Hope 2003: plate 48); Room 2 is painted yellow. The neighbouring Tomb 2 yielded fragments of painted cartonnage and a funerary bed (Hope 2003: 272-277). These two tombs have provided five pigment samples.

The South Tomb Group, is located at the southern edge of the settlement. These tombs are not well preserved.   A three-room monumental tomb, ST4, is the most elaborate of the better-preserved tombs and is the only one to have been excavated (Hope 2003: 282-284).

Kellis Cemeteries

  The two cemeteries associated with Kellis are located north of the settlement and on either side of the northwest *wadi* which runs from the northeast to the west of the settlement boundary. The west cemetery (DOP number 31/420-C5-1), referred to as Kellis 1, consists of a significant number of small chambered tombs which are cut into a series of low-rise mounds on the west of the *wadi*. Twenty-six have been excavated and a large number of mummified bodies covered with painted cartonnage were found (Birrell 1999; Hope 2014); the cartonnage has provided a number of the 'forensic' samples for analysis. The cemetery has been dated to be in use from the Ptolemaic period to the 3rd century CE.

The east cemetery, Kellis 2 (31/420-C5-2) is located some 200 m north-east of the northernmost mud- brick mausolea in the North Tomb group and on a low, undulating rise. The cemetery extends for at least 150 m east-west and 60 m north-south and there are an estimated 3,500 – 4,000 burials in pit graves (Bowen 2003a).   Thirteen small mudbrick mausolea have been identified within the cemetery and six have been excavated. In excess of 750 pit graves have been excavated, many of which are intact. The burials are all oriented east-west with the head of the deceased placed to the west: this is typical of Christian burial practice. The cemetery was in use from the late 3rd century and throughout the 4th century.

1.1.1.2.2 Mut al-Kharab

Mut al-Kharab (Mut the Ruined) is located to the south-west of Mut, the modern capital of Dakhleh Oasis and occupies a large mound, the dominant feature being a substantial mudbrick enclosure measuring ~240 m north/south X 180 m east/west, which housed the temple of Seth, Lord of the Oasis (Hope 2001; Hope 2009).

Excavations have been underway since 2001 and are continuing. The stone from the temple was mostly robbed but sections from the lower wall have been uncovered. The surrounding shrines and ancillary buildings are of mudbrick and several have been excavated, as have a number of trenches. Ceramics and architecture from the Old Kingdom, as well as ceramics from the indigenous Sheikh Muftah culture, have been uncovered at the site and material remains from the Middle and New Kingdoms, the Third Intermediate, Late, Ptolemaic and Roman and Late Roman periods has been found. The site has also yielded quantities of Islamic glazed ware, the earliest being from the Mameluk period. In the south west corner of the enclosure is a large open well with significant quantities of yellow and red ochre deposits. Samples of raw pigment were found here.

1.1.1.2.3 Dayr Abu Matta

Dayr Abu Matta is located in western region of Dakhleh Oasis, and is situated on a low mound 2.5 km north-west of the village of Rashda. The site comprises a triconch church and a tower-like building to the west which probably identifies it as a small monastic settlement (Bowen 2013). There are remains of structures to the north of the church and to the south of the tower-like building. The full extent of the site cannot be determined due to the encroaching cultivation. The church has been excavated in full and select sections of the west building, as well as structures to the immediate north of the church have also been investigated. Numerous Christian graves were found both within the church and to its north and west.

Coins, the ceramic and glass assemblage, as well as ostraka, indicate that the settlement was occupied from the late 4th century to the 6th century. The small glass boss analysed in this thesis has been dated to 5th or 6th century CE.

1.1.1.2.4 Qasr al-Dakhleh

The Islamic town of el-Qasr (the Fortress) located in Western Dakhleh, was probably founded at the end of the 12th century over the remains of an earlier Roman-period settlement. The Qasr Dakhleh Project was commenced in 2005, for the purpose of restoring and preserving abandoned mudbrick houses of the Islamic period (Qasr al-Dakhleh Project http://artsonline.monash.edu.au/ancient-cultures/files/. In 2008 permission was granted to undertake excavation on a Roman-period structure, which revealed the walls of a strong fortress with walls up to six metres thick; it probably dates to the late 3rd century CE (Kucera 2012: 305-3160). The site has provided Islamic opaque glass bracelets and glazed pottery sherds but not provided within this thesis.

1.1.1.3.1 Dakhleh Oasis sample find locations

Other than surface finds which are identified by their general location, the context of each sample is discussed in the respective Chapter and together with an identifying image in the respective Appendix.

As stated, the samples from the Western Desert which were analysed were recovered from the Dakhleh Oasis at Mut al-Kharab, Dayr Abu Matta, Qasr al-Dakhleh and principally from ancient Kellis (Ismant al-Kharab). One alum sample was obtained from Kharga Oasis.[1]
All find locations are provided in the appropriate Appendix.

Forty-six samples of pigments applied to walls and cartonnage from Kellis dated to 2nd century CE, are discussed in the respective Chapters and Appendices. A link to all of the raw data and additional information is provided:

https://drive.google.com/drive/folders/0B1MXnIeNTO4icGV6dTFSaXhOQU0?usp=sharing

The Western Desert finds at ancient Kellis (Ismant al-Kharab) and Mut al-Kharab within the Dakhleh Oasis are listed below and in Appendix A3. They are generally dated to the 4th century CE, although one Ramesside period (1295-1186 BCE) blue-painted pottery sample and an additional sherd from the Ptolemaic period (332-30 BCE) were provided. All sherds were from excavations conducted at Mut al Kharab or from the ancient village of Kellis.

Mut al-Kharab – pigments on pottery

Eight samples of pigments on pottery from Ramesside, Ptolemaic and 4th century CE periods.   All are surface finds and are as follows:

Blue painted	1 sherd – Ramesside period
Egyptian blue	1 sherd – Ptolemaic period
Monochrome decorated	6 sherds – 4th century CE

Six trench micro samples of raw pigments not attached to any medium and tentatively dated to 747 to 525 BCE, as follows:

Mut al-Kharab, trench pigment samples.

Trench 18	1 micro-sample - Egyptian blue
Trench 29	1 micro-sample, pigment – yellow ochre
Trench 35	1 micro-sample, pigment - red
Trench 36	1 micro-sample, pigment, 25/26th Dynasty - red
Trench 38B	1 micro-sample, pigment – red ochre
Trench 38	1 micro-sample – Egyptian blue

---

[1]Dr. Andrew Shortland, Cranfield University is thanked for supplying the sample

Forty-six samples of pigments applied to walls and cartonnage from Kellis dated to 2nd century CE, as follows:

Kellis – pigments, and pigments on plaster and cartonnage

	Main Temple Complex, Area D
Shrine I	8 samples pigmented surface
Shrine IV	2 samples pigmented surface
Shrine IV	1 sample – Egyptian blue

	Large East Church, Area A
Church A/7	2 micro-samples, pigment

	Painted wall decoration in B/3/1.
Wall samples	20 micro-samples, pigment

Pigments on Cartonnage

	Kellis
North Tomb 1	4 samples pigmented surface
North tomb 2	1 sample – Egyptian blue
	Kellis 1 cemetery
Tomb 16	1 sample, pigment
Tomb 16	1 sample - Egyptian blue
Tomb 20	2 samples, pigment
Tomb 21	2 samples, pigment
Tomb 22	1 sample – Egyptian blue
Tomb 23	1 sample, pigment

1.1.2 Nile valley and North Sinai Regional and samples

For comparative purposes, 34 sherds obtained from random surface finds within the Nile valley and North Sinai were analysed and their general find locations are listed below. A map for their location is provided in Figure 1.1. The Nile valley sherds were all surface finds which were recovered from various sites in the floodplain and south to Thebes (Malkata/Karnak/Deir el-Medineh/Luxor), and at both Amarna and North Sinai. Many of these Nile valley sherds were blue painted pottery from the New Kingdom (18th-20th Dynasties). The samples are discussed in Chapters 3 to 5 and all analytical data is provided in Appendices A3 to A5 in the link:
https://drive.google.com/drive/folders/0B1MXnIeNTO4icGV6dTFSaXhOQU0?usp=sharing

Nile valley samples analysed included:
- Malkata ("the place where things are picked up") which was the site of the palace-city of Amenhotep III (c. 1390-1352 BCE) on the West Bank of the River Nile at Thebes (Luxor) (Hayes 1951a-1951d); Hope 1989: 3-4); Wypyski 1998); Nicholson and Peltenburg 2000). Between 1910 and 1922 the Museum of Art, New York undertook excavations at Malkata, with later excavations being conducted by the University of

Pennsylvania during the years 1971-1974.   These excavations provided evidence of faience and glass production including numerous fired clay moulds, faience objects and lumps of colouring matter. As discussed by Nicholson and Peltenburg (2000) whilst the Malkata site is chronologically earlier than Amarna, the production is not as well documented as the Petrie finds at Amana. They noted that the workshops at Malkata probably directly preceded the workshops at Amarna.

- Amarna is situated approximately half-way between the ancient capitals of Memphis and Luxor. It was the 18th Dynasty capital city occupied by Akhenaten (1352-1336 BCE) and as such, is chronologically later than Malkata.
- Other samples were provided from Karnak North, Deir el-Medineh, Dendera and North Sinai and are listed below.

Samples analysed are as follows:

Anubieion, Saqqara

Anubieion is located on the desert edge overlooking the Nile valley. It is the site of a mainly Ptolemaic temple, Mastaba tombs, pyramids and their associated temples. Anubieion has been described by Smith and Jeffreys (1979) and the actual sample analysis is provided in by French (2013: 343).

Blue painted   1 micro-sample, probably 19th Dynasty

Amarna

Located on the east bank of the River Nile, the city is situated approximately half-way between Memphis and Luxor. It was the 18th Dynasty capital city occupied by Akhenaten (1352-1336 BCE) and abandoned shortly after his death. As such, it is chronologically later than Malkata by a period of 15 to twenty years.

Monochrome painted   1 sherd – late 18th Dynasty, surface finds
Blue painted   8 sherds – late 18th Dynasty, surface finds

Deir el-Medineh

This was the village occupied by the artisans who worked on the tombs in the Valley of the Kings during the 18th and 20th Dynasties. The site is on the west bank of the Nile, south of the Valley of the Kings. The tombs of the workmen themselves are located just outside the village walls and are richly decorated.

Blue painted   1 sherd – Ramesside, surface find

Dendera

Large temple complex, dedicated to Hathor. The temple that stands today was built by Kleopatra VII but there is evidence for an 18th Dynasty temple. It is located in Upper Egypt near Qena, midway between Abydos and Luxor.

Blue painted   1 sherd – New Kingdom, surface find

Karnak North

Temple complex, located 2.5 km north of Luxor and is the location of the Temple of Montu and the Treasury of Thutmose I plus other structures. It was the main place of worship of the god Amun, in the 18th Dynasty. It is adjacent on the north to the enclosure wall around the temple of Amun complex proper.

Blue painted	3 sherds - probable late 18th Dynasty, possibly 19th Dynasty. From a sherd dump over the remains of the Treasury of Thutmose I that also contained some inscribed material of Akhenaten; stylistically the pieces are late 18th Dynasty

Malkata

Hope reported that the available evidence would suggest that the site at Malkata was occupied only during the late 18th Dynasty, and most of the recovered pottery can be dated to the last decade of the reign of Amenhotep III.

Egyptian green	1 sherd – late 18th Dynasty, surface find
Yellow, orpiment	1 sherd - late 18th Dynasty, surface find
Monochrome painted	3 sherds - late 18th Dynasty, surface find
Blue painted	9 sherds - late 18th Dynasty, west of the palace complex
Egyptian blue	2 sherds – late 18th Dynasty

Saqqara.

Saqqara is the Memphis cemetery, Memphis being the main administrative centre throughout much of the Pharaonic period and sole capital of the early Dynastic and Old Kingdom. It is located at the mouth of the Nile delta, and served as a regional centre for commerce, trade and religion. Memphis was under the protection of the god Ptah, the patron of craftsmen. It was at Memphis that the kings were crowned.

Blue painted	2 micro-samples, Ramesside. Sherds from contexts assigned to phase IIa at Kom Rabia (Jeffreys 2006: 12-24).

North Sinai, Bir al-Abd

Blue painted	1 sherd late 18th Dynasty. Exact find spot is unknown

CHAPTER 2. ANALYTICAL METHODS

(a)   FEI Quanta 3D FEGSEM™ Focussed Ion Beam electron microscope (Monash Centre for Electron Microscopy)
(b) Renishaw Raman spectrometer

2.1 Methodology

The prohibition on removal of archaeological material from Egypt places a greater emphasis on the preservation of the material held outside of Egypt. Thus, a greater emphasis is now required to ensure that the maximum information is gained from objects without resorting to destructive analytical methods. Museums worldwide are now very reluctant to allow any physical damage to occur to items now in their possession, or to allow artefacts to leave their premises. For this reason, modern analytical instruments which meet the non-destructive requirement have been adopted in conducting this research program. The results obtained clearly identify the claim that such methods are capable of providing in-depth analyses of these varying types of artefacts.

In order to understand the chemical construction of a pigment, both its elemental composition and its mineralogy are required. Previous researchers have used both XRD and electron microscopy to garner this information, techniques which in the past have required sample removal. The approach being adopted in this research is to use low vacuum electron microscopes which alleviate the need for carbon or precious metal coating or sample removal and the synchrotron for large area mapping for elemental analysis. Raman spectroscopy has been adopted to non-destructively determine the mineralogy of all samples.

Each of the instruments used are described below.

By understanding which trace elements are present and their mineralogical form so an understanding of their thermal history can be gained. Dehydroxylation of minerals occurs at varying temperatures.   Changes in mineral structure can also occur at known temperatures. Thus, Raman spectroscopy by determining which minerals are present and in which form has enabled their thermal history to be mapped. Mössbauer spectroscopy can

determine which iron phases are present in a sample and therefore its thermal and the environmental conditions present during its manufacture and/or during sub-surface burial.

2.2 Instruments employed

2.2.1 Optical microscopy

Optical microscopy, first developed in the early 1600s, involves the interaction of visible light with an object or sample coupled with the magnification of the area under investigation to provide greater surface information. Thus, objects smaller than that visible by the human eye may be examined in some detail. Light-optical microscopes are available in two basic forms.   Namely, the biological microscope which requires an optically transparent specimen and the metallurgical microscope in which light is reflected from the surface of the specimen.

An Olympus SZX16 optical microscope fitted with an Olympus DP71 camera and with the output signal being sent to a computer for data collection was used in this study. Stage illumination was achieved using a Leica KL1500 LCD white light source. This instrument is located in the Monash Centre for Electron Microscopy (MCEM).

Images were obtained at various magnifications to enable the objects under examination to be recorded in sufficient detail appropriate for the purpose. A scale bar correct for that specific magnification was fitted to the recorded images.

2.2.2 Scanning Electron Microscope (SEM)

A Scanning Electron Microscope provides an image of the surface of the object under examination using a beam of energetic electrons (Egerton 2005; Stuart 2007; Powell 1990). When the electron beam strikes the surface of a sample some electrons are elastically scattered by the atoms within the sample without a significant loss in energy. These electrons are at a slightly lower energy than the ionising electron beam and are referred to as back-scattered electrons (BSE). Other electrons produce an inelastic collision and are known as secondary electrons (SE). BSE electrons whilst within the sample may result in inelastic collisions and generate SEs. Electrons from within the outer energy atomic shells then fill the vacant holes produced by this emission of SEs from the inner energy shells. This results in energy being released in the form of characteristic X-rays. When fitted with a suitable energy dispersive detector (EDS), the analysis of these X-rays enables elemental analyses down to $Z \leq 4$ to be achieved.

Previously, samples were normally in a dry state surrounded by a high vacuum.   Non-conductive samples such as pigments and pottery required the application of a thin layer of a conductive material such as carbon, gold or other suitable vacuum-applied coating, the choice of type being determined by the elements under investigation. However, modern instruments can be operated under low vacuum (~50 Pa) using water vapour or other gas to remove excessive sample surface charging. Such instruments, as used in this thesis, are of particular importance in the study of archaeological materials as they remove the need for

coating. Furthermore, their design enables much larger samples to be non-destructively analysed.

Semi-quantitative analyses were originally conducted within the Monash Centre for Electron Microscopy (MCEM) using a JEOL 840A SEM fitted with an Oxford Instruments 10 mm^2 Si(Li) X-ray detector with ultra-thin window (UTW) and Inca analysis and imaging system. The microscope was operated at 20 keV, the probe current set at 1 nA and a working distance of 39 mm. The unpolished samples, previously examined by Raman spectroscopy, were carbon coated prior to examination using a Cressington 208 carbon evaporative carbon coater. The instrument was calibrated daily using a copper screen mounted on a standard 12.6 mm diameter SEM sample stub. The electron beam was rastered over a sample surface area of 3,600 μm^2. Whilst the micro-samples were unpolished, they advantageously do not contain contamination from the use of a lead-containing lapping medium as is often the case with polished samples. In a previous study (Jay and Cashion (2013), analysis of ceramic sherds from Limehouse, London, using this sample preparative technique were compared with published results obtained from similar but polished samples from Limehouse, UK analysed by the British Museum. The two methods gave very comparable results confirming the accuracy of this unpolished technique. Spataro *et al.* (2009) conducted comparative analyses at the British Museum using a polished sample of Dehua porcelain, uncoated and under low (30Pa) vacuum and the same sample carbon coated under high vacuum. They stated that the same results were obtained within statistical analytical errors. They then repeated this work under low vacuum using the polished Dehua sample and another sample of porcelain from the same piece but with a fractured surface and reported that the results were virtually the same.

Backscattered electron images (BSE) of the microstructures of the different phases are clearly visible. Elements with low atomic numbers show up dark, high atomic numbers light; thus quartz will appear dark, lead light.

2.2.2.1 FEI Nova NanoSEM 450

After decommissioning of the JEOL 840A an FEI Nova NanoSEM 450™ Field Emission Scanning electron Microscope, which is fitted with a Schottkey-type field gun has been installed by MCEM and has been employed for the later work described within this thesis. The instrument is capable of providing both high resolution images and EDS analyses under both high and low vacuum settings. This instrument is fitted with a Field Emission Gun, a 5-axis stage, IR chamber camera; oil-free pumping system and a retractable DBS annular BSE detector. Low vacuum imaging, LV-BSE detector is also fitted. When used under low vacuum operation, no surface coating of the sample to eliminate surface charging is required. The beam landing energy is continually variable over the range of 30 keV down to 0.05 keV. Beam deceleration; in-lens detectors; NavCam; Helix detector; plasma cleaner; cryo-trap together with Bruker Quantax 400 X-ray analysis system and 60mm^2 Silicon Drift Detector (SDD) with super light element window (SLEW). In the present research, the microscope was normally operated under low vacuum mode at 50 Pa and with a spot size of 5.0 with the working distance set to between 5 and 7 mm.

In conducting the elemental analyses a number of factors were given particular attention, namely:

1. The instrument was calibrated daily using a pure copper grid.

2. Accelerating voltage. An accelerating voltage of 20keV was selected to meet the requirement for exceeding the critical ionisation energy. In some samples, lead could exist at significant percentages. Thus, to excite the Pb Lα X-ray line by a factor of 1.5, a beam energy of 20 keV was selected. However, the higher the accelerating voltage, the larger the interaction volume and therefore the greater the interference from subsurface elements. Thus, as beam electrons enter a sample they interact as negatively charged particles with the electrical fields of the specimen atoms. This interaction can deflect beam electrons along a new trajectory, known as "elastic scattering". The probability of elastic scattering strongly increases with increasing atomic number because heavier atoms have a much stronger positive charge on the atomic nucleus, and decreases as the electron energy increases. The Back Scattered Electron (BSE) signal at conventional SEM beam energies (>10 keV) is not a surface-sensitive signal. However, as the beam energy is decreased, the range decreases rapidly and the BSE signal becomes much more surface-sensitive at low energy (smaller interaction volume). Opposite to BSE signal yield which increases nearly monotonically with the specimen atomic number, the Secondary Electrons (SE) from pure elements are relatively insensitive to atomic number. The probability of inner shell ionisation is discussed by Powell (1990). Ionisation when plotted as a function of overvoltage increases rapidly from an overvoltage of 1 to a maximum of about 3. As beam electrons lose their energy because of inelastic scattering, they can interact with atomic inner shells down to overvoltages as low as 1. Thus the most important factor in determining the limits of detection in X-ray analysis is the presence of a continuum background. That is, non-characteristic radiation at the same energy as the characteristic radiation of interest. In considering the maximum overvoltage it must be noted that increasing the incident energy as large as possible for a specific excitation energy of an element in a specimen ensures that it is possible to measure a smaller elemental mass fraction. However, such high beam energies enable beam electrons to penetrate deeper into the sample under analysis. Thus, X-rays are produced deeper in the specimen, increasing the interaction volume. This can therefore degrade the spatial resolution of analysis and by increasing the path length within the specimen increase the absorption of X-rays within the specimen before they are measured.by the X-ray detector. This absorption reduces the measured X-ray intensity, degrades the limits of detection and increases the uncertainty of the correction for absorption that must be applied in the ZAF quantitative analysis procedure. Therefore, as the samples under analysis in the present research program may be considered to be thick, bulk specimens, the optimum beam energy beyond which further increases in beam energy would reduce the analytical performance was considered to be 20 keV. This was based upon the likelihood that the highest atomic number element would be lead (Z = 82) (Goldstein *et al*. 2003). At this voltage, the Pb Lα line is activated and this is well separated from the Pb Mα line and well distant from sum peaks and pile up. At this beam energy, all possible peaks of an element in the range 0.1 - ~15 keV will be excited with increasing

efficiency as the photon energy decreases. It should be noted that the As Kα line overlaps the Pb Lα line and this overlap needs to be considered in any analysis in which both elements are present.

3. Count rates in excess of 10,000 cps with a dead time of 10 – 30 % and a minimum beam time of 60 seconds was selected.

4. To minimise the known interference effect of sum peaks (pulse pile-up) caused when X-ray photons reach the detector at nearly the same time, and the pulse processing electronics erroneously record the sum of their energies rather than each one individually. This is a particular problem for samples containing high silica due to the sum of the Si and O energies distorting the shape of the overlapping S Kα and the Pb Mα lines. In the present analyses the Pb Lα energy line was selected. However, for comparative purposes, the data was also constrained to the Pb Mα line and is similarly provided. Thus, pulse pile-up occurs if a photon arrives at the detector before the linear amplifier is finished processing the preceding phonon. Pulse pile-up can be reduced by decreasing the processing time for each phonon because shorter linear amplifier output pulses are less likely to interfere with each other. Thus, pulse pile-up will lead to incorrect phonon energy assignment because of inaccurate pulse light measurement. Sum Peaks occur if two phonons arrive at the detector almost simultaneously and the output is a single combined peak corresponding to the sum of the phonon energies.

5. It should also be noted that there is overlap of the Pb Lα line with the As Kα line. Also, the overlap of the As Lα line with the Mg Kα line.

2.2.2.2 FEI Magellan 400 XHR FEGSEM

The Magellan 400 FEGSEM is an extreme high resolution (XHR) instrument equipped with a monochromator allowing improved resolution at low accelerating voltages. This system is fitted with a Quickloader sample loading station allowing for fast transfer of samples without compromising the vacuum. Also equipped with a large area SDD x-ray detector, the instrument comprises an FEG; 5-axis piezo stage; IR chamber camera; oil-free pumping system; retractable DBS annular BSE detector; retractable STEM3 detector; quick loader; beam deceleration; in-lens detectors; NavCam camera; plasma cleaner; cryo-trap; Bruker Quantax 400 X-ray analysis system and 30mm^2 SDD with(SLEW.

The sample was carbon coated as described above before examination in the microscope.

2.2.2.3 FEI Focussed Ion Beam microscope (FIB)

The FIB can be used under low vacuum or high vacuum. In this instrument, an accelerated beam of electrons is used to examine the sample and provide elemental information via an SEM-EDS detector. The method can be non-destructive and under low vacuum mode does not require the application of a conductive coating to the surface under examination.

In this study the Quanta™ 3D FEG DualBeam technology microscope manufactured by FEI Company™ located in MCEM, was used under low vacuum conditions to avoid the need for carbon or other coating. To achieve the prevention of surface charging of the sample, water vapour was introduced into the sample chamber to remove excess charge. The instrument is fitted with an SEM-EDS detector for elemental analysis. It was normally operated in Backscattered Secondary Electron (BSE) mode and at a working distance (WD) of approximately 10 mm and an accelerating voltage of either 15 keV accelerating voltage, ~1.7 nA beam current or 20 keV with ~4 nA beam current in low vacuum mode at a pressure of 60 to 100 Pa. Imaging was conducted using either 4Q BSED for BSE compositional analysis, or LVSED for SE topographical analysis. EDS analysis was conducted by means of EDAX Apollo SDD plus EDAX Genesis analysis software. Because of the low vacuum operation, the electron beam exhibits slight coning or skirting and therefore together with the interaction volume the results obtained for the spot analyses as reported herein are considered to be semi-quantitative. However, by directly examining the surface of the sample, features removed in sample polishing become visible. The instrument was calibrated daily using a pure copper disk. As has been previously reported, sodium can migrate under the electron microprobe. To minimise this, and other potential errors, several analyses were conducted over areas of approximately 1-2mm² and the results averaged. Previous studies have shown that this technique provides a sufficiently high degree of accuracy (Shugar and Rehren 2002; Spataro *et al*. 2009; Jay and Cashion 2013).

The FIB was used to "mill" material from the sample with nanometre precision using a beam of positively charged gallium (Ga⁺) ions.   Because the ions are much more massive than electrons, the higher-mass ions dislodge neutral and charged particles (atoms, molecules, and multi-molecular particles) from the sample surface.   In this instrument, the electron and ion beams intersect at a 52° angle at a coincident point near the sample surface, enabling SEM imaging of the FIB-milled surface.

2.2.3 Synchrotron X-ray fluorescence microscopy

The XFM beamline of the Australian Synchrotron used in this research relies on x-ray fluorescence (XRF) to obtain ppm level detectability for elements with atomic numbers (Z) ≥ 19. In this instrument, electrons produced by the electron gun by thermionic emission, pass to the linear accelerator operating at a frequency of 3 GHz to accelerate the electron beam to 100 MeV.   The booster ring, which is 130 metres in circumference, is the electron synchrotron. It takes the 100 MeV beam and increases its energy to 3 GeV. The booster ring contains 60 combined function (steering and focussing) electromagnets to keep the electrons inside the stainless steel vacuum chamber circulating at high speed.   The accelerated electrons then pass to the 216 metre in circumference storage ring which consists of 14 nearly identical sectors. The centripetal acceleration of the electrons results in the emission of bremsstrahlung or braking radiation X-rays. An electron spends about half a second in the booster ring and completes over one million laps. Synchrotron radiation is created when electrons are accelerated to nearly the speed of light. It is this light (X-rays) that are used to excite the sample.

When an electron beam of high energy strikes a material and photons are emitted, this radiation is called bremsstrahlung or "braking radiation". This results from the deceleration

of the electrons inside the material.   When an individual atom is excited (irradiated) by a sufficiently high external energy source it emits x-ray photons from an inner shell (usually a K or L shell) of a characteristic energy or wavelength.   Thus, the interaction between the X-ray beam generated by the synchrotron and the material is this ejection of photoelectrons from the inner shell of the atoms forming the material undergoing analysis.   These photoelectrons leave with a kinetic energy which is described as the difference in energy between that of the incident particle and the binding energy of the atomic electron.

When the ejected electron (photoelectron) leaves the inner shell, a vacancy is created in the electronic structure of the atom. An electron from a higher energy shell will then move to fill the created vacancy. In this relaxation, the atom undergoes fluorescence, or the emission of an X-ray photon whose energy is equal to the difference in energies of the initial and final states. Detecting this photon and measuring its energy enables the determination of the element and the specific electronic transition from which it originated (Jenkins 1988: 4-6). This is the basis for X-ray fluorescence spectroscopy, where elements may be quantified based upon the rate of emission of their characteristic X-rays from a sample being excited. Thus, by counting the number of photons of each energy emitted from a sample the elements present may be identified and quantified.

Another mechanism for the dissipation of the excess energy is through another outer shell electron. This leaves the outer shell in a doubly ionised excited state. The emission of a second photoelectron to regain stability is known as the Auger effect as discussed by Jenkins (1988:6). When an X-ray is scattered with no change in energy this is called Rayleigh scattering, and when a random amount of energy is lost this is known as Compton scattering. Scattered X-rays in XRF create high levels of background radiation (Anzelmo and Lindsay 1987: A181-A185).

Elemental maps were obtained of the samples by raster scanning at an incident energy of 15.75 keV, which is above the binding energy of the elements of interest. The beam was focused using a Kirkpatrick-Baez (KB) mirror system to a 2 μm spot size.   These images show 100 X 100 μm pixels. The resultant fluorescence from the sample was collected using the 384-element Maia detector, operating in fly-scanning mode. The collected data were analysed using the software package GeoPIXE.

2.2.4 Mössbauer spectroscopy

Mössbauer spectroscopy enables the electronic environment of atoms in the element of interest to be investigated. A suitable source nucleus emits γ-rays which are then reabsorbed by the nuclei of the same element present in a solid sample under investigation. Thus, in the proposed study the radioactive source ^{57}Co decays to ^{57}Fe by electron capture. Hyperfine interactions of the nuclei with their environment in a solid result in shifts and splittings of the Mössbauer lines observed in the spectra. The chemical or isomer shift is proportional to the product of the electron density at the site of the nuclei and the change of the nuclear charge radius during the Mössbauer transition. Electronic quadrupole splitting results from the differing spins in the ground and excited states. The quadrupole spitting in iron compounds is different for Fe^{3+} and Fe^{2+} and can be used, together with the isomer shift to distinguish between the two oxidation states (Stuart 2007). With ceramic materials,

Mössbauer spectroscopy can provide information regarding the firing technology and the colour of these materials. Although iron is often only a minor component in ceramics, often in the form of oxides and oxyhydroxides it undergoes a range of transformations during the firing process. Thus, by using the intensities, the magnetic component and the quadrupole splitting of Fe^{3+} and Fe^{2+}, the original firing conditions can be estimated. Furthermore, Mössbauer spectroscopy is able to determine if the firing process was conducted under oxidising or reducing conditions. This can be used to determine if the colour of the artefact is caused by the clay itself or by the redox conditions present during the firing process.

In a similar manner, Mössbauer spectroscopy can be used in the study of glasses containing iron contamination.

2.2.5 Raman Spectroscopy

Micro-Raman spectroscopy is a fast and non-destructive method which can be used for the spot identification of a wide range of materials. This identification depends on spectrum interpretation and on the comparison of the unknown spectrum with an extended library of known spectra. Raman spectra can be recorded by the direct analysis of the artefact or of microscopic samples removed for transportation to a dedicated instrument. The coupling of the spectrometer with a microscope reveals a high spatial resolution, which allows spectra of individual grains with dimensions down to 1 micron to be recorded. Therefore a non-destructive micro-sampling method can be used. Raman spectroscopy can be applied to organic and inorganic materials in solid, liquid or vapour states. It is equally applicable to ancient objects as it is to modern objects of art where it can provide mineralogical information without the need for any sample removal (as opposed to XRD which does require removal of a small sample for analysis). It can provide useful information about amorphous materials (glasses and glazes), not able to be achieved by other instruments.

The Raman Effect, named after Sir C. V. Raman (Nobel Prize 1930) who first established the principle in 1928, is a spectroscopic technique in which radiation in the form of monochromatic light, usually from a laser in the visible, near infrared, or near ultraviolet range, is used to study vibrational, rotational, and other low-frequency modes in a system. The light generated by the laser interacts with molecular vibrations, phonons or other excitations in the system. Not all vibrations are Raman active, there must be a change in the polarisability of the molecule with the vibrational motion (i.e., the polarisability must be strain-dependent), rather than a change in dipole moment. Thus when this radiation is applied to a molecule and which does not correspond to an absorption process, it is scattered. Most of the scattered radiation is unchanged in wavelength and is known as Raleigh scattering. A small portion of the scattered light is slightly increased or decreased in wavelength and this is termed Raman scattering. The resultant shift in energy of the laser photons gives information about the vibrational modes in the system (Edwards and Chalmers 2005; Stuart 2007). This change in energy corresponds to the energy of the vibration. Both energy and momentum must be conserved.

All sherds and wall samples were examined using the Renishaw inVia Raman spectrometer located within the Department of Chemistry, Monash University. The results were obtained at room temperature generally using the 514.5 nm line of a Coherent Innova®70C Spectra

Physics argon and krypton (Kr+-Ar+ ion) mixed gas laser capable of providing blue (413 nm), green (514.5 nm) wavelength light as the excitation source. The red laser (633 nm) also fitted to this instrument was trialled as required.   Some samples were analysed using the 782 nm solid-state laser fitted to the Renishaw RM 2000 instrument.   The beam was focussed down to an approximate 2 μm spot on the sample using an Olympus X50 microscope objective of a Leica DMLP confocal microscope.   Advantageously, such a small spot size minimises any signal being received from adjacent minerals thereby compromising the analysis.   The backscattered light was collected through the same objective.   The Renishaw inVia micro-Raman spectrophotometer was fitted with a thermoelectrically cooled charge coupled device (CCD) array detector and a confocal aperture of 10-100 μm was used; number of pixels on the CCD array was 10. Power at the sample was 1 mW or less to ensure no change in mineral composition during examination. The instrument was calibrated daily using the 520.5 cm^{-1} first order silicon line. Raman data was baseline subtracted and fitted using the Bruker OPUS Ver. 6 software developed by Bruker Optik GmbH.

Up to 50 scans were collected from each sample and a representative number of spectra confirming the mineral composition were then plotted. The sample spot analysed was inspected after each analysis to ensure that no degradation of the sample had occurred. Where fluorescence was encountered it was found necessary to reduce the power at the sample; in turn, this generally resulted in a poorer spectrum.

In stacking the Raman spectra for comparative and data presentation, some loss in detail may occur. The original spectra were always analysed to ensure that maximum data interpretation was made.

2.2.5.1 Raman Spectral database assignment

The major Raman bands indicative of the various mineral species encountered during the various analyses are provided in Appendix A2. Their respective individual major peaks employed in the individual mineralogical determinations are provided in the relevant tables provided in this Appendix.

CHAPTER 3.   PIGMENTS ON POTTERY, WALLS AND CARTONNAGE

3.0   Introduction

The major focus within this chapter is to determine the chemical and mineralogical compositions of the iron oxide-based reds and yellow, arseno-sulphide-based yellow, black, white and green mineral pigments applied to a range of sherds, cartonnage and walls dating from the New Kingdom to 4th century CE.

Egyptian blue decoration and Egyptian green (Green frit) pigments are discussed in Chapter 4, Appendix A4 and cobalt-based pigments are discussed in Chapter 5 and Appendix A5.

The pottery fabrics and the wall and the cartonnage plasters are discussed in detail in Appendix A3. Only a brief summary is provided below. All of the supporting data is provided in:
https://drive.google.com/drive/folders/0B1MXnIeNTO4icGV6dTFSaXhOQU0?usp=sharing

3.1 Pottery samples

The pottery samples examined were recovered more than 30 years ago from the Nile valley and dated to the 18th/19th Dynasty or more recently from the Dakhleh Oasis and dated from the 19th Dynasty to the 4th century CE.

The Nile valley sherds were all surface finds which were recovered from various sites in the floodplain and south to Thebes (Malkata/Karnak North/Deir el-Medineh/Luxor), and at both Amarna and North Sinai. They are described in Chapter 1 and in Appendix A3.

3.1.1 Resumé, pottery fabric

The chemistry and mineralogy of the aluminosilicate pottery is provided in detail in Appendix A3. In the present study, Raman spectroscopy has clearly identified the presence of diopside within the body of almost every sherd. The formation of diopside indicates a firing temperature in the order of 900°C. As shown by Deer *et al.* (1992: 243) it is possible that diopside could have resulted from dolomite reacting with quartz to form tremolite and calcite and then reacting with additional silica to form diopside. However Raman spectroscopy only identified the presence of dolomite in one sherd, suggesting that in the present range of pottery samples this reaction did not occur, or the reaction had gone to completion. It is likely that magnesium was derived from either the clay raw materials selected or from plant ash biomass including kiln and cooking oven ash.

Raman spectroscopy analyses did identify anatase in most of the body analyses.   As rutile is formed at temperatures approaching 1000°C, its non-detection would suggest a firing temperature below this transition point. Although, the reaction rate for rutile formation can be slow and according to Murad (2003) two factors may be responsible for the high thermal stability of anatase, namely coarse particle size and possible reactions with aluminium and silica liberated during the thermal breakdown of kaolin.

Whilst the number of samples available for analysis was limited, Tables 3.1 and 3.2 clearly indicate differences between the earlier Nile valley pottery fabrics and the later Western Desert fabrics at Dakhleh Oasis. Other than one very high calcium-containing fabric from the Ramesside period, the Dakhleh Oasis fabrics are all higher in alumina and silica than the fabrics analysed from the Nile valley. The lime content of the Dakhleh fabrics is low, suggesting that either the silica selected was lower in lime, addition of lime as limestone was discontinued or an alternative source of silica was selected and pulverised. The analysis of a random sample of sand from Dakhleh Oasis is provided in Chapter 4, Section 4.5.1.1. The analysis indicates a low CaO concentration and minor feldspar in the sand, which supports the low lime concentration in the pottery fabric. Some of the Raman data indicate the presence of moganite and this would suggest that chert (flint) may have been ground and used as the silica source. Moganite in chert or flint is discussed in detail by Jay *et al*. (2015). This possibility requires further investigation. Malkata and Amarna fabrics can be separated based upon their alumina content, Malkata being lower in alumina and higher in lime than the Amarna fabrics. Karnak North fabric samples are similar to Amarna fabrics.

3.1.2 Cream slip

The cream surface appearance is directly related to the burnishing process with finer-sized particles present in the body fabric migrating to the surface. As provided in Table 3.3 and Appendix A3, the feldspars of varying composition have been detected within most of the surface analyses. Gypsum, or its anhydrous form, anhydrite, were also detected in the surface of most sherds. This would suggest that as part of the burnishing procedure, gypsum was also rubbed into the surface of the vessel. This would assist in creating the pleasing appearance and a surface suitable for decorating. When fired, the gypsum would convert to anhydrite and thus, the detection of its Raman signature would confirm that the slip coating was applied pre-firing to the pottery vessel. If calcite had also been used, it would have decarbonated on firing, losing its Raman ν_1 symmetric stretching band at 1086 cm^{-1}.

Upon burial, the anhydrite could undergo rehydration and with the known levels of calcium in the sand and soils, under moist conditions either vaterite or calcite could be deposited on to the sherd surface. This could account for the detection of calcite in rare instances.

Table 3.1. Nile valley produced pottery body elemental analysis comparison.

Sample	Al_2O_3		SiO_2		CaO		
	Low (<15%)	High (>15%)	Low (<50%)	High (>50%)	Low (<10%)	Intermed. (10-20%)	High (>20%)
Malkata							
M1	13.0		44.3				22.8
M2	14.1		44.1				22.6
M3	0.3		48.7				49.4
M4		17.3	46.0			13.1	
M5		19.6	48.2		6.0		
M6		15.0		53.6	7.1		
M7	14.2			52.8		18.9	
M8		17.3	49.9			15.5	
M9	11.4		44.7			19.7	
M10	12.7			56.2		17.2	
M11	14.8		49.2			19.8	
M12		16.9		54.1	4.4		
M13	12.2		46.8				21.5
M14	11.8		45.0				24.4
M15	12.8		47.9			15.9	
M16	11.4			50.1		17.3	
Amarna							
A1		17.4		53.2	6.9		
A2		16.2	44.3			12.0	
A3		16.3	42.4			1.4	
A4		20.9		52.3	4.0		
A5		16.7		51.9	5.3		
A6	10.8		41.6				30.9
A7		16.6		56.8	4.5		
A8		15.6		52.3	6.6		
A9	14.1		45.2				22.3
North Karnak							
NK1		16.6		57.4	3.9		
NK2		15.9		51.1	5.8		
NK3		18.3		52.8	4.4		
Dendera							
DE1		17.5	40.0			17.2	
Deir el-Medineh							
DM1		16.4	44.3			12.2	
Sinai							
S1		15.5		54.7	5.3		

Table 3.2. Dakhleh Oasis produced pottery body elemental analysis comparison

Sample	Al₂O₃		SiO₂		CaO		
	Low (<15%)	High (>15%)	Low (<50%)	High (>50%)	Low (<10%)	Intermed. (10-20%)	High (>20%)
Ramesside period							
D7	14.9		33.7				30.6
Ptolemaic period							
D8		20.2		55.3	7.7		
Roman period							
D1		28.9		56.9	1.7		
D2		24.2		60.6	1.9		
D3		24.1		62.6	1.2		
D4		22.3		61.5	1.5		
D5		20.6		59.7	4.5		
D6		21.7		55.8	5.1		

Table 3.3. Elemental analyses of the major elements present in the cream burnished surface found on samples from the Nile valley and the Dakhleh Oasis. Note the effect of substrate elements on the accuracy of the provided information. The analyses closely replicate the results provided for the pottery fabric.

Sample	Al₂O₃	SiO₂	FeO	CaO	MgO	SO₃	Remarks
Malkata							
M2	13.3	45.4	6.4	20.3	1.9	2.8	gypsum
M5	13.6	60.4	8.9	3.8	2.8	0.7	feldspar
M6	15.0	40.6	7.7	22.4	4.0	2.6	feldspar
M7	8.7	4.0	1.0	28.4	38.8	13.1	huntite, gypsum
M8	7.1	46.0	1.9	16.3	18.4	1.7	huntite, gypsum
M9	12.7	41.6	8.0	23.1	3.8	1.5	burnished
M10	14.8	40.8	9.2	22.8	3.1	1.7	calcite, trace gypsum
M11	18.2	44.4	8.6	18.3	4.9	0.3	burnished
M12	8.4	24.6	5.0	22.1	2.9	26.5	gypsum
Amarna							
A2	13.7	39.3	7.2	20.8	4.1	7.0	gypsum, quartz
A3	10.8	34.0	7.0	20.9	4.6	11.4	anhydrite, quartz
North Karnak							
NK1	15.3	50.6	8.5	10.8	4.3	2.8	anhydrite, trace calcite
NK2	15.7	49.7	9.0	8.4	4.8	3.9	calcite
NK3	8.6	29.9	11.5	27.8	1.9	6.4	gypsum or anhydrite
Dendera							
DE1	12.1	27.6	7.5	11.9	2.4	4.6	anhydrite
Dakhleh Oasis							
D2	30.2	50.8	7.2	1.9	2.3	1.6	gypsum, feldspar, silica
D3	25.8	46.9	4.9	6.5	1.2	8.3	gypsum, quartz
D5	28.5	50.5	8.6	2.8	1.9	1.7	quartz
D7	15.3	25.4	4.8	36.6	5.8	2.5	anhydrite, gypsum, quartz, huntite or dolomite, calcite
D8	4.3	6.5	0.6	63.9	3.1	7.1	gypsum

3.1.3 Evidence for post-firing pigment application

In a study conducted by Eliyahu-Behar *et al.* (2016) these researchers investigated the variously termed 'white slip', 'white limey-slip', 'lime wash' and 'lime or white coated' coatings to the exterior and occasionally to the interior of pottery vessels such as those reported from Egypt at Giza and at Abydos during the Early Bronze Age. They proposed that these post firing applied lime-plaster coatings were functional and intended to decrease permeability and protect the contents of these vessels. In their study, they studied the interface between the white coating and the pottery vessel and demonstrated that the SEM images and analyses supported a post-firing regime. And, FTIR supported the pottery to have been fired at a temperature lower than that required to convert limestone into a lime-plaster. Thus, the lime-plaster coating must have been applied post firing to the pottery vessel.

Huntite, was found on the surface of two sherds from Malkata, the Raman spectra of one is shown in Figure 3.1. The presence of huntite would confirm a pigment post firing, otherwise the carbonate anion would have volatilised during any firing process and the calcium and magnesium ions would have entered into a chemical reaction with the underlying pottery. It is unlikely that such a fired coating would have been able to undergo a further reaction with carbon dioxide in the atmosphere and restore the original mineral structure.
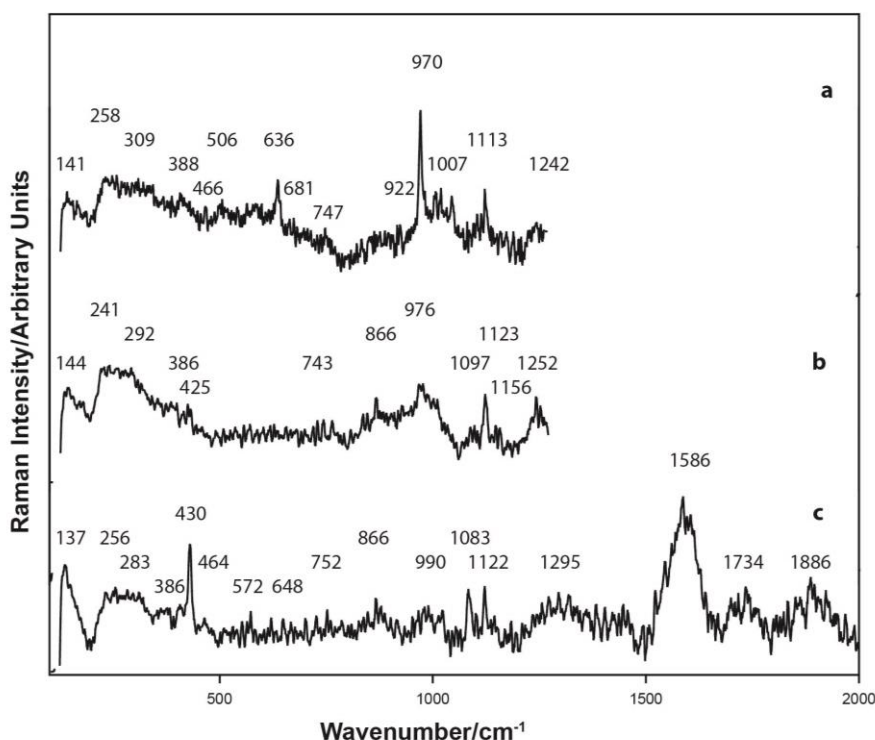
Figure 3.1. Raman spectra, white slip coating on pottery Malkata sherd M8 (M73/K/1406). In spectrum (a) the Raman band at 1007 cm^{-1} is gypsum and the bands at 636 and 970 cm^{-1} show the presence of para wollastonite-*2M*; in (b) the Raman bands at 292 and 386 cm^{-1} is indicative of either traces of goethite (α-FeOOH) or ferroxyhite (δ-FeOOH) and in (b) and (c) the 1122 cm^{-1} band is huntite, (c) the Raman band at 1083 cm^{-1} is calcite; the Raman bands at 430 and 1083 cm^{-1} is indicative of traces of Egyptian blue (λ = 514.5 nm).

3.2 Wall plasters

The chemistry and mineralogy of the wall plasters is provided in Appendix A3.

3.2.1 Samples

As discussed in Chapter 1, all wall samples are from Kellis. The actual data generated for each sample is illustrated within Appendix A3. Appendix A3 also contains the results obtained from cartonnage samples and also from forensic sampling of walls, and from pigments located in trench excavations from Kellis, and Mut al-Kharab. Trench samples[1] and the micro (forensic) samples were obtained by collection directly on to double sided carbon tape applied to 13.5 mm SEM aluminium stubs. As such, this method demonstrates the significant analytical detail able to be derived from such a micro-sampling regime. An image of each micro-sample is provided in Appendix A3.

3.2.2 Resumé, wall decoration plaster

Where plaster was attached to the pigment sample it has been analysed and is reported upon in Appendix A3. It is evident that the wall plaster has been formed using lime water to form calcite as discussed in Appendix A3. And, gypsum was detected in all samples indicating that it either formed part of the plaster composition or has formed by reaction with atmospheric sulphur oxides probably from cooking fires. Cristini *et al*. (2010) observed that a humidity of >40% is essential for calcite to be transformed into gypsum in the presence of sulphur in the local atmosphere. And in their studies of samples stored or located in humid areas, the surface formation of gypsum was only to a depth of 1-3 μm. This may well form part of the gypsum formation observed in a number of sherds within this study. In two of the wall samples (Samples 1 and 7) anhydrite has been observed. This is a clear indication that gypsum has been heated to dehydrate it as part of the plaster composition as it is unlikely that gypsum would dehydrate even under arid conditions. Most plasters show the presence of clays in the form of added feldspars. Sub-rounded coarse silica particles and plant material has been added as extenders within the plaster as clearly evident in the wall plaster images provided in Appendix A3.

A typical Raman spectra of the plaster applied to the south wall, North Tomb, Kellis, and throughout the Dakhleh Oasis, is provided in Figure 3.2. It contains quartz, calcite, siderite [$FeCO_3$] and feldspar (probably as orthoclase or labradorite). The bands at wavenumbers 204 and 278 cm^{-1} indicate the presence of tridymite, a silica polymorph which will form at approximately 1000°C and as such, indicates a high temperature calcination of limestone or other form of calcium carbonate and which must have contained residual quartz in the calcium-containing mineral at the time of calcination.

---

[1]A/Prof. Hope is thanked for sourcing these samples and arranging for their removal from Egypt.
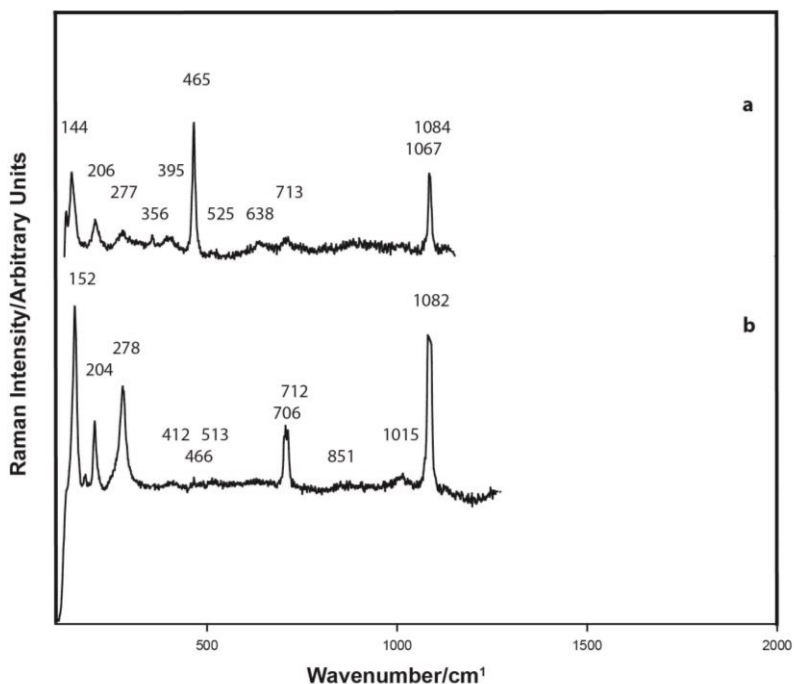
Figure 3.2. Raman spectrum, plaster attached to wall Sample 7, south wall, North Tomb 1, Kellis. The plaster contains quartz, calcite and siderite [$FeCO_3$]. The bands at wavenumbers 204 and 278 cm^{-1} indicate the presence of tridymite, a silica polymorph which will form at approximately 1000°C (λ = 514.5 nm).

3.3 Cartonnage

The chemistry and mineralogy of the cartonnage plaster is provided in Appendix A3.

3.3.1 Samples

As described in Chapter 1 and Appendix A3, five pigmented cartonnage samples were obtained from Kellis North Tombs 1 and 2 and eight pigmented samples from Kellis 1 cemetery. The pigments applied to these samples included three decorated with Egyptian blue and these samples are discussed in Chapter 4 and Appendix A4.

3.3.2 Results and discussion

All of the cartonnage samples examined have used gypsum as the sole plaster composition. Raman spectra to support this determination are provided in Figure 3.3 below.
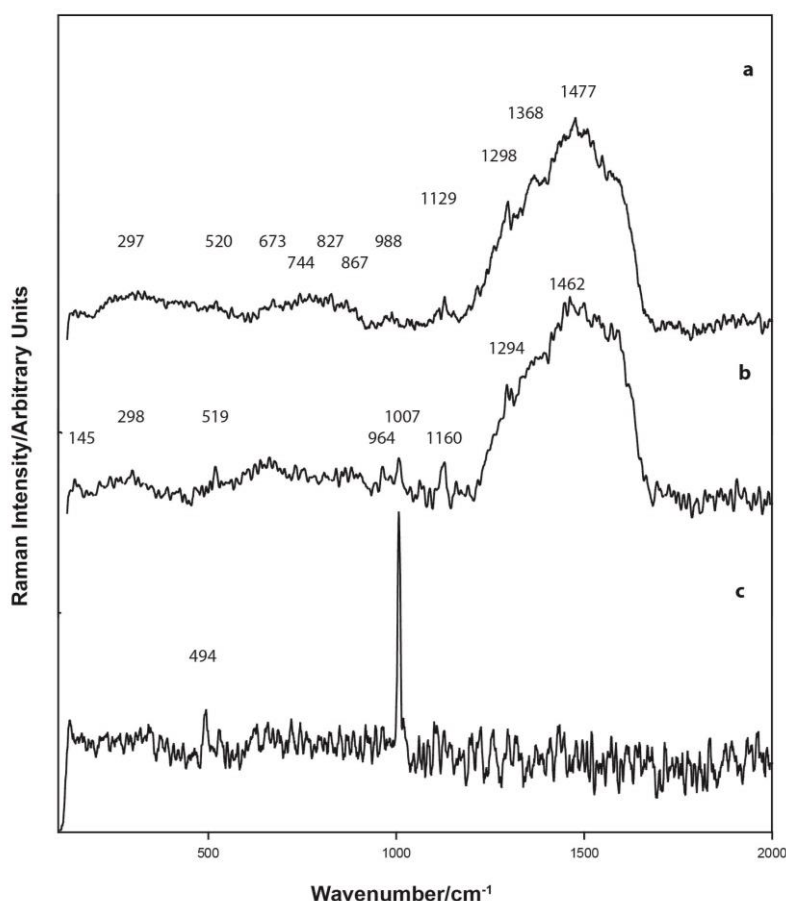
Figure 3.3. Raman spectra of (a) and (b) the green pigment and (c) plaster applied to cartonnage, Tomb No 20, Kellis 1 cemetery. Additional data is provided in Appendix A3 ($\lambda = 514.5$ nm).

3.4 Pigments

The use of inorganic pigments by the ancient Egyptians for the decoration of pottery or mural paintings on the walls of buildings and tombs attest to their careful preparation and usage. These pigments are naturally-occurring and have been widely utilised during all of the Dynastic periods under examination. Lee and Quirke (2000: 105) summarised the principal colours used during the Dynastic period into three pairs, namely black and white, red and yellow and blue and green. Variants to this palette include brown, grey, orange, pink and purple. The surface (ground or slip) on to which the colourant has been applied can influence the pigment choice. For example, the choice of pure orpiment on New Kingdom royal red quartzite sarcophagi as compared with mixed orpiment and ochre on limestone and sandstone temple reliefs from the same period.

Egyptian blue and Egyptian green samples are reported in detail in Chapter 4 and Appendix A4 and cobalt blue pigments are discussed in Chapter 5 and Appendix A5. The raw data for all other pigments discussed in this chapter are provided in detail in Appendix A3.

The Raman spectra produced by naturally occurring pigment materials and used by Egyptian workers are listed in Chapter 2. In this database, the various minerals, compounds and their respective chemical formulae are given. And, the type and style of decoration applied to pottery vessels during the 18th Dynasty have been discussed in detail by Hope

(1989), Shortland *et al*. (2006), Abe *et al*. (2009).   The style of decoration has been used as a method for dating.

Analysis of the various iron oxide and arsenic sulphide pigments is influenced by their applied thickness.   Reference to the individual optical microscope images provided in Appendix A3 will clearly indicate the inhomogeneity within the deposition of the application and/or remaining on the pottery surface after long-term burial or weathering. The electron beam can penetrate the surface under examination by about 5 μm and this is likely to be sufficient, particularly where surface coverage is <100 percent, to enable substrate minerals to form part of the obtained analysis. Whilst every effort was taken to carefully select areas for analysis, the results can only be considered to be indicative of composition and not absolute. This is clearly evident in analyses in which the elements found in cobalt blue (Co, Ni, Zn) are reported in browns and reds (these pigments have been applied over or under the cobalt blue).   A similar outcome could be expected where magnetite-containing black has been applied over brown, or where pigments have been applied over slip coatings. High iron has been reported present in white lines applied over a red substrate. This particular concern was addressed by careful analysis of the pigment substrate as summarised in Sections 3.1 to 3.3.

Iron oxides, the major pigments utilised for reds, brown, black and yellow, are good absorbers in the range of the wavelengths of excitation lasers and therefore become materials which are liable to thermal change. This is particularly important in studies of divalent iron such as wüstite and magnetite (wüstite decomposing at 570°C to form magnetite (West *et al*. 2005). Thus, the laser source used in the Raman spectroscopy analyses can also change the composition of the iron oxyhydroxides by dehydroxylation.   To minimise the effect, low power settings were employed and the spot analysed was inspected for visual change in colour immediately after the spectrum was obtained and the result rejected if any visible change was observed. Thus, some of the oxyhydroxides could contain minor percentages of oxide, that is, portion of the goethite could have changed to hematite but which was not visually evident.   And, the hydration of hematite crystals, which in the presence of water molecules, can interact with the hematite to create OH$^-$ ligands thereby reducing the symmetry around the Fe^{3+} ions.   The greater the distortion around the Fe^{3+} ions, the less saturated is the hue of the red (Cristini *et al*. 2010; Pailhé *et al*. 2008). Parras *et al.* (2010) alternatively proposed goethite can originate from a hydration of hematite. This is not supported by Cornell and Schwertmann (1996: 207) who indicate that under dry conditions, surface Fe atoms may be co-ordinatively unsaturated and because they carry unoccupied atomic orbitals, surface Fe atoms are Lewis acids. As water can donate an electron pair it is a Lewis base. Therefore, in aqueous systems they coordinate with hydroxyl ions or water molecules which share their "lone" electron pairs with Fe. Following adsorption, the water molecules are capable of dissociation, rapidly resulting in a surface covered by hydroxyl groups coordinated to the underlying Fe atoms. This is followed by further adsorption of water molecules which hydrogen-bond to the surface OH groups. These surface hydroxyl groups are the functional groups of iron oxides and are chemically reactive entities.   They possess a double pair of electrons together with a dissociable hydrogen atom and are thus amphoteric, which enables them to react with both acids and bases.   This needs to be borne in mind in considering the published results provided in Appendix A3.

Amorphous carbon has been reported to be present in most samples. Part of this carbon could be directly related to soil from burial and again, this needs to be borne in mind when considering the results provided in Appendix A3.

3.4.1 Black

The Raman signatures for the black pigments used to decorate vessels are summarised in Tables 2.4 and 2.7, Appendix A2. Table 3.4 provides a summary of the iron oxides located on various pottery sherds. Generally, the black lines were the final decorative pigment to be applied to the surface being decorated. They were not fired onto the pottery body.

As provided in Appendix A3, all black pigments applied to pottery were found to contain amorphous carbon and magnetite. The high iron content of the black lines is clearly evidenced in the synchrotron images provided in Figures 3.5-3.7. Only two sherds indicated the presence of a manganese-containing mineral, although minor traces of manganese are located in almost every analysis. Lucas (1989: 340) identified pyrolusite (MnO_2) and this is a possible raw material suitable for such purposes. The Raman signature for pyrolusite provides strong bands at 534 and 664 cm^{-1}, with evidence that the 664 cm^{-1} band can split to form bands at 667 and 671 cm^{-1}. As such, the higher wavenumber band conflicts with the diopside/enstatite Raman signature, making identification of this mineral difficult. Manganese concentrations of up to 4.5% MnO were detected in North Karnak Sample NK2 and at a slightly lower concentration in Dendera sherd Sample DE1.
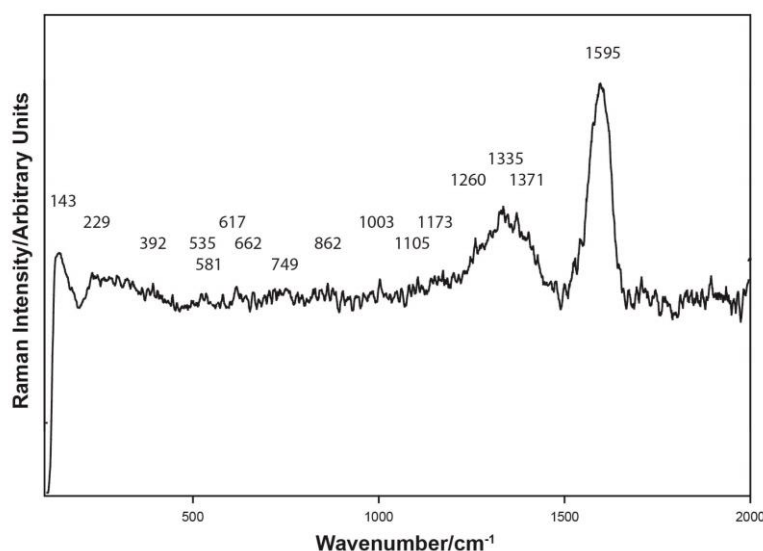
Figure 3.4. Raman spectrum, black line, Malkata sherd M8 (M73/K/1406). This sample contains magnetite (662 cm^{-1}), goethite and amorphous carbon together with diopside and probably feldspar (λ = 514.5 nm).

Relative Concentration Legend

Zero   Maximum
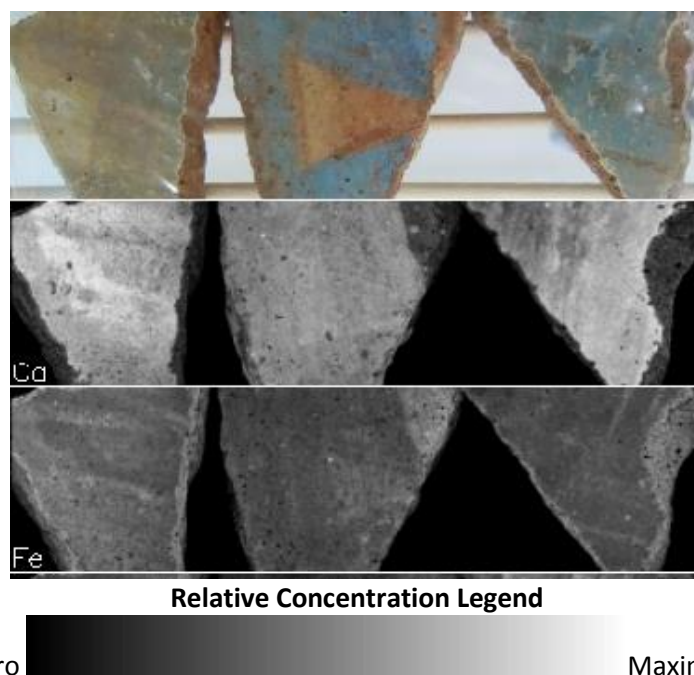
Figure 3.5. Synchrotron elemental maps showing the relative concentrations of elements Ca and Fe which were generated using the XFM beamline for sherds Amarna A2, Malkata M3 and Malkata M5. The additional elements detected are provided in Appendix A5.

Relative Concentration Legend

Zero   Maximum
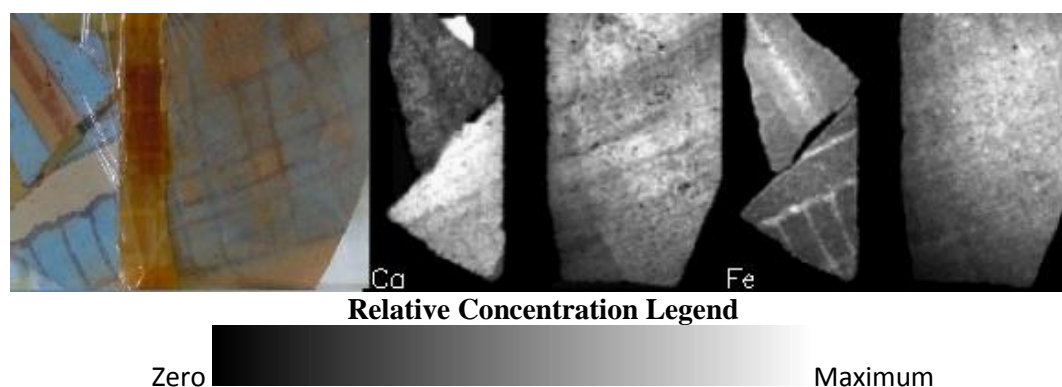
Figure 3.6. Synchrotron elemental maps generated using the XFM beamline for sherds North Sinai (upper left), Deir el Medineh (Lower left), Amarna 4 (Right) and showing the relative concentrations of Ca and Fe. The additional elements detected are provided in Appendix A5.

Relative Concentration Legend

Zero   Maximum
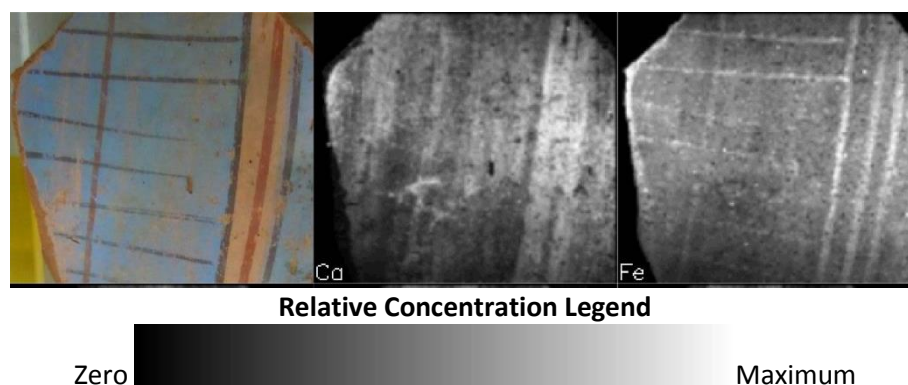
Figure 3.7. Synchrotron XFM beamline element maps of Ca and Fe within a region in North Karnak sample NK3. The additional elements detected are provided in Appendix A5.

The higher iron concentrations obtained from the analysis of the North Karnak sherds is probably explained by the thicker, more uniform pigment decoration applied, or remaining on the surface of these sherds.

The present research would conflict with the statement by Lee and Quirke (2000: 108) that "there is almost no evidence for the use of materials other than carbon for obtaining black in painting during the Dynastic period". The present findings are in accordance with Sabbatini *et al.* (2000) who determined that the black coloured pigment on pre-Roman pottery was either magnetite or carbon of vegetable origin. De Benedetto *et al.* (2010) concluded that if the carbon black was derived from either animal or vegetable matter it would not provide a Raman peak at 960 cm^{-1} indicative of phosphorus (the $\nu(PO_4)^{3-}$ symmetric stretching vibration). Distinguishing 'bone black' from other types of carbon is discussed by Cavalheri *et al.* (2010) and Parras *et al.* (2010) both of whom concluded that if no peak at 960 cm^{-1} is observed to indicate bone material, then either soot or plant ash was used as the carbon black. This conclusion ignores the possibility for magnetite to be present. When the elemental phosphate analyses are sufficiently low or in cases where bone ash has not been detected by its Raman signature, the small spot size of the Raman laser (lens dependent) may account for the non-observance of the 960 cm^{-1} band.

Table 3.4. Elemental analyses of the major elements present in the black pigment on pottery sherds. Note the potential effect of substrate elements on the accuracy of the provided information.

Sample	FeO	SiO$_2$	Al$_2$O$_3$	CaO	MgO	Mineral					
	%	%	%	%	%	1	2	3	4	5	6
Malkata											
M9	7.7	32.3	35.5	6.3	4.5	■	■	■	■		■
M15	6.5	47.8	13.4	9.7	7.7						■
Amarna											
A3	6.8	32.5	8.8	22.2	5.0	■	■	■	■	■	■
A4	9.9	12.3	25.5	14.5	2.8	■			■		■
A6	2.1	15.1	12.9	48.8	1.3				■		
North Karnak											
NK1	24.2	22.8	9.3	16.4	2.2	■	■	■	■	■	■
NK2	24.0	19.5	31.7	3.3	7.3	■	■		■	■	■
NK3	11.5	29.9	8.6	27.8	1.9		■		■	■	■
Dendera											
DE1	17.5	21.8	14.0	17.2	2.2	■			■		
Deir al-Medineh											
DM1	5.8	20.0	7.3	25.4	1.6	■	■		■		■
Sinai											
S1	12.3	54.7	15.5	5.3	3.0	■	■		■		
Dakhleh Oasis											
D1	7.1	50.2	29.3	1.5		■	■	■	■		■
D6	10.9	49.0	27.3	1.4		■	■	■	■		■
D8	3.0	17.0	8.1	52.7	3.4	■			■	■	

1= magnetite   2=hematite   3=goethite   4=amorphous carbon   5=apatite   6=MnO

Dendera sherd DE1 has the residues indicative of a very thin black line drawn on its surface. As such, the pigment analyses are strongly modified by the substrate. However, as shown in Raman Figure 3.8, and in the EDS data provided in the Area and spot analyses in Appendix A3 indicate a high concentration of iron oxide and applied to an aluminosilicate body or surface containing gypsum. This data is summarised below. The Raman signature for magnetite is observed in Figure 3.8.

Area analysis, black line applied to Dendera sherd DE1.

Na$_2$O	MgO	Al$_2$O$_3$	SiO$_2$	P$_2$O$_5$	SO$_3$	Cl	K$_2$O	CaO	TiO$_2$	MnO	FeO	CoO	NiO	CuO	ZnO
6.1	2.2	14.0	21.8	0.1	11.5	4.8	1.8	17.2	0.7	1.0	17.5	0.6	0.3	0.0	0.3

Whereas, as provided in Appendix A3, and in Figures 3.9 and 3.10, the thicker black pigments found on North Karnak, Amarna and Deir al-Medineh and sample D6 from Dakhleh Oasis all contained amorphous carbon and significant hydroxyapatite indicative for the use of bone ash or from a similar animal origin, such as ivory. The Raman band at 958 cm^{-1} in Figure 3.10 can be ascribed to phosphate. Caggiani and Colomban (2011) have discussed in detail the identification of black pigments.
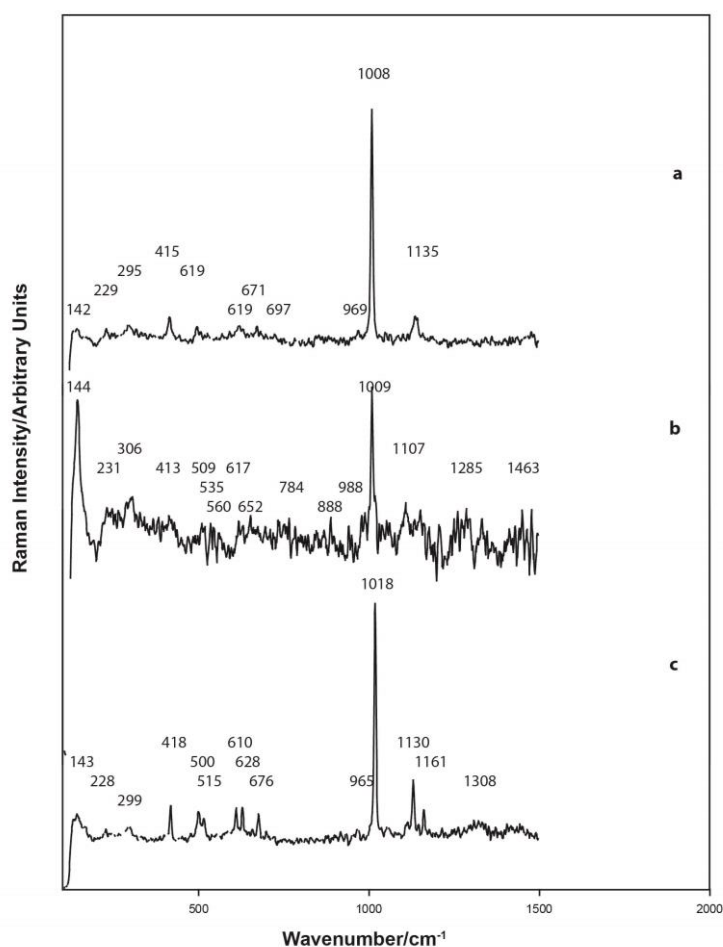
Figure 3.8. Raman spectra, black pigment on pottery surface of Dendera sherd DE1 The black line contains gypsum and anhydrite, magnetite, feldspar, amorphous carbon, and probably diopside ($\lambda = 514.5$ nm).
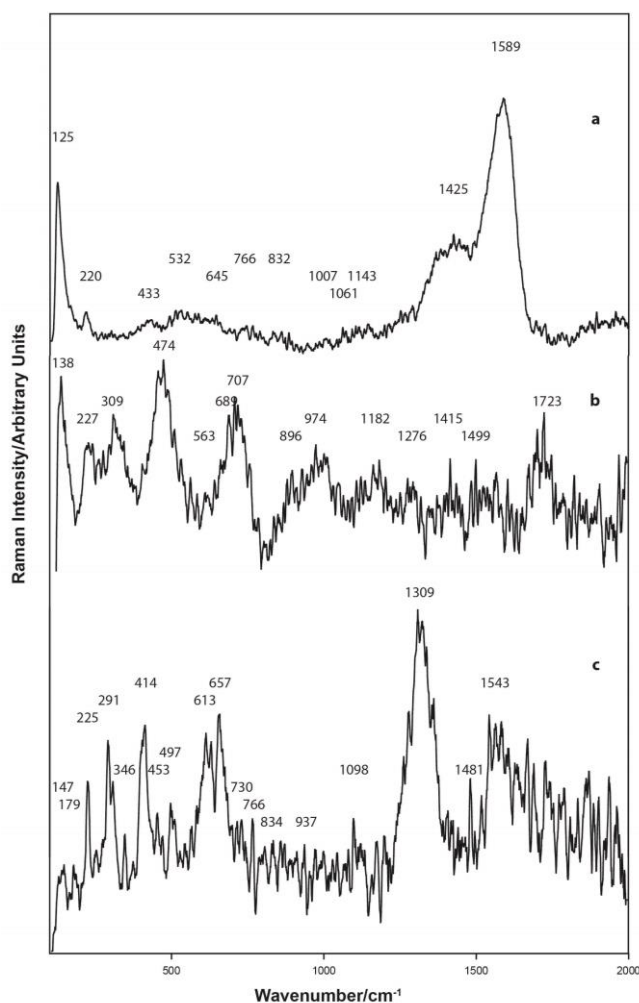
Figure 3.9. Raman spectra, black line on pottery surface of North Karnak sherd NK2. The black line contains amorphous carbon, magnetite and hematite together with gypsum and anhydrite, orthoclase feldspar, quartz, and possibly hedenbergite ($\lambda = 514.5$ nm).
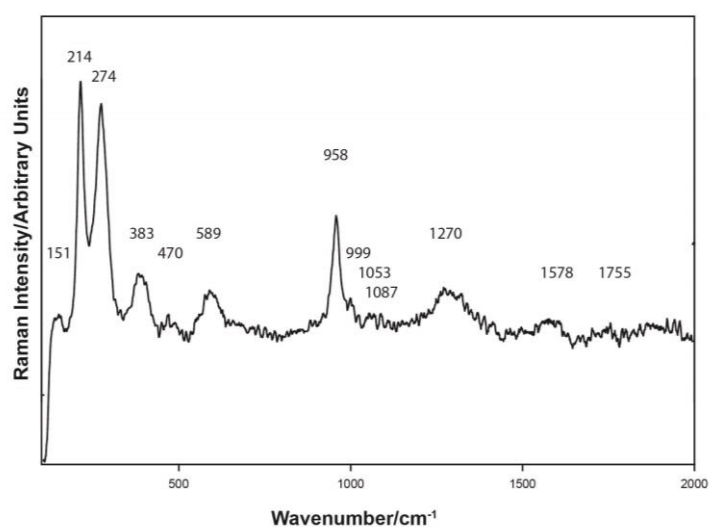
Figure 3.10. Raman spectrum, black line on North Karnak sample NK3. The band at 958 cm^{-1} is ascribed to either hydroxyapatite or to whitlockite or other phosphate minerals as listed in Table 2.24, Appendix A2. Other minerals present are quartz, hematite, goethite and amorphous carbon   ($\lambda = 514.5$ nm).

The presence of phosphosiderite and magnesioaxinite are both indicated within various black pigmented lines as provided by their respective Raman signatures provided in Figure 3.11. And, the iron phases present in Dakhleh Oasis sherd D8 also contained siderite and lepidocrocite.

And, the presence of hydroxyapatite clearly supports the evidence obtained throughout this thesis that ash was utilised in various ways, including its use in pigments, and as an alkali flux. Thus, to find bone ash in the pigments and in body fabrics is not unexpected.

Most black pigment samples applied to pottery also contain feldspars, including the plagioclase feldspar anorthite, pseudowollastonite and both ilmenite and rutile, refer to Figure 3.10. The titanium can be indurated into the iron mineral structure.
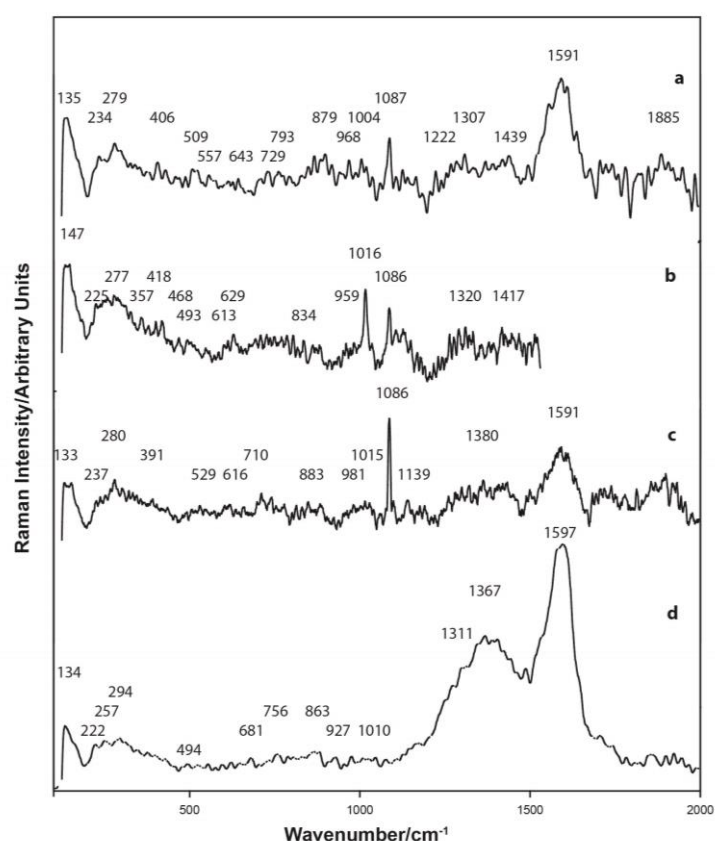
Figure 3.11. Raman spectra, black line on Mut al Kharab sherd D8, dated to the Ptolemaic period. The black line contains hydroxyapatite (bone ash) amorphous carbon and carbonised carbon. Hematite, possibly maghemite which may have formed from the dehydration of lepidocrocite; feldspar, brookite, calcite and anhydrite are present (λ = 514.5 nm).
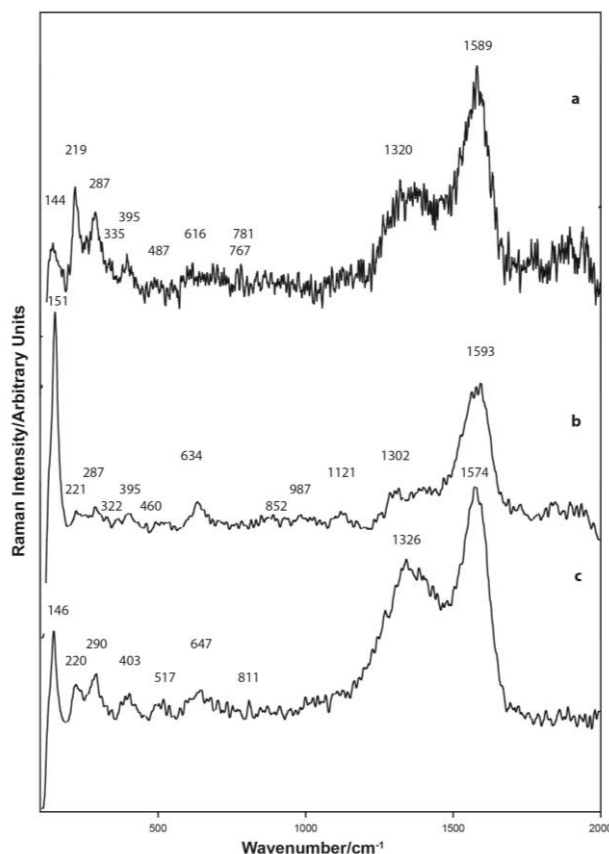
Figure 3.12. Raman spectra, black line on Dakhleh Oasis sherd D1. The black line contains high alumina and high iron. It is a mixture of amorphous carbon and iron oxide, together with anatase, feldspar and pseudowollastonite. The iron is a mixture of magnetite, hematite and goethite (λ = 514.5 nm).

The black pigment on Mut al-Kharab sherd D8 provided in Figure 3.11 has been applied over gypsum. Traces of phosphate are also observed. The presence of calcite is probably from post-production, from burial deposition.

Similarly, the Raman spectra for the black line decoration on Dakhleh Oasis sherds D1 and D6 are provided in Figures 3.12 and 3.13, the mineralogy associated with each sherd is provided with the Raman data interpretation. Both sherds contain potash feldspar as indicated by the high K_2O analyses and supported by the Raman spectra.

As provided in Table 3.5, the elemental and mineralogical data for each of the black and grey pigments applied to walls at Kellis is provided in Appendix A3. As shown, carbon black has been the major source for this pigment. There are minor quantities of various iron oxides present and rhodonite [$MnSiO_3$] was detected in one sample.

And, in Table 3.5 and Figure 3.14 the black iron oxide, magnetite was employed as the black pigment on cartonnage sample C5 from Tomb 16, Kellis 1 cemetery. The Raman spectra of the black cartonnage sample also indicates the presence of an organic complex, probably a mixture of Gum Arabic and a diterpenoid resin, probably from *Pinus pinea* or *P. haleopennsis*. The Raman data for the organic complexes is provided in Table 2.5, Appendix A2.
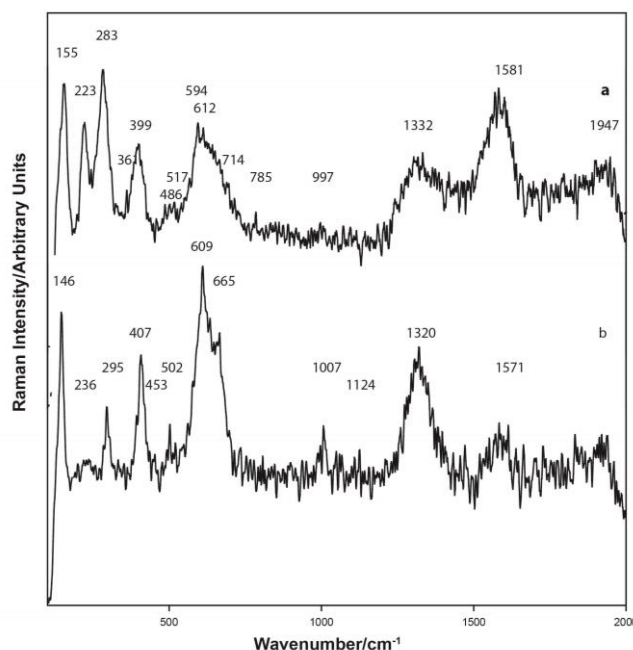
Figure 3.13. Raman Spectra, black line on Dakhleh oasis sherd D6. The black line is composed of amorphous carbon together with iron minerals including magnetite, hematite and goethite. Orthoclase feldspar, probably anorthite and possibly labradorite, together with diopside and possibly diaspore [AlO(OH)]. Both anatase and ilmenite were detected. The EDS analyses indicate a high potash concentration supporting the Raman spectra for potash feldspar ($\lambda = 514.5$ nm).

Table 3.5. Black, grey, cream and white pigment wall decoration, cartonnage and trench sample mineralisation. The individual sample numbers are as listed in Chapter 1 and Appendix A3.

Wall decoration													
Sample	**Mineral**												
	1	**2**	**3**	**4**	**5**	**6**	**7**	**8**	**9**	**10**	**11**	**12**	**13**
Main Temple, D/2 Shrine 1, Kellis													
6	■	■											■
8	■	■	■										■
9		■		■									
Forensic wall samples, Area B/3/1 Kellis, refer Appendix A3													
K2		■			■	■	■						
K4		■		■				■	■				
K5		■		■									
K7		■				■				■			
K9	■	■								■			
K10	■	■								■			
K12	■	■											■
K13	■					■							
K15					■	■							
Cartonnage Kellis 1 cemetery, Tomb 1													
C5													■

1 = iron oxide (including hematite)   2 = amorphous carbon   3 = hypersthene   4 = gehlenite   5 = jarosite
6 = goethite   7 = ferricopiapite   8 = hedenbergite   9 = ferrogedrite
10 = siderite   11 = celadonite   12 = natrojarosite   13 = magnetite
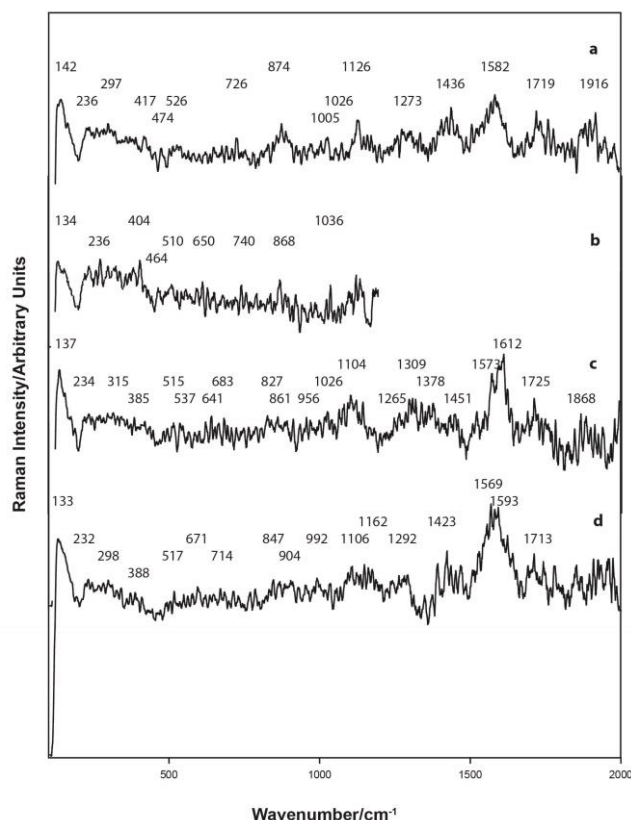
Figure 3.14. Raman spectra of the black pigment and plaster on cartonnage sample C5, Tomb 16, Kellis 1 cemetery. The black pigment as applied was amorphous carbon into which the feldspars orthoclase and/or sanidine [$KAlSi_3O_8$] were detected, together with anatase [TiO_2], contaminated iron-containing mineral such as magnetite, an iron ochre mineral, and a ferro-aluminate. Traces of forsterite are present. The poor quality of the spectra has resulted from fluorescence which most likely emanated from the addition of an organic complex as part of the pigment coating. A very low powered laser was required to be employed in an effort to obtain a useful Raman signal and to not degrade any iron oxides ($\lambda = 514.5$ nm).

3.4.2 Brown

Lucas (1989: 144) reported that good quality brown ochres occur within the Dakhleh Oasis. He also reported that the brown pigment applied during the fourth Dynasty and to an 18th Dynasty box consisted of an iron oxide and gypsum. An early papyrus examined by the British Museum conservation project indicated that the brown pigment was a mixture of hematite, orpiment and carbon black; on a nineteenth Dynasty papyrus was a mixture of realgar and carbon black. Hematite, together with carbon black was found on a 21st or 22nd Dynasty papyrus.

As reported by Lee and Quirke (2000: 111) the analysis may not always clearly indicate the original hue intended by the artist at the time of application. A large number (~30) of black/brown manganese oxides/oxyhydroxides exist. Their identification is made more difficult by the potential for many of these minerals to undergo thermal laser-induced transformations (Bersani and Lottici 2016). Thus, the present interpretation may not fully reflect the original colour of the pigment decoration and in particular, of the various iron oxides and oxyhydroxides.

A summary of the brown pigment analyses is provided in Table 3.6. As shown, the brown pigments from Malkata also regularly contain gypsum, feldspars, phlogopite, quartz, barium, arsenic and grog, all of which are reported in more detail in Appendix A3.

Table 3.6. Elemental analyses of the major elements present in the brown pigment on a range of pottery sherds. Note the effect of substrate elements on the accuracy of the provided information.

Sample	FeO	SiO$_2$	Al$_2$O$_3$	CaO	MgO	Mineral					
	%	%	%	%	%	1	2	3	4	5	6
Malkata											
M3	8.4	43.8	12.0	10.6	3.1	■	■		■		■
M4	10.4	40.4	17.0	14.2	4.6	■	■				■
M5	8.9	60.4	13.6	3.8	2.8		■			■	■
M6	6.7	25.3	27.4	19.4	5.8		■	■	■		■
M9	26.7	35.4	12.8	10.9	3.8		■		■		■
M10	21.2	37.1	11.9	18.7	3.7	■	■				■
M11	17.7	40.2	19.4	11.2	2.7	■	■		■		■
M13	17.6	22.7	7.0	24.2	6.0						■
Amarna											
A3						■	■	■	■		
A5						■	■		■		
A6	5.7	40.6	9.6	31.6	7.0	■	■	■		■	
North Karnak											
NK1	24.2	22.8	4.3	16.4	2.2	■	■		■	■	
North Sinai											
S1						■	■			■	
Dakhleh Oasis											
D2	19.9	33.5	37.8	1.1	1.4	■	■	■			■
D3	6.5	42.7	23.9	8.4	2.4			■			
D4						■	■	■	■		

1= magnetite   2=hematite   3=goethite   4=amorphous carbon   5=apatite   6=MnO
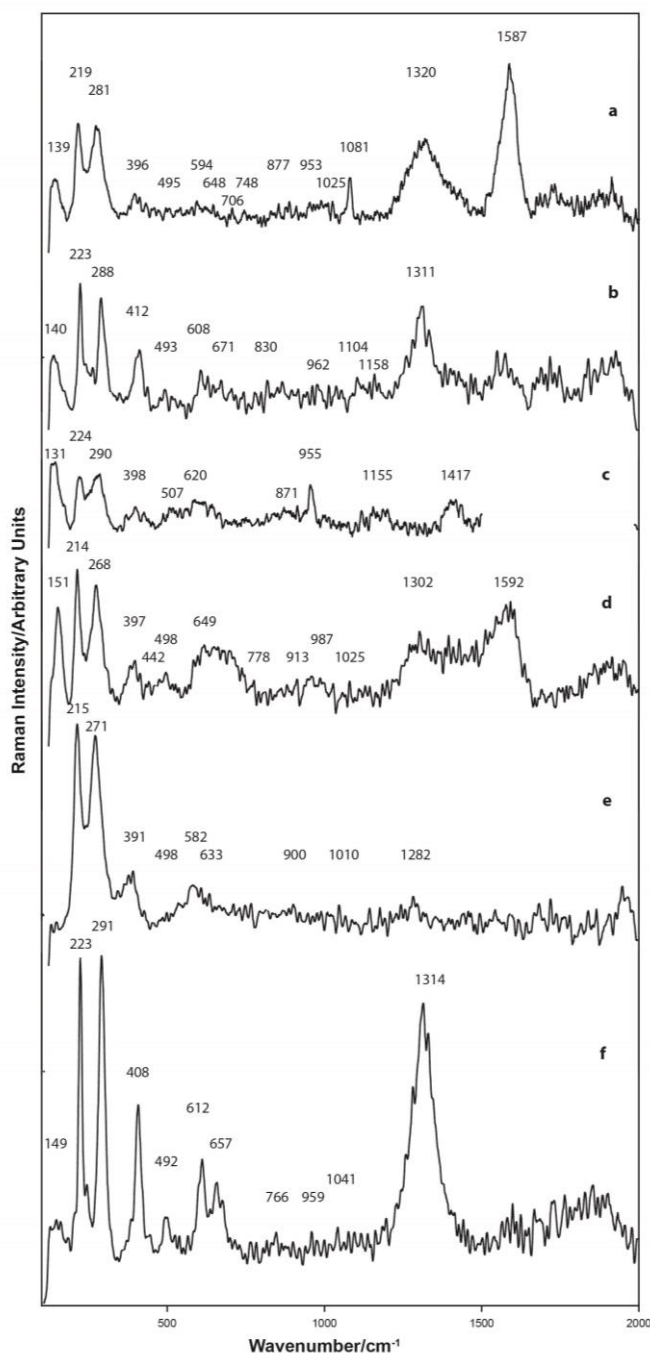
Figure 3.15. Raman spectra, red/brown pigment on pottery surface of Malkata sherd M9. The red/brown line is a mixture of iron ores of varying quality, some of which are highly crystalline, others, less so but including hematite and magnetite, together with amorphous carbon, feldspar, diopside, hydroxyapatite and natrite (λ = 514.5 nm).

The Raman spectra of the brown line on Malkata sherd M4 indicate that it comprises a mixture of low crystalline hematite, magnetite, probably amorphous carbon, feldspar, calcite, diopside and forsterite, and ilmenite together with anatase. A large particle of 'grog" is visible in Figure A3.M4.14. The elemental analyses provided in Appendix A3 indicate the presence of traces of arsenic on this sherd. And, the synchrotron images provided in Chapter 5, Figure 5.38 identify the presence of arsenic in Malkata sherds M3 and M5 particularly associated with the applied cobalt blue pigment and spots of arsenic are visible in Malkata M9.

The source of the arsenic in Malkata sherd M4 has not been determined. The synchrotron images in Chapter 5, Figures 5.38 (Malkata M9, arsenic spots only), 5.39 (Malkata M3 and M5 show a large area of arsenic) and in Figure 5.41 (Deir el-Medineh sherd DM1) large areas of arsenic are clearly associated with the cobalt blue pigment. In Malkata sherds M3 and M5 the arsenic would appear to be associated with the cobalt blue pigment. The presence of arsenic was also detected in the red pigment applied to Amarna sherd M9 and in Deir el-Medineh sherd DM1.
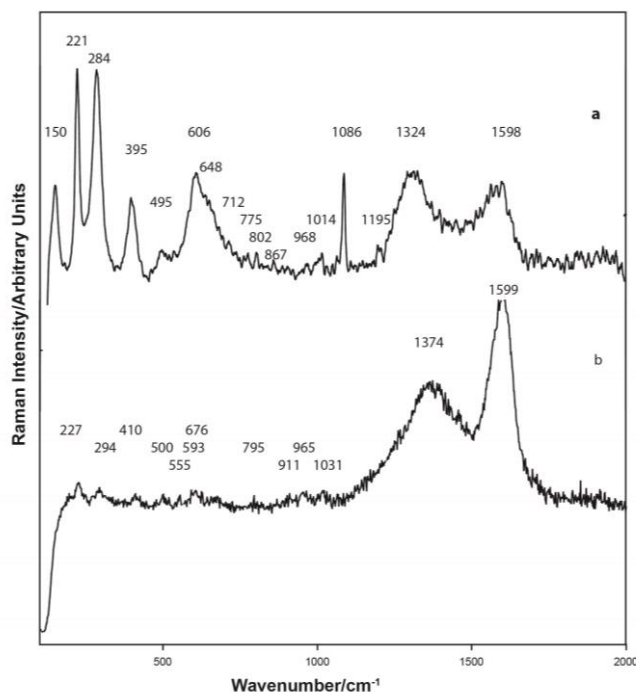
Figure 3.16. Raman spectra, dark brown decoration on Malkata sherd M10. The dark brown line is a mixture of magnetite, crystalline hematite and amorphous carbon. It also contains calcite and spinel ((a) $\lambda = 514.5$ nm, (b) $\lambda = 413$ nm).
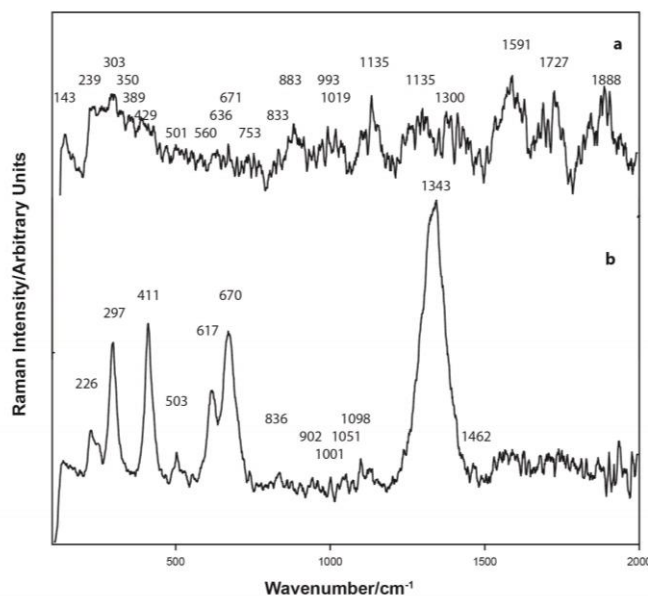
Figure 3.17. Raman spectra, brown line on pottery surface of Amarna sherd A3. The brown line is a mixture of goethite together with hematite and magnetite combined with a highly ordered crystalline source of carbon. Feldspar and traces of anhydrite were detected. Raman spectra would indicate the probability of an organic binder being present in the pigment ($\lambda = 514.5$ nm).
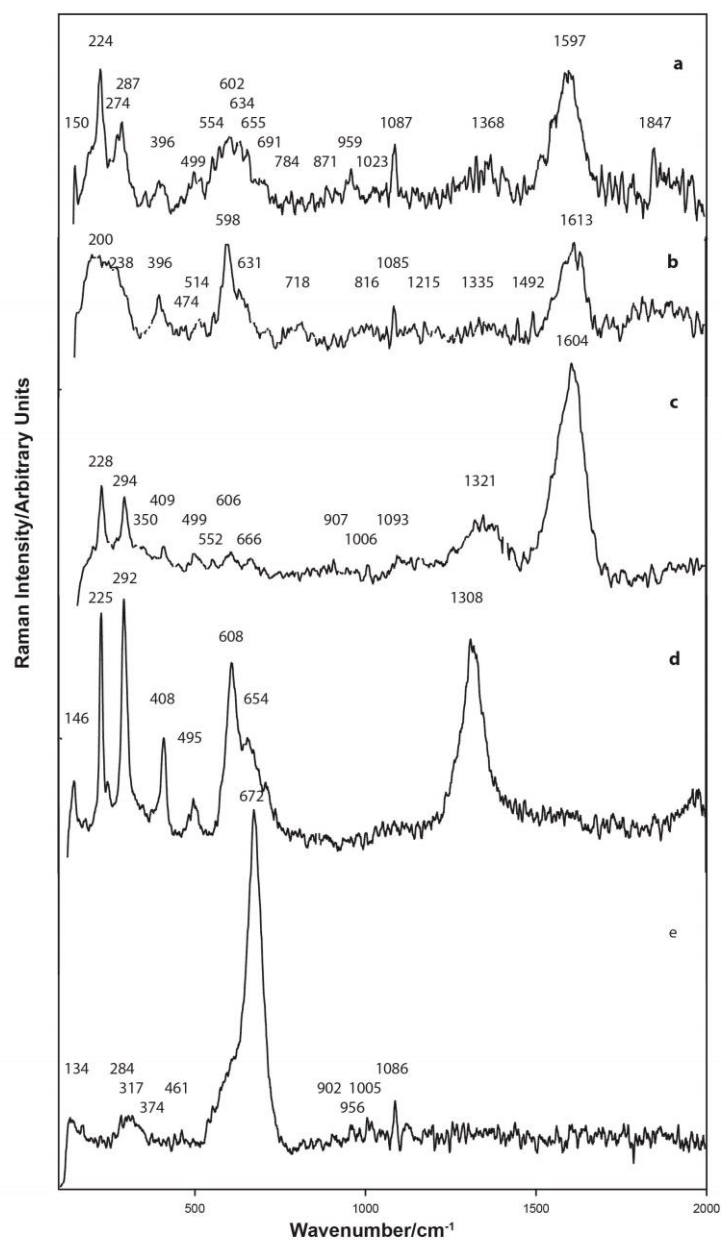
Figure 3.18. Raman spectra, brown line on the pottery surface of Amarna sherd A6. The dark brown/black line contains calcite, magnetite, hematite, goethite, gypsum, whitlockite or another phosphate, and amorphous carbon ($\lambda = 514.5$ nm).
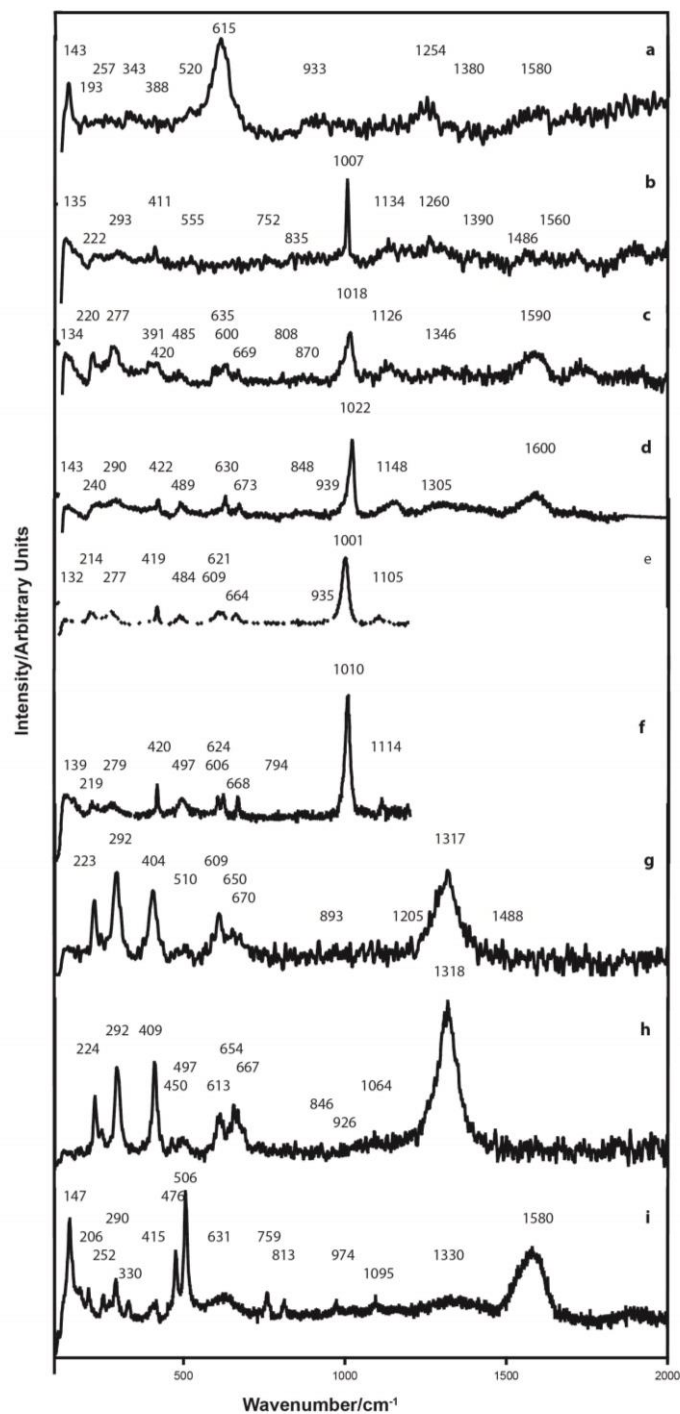
Figure 3.19.   Raman spectra, brown-black line on pottery surface of North Karnak sherd NK1.   The brown/black line contains magnetite, hematite and possibly magnesioferrite [$MgFe^{3+}_2O_4$] together with gypsum, feldspar, amorphous carbon, diopside, enstatite and probably forsterite, wollastonite, traces of whitlockite or other phosphate as listed in Table 2.24, Appendix A2, probably illite and possibly natroalunite [$NaAl_3(SO_4)_2(OH)_6$] ($\lambda = 514.5$ nm).
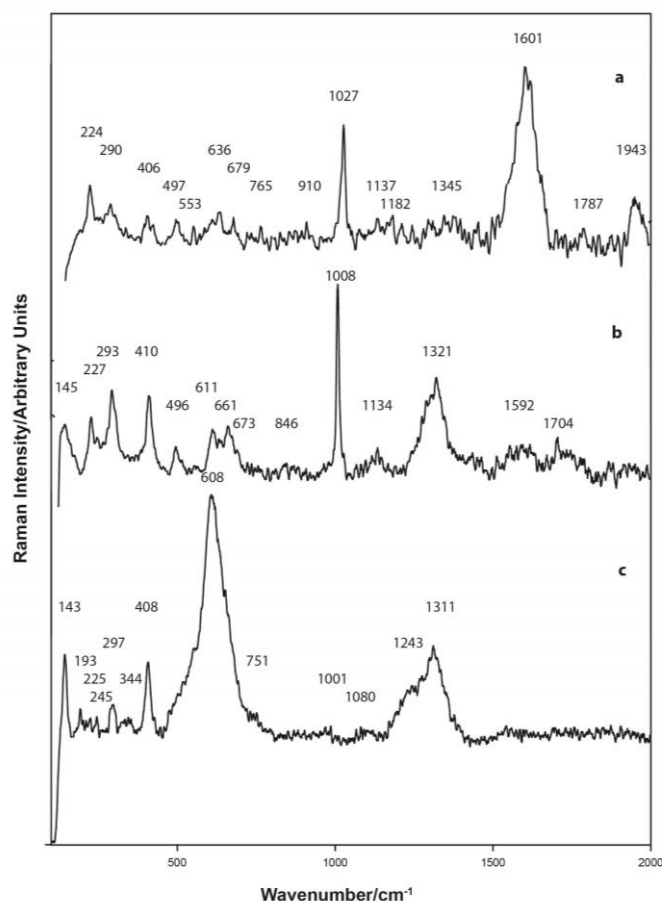
Figure 3.20. Raman spectra, brown/black line on Bir al-Abd sherd, North Sinai. The brown-black line contains amorphous carbon, hematite, magnetite and probably feldspar, phlogopite, magnesite, anatase and variscite [AlPO$_4$.2H$_2$O] ((a) λ = 413.2 nm; (b) and (c) λ = 514.5 nm).
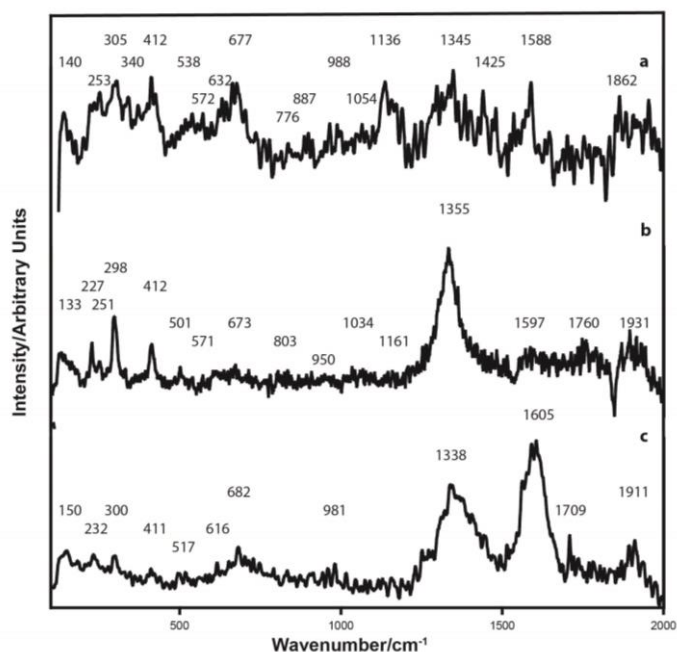
Figure 3.21. Raman spectra, brown decoration on Dakhleh Oasis sherd D2. The brown line is composed of hematite containing magnetite and probably goethite. Feldspar, wollastonite, pseudowollastonite, apatite and mullite are also present. There are areas within the EDS analyses indicative of higher alumina, probably associated with adsorption of an unidentified carbonate and traces of gypsum (λ = 514.5 nm).

The probability of the formation of variscite [$AlPO_4.2H_2O$] as indicated in Figure 3.20 is indicative of the heating of an aluminium source, such as a clay mineral including a member of the feldspar family or the alumina formed during the cobalt pigment production with a source of phosphorus such as provided by urine as discussed in Chapter 5. And, as discussed in Chapter 5 and Appendix A5, this mineral is also suspected of being formed in Malkata sherd M3.

There is evidence that the Dakhleh Oasis Sample D2 brown pigment was possibly heated to 1000°C, or more likely the pottery fabric underlying the pigment was fired to this temperature. This is based upon the determination of mullite in the Raman signature. Mullite would only commence forming at this temperature and requires 1200°C to fully form. The presence of goethite, magnetite and traces of an unidentified carbonate would eliminate the pigment itself from being high fired or fired on to the pottery vessel.
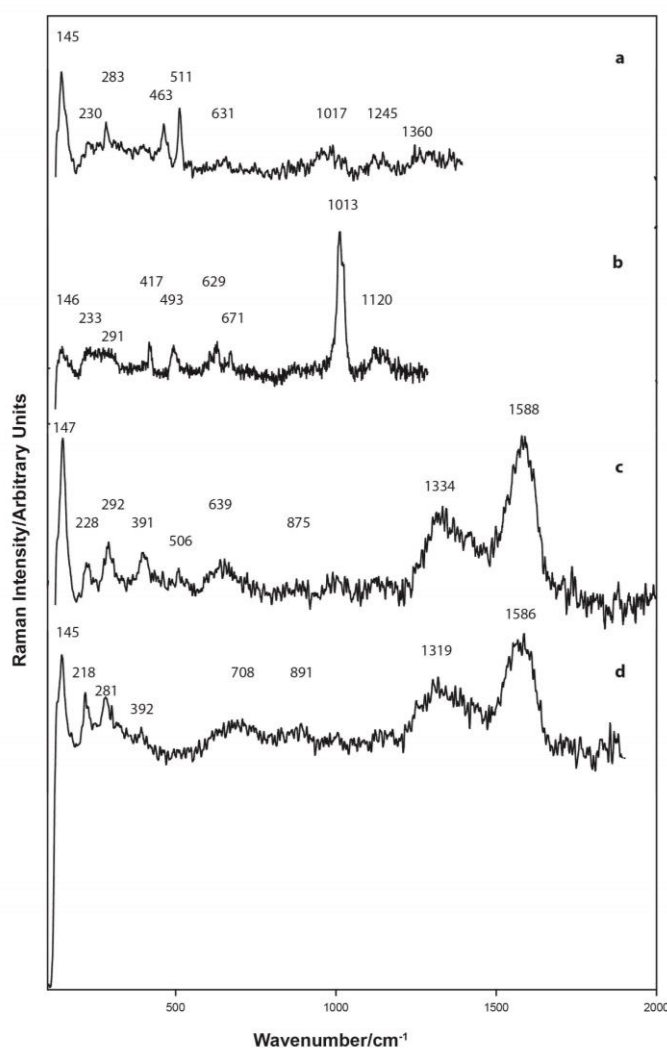
Figure 3.22. Raman spectra, brown pigment on Dakhleh Oasis sherd D3. The brown pigment is based on goethite together with quartz, amorphous carbon, feldspar (probably as either labradorite or orthoclase), ilmenite, anatase, diopside and with the probability of traces of hematite. Gypsum is present, probably as a slip coating. The Raman spectrum provides the possibility for the pigment to contain braunite ($Mn^{2+}Mn^{3+}_6O_8.SiO_4$), however manganese was not detected in the EDS analyses ($\lambda = 514.5$ nm).
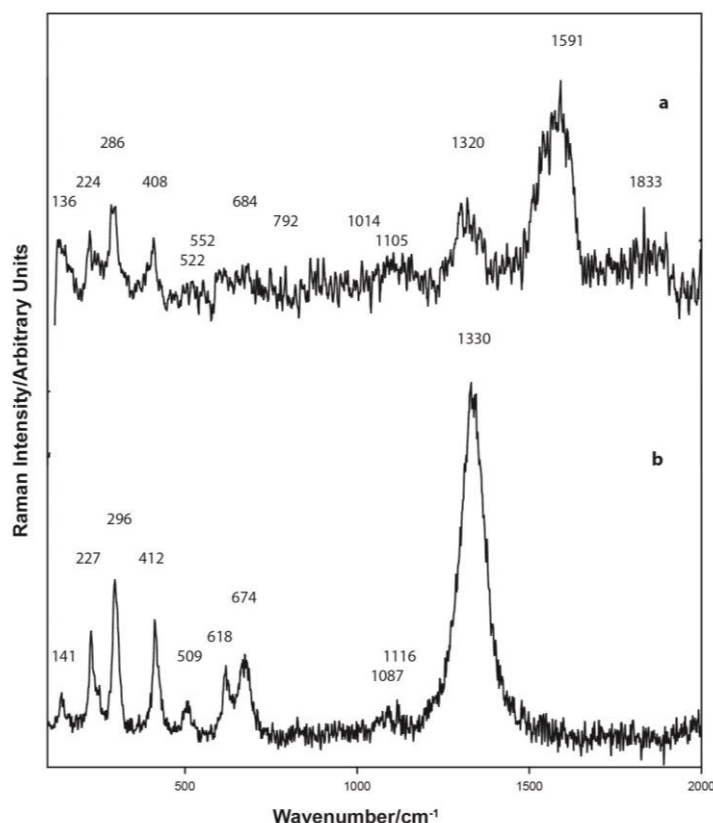
Figure 3.23.   Raman spectra, red-brown pigmented area, Dakhleh Oasis sherd D4.   The pigmented surface contains hematite and possibly a trace of magnetite and goethite, feldspar, amorphous carbon and a trace of calcite ($\lambda = 514.5$ nm).

The broad Raman hematite peaks evident in Figures 3.21 to 3.23 would suggest that a different source of hematite, namely one containing aluminium or titanium (refer EDS analyses such as for sample D8), was selected for decoration within the Dakhleh Oasis as opposed to that used to decorate the Nile valley samples.

The EDS analyses reported in Table 3.6 indicate that apatite was not found in any sample from Dakhleh Oasis and in only one sample, (D4), was either amorphous carbon or manganese observed. Although, three samples is a limited number for such an observation to be considered definitive. Other than the iron-containing minerals and amorphous carbon, all other minerals detected are more likely to be from the pottery fabric or the underlying slip coating.

Goethite has been detected, particularly in the brown pigments found on sherds excavated within the Dakhleh Oasis. The difficulty in examining goethite using Raman spectroscopy is complicated by the potential for silica to be present both by admixture and as an impurity, often with hematite, aluminium and water, or manganese substituting for Fe^{3+} in the mineral structure.   Goethite tends to be a more yellowish-brown ochre than the more reddish lepidocrocite.   On heating, leading to dehydration, goethite forms hematite, whereas lepidocrocite on heating forms the magnetic spinel maghemite. Goethite can also occur as a weathering product of iron-bearing minerals such as siderite, magnetite, pyrite, etc. Deer *et al*. 1992: 578).

An additional complexity is introduced into the analysis by the possible catalytic effect of hydroxyl groups adsorbed on the iron surface, particularly on magnetite, a black mineral generally found in the pottery black and brown decorations as noted in Tables 3.4 and 3.6. The occurrence of hydroxyl groups can directly result from the dissociation of water molecules interacting with the iron surface, such as magnetite. As discussed by Shebanova and Lazor (2003), although the role of electron-transfer oxidation is well-known, its role in the case of the semi-conducting mineral magnetite, is yet to be established.

3.4.3 Red

As suggested by Lucas (1962: 346) the red coloured pigments can be generally divided into two groups, the red anhydrous iron oxides and the hydrated iron oxides (oxyhydroxides) although such a division ignores the potential for the inclusion of vermilion, which has been reported in pink pigments (Lee and Quirke 2000: 114), amorphous carbon or realgar. Lucas (1962: 348) proposed that the term hematite should be restricted in Egyptology to the black metallic-looking mineral employed for carving into beads and other small objects. Lee and Quirke (2000: 113) proposed that in accordance with Lucas (1962: 348), the term 'haematite' (the US spelling of 'hematite' is now adopted throughout this thesis) was stated to be reserved in Egyptology for the mineral with a metallic black appearance.   Certainly, hematite can vary from black through shades of grey, brown, reddish brown to red. Depending upon its hydration, or inclusions of other elements into the mineral structure, particularly titanium or aluminium this can modify its visual appearance and its Raman spectrum.

Yellow oxyhydroxy iron oxides when heated change colour. Thus, at about 300°C, iron hydroxides will lose their water of hydration and at a slightly more elevated temperature the recrystallization of amorphous and/or poorly crystallised iron oxyhydroxides begins. At 600°C, the pigment turns bright red in colour and the spectrum is similar to that of hematite, Fe(III) oxide (Sabatini *et al*. 2000). Lucas dismissed the heating of yellow ochre to produce red ochre as had previously been postulated because good quality ochre, deep red in colour, is found both in the Nile valley near Aswan and in the Western Desert oases. Red lead pigments were not reported before the late Ptolemaic or Roman period (Blom-Böer 1994: 66).

The major minerals detected in the red pigment on various pottery sherds are from iron oxides and oxyhydroxides as provided in Table 3.7 with the pigment shade modified by traces of amorphous carbon.   Additional minerals detected included feldspar in most pigments, diopside, enstatite and forsterite, quartz, anhydrite, calcite, hydroxyapatite, whitlockite or other phosphate-containing mineral, natrite, ilmenite, anatase and rarely rutile, brookite and pseudobrookite, phosphosiderite, wollastonite and traces of copper. Other than the titanium minerals and iron-containing minerals all of the other minerals can potentially be traced to the pottery fabric. This can therefore explain the presence of the high temperature minerals such as wollastonite, diopside, rutile and other magnesium based minerals. Quartz, which is regularly detected, is suggested by David *et al.* (2001) to have been added to the pigments to act as a grinding aid in the fine grinding of the iron oxide pigments. It is also proposed in this thesis at Section 3.4.4 that quartz was used as a grinding aid for orpiment.

The Raman spectrum for hematite varies with the composition (quality) of the pigment. This also introduces changes in its brightness and shade. By reference to many of the Raman signatures given in Appendix A3 it is evident that the narrow bands at 227, and 245 cm^{-1} and the strong band at 293 as well as the peaks at 414, 495, 610 and 1315 cm^{-1} are indicative of high quality hematite and are characteristic of the hexagonal-structured hematite. Broadening and upshifting (red shift) of these hematite bands is accompanied by the substitution of aluminium and/or titanium cations (Leon *et al.* 2010; De Benedetto *et al.* 2010) including the appearance of a band at about 645 cm^{-1} and according to Froment *et al.* (2008) particularly of the ~405 cm^{-1} peak. Whereas, crystallinity or particle size can lead to a downshift 225/294 cm^{-1} to 214/274 cm^{-1} (Wang *et al.* 1998) and is indicated in Figures 3.27 and 3.31. The simultaneous presence of a Raman band at about 670 cm^{-1} is observed in the aluminium-substituted hematite minerals. Thus the Raman spectra of iron oxides always provide bands related to Fe-O stretching modes of the basic FeO_4 tetrahedral unit, giving rise to a strong band between 550 (Fe^{2+}) and 725 (Fe^{3+}) cm^{-1}. The strong bands between 200 and 300 cm^{-1} are lattice mode bands characteristic of the layer structure (Cristini *et al.* 2009). Consideration must also be given to the unlikely potential for goethite to have originated from a hydration process of hematite as proposed by Parras *et al.* (2010). As shown in Figures 3.24 (Malkata), 3.25 (Amarna) and 3.26 (Dendera) highly crystalline hematite was employed at these sites. Whereas, as provided in Figure 3.27, the Raman spectra for Deir el-Medineh sherd DM1 shows both peak broadening and downshift indicative of the presence of aluminium and/or titanium in the mineral structure.

And as reported by Cristini *et al.* (2010) and by Pailhé *et al.* (2008), the saturation of the red colour in hematite depends upon a low average trigonal distortion exerted on the distortion of the Fe^{3+} octahedral sites. They reported, and as seen in the various hematite spectra provided in Appendix A3, the changes in pigment colour can be attributed to hydration of the hematite crystals. In effect, water could interact with hematite by creating OH^- ligands thereby reducing to symmetry around to Fe^{3+} ions and the greater distortion around the Fe^3 ions reducing the saturation and therefore the hue of the red pigment. This change could explain changes in the hue of the pigment from red to orange.

Hematite being an antiferromagnetic material, the Raman peak at 1315 cm^{-1} as shown for example in Figures 3.25 and 3.26 is often assigned to a two-magnon scattering process as discussed by Bernal and Bello (2003). Whilst this peak is absent in magnetite, in minerals containing both hematite and magnetite, the peak at 660 cm^{-1} link it to the presence of the cubic-structured magnetite and/or to a disorder effect in the crystalline structure of the hematite (De Faria *et al.* 1997).

Mazzetti and Thistlethwaite (2002), discussed the loss of OH^- ions and the resultant rearrangement of ligands around Fe^{3+} ions when oxyhydroxide iron minerals such as ferrihydrite, schwertmannite or goethite are heated; this results in a fraction of Fe^{3+} achieving the tetrahedral coordination that is associated with maghemite. De Faria *et al.* (1997) demonstrated that maghemite is stable at 200°C but at 300°C, hematite is readily observed. Such changes are liable to occur even at low power laser settings. In this respect, Worobiec *et al.* (2011) stated that a laser excitation of 514.5 nm was proven to provide optimal molecular and crystalline information from iron-rich particles, justifying the employment of this laser excitation wavelength for most of this thesis. However, some results were also

obtained at other laser settings and these are noted within the relevant Raman spectral details.

The oxidation of iron itself depends upon both the treatment temperature an on the annealing conditions. In air, at temperatures above 200°C, the oxide films consist of a duplex structure, magnetite in contact with the iron substrate and hematite as an outer layer in contact with air. Whilst iron is not encountered in the pigments under examination, reactions occurring on iron oxides are applicable in the present research. Thus, it is possible for magnetite, hematite and maghemite to co-exist. And at temperatures below 200°C iron, in the presence of water vapour produces an oxide layer which consists of a film of magnetite upon which a thin maghemite overlayer is formed (Pérez-Robles *et al*. 1999; West *et al*. 2005). Thus, the formation of maghemite requires the presence of water and is therefore difficult for it to exist as the only oxide phase. Maghemite has an inverse spinel structure and can therefore be seen as an iron-deficient form of magnetite with iron vacancies in the octahedral spinel sites.
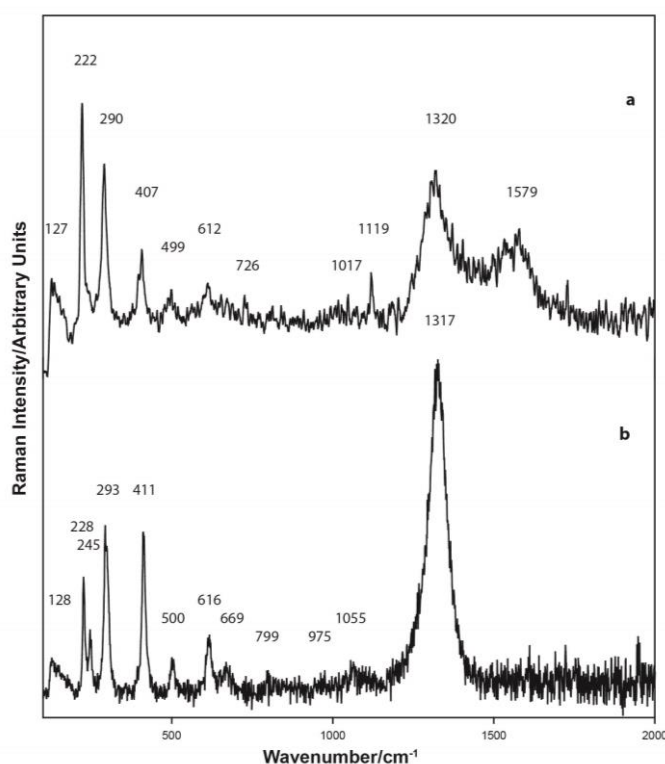
Figure 3.24. Raman spectra of the red pigment on Malkata sherd M7. This red pigment is a highly crystalline ematite together with traces of amorphous carbon, probably diopside, anhydrite and hydromagnesite (λ = 514.5 nm). The elemental analysis of the pigment is provided below,

Elemental analysis, Red pigment FIB-EDS Spot 1 analysis in Figure A3.M7.2.

Na$_2$O	MgO	Al$_2$O$_3$	SiO$_2$	P$_2$O$_5$	SO$_3$	Cl	K$_2$O	CaO	TiO$_2$	MnO	FeO	CoO	NiO	CuO	ZnO
0.6	9.3	4.0	5.2	0.4	6.4	1.3	0.7	9.5	0.4	0.0	62.3	0.0	0.0	0.0	0.0
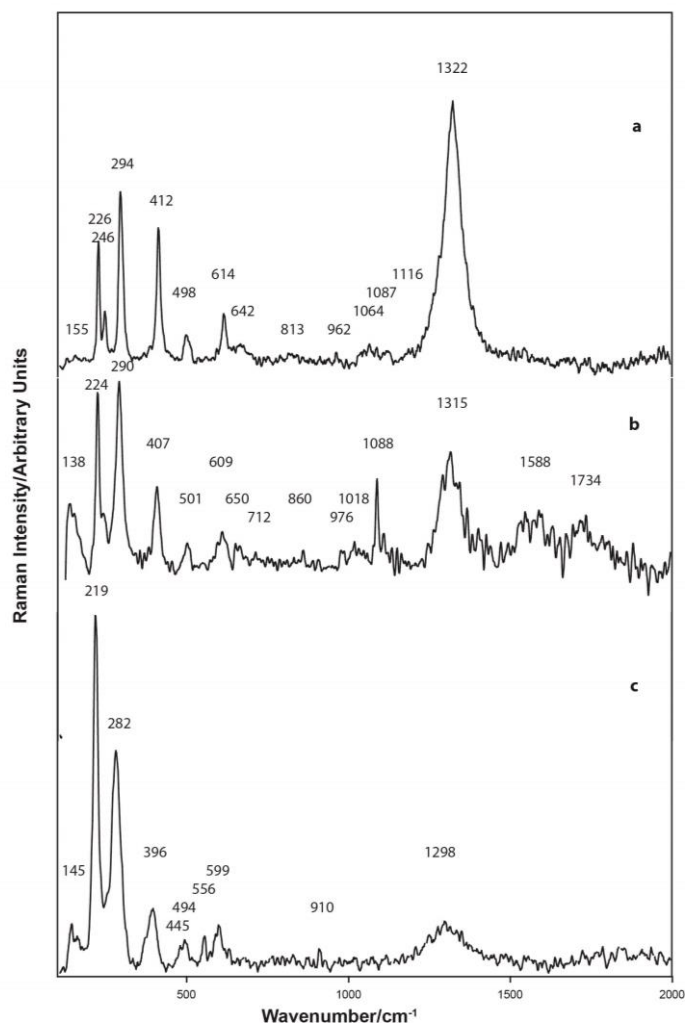
Figure 3.25. Raman spectra, red pigment on Amarna sherd A9 ((a) and (b) λ = 514.5 nm; (c) λ = 413.2 nm). The red pigment is a highly ordered crystalline hematite as shown by the narrowness of the Raman bands. Traces of calcite, anhydrite, feldspar, arsenic and probably red/brown crystals of spessartine [$Mn^{2+}_3Al_2(SiO_4)_3$] were detected. The average elemental analysis of the red pigment on this sherd is provided below.

Average elemental analysis, red surface coating on Amarna shed A9. JEOL 840A Area analyses.														
Na$_2$O	MgO	Al$_2$O$_3$	SiO$_2$	P$_2$O$_5$	SO$_3$	Cl	K$_2$O	CaO	TiO$_2$	MnO	FeO	CoO	NiO	CuO	ZnO
1.3	1.1	9.1	14.0	0.5	5.9	0.2	0.4	8.0	0.3	0.4	54.4	0.0	0.0	1.4	0.3
#+As$_2$O$_3$ = 2.1% average														

Table 3.7. Elemental analyses of the major elements present in the red pigment. Note the effect of substrate elements on the accuracy of the provided information.

Sample	FeO %	SiO$_2$ %	Al$_2$O$_3$ %	CaO %	MgO %	Mineral 1	2	3	4	5	6
Malkata											
M7	62.3	5.2	4.0	9.5	9.3		■		■		
M8	17.4	9.6	18.8	14.1	27.3		■				
M9	9.6	45.8	`14.0	13.5	4.7						■
M12	9.4	40.8	14.2	13.5	3.7						■
M14	12.5	40.8	15.2	15.0	5.7						■
Amarna											
A7	11.1	34.2	24.8	9.8	4.2						■
A8	6.9	39.6	19.3	12.8	3.6						■
A9	54.4	14.0	9.1	8.0	1.1						■
North Karnak											
NK1	9.3	21.9	43.0	3.5	6.0	■	■	■		■	■
NK3	20.4	23.7	8.9	26.7	0.6		■			■	■
Dendera											
DE1	25.3	26.7	15.2	12.6	1.7		■				■
Deir al-Medineh											
DM1	7.0	35.4	13.3	13.4	4.2	■	■			■	■
Sinai											
S1	11.8	46.9	15.8	8.6	3.9		■		■		■
Dakhleh Oasis											
D1	3.7	42.1	27.1	14.4	1.6	■	■		■		
D6	9.0	49.5	28.6	3.1	2.2		■	■	■	■	

1= magnetite   2=hematite   3=goethite   4=amorphous carbon   5=apatite   6=MnO
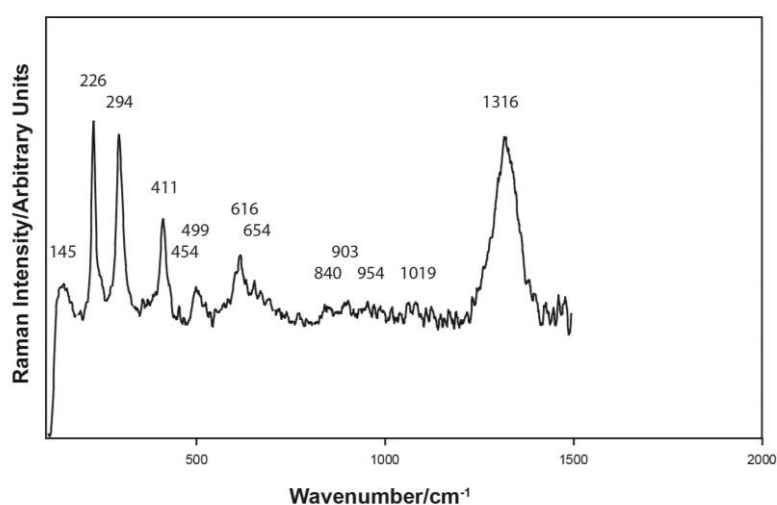
Figure 3.26. Raman spectrum, red pigment on the pottery surface of Dendera sherd DE1 (λ = 514.5 nm). The red pigment is a highly crystalline hematite indicated by the narrowness of the Raman bands. It contains feldspar, possibly diopside, anhydrite and possibly anatase. The average elemental analysis is provided below.

Average elemental analysis, red pigment, Dendera DE1, Nova analyses Figure 3.26 and Appendix A3 Figure A3.DE1.3

Na$_2$O	MgO	Al$_2$O$_3$	SiO$_2$	P$_2$O$_5$	SO$_3$	Cl	K$_2$O	CaO	TiO$_2$	MnO	FeO	CoO	NiO	CuO	ZnO
4.0	1.7	15.2	26.7	0.0	7.1	3.2	2.7	12.6	0.8	0.2	25.3	0.2	0.1	0.1	0.1
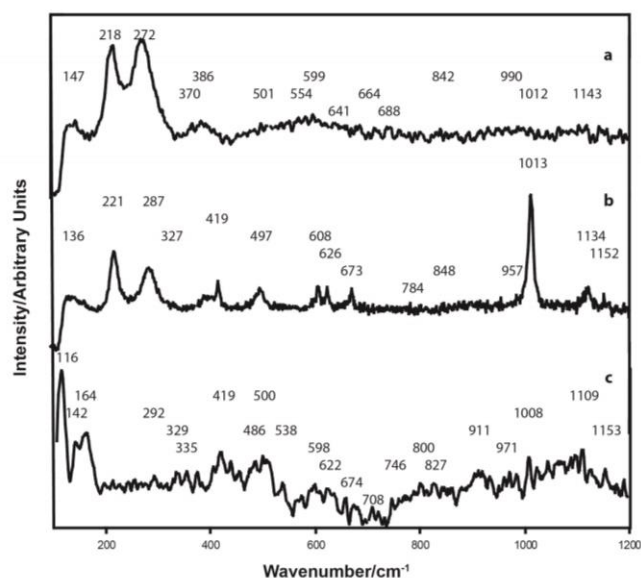
Figure 3.27.   Raman spectra, red pigment on pottery surface of sherd Deir al-Medineh sherd DM1 (λ = 514.5 nm). The Raman spectra shown for the red or brown pigments indicate that they are poorly ordered hematite containing titanium and/or aluminium, magnetite, goethite, pseudobrookite and anatase, gypsum, feldspar, wollastonite, diopside and winchite [$\square$Na,Ca[Mg$_4$Al]Si$_8$O$_{22}$(OH)$_2$], anomalous phosphorus, lead and arsenic and possibly siderite. The elemental analysis is provided below.

Elemental analysis, red pigment , Deir el-Medineh sherd DM1, JEOL 840A Area analyses.

Na$_2$O	MgO	Al$_2$O$_3$	SiO$_2$	P$_2$O$_5$	SO$_3$	Cl	K$_2$O	CaO	TiO$_2$	MnO	FeO	CoO	NiO	CuO	ZnO
3.2	4.2	13.3	35.4	1.2	14.4	0.0	2.2	13.4	0.5	0.1	7.0	0.0	tr	0.6	tr

+PbO = 3.8%, +As$_2$O$_3$ = 0.7%

Red hematite requires an oxidising environment to form, whereas black magnetite requires reducing conditions. It has been shown that the Raman band at ~670 cm^{-1} could be present in disordered or impure hematite. If the 670 cm^{-1} band is always present together with other hematite bands and never alone, the presence of magnetite should be considered doubtful (Bersani and Lottici 2016). Only when present as a lone band, and closer to slightly lower wavenumbers (~660 cm^{-1}) the attribution to magnetite can be considered certain.

The red pigment applied to the North Karnak sherds as provided in Figure 3.28 varies in quality from highly crystalline to a more amorphous quality. And, as shown in Figure 3.29, the Bir al-Abd sample from North Sinai is highly crystalline.   In the red pigment samples, as typically provided in Figures 3.30 and 3.31 from Dakhleh Oasis, , the hematite peaks are broadened by the presence of either aluminium or titanium. Several of the red pigments contain goethite or other oxyhydroxide iron minerals or the iron carbonate, siderite.   This would indicate that different sites were used to obtain the raw material in the Nile valley and also different again in Dakhleh Oasis.
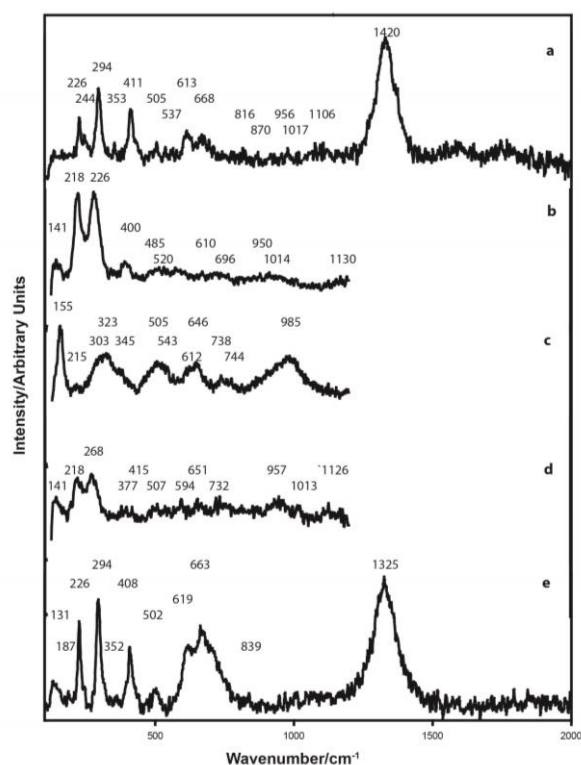
Figure 3.28. Raman spectra, red pigment on North Karnak pottery sherd NK1 (λ = 514.5 nm). The red pigment contains hematite, a portion of which is crystalline, goethite, magnetite, feldspar, anhydrite, hydroxyapatite and possibly phosphoferrite.
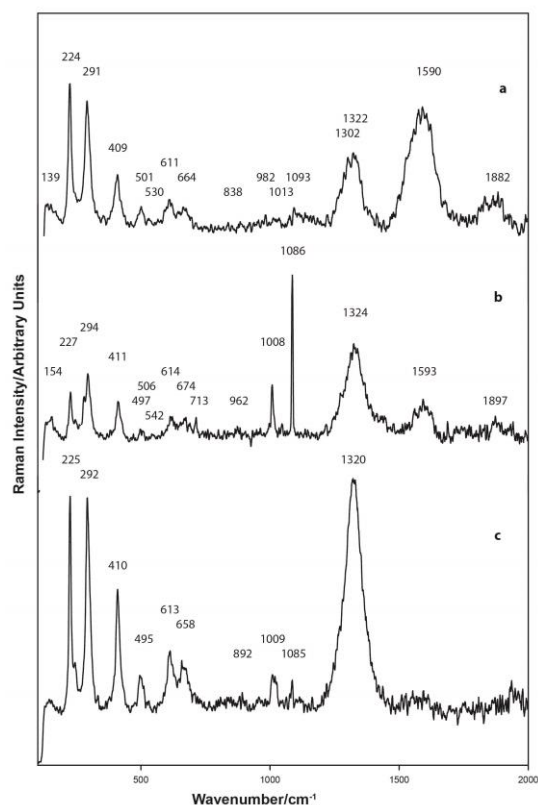
Figure 3.29. Raman spectra, red pigment on North Sinai sherd S1 (λ = 514.5 nm). The red pigment is highly crystalline hematite together with calcite, gypsum, feldspar, diopside and forsterite, lepidolite, magnesioaxinite and either dolomite [$CaMg(CO_3)_2$] or magnesite [$MgCO_3$].
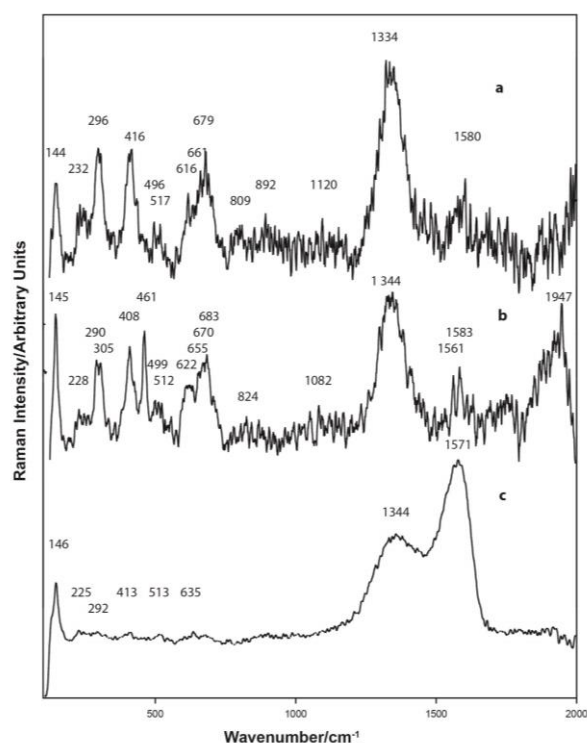
Figure 3.30. Raman spectra, red pigmented surface of Dakhleh Oasis sherd D1 (λ = 514.5 nm). The red surface coating is primarily hematite together with traces of magnetite. And the pigment contained significant amorphous carbon together with silica and feldspar. The SEM analysis indicated the presence of high alumina and high lime, along with the iron oxide minerals.
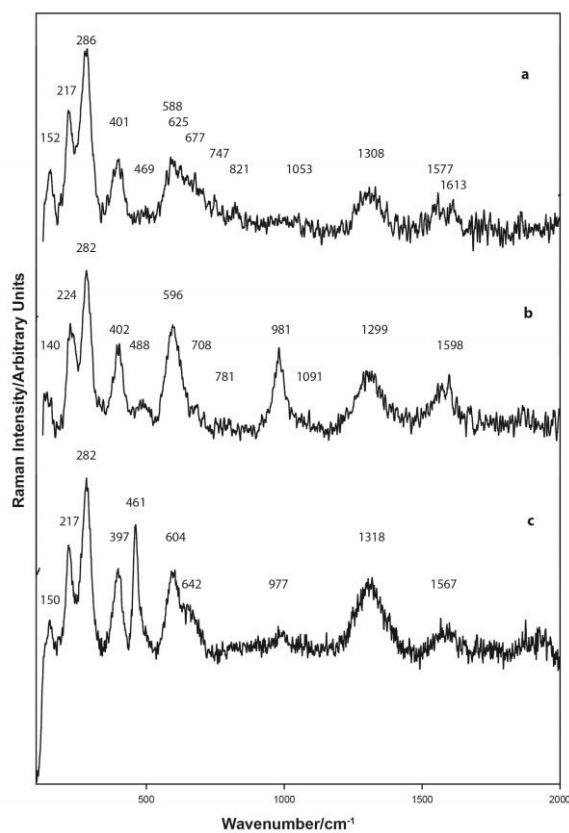
Figure 3.31. Raman spectra, red surface on a 4th century CE Roman sherd D6, from Dakhleh Oasis. The red pigment is hematite where variability in crystallinity or grain size has resulted in a downshift (or blue shift). Al and/or Ti are also present as shown by their elemental analysis and these would be expected to cause a red shift

in the spectrum.   Thus, a contaminated hematite, together with goethite, amorphous carbon and possibly phosphosiderite form the red pigment.   Anatase and ilmenite are both present in the red pigment. Hydroxyapatite is present as shown from its Raman signature and from the bone ash particle analysed in Figure 3.42 and as such, would suggest the use of kiln or similar type ash in preparing the pigment and this may have contributed to the elevated potash in the analyses.   It is also possible that the hydroxyapatite could be associated with the pottery fabric, and the addition of kiln ash to the fabric is considered to have formed part of the fabric construction. ($\lambda = 514.5$ nm)

As indicated in Table 3.8 and Figure 3.32, the red pigments on wall and cartonnage are also based upon hematite. Sample 14 is a high quality hematite as indicated by the narrowness of the respective Raman signature peaks and from the SEM-EDS elemental analysis provided in Appendix A3.
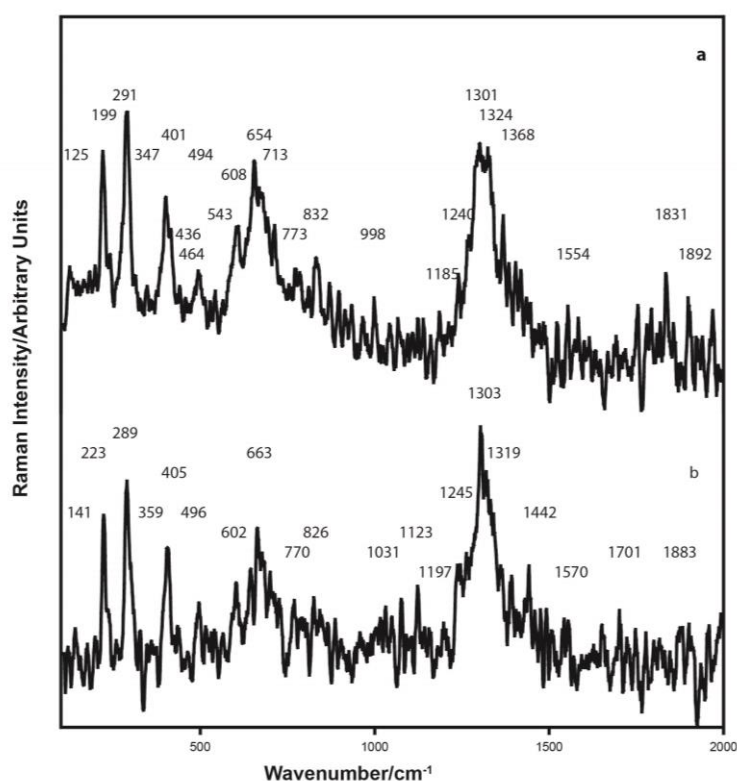
Figure 3.32. Raman spectra, Dakhleh Oasis, Pharaonic red pigment, Sample 14, Main Temple D/2 Shrine 1 floor. The red pigment is hematite containing traces of goethite and quartz. The hematite does not exhibit the presence of aluminium or titanium elements in its structure. ($\lambda = 514.5$ nm).   As shown in the following elemental analysis, the pigment contains almost no contaminants.

Average elemental analysis Sample 14, Shrine I floor Pharaonic (JEOL 840A analysis)													
Na_2O	MgO	Al_2O_3	SiO_2	P_2O_5	K_2O	CaO	TiO_2	MnO	FeO	CuO	SO_3	Cl	SnO_2
0.2	0.2	0.7	3.6	0.4	tr	1.6	tr	0.2	87.6	2.0	0.9	1.2	0.0
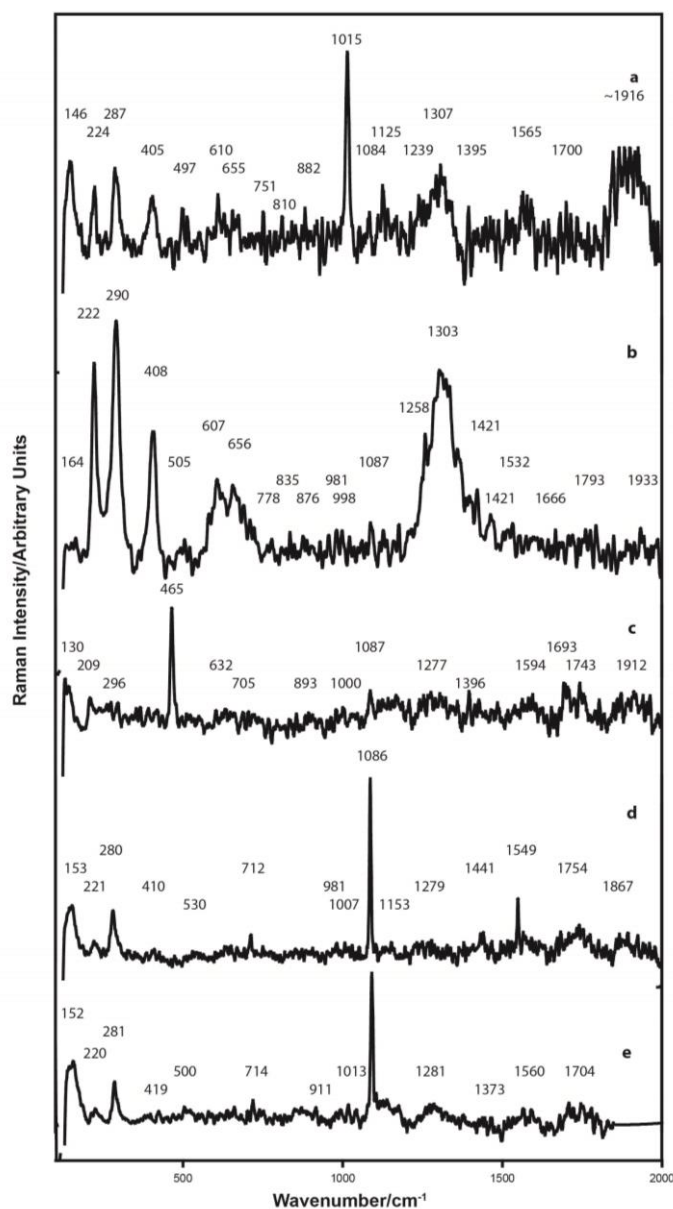
Figure 3.33.   Raman spectra, pigment 1, red applied to wall at Kellis. (d) and (e) are plaster (λ = 514.5 nm). Red pigment is hematite. The pigment also contains anhydrite, gypsum, quartz, amorphous carbon and feldspar, possibly as oligoclase. Elemental analyses of pigment and plaster are provided below.

Average elemental analysis, red, NT1, South wall (JEOL 840A analysis)

Na$_2$O	MgO	Al$_2$O$_3$	SiO$_2$	P$_2$O$_5$	K$_2$O	CaO	TiO$_2$	MnO	FeO	CuO	SO$_3$	Cl
0.6	1.0	5.3	21.9	0.2	0.5	65.7	0.1	0.2	1.8	0.3	1.7	0.9

Average elemental analysis plaster (very approximate) (JEOL 840A analysis)

Na$_2$O	MgO	Al$_2$O$_3$	SiO$_2$	P$_2$O$_5$	K$_2$O	CaO	TiO$_2$	MnO	FeO	CuO	SO$_3$	Cl
2.5	1.6	5.8	20.5	0.5	0.0	64	0.6	0.0	1.9	0.0	1.3	1.6
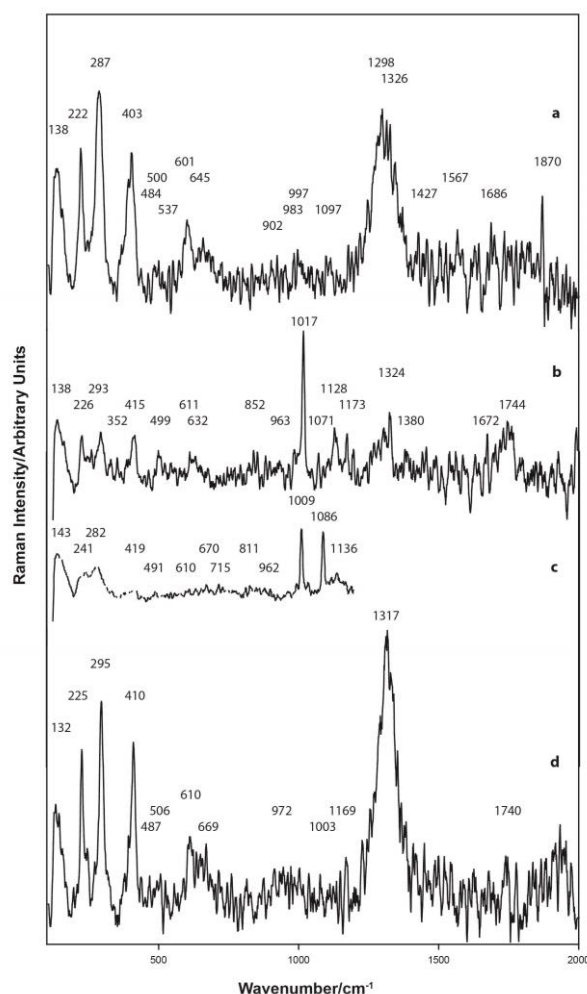
Figure 3.34.   Raman spectra, red pigment, forensic sample K27, Large East church, Kellis, 4th century C.E. (λ = 514.5 nm). The SEM-EDS analysis indicates that the pigment is composed of sulphate, calcium and iron oxide. Raman spectroscopy is indicative of calcite, aragonite, gypsum, anhydrite, and a highly ordered hematite similar to that observed in Sample K20 and some amorphous carbon. Elemental analysis of the red pigment is provided below.

Average elemental analysis, Sample K27 Kellis A/7 from capital new bema, red pigment (Nova analysis)														
Na_2O	MgO	Al_2O_3	SiO_2	P_2O_5	SO_3	Cl	K_2O	CaO	TiO_2	MnO	FeO	CoO	CuO	ZnO
0.7	0.5	2.8	6.9	0.1	21.5	0.1	0.4	26.3	0.1	0.0	40.5	0.0	0.0	0.0

As shown in Figures 3.32 to 3.36, the quality of the hematite selected for application to the walls at Kellis and on the sherds from Dakhleh Oasis would appear to have been obtained from the same iron deposit.

Table 3.8. Red, brown and pink pigment wall decoration, cartonnage and trench sample mineralisation. The individual sample numbers are as listed in Chapter 1 and Appendix A3.

Wall Decoration – Kellis, 4th century CE.																		
Sample	Mineral																	
	1	2	3	4	5	6	7	8	9	10	11	12	13	14	15	16	17	18
1	■																	
3			■		■	■	■	■	■									
13			■	■														
14	■		■															
K3	■																	
K8										■	■	■						
K9	■												■					
K11	■													■				
K16	■																	
K18	■													■	■	■		
K27	■																■	
Cartonnage – Kellis, 2nd century CE																		
C3	■																	■
C7	■																■	
C10	■			■														■
Trench samples – Mut al Kharab, 25/26 Dynasty to 200 BCE																		
21	■		■							■							■	
22	■									■							■	
23	■						■										■	

1 = hematite   2 = magnetite   3 = goethite   4 = natrojarosite
5 = ferrihydrite   6 = lepidocrocite   7 = jarosite   8 = schwertmannite
9 = maghemite   10 = siderite   11 = celadonite   12 = natrojarosite
13 = hastingsite   14 = gehlenite   15 = coquimbite   16 = grunerite
17 = amorphous carbon   18 = ankerite
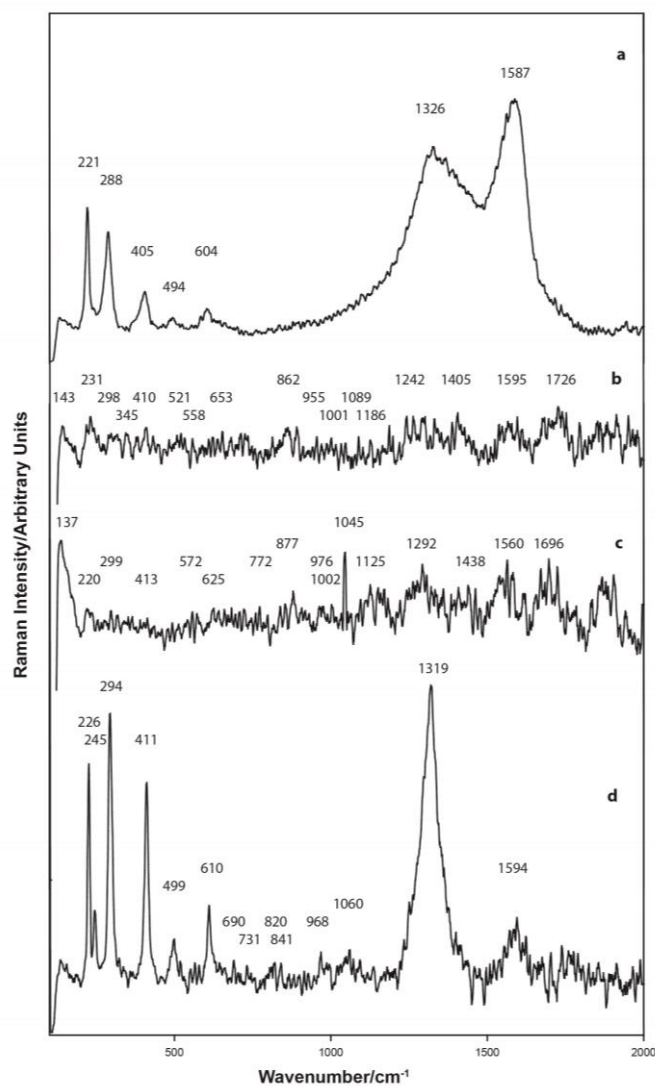
Figure 3.35. Raman spectra, red pigment, Mut al-Kharab trench Sample 21, context 29, trench 35. (λ = 514.5 nm). The pigment contains highly ordered hematite similar to that used for Samples K20 and K27. The Raman spectra of the pigment indicates the presence of amorphous carbon and traces of goethite, wollastonite and possibly siderite. The pigment elemental analysis is provided below.

Average elemental analysis Sample 21, Mut al Kharab, T35 (29) red pigment (Nova analysis)

Na$_2$O	MgO	Al$_2$O$_3$	SiO$_2$	P$_2$O$_5$	SO$_3$	Cl	K$_2$O	CaO	TiO$_2$	MnO	FeO	CuO	SnO$_2$	As$_2$O$_3$
7.9	4.1	21.5	42.2	0.3	1.8	0.3	2.6	9.0	0.9	0.0	9.2	tr	0.0	0.0
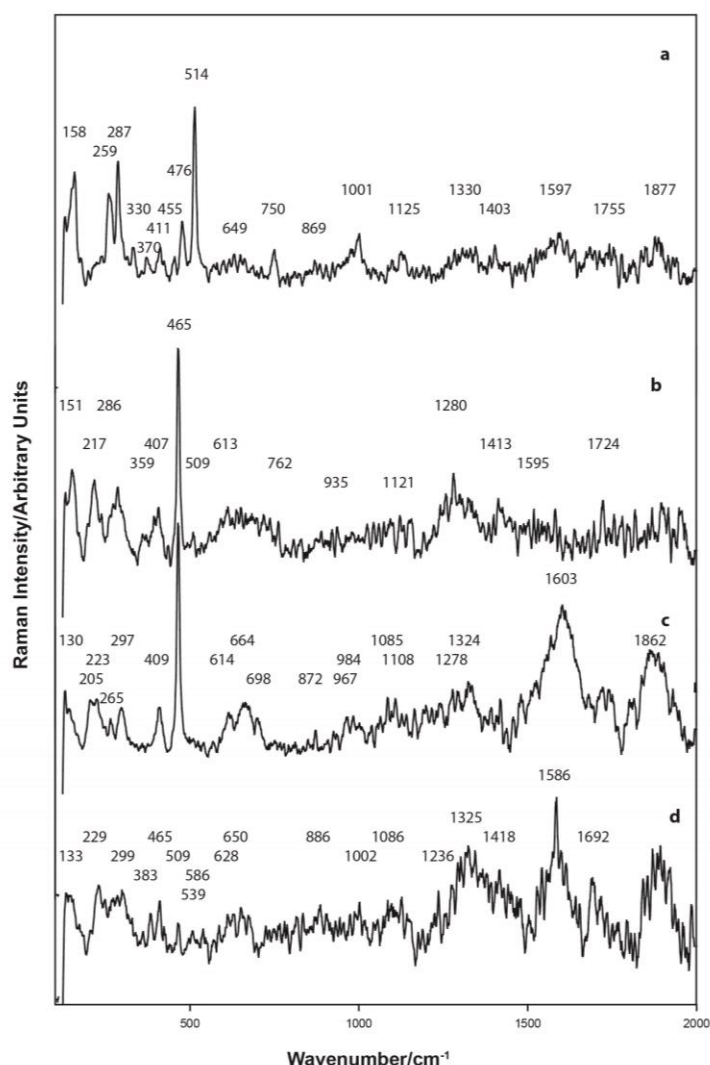
Figure 3.36.   Raman spectra, red ochre pigment Sample 23, Mut al-Kharab trench sample 38B, Context 58 (λ = 514.5 nm).   The red pigment contains hematite, jarosite, amorphous carbon, calcite feldspar (orthoclase and labradorite) and possibly ferrogedrite. Pigment elemental analysis is provided below.

Average elemental analysis Sample 23, red ochre pigment (Nova analysis)

Na$_2$O	MgO	Al$_2$O$_3$	SiO$_2$	P$_2$O$_5$	SO$_3$	Cl	K$_2$O	CaO	TiO$_2$	MnO	FeO	CuO	SnO$_2$	As$_2$O$_3$
1.5	1.1	4.3	52.3	0.6	0.6	0.4	0.7	0.4	0.3	0.3	37.2	0.3	0.0	0.0

Pink pigments have been found by other workers to have often been based upon vermillion. The Raman spectrum for vermillion as given by Burgio and Clark (2001) does not accord with any of the Raman spectra obtained. Whereas, in the present study, the pink colour on walls at Kellis has been found to be hematite-based, modified by the addition of goethite, natrojarosite or ankerite and lightened by the addition of a significant addition of orthoclase feldspar and possibly augite. Their Raman spectra are provided in Figures 3.37 and 3.38. The hematite selected for this shade was amorphous and of a lower quality than that used as a red pigment.
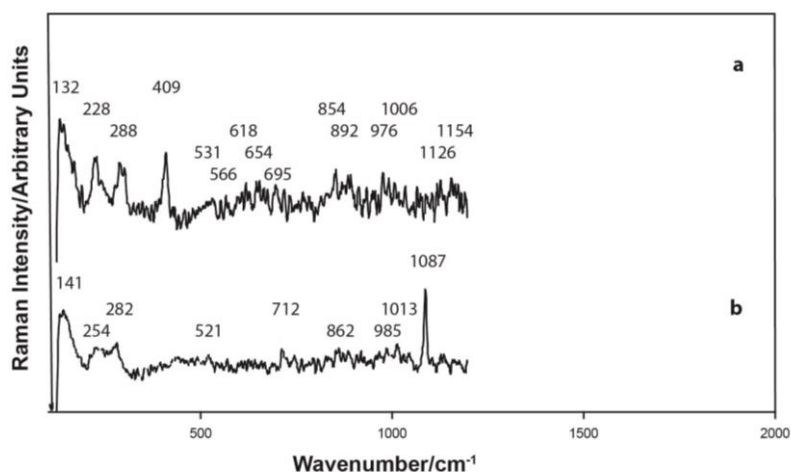
Figure 3.37.   Raman spectra of pink wall pigment, Kellis, location Area B, Painted Villa (λ = 514.5 nm). The pink pigment has been achieved by mixing a low quality iron oxide, (hematite containing alumina and titanium) with calcite; gypsum, anhydrite and hastingsite [$Na,Ca_2(Fe^{2+}_4Fe^{3+})(Si_6Al_2)O_{22}(OH)_2$] were also observed. The elemental analysis is provided below.

Average elemental analysis, Sample K9 Kellis 3/3/1 Area B pink pigment (Nova analysis)

Na₂O	MgO	Al₂O₃	SiO₂	P₂O₅	SO₃	Cl	K₂O	CaO	TiO₂	MnO	FeO	CoO	CuO	ZnO
3.2	2.5	8.3	18.0	0.6	7.1	2.9	1.0	49.4	0.3	0.0	6.3	0.0	0.3	0.0
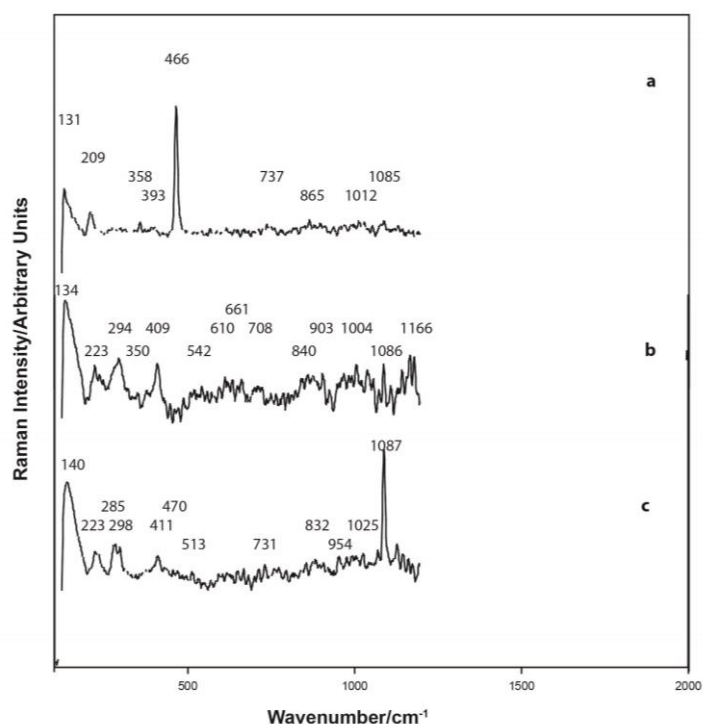
Figure 3.38.   Raman spectra, dark pink wall pigment Sample K18, Kellis, location B/3/1 (λ = 514.5 nm). Raman spectroscopy indicates that the sample contains silica, calcite, the pyroxene diopside, gypsum, feldspar (possibly anorthite and labradorite) gehlenite, hematite containing aluminium and titanium, probably coquimbite [$Fe^{3+}_2(SO_4)_3.9H_2O$] and possibly grunerite [$\square Fe^{2+}_2Si_8O_{22}(OH)_2$]. Pigment analysis is provided below.

Average elemental analysis, Sample K18 Kellis B/3/1 Area J ?(14) dark pink pigment (Nova analysis)

Na₂O	MgO	Al₂O₃	SiO₂	P₂O₅	SO₃	Cl	K₂O	CaO	TiO₂	MnO	FeO	CoO	CuO	ZnO
5.0	5.2	18.7	37.7	0.7	9.4	2.9	2.8	9.4	0.7	0.0	7.0	0.0	0.5	0.0

Amorphous carbon was present in a number of the samples. It is not known whether this has come from contamination or from a deliberate addition to darken the appearance of the red. This is particularly evident for the reds applied to cartonnage samples as indicated in Figure 3.39.
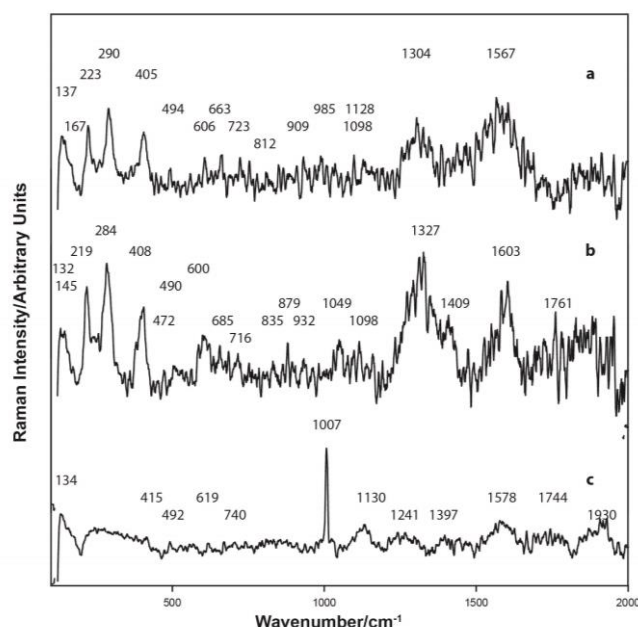
Figure 3.39. Raman spectra of a red pigment and plaster applied to cartonnage sample C7. The red pigment is hematite containing either or both alumina [Al_2O_3] and anatase [TiO_2]. The Raman band at 663 cm^{-1} is likely to be related to disorder effects and/or nanocrystals. Amorphous carbon is present in the sample.   The elemental analysis is provided below.

Average elemental analysis sample C7, Tomb 21 red pigment (Nova analysis)

Na$_2$O	MgO	Al$_2$O$_3$	SiO$_2$	P$_2$O$_5$	SO$_3$	Cl	K$_2$O	CaO	TiO$_2$	MnO	FeO	CuO	SnO$_2$	As$_2$O$_3$
2.2	2.7	6.0	45.2	0.0	8.2	0.5	1.1	7.7	0.7	0.0	25.7	0.0	0.0	0.0

The pigment has been applied on to a gypsum-silica cartonnage plaster surface as shown in Figure 3.39 and Figure A3.C7.1(c) and treated with an organic complex of unknown composition. There are a number of Raman bands which as indicated from the organic signatures provided in Table 2.5, Appendix A2, would suggest that the organic material is a mixture of Gum Arabic and a diterpenoid resin probably from the resin collected from *Pinus pinea* or *P. haleopennsis*.

Cartonnage pink sample C3 shown in Figure 3.40 and Appendix A3.C3 has again been applied using a highly fluorescent organic binder and this has rendered it difficult to obtain quality spectra.
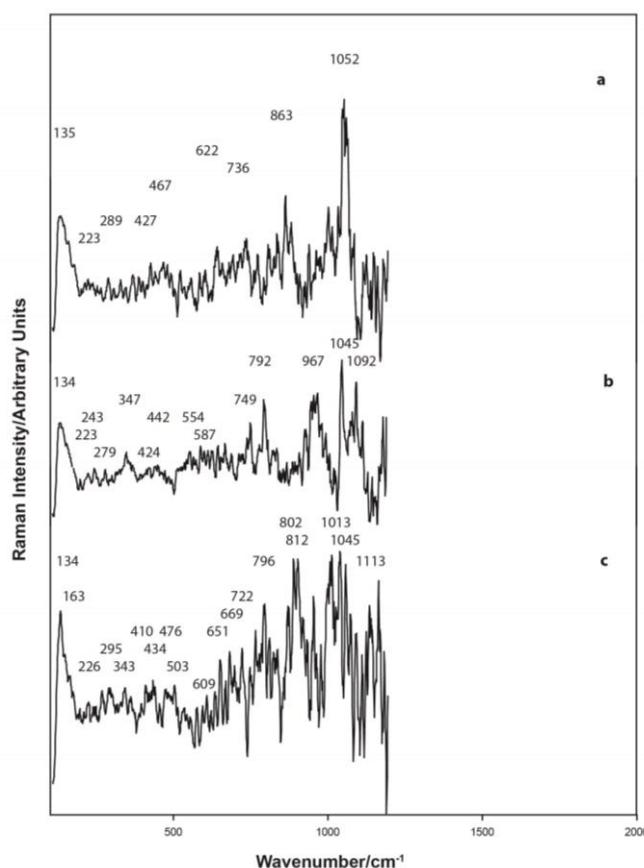
Figure 3.40.   Raman spectra of the pink pigment and plaster applied to cartonnage sample C3 (λ = 514.5 nm). The pink pigment as applied was most likely a mixture of hematite [Fe_2O_3] containing titanium dioxide (probably as anatase [TiO_2]), a feldspar (probably labradorite [$(NaCa)(AlSi)_4O_8$]), starkeyite [$MgSO_4.4H_2O$] and the carbonate minerals dolomite [$CaMg(CO_3)_2$] and ankerite [$CaFe^{2+}(CO_3)_2$] blended to obtain the desired shade of pink.   This pigment has been applied on to a gypsum plaster surface, and treated with an organic complex of unknown composition.   There are a number of Raman bands, which as indicated from the organic signatures provided in Table 2.5, Appendix A2, would suggest that the organic material is probably a mixture of Gum Arabic and a diterpenoid resin probably from the resin collected from *Pinus pinea* or *P. haleopennsis*. The elemental analysis is provided below.

Average elemental analysis sample C3, Tomb 23, pink pigment   (Nova analysis)

Na$_2$O	MgO	Al$_2$O$_3$	SiO$_2$	P$_2$O$_5$	SO$_3$	Cl	K$_2$O	CaO	TiO$_2$	MnO	FeO	CuO	SnO$_2$	As$_2$O$_3$
3.4	2.2	39.4	8.5	0.3	26.6	3.1	2.4	12.2	0.1	0.0	1.2	0.4	0.0	0.0

The purple pigment used on a wall decoration, Main Temple, Kellis, would appear to be a mixture of various iron oxides, including goethite, together with a mixture of other iron oxides probably derived from heating hydrated iron oxides to >300°C. Amorphous carbon has also been added. The sample is poorly crystalline and as such, it is difficult to differentiate the various iron oxides formed. It is shown and discussed in Figure 3.41.
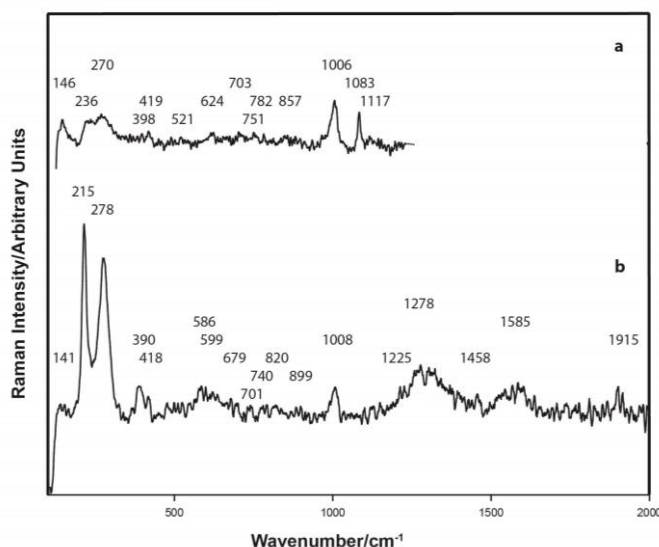
Figure 3.41.   Raman spectra, purple wall pigment, Sample 3, Main Temple, Kellis (λ = 514.5 nm). The applied pigment is a mixture intended to provide a shade of red and mixed with amorphous carbon. The red pigment has probably been derived from heating limonite a mixture of hydrated iron oxide minerals [FeO(OH).nH_2O] and including goethite, akagenéite, ferrihydrite, lepidocrocite, jarosite and schwertmannite to form intermediate minerals and which may include maghemite, hematite, etc.   Such thermal transformations can occur at temperatures >300°C. Thus, the phases present in this pigment are poorly crystallised and it is therefore difficult to discriminate one phase from another. The elemental analysis is provided below. The Raman spectrum in Figure A3.3.2(a) indicates the presence of an indeterminate organic compound probably added as a binder.

Average elemental analysis, Shrine IV Room 1 South Wall (JEOL analysis)													
Na_2O	MgO	Al_2O_3	SiO_2	P_2O_5	K_2O	CaO	TiO_2	MnO	FeO	CuO	SO_3	Cl	ZnO
0.9	1.1	6.0	13.3	0.5	1.0	40.5	0.2	0.0	30	0.2	4.6	1.4	0.2

The SEM-BSE image of a large particle of hydroxyapatite in Dakhleh Oasis sample D6 appears to have reacted with silica and alumina and is shown in Figure 3.42 together with its SEM-EDS spectrum indicating phosphorus. The analysis of the minerals surrounding this particle is phosphorus free as provided in Appendix A3.D6.18. Thus, as indicated in Table 3.7, apatite is present in several of the red pigmented pottery analyses. Such presence would again suggest the presence of kiln ash or fuel ash either in the pigment itself, or more likely in the pottery fabric. A reasonable possibility is that the kiln ash may have formed part of the burnishing process.
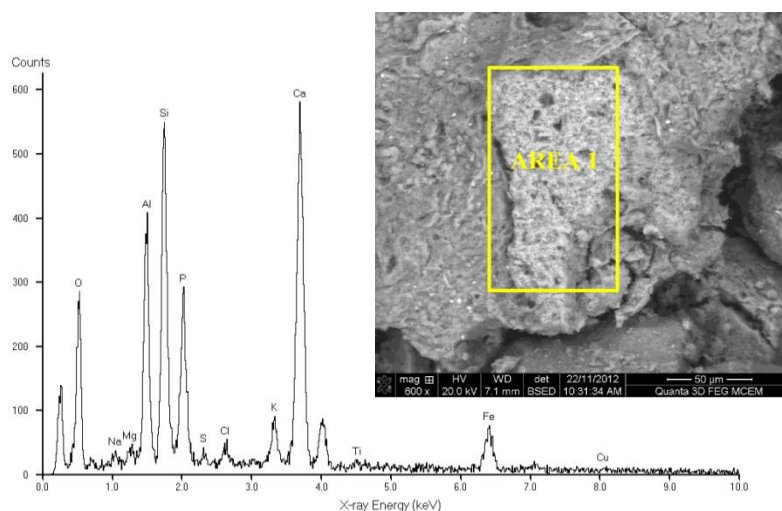
Figure 3.42. FIB EDS spectrum together with the FIB BSE image for the analysis of Area 1, being the calcium phosphate particle in the red pigment applied to Dakhleh Oasis sample D6 displayed and which particle is further discussed in Appendix Figure A3.D6.18.

3.4.4 Yellow

Orpiment, a yellow arsenical sulphide pigment (As_2S_3) was often employed in Egypt from the 12th Dynasty to at least the Ptolemaic period (Lee and Quirke 2000: 116). The Raman spectra for the orpiment applied on the Malkata pottery Sample M8 is shown in Figure 3.43 and for Malkata M2 in Appendix A3.M2.1. Additional data for both sherds is provided in Appendix A3. In both samples, significant quartz was present (45 and 46%) suggesting that the yellow was derived from or blended to obtain a similar composition, or more likely, that silica was employed as a grinding aid. In both sherds the presence of feldspar was detected; Sample M2 also contained spinel, diopside, and traces of huntite and realgar.

The underlying slip on Malkata Sample M2 was gypsum with traces of huntite. Or huntite with traces of wollastonite, diopside, goethite and possibly hydroxyapatite in the case of Malkata Sample M8. The Raman spectra for the slip (refer to Appendix A3, Figure A3.M8.29(c)) has a strong band at 1083 cm^{-1} indicative of calcite. However, there is also a strong band at 430 cm^{-1}, indicative of Egyptian blue (bands at 431 and 1086 cm^{-1}), and for this reason, calcite is not considered to be proven to be present. An accompanying band at 1122 cm^{-1} indicates the presence of huntite. Malkata sample M8 also contained anomalous copper and arsenic mineralisation and as shown in Figure A3.M8.29, the presence of an organic binder.
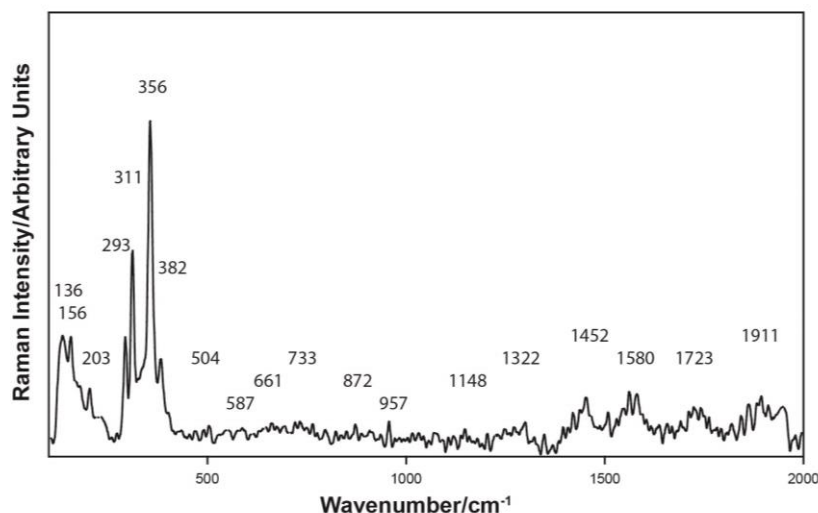
Figure 3.43. Raman spectrum, yellow pigment confirming its composition to be orpiment on Malkata sherd M8. The yellow pigment is orpiment (As_2S_3) and intermixed with the orpiment is quartz, an unidentified iron-based mineral, and traces of feldspar. The Raman spectrum in Figure A3.M8.5 provides some evidence for the possible use of an unidentified organic binder. ($\lambda = 514.5$ nm).

The yellow wall decoration samples found at Kellis are generally based upon a range of iron oxide minerals as provided in Table 3.9 and in Appendix A3, to obtain the various shades of yellow applied. The oxyhydroxides including goethite, lepidocrocite and akaganéite have been observed in various samples. Jarosite and natrojarosite have also been observed together with minor hematite. The term 'limonite' as used by Lee and Quirke (2000: 105) is rapidly being dispensed with from mineralogical terminology and is not used in this thesis.

A dark yellow pigment, Kellis wall Sample K14, find location B/3/1, is provided in Figure 3.44, and a contrasting pale yellow pigment sample from Kellis, Sample K6, find location B/3/1, is shown in Figure 3.45. An additional shade of yellow, Figure 3.46, is provided in wall Sample 11, find location, north wall, North Tomb 1, Kellis. Each pigment type, as identified in Table 3.9, shows the variation in shade; the more orange yellow being a blend of goethite plus hematite and amorphous carbon. Whereas the light yellow is jarosite and the dark yellow a mixture of jarosite, natrojarosite and lepidocrocite, the red shade introduced by the presence of lepidocrocite would also darken the shade of the yellow pigment.
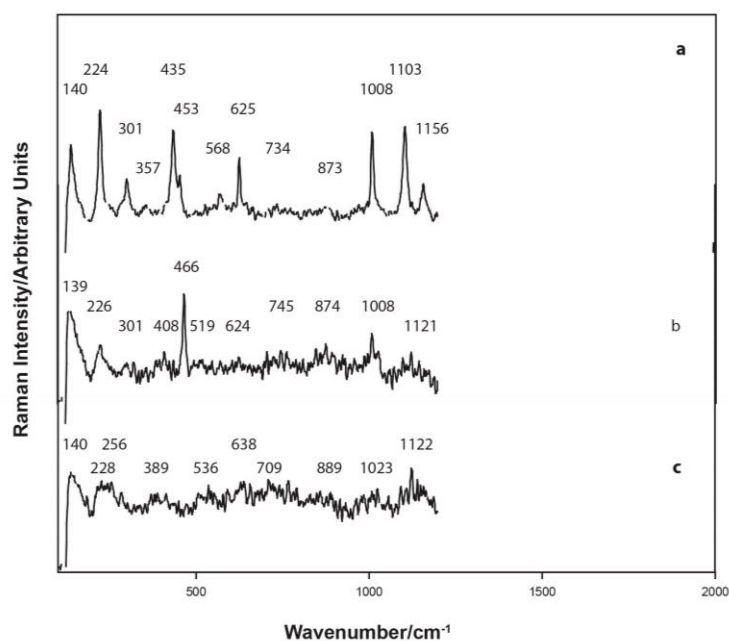
Figure 3.44. Raman spectra, dark yellow pigment applied to Sample K14, find location B/3/1, Area G, Kellis. As shown by the SEM-EDS analysis, the sample is high in sulphate, calcium, silica and iron oxide and contains gypsum, a trace of anhydrite, silica, jarosite, and possibly natrojarosite and probably lepidocrocite [γ-FeO(OH)]. (λ = 514.5 nm). The elemental analysis is provided below.

Average elemental analysis, Sample K14 Kellis 3/3/1 Area G dark yellow pigment (Nova analysis)													
Na_2O	MgO	Al_2O_3	SiO_2	P_2O_5	SO_3	Cl	K_2O	CaO	TiO_2	MnO	FeO	CoO	CuO	ZnO
2.0	0.5	2.8	29.4	0.2	18.7	0.7	3.0	16.0	0.5	0.0	25.8	0.1	0.3	0.0
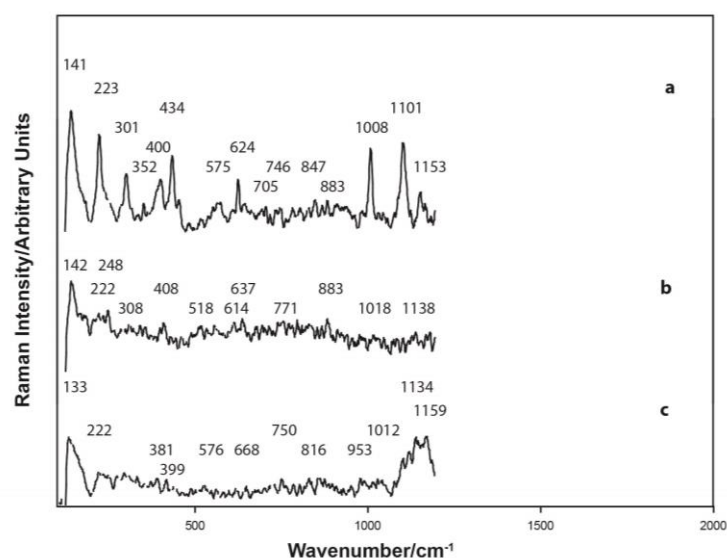
Figure 3.45. Raman spectra, pale yellow pigment, Kellis Sample K6, find location B/3/1, Area G. The yellow mineral is primarily jarosite [$KFe^{3+}_3(SO_4)_2(OH)_6$] which contains silica, feldspar, gypsum, anhydrite and the pyroxene diopside. (λ = 514.5 nm). The elemental analysis is provided below.

Average elemental analysis, Sample K6 Kellis 3/3/1 Area B pale yellow (Nova analysis)													
Na_2O	MgO	Al_2O_3	SiO_2	P_2O_5	SO_3	Cl	K_2O	CaO	TiO_2	MnO	FeO	CoO	CuO	ZnO
2.3	0.5	2.0	34.6	tr	14.4	0.8	2.0	4.6	0.8	0.0	37.9	0.0	0.2	0.0
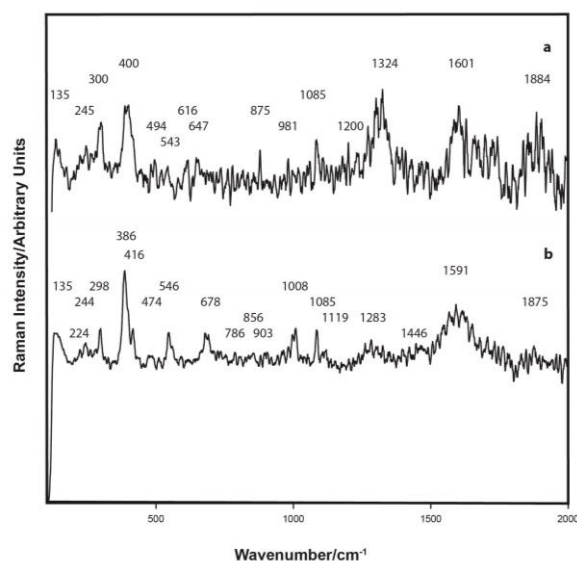
Figure 3.46. Raman spectra, yellow cartonnage sample, Sample 11, find location, north wall, North Tomb 1, Kellis. The yellow pigment consists of a mixture of the iron oxides hematite and goethite together with ilmenite, calcite, gypsum and amorphous carbon. ($\lambda = 514.5$ nm). The elemental analysis is provided below.

Average elemental analysis, NT1 North Wall (JEOL 840A analysis)													
Na_2O	MgO	Al_2O_3	SiO_2	P_2O_5	K_2O	CaO	TiO_2	MnO	FeO	CuO	SO_3	Cl	SnO_2
0.4	1.2	3.6	9.5	0.1	0.7	76.7	0.2	0.0	3.0	0.0	2.8	1.8	0.0
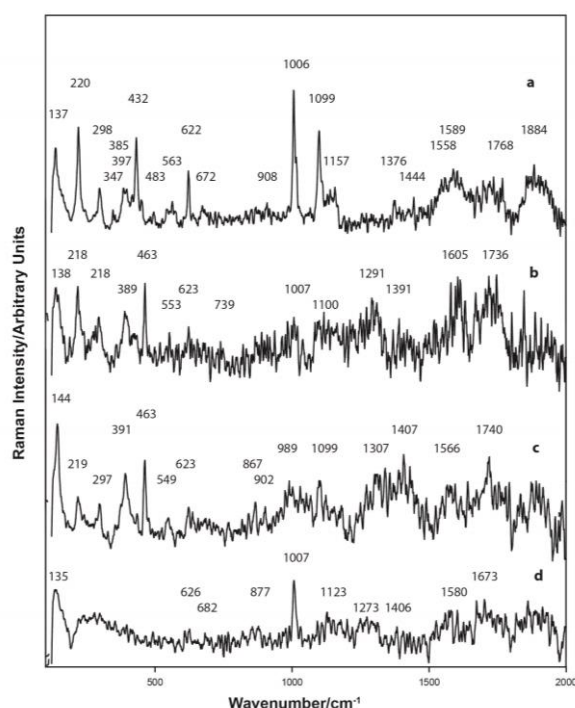
Figure 3.47. Raman spectra of a yellow pigment and plaster on cartonnage C8 ($\lambda = 514.5$ nm). The yellow pigment is jarosite [$KFe^{3+}_3(SO_4)_2(OH)_6$]. Quartz and a carbonaceous matter are also present.   The quartz is more likely to be associated with the jarosite possibly as a grinding aid, rather than part of the plaster. The pigment has been applied on to a gypsum plaster surface, and treated with an organic complex of unknown composition. There are a number of Raman bands which, as indicated from the organic signatures provided in Table 2.5, Appendix A2, would suggest that the organic material is a mixture of Gum Arabic and a diterpenoid resin probably from the resin collected from *Pinus pinea* or *P. haleopennsis*. The elemental analysis is provided below.

Average elemental analysis sample C8, Tomb 21 yellow pigment (Nova analysis)														
Na$_2$O	MgO	Al$_2$O$_3$	SiO$_2$	P$_2$O$_5$	SO$_3$	Cl	K$_2$O	CaO	TiO$_2$	MnO	FeO	CuO	SnO$_2$	As$_2$O$_3$
1.3	1.1	2.5	22.2	0.0	12.4	1.0	2.5	2.3	1.5	0.0	53.3	0.0	0.0	0.0
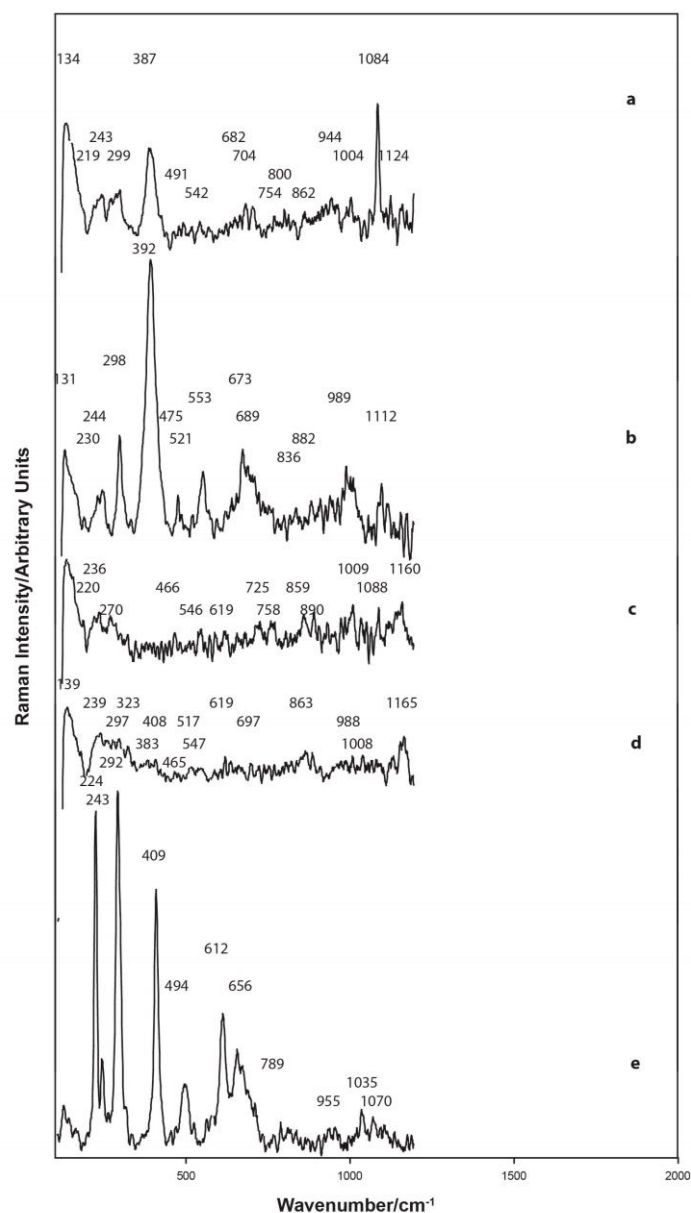
Figure 3.48.   Raman spectra, saffron yellow pigment on trench sample K20 (λ = 514.5 nm). As shown by the SEM-EDS analysis, the sample consists primarily of alumina (clays), silica and calcium. Raman spectroscopy indicates the presence calcite, gypsum, a highly crystalline hematite, (particularly evident by the narrow peaks in Figure 3.48(e), goethite and traces of brochantite [CuSO$_4$(OH)$_6$]. The elemental analysis is provided below.

Average elemental analysis, Sample K20 Kellis B/3/1 Area J saffron yellow pigment (Nova analysis)														
Na$_2$O	MgO	Al$_2$O$_3$	SiO$_2$	P$_2$O$_5$	SO$_3$	Cl	K$_2$O	CaO	TiO$_2$	MnO	FeO	CoO	CuO	ZnO
5.6	4.7	16.8	36.6	0.7	5.8	3.4	2.1	15.2	0.7	0.0	8.3	0.0	0.3	0.0

The variation in the mineral, or of the mineral blend selected is reflected in the final shade of the yellow pigment obtained and identified in the Raman signatures provided in Figures 3.44 to 3.48 and in Table 3.9.

Table 3.9. Yellow pigment wall decoration, cartonnage and trench sample mineralisation. The individual sample numbers are as listed in Chapter 1 and Appendix A3.

Wall decoration									
Sample	Mineral								
	1	2	3	4	5	6	7	8	9
5	■	■	■	■					
11		■	■		■				
12			■			■			
15		■				■			
K6							■		
K14	■				■	■	■		
K17		■			■				
K20		■			■			■	
Cartonnage									
C8							■		
Trench samples									
24 Mut	■	■							

1 = lepidocrocite   2 = goethite   3 = amorphous carbon
4 = oxidised iron pyrite   5 = hematite   6 = natrojarosite
7 = jarosite   8 = brochantite   9 = akaganéite

3.4.5 Green

An unusual form of Egyptian green from the wall of the Main Temple, Kellis and which has undergone lichen attack is discussed in Chapter 4 and Appendix A4. Degradation of this sample by lichen reaction to form copper oxalates has been detected by Raman spectroscopy.

All of the elemental and mineralogical details in respect of the other green pigments are provided and discussed herein and in more detail in Appendices A3 and A4. The green minerals encountered include a mixed red and blue pigment comprising possibly lazurite plus hematite at Kellis site B/3/1 as shown in Figure 3.49 and a mixture of brochantite and hematite as shown in Figure 3.50 which was applied to the wall of a villa at Kellis. A "green earth" pigment, Sample 7, was applied as the wall decoration of North Tomb 1, Kellis and Sample 2, a grey-green pigment was applied on the Main Temple wall at Kellis. Copper carbonate (malachite) provided the green pigment on cartonnage sample C1.

The green earths comprised clayey micas of either celadonite and/or glauconite. The celadonite being associated with fractures in volcanic rocks and glauconite is found in marine sedimentary rocks. The signatures of the Raman spectra are discussed in detail by Cristini *et al*. (2010). These authors also reported that the 514.5 nm laser excitation, as employed in the present research, uniquely shows many bands in the range 1200 – 1600 cm^{-1}

similar to that of ferroceladonite. They attributed these bands to the presence of minor concentrations of interlayer molecules or cations. Green earths have been positively identified in wall decoration at Kellis as provided in Figure 3.51 and as discussed within each figure.
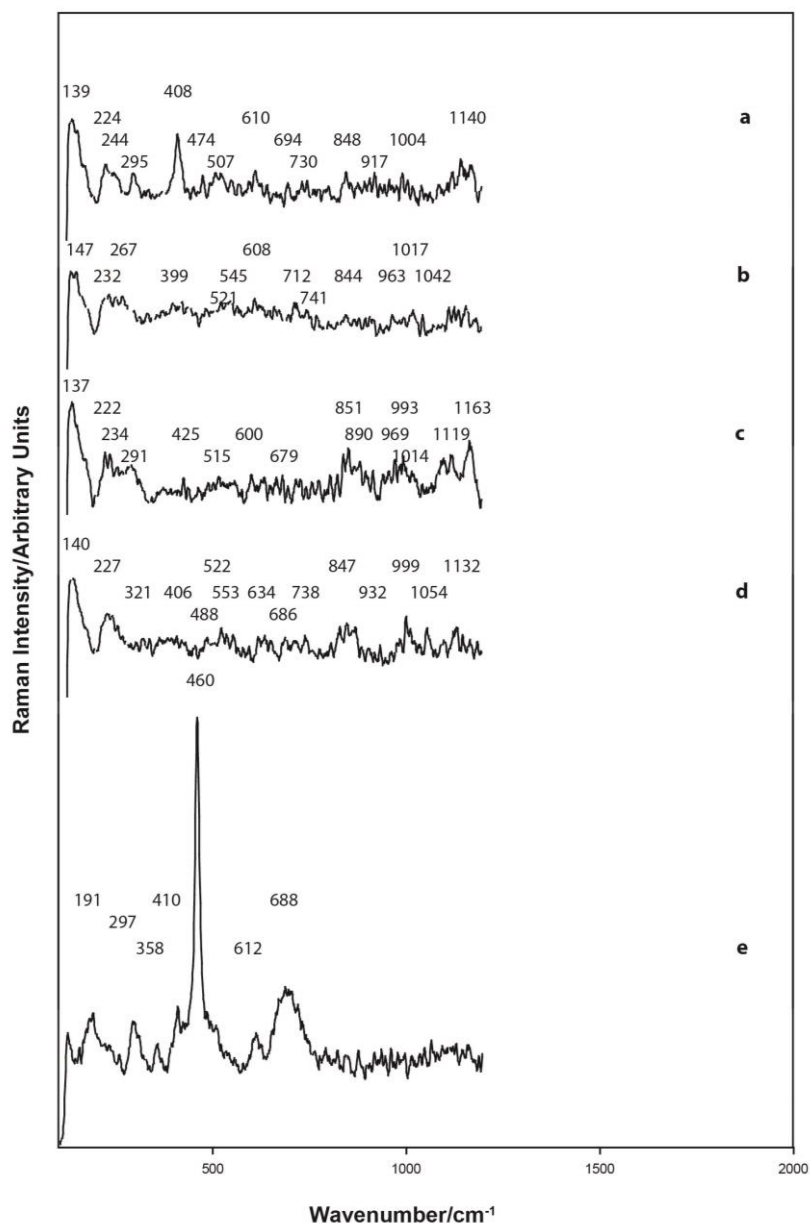
Figure 3.49. Raman spectra, pale green pigment on sample K19, Painted villa wall, Kellis ($\lambda = 514.5$ nm). The pigment consists of anhydrite, quartz, feldspar as microcline, hematite and possibly lazurite $[Na_3Ca(Si_3Al_3)O_{12}S]$ although an alternative pigment may be present. The elemental analysis is provided below.

Average elemental analysis, Sample K19 Kellis B/3/1 Area J green pigment (Nova analysis)														
Na_2O	MgO	Al_2O_3	SiO_2	P_2O_5	SO_3	Cl	K_2O	CaO	TiO_2	MnO	FeO	CoO	CuO	ZnO
8.9	3.9	18.7	39.9	0.9	5.8	4.7	2.8	6.4	0.8	0.0	6.5	0.0	0.7	0.0
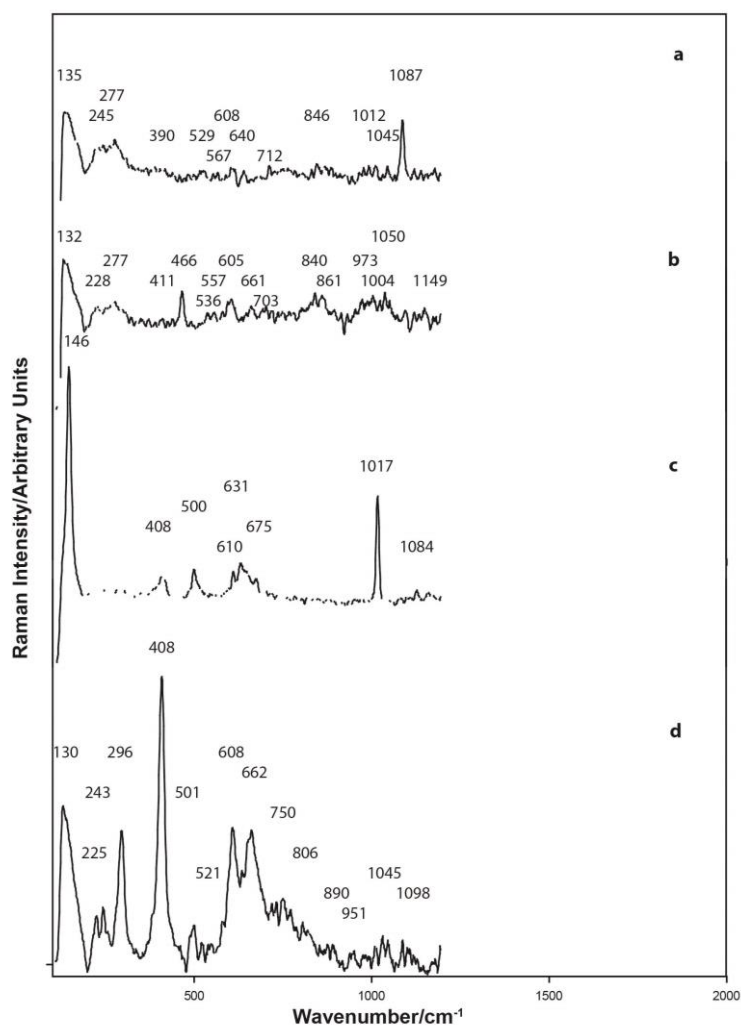
Figure 3.50. Raman spectra of a forensic sample of green pigment, Sample K1, Area B, Structure 3/1, Painted villa, side room west, Kellis ($\lambda = 514.5$ nm).   The sample contains anhydrite, calcite, quartz, hematite indurated with anatase and alumina, magnesiospinel [$MgAl_2O_4$] (spinel, *sensu stricto*), the pyroxene diopside and brochantite [$Cu_4SO_4(OH)_6$].

Average elemental analysis, Sample K1, Kellis B/3/1 Area B pale green (Nova analysis)

Na$_2$O	MgO	Al$_2$O$_3$	SiO$_2$	P$_2$O$_5$	SO$_3$	Cl	K$_2$O	CaO	TiO$_2$	MnO	FeO	CoO	CuO	ZnO
6.9	1.8	4.5	17.3	0.7	3.4	7.8	2.6	46.9	0.1	0.0	7.5	0.0	0.4	0.0
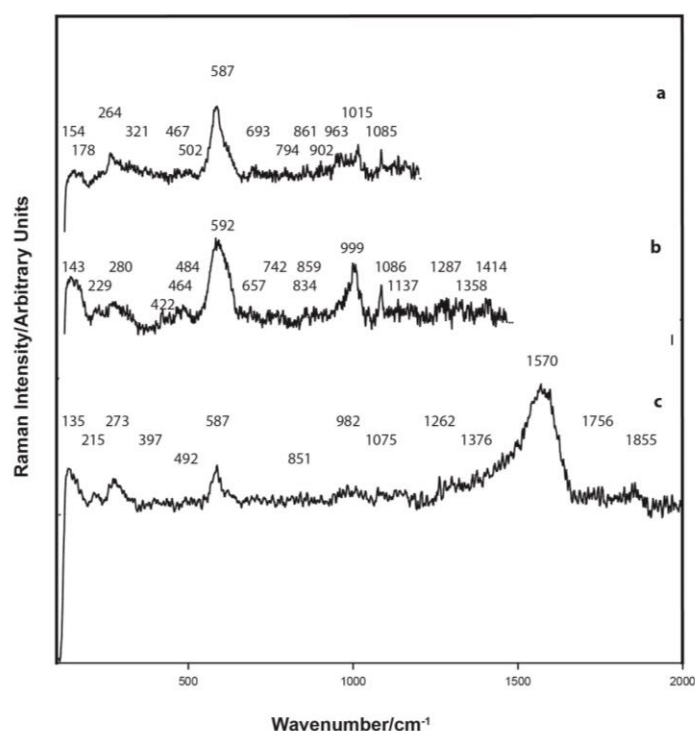
Figure 3.51 Raman spectrum, "green earth" pigment, Sample 7, find location, south wall, North Tomb 1, Kellis. The green pigment is the "green earth" mineral glauconite, together with calcite, anhydrite and feldspar (probably orthoclase or labradorite). (λ = 514.5 nm).

Average elemental analysis, NT 1 South Wall, Kellis (JEOL 840A analysis)

Na$_2$O	MgO	Al$_2$O$_3$	SiO$_2$	P$_2$O$_5$	K$_2$O	CaO	TiO$_2$	MnO	FeO	CuO	SO$_3$	Cl	SnO$_2$
0.4	0.9	4.6	35.1	0.1	0.5	51.5	0.1	tr	2.0	0.2	1.0	0.5	0.0

Cristini *et al*. (2010) reported that not every sample of green pigment used was able to be identified; in one instance it was Egyptian blue mixed with orpiment, goethite in another case and one object was painted with a lower layer of orpiment and an upper layer of Egyptian blue; green earths, as the iron-rich celadonite/glauconite clay minerals were also identified.   According to these authors, they were only aware of three examples of green earths being used in Egyptian art, namely a wall-painting in a Roman-Egyptian shrine, a Graeco-Roman cartonnage fragment and a Roman-Egyptian mummy cloth. As is reported herein and in Appendix A3, the present thesis has extended this number of green earth pigments being used in both wall decoration and on cartonnage.
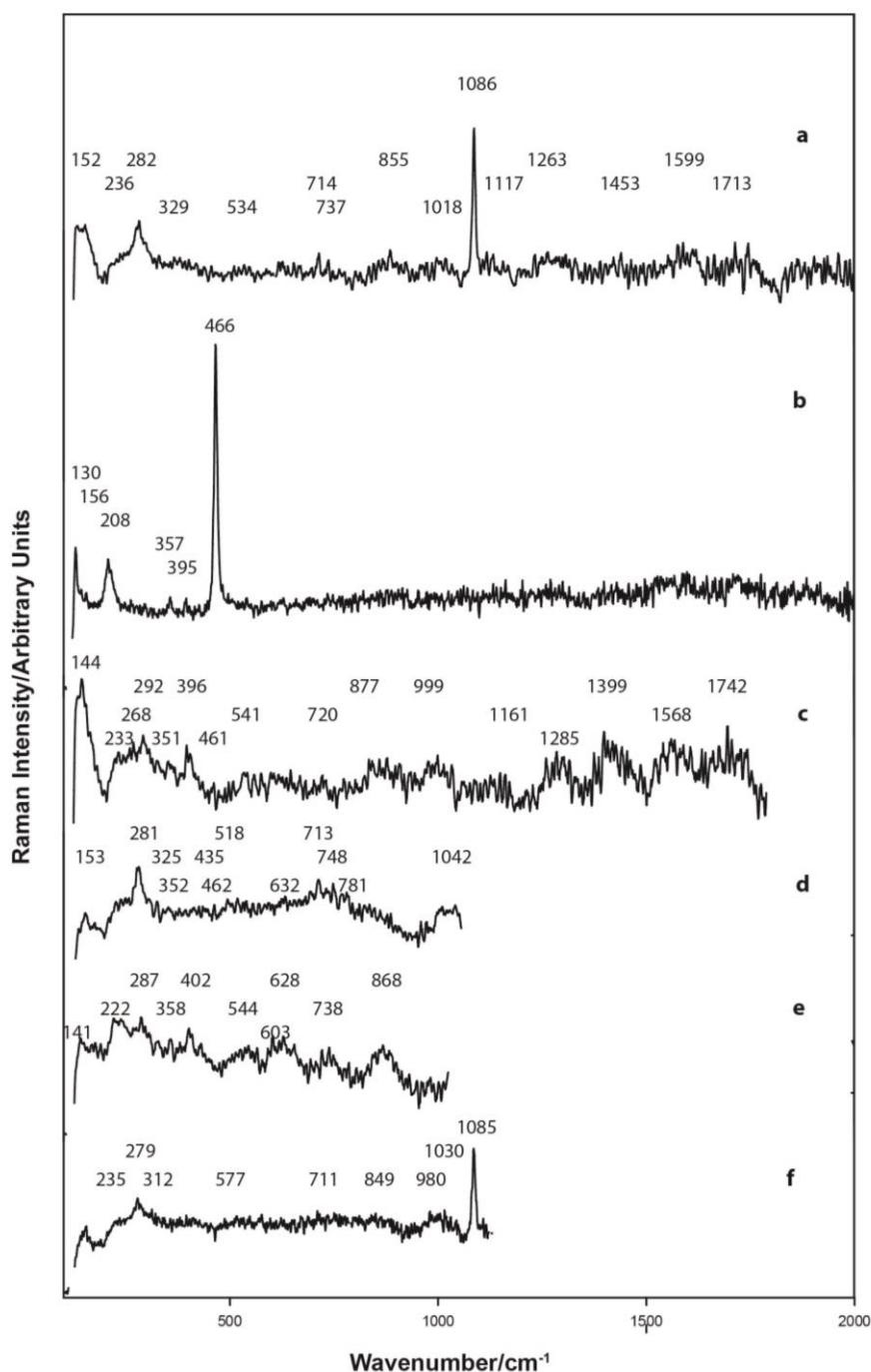
Figure 3.52. Raman spectra of the green-grey pigment, Sample 2, Main Temple, Kellis, the elemental analyses of which are provided above. The pigment contains quartz, gypsum, feldspar and calcite. The pigment does not contain Egyptian green, although the band at 1086 cm^{-1} can be assigned to either ν_1-symmetric stretching mode of CO_3 or Si-O$_{nbr}$ stretching mode (Si-O-Si stretching) indicative of part of the Raman signature for Egyptian green. As provided in Figure 3.52, Appendix A3.2.5 and in Figure 3.55, a region containing metallic particles of a copper-zinc-bismuth alloy was located. And, the presence of high calcium and high silica would provide the necessary raw materials to manufacture Egyptian green. Phosphorus, indicative of bone ash, or as a trace element in brass and bronze, was also present with this metal alloy. In other Egyptian green pigments, copper and tin (indicative of bronze) were used as starting raw materials. Copper-zinc mineralisation, indicative of brass, was introduced more recently than bronze production, indicative that this pigment may have been a failed attempt to produce Egyptian green from an alternative metal source. Very slight traces of possibly malachite or the green earth, glauconite, together with amorphous carbon is suggested to be present in the pigment from their respective Raman signatures; Figure 3.52(f) plaster is calcite containing traces of feldspar and goethite. (λ = 514.5 nm).

Calza *et al*. (2007), separately reported green earths to have been used on a sarcophagus cartonnage of the mummy n.158 in the National Museum, Brazil. From the presence of tricalcium phosphate together with carbon and magnesium sulphate, the black pigment was found to probably be ivory black. The brown pigment was either ivory black or magnetite and the red to be a red ochre. The white pigment was not positively identified, the authors providing a range of possible minerals, including sulphates, carbonates, or bone white.

Bonizzoni *et al.* (2011) reported that the strong fluorescence exhibited by the entire sarcophagus surface (26th Dynasty) prevented them from directly observing any Raman bands from the pigments in-situ using a hand held Raman instrument. Green was unable to be analysed using 1064 nm laser. Edwards *et al.* (2004) also reported strong fluorescence also using a 1064 nm laser. A high background emission prevented them from obtaining a spectrum for a suspected sample of Egyptian blue.
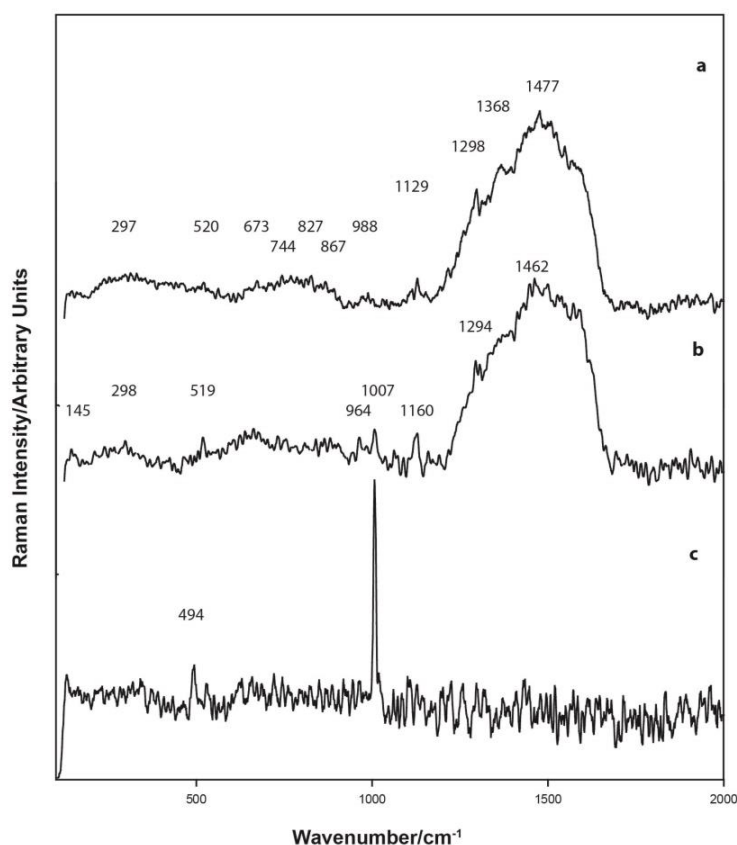
Figure 3.53. Raman spectra of the green pigment and plaster on cartonnage sample C1, Tomb 20, Kellis 1 cemetery ($\lambda = 514.5$ nm). The green pigment as applied was most likely a mixture of malachite [$Cu_2CO_3(OH)_2$] and carbonatecyanotrichite [$Cu_4Al_2CO_3(OH)_2.2H_2O$]. The mineralogical form of the arsenic has not been determined. Deterioration of the pigment has formed anatacamite [$Cu_2Cl(OH)_3$] antlerite $Cu^{2+}_3SO_4(OH)_4$] and a carbonaceous matter. The pigment has been applied on to a gypsum plaster surface, and treated with an organic complex of unknown composition. There are a number of Raman bands which as indicated from the organic signatures provided in Table 2.5, Appendix A2, would suggest that the organic material is a mixture of Gum Arabic and a diterpenoid resin probably from the resin collected from *Pinus pinea* or *P. haleopennsis*. The elemental analysis is provided below.

Average elemental analysis sample C1, Tomb 20 green pigment (Nova analysis)														
Na_2O	MgO	Al_2O_3	SiO_2	P_2O_5	SO_3	Cl	K_2O	CaO	TiO_2	MnO	FeO	CuO	SnO_2	As_2O_3
2.4	0.8	3.2	5.7	0.9	34.1	0.7	1.1	27.8	0.1	0.0	2.4	17.2	2.9	0.9
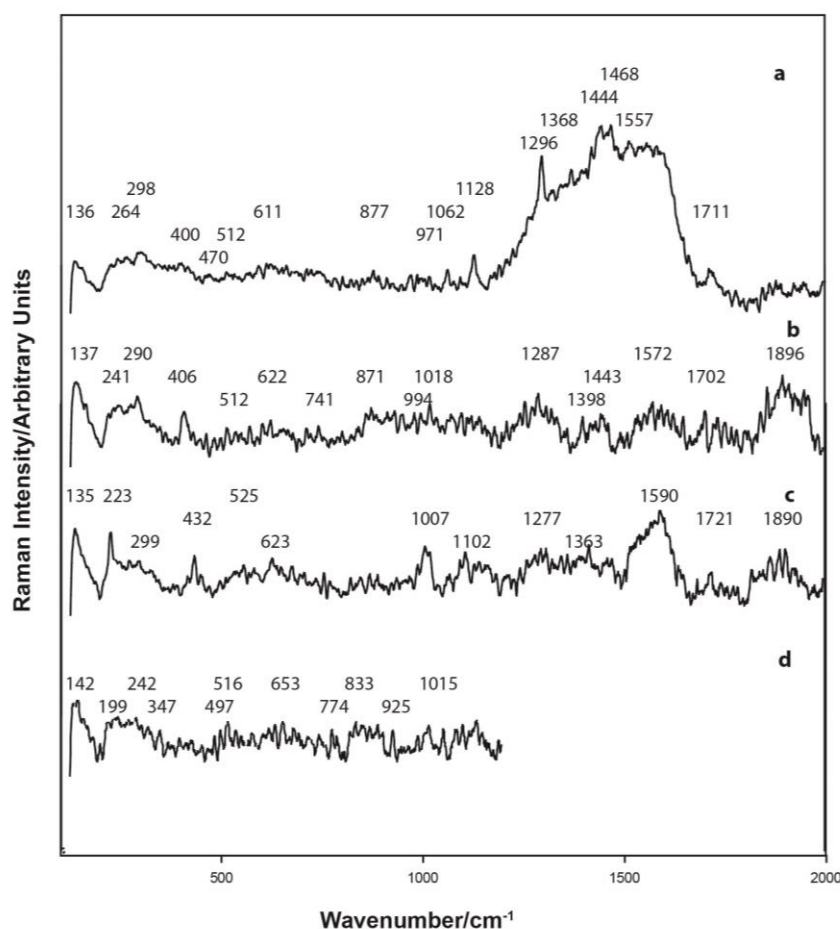
Figure 3.54. Raman spectra of the green pigment (a) and (b), and plaster (c) and (d) Sample C4, Kellis 1 cemetery, Tomb 20. The pigment has been applied on to a gypsum plaster surface, and treated with an organic complex of unknown composition. There are a number of Raman bands which as indicated from the organic signatures provided in Table 2.5, Appendix A2, would suggest that the organic material is a mixture of Gum Arabic and a diterpenoid resin probably from the resin collected from *Pinus pinea* or *P. haleopennsis.* (λ = 514.5 nm).

Average elemental analysis sample C4, Tomb 20, green pigment (Nova analysis)

Na_2O	MgO	Al_2O_3	SiO_2	P_2O_5	SO_3	Cl	K_2O	CaO	TiO_2	MnO	FeO	CuO	SnO_2	As_2O_3
3.4	5.2	8.2	17.3	0.7	19.7	1.5	1.6	15.4	0.4	0.0	5.6	19.0	1.9	0.0

Thus, the green pigment applied to cartonnage at Dakhleh Oasis as determined from the analysis of Samples C1 and C4, Kellis 1 cemetery, Tomb 20 was most likely a mixture of the green pigment, malachite [$Cu_2CO_3(OH)_2$] and carbonatecyanotrichite [$Cu_4Al_2CO_3(OH)_2.2H_2O$] as shown in Figures 3.53 and 3.54. Deterioration of the pigment has formed anatacamite [$Cu_2Cl(OH)_3$] antlerite $Cu^{2+}_3SO_4(OH)_4$] and a carbonaceous matter. The mineralogical form of the arsenical mineral detected in the SEM-EDS analysis, has not been determined.

Edwards *et al.* (2007) applied Raman spectroscopy to determine the composition of a pale yellow and of a dark brown staining on two Egyptian sarcophagi in the Manchester Museum collection dated to ca. 2200 y BP. The substrate comprised linen in a gypsum and

limewash plaster matrix. Examination of the resinous material and the resin specimen and they reported that it is closely related to a *Pistacia* species as presently observed at Dakhleh oasis. Edwards *et al*. (2004) examined twenty-nine pigment specimens from nine coffins, coffin lids and associated funerary artefacts using Raman spectroscopy. Quartz from fine river sand, used as a grinding aid was detected in several pigments. The red was considered to be either pure hematite or hematite mixed with clays, or alternatively obtained from heating goethite to temperatures above 300°C. Black was amorphous carbon, pink to be a mixture of calcite and minium (red lead), and in one 21st Dynasty Theban coffin base to be anhydrite, in admixture with calcite and hematite. The red pigment on another coffin was a mixture of calcite, hematite and pararealgar. Yellow was normally goethite but a Rishi 17th Dynasty coffin lid from Qurneh was an unusual mixture of crocoite (lead (II) chromate), limonite (iron(III) oxide) and calcite. Egyptian blue and lazurite, which may have originated from restoration were both present.   These authors proposed that the new pigments in the funerary artefacts from the Ptolemaic and Graeco-Roman periods points to a trade between Egypt and Rome from about 300 BCE to 300 CE.

Bone ash particles, some of which have adsorbed sodium chloride to form a coating on their surface were observed within the blue/green pigment applied to the surface of the Main Temple, D/5, Shrine IV Room 1 Kellis (refer Appendix A3, Sample 2, Figure A3.2.4).   This sample, as provided in Figure 3.55, is a mixture containing significant particles of silica, copper, calcium, zinc and bismuth within the green mineralisation. These elements are indicative of Egyptian green manufacture or its attempted manufacture, using scrap brass shavings (brass is a copper/zinc alloy) rather than bronze shavings and as such, is in accordance with the time period indicated (2nd century CE).   The Raman spectra are provided in Figure 3.52. It is not immediately evident as to the source of the bone ash, however, it does contain amorphous carbon and this may indicate that it has been derived from an organic source. The average elemental analyses are provided in Table 3.10.

Table 3.10. FIB BSE elemental analyses of Area 1 and spot 1 provided in Figure 3.55 below. The pigment is Sample 2, a grey-green pigment , Main Temple, D/5, Shrine IV, Room 1, upper wall, Kellis.

Average elemental analysis, Grey-Green Sample 2, Kellis. Shrine IV Room 1 Roof? Upper wall (metallic inclusions in the FIB analysis, namely in Area 1 analysis, refer Figures A3.2.1 and A3.2.2)

Na_2O	MgO	Al_2O_3	SiO_2	P_2O_5	K_2O	CaO	TiO_2	MnO	FeO	CuO	SO_3	Cl	ZnO
0.0	2.3	6.2	15.5	1.6	1.1	17.9	0.0	0.0	3.4	28.1	4.6	1.5	17.9

Average elemental analysis, Grey-Green Sample 2, Kellis. Shrine IV Room 1 Roof? Upper wall (metallic inclusions in the FIB analysis, Spot 1 analysis, refer Figures A3.2.1 and A3.2.3)

Na_2O	MgO	Al_2O_3	SiO_2	P_2O_5	K_2O	CaO	TiO_2	MnO	FeO	CuO	SO_3	Cl	ZnO	Bi_2O_3
0.0	1.8	4.4	10.2	1.6	0.7	9.0	0.0	1.2	3.0	34.0	4.3	1.1	21.0	6.7
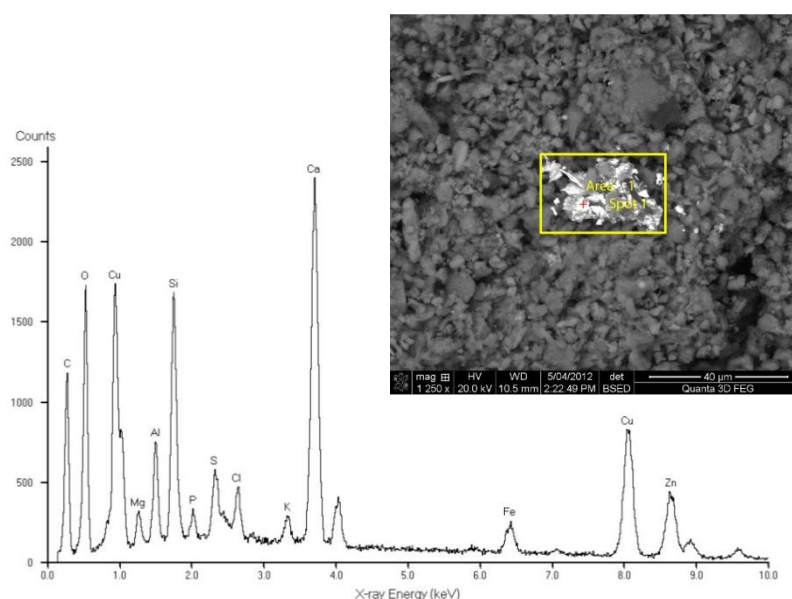
Figure 3.55. FIB BSE image showing the position of Area 1 and spot 1 analyses for Sample 2, and the FIB EDS spectrum for Area 1 and Appendix A3, Figure A3.2.1. Grey-green pigment , Main Temple, D/5, Shrine IV, Room 1, upper wall, Kellis. The analyses are provided in Table 3.10 and discussed in Appendix A3. The analyses provide a significant indication of copper and zinc being present. Thus, brass (a copper-zinc alloy), rather than bronze was used as the copper source. A strong indication for the presence of phosphorus is also indicated.

3.4.6 White

As shown in Table 3.11, and in Figures 3.56 and 3.57, the white minerals selected for application as slip coatings were calcite, gypsum and/or huntite. The choice of huntite as a white pigment was considered by Ambers (2004) to be related to artistic purposes only and not restricted in its use to any religious or societal group. It has the positive ability to affect the brightening of reds and other more translucent pigments.

The presence of calcite or huntite would indicate a post-firing application. Bone ash may well have formed part of the fabric or to have been incorporated into the pigment during the formation of anhydrite. The presence of anhydrite would suggest a pre-firing application of this pigment.
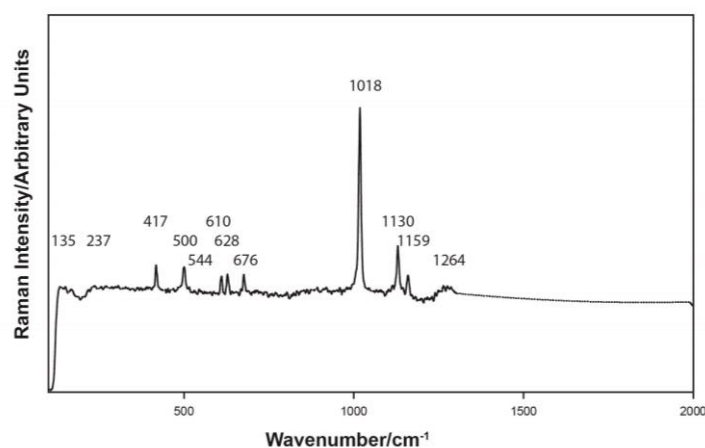
Figure 3.56. Raman spectra, white area on body surface of sherd Sample D5, Dakhleh Oasis 4th century Roman. The Raman spectrum is that of anhydrite (λ = 514.5 nm).
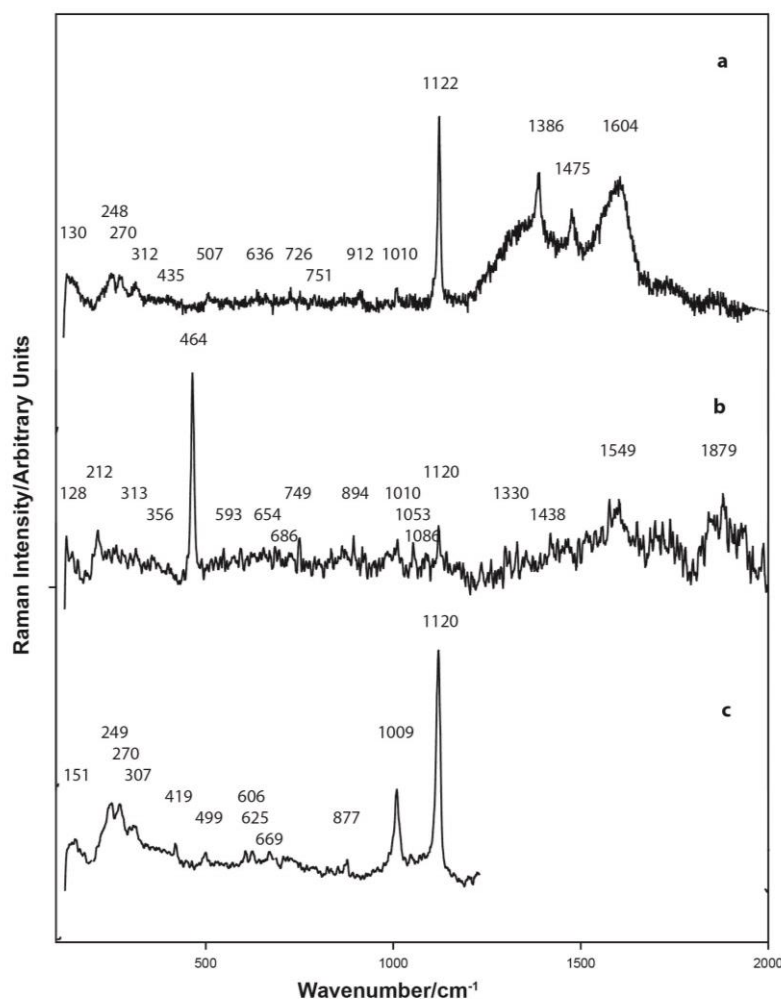
Figure 3.57. Raman spectra, white slip surface coating on Malkata Sample M7, (Malkata sherd M73/K/5). The white slip is a mixture of gypsum and huntite together with quartz, feldspar, hematite, diopside and/or enstatite and amorphous carbon. As shown by its elemental analysis, the slip contains anomalous copper and arsenic. There is an indication for the presence of an organic complex, however, the sample fluorescence has prevented obtaining a portion of the required spectrum (λ = 514.5 nm).

Table 3.11. Elemental analyses of the major elements present in the white pigment found on samples from the Dakhleh Oasis. Note the effect of substrate elements on the accuracy of the provided information.

Sample	FeO %	SiO$_2$ %	Al$_2$O$_3$ %	CaO %	MgO %	Mineral
Dakhleh Oasis						
D2	7.2	50.8	30.2	1.9	2.3	gypsum, quartz
D4	5.6	52.7	21.8	6.5	2.5	quartz (prob. as flint), gypsum
D7	4.8	25.4	15.2	36.6	5.8	gypsum, bone ash
D8	0.6	6.5	4.3	63.9	3.1	gypsum, bone ash

Importantly, the white line on Sample D4 (Dakhleh Oasis sherd S2) is principally silica and the presence of residual skeletal silica from plant fibres such as straw or chaff are evident in the BSE image provided in Figure 3.58. This would confirm that the pigment has been heated to at least 600°C but below 1000°C as there is no evidence to confirm the presence of either tridymite or cristobalite. It is possible that flint or chert was used as a silica source. Moganite is present as shown by the strong silica Raman signature and an accompanying Raman band at 503 cm^{-1} within the pigment. Moganite in silica has been described in detail by Jay *et al*. (2015) and moganite has certainly been detected in lithics found at Dakhleh Oasis in the Western Desert (unreported Raman data, not included in this thesis). A brief discussion is provided in the accompanying information A7 within the data link provided. The indication of a high temperature firing of the silica is supported by the presence of phosphorus (as bone ash) from kiln ash.
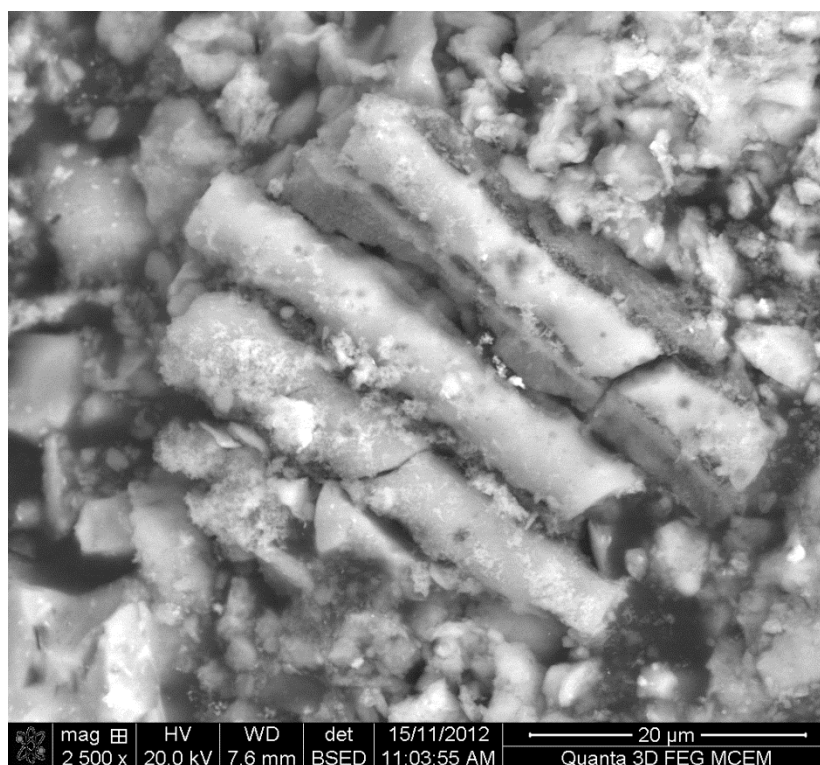
Figure 3.58. FIB EDS image of the skeletal silica present within the white pigment applied to the surface of Sample D4, Dakhleh Oasis, 4th century Roman.

Table 3.12. Average elemental analysis of the white pigment applied to the surface of Dakhleh oasis sherd D4.

Average elemental analyses, white pigment, FIB EDS average Area analyses, Figures A3.D4.1,A3.D4.4, A3.D4.6

Na$_2$O	MgO	Al$_2$O$_3$	SiO$_2$	P$_2$O$_5$	SO$_3$	Cl	K$_2$O	CaO	TiO$_2$	MnO	FeO	CoO	NiO	CuO	ZnO
3.5	2.5	21.8	52.7	0.5	1.4	1.3	2.3	6.5	1.3	0.0	5.6	0.0	0.0	0.6	0.0
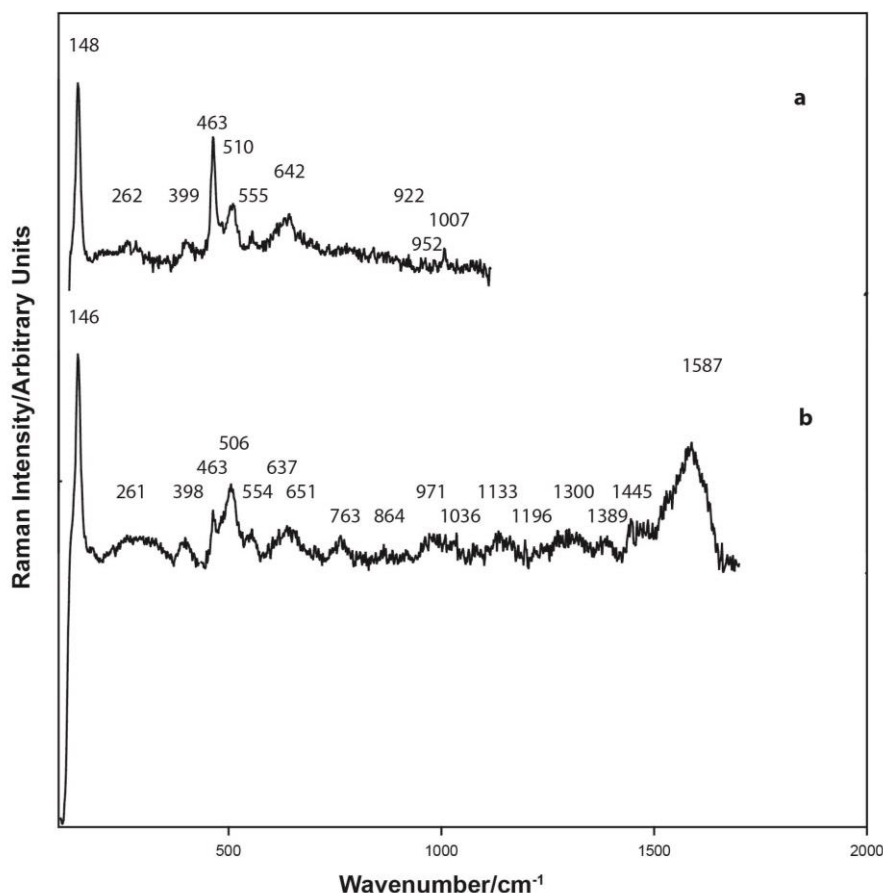
Figure 3.59. Raman spectra, white pigment on Sample D4, Dakhleh Oasis 4th century Roman sherd. The white pigment applied as a white line is principally quartz and which has been heated to an elevated temperature as shown by the presence of residual silica in the form of tubes created when straw-like vegetation has undergone combustion with the silica as shown in Figure 3.58, the analysis of which is provided in Appendix A3.D4.6, Spot 1. Importantly, whilst slight skirting of the electron beam and/or penetration of the beam to below the surface, it is instructive to examine the analysis of these particles. They contain approximately 89.8% SiO$_2$ together with soda and potash (0.7% and 0.5% respectively) and a slightly higher concentration of magnesia (1.0%). Alumina, lime and iron may have been elevated by the surrounding pottery white pigment and/or body but, the analysis would also indicate their presence in the plant matter prior to calcination. The presence of wollastonite would support a high temperature firing of the silica. ($\lambda = 514.5$ nm).

It is conjecture, however, flint (or chert) is available in the region and is a readily available source of silica. The Raman band at 504 cm^{-1} in association with a strong silica peak at 464 cm^{-1} has been occasionally observed in other analyses, indicating the presence of moganite and thus, flint (chert). It is known, and certainly practiced elsewhere, that heating flint in the region of 600°C will rapidly cause the silanol within its structure to rapidly expand, shattering the flint and creating a fine silica powder (Jay *et al*. 2015). The presence of feldspar, probably as labradorite and/or oligoclase and anatase were also detected.

Calcium phosphate particles were detected in the white pigment present on the surface of sherd Sample D7, Mut al Kharab, Ramesside period and shown in Figures 3.60 and 3.61.
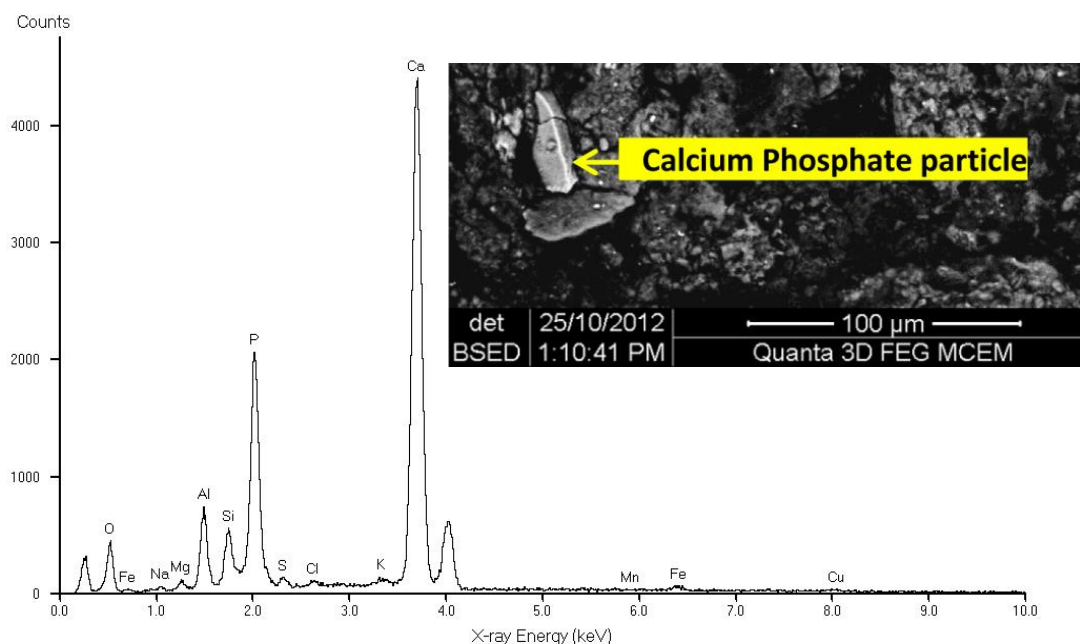
Figure 3.60. FIB EDS spectrum, for the analysis of Spot 1, a calcium phosphate (whitlockite or bone ash) particle observed in the white pigment applied to the surface of Sample D7, Mut al Kharab, Ramesside period.
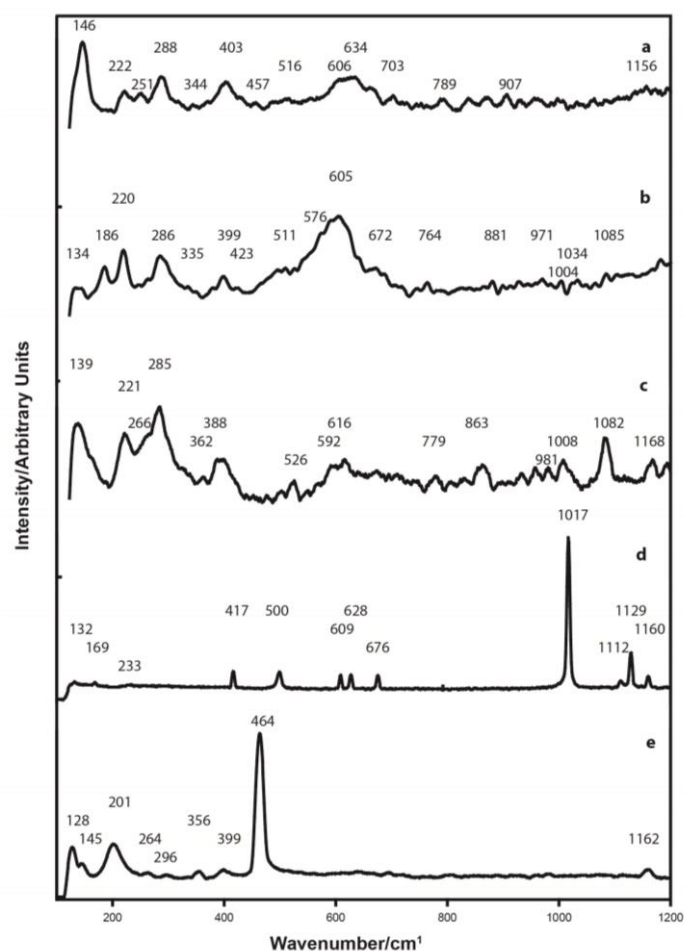
Figure 3.61. Raman spectra, white surface (λ = 514.5 nm). The EDS analyses indicate that the calcium concentration is an average of 36.6%. Part of the calcium can be attributed to the probable tricalcium phosphate (average of 3.8% P_2O_5 determined by analysis), although the actual calcium:phosphorus ratio can vary

3.62

depending upon the history of the bone prior to calcining, but it would be in the order of 30% of the CaO analysis. The sulphate content as provided by the EDS analyses is low, however, the Raman spectra in Figure 3.61 indicates the presence of both anhydrite and gypsum together with calcite. Calcite when heated to 850°C (Rodriguez-Navarro *et al*. 2009) will evolve its carbonate as carbon dioxide and this, together with the anhydrite would indicate that both gypsum and calcite have undergone a thermal cycle. The presence of calcite is most likely a post-deposition during sherd burial. The elevated MgO (5.8%) would suggest the presence of some huntite and this is confirmed from the Raman band at 1129 cm^{-1}. The presence of hydroxyapatite (bone ash) would indicate that kiln ash was employed in the production of this pigment. Anatase and rutile are both present confirming the exposure of this mineral to a temperature above 850°C. Feldspar, hematite containing aluminium and/or titanium, quartz, and traces of diopside are present. A band at 863 cm^{-1} in Figure 3.61(c) is attributed to $[CO_3]^{2-}$ weakly bonded to cations as discussed by Chiriu *et al*. (2014). The presence of quartz, rather than tridymite or cristobalite would indicate that the heating did not exceed 1000°C.

3.4.7 Pigment Binders

Egg white, animal glue and plant gum were variously detected as the binder used to fix the pigment to the substrate. These binders are illustrated in Figures 3.62 and 3.63. Visually, there is no indication of their presence. However, as provided in Chapter 4, beeswax was certainly used to overcoat Egyptian green pigments applied to pottery and this had a significant binding effect in fixing coarse pigments to the pottery surface.
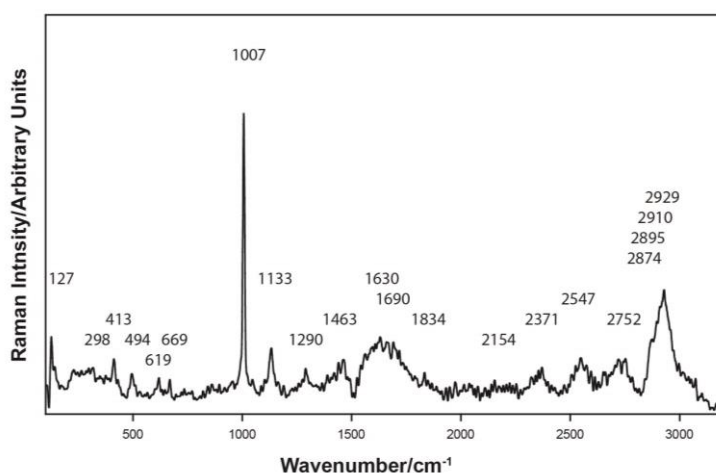
Figure 3.62. Raman spectrum, Malkata sample M5, indicating the gypsum slip to which gum Arabic and egg protein binders have been used in the application of the cobalt blue pigment to the slip surface. This has been subsequently coated with beeswax ($\lambda = 514.5$ nm).
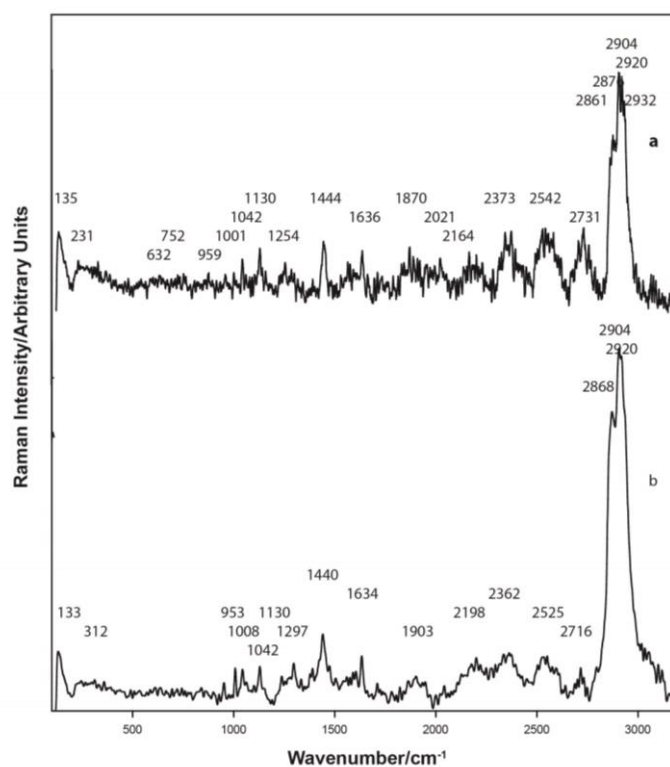
Figure A3.63. Raman spectra, egg protein used to fix the pigments to the pottery vessel surface, Amarna Sample A1, Nile valley, New Kingdom, (λ = 514.5 nm).

3.4.8 Surface deposits

These surface deposits are probably related to the vessel usage. Inside sherd surface coating on Malkata sherd M3 is provided in Figure 3.64.
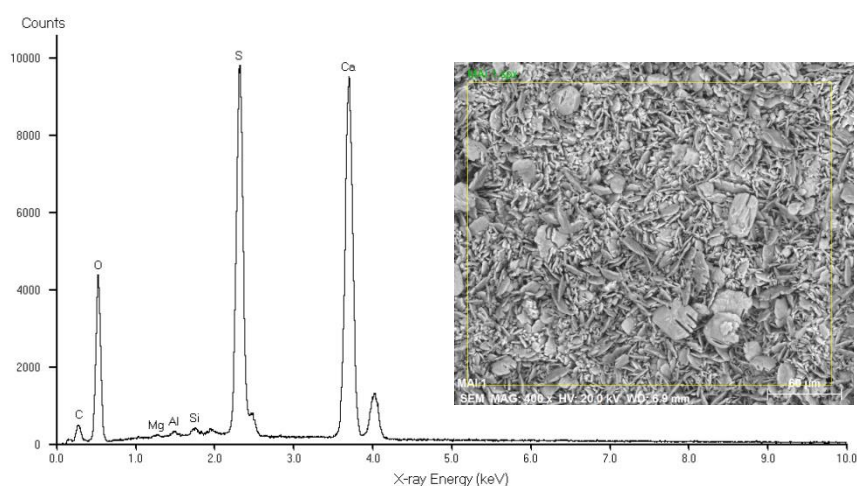
Figure 3.64. BSE-EDS spectrum for the analysis of the area on the surface of Malkata sherd M3 confirming it to be gypsum. The Nova SEM-BSE image is of the deposit on the surface of this Malkata sherd.

And, an organic complex, probably related to palmatine was found present on the internal surface of North Karnak sherd Sample NK3. Its Raman signature is provided in Figure 3.65. This internal vessel coating may directly relate to its previous usage.
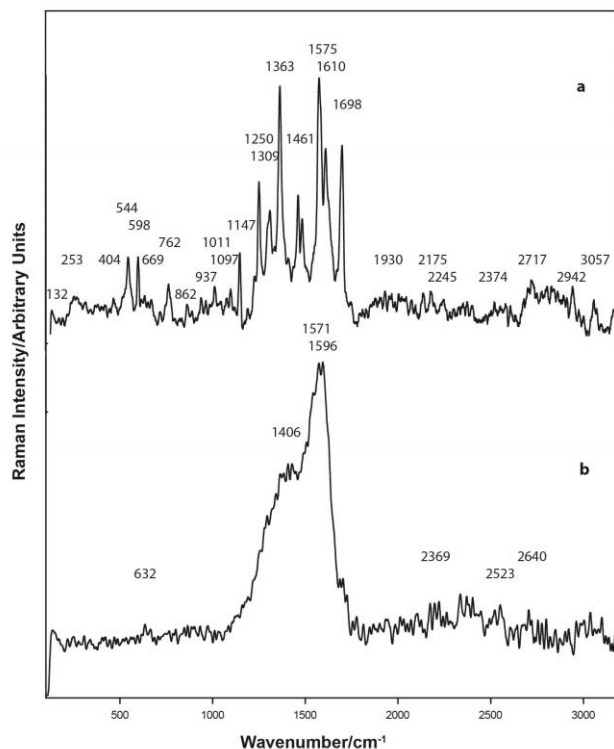
Figure 3.65. Raman spectra, residual organic matter on the internal vessel surface of North Karnak Sample NK3. Possibly related to the original vessel usage. The Raman spectrum of the organic complex indicates that it may be related to palmatine ($\lambda = 514.5$ nm).

3.5 Chapter summation

As demonstrated in this Chapter, Raman spectroscopy is a highly efficient research instrument for the examination of inorganic pigments. It has also been demonstrated that Raman spectroscopy is capable of determining the presence of residual organic complexes. As such, this indicates the need for wearing gloves when handling artefacts to minimise surface contamination. Coupling this instrument with electron microscopy has extended the understanding of the pigments under examination. Problems created by the potential contamination of micro-samples during their removal from sherd surfaces, even using a diamond tipped instrument, has been demonstrated. General conclusions with respect to this chapter are provided in Appendix A3.

CHAPTER 4.   EGYPTIAN BLUE and EGYPTIAN GREEN

4.1   Introduction

In ancient cultures, art and science were a single entity due mainly to their early stage of development. They were defined by the necessities of life and their technical possibilities (Berke 2007).   Thus, Egyptian blue, first developed in Egypt during the Old Kingdom is considered by many to be the very first chemical synthesis process to be developed by human endeavour.   However, Egyptian faience has also been referred to as the 'first high-tech ceramic' the production of which spans up to 5000 years, with extant examples dating from the Predynastic period (Vandiver and Kingery 1987; Clark and Gibbs 1997).   There is strong evidence that the glazing of stones and steatite originated in the Near East in about 4000 BCE (McCarthy *et al*. 1995) and with time developed into the glazing being applied to clay and silica-based objects.

The Egyptians attached a special significance to the colour green (MacKenzie 1922). It is believed that the colour was most likely associated with life itself because of the association of green with the propagation of plants and crops. It was also seen as a sign of resurrection and early Egyptian texts refer to the afterlife as the "field of malachite". The colour is also closely associated with water (Wilkinson 1843). Consequently the colour green was highly prized in both natural and manufactured forms (Ragai 1986).

4.2 Egyptian blue

Egyptian blue pigment probably developed during the 4th Dynasty (2613-2494 BCE) (Riederer 2012), came into widespread use during the New Kingdom (18th Dynasty) and in subsequent periods for the decoration of a range of objects and walls. Hatton (2008: 146) however proposed that Egyptian blue was first synthesised in Egypt during First Dynasty (c. 3000-2890 BCE) as shown by its usage in Tomb 3121 at Saqqara which is dated to the reign of Qa'a ('Ka-sen'), the last king of the First Dynasty (c. 2900 BCE). And more recently, a small alabaster bowl in the Museum of Fine Arts, Boston, which is decorated with Egyptian blue has been dated to the formative years of Nagada III A-B (c. 3300-3200 BCE).   David *et al.* (2001) stated that Egyptian blue has been identified in early Pharaonic burial sites dating from the 4th Dynasty (2613-2494 BCE). Mirti *et al*. (1995), Lee and Quirke (2000: 109) and Pradell *et al*. (2006) all suggested that the usage of Egyptian blue commenced around 2300 BCE. Pigment cakes of both Egyptian blue and Egyptian green were found by Bruyère in 1927 and 1935 at Deir el Medineh dated to the New Kingdom (c. 1567 – 1085 BCE) and these pigments have been studied and reported on by Pagès-Camagna and Colinart (2003). Lucas and Harris (1989: 342) reported that the 5th Dynasty tomb of Perneb as the earliest certain occurrence and this chronology is supported by Baraldi *et al*. (2001). Lucas also reported that the green used in decorating the tomb of Perneb was malachite. El Goresy *et al*. 1986) suggested that the earliest use of Egyptian blue was during the 5th and 6th Dynasties in tomb paintings at Saqqara. Riederer (2012) in suggesting that the first usage was on tomb reliefs, sarcophagi, stone and wooden figures, cloth and papyrus and in particular the sculpture of Rahotep in the Egyptian Museum, Cairo, noted that by the beginning of the 5th Dynasty there are numerous objects painted with Egyptian blue and therefore this pigment was the blue paint used almost exclusively on both inorganic and organic materials. He also noted

Chapter 4
Copper-based pigments
Egyptian blue and Egyptian green

the deeply etched hieroglyphs on the reliefs in the pyramid of Unas at Saqqara, which are filled with solid masses of Egyptian blue. This indicates that by now, there must have developed a significant industry manufacturing the pigment.

Hatton (2008: 168) stated that the surface coverage of Egyptian blue when mixed in water is 17.5 cm²/g. Thus, the New Kingdom temple of Medinet Hebu at Thebes which had an area of 2500 m² required 1400 Kg of pigment. Assuming a cake diameter of 100 mm and a thickness of 20 mm, then this would be equivalent to the production of some 6300 primary cakes. The technology then rapidly spread to Mesopotamia and Greece and eventually throughout the Roman Empire.

Mirti *et al*. (1995) reported that development of a pigment similar to Egyptian blue, may have occurred at the same time, or even earlier in Mesopotamia. However, it is more generally accepted that its use spread from Egypt. Its usage continued in Turkey and almost exclusively in Italy and central Europe until the Middle Ages. In Egypt, azurite, lapis lazuli, ultramarine, indigo, glaucophane (found on the Greek islands) and cobalt blue were less frequently used as a blue pigment.

The carved and painted and limestone blocks from the 19th Dynasty tomb of *hwi nfr* at Saqqara contained Egyptian blue, Egyptian green (parawollastonite), together with red ochre and orpiment. Egyptian blue has also been found on the blue-coloured wall surfaces in the temple of Seti I at Abydos. Pavlidou *et al*. (2008) reported that an FTIR peak at 1319 cm⁻¹ was seen as a strong indication that calcium oxalate had formed from biodegradation processes within the Egyptian blue wall decoration in this temple. This is discussed in Section 4.6.3.

Riederer (2012), in a review article suggested that Egyptian blue was rarely used to decorate pottery; he cited the work of Arnold (1972) who had reported its use on pottery vases from the 11th Dynasty tomb of Saff el-Dawaba at el-Târif in western Thebes and the report of Miller (1986) for its use on a 12th Dynasty alabaster jar. These vases were painted using Egyptian blue on to a white ground (slip) after firing; a technique different from the vases of the 18th Dynasty blue painted pottery which according to Riederer (1974) were painted with a mixture of clay and a cobalt compound and then fired. An alternative application method for the cobalt blue pigment is reported in Chapter 5 of this thesis.

Uda *et al*. (2000) conducted a study of seven fragments of the blue from painting on the walls of the Malkata palace of Amenhotep III using PIXE analysis. He showed that the composition of the pigments was in all cases consistent with cuprorivaite, cuprowollastonite and a copper-rich glass. Egyptian blue from the tomb of Mereruka in Saqqara (6th Dynasty) contained only minor concentrations of wollastonite, glass and cristobalite indicating that the workers were preparing the pigment according to a well-established recipe (Jaksch *et al*. 1983).

During the Ptolemaic and the Roman periods the extensive production of Egyptian blue decreased, but it remained the pigment of choice for blue decoration particularly in Italy as shown by the extensive recovery of sherds dated to 90-60 BCE (Grifa *et al*. 2016). After the

Roman period, Egyptian blue was rarely used (Riederer 2012). Other changes, particularly the source of the copper raw material occurred over this long production period. The presence of traces of arsenic in Egyptian blue was suggested to have come from the copper ore used to produce the pigment (Mahmoud *et al*. 2011; Schiegl *et al*. 1990). These changes will be discussed within this chapter.

4.3 Egyptian green

Different methods for obtaining a green decoration were adopted throughout Egypt; a synthetic green produced from copper in a manner similar to that used for Egyptian blue production; the application of a green mineral such as malachite or the Green earths, which are naturally occurring clay minerals. Green earths are discussed in Chapter 3. Egyptian green (mainly parawollastonite), has received significantly less reporting in the published literature. The term Egyptian green will be used throughout this thesis rather than "Green frit".

Malachite can be found in a number of places in Egypt; it was important to the Egyptians because of its use in copper production (Barrois 1932; Lucas 1927: 199). The word *w3D* meaning "green stones" has been found in reference to a number of sites within Egypt, such as the Gebel Zebara on the Red Sea (Iversen 1955) and, it is believed to be a reference to the green kohls and to the mineral malachite as eye pigments (Harris 1961; Iversen 1955). It is to be found within a number of different literary contexts, such as lists of precious stones, and as reference to a pigment within the Book of the Dead (Iversen 1955).

Lucas and Harris (1989: 345) observed that the green in paintings from the 4th Dynasty to the New Kingdom were malachite or chrysocolla, the former dominating. According to Lucas (1989: 345), F.C.J. Spurrell recorded the use of malachite, or malachite and gypsum and/or malachite over yellow in 4th Dynasty tomb paintings. In paintings from the Middle and New Kingdoms; both malachite and chrysocolla were employed.

Pagès-Camagna *et al*. (1999) stated that there are no ancient texts which discuss the preparation of Egyptian green pigment, whereas Egyptian blue has recipes written in Latin by Vitruvius and Pliny and in Greek by Theophrastus as provided in Appendix A4. Early studies suggested that it was an alteration product induced by the presence of iron. In the case of Egyptian green, the historical usage of this pigment is disputed by several writers. Noll and Hangst (1975) and Noll (1981) suggest that a green pigment containing wollastonite (Egyptian green) was possibly an accidental by-product from the synthesis of Egyptian blue. However, a similar wollastonite-containing pigment, called "Green frit" was intentionally produced according to Jaksch *et al*. (1983). Wollastonite, together with glass, are major phases in numerous Egyptian green pigments (Jaksch *et al*. 1983). These researchers also stated that the manufacture of Egyptian blue under reducing conditions will lead to the formation of Egyptian green, the major phase consisting of copper wollastonite.

As discussed by Noll and Hangst (1975), Egyptian green production was achieved by the Egyptians prior to, or during the 5th Dynasty. Without providing supporting analytical data, Pagès-Camagna and Colinart (2003) proposed that tomb paintings and on stone statues

occurred during the First Intermediate Period (c 2200 BCE).   According to Ullrich (1987) Egyptian green was developed during the 6th Dynasty and Jaksch *et al.* (1983) claim that it has been found in many 5th and 6th Dynasty sites. The use of green frit or Egyptian green was recorded by Lucas (1989: 345) in an unnamed 6th Dynasty tomb together with six specimens from the 18th Dynasty and one from a 26th Dynasty tomb. According to Lucas (1989: 345), Layard stated that the Egyptian green was 'a mixture of yellow ochre with vitreous blue' and that a green examined by John (an analyst) was reputed to be 'blue frit mixed with a vegetable yellow'.   A green tone in Egyptian blue was alternatively said to be introduced by the presence of iron in the raw materials (Ullrich 1987; Le Fur 1994; Weatherhead and Buckley 2008: 208).

Archaeological evidence has suggested that malachite was also mined in the Timna valley and in the Eastern Desert and the Sinai Peninsula at Wadi Maghara, Serabit el-Khadim and Bir Nasib (Aston *et al*. 2000: 43).   Harris (1961) believed that during the Old Kingdom the Eastern Desert rather than the Sinai Peninsula was the main source of malachite. The earliest known record of a mining expedition for malachite is from the First Dynasty (Lucas and Harris 1989: 202) although malachite has been found in graves dating from the Predynastic period suggesting a much earlier usage (Debb *et al*. 2004; Diamandopoulos 1996; Ead 2006; Lucas and Harris 1989: 210).

Pagès-Camagna (2003), Pagès-Camagna *et al* (2006) and El Goresy (2000) suggest that this pigment was only used during the Middle and New Kingdoms (2100-1069 BCE) and was confined to Egyptian territory (Nubia, Sinai, Egypt). Hatton (2008: 147) agreed with these workers and stated that the use of Egyptian green commenced sometime between the second half of the 3rd and the mid-2nd millennium BCE. However, the excavations conducted at Cuma, Italy by Grifa *et al*. (2016), indicate an extensive use of Egyptian green during the period 90-60 BCE and as such, refutes this geographical limitation.

El Goresy (2000) stated that these early green pigments consisted of a copper-blue glass with a low calcium concentration which has weathered to form atacamite. He then proposed that the copper-bearing wollastonite, which he termed "green frit" was used at the beginning of the 18th Dynasty on tomb paintings at Edfu and El Kab.

4.2 Historical textural background
Refer Appendix A4 in link:
https://drive.google.com/drive/folders/0B1MXnIeNTO4icGV6dTFSaXhOQU0?usp=sharing

4.3 Historical overview
Refer Appendix A4 in link:
https://drive.google.com/drive/folders/0B1MXnIeNTO4icGV6dTFSaXhOQU0?usp=sharing

4.4   Egyptian blue samples examined

The samples provided were ready-for-use pigments held in museums as indicated in Tables 4.1 and 4.2 or from vessel sherds, or samples which have become detached from wall murals or cartonnage.

A list of the samples of Egyptian blue pigment and their holding is provided in Table 4.1 below. A number of these samples were recovered during the course of Petrie's excavations at Amarna in 1891-2 (Petrie 1894) and are now held either in the Petrie Museum, University College, London or the Bolton Museum. Additional samples were also obtained from other sources which are also listed in Table 4.1. The contexts in which some of the samples were obtained are provided by Weatherhead and Buckley (1989 Tables 10.1-10.6, 223-240), French (2013: 1.4) or A/Prof. Hope as provided in Table 4.2.

All samples have been non-destructively examined using Raman spectroscopy, electron microscopy and one by the XFM beamline at the Australian Synchrotron.   The detailed analyses for each sample are provided in totality in Appendix A4. Refer link:

https://drive.google.com/drive/folders/0B1MXnIeNTO4icGV6dTFSaXhOQU0?usp=sharing

Table 4.1.   Samples of Egyptian blue provided by A/Prof. C. Hope.

	Sample No.	Place of excavation	Museum holding
E1	A22/1/1966(4)	Amarna	Bolton Museum
E2	A22/6/1966(2)	Amarna	Bolton Museum
E3	A22/12/1966(1)	Amarna	Bolton Museum
E4	UC24684	Amarna	Petrie Museum, University College London
E5	UC24685	Amarna	Petrie Museum, University College London
E6	UC24686a	Amarna	Petrie Museum, University College London
E7	8979b	Amarna	Petrie Museum, University College London
E8	8979c	Amarna	Petrie Museum, University College London
E9	A4901 KN	Karnak North, Luxor	
E10	EB1#3463	Tell esh-Shariya, Gaza Strip	Sample provided by Prof. Eliezer Oren who excavated the site.

Table 4.2. Samples of pottery, cartonnage or wall decoration on which Egyptian blue has been located and analysed and provided by A/Prof. C. Hope.

	Sample No.	Place of excavation	Museum holding
M 7	M73/K/5	Malkata	Monash University
M8	M73/K/1406	Malkata	Monash University
D8	D8, Mut	Mut al-Kharab	Monash University
E11	DAF 124	Anubieion, Saqqara	Monash University
C2	Cartonnage C2	Kellis 1 Tomb cemetery	Monash University
C10	Cartonnage C10	Kellis 1 Tomb cemetery	Monash University
C17	Cartonnage C17	Kellis North Tomb 2	Monash University
W16	Wall, W16	Main Temple, Area D, D/5, Kellis	Monash University
MUT25	Pigment, MUT25	Mut al-Kharab, Trench 38	Monash University
MUT26	Pigment, MUT26	Mut al-kharab, Trench 18.	Monash University

4.5   Egyptian blue, Results and Discussion

All of the original research data applicable to this chapter is provided in Appendix A4. Each sample analysed is individually reported and commented upon as necessary. Only specific data in respect of the relevant research results are provided or alternatively are summarised and provided within the body of this thesis.

In reviewing the work conducted by the Hatton *et al*. (2008) and in the present thesis, it should be noted that in SEM analyses, the sulphur line and the lead lines overlap. Similarly, the arsenic and the lead lines overlap making the analysis reliant on the software package and the skill and understanding of the analyst or researcher for final determination. The Pb Mα = 2.5010 kV, Pb Mβ = 2.4420 kV and Pb Lα = 10.551 kV, the As Kα = 10.532 kV and the S Kα = 2.3070 kV, S Kβ = 2.4640 kV line overlaps are clearly evident. Furthermore, the As Lα line (1.2820 kV) overlaps the Mg Kα line (1.2540 kV). The comments in respect of the limitations of EDS analyses contained in Chapter 2 are pertinent.

SO$_x$ was observed by the present researcher but not by Hatton *et al*. (2008). Therefore, it is feasible that the sulphur analysis reported in this thesis could account for the lead concentration observed by Hatton *et al*. (2008). The 20 kV accelerating voltage used in the present research, would activate the Pb Lα line, but the 15 kV accelerating voltage used by Hatton would not activate this line. No Pb Lα peak was observed in the present study, thus casting doubt upon the Hatton lead analyses.

Limitations created by the lack of availability of any actual vessels in which the Egyptian blue was manufactured necessitated that this research rely upon identifiable diagnostic traces present within specific pigment samples. The forthcoming publication alluded to by Pusch and Rehren (2007: 129) for the production of Egyptian blue at Qantir-Piramesse may further elucidate the manufacturing process and particularly the vessels in which the pigment was produced at this specific site. This could provide additional information to support one or more of the hypotheses advanced within this chapter.

Comparative Raman spectra for the Egyptian blue raw material samples listed in Table 4.1 are provided in Figures 4.1 – 4.3 and Table 4.3. The Egyptian blue and Egyptian green pigments applied to pottery and other surfaces listed in Table 4.2 are discussed in Section 4.8. Table 2.20, Appendix A2 provides the RRUFF Raman spectral data for various minerals which may be encountered in the various samples of Egyptian blue. Tables 4.3 and 4.4 summarises the mineralogy as provided by Raman spectroscopy. More detailed Raman spectra which form the basis for these tables are located in Appendix A4. These spectra indicate the individual minerals present in each sample listed in Table 4.4. Section 4.6 describes the Egyptian green pigment. Tables 4.6 to 4.8 provide the SEM-EDS analyses for the Egyptian blue samples.

4.5.1 Egyptian blue (cuprorivaite) mineralogy and formation

Egyptian blue is very closely related to the naturally occurring mineral cuprorivaite (calcium copper tetrasilicate) having the formula $CaCuSi_4O_{10}$ (or $CaO.CuO.4SiO_2$) with variable

amounts of wollastonite, silica phases (quartz, tridymite, and cristobalite), a copper-rich glass, ionic copper, alkali and chlorine-bearing silicate glass, a copper oxide phase and often containing either cuprite or tenorite, and generally bronze residues which had not reacted with the surrounding phases (Minguzzi 1938; Bianchetti *et al* 2000). Von Strunz (1957) stated that they considered cuprorivaite to be a mixture of wollastonite and glass. However, Mazzi and Pabst (1962) then re-examined the remainder of the sample analysed by Minguzzi and after using heavy liquids to fractionate the sample, employed XRD to determine its mineralogy. They confirmed that the material is cuprorivaite with a formula of $CaCuSi_4O_{10}$.

According to Jaksch *et al.* (1990) in studying monuments from the Old Kingdom until the commencement of the New Kingdom, Egyptian blue was originally prepared by reacting ("fritting") a rich copper-containing mineral and a calcium-phosphate-arsenate phase. Later, during the 18th Dynasty, scrap metal from copper and bronze (copper-tin alloy) production, together with desert sand, lime and an alkali flux (as discussed in Section 4.5.2.5) at a temperature below 742°C (Jaksch *et al*. 1983; Lee and Quirke 2000: 109), at 750°C (Turner 1956), at 850°C (Lucas 1989: 342; Laurie 1914) or 850-1000°C (Hatton 2008: 155; Pagès-Camagna and Colinart 2003; Ullrich 1979) and below 1050°C (Hatton *et al*. 2008), then cooling, pulverising and probably reheating and subsequently additional grinding to produce the final pigment. As will be reported below, various researchers claim the need for either oxidising or reducing conditions in the heating process. The cuprorivaite is then ground to a variable particle size, this size reduction influencing the final visual colour. A 4th century Roman period Egyptian green (now grey-green) wall sample (Sample 2) from Kellis was found to contain brass (copper-zinc alloy) is discussed in Appendix A3 and is suggestive of a further and thus later change in the reaction chemistry.

Whilst Egyptian blue has been studied (Hatton 2008); Bianchetti *et al*. 2000); Ambers 2004); David *et al*. 2001); Jaksch *et al*. 1983); Pagès-Camagna and Colinart 2003); Tite 1987), there is still some disagreement amongst several authors in respect of the raw materials employed and the reaction conditions adopted. The copper minerals malachite and/or chrysocolla were probably an essential ingredient in the early manufacture of both the blue and the green versions of this pigment from at least the 4th Dynasty onwards (Lee and Quirke 2000: 109). During the reign of Thutmose III (c. 1479-1425 BCE), copper and bronze filings or bronze scrap as evidenced by the presence of tin, replaced the copper minerals in the manufacture (Jaksch *et al*. 1983). Tin continued to be found in Egyptian blue pigment throughout the New Kingdom and to Ptolemaic and Roman times (Hatton 2008: 161). Interestingly, tin was not present in the pigment samples analysed from constructions in Karnak temple and at the temple of Hatshepsut in Deir el Bahari (Jaksch *et al*. 1983). As stated by Hatton (2008: 161) and by Schiegl *et al*. (1990), leaded bronze was introduced during the 19th Dynasty, although as stated above, tin, indicative of bronze, was in use through to the Ptolemaic and Roman periods (Jaksch e*t al*. 1983). This does indicate a degree of uncertainty into dating objects based solely upon the bronze composition present in Egyptian blue.

Jaksch *et al*. (1983) stated that the presence of pyrite crystals found in an Egyptian blue sample from the tomb of Akhethotep (c. 2400 BCE) and also in an Egyptian green pigment from the tomb of Neferronpet (reign of Rameses II) can be seen as no more than a possible

use of a copper sulphide mineral. An analysis by Saleh *et al.* (1974) of a sample taken from a pigment cake found in the tomb of Kheruef (reign of Amenhotep III) showed the presence of 1.7% of tin oxide. They dismissed the result suggesting that the copper used to make the Egyptian blue had been contaminated. Jaksch *et al.* (1983) found tin present in numerous samples from a range of temple and tomb sites but did not specifically nominate the sites at which tin was found in the pigments. They also proposed that the mode of occurrence within the glass is indicative of crystallisation from a melt since both cuprorivaite and the tin appear as clusters of idiomorphic crystals.

According to Pagès-Camagna and Colinart (2003) and Riederer (2012), cuprorivaite exists between 870 – 1080°C. Quartz disappears above 950°C and is slowly replaced by cristobalite or tridymite, the tridymite only existing up to 1100°C. Riederer (2012) stated that Egyptian blue decomposes at 1080°C to form glass, high temperature silica polymorphs and either Cu^{2+} oxide in an oxidising atmosphere or Cu^{+} oxide in a reducing atmosphere. In the phase diagrams provided by Morey (1930) and by Phillips and Muan (1959), they indicate that tridymite can exist to a temperature of 1475°C and therefore, cristobalite would not be expected to be found in Egyptian blue. Therefore, if tridymite is present then the temperature reached would be in the order of 1000°C. Note that the pottery reaction vessels in which the Egyptian blue and green reactions were conducted will collapse at <1100°C. Parawollastonite would only form if the mixture was not well mixed, leading to an excess of calcium in regions within the melt, and if the firing temperature was above 950°C. They reported that very few samples examined showed the presence of cristobalite. Furthermore, their research suggested that the total flux ($Na_2O + K_2O$) in Egyptian blue frit is never more than 5%, and at higher flux content of between 5.7% and 10% a turquoise colour results. And, tridymite is only formed at flux concentrations of <7%, and that >8% flux is required for cristobalite crystallisation. The present results support this proposal as (other than sample DAF 124) the total flux as provided in Table 4.11 indicates a concentration of <7% and as given by Raman in Table 4.4, tridymite was present, not cristobalite. The polymorphs quartz, tridymite and cristobalite all give excellent Raman signatures. Pagès-Camagna and Colinart (2003), stated that the bulk CaO/CuO ratio is about 0.7 and the SiO_2/CuO is approximately 3. These results are confirmed in Table 4.11 for the samples examined.

Baraldi *et al*. (2001) reported that the reaction(s) should be conducted under an oxidising atmosphere. These workers proposed the following reaction steps:

    250-350°C:
$$Cu_2(OH)_2CO_3 \rightarrow 2CuO + H_2O + CO_2\uparrow$$
malachite decomposition is evidenced by a sharp endothermic peak in the DTA curve;

    600-700°C:
$$CaCO_3 \rightarrow CaO + CO_2\uparrow$$
calcite decomposition is evidenced by a sharp endothermic peak in the DTA curve;

    750-900°C:
pigment formation, ($CaCuSi_4O_{10}$) $\rightarrow$ exothermic peak in DTA curve;

>1040°C:
$$2CaCuSi_4O_{10} \rightarrow 2CaO + Cu_2O + 8\ SiO_2 + \tfrac{1}{2}O_2$$
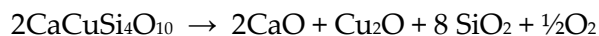
Ingo *et al*. (2013) claim that the raw materials must have been heated to a molten state because the observed microstructure cannot be produced by solid-state reactions either during sintering, or from simple heating of the pigment below its melting temperature. They also favoured natron as the flux because of the absence of phosphorus, which they considered to be diagnostic for plant ash. This is discussed in more detail in Section 4.5.2.5.3.

The mineralising effect reported by Deer *et al.* (1992: 561) with respect to spinel formation equally applies to the synthesis of ceramic minerals with the diopside and anorthite structure based on wollastonite, proceeds according to the following reactions:

$$CaSiO_3 + MgO + SiO_2 \rightarrow CaMgSi_2O_6$$
$$CaSiO_3 + Al_2O_3 + SiO_2 \rightarrow CaAl_2Si_2O_8$$

This discussion is amplified within Appendix A4 under the heading Mineralogy Overview.

Table 4.3. Raman spectral comparison, major Egyptian blue bands for the samples in Table 4.1 and provided in Appendix A4, together with other published Raman spectral results.

Reference	Laser, nm	Wavenumber assignment cm^{-1}
Egyptian blue sample:	514.5	
A22/1/1966 (4)		**1086**, 1015, 991, 970, 790, 763, 573, 475, 466, **431,** 379, 360, 232, 196, 165, 138, 114
A22/12/1966 (1)		**1083,** 1010, 972, 788, 755, 641, 570, 472,**430,** 376, 360, 229 , 197, 136, 111
8979b		**1082**, 1010, 983, 787, 567, 474, **430,** 377, 192, 135
8979c		**1083,** 1009, 744, 570, 474, **429,** 376, 360, 196, 136
UC24684		**1085**, 1042, 1009, 969, 735, 637, 569, 476, **432**, 378, 324, 231, 197, 137
UC24685		**1082**, 1009, 984, 789, 569, 472, **430**, 376, 197, 162, 135
UC24686a		**1084**, 1005, 647, 631, 622, 453
DAF 124		**1085**, 1012, 991, 788, 763, 570, 475 **430,** 377, 360, 231, 197, 137, 112
EB1#3463		**1084**, 1011, 984, 965, 789, 762, 570, 474, **430,** 378, 359, 229, 163, 136
A4901KN		**1082**, 1009, 967, 931, 739, 633, 569, 511, **431,** 377, 360, 321, 227, 193, 135, 110
Bell *et al*. (1997)	514.5	**1086**, 1012, 992, 789, 762 571, 475, **430,** 377, 358, 230, 200, 137, 114
Bordignon *et al*. (1997)	632.8	**1085**, **430**, 376, 358, 137
Bruni *et al*. (1999)	488	**1085** 793 572, 478, **432**
Burgio and Clark (2001)	1064	**1086,** 465, **431**
David *et al*. (2001)	514.5	**1086**, 1012, 992, 789 572, 470 **430**
Edwards *et al*. (2004)	unstated	**1086**, 571 **430** 360 162, 139
Mahmoud (2011)	632.8	1086, 985, 574, 470, **432**, 382, 229

Table 4.4. Minerals detected in the Egyptian blue samples listed in Table 4.1

Mineral	Formula	Wavenumber (cm^{-1})	1	2	3	4	5	6	7	8	9	10	11
α-quartz	SiO_2	357, **464**, 1084, 1160	●	●	●		●		●	●	●	●	●
tridymite	**SiO_2**	**209, 301, 355, 433, 1071**	●	●				●	●	●	●	●	●
cristobalite	SiO_2	**229, 471**											
magnesite	$MgCO_3$	330, **1095**									●		
enstatite	$MgSiO_3$	**660, 682, 1010**						●					
wollastonite	$CaSiO_3$	**635, 970**	●	●	●	●	●	●		●	●	●	·
pseudowollastonite	$CaSiO_3$	**372, 580, 982**		●		●	●						
anhydrite	$CaSO_4$	**1018,** 1163			●								
gypsum	$CaSO_4.2H_2O$	**1007**						●	●	●	●		
aragonite	$CaCO_3$	**1084**	●	●	●	●	●	●	●	●	●	●	●
apatite	$Ca_5(PO_4)_3(OH)$	430, **960**	●										
clinozoisite	$Ca_2Al_3(Si_2O_7)(SiO_4)O(OH)$	351, **570**, 603, **912**, 985, 1093											●
gehlenite	$CaFeSi_2O_6$	**661, 1013**			●							●	
ankerite	$CaFe^{3+}(CO_3)_2$	**1102**									●		
marialite	$(Na,Ca)_4(Si,Al)_2O_{24}.Cl,CO_3,SO_4$	164, 263, **459, 537, 773,** 1099	●	●									
albite	$NaAlSi_3O_8$	172, **290, 480, 508,** 788, 814, 1110						●		●	●		●
labradorite	$Na_{0.5-0.3}Ca_{0.5-0.7}Al_{1.5-1.7}Si_{2.5-2.3}O_8$	480, **507**, 563, 1112											●
microcline	$KAlSi_3O_8$	283, 453, 476, **514**, 1102					●						●
oligoclase	$Na_{0.9-0.7}Ca_{0.1-0.3}Al_{1.1-1.3}Si_{2.9-2.7}O_8$	**291**, 417, 456, **480, 507**, 763, 807						●					
orthoclase	$KAlSi_3O_8$	154, 278, 474, **511,** 1124		●	●		●						
riebeckite	$□Na_2(Fe^{2+}_3Fe^{3+}_2)(Si_8O_{22})(OH)_2$	**143, 160, 195, 577, 666, 967**	●										
hastingsite	$NaCa_2(Fe^{2+}_4Fe^{3+}_2)(Si_6Al_2)O_{22}(OH)_2$	430, **526, 695**	●										
antlerite	$Cu^{2+}_3SO_4(OH)_4$	**416, 989**						●		●			
brochantite	$Cu_4SO_4(OH)_6$	384, 481, 609, **971**						●	●				
chalcanthite	$CuSO_4.5H_2O$	**984**		●									
dioptase	$CuSiO_3.H_2O$	**223**, 266, **356, 395, 659**		●						●	●		
langite	$Cu_4SO_4(OH)_6.2H_2O$	235, **431, 971**		●	●	●	●	●		●	●		
pseudomalachite	$Cu_5(PO_4)_2(OH)_4$	**368, 447, 480, 609, 972**	●				●						
malachite	$Cu_2CO_3(OH)_2$	**179**, 218, **263, 430, 534**	●								●		
connellite	$Cu_{36}(SO_4)(OH)_{62}Cl_8.6H_2O$	194, 263, **401**, 872, **981**	●										●
chalconatronite	$NaCu(CO_3)_2.3H_2O$	**317**, 763, **866**, 1071	●										

mineral	formula	Raman shifts	1	2	3	4	5	6	7	8	9	10	11
natrochalcite	$NaCu_2(SO_4)_2(OH).H_2O$	212, 637, **999**, **1048,** 1209										●	●
sampleite	$NaCaCu_5(PO_4)_4Cl.5H_2O$	194, **452**, 553, **642**, 923, **995**, 1081		●									●
chalcocite	Cu_2S	**218, 281,** 393, 594, 1038						●					
cuprite	Cu_2O	110, 143, **216**, 406, 624											
tenorite	CuO	**105, 190, 212**, 336, 366, 640									●		
chalcopyrite, or	$CuFeS_2$	203, **290**, 470						●			●		●
isocubanite	$CuFe_2S_3$	287, 172									●		
pyrite	FeS_2	**355, 390**											
hematite	Fe_2O_3	225, **290, 410, 1320**	●								●		
pseudobrookite	$Fe^{3+}_2TiO_2$	**195, 218, 336, 654**								●			
brookite	TiO_2	**151**, 639 (Br)					●	●					
cassiterite	SnO_2	**634**, 776				●					●	●	
malayaite	$CaSnO(SiO_4)$	**323, 465, 573**	●			●					●		
thénardite	Na_2SO_4	453, 466, 624, 632, 650, **994,**1130									●	●	
hanksite	$KNa_{22}(SO_4)_9(CO_3)_2Cl$	467, 471, 623, 628, **990**, 1081	●										

1. DAF 124   Anubieion, Saqqara
2. EB1#3463   Tell esh-Shariya, Gaza Strip
3. A4901KN   Karnak North
4. 8979b   Amarna, Petrie Museum
5. 8979c   Amarna, Petrie Museum
6. UC24684   Amarna, Petrie Museum
7. UC24685   Amarna, Petrie Museum
8. UC24686a   Amarna, Petrie Museum
9. A22/1/1966(4)   Amarna, Bolton Museum
10. A22/6/1966(2)   Amarna, Bolton Museum
11. A22/12/1966(1)   Amarna, Bolton Museum

Table 4.5. Raman spectroscopy assignment for the slip coatings encountered on various samples.

Mineral	Formula	Laser, nm	Sample DAF 124	Egyptian blue A22/1/1966	Egyptian blue UC24686a
α-quartz	SiO_2	514.5	464	266, 128	
devitrite	$Na_2Ca_3Si_6O_{16}$		991, 671, 608, 408, 291		
sodalite	$Na_4Si_3Al_{12}Cl$		992, 464		
albite	$NaAlSi_3O_8$		506, 483, 291		
hematite	Fe_2O_3		608, 407, 291, 231	404, 290, 224	
aragonite	$CaCO_3$		1084		1087
huntite	$CaMg_3(CO_3)_4$				
burkeite	$Na_4(SO_4)CO_3$		995, 1063		995, 1063
pectolite	$NaCa_2Si_3O_8(OH)$			1172	
glauberite	$Na_2Ca(SO_4)_2$			1143	
muscovite	$KAl_2(Si_3Al)O_{10}(OH)_2$			699	

Table 4.6.   FIB, SEM- EDS average analytical data for Egyptian blue samples provided.

	Na2O	MgO	Al2O3	SiO2	P2O5	SO3	Cl	K2O	CaO	TiO2	MnO	FeO	CoO	NiO	CuO	ZnO	BaO	PbO	SnO2	As2O3	Cr2O3	F
A22/1/1966	2.2	0.9	2.2	64.4	0.1	0.8	0.2	0.5	10.4	0.0	0.0	1.4	0.0	0.0	17.1	0.0	0.0	0.0	0.0	0.0	0.0	0.0
A22/6/1966	2.9	0.1	1.1	63.5	0.2	0.6	0.5	0.4	18.3	0.0	0.0	0.7	0.0	0.0	11.3	0.0	0.0	0.0	0.0	0.0	0.0	0.0
A22/12/1966	1.6	9.8	1.8	55	0.0	1.5	1.1	0.7	11.4	0.0	0.0	1.2	0.0	0.0	14.8	0.0	0.0	0.0	1.4	0.0	0.0	0.0
8979b	0.8	1.1	4.1	53.9	0.5	1.7	0.2	0.4	17.0	0.5	0.0	2.0	0.0	0.0	16.6	0.0	0.0	0.0	1.6	0.0	0.0	0.0
8979c	2.7	1.1	2.6	57.1	0.9	1.0	0.4	0.5	12.4	0.2	0.0	1.5	0.0	0.0	18.5	0.0	0.0	0.0	1.6	0.0	0.0	0.0
UC24684	3.3	1.2	4.0	57.2	1.0	3.0	1.0	1.4	12.1	0.2	0.0	1.9	0.0	0.0	13.7	0.0	0.0	0.0	0.0	0.0	0.0	0.0
UC24685	1.0	1.1	1.8	56.6	tr	1.0	0.2	0.0	12.5	0.1	0.0	0.7	0.0	0.0	24.7	0.0	0.1	0.0	0.0	0.0	0.0	0.0
UC24686a	5.6	0.2	2.4	59.0	0.0	3.8	0.0	1.2	9.3	0.0	0.0	0.2	0.0	0.0	18.5	0.0	0.0	0.0	0.0.	0.0	0.0	0.0
DAF 124	8.1	1.4	3.5	53.9	0.3	1.1	0.5	0.5	12.3	0.3	0.0	1.2	0.0	0.0	16.1	0.0	0.0	0.0	1.3	0.0	0.0	0.0
#3463	1.3	2.5	1.8	58	0.0	0.5	0.5	0.8	12.5	0.0	0.0	0.9	0.0	0.0	20	0.0	0.0	0.0	1.2	0.0	0.0	0.0
A4901 KN	2.1	0.8	2.2	64.3	tr	0.6	0.6	0.5	10.3	0.0	0.0	1.1	0.0	0.0	16.2	0.0	0.0	0.0	1.5	0.0	0.0	0.0
Average	**2.9**	**1.0**	**2.5**	**58.4**	**0.3**	**1.4**	**0.5**	**0.6**	**12.6**	**0.1**	**0.0**	**1.2**	**0.0**	**0.0**	**17.0**	**0.0**	**0.0**	**0.0**	**0.8**	**0.0**	**0.0**	**0.0**

EDS analyses of various inclusions in Egyptian blue sample A22/1/1966 (4).

Table 4.7.   Analysis of various bone ash particles in sample A22/1/1966(4).

	Na2O	MgO	Al2O3	SiO2	P2O5	SO3	Cl	K2O	CaO	TiO2	MnO	FeO	CoO	NiO	CuO	ZnO	BaO	PbO	SnO2	As2O3	Cr2O3	F
Bone ash 1	0.0	0.0	0.0	6.7	5.7	0.0	0.0	0.0	0.0	0.0	0.0	83.5	0.0	0.0	4.2	0.0	0.0	0.0	0.0	0.0	0.0	0.0
Bone ash 2	0.7	0.0	2.4	24.4	24.5	0.2	1.3	0.0	33.6	0.0	0.0	0.9	0.0	0.0	8.3	0.0	0.0	0.0	0.0	3.8	0.0	0.0
Bone ash 3	0.6	0.0	2.9	25.6	17.0	0.0	1.2	0.5	34.6	0.0	0.0	1.3	0.0	0.0	11.1	0.0	0.0	0.0	0.0	4.9	0.0	0.4
Bone ash 4	0.6	0.0	2.9	24.2	22.9	0.0	1.0	0.3	32.5	0.0	0.0	0.9	0.0	0.0	10.2	0.0	0.0	0.0	0.0	3.8	0.0	0.9
Bone ash 5	0.0	0.0	1.1	17.0	27.5	0.0	1.7	0.4	41.8	0.0	0.0	0.0	0.0	0.0	6.2	0.0	0.0	0.0	0.0	4.5	0.0	0.0
Bone ash 6	4.0	0.0	2.4	29.5	20.9	0.1	1.4	0.6	27.8	0.0	0.0	1.3	0.0	0.0	6.9	0.0	0.0	0.0	0.0	3.9	0.0	1.3
Bone ash 7	0.0	0.0	1.4	19.3	26.8	0.3	1.1	0.0	37.2	0.0	0.0	0.9	0.0	0.0	7.4	0.0	0.0	0.0	0.0	4.4	0.0	1.2
Bone ash 8	0.0	0.0	2.5	23.2	24.1	0.6	1.1	0.0	33.5	0.0	0.0	0.8	0.0	0.0	8.4	0.0	0.0	0.0	0.0	4.9	0.0	1.5
Bone ash 9	0	0	1.5	15.8	28.3	1.1	1.5	0	41.5	0	0	0	0	0	4.5	0	0	0	0	4.4	0	0.9
Bone ash 10	0.0	0.0	0.8	32.0	17.1	0.4	1.1	0.0	32.9	0.0	0.0	0.0	0.0	0.0	11.2	0.0	0.0	0.0	0.0	4.4	0.0	0.0
Bone ash 11	0.0	0.0	1.4	15.8	28.5	1.1	2.1	0.0	41.4	0.0	0.0	0.0	0.0	0.0	5.3	0.0	0.0	0.0	0.0	4.4	0.0	0.0
Bone ash 12	0.0	0.0	1.9	34.2	14.1	0.2	0.9	0.0	30.8	0.0	0.0	1.3	0.0	0.0	12.5	0.0	0.0	0.0	0.0	4.1	0.0	0.0
Bone ash 13	0.0	0.0	2.7	38.6	13.6	0.2	1.1	0.0	26.4	0.0	0.0	1.8	0.0	0.0	12.9	0.0	0.0	0.0	0.0	2.8	0.0	0.0
Bone ash 14	0.0	0.0	1.8	27.3	20.1	0.2	1.2	0.0	34.6	0.0	0.0	0.9	0.0	0.0	9.5	0.0	0.0	0.0	0.0	4.4	0.0	0.0
Bone ash 15	0.0	0.0	1.5	28.7	18.3	0.4	1.0	0.0	34.3	0.0	0.0	0.9	0.0	0.0	10.7	0.0	0.0	0.0	0.0	4.2	0.0	0.0
Bone ash 16	0.0	0.0	1.9	41.6	10.3	0.1	0.6	0.0	26.4	0.0	0.0	1.0	0.0	0.0	15.4	0.0	0.0	0.0	0.0	2.7	0.0	0.0

Table 4.8. Analysis of various metal, oxide and sulphate inclusions in sample A22/1/1966(4).

Sample A22/1/1966 (4)

	Na2O	MgO	Al2O3	SiO2	P2O5	SO3	Cl	K2O	CaO	TiO2	MnO	FeO	CoO	NiO	CuO	ZnO	BaO	PbO	SnO2	As2O3	Cr2O3	F
Pb	0.0	1.2	3.1	30.6	27.4	0.0	1.5	0.5	17.7	0.0	0.0	0.0	0.0	0.0	12.3	0.0	0.0	5.7	0.0	0.0	0.0	0.0
Ti	0.0	0.6	1.1	12.9	0.0	0.0	0.0	0.0	2.1	79.0	0.0	0.5	0.0	0.0	3.9	0.0	0.0	0.0	0.0	0.0	0.0	0.0
Sulphate	0.0	0.5	3.4	45.5	0.0	12.5	0.0	0.0	6.9	0.0	0.0	0.6	0.0	0.0	10.8	0.0	20.0	0.0	0.0	0.0	0.0	0.0
Sn	0.0	0.7	1.9	56.1	0.6	0.0	0.2	0.0	10.5	0.0	0.0	1.1	0.0	0.0	10.7	0.0	0.0	0.0	18.1	0.0	0.0	0.0
Cu-Sn	0.0	0.4	1.3	11.6	0.0	0.0	0.0	0.2	1.6	0.0	0.0	0.7	0.0	1.2	82.4	0.0	0.0	0.0	0.6	0.0	0.0	0.0
Cu 1	0.4	0.4	1.3	12.9	0.0	0.2	0.0	0.1	1.8	0.0	0.0	0.0	0.0	0.0	82.9	0.0	0.0	0.0	0.0	0.0	0.0	0.0
Cu 2	0.0	0.0	1.6	17.2	0.0	0.0	0.0	0.0	2.0	0.0	0.0	0.0	0.0	0.0	79.2	0.0	0.0	0.0	0.0	0.0	0.0	0.0
Cu 3	0.0	0.5	1.7	15.7	0.0	0.0	0.2	0.0	3.5	0.0	0.0	0.5	0.0	0.0	77.9	0.0	0.0	0.0	0.0	0.0	0.0	0.0
Cu 4	0.0	0.7	3.4	19.0	0.4	0.5	0.0	0.0	2.8	0.0	0.0	1.0	0.0	0.0	72.2	0.0	0.0	0.0	0.0	0.0	0.0	0.0
Cu 5	0	0	0.8	55.4	0	0	0	0	16.9	0	0	0	0	0	27	0	0	0	0	0	0	0
Cu 6	0.0	0.0	3.8	49.5	1.0	1.2	0.0	0.0	7.8	0.0	0.0	1.9	0.0	0.7	33.6	0.0	0.0	0.2	0.0	0.0	0.4	0.0
Cu 7	0	0	2.3	47.4	1.9	0	0.1	0	18.4	0	0	1.1`	0	0	27.3	0	0	0	0	1.4	0	0
Cu-As$_2$O$_3$	0.0	0.0	12.7	33.3	0.0	0.0	0.0	0.3	11.3	0.0	0.0	2.3	0.0	0.0	26.2	0.0	0.0	0.0	0.0	13.9	0.0	0.0
Ag 1	0.7	0.4	0.4	12.6	0.0	0.4	10.5	0.3	3.6	1.6	0.0	42.0	0.0	0.0	9.1	0.0	0.0	0.0	0.0	0.0	5.8	0.0
Ag 2	0.9	0.6	1.4	27.1	0.0	0.9	17.3	0.4	3.7	0.3	0.0	33.6	0.0	0.0	8.6	0.0	0.0	0.0	0.0	0.0	5.2	0.0

SAMPLES FROM BOLTON MUSEUM, – RAMAN SPECTRA
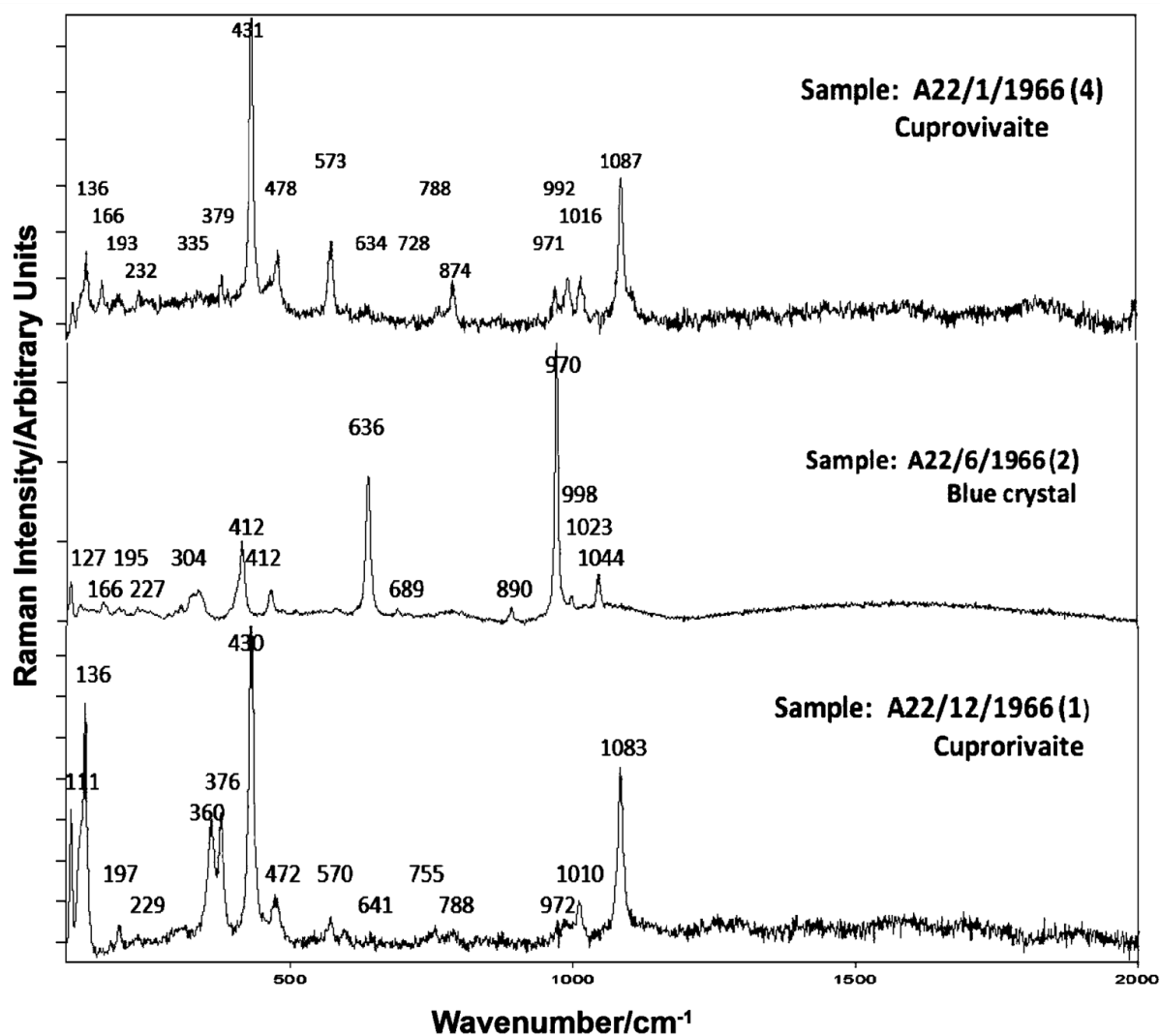
Figure 4.1. Composite Raman spectra of the Egyptian blue samples held by the Bolton Museum, Manchester. Sample obtained from Amarna (λ = 514.5 nm).

COMPOSITE OF SAMPLES, PETRIE MUSEUM, UNIVERSITY COLLEGE, LONDON – RAMAN SPECTRA
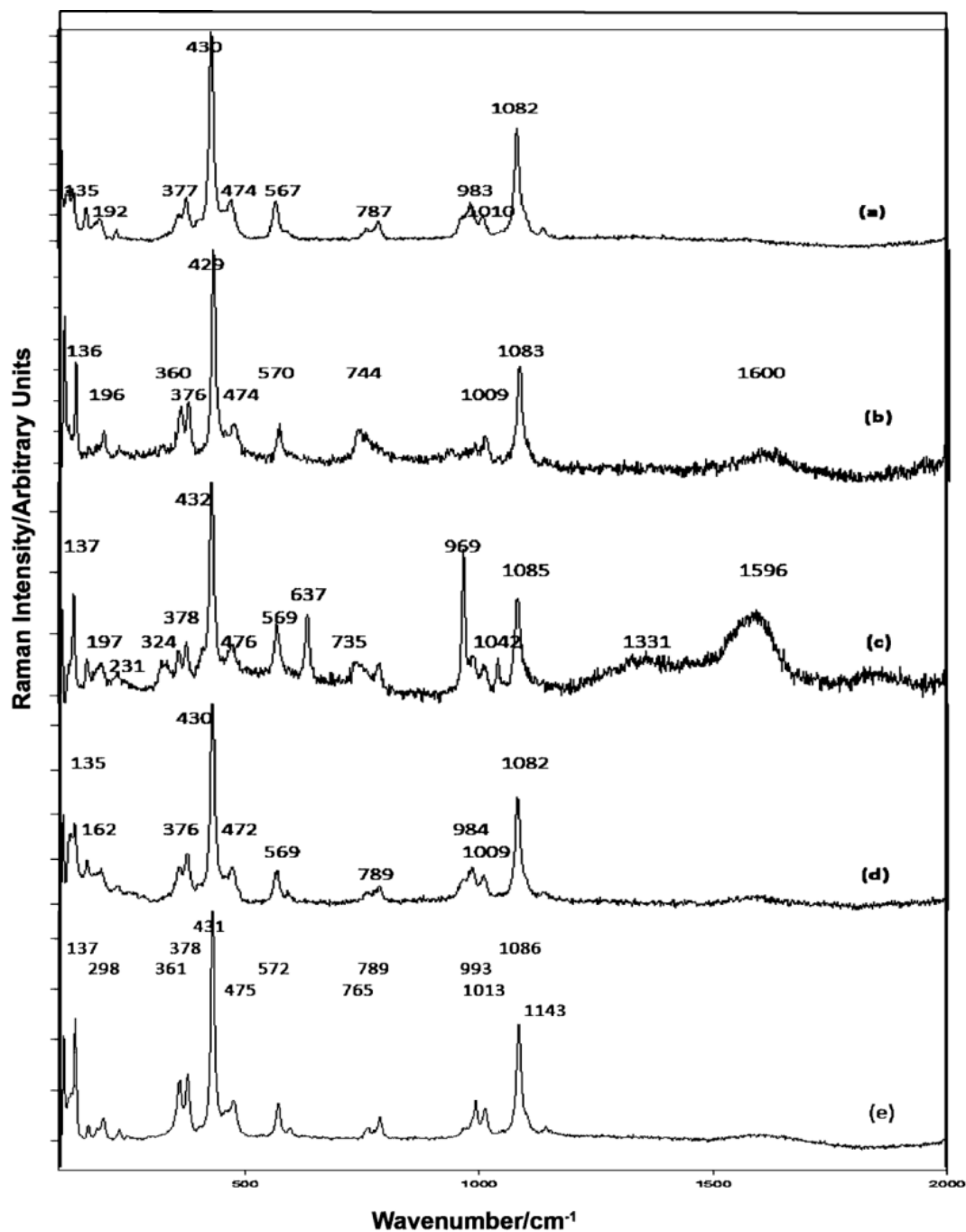
Figure 4.2. Composite Raman spectra of the Egyptian blue samples held by the Petrie Museum, University College London. Samples obtained from Amarna. Sample (a) is 8979b; (b) is 8979c; (c) is UC24684; (d) is UC24685; (e) is UC24686a (λ = 514.5 nm).

COMPOSITE OF OTHER EGYPTIAN BLUE SAMPLES –RAMAN SPECTRA
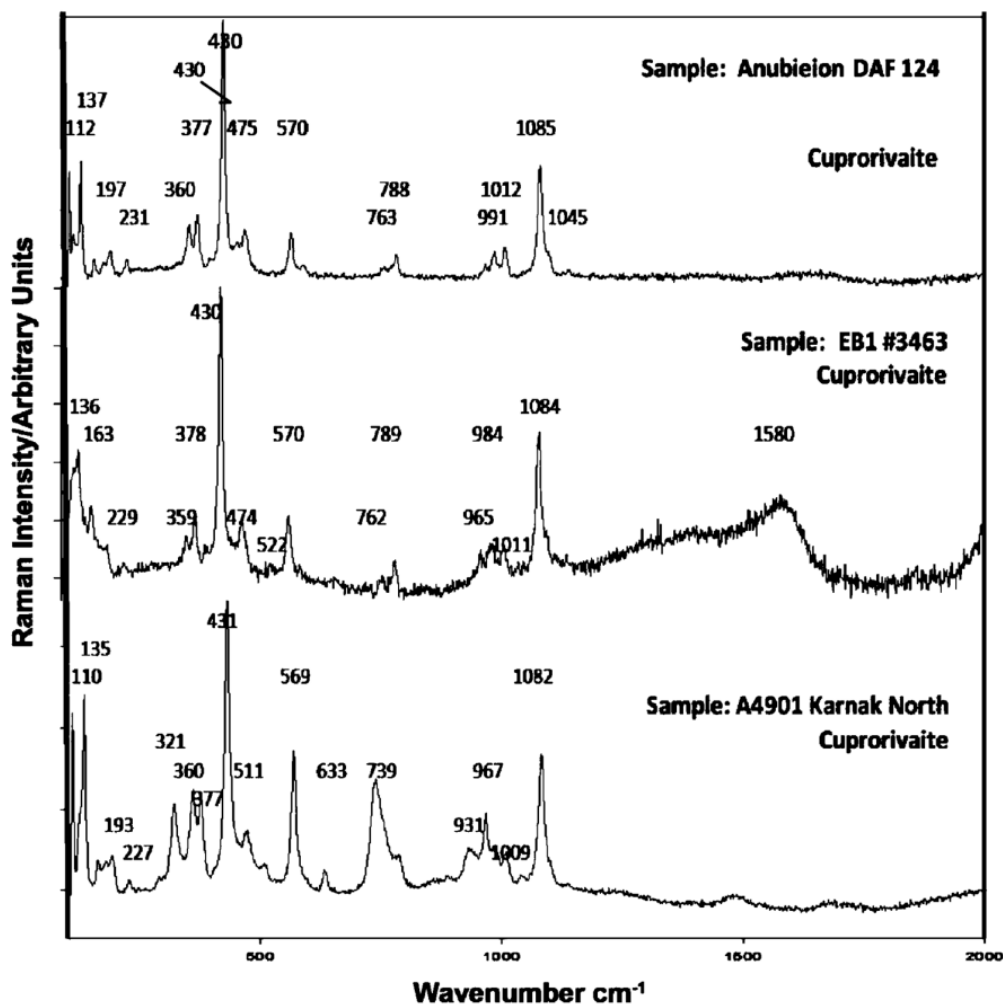
Figure 4.3. Composite Raman spectra of the Egyptian blue samples. Samples analysed as marked ($\lambda = 514.5$ nm).
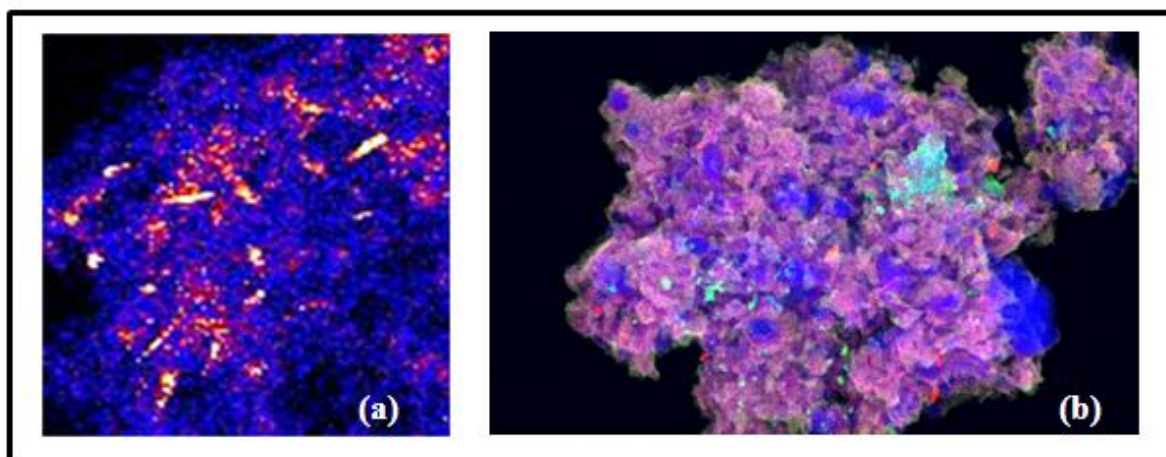
Figure 4.4. Synchrotron high energy XFM-generated beamline images. (a) shows the presence of bright (white) rod-shaped, arsenic-containing particles. (b) is a CuCaCompton composite image of the relevant elemental maps.
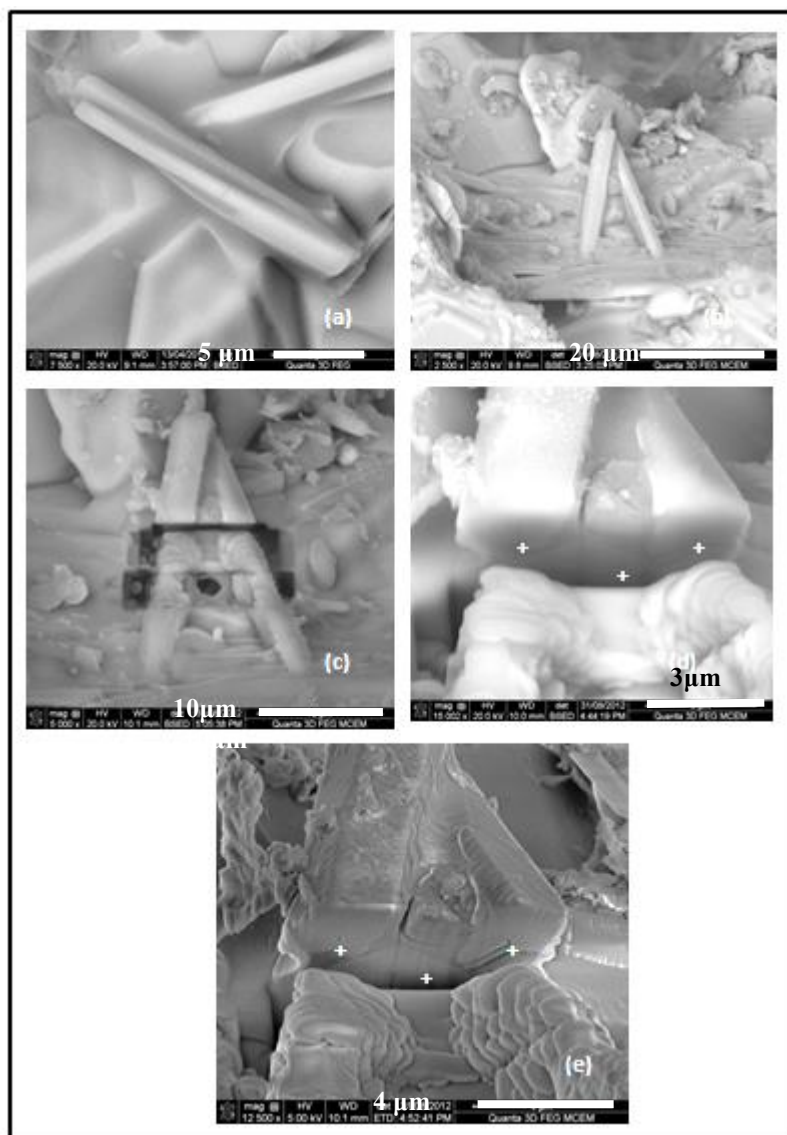
Figure 4.5.   (a) and (b) are FIB BSE images of two of the calcium-phosphorus (bone ash) particles analysed, (a) being in the white surface coating to sample 24685; (c), (d) and (e) show the Ga^+ ion milling of two of the bone ash particles. The + marks indicate analysis spots following rotation of the sample.
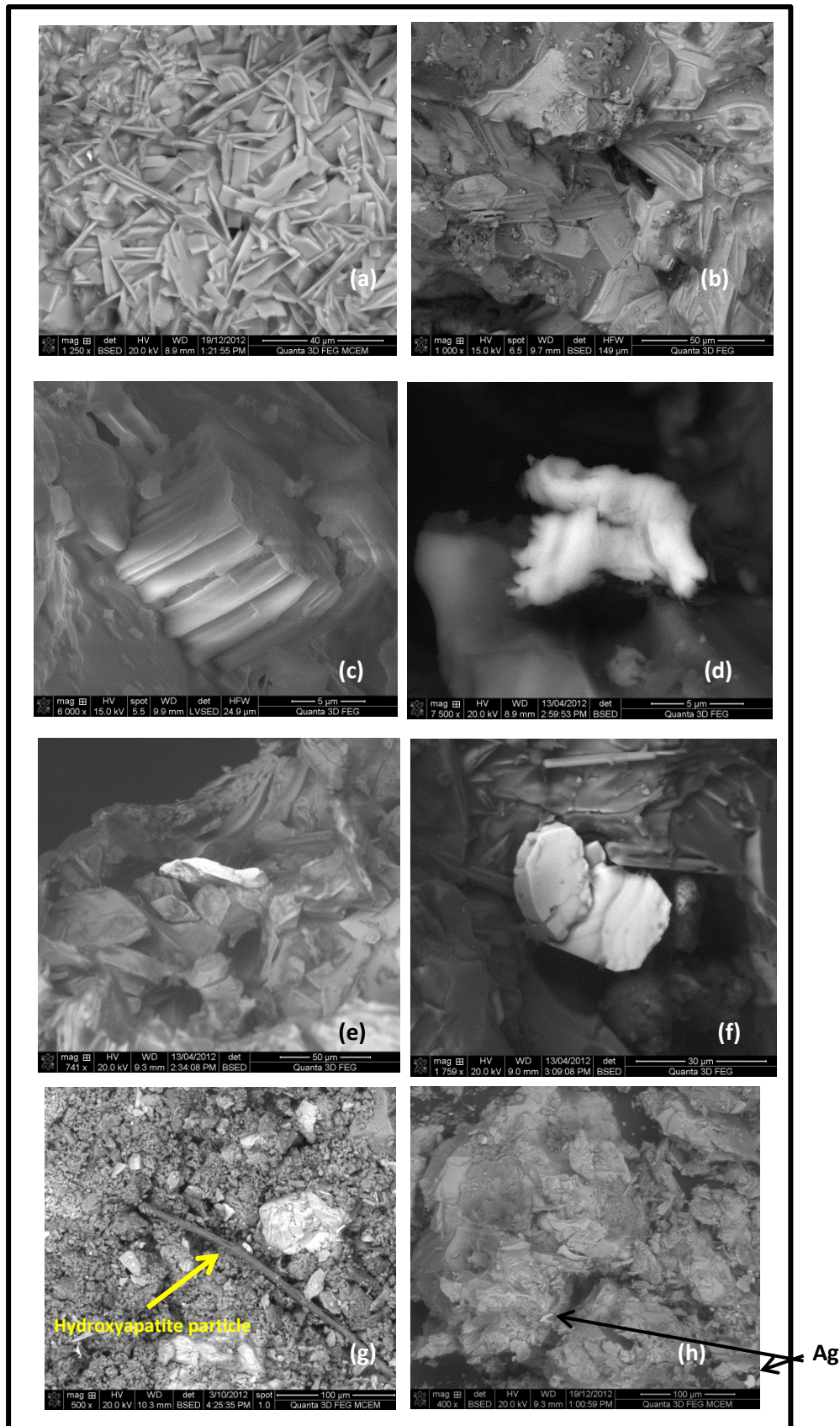
Figure 4.6. (a) is FIB SE image of sample A22/6/1966 (b) and (c) are SE images of A22/1/1966 analysed. (d) is a titanium-based particle; (e) and (f) are of a copper particle;(g) is Amarna sample UC24684 showing the presence of hydroxyapatite (bone ash); (h) are two silver particles in A22/1/1966 (probably derived from the diamond sampling tool, refer Appendix A3).

Table 4.9. Comparison of the SEM-EDS analyses for Egyptian blue and of other researchers with the theoretical composition of cuprorivaite.

Element Oxide	Element percentage reported in cuprorivaite samples analysed							
	Theoretical	This study		Mahmoud (2011)	Pavlidou (2008)	Pagés-Camagna (2003)	Ullrich (1983)	Jaksch *et al.* (1983)
CaO	14.92	12.6	14.5*	22.04 (Ca)	12.0 (Ca)	15.2	12.0	14.9
CuO	21.15	17.0	19.3*	14.54 (Cu)	15.0 (Cu)	21.5	19.0	21.3
SiO$_2$	63.93	58.4	66.4*	54.25 (Si)	33.0 (Si)	62.8	63.0	63.6

*Normalised.

Table 4.10. EDS average data for the principal elements comprising cuprorivaite in the samples provided.

Element Oxide	Percentage in Cuprorivaite samples analysed									
	#3463	4901	8979b	8979c	24684	24685	24686a	A22/1	A22/6	A22/12
CaO	12.5	10.3	17.0	12.4	12.1	12.5	9.3	11.5	18.3	11.4
CuO	20.0	16.2	16.6	18.5	13.7	24.7	18.5	20.1	11.3	14.8
SiO$_2$	58.0	64.3	53.9	57.1	57.2	56.6	59.0	59.7	63.5	55.0

Table 4.11. Calcium to silica, calcium to phosphate (P$_2$O$_5$) silica to copper and tin to copper ratios based upon the average percentage (normalised) of the element present, FIB analyses.

Sample	SiO$_2$	CaO	CuO	CaO/CuO	P$_2$O$_5$	Na$_2$O/K$_2$O	Na$_2$O/MgO	Total% alkali	CaO/SiO$_2$	SiO$_2$/CaO	CaO/P$_2$O$_5$	SiO$_2$/CuO	SnO$_2$/CuO
A22/1/1966	64.4	10.4	17.1	0.6	0.1	4.4	2.4	2.7	0.16	3.8	104	3.8	-
A22/6/1966	63.5	18.3	11.3	1.6	0.2	7.3	29	3.3	0.29	5.6	915	5.6	-
A22/12/1966	55	11.4	14.8	0.8	0	2.3	0.2	2.3	0.21	3.7	-	3.7	0.095
UC 24684	57.2	12.1	13.7	0.9	1.0	2.0	0.7	4.7	0.21	4.2	121	4.1	-
UC 24685	56.6	12.5	24.7	0.5	tr	5.4	2.5	1.0	0.22	2.3	-	2.3	-
UC 24686a	59.0	9.3	18.5	0.5	0.0	2.4	2.8	6.8	0.16	3.2	-	3.2	0.086
8979b	53.9	17.0	16.6	1.0	0.5	---	0.9	1.2	0.32	3.2	34	3.2	0.096
8979c	57.1	12.4	18.5	0.7	0.9	4.7	28	3.2	0.22	3.1	138	3.1	0.086
EB1#3463	58.0	12.5	20.0	0.6	0	1.6	0.5	2.1	0.22	2.9	-	2.9	0.06
A4901KN	64.3	10.3	16.2	0.6	tr	4.2	2.6	2.6	0.16	4.0	-	4.0	0.093
DAF 124	53.9	12.3	16.1	0.8	0.3	16.2	5.8	8.6	0.23	3.3	41	3.3	0.081
M73/K/5*	22.4	8.5	46.0	0.2	0.0	4.7	0.1	1.7	0.38	2.6	--	3.70.5	---
M73/K/1406	52.1	11.9	8.4	1.4	0.2	2.6	0.7	4.3	0.23	4.4	59.5	6.2	---

*Two of the three copper analyses were eliminated from the analyses provided in Tables in Appendix A4.M7 as they were of copper metal shown by analyses of 55.0 and 69.0% CuO. The results were highly variable and probably significantly influenced by their small size and the interaction volume generated in the electron beam creating X-rays from the slip coating. This is evident from the high magnesium results reported in Appendix A5 Sample M7. Whilst no tin was detected in the FIB analyses of the two Malkata samples, it was however detected in later analyses conducted using the Nova electron microscope at an accelerating voltage of 15 kV in Malkata sample M7 (M73/K/5) but not in Malkata sample M8 (M73/K/1406)..

The high energy synchrotron beamline results are provided in Figure 4.4. The beam is able to analyse larger areas than that capable of being conducted in electron microscopes. It was this analysis that provided the initial evidence for the presence of a previously unreported arsenical mineral complex in Egyptian blue. As shown in Figure 4.5(a), there are a number of rod-shaped inclusions of calcium-phosphorus-arsenic complexes often containing fluorine which are approximately 10-20 μm long and about 2 μm wide. These particles have now

undergone further analysis under low vacuum in either a Focussed Ion Beam (FIB) or a Nova NanoSEM electron microscope. The results of these analyses provided herein shed an alternative concept in respect of the internal slip lining to the pottery reaction vessels and of the possible incorporation of kiln ash as the plant ash flux in late Roman production.

In Figure 4.4(b) the false colour red-green-blue CuCaCompton composite image of the relevant maps shows calcium is present in the copper-containing phase i.e., copper in a wollastonite phase. Compton scattering (inelastic scattering), is relatively sensitive to lighter (low-Z) elements and provides information regarding the morphology of the particle. Figures 4.5(a) and (b) and Figure 4.6(g) provide images of the calcium-phosphorus-fluorine-arsenic-containing particles displayed in Figure 4.4(a). Additional data and images are provided in Figure 4.11 to 4.15 and in greater detail in Appendix A4, Figures A4.E1.75 to A4.E1.94; in Appendix A4 for samples E5 (UC24685), E8 (8979C), E11 (DAF124) and cartonnage samples C2, C10 and C17. Figures 4.5(c) to (e) are images of the Ga^+ ion milling of the sample as will be discussed below. Additional images of these arsenical particles are provided in Appendix A4; the arsenical particles found in sample E5 are all located within a white surface coating or incrustation and discussed in Section 4.5.2.5.2. Interestingly, as shown in Figure A4.E1.95, a 50 μm long particle was identified coated with gypsum and containing ~1% As_2O_3.

EDS-generated elemental data for these Egyptian blue samples is summarised in Table 4.6 and a number of the inclusions located in various samples are provided in Tables 4.7 and 4.8. Comparative Egyptian blue (cuprorivaite) analyses are given in Table 4.9. The Mahmoud (2011) published analyses in Table 4.9 appear to be incorrect, the calcium and copper analyses should be reversed. The EDS elemental analytical data obtained by area analysis in the present research are given in Appendix A4. The average SEM-EDS analyses for all of the samples provided, together with a comparison with results from alternative studies and given in Table 4.9 confirms the theoretical analysis for cuprorivaite. When the presence of other elements is eliminated and the results normalised, the CaO concentration of 14.3% and CuO of 19.3% compares favourably with a theoretical concentration of 14.92% CaO and 21.15% respectively.

As shown in Table 4.3 and by reference to Figures 4.1-4.3, all of the bands for the Raman signature for the mineral cuprorivaite are present in all samples other than the turquoise sample E2 (A22/6/1966(2)). This sample, in Figure 4.1, shows a strong Raman signature for wollastonite indicated by the Raman bands at 636 and 970 cm^{-1}. A comparison with the analyses of other Egyptian blue pigments by other workers is also provided in Table 4.3. The interpretation of the Raman spectral information is given in Table 4.4. Pagès-Camagna *et al*. (1999) observed that large variations in the Raman signatures obtained from various samples, some bands decrease in intensity and become too weak to be observed. They attributed the differences to a possible polarisation effect and did not consider different fabrication processes or the formation of other mineral complexes.

As provided in Tables 2.20, Appendix A2 and 4.4, the Raman bands at 637 and 971 cm^{-1} are assigned to wollastonite-$2M$ (parawollastonite) and the bands at 984, 578 and 371 cm^{-1} to

pseudowollastonite (β-wollastonite). Egyptian blue sample E5 (UC 24685) from Amarna was the only sample which did not provide a signature for any form of wollastonite.

Comparative data from other researchers for EDS analyses of Egyptian blue and of the principal elements in cuprorivaite are summarised in Tables 4.9 and 4.10. Table 4.11 provides a number of elemental ratios for the various Egyptian blue samples analysed.

4.5.2 Raw materials employed in the production of Egyptian blue

4.5.2.1 *Quartz/silica*
Discussed in detail in Appendix A4.

A random sample of sand from Dakhleh Oasis was crushed and analysed to provide the following SEM-EDS analyses. Additional data is provided in Appendix A5.

Elemental analysis, ground silica particles, Nova-EDS Area analyses, refer Figures A5.D10.5 and A5.D10.6.

Na_2O	MgO	Al_2O_3	SiO_2	P_2O_5	SO_3	Cl	K_2O	CaO	TiO_2	MnO	FeO	CoO	NiO	CuO	ZnO
0.2	0.3	2.1	94.3	0.0	0.5	0.0	0.1	0.4	0.0	0.0	2.0	0.0	0.0	0.0	0.0
0.3	0.4	1.8	94.9	0.0	0.6	0.1	0.1	0.8	0.1	0.0	0.9	0.0	0.0	0.0	0.0
Average analysis															
0.3	**0.4**	**2.0**	**94.6**	**0.0**	**0.6**	**tr**	**0.1**	**0.6**	**tr**	**0.0**	**1.5**	**0.0**	**0.0**	**0.0**	**0.0**

4.5.2.2 *Lime*
Discussed in detail in Appendix A4.

4.5.2.3 *Copper*
Discussed in detail in Appendix A4.

4.5.2.4 *Tin (bronze)*
Discussed in detail in Appendix A4.

4.5.2.5 *Alkali flux*

There is considerable disagreement in the published literature as to whether natron (trona), plant ashes, or the salts evaporated from the River Nile waters provided the source of the alkali flux. As reported, the sodium flux is possibly supplied from natron from the natural evaporate deposit of the ancient lakes at Wadi Naturn and El Kab (Lucas 1989: 263; Kaczmarczyk and Hedges 1983: 134; Tite *et al*. 2006; Pagès-Camagna and Colinart 2003; Shortland *et al*. 2011). Natron (trona), was considered to be the original source of the flux for glass manufacture as the original Egyptian blue and green fluxes had been based upon natron. These various mineral salt deposits within this region have been mined from about 3000 BCE onwards (Lucas and Harris 1926: 263; Garrett 2001; Edwards *et al*. 2007; Shortland *et al*. 2011) and used in applications such as mummification, food preparation, animal

purgative, glass making, dyeing, and tanning (after being reduced). They are uniformly low in potash.

Alternatively, plant ashes growing in semi-desert environments may have been the source of the flux. This biomass when fired has widespread usage, including the production of soap and glass. Thus, it is conceivable that this was a source of the alkali flux. Because of the disputation within the published literature, both sources of alkali flux will be discussed.

In considering the alkali flux used in glass manufacture, the question must be asked as to how relevant is the type or source of this alkali to Egyptian blue manufacture; the production of Egyptian blue having commenced well prior to glass manufacture? According to Barkoudah and Henderson (2006), glasses, thought to have been made from halophytic plant ashes, date mainly to the Bronze Age, the Sasanian and Islamic periods. Between 800 BCE and 800 CE, natron was used as a flux in large parts of Western Asia and Europe for glass production. Therefore, is it reasonable to relate potash, magnesium and phosphorus concentrations present in Egyptian blue directly to the use of plant or vegetable ash as has been the case for glass? This will be discussed below.

The alumina content is probably associated with feldspar impurities present in the sand. Limestone or shell fragments in the sand were suggested by Pagès-Camagna and Colinart (2003) as the calcium source. Pagès-Camagna and Colinart (2003) also considered that any magnesia would not have come from dolomitic limestone since the bulk lime and magnesia concentrations do not correlate. Jaksch *et al*. (1983), supported by Pagès-Camagna and Colinart (2003) reported that the soda, potash, magnesia and phosphorus contents are each in the range 0.1-0.2%. On the basis of the low $Al_2O_3/(Na_2O + K_2O)$ ratios they suggested that feldspars were not the source of the alkali flux. Therefore these authors concluded that plant ash was the most likely source for the alkali. However, Tite *et al*. (1984) conjectured that in samples containing very low alkali concentrations (<1.0% $Na_2O + K_2O$) and with molar concentrations of $Na_2O + K_2O \leq Al_2O_3$ concentration, that the alkalis were introduced with the silica sand as feldspars and clay minerals.

Raman spectroscopy failed to detect the signature of various feldspars (other than albite which was most likely formed in the Egyptian blue reaction), indicative that feldspars were not part of any flux. And, Hatton *et al*. (2008) considered that the Na_2O/K_2O ratios in the resulting glass phase will be significantly reduced because of the contribution to the overall potash content from feldspars. This would assume that the feldspars were alkali feldspars rather than plagioclase.

4.5.2.5.1 *Sodium sulphate, sodium carbonate (natron or trona)*

Mineralisers (alkali flux) can have a significant effect on the crystal lattice of sintering material. They cause a relaxation in the crystal structure thereby increasing its activity. Furthermore, mineralisers work best at very low concentrations. (<1-3%). Investigation into the mineralising effect of additives such as fluorine, boron or even water vapour on the synthesis of calcium aluminosilicates or of spinel has been shown to be beneficial (Deer *et al*. 1992: 561). This is likely to occur during the initial Egyptian blue fritting reaction.

Mazzochin *et al.* (2004) concluded that cuprorivaite can be produced using sodium carbonate as the sole flux in the temperature range of 800-900°C. As discussed below, Pradell *et al.* (2006) recommended the addition of 3 wt% of Na_2CO_3 as a suitable flux. And Baraldi *et al.* (2001) stated that pure natron melts at 853°C, but at lower temperatures when impurities are present. On melting, natron behaves as a solvent for the other components.

Sodium sulphate is the second most common water-soluble mineral found in nature. Very substantial deposits of thénardite (sodium sulphate) occur together with natron, crude soda ash or trona in the 2-20 playa lakes (depending upon the dryness of the season) at Wadi Natrun. This deposit, located 80 km northwest of Cairo is at a negative elevation of 23 m and is 32-38 m below the River Nile and extends in an arc for about 25 km within a 5 km wide band. It appears that sulphate reducing bacteria have formed the deposit from probably Nile waters flowing through subterranean limestone deposits. Among these various sub-basins, all of which are brine rich in carbonate, sulphate and chloride, some contain almost pure halite, others contain trona, often containing burkeite and occasionally hanksite.   The lakes at either end are higher in elevation and crystallise principally trona or natron. The next lower lakes contain principally halite and Beida Lake is the lowest elevation and contains massive thénardite (Garrett 2001). The evaporite deposits at Lake Fazda (Wadi Natrun) examined by Shortland *et al.* (2011) indicated that the deposits contained minimal sodium carbonate in the form of natron or trona, but mainly consisted of burkeite and halite.   And Edwards *et al.* (2007) reported the natron specimens are of indefinite composition, comprising sodium sulphate, sodium carbonate, with several containing sodium bicarbonate and gypsum. Unlike the carbonates which dissociate to form oxides and are then able to be readily incorporated into a glass matrix, chlorides and sulphates are almost insoluble in glass-like structures.   These latter minerals form an immiscible melt that remains separate from the glass. It should be noted that halite does not provide a Raman signature.

Pagès-Camagna and Colinart (2003) reported that in the samples of Egyptian blue examined the total flux concentration (Na_2O + K_2O) never exceeded 5%. However, in turquoise samples the flux concentration varied between 5.7% and 10%. In the present research, the turquoise sample E2 (A22/6/1966) contained a total flux of 3.3% but a significantly higher CaO concentration (18.3%) which would have significantly contributed to the overall flux. Sample E 11 (DAF 124) has a much higher total flux content averaging ~9.5%, but very variable and sample E6 (UC24686a) contains a total flux concentration of 6.8%. Appendix A4 data for sample E11 indicates a very wide range of Na_2O concentrations probably emanating from soda-based minerals. Concentrations range from <2% to as high as 37% Na_2O and the accompanying Cl concentrations are ~0.5% indicating that the white surface incrustation is not NaCl.   In both samples, the higher flux concentration is principally provided by the sodium source. When viewed under an optical microscope, sample UC24686a has a significant percentage of crystals which appear to be green.

Weatherhead and Buckley (1989: 206) in their EDS analyses of Egyptian blue from Amarna reported the absence of sodium (with one noticeable exception being a turquoise pigment). To them, this suggested that the low sodium levels at Amarna previously reported by Tite *et*

al. (1981); (1984), Lucas and Harris (1962: 495), Kaczmarczyk and Hedges (1983: 134), Dayton (1978: 31-2) were due to contamination by other materials in the sample, possibly glass or unreacted natron or that the samples examined had been prepared in a different manner, or a different stage in the pigment manufacture.

In the pigment samples under investigation, as shown in Table 4.11, the total flux concentration ranges from 1.0 to ~ 9.0%, averaging 3.5% and as stated above, tridymite but not cristobalite together with wollastonite formed as shown by their Raman signatures.

The very high sodium concentration in the Anubieion sample E11 and in the Amarna sample E6 is a further indication that natron may have been employed in these specific instances. Based upon the presence of thénardite and the high sulphate analyses recorded in Table 4.6, and the low potash analyses, it is more likely that natron (trona) was the alkali flux selected. However, some plant ash could have been added in specific instances, or added as a minor portion of the alkali flux.

Delamare (1998) suggested that two different physical processes may be involved in the formation of Egyptian blue depending upon the percentage of alkali flux included in the recipe. When only a few per cent of alkali is present a liquid or glass phase is formed from which the Egyptian blue crystals nucleate and grow. And, when the alkali content is insufficient to produce significant liquid or glass phase, the Egyptian blue crystals were formed from surface diffusion by solid state sintering between the three major components. Delamare then argued that it would be likely that Egyptian blue would contain non-stoichiometric Egyptian blue crystals.

To test the Delamare theory, Pradell *et al*. (2006) investigated the use of high temperature XRD analysis at varying alkali concentrations and temperatures. They conducted their study using the high proton flux provided by synchrotron radiation. Their base mixture employed a synthetic malachite, silica and calcium carbonate with variable soda as a flux. With a high alkali mixture (3% Na_2O) the first major phase change occurred in the 700-800°C range with the decomposition of the sodium carbonate. At about 850°C the calcite commenced to decompose to form CaO and Ca_2CuO_3, and is completed by 900°C. Then, at about 950°C the calcium oxide reacts with silica to form wollastonite thereby decreasing the amount of quartz and tenorite remaining in the system. Between 950 and 1000°C the sodium silicate disappears and the corresponding decrease in the total crystalline phases suggests that a melt is formed from which the cuprorivaite crystallises. They then suggested that at about 1000°C some of the quartz then converted to cristobalite. According to phase diagrams such as provided by Kracek (1932) and by Morey and Bowen (1925) the more likely silica phase to form would be tridymite. (XRD is not the preferred instrument for conducting this analysis.) As the temperature cools, crystals continue to grow down to a temperature of about 700°C, with some increase in the wollastonite formation. The high alkali mixture producing significantly more Egyptian blue than the low alkali mixture and the unreacted tenorite is also higher in the low alkali mixture.

In the case of a low alkali formulation (0.3% Na_2O), the CaO reacts to form Ca_2CuO_3, the reaction peaking at 950°C. Above 950°C sodium calcium silicate is formed. As stated above,

regardless of the percentage of alkali selected, when formed, this phase in turn disappears at about 1000°C when wollastonite is formed. Again, they also propose that between 950 and 1000°C some quartz transforms to cristobalite. This formation is again questioned as phase diagrams would again indicate that tridymite would be the more likely phase to form. They reported that little crystal growth was observed on cooling. Pradell *et al*. (2006) then suggested that Delamare is incorrect in his proposed hypothesis of crystal growth formation by solid-state sintering. They proposed that Delamare's non-stoichiometry was due to the surface irregularity and contamination of the unpolished Egyptian blue particles he analysed. These researchers also considered that high alkali mixtures produced significantly more Egyptian blue than low alkali concentrations. Furthermore, the tenorite concentration is also higher in the low alkali flux mixtures.

4.5.2.5.2 *Alkali surface deposit*

The surface of samples Anubieion E11 and E6 (UC24686a) shown in Figure 4.7 indicate the presence of a white mineral deposit. The reason for the presence of the deposit is unknown; and, the sample history is also not known. It may be contamination from burial or from contact with other sodium-containing minerals but this is considered to be unlikely. It is more likely, as discussed below, to result from the Egyptian blue production and the use of trona containing thénardite as the alkali flux.   As provided in Tables 4.12 and 4.13 the elemental analysis of each deposit indicates the presence of high sodium and in the case of UC24686a, also high sulphur. Raman spectra provided in Figure 4.8 indicate that the deposit in the case of DAF 124 is hanksite, gaylussite, thénardite and natrite. These soda-based minerals account for the very high Na_2O concentrations recorded. On Sample E6, the white deposit is thénardite. These minerals are reported to be found in the Wadi Natrun mineral deposit (Garrett 2001) and this indicates that natron and associated minerals formed the alkali flux in these two samples.

Thénardite has a melting point of 884°C, a decomposition point of ~1100°C and a Specific Gravity = 2.698. Wollastonite has a melting point of 1100°C, and S.G. = 2.915 (Perry and Greene 1984: 3.10-3.22), whilst Tite *et al*. (2006) suggest a thénardite decomposition temperature of ~1200°C. Therefore, the thénardite would be stable, melt and float to the surface of the Egyptian blue during cooling. Unlike the carbonates, such as trona or natron, which dissociate to form oxides and are then able to be readily incorporated into a glass matrix, chlorides and sulphates, including thénardite, are almost insoluble. These latter minerals form an immiscible melt that remains separate from the glass.   Therefore, it is reasonable that if trona was used as the alkali flux in the manufacture of sample UC2486a, then thénardite could remain on the sample surface.
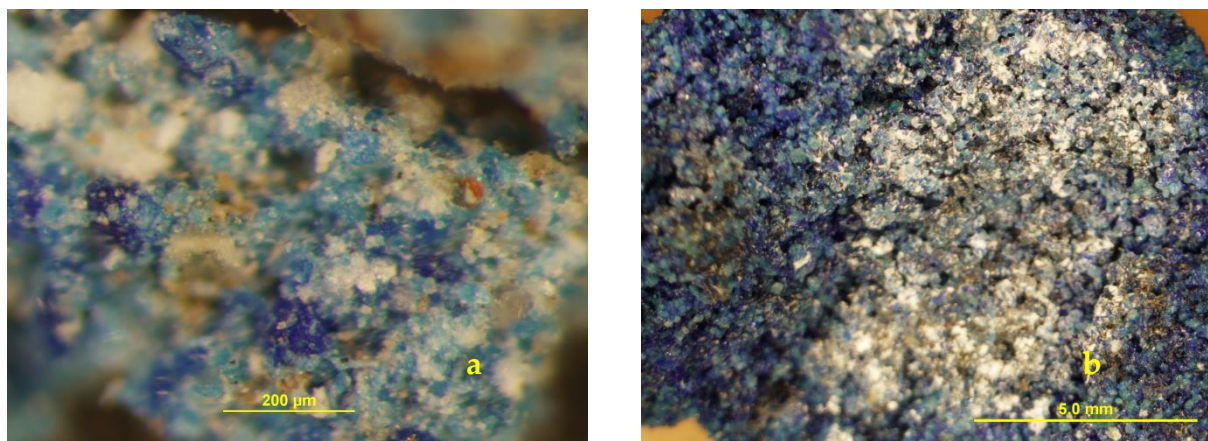
Figure 4.7. Optical microscope images of the white deposit present on the surface of (a) E11(DAF 124) and (b) E6 (UC24686a).
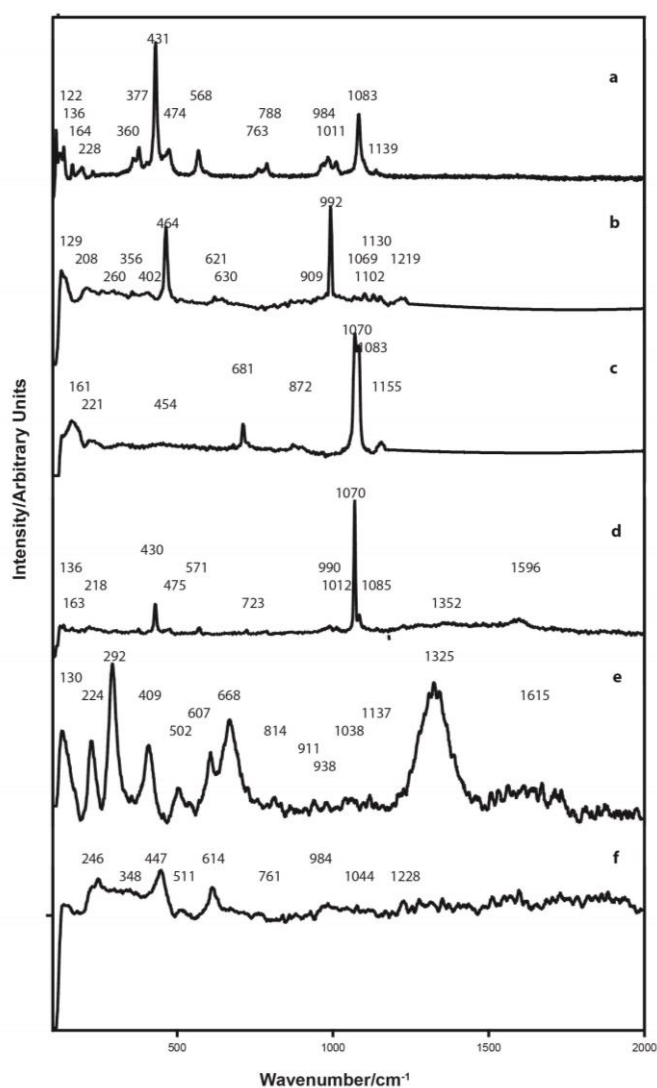
Figure 4.8 Raman spectra for various crystalline materials observed within Anubieion sample E11 (DAF 124). The blue pigment was identified as Egyptian blue (cuprorivaite) together with calcite, malachite, pseudomalachite, connellite, chalconatronite, hydroxyapatite, quartz, tridymite, wollastonite, aragonite, marialite, magnesioriebeckite, hastingsite, hematite, malayaite and hanksite. Bronze scrap was the main copper source as shown by the presence of tin ($\lambda = 514.5$ nm)

4.29

Table 4.12. FIB SEM-EDS analysis of the white mineral at the surface of Egyptian blue sample UC24686a.

	Na2O	MgO	Al2O3	SiO2	P2O5	SO3	Cl	K2O	CaO	TiO2	FeO	CuO	SnO2
UC24686a1_S2	26.9	0.0	0.2	7.0	0.9	52.0	0.0	6.2	3.8	0.0	0.4	2.7	0.0
UC24686a1_S3	35.1	0.1	0.8	4.6	0.4	51.1	0.3	0.0	2.8	0.0	0.2	1.5	0.0
UC24686a2_S3	33.1	0.0	0.4	5.5	0.4	50.5	0.0	5.0	3.2	0.0	0.3	1.5	0.0
Average	**31.7**	**tr**	**0.5**	**5.7**	**0.6**	**51.2**	**0.1**	**3.7**	**3.3**	**0.0**	**0.3**	**1.9**	**0.0**

Arsenical copper as shown by the absence of tin and the presence of CuO = 22.6% and As₂O₃ = 2.4% was used as the copper raw material in Sample E6. According to the Jaksch *et al*. (1983) dating proposal, this would suggest an early New Kingdom date for its production.

Table 4.13. Nova SEM-EDS average analysis of the white mineral at the surface of Anubieion, Saqqara, Egyptian blue sample E11, together with the average analysis of the high soda surface deposit and the analysis of a bone ash particle contained therein.

	Na2O	MgO	Al2O3	SiO2	P2O5	SO3	Cl	K2O	CaO	TiO2	FeO	CuO	SnO2
DAF124-15keV	8.9	5.8	4.1	57	tr	0.4	0.7	0.6	6.3	0.2	2.3	13.3	0.4
DAF124 high soda	27.1	6.1	4.3	28.6	0.0	1.2	0.7	1.0	22.9	0.0	2.4	5.8	0.0
Bone ash particle	2.0	1.8	0.4	5.9	29.9	0.0	0.7	0.1	53.5	0.0	0.2	2.5	0.0 +**F** = 2.9

Shortland *et al*. (2011) found thénardite present in three of the nineteen samples analysed from Wadi Natrun. This mineral would give a strong Raman signature as provided in Table 2.20, Appendix A2 and therefore its Raman signature in Figure 4.8 would indicate its presence.   The high sodium, potassium and sulphur concentrations provided in Table 4.12 in the elemental analysis of sample UC 24686a would confirm that thénardite and hanksite are the principal minerals present in the white coating on the surface of this sample.

Spot elemental analyses within the white surface deposit on Sample E5 are provided in Table 4.14. Spot 1 is of a long material of unknown composition but coated in gypsum. Spot 2, a rhombohedral crystal is diopside, although dolomite cannot be excluded. Leichmann (2006) proposed the use of either dolomite or magnesite as part of the minerals used in the production of Egyptian blue. He noted that the high magnesium found in one analysis was indicative of diopside formation. A crystal of diopside was detected in Sample E5 and its Raman signature is shown in Figure A4.E5.33(c).   And, it should be noted that in sample UC 24685 a rhombohedral crystal of dolomite was observed and analysed, as provided in Figure A4.E5.23, providing some support for the Leichmann proposal.

The analysis of the white surface coating is provided in Table 4.14, and indicates that very low fluxing minerals are present, but confirm that natron (trona) was the source of the flux. Raman spectra for white surface contamination on sample E5 is provided at Figure A4.E5.33 and summarised in Table 4.15. The Raman spectra indicate the presence of silica, diopside, starkeyite, gypsum, pentahydrite, calcite, probably pseudowollastonite and aragonite.

4.5.2.5.3 Alkali flux, plant or kiln ash

The case for plant or vegetable ash being used in Egyptian blue and green production largely revolves around the trace elements, particularly potash, magnesium and phosphorus. Thus, the possible sources for this form of alkali flux will be discussed in an attempt to provide a firm basis for decision-making in respect of its possible use in Egyptian blue production.

Gur-Arieh *et al*. (2014) have reported that information can be obtained from cooking installations by analysis of the phytolith component. Furthermore, wood ash may undergo chemical diagenesis to various degrees. These workers proposed a method to differentiate between wood ash and cattle dung, both of which were reported as fuel materials in Late Bronze Age ovens excavated from an Egyptian building complex at Qubur el-Walaydah. Charred botanical and microfauna, including bone fragments and anhedral calcite associated with phytoliths were recovered. The presence of dung spherulites indicated that dung was used as a fuel at all sites. They reported that dung-dominated fuel is not as common as wood-dominated fuel at all of the sites and at all time periods they investigated.

Importantly, Nicholson (2007: 121) noted that at Amarna, no facilities for natron storage have been located. He suggested that plants could have been ashed close to their source and the ash then transported to Amarna. This has been also discussed by Brill (1970: 124), Tylecote (1986: 226), Barkhoudah and Henderson (2006), Colomban *et al*. (2010/11), and Tite *et al*. (2006), particularly with respect to glass production within the Middle East and Europe. Kato *et al*. (2010) observed that a transition from natron to plant ash occurred in glass production in the Islamic world between the 8th and the 10th century CE. As such, this would suggest that the more recent discussion of glass production at Herat, Afghanistan, by Brill is not relevant to the present discussion with respect to Egyptian blue and green.

Nicholson (2007: 123) proposed that the plant ash would require sieving to remove stones or other larger material. He proposed that the ash would then have been finely ground and sieved prior to its use. If this process was followed, small particles of bone material would then be capable of entering an ash-containing reaction process.

As previously stated, natron contains few impurities, the potash, magnesia and phosphorus contents each being 0.1-0.2% (Pagès-Camagna and Colinart 2003; Hatton *et al*. 2008). Therefore Pagès-Camagna and Colinart (2003) concluded that based upon the soda, potash, magnesia and phosphorus concentration in the New Kingdom Egyptian blue samples from Karnak they analysed, (their result P10 is provided in the accompanying table), that plant ash was the most likely source for the alkali flux.   They did not consider that the potash could have been derived from the feldspars present in the sand used as the silica raw material.

Sample	Na_2O	K_2O	MgO	P_2O_5
Pagès-Camagna *et al*. (2003), Karnak sample P10	2.8	0.5	0.2	0.4
Karnak Sample A4901KN	2.1	0.5	1.0	tr
DAF124	8.1	0.5	1.4	0.3

Hatton *et al*. (2008) concluded that based upon the Na_2O/K_2O ratios which are typically in the range from 3 to 11 and Na_2O/MgO ratios typically in the ratio of 6 to 25 then the source of the soda rich ashes are derived from the halophytic plants such as *Salsola soda* and *Anabasis articulata* growing in coastal and salt marsh desert regions. In considering plant ash as the source of the alkali flux from plant it must be noted that the composition of plant ashes can vary depending upon the plant type, location and growing season. Therefore, because the Na_2O/K_2O ratios in the glass phase of all Egyptian blue samples and in more than half of the Egyptian green samples they analysed are <6 then this was considered by these workers to support the source of the alkali flux to be soda-rich plant ash. Presuming that this assumption is correct, the present results provided in Table 4.12 indicate Na_2O/K_2O ratios of 1.6 to 5.4 except for two cases, a turquoise appearing sample E2 and the powdered sample E11 which is significantly contaminated with a white slip. This would suggest that soda-rich plant ash was the source of the alkali flux, or, as propounded in this thesis, the use of readily available kiln ash. However, this use of plant ash is discounted, based upon the analyses provided in Table 4.12 and in the above table. The earliest date which can be ascribed to plant ash being the flux in Egyptian blue within the Dakhleh Oasis is after 200 BCE and before 2nd century CE.

The evidence developed in this thesis has indicated that, contrary to the opinion of Jaksch *et al.* (1983) and Pagès-Camagna and Colinart (2003), natron (trona) was the more probable alkali flux employed during the New Kingdom and to the Roman period with the proviso that in, or by, the 2nd century CE, Egyptian blue changed to using a plant ash flux. This change is predicated on the high potash concentration in a 2nd century cartonnage sample and which is supported by high potash in an Egyptian green applied to a 4th century Roman period (now grey-green) wall sample (Sample 2) from Kellis.   The flux change possibly corresponds to a change to a lead-containing copper ore and/or zinc-containing alloy (brass) as indicated in more detail in Appendix A3.

In the sample analyses provided in Table 4.6, the potash concentrations are uniformly low, being <1% K_2O, with only two samples being slightly higher at < 1.5%. Feldspars are the most likely provider of the potash.   However, Egyptian blue on pottery samples from 4th century Kellis contained <1% to <2% K_2O. And, the 2nd century CE cartonnage samples from Kellis provided analyses of 1.0%, 1.4% and 3.7% K_2O and these potash concentrations support plant ash as the alkali flux. The cartonnage sample C2 from Tomb 22, Kellis 1 cemetery was high in arsenic (7.5% As_2O_3) and high in potash (K_2O = 1.4%). Cartonnage Sample C17 from North Tomb 2 contained 3.7% K_2O, together with very small particles of lead (up to 43% PbO) as cotunnite and a particle of bone ash (P_2O_5 = 13.3%, CaO 17.9%). As such, the presence of lead would indicate a probable change in both the composition of the copper source material and in the use of plant ash as indicated by the high potash and hydroxyapatite within the Dakhleh Oasis samples. The two earlier dated trench samples of Egyptian blue from Mut al Kharab (25/26th Dynasty to c. 200 BCE), contain a natron–based flux.

Table 4.14. FIB EDS analyses of Spots 1 and 2 provided in Figure 4.11 and in Appendix A4, Figure A4.E5.23. The spots are from within the slip coating visible on the surface of sample E5 (UC24685).

	Na2O	MgO	Al2O3	SiO2	P2O5	SO3	Cl	K2O	CaO	TiO2	MnO	FeO	CoO	NiO	CuO	ZnO	BaO	PbO	SnO2	As2O3	Cr2O3	F
Spot 1	0.0	0.9	1.7	14.6	0.0	41.4	0.0	0.4	34.0	0.1	0.0	0.9	0.0	0.0	5.9	0.0	0.0	0.0	0.0	0.0	0.0	0.0
Spot 2	0.0	19.0	4.3	22.4	0.0	2.8	0.1	0.6	42.4	0.3	0.0	1.4	0.0	0.0	6.8	0.0	0.0	0.0	0.0	0.0	0.0	0.0

Table 4.15   Minerals detected in the slip on the surface of Egyptian blue sample E5 (UC24685).

Mineral \ Sample	Formula	Wavenumber/cm^{-1}		Database Reference
		Database	**Observed**	
apatite	$Ca_5(PO_4)_3(OH,F,Cl)$	960, 1059	965	RRUFF
calcite	$CaCO_3$	149, 276, 708, 1012, **1087**	276, 714, 1087	RRUFF
aragonite	$CaCO_3$	155, 208, **1085/1088**	154, 1087	RRUFF
magnesite	$MgCO_3$	212, 330, 1094	330, 1090	RRUFF
siderite	$FeCO_3$	283-305, **1090**	285, 1090	RRUFF
anhydrite	$CaSO_4$	417, 499, 601, 676, **1017**, 1129	1019	RRUFF
gypsum	$CaSO_4.2H_2O$	414, 493, 670, **1007,** 1116	414, 494, 622, 665, 1004	RRUFF
diopside	$Ca(Mg,\square)Si_2O_6$	323, 356, 391, 666, 1012, 1026	666, 1013	RRUFF
quartz	SiO_2	266, 357, 402, **467**, 699, 810, 1162	263, 464	RRUFF
Na-gmelinite	$Na(Si_8Al_4)O_{24}.11H_2O$	323, 411, **495,** 1108	418, 494	RRUFF
muscovite	$NaAl_2(Si_3Al)O_{10}(OH)_2$	263, 407/420, 703, 915, 950	263, 703	RRUFF
paragonite		265, 403, 656, 702, 750		RRUFF
pyrophillite	$Al_2(Si_4O_{10})(OH)_2$	261, 705	262, 706	RRUFF

4.5.2.6 *Phosphate*

Because of the close relationship of glass production with that of cuprorivaite, Tite *et al*. (2006), Hatton *et al*. (2008: 1601) and Vandiver (2008: 40) provided phosphate concentrations for a wide range of plant matter. Generally, these P_2O_5 analyses were much less than 2.0% except for an analysis of *Suaeda* from Barnug, Egypt which contained 4.6 and 5.3% P_2O_5 as provided in Chapter 5, Table 5.11.   This small percentage of phosphate reported would be insufficient to react with calcium to form the percentages of P_2O_5 and CaO to form the hydroxyapatite particles observed in the present study. In blast furnace slags, the phosphorus in the ore follows the slag formed in the reduction process, again indicating that the phosphate would enter the calcium silicate formed rather than entering into a separate reaction with the lime. Importantly, Vandiver reported that three samples of natron from Egyptian tombs (Brill-655, -657, -658) were not analysed for P_2O_5 (the notation "na", "not analysed" being used). Hatton *et al*. (2008: 1601) largely reproduced the Vandiver table but did not report the notation "na" to indicate "not analysed". This limited reporting has significance as discussed below at Section 4.5.2.6.3.

Western Desert plant ash could be significantly different in chemical composition, from many of the types of plant ash provided in the literature and summarised in Table 5.11, and specifically Table 5.12 in Chapter 5, with the potential for the trees, grasses and other plants growing in the oases to be higher in magnesium due to the plants growing in magnesium-rich ground-waters. Phosphate beds are also located in desert regions, potentially rendering Western Desert plant ash different from coastal regions. One sample of ash from a composition comprising a mixture of *Acacia nilotica*, controversially known as *Vachellia nilotica* or gum Arabic tree and *Tamarix aphylla* (Tamarisk) from the Dakhleh Oasis was analysed providing the data in Chapter 5, Table 5.12. The ash sample is high in soda, calcium and magnesia at a concentration higher than that reported for any other plant type given in Table 5.11, probably all or any of these minerals being present as chlorides or sulphates. Plant ash is discussed in more detail in Chapter 5, Section 5.4.2.2.

Jaksch *et al*. (1983) reported the presence of phosphorus (up to 2 wt.%) in the glass phase in Egyptian blue and as they considered phosphorus to be diagnostic for plant ash, they proposed that plant ash rather than alkali salts was the flux.   Ingo *et al*. (2013) also claimed that phosphorus is diagnostic for plant ash. However, Colomban *et al*. (2010/11) disputed the presence of phosphorus as being proof of plant or vegetable ash, noting that the phosphorus concentration depends upon seasonal growth conditions and the ripeness of the grain at the time of ashing. Barkoudah and Henderson (2006) also reported that wide compositional variation occurs for the same species, the parts of the trees selected, and the geological zones in which the trees were growing.

An alternative proposal for the presence of this concentration of phosphorus is directly related to the presence of hydroxyapatite (bone ash). As will be discussed in Section 4.5.2.6 and in Chapter 5, bone ash can be present in kiln ash and thus kiln ash, rather than specially prepared plant ash is the more likely source of the alkali component, if such a flux is employed. The published data in respect of the elemental composition of plant ash is limited, confined to plants from coastal areas of Egypt, or to third counties and thus, is considered to be tenuous and of limited applicability, particularly to desert regions of Egypt. The present results provide an alternative proposal for the

presence of, and the source of this concentration of phosphorus, namely, it is directly related to the presence of hydroxyapatite (fluoroapatite or bone ash)   .

The presence of calcium-phosphate-arsenate mineralisation in almost all Egyptian blue samples from monuments from the Old Kingdom up until the commencement of the New Kingdom was observed in polished sections in a significant number of samples examined by Schiegl *et al*. (1990), (1992) and which is demonstrated in Figure 4.10.

Minerals containing calcium-arsenic-phosphorus complexes were also observed in two samples analysed by Leichmann (2006).   The explanation given by Leichmann that arsenic was unconsciously added to the sample to alloy with the copper; whereas, the arsenic may well have been a deliberate addition to harden the copper.   However, the comment that the arsenic-rich phosphates are products of firing is now considered to be unconvincing.

Anomalous levels of phosphorus (generally present as Ca-P-F-As particles) were detected in Amarna samples E1 (A22/1/1966), E5 (UC24685) and E8 (8979c) together with arsenic as As_2O_3 in E4 (UC24684), and Karnak North sample E9 (A4901KN).   Similarly, anomalous, arsenic-free, calcium phosphate was detected in Anubieion sample E11 (DAF 124) from Saqqara as provided in Figure 4.29, and in Table 4.16.

Table 4.16. A selection of particular discrete calcium phosphate particles and their associated element analyses found in various Egyptian blue samples examined.

Element	A22/1/1966	UC24685	8979c	DAF124	C17 (NT2)
P_2O_5	27.1	19.9	24.1	29.9	13.3
CaO	41.2	33.5	34.9	53.5	17.9
As_2O_3	4.5	1.3	2.7	-	-
F	0.4	1.6	-	2.9	-
PbO	-	-	-	-	31.8

The extensive electron microscopy analyses conducted in the FIB, particularly for sample A22/1/1966 (E1) are reported in Appendix A4, as are the gallium ion milling and analysis of two of these particles commencing at Figure A4.E1.74.

The evidence provided in this thesis supports the addition of arsenical bronze, tin bronze and leaded bronze scrap in the manufacture of Egyptian blue over an extended time-frame.   The bronze metal would have been manufactured in lined pottery vessels.   Thus, if bone ash formed part of the crucible lining, then any arsenic which was released could have been adsorbed by the bone material.   It is known that arsenic was deliberately added to copper to harden it. Alternatively, the use of kiln ash containing phosphorus (as hydroxyapatite) as the flux component would provide an additional route for the entry of phosphorus into the Egyptian blue. Ogden (2000: 150) stated that traces of phosphorus may result from contamination of the raw materials with ash from the fuel during fritting thereby supporting this contention. Lucas (1962: 187) noted that the presence of phosphate and potash in glass cannot be readily explained. And, Lucas hypothesised that contamination could be caused by the corrosion of the refractory crucible material.

However, it is also possible that bone ash if used say with gypsum to manufacture the slip lining on the inside of bronze reaction vessels could have adsorbed arsenic in a previous reaction. Or alternatively, during Egyptian blue production, if arsenic-containing bronze scrap was employed. This suggestion is supported by Merkel and Rehren (2007) who suggested the reuse of finely ground ash tray material with slaked lime, silica and possibly carbon. There is also the possibility for arsenic to be adsorbed by the hydroxyapatite particles present in the Egyptian blue from the soil profile if the samples were recovered from an excavation. As the precise find spot is unknown, this possibility cannot be further examined.

Rehren (1997) examined the fabric of the crucible fragments recovered at Qantir and which had been used for glass production and for bronze melting. He reported that there was a considerable difference in the phosphorus content in the two vessel types, with the glass vessels having the higher phosphorus content. He attributed this observation to contamination by the fuel ash during the use-related firing of the crucibles. Rehren also related the higher sodium and in particular, the high potassium in these glass-working crucibles to fuel ash dust rather than the charge. Also, the elevated level of lead in the glass crucibles when compared with the bronze crucibles, whilst unexplained, was claimed to not be related to the charge. The presence of bone ash and the reaction of phosphorus with the alumina present in cobalt pigments is discussed in Chapter 5.

Some phosphorus was suggested by Rehren (1997) as having been derived from soil during burial in accordance with the work of Freestone *et al*. (1985). Freestone and co-workers had reported that there is a close relationship between the glass phase in the ceramic body and the increase in phosphorus up-take. And, Rehren reported that these ceramic vessels were highly vitrified, which, based upon the Freestone *et al.* (1985) proposal, would not be capable of adsorbing phosphates as discussed below.

4.5.2.6.1 *Possible phosphate deposition from ground-waters*

Duma (1972) studied the phosphate concentration in ancient pottery. He suggested that almost all igneous rocks undergo weathering, and therefore their residues, namely clays, are the primary component required for the manufacture of pottery. Thus, as most igneous rocks also contain phosphates they can enter into the fabric of the pottery vessel. Furthermore, because phosphorus is an important component of most living organisms, enrichment of the phosphate content of the soil can be due to local biological factors, often of anthropological origin. On their decomposition, phosphoric acid is formed and this can result in the transport of phosphorus though the soil profile. Adsorption, chemical bonding and ion exchange reactions can then lead to fixation of the phosphate on clays and other reactive surfaces. Duma reported that the unglazed pottery he examined indicated increasing concentrations of phosphate from the rim to the internal base, indicating that at least part of the phosphate can be attributed to usage factors.

In the Duma (1972) study, he reported that the phosphorus uptake on fired products of china clay was found to increase with firing temperature, preferably over the range of 600-800ºC in association with the solubility of its alumina content and despite a continuously decreasing specific surface. This led him to postulate that the bonding of phosphate ions in fired china clay products is different to the bonding observed on raw china clay. Whilst kaolinite, the major

constituent in china clay and dehydrated kaolinite is chemically highly reactive, he was unable to establish that aluminium phosphate was formed. Thus, he hypothesised that phosphorus from the organic substances once contained in the pot passes into the very porous pot material and through it into the surrounding earth. It also assumed that clays, even when fired, are able to bind phosphate ions permanently. Franklin and Vitali (1985) confirmed this finding; they prepared briquettes using an illitic, kaolinitic, feldspathic clay to which was added 10% CaO and fired them at 950°C. As such, this pottery would have generally replicated Malkata pottery bodies. After long-term soaking in phosphatic solutions of variable pH, acidity, buffered or unbuffered and room temperature or 90°C they reported that following a rapid dissolution of cations from the briquette surfaces a diffusion barrier developed which protected the briquette surfaces from further chemical attack. The presence of Ca- and Fe-phosphates is consistent with the solution changes reported.

Bolleng *et al*. (1993) conducted a series of experiments into phosphate concentrations on early pottery (1120-200 BP) from Basarwa, South Africa. The pottery was heated to between 300 and 800°C and then stained using Feigel's solution to determine if the calcium present was from bone, shell or from caliche inclusions in the pottery. They anticipated that whilst the samples had been heated to 800°C, that vessel channels would still be visible, especially in larger particles. This anticipated visual structure is contrary to the views reported by Abouzeid (2008) who reported that heating calcium phosphate minerals leads to minimal change in particle density below 750°C; however, above this temperature, the internal collapse in the particle porosity which commenced at 650°C, leads to an increase in density. Thus, it is unsurprising that no vessel channels were visible.

Bolleng *et al.* (1993) reported that their XRF analyses indicated high Ca and high P supporting a proposition that crushed bone had been included with the grass fibre as temper. However, their SEM results suggested to them that the Ca had been derived from caliche and therefore, the P must have been derived from either select clays, ashed grass or absorbed blood. They concluded that because P was not observed, unless the anomalous calcareous inclusions were derived from heavily burned bone particles which eliminated channel structure and eliminated P, then bone was not added as temper and these calcareous fragments were caliche. This loss of P would not occur at the reaction temperatures under consideration and is discussed below. Thus, as visual inspection eliminated cattle dung as temper, they therefore concluded that the only other source for the elevated phosphate would therefore be residual blood and fat adsorbed in the fibre temper and in fabric pores. In doing so, they misquoted Freestone *et al* (1987), indicating that Freestone would support their findings. In this document, they reported that they still needed to investigate ashes such as wood ash, leaf ash or dung ash, all of which could potentially have been added into the pottery fabric and therefore provide additional sources of P and Ca.

Freestone *et al.* (1994) took exception to their prior work being quoted in support of the Bolleng *et al*. findings and in particular that "P is an established marker element for the presence of these substances {i.e., fats, blood, etc.} in fired clay". Freestone and co-workers then quoted a number of other researchers to support their argument that the presence of phosphate is a post-depositional phenomenon and furthermore, post-burial deposition of phosphate is not confined to pottery. Previously, in a thought-provoking paper, Freestone *et al*. (1985) had studied the adsorption of phosphorus on to pottery, slag and glass surfaces. They reiterated that disordered silicates such as

the less-common clay minerals allophanate and imogolite, weathered glass and slag and fired clay, show a much greater capacity to adsorb phosphate than typical unfired soil clays. Low fired potsherds with open sponge-like internal structures, are particularly prone to adsorb phosphate. Freestone *et al.* concluded that elevated phosphate in archaeological pottery may not be taken as an indicator of use. They made no comment in respect of the calcium or bone particles observed by Bolleng. This Freestone research is discussed more fully in Chapter 5, Section 5.4.2.7.2 in respect of the analyses of the sherd fabrics in the present research.

Clearly, the fluorine-containing hydroxyapatite particles encountered in the present research and discussed in Section 4.5.2.6.3 are significantly different to the phosphate encountered by Freestone and co-workers from burial conditions discussed herein and in Chapter 5, Section 5.4.2.7.2. These discrete particles are isolated, readily located on the surface, with a definite mineral structure in accordance with a molar Ca/P ratio for apatite or whitlockite, generally contain fluorine and not that of a calcium-deficient mineral as described by Freestone *et al.* (1987). They are able to be milled in the FIB with a gallium ion beam and analysed within the electron microscope. As such, they do not fit the description for phosphate adsorption from soil as described by Freestone. These hydroxyapatite particles are not directly related to either silica or alumina.

During fritting or in the subsequent thermal cycle (if a two-stage heating process was adopted), it could be conjectured that phosphorus present in plant ash , if it formed part or all of the alkali flux, could react with excess calcium oxide to form a calcium phosphate mineral. Equally possible would be for the phosphorus to react with aluminium. These suggestions are rejected on the basis of the presence of fluorine in the hydroxyapatite particles analysed as provided in Table 4.16, the significant level of arsenic adsorbed on to their surface and throughout the particles, and the determination that plant ash was not the flux selected. And, as shown in the various tables in Appendix A4, no aluminium phosphate complexes were found. Neither phosphorus nor arsenic was detected in the immediate surrounds to these hydroxyapatite minerals as provided in Appendix A4 commencing at Figure A4.E1.74. This would suggest that the arsenic has been previously adsorbed on to the calcium phosphate surfaces rather than chemically formed during the Egyptian blue reaction. The presence of fluorine, which is diagnostic for bone material, would of itself dismiss any suggestion of the formation of a Ca-As-P complex by a high temperature chemical reaction.

4.5.2.6.2 *Discrete calcium phosphate particles and their calcination*

The source of phosphorus detected in the present research has no relationship with burial conditions. These particles show a clear P-Ca-F mineral composition and at concentrations strongly suggestive of bone ash. In fact, no alternative explanation for these particles can be advanced. As is shown in this chapter in Figures 4.11, 4.12 and 4.16 and in Chapter 5, Figures 5.44 to 5.47, this can be attributed to hydroxyapatite or fluoro-apatite particles, a number of which are shown in Appendix A5 and particularly in sample D7 from Mut al-Kharab and discussed in Chapter 5, Section 5.4.3.

Bone, is predominately hydroxyapatite $[Ca_{10}(PO_4)_6(OH)_2]$ and when heated in the absence of a flux or competing reactant, undergoes thermal decomposition to form β-tricalcium phosphate, lime

and water. The reaction commences at around 775°C, (Mukhopadhyay *et al*. 2011), or >775°C (Iqbal *et al*. 2000), according to the following reaction:

$$Ca_{10}(PO_4)_6(OH)_2 \quad \xrightarrow{\Delta} \quad 3\beta\text{-}\ Ca_3(PO_4)_2\ +\ CaO\ +\ H_2O$$
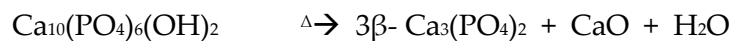
and, at 1000°C, only calcium phosphate was detected by XRD (Iqbal *et al.* 2000). The highly reactive CaO formed is then capable of reacting with metakaolin in pottery to form anorthite. Furthermore, the amorphous silica discarded from clay relicts during metakaolin formation may assist melt formation at ~985°C providing sufficient potash is present, as for example if nepheline syanite (feldspar, a mixture of microcline and nephelene crystals) is present. Alternatively, the lime (Ca^{2+} or O^{2-}) may diffuse into the silica within the forming Egyptian blue, Egyptian green or cobalt blue aiding liquid formation at lower temperatures and the formation of wollastonite. Iqbal *et al.* indicated that in low concentrations, bone ash acts as a flux (Iqbal *et al*.(2000a) and which is in accordance with the work of Franklin and Forrester (1975) who stated that between 2-20% bone ash acts as a vigorous flux in combination with silicate materials.

According to Thompson *et al*. (2013) the process of heating bone is complex, producing a range of complicated changes within this material. Dehydration occurs between 100 and 600°C, Decomposition (loss of organic component) 300-800°C, inversion (alteration of the inorganic phase) 500-1100°C and fusion (coalescence of crystal structure >700°C. By 900°C the porous texture formed by the previous losses is altered to produce a closely interlocking texture. Thus, during the heating and burning process, the crystal structure of bone becomes better ordered and characterised by larger crystals and less strain, and as such, the Crystallinity Index (CI) increases.

It should be noted that some loss of fluorine can occur during calcining of hydroxyapatite (in the form of fluoro-apatite) at about 1000°C in forming bone ash. Chen and Miao (2005) observed that the fluorine content can modify the rate of decomposition and result in the densification of the fired material. This would suggest that in the bone ash particles reported in this chapter and in Chapter 5 that no significant structure would be expected to be evident in any of these particles. Chen and Miao (2005) noted that in the thermal treatment of hydroxyapatite and fluoro-apatite [$Ca_{10}(PO_4)_6(OH)_{2-2x}F_{2x}$] the fluorinated product can increase its crystallinity and the strong ionic bonding within the crystal structures leading to increased density, chemical and thermal stability. This change in chemical properties, leading to stabilisation of the crystal structure was considered to result from the partial substitution of the existing hydrogen ions in the OH^- groups by F^- ions. The higher affinity of the F^- ions with respect to the oxygen ions produces a well-ordered apatite crystal structure. They proposed that the two step thermal decomposition reaction:

        at about 800°C
$$Ca_{10}(PO_4)_6(OH)_2 \ \rightarrow\ Ca_{10}(PO_4)_6(OH)_{2-2x}O_x + xH_2O$$

        before 1220°C
$$Ca_{10}(PO_4)_6(OH)_{2-2x}O_x \ \rightarrow\ 3Ca_3(PO_4)_2 + CaO + (1-x)H_2O$$
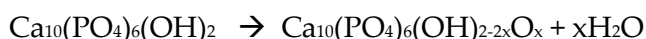
They established that the sintering reaction commenced at about 1000°C, and within the thermal range 1000-1100°C, the shrinkage rate or densification proceeded rapidly with maximum

densification occurring at 1100°C, slowing down to finally zero at 1450°C.. These workers clearly established that the presence of fluorine will aid the densification of hydroxyapatite when heated above 1000°C. In their experiments, the onset sintering commenced at about 1150°C and within the thermal range from 1150-1250°C the rate of densification increased rapidly. The loss of visible structure is clearly shown in Figure 4.9 below. This would indicate that no visible structure is likely to be seen in the approximately 2μm in diameter fluoro-hydroxyapatite samples on the surface of Egyptian blue pigments when they were examined under the electron microscope.
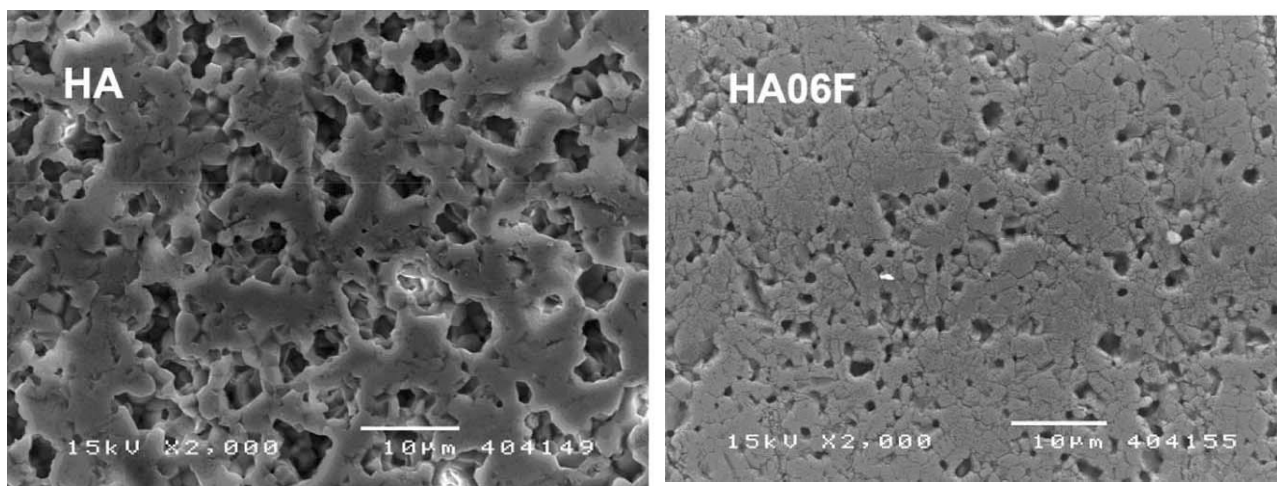
Figure 4.9. Surface morphologies of hydroxyapatite and fluoro-hydroxyapatite in which the F content was x = 0.6 in the above formula. Following sintering at 1300°C then polishing and etching for 10 minutes in a 2.5% solution of citric acid the above images were obtained. The scale bar is 10 μm. They clearly indicate the densification and loss of skeletal structure in fluoroapatite (Chen and Miao 2005).

Orlovskii *et al*. (2002) proposed slightly different two-step reactions occurred during the sintering of hydroxyapatite. At 900°C or at 850°C in a moisture vapour free atmosphere, oxyhydroxyapatite [$Ca_{10}(PO_4)_6(OH)_{2-2x}O_x\square_x$] (where $\square_x$ represents a vacancy and x <1) forms, followed by its further decomposition to $Ca_3(PO_4)_2$ and $Ca_4P_2O_9$.

Welch and Gutt (1961) investigated the volatilisation of phosphorus pentoxide from substances varying in composition between $2CaO.P_2O_5$ and $3CaO.P_2O_5$ and reported that their work reaffirms by direct observation the congruent melting of $2CaO.P_2O_5$ (1355°C) and the incongruent melting of $4CaO.P_2O_5$ (1720°C) with the liquidus curve reaching a maximum near the composition $53CaO.47P_2O_5$ (wt.%) (1777°C) and that there is limited miscibility between $2CaO.P_2O_5$ and $3CaO.P_2O_5$.

The presence of arsenic in the bone ash can be explained by considering the behaviour of bone ash in the presence of certain metallic elements. Bone ash is highly absorbent for a number of elements as shown by its usage in cupellation to absorb the lead oxide leaving behind the gold (or electrum) bead. Bone ash will absorb arsenic as seen in these particles and adsorb sodium chloride and gypsum as shown by the external coating on a number of other particles. Furthermore, bone ash is able to withstand high temperatures (>1400°C) as shown by its continued use in the construction of cupellation cups used for gold analysis by fire assay. Its use in cupellation continued into the late Roman period as shown by 31% tricalcium phosphate (bone ash) being found present in a Roman

cupellation hearth clearly indicating that this cupellation vessel was lined with bone ash (Owen and Hillis 2003).

The analytical results provided in Appendix A4 indicate that these particles are therefore arsenic adsorbed onto hydroxyapatite confirming that bone ash may have formed part of the slip used to line the fritting pans or the small vessels prior to the manufacture of this pigment or in copper or bronze production. The bone ash particles found in the analysis of UC24685 were all in the white complex on the surface of this pigment and therefore support this hypothesis.

In an important, but largely unrecognised research conducted by Schiegl *et al.* (1990), they identified similar Ca-P-As particles in Egyptian blue pigments. The samples were from monuments from the Old Kingdom to the commencement of the New Kingdom and this arsenical phase was located in almost every sample analysed. They provided the BSE image, Figure 4.10, to support their work. As such, these particles bear a striking similarity to the particles detected and discussed within this thesis.

According to Schiegl *et al.* (1990; 1992), and shown in Figure 4.10, Egyptian blue frit contains residues of arsenic, tin and lead and which exhibit a distinct chronological distribution pattern. They reported that in the Old Kingdom until the commencement of the New Kingdom, a calcium-phosphate-arsenate phase was encountered in almost every pigment sample they examined. No tin was found in samples before the 18th Dynasty. They therefore proposed that prior to the 18th Dynasty only arsenical bronze or possibly arsenical copper was in use as the copper raw material source. Tin bronze first appeared in the 18th Dynasty during the reign of Thutmose III indicated by the tin-bearing compounds cassiterite [SnO_2] and malayaite [$CaSnSiO_5$]. Lead-bronze was introduced prior to, or early in the 19th Dynasty. Thus, according to Schiegl, this chronological distribution pattern of As, Sn, and Pb in pigments from well-dated monuments decorated with Egyptian blue pigments allows for a more accurate method for dating bronze artefacts.

The Schiegl *et al.* (1990) hypothesis may be correct as these micron-sized Ca-P-As particles may have been derived from more than one source; however, Schiegl *et al.* ignored the role of calcium and phosphorus in their discussion and concentrated on the importance of tin, arsenic and lead, all of which they reported to be present in Egyptian blue over various Dynasties. And, the change in the concentration of tin, arsenic and lead was, in their consideration, the important factor which directly related to the type of bronze metal being manufactured in various epochs.

The present results would not necessarily question the reliability of this proposed bronze dating method. The late 18th Dynasty Amarna sample E6 was produced using arsenical copper/bronze as shown by its lack of tin and an elemental analysis containing 22.6% CuO and 2.4% As_2O_3. Furthermore, the combination of arsenic, phosphorus, calcium and fluorine (Ca-P-As-F) in the Egyptian blue samples analysed in the present study has not been previously recognised. These results will be discussed further at Section 4.5.2.6.3 and would tend to question the reliability of this dating method.

Indirectly, the work of Leichmann (2006) in reporting the presence of As-P particles in Egyptian blue samples prepared during the Old Kingdom is in accordance with this proposal. This mineral reported by Leichmann indicated a composition approaching that of arsenocrandallite in a sample

of Egyptian blue from the funerary temple of Raneferef (Leichmann 2006: 58).   No Raman signature for this mineral or other arsenate minerals was detected by their Raman signature in any sample examined.
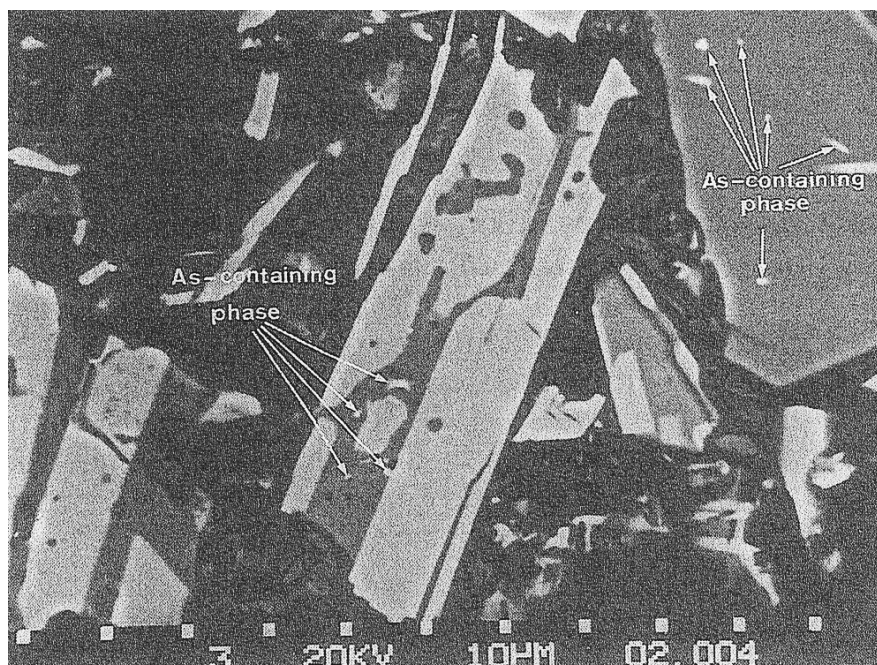
Figure 4.10. BSE image of the white, micron-sized particles (marked as As-containing phase) located in the dark grey glass phase.   The light grey regions are cuprorivaite. [Image from Schiegl *et al.* (1990).]

As calcium phosphates, particularly in the form of bone, are highly absorbent for a range of elements including arsenic, it is a reasonable supposition that slag generated from bronze production could contain Ca-P-As particles particularly if bone material, potentially present in the kiln ash, formed part of the flux used in the preparation of bronze metal, or alternatively, from the pottery inner surface lining. And, this proposal would be supported if arsenical bronze had been manufactured using hydroxyapatite-containing kiln ash as a flux. This proposition would also be enhanced if it was able to be determined that bronze production had been conducted in white, high calcium (hydroxyapatite or bone ash) lined vessels, with, or without added gypsum, as described by Turner, Rehren and others for glass or Egyptian blue production (refer Section 4.7). If this usage occurred, then any liberated arsenic from arsenical copper or arsenical bronze would be adsorbed on to the phosphate particles and more likely report in the slag formation.   The subsequent use of such slags in Egyptian blue production could then give rise to these Ca-As-P particles being incorporated into the Egyptian blue pigment.

In a later publication, Schiegl *et al.* (1992) hypothesised that in the deterioration of As-bearing Egyptian blue pigment layers the primary relic Ca-P-As crystals are dissolved and As- and P-bearing solutions migrate into the substrate and then precipitation of secondary Ca-As-P takes place. The formation of the secondary precipitated Ca-P-As accelerates the spalling of the residual components of the pigment layer as a result of this recrystallisation. The aggressive phosphate-bearing material was then considered to be capable of penetrating the painted decorations from their surface to the substrate. In this hypothesis, Schiegl *et al.* (1992) then proposed that calcite and

dolomite crystals were then replaced by the phosphate-based material in both the pigment and in the stucco. Repeated additions of this phosphatic material then led to the formation of successive phosphate layers in which pseudomorphs of carbonate rhombohedra are usually well preserved. Furthermore, due to their compactness these secondary phosphate layers are resistant to crumbling. Schiegl and co-workers then stated that their results fully support the proposal of Wilson-Yang and Burns (1988) that bat droppings are the source of the phosphorus; such defecation having been observed on the walls of the Beni Hasan tombs.

It should be noted however, that calcium arsenate compounds are unstable in the presence of air and water as CO_2 will react with the arsenate to form calcium carbonate and release the arsenical complex back into solution. And, in a joint study between the University of Montana and SME Technology Applications Inc. on behalf of the U.S. EPA it was demonstrated that if a P/As mole ratio ≥ 5 and the Ca/(As+P) mole ratio is >1.5 then these apatite-like compounds such as $Ca_{10}(As_xP_yO_4)_6(OH)_2$ are extremely stable (Anon. 1998)[1]. In the present study, the arsenoapatite particle P/As ratio is ~8 and the Ca/(P+As) ratio is ~1.8. Therefore the fluoro-bone ash material is from a primary source and not the result of phosphorus dissolution and reprecipitation. Therefore, if in the case of wall decoration using Egyptian blue pigments the phosphorus was derived from bat droppings then once the phosphorus precipitated on the calcite it would become insoluble and unlikely to enter into further dissolution and precipitation reactions.

As reported by Nicholson and Henderson (2000: 127) the presence of potash has been proposed to result from contamination of the frit by fuel ash. Caley (1962: 81) suggested that perhaps the ash from the fuel employed to melt the glass was incorporated into successive batches as one of the raw materials. In light of the present research, the location of discrete particles of hydroxyapatite provides support for this hypothesis.

Henderson *et al*. (2004) observed that it is possible that the discovery of bone fragments in the glassy matrix of what they described as type 4 frit and in the fills of three out of the four chamber furnaces from Tell Zujaj that hydroxyapatite would provide the calcium and phosphorus for oxidation within the melt.

It is now hypothesised that the observed hydroxyapatite particles result from either the use of bone ash to line the fritting pans, or alternatively, from the use of kiln ash flux which may arbitrarily contain bone material, possibly in an earlier chemical process such as bronze production, to enter the Egyptian blue formulation. This hypothesis thereby provides an additional layer of uncertainty. The single Western Desert plant ash analysis from Dakhleh Oasis provided in Table 5.12 suggests that $P_2O_5 < K_2O \ll MgO < Na_2O$, CaO. To date, no sites for the specific ashing of plant material, or its storage, has been discovered within Egypt. Plant ash is therefore not considered to have formed the major part of any flux.

---

[1]This research was conducted as part of the required stabilisation of the highly acidic and toxic water present in the Berkeley Pit, Butte, Montana, USA, following the cessation of copper mining. As such, no release of this water was contemplated until the water was of potable quality and the copper, arsenic and other heavy metals present in the pit water had been removed and stabilised for suitable placement in on-land tailings dams. The work reported upon above, was conducted as part of this precipitate stabilisation project. I visited the site in September 2003 for technical discussions with the proponents as part of the on-going research.

4.5.2.6.3   Calcined hydroxyapatite (bone ash)

As previously stated, the synchrotron XFM beamline analysis of the Egyptian blue particle revealed the presence of a significant number of arsenic-rich, rod-shaped particles, generally 10-20 μm long by about 2 μm wide ("diameter") and which are present on the surface of the Egyptian blue particle A22/1/1966(4) (E1) as shown in the synchrotron arsenic elemental map, Figure 4.4.

As the smaller dimension of the particles are approximately 2 μm, it is comparable to that of the X-ray spot size of the XFM configuration used; the higher resolution FIB BSE detector was then employed to locate and analyse several of these particles. Much larger particles located on the surface of Egyptian blue sample UC24685 are shown in Figures 4.13 and 4.16.

FIB BSE images of these arsenic-rich particles are provided in Figure 4.6(a) and (b). To analyse the composition of the arsenic-rich particles, channels up to 10 μm deep, were milled using the Ga^+ (ion) beam fitted to the FIB microscope. Milled particles are shown in Figure 4.6(c), (d) and (e). Analysis spots are marked by the + marks. Sixteen elemental analyses of these particles were conducted, with the results presented in Table 4.7.   These results indicate a CaO composition ranging from about 26-42% CaO with a commensurate P_2O_5 content ranging from 10.3 to 28.5%.

Fluorine was detected in five of these analyses, providing a strong confirmatory diagnostic indication for the presence of hydroxyapatite. According to Kamino *et al*. (2007) hydroxyapatite is one of the most sensitive materials to electron beam irradiation and is therefore considered to be difficult to thin for TEM examination without causing damage. Thus, the Ga^+ ion was used directly at the required milling spot to ensure support for the particles under analysis.

The Ca:P ratio found is comparable to that of hydroxyapatite a major component of bone, any difference from theoretical most likely results from the temperature of calcination of the hydroxyapatite, which progressively dehydrates to β-tricalcium phosphate (bone ash) over the temperature range 1000-1400°C concomitantly releasing about 10% of its CaO which is consistent with the present analyses (Owen *et al*. 2000; Owen and Hillis 2003; St. Pierre 1955).   Refer also to Section 4.5.2.6.2. As noted by Owen *et al*. (2000) and Owen and Hillis (2003), this makes it similar to whitlockite particularly since the CaO/P_2O_5 ratio of whitlockite in ceramics can vary significantly from its naturally occurring counterpart.

St Pierre (1955) indicated that at about 1000°C hydroxyapatite will gradually break down to form tricalcium phosphate, release lime and water as follows:
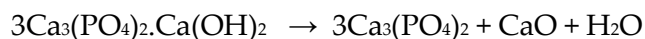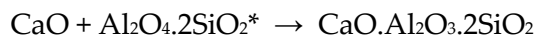
$$3Ca_3(PO_4)_2.Ca(OH)_2 \ \rightarrow \ 3Ca_3(PO_4)_2 + CaO + H_2O$$
and,
$$CaO + Al_2O_4.2SiO_2* \ \rightarrow \ CaO.Al_2O_3.2SiO_2$$
*indicative formula only.

Kaolin will dehydroxylate to metakaolin at 650°C, and the reaction of the lime with metakaolin is rapid. Tricalcium phosphate will remain stable until well above 1370°C, a temperature which is significantly higher than the temperature at which the pottery vessel would have failed. Furthermore, the liberated CaO is highly reactive and can readily react with clay and silica

polymorphs to form gehlenite and thence anorthite (Owen *et al*. 2000); Owen and Hillis 2003); St. Pierre 1955). Gehlenite and anorthite will only form with highly calcined bone ash if an additional source of CaO is available. However, the Raman signatures for these minerals were not detected in the Egyptian blue pigments from Amarna. Gehlenite was detected in a sample from Karnak North and in the turquoise sample E2 (A22/6/1966(2)).

Hatton *et al*. (2008: 1594) observed that in their analyses of their samples AM4 and AM9 from Amarna that these two samples were contaminated by lime from the substrate. Unfortunately, they did not analyse for phosphorus or sulphur (refer to their Table 7). They suggested that the CaO/CuO ratios of 1.5 and 1.7 differed from what they saw as "normal", namely 0.6-1.0. However, without the phosphorus or the sulphur analyses it is conjecture that the CaO analysis is obtained from lime; it may well be from this source, but lack of data precludes acceptance of their proposed source for the calcium reported. The Amarna samples examined in the present research, results of which are provided in Table 4.11 agree with this "normal" CaO/CuO ratio, the ratio for the present samples was found to be between 0.6 and 1.0 except for the turquoise sample E2 (A22/6/1966(2)) in which this ratio is 1.6.

Figures 4.11 to 4.16 provide images and their respective SEM-EDS spectrum which identify the shape and composition of these fluorine-containing hydroxyapatite particles and of the arsenic or gypsum adsorbed thereon. Nicholson (2007: 121,127) and Nicholson and Peltenberg (2000: 192) noted that there are fragments of bone with signs of burning from the upper fill of one of the kilns (Kiln 1) indicating to him that this at least was an occasional practice for the potters, if not the glass makers for this to have been a method for refuse disposal, but no evidence can be mounted to establish whether this was practice or whether it was in fact conducted for the production of bone ash. Bone ash has also been reported in kilns associated with cooking at Soknopaiou Nesos.[2]
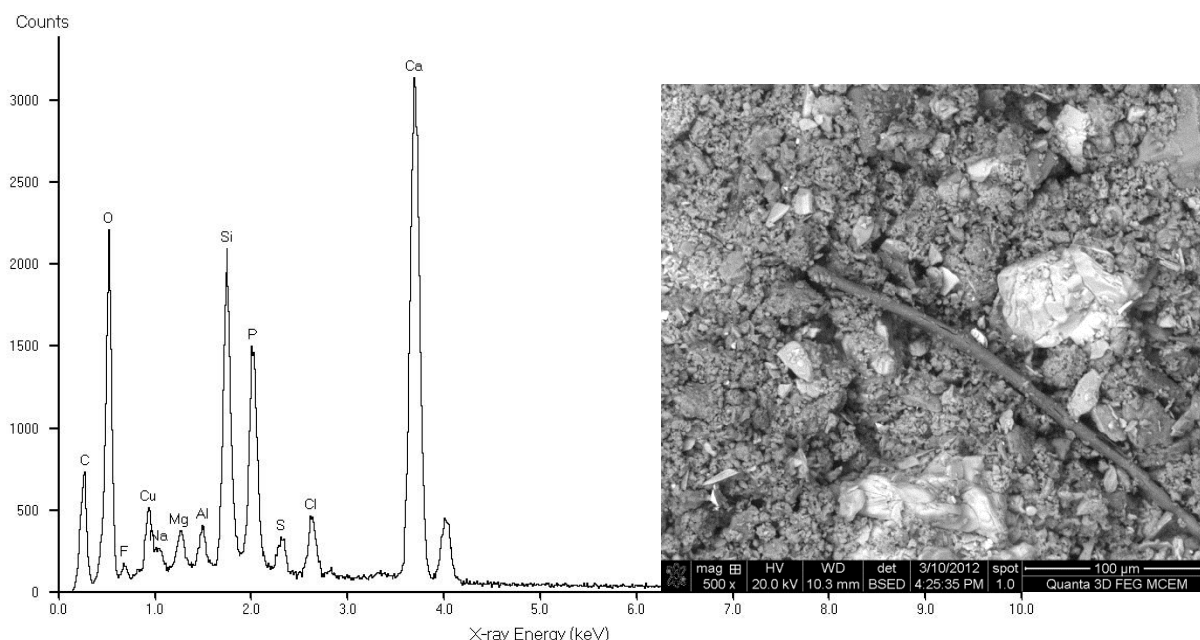
Figure 4.11. Data from sample E5 (UC24685). Refer Figure A4.E5.14. FIB EDS spectrum for the analysis of the approximately 250 μm long hydroxyapatite particle shown in the accompanying BSE image. Hydroxyapatite (bone ash) is shown by the high peaks for P and Ca together with a peak indicative of the presence of fluorine. Similar bone ash particles are observed in Figures A4.E5.21, A4.E5.23 and A4.E5.28.

_____

[2] Dr. A. Connor, pers. comm. (23 Oct. 2015).
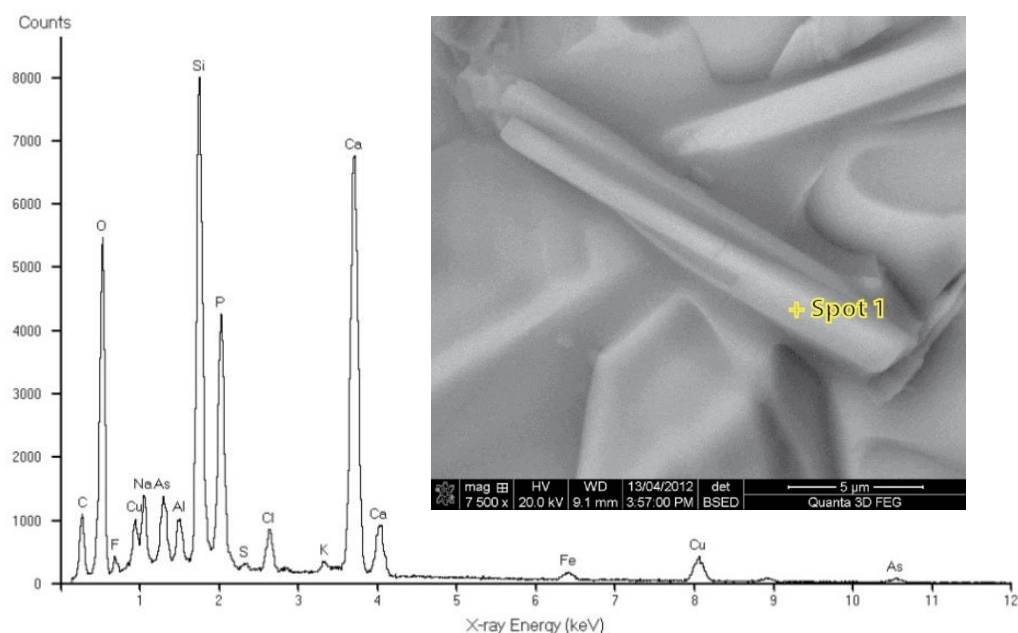
Figure 4.12. Sample E1. (Data from Appendix A4, Figure A4.E1.62.) FIB BSE image of an approx. 15 µm long rod-shaped, arsenic-containing, hydroxyapatite (bone ash) particle, the analysis for which is marked as Spot 1 and as Spot 1 in Figure A4.E1.61 and A4.E1.62. Again, a fluorine peak is observable in the above spectrum.
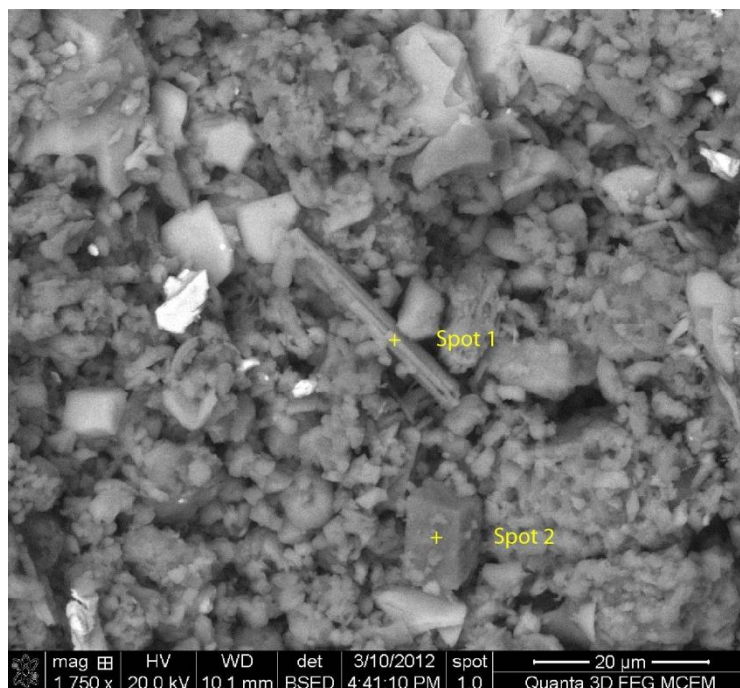
Figure 4.13. Sample E5 (UC24685). FIB BSE image showing the position of a particle of gypsum (Spot 1) and of a diopside crystal (Spot 2) in the surface slip coating. The spot EDS spectra are provided in Figures 4.14 and 4.15 and their elemental analyses are provided in Table 4.14.
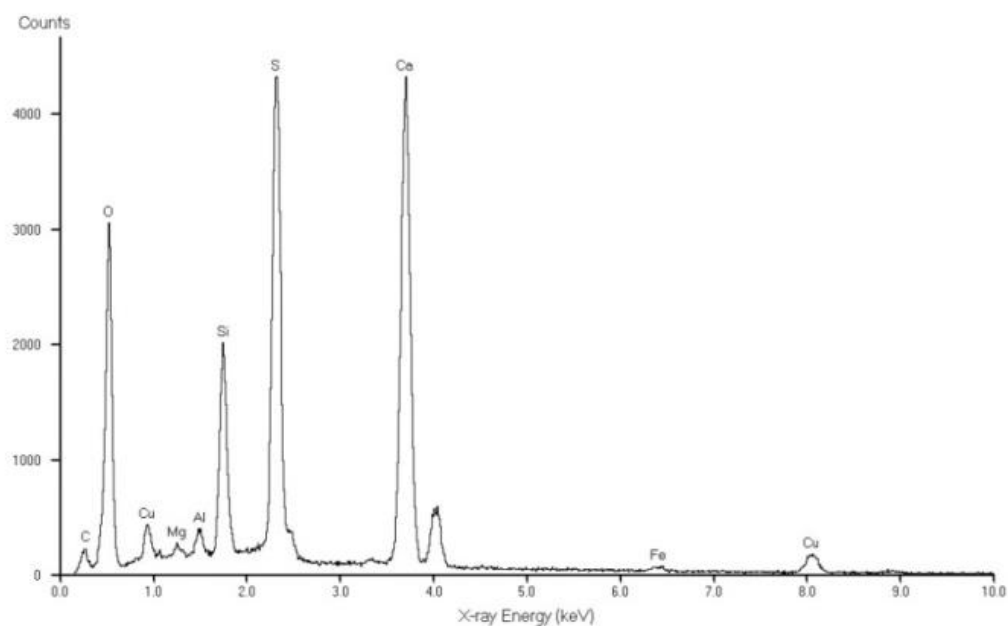
Figure 4.14. FIB EDS spectrum for the analysis of Spot 1 in Figure 4.13.   The spot is located in the slip coating adhering to sample E5 (UC 24685).
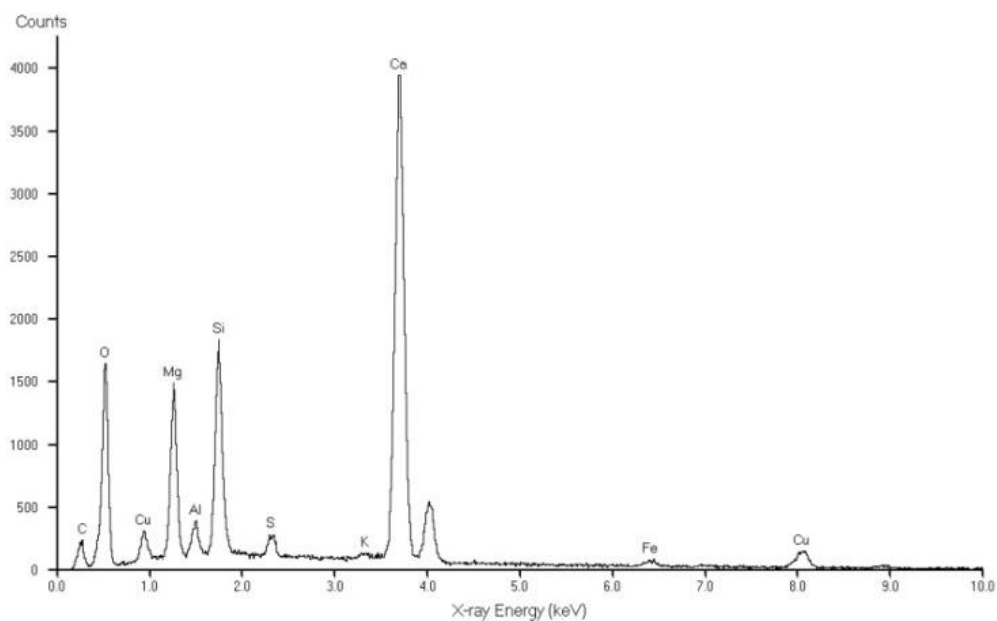
Figure 4.15. FIB-EDS spectrum for the analysis of Spot 2 in Figure 4.13. The spot is located in the slip coating adhering to sample E5 (UC 24685).
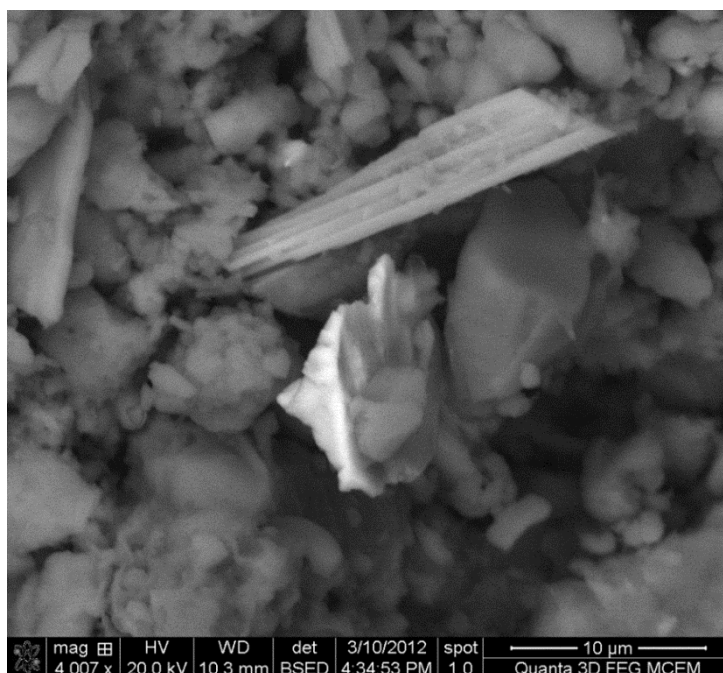
Figure 4.16. FIB BSE image of a hydroxyapatite particle and a bright metallic copper particle in the slip coating on the surface of sample E5 (UC24685). The silica and calcium accompanying this particle would suggest that it is from slag.

4.5.2.7 Lead

Table 4.8 provides the analysis for a copper-lead particle in sample E1 (A22/1/1966) probably adsorbed onto bone ash as shown by the high Ca and P_2O_5 analyses. The source of the lead cannot presently be determined. It may well have come from a trace of lead-bronze metal present in the bronze slag, or from a cupellation process and the cupel material recycled, but this is presently speculative. Other workers studying Egyptian blue have also reported the presence of lead in rare instances. Lucas (1989: 243) suggested that the principal Egyptian source of lead is Gebel Rosas.

Particles of lead were detected in cartonnage sample C17 obtained from the North Tomb 2. These particles were accompanied by high (up to 6.6%) potash, together with high sulphate and two of the particles contained high phosphate (up to 13.3% P_2O_5). The evidence does not suggest that the lead is adsorbed on to the hydroxyapatite, rather, the individual hydroxyapatite particles are directly adhering to the lead, indicative that they may have come from a related production cycle.

4.5.2.8 Cobalt

According to Tite *et al*. (1984), samples of Egyptian blue from Nimrud and Nineveh and also occasionally in samples from Egypt, contain cobalt at a concentration of 0.01-0.1%. They considered that at the concentrations observed that a maximum of 5% of cobalt blue glass could have been added to the Egyptian blue. Cobalt was not detected in any of the samples analysed.

4.5.2.9 Silver

The presence of silver in two Egyptian blue samples is indicative that these silver particles were derived from sampling contamination from the use of a diamond sampling tool as discussed in Appendix A3. Jaksch *et al*. (1983) reported that one sample of Egyptian blue from the 19th Dynasty tomb of Queen Nefertari contained inclusions of gold.

4.5.2.10 Chromium

EDS analysis revealed the presence of significant Cr_2O_3 (~5-16%) in samples E1 (A22/1/1966), E2 (A22/6/1966) and sample E4 (UC24684). Each reading was accompanied by the presence of very high iron concentrations. It is considered that it is likely that a chromium steel knife blade was used to remove the sample from the bulk material. The chromium in sample E1 was accompanied by nickel and high iron, indicative of contamination by stainless steel. Chromium, accompanied by high iron was also detected in sample E3 (A22/12/1966).

4.5.2.11 Titanium

Titanium, when present in the pigment is generally associated with the iron oxide. A particle within sample E1 is shown in Figure 4.6(d) and its analysis is provided in Table 4.8. This particle contains 79% TiO_2 and very low iron, indicative of rutile. The high reaction temperature used to form the Egyptian blue pigment would normally ensure that rutile would be the dominant mineral rather than brookite or anatase. However, no Raman signature for any titanium mineral was observed. Tite and Shortland (2003) in studying cobalt and copper-based blue frits suggested that in one copper-blue frit particle, highly contaminated by aluminium, iron and titanium oxides that these elements had diffused from the adhering ceramic vessel into the glass. In the present particle, generally alumina and iron are present as traces suggesting that the vessel was not the source for the titanium oxide particle. It is therefore hypothesised that the titanium was derived from the sand used as a raw material. The presence of titanomagnetite as an accessory mineral in desert sands was confirmed by Nicholson (2007: 119) and by Lee and Quirke (2000: 109).

4.5.2.12 Carbon

As discussed by David *et al*. (2001), amorphous carbon exhibits broad Raman bands at ~1340 cm^{-1} and ~1580 cm^{-1}.   Samples which exhibit only one band at ~1580 cm^{-1} and which is normally narrower in spectral band width is indicative of a highly crystalline ordered graphite. Samples which indicate different carbon bands would suggest that the carbon may have been derived from different sources. Some of the carbon could have been derived from soil contamination.

4.5.2.13 Arsenic

In addition to the arsenic adsorbed on to fluoro-hydroxyapatite particles discussed above, an Egyptian blue cartonnage sample C2 (Tomb 22) from Kellis 1 cemetery were found to contain arsenic; the arsenic concentration of 7.5% does not have any apparent other related mineral association. Its mineralisation has not been determined.

Chapter 4
                                                    Copper-based pigments
                                                    Egyptian blue and Egyptian green

4.5.3 Egyptian blue summary

The Egyptian blue mineral seen in the BSE images provided in Figures 4.4 to 4.6 and throughout Appendix A4 are of a flat tabular shape with a composition approximating that of cuprorivaite (refer Tables 4.9 and 4.10). Importantly, the presence of both metallic copper and bronze particles (data given in Table 4.8 and throughout Appendix A4) support the proposition that scrap metal oxide or slag from the manufacture of copper and bronze provided the copper source used in the manufacture of this pigment during the 18th Dynasty.   This is in accordance with previously published literature and discussed by Hatton (2008); El Goresy *et al*. (1986), and El Goresy (2000).

Examination of sample E1 (A22/1/1966(4)) using the high energy Synchrotron XFM beamline supports the evidence that elements with atomic numbers (Z) lower than calcium are present within the particle. The CuCaCompton composite image of the relevant maps shows the calcium is in the copper phase.   Compton scattering is inelastic scattering, and is useful to see where light (low-Z) elements are located (lighter elements = less self-adsorption), thus, relatively the scatter seems higher.   As shown in Figures 4.4, 4.5 (a) and (b), there are a number of rod-shaped inclusions of arsenic, approximately 10-20 μm long and about 2 μm wide.   Figure 4.6(g) and Figures 4.11 and 4.12 indicate that some of these arsenic-containing hydroxyapatite particles in other samples are up to 250 μm in length.

As reported by David *et al*. (2001), the Raman signature bands for cuprorivaite provided in Table 4.3, all of which are present in the samples examined. The band at 630/637 cm^{-1} can be ascribed to cassiterite; at 430 cm^{-1} to tridymite; 465 cm^{-1}to α-quartz; and the bands at 637 and 971 cm^{-1} to β-wollastonite.   The EDS analysis confirms the average sample composition to closely match that of the theoretical analysis for cuprorivaite, generally having an average normalised CuO concentration of 19.3% against a theoretical concentration of 21.15%, CaO concentration of 14.3% against a theoretical concentration of 14.92% and a slightly higher SiO_2 concentration of 66.4% against a theoretical concentration of 63.93%. These minor differences can be explained from the presence of non-cuprorivaite derived matter on the surface of the particles thereby acting as a modifier. Carbonaceous matter, particularly graphitic carbon is present in most samples as shown by their Raman bands. Carbon is deleted from all analytical results. Other elements present at a significant concentration include alumina, soda, iron and tin as shown in Figure 4.17.
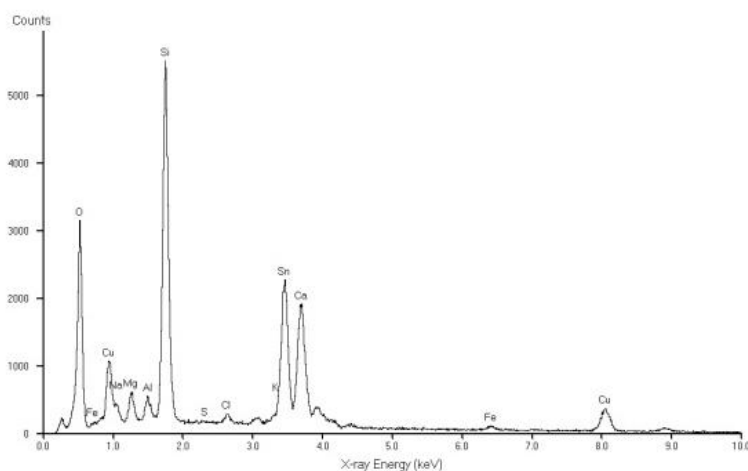
Figure 4.17. EDS spectrum of Egyptian blue sample E1 (A22/1/1966) and similarly in Figures A4.E1.33 and A4.E1.66 indicative of a bronze particle as shown by the high Sn peak.

As noted by Hatton *et al*. (2008), the principal distinguishing feature for Egyptian blue is the bulk copper oxide content exceeding that of the bulk lime to give a CaO/CuO ratio in the range of 0.6 to 1.0. The present research as provided in Table 4.11 supports this outcome.

The CaO/CuO ratio of an average of 0.7 provided in Table 4.11 is similar to that for the faience samples as reported by Hatton *et al*. (2001). Pagès-Camagna and Colinart (2003), confirmed that the bulk CaO/CuO ratio is about 0.7 and the SiO_2/CuO is approximately 3. As shown in Table 4.11 the present research is in good agreement, providing averages of approximately 0.8 and 3.6 respectively and confirm that all Egyptian blue samples contain a greater concentration of copper than calcium (refer Table 4.6).

Noll and Hangst (1975) observed that Egyptian blue is normally relatively coarse in particle size, namely 5-50 µm and therefore can only be applied in thick layers. As shown in Figures 4.5 and 4.6 and throughout Appendix A4, all samples are highly variable in particle size approximating that described by Noll and Hangst.

The plot provided in Figure 4.18 of the elemental oxide ratios of copper to calcium and to silica for the Egyptian blue samples analysed fit a tight envelope indicating that a reasonably constant batch to batch raw material formulation was maintained at the various sites at which this pigment was made. The outlier sample number 2 is turquoise in colour with a calcium oxide percentage of 18.3% is higher than the copper oxide percentage at 11.3%. The other outlier is M8 (M73/K/1406) (Sample 13) and in this instance, the highly variable analyses results from the micron-sized residual pigment remaining on the sherd significantly reducing the analytical reliability. Thus, the residual size of generally < 20µm made it difficult to comment upon the shade of blue in either of the two Malkata sherds. Malkata sample M7 (M73/K/5) (Sample 12) contained a very high magnesium concentration of 16.8% (37% MgO in white surface coating), indicative of probable contamination of the cuprorivaite by the substrate.
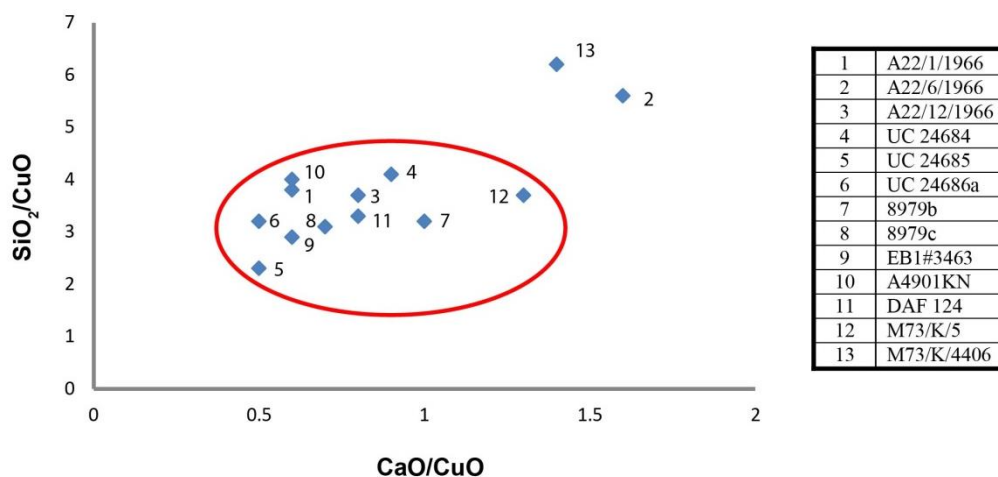
Figure 4.18. Plot indicating the effect of variation in the ratio of reactants within Egyptian blue. The outlier samples 13 and 2 both indicate a turquoise shade of blue. (Note that sample 9 in the identifying sample table is renumbered to #3463 and sample 13 is now renumbered as M73/K/1406 in accordance with the sample number in Hope (1980).) Samples 2 and 12 are significantly higher in magnesium than other samples analysed.

4.6   EGYPTIAN GREEN

Only aspects specifically relevant to Egyptian green pigments and not discussed in respect of Egyptian blue will be discussed in this section.   "Green Earths" and green minerals such as malachite when used as pigments are discussed in Chapter 3. The raw data is provided in: https://drive.google.com/drive/folders/0B1MXnIeNTO4icGV6dTFSaXhOQU0?usp=sharing
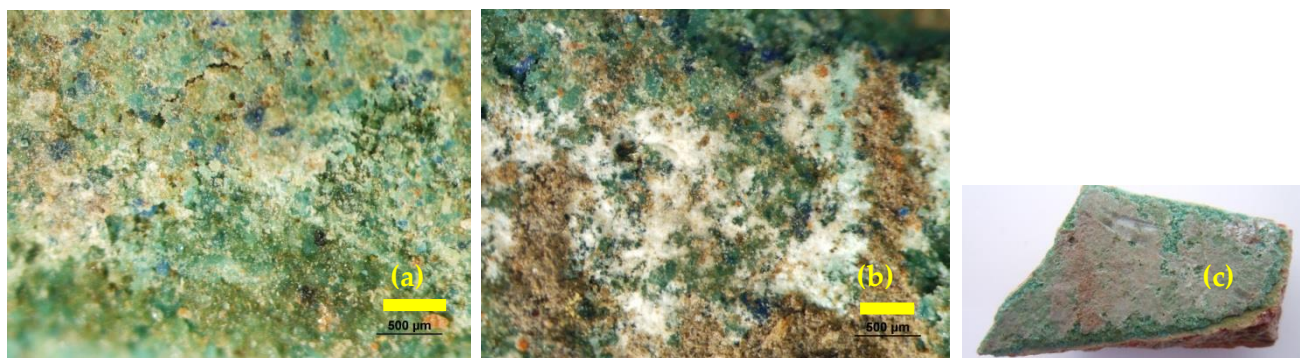
Figure 4.19. Surface of sherd M1. Note the occasional blue crystal. The white slip is clearly visible in (b). The yellow scale bar is 500μm. (c) Sherd M1 coated with Egyptian green, beeswax overcoated.

Egyptian green was also examined from a sample derived from the Main Temple, D/2 Shrine 1 vault,   Kellis and is discussed in Chapter 3.

4.6.1   Mineralogy

It has been postulated that Egyptian green was synthesised soon after the discovery of Egyptian blue (Pagès-Camagna and Colinart 2003).   These researchers reported that Egyptian green is characterised by the presence of parawollastonite crystals smaller than 10μm and residual silica (quartz and/or tridymite or cristobalite) embedded in an amorphous, silica-rich glass phase. They also observed firing residues of tenorite, which they proposed indicated that this pigment was synthesised under oxidising conditions, because under reducing conditions red cuprite would have formed.   Tin was found, the form of which was unable to be identified by these workers; they suggested that it was present either as cassiterite or as an unidentified Ca-Si-Sn complex (60% SnO_2, 20% SiO_2 and 19.6% CaO), which is structurally different from malayaite as discussed by Groat *et al.* (1996).

Thus, Egyptian green is obtained by modification of the proportions of the compounds (Ullrich 1987; Le Fur 1994; Schiegl *et al.* 1989), or by variation in the firing conditions, namely temperature and atmosphere in the furnace (Ullrich 1987; Jaksch *et al*. 1983; Noll and Hangst 1975) or by temperature and the quantity of the added flux (Pagès-Camagna and Colinart 2003).

Noll and Hangst (1975) first identified Egyptian green as a distinct pigment rather than a decomposition product. Subsequently, El Goresy *et al*. (1986) and Tite (1987) established that the Egyptian green pigment contained a higher calcium content relative to the copper content and that the alkali was normally greater than that found in Egyptian blue pigments. And, Hatton *et al*. (2008) stated that the bulk copper oxide content of Egyptian blue is normally greater than the bulk

lime contents whereas the bulk lime contents of the green frits are greater than the bulk copper oxide contents.   Thus the Egyptian blue CaO/CuO ratio is in the range 0.6-1.0 and for Egyptian green the CaO/CuO ratio is >1.8.   These researchers state that they found two exceptions to this 'rule' being samples AM4 and AM9 (both from Amarna) and which are discussed in Section 4.6.4. Since the lime contents of Egyptian blue (11-13% CaO excluding the two contaminated residues) and green frit (8-24% CaO) overlap, the change from producing Egyptian blue to Egyptian green was therefore most probably achieved by reducing the copper oxide in the recipe.

Pagès-Camagna *et al*. (2006) conducted a series of syntheses and suggested that both pigments can be obtained by heating a mixture of silica, calcium carbonate, copper and a sodium salt to temperatures between 870 and 1100°C for 15 – 72 hours. The green pigment was prepared by heating the same raw materials but in different proportions and at higher temperatures of between 950 and 1150°C.   Furthermore, the colour of the synthesised product was influenced by both temperature and the added flux.

Thus, whilst Egyptian blue and Egyptian green can be considered to be two different pigments, they share many common features, primarily that both pigments were produced from the same raw materials and under similar firing conditions. Thus, much of the applicable mineralogy has been discussed in Section 4.5 and will not be repeated within this section.

4.6.2 Egyptian green colour development

Pagès-Camagna and Colinart (2003) indicated that they were of the opinion that Kaczmarczyk and Hedges (1983) and Le Fur (1994) were incorrect in suggesting that the colour could have resulted from the presence of iron coming from the sand used in the pigment production; or that the colour is generated by the weathering of Egyptian blue. This suggestion was discounted on the basis that degradation of Egyptian blue leads to the formation of copper chloride or copper carbonates as discussed by Schiegl *et al*. (1992). Others have considered Egyptian green to be a pale Egyptian blue or even considered to be a misfired Egyptian blue (Tite 1987; Weatherhead and Buckley 1988: 208; Pagès-Camagna 1998).

If the CaO concentration exceeds that of the CuO, the excess calcium precipitates from the glass typically as wollastonite (calcium silicate) and the remainder of the copper remains dissolved in the glass to produce the turquoise/pale blue colour. As reported by Tite *et al*. (1998) turquoise/pale blue pigments were also produced if the alkali flux concentration in Egyptian blue was increased from the usual concentration 0.4-2.4% Na_2O to 5-7% Na_2O. And, Weatherhead and Buckley (2008: 206) reported that the most significant difference between Egyptian blue and the turquoise variant is the relatively high sodium content of the latter: (they incorrectly reported that elements higher than sodium cannot be determined by SEM-EDS analysis).

According to Pagès-Camagna and Colinart (2003), a series of Egyptian green samples were analysed by XAFS (X-ray Absorption Fine Structure) analysis. They established that four oxygen ions are around the Cu^{2+} ions at 1.82Å and two others at 2.29Å in a distorted octahedral site. These results are consistent with the work of D'Angelo *et al*. (1979) for second neighbours and support the work of Nakai *et al*. (1999) in respect of copper ions in glasses. The green colour results from the copper ion being in this octahedral configuration in the silica-rich glass phase. In Egyptian

blue the copper is in a square planar structure in the cuprorivaite and therefore blue. Thus copper can produce different colours even when in the same oxidation state. Furthermore, as has been demonstrated, divalent copper ions and not divalent iron ions create the colour. Raman spectra are all consistent with the reference spectrum for β-wollastonite, and the Raman spectrum does not allow β-wollastonite and cuprowollastonite to be distinguished from each other. According to Bianchetti *et al*. (2000) the Egyptian green owes its colour to the Cu-wollastonite. Whereas, at Karnak, these authors reported that the green pigment is chrysocolla.

4.6.3 Egyptian green and Egyptian blue colour deterioration

As described above, the disastrous and well advanced deterioration of Egyptian blue and green pigments has been investigated in detail. One explanation given is that the process commences with the devitrification of copper- and chlorine-bearing glass and glaze. The copper ions leach from the glass and basic copper chloride (atacamite or paratacamite) forms and then precipitates by the reaction of these solutions with the calcium carbonate in the stucco or plaster base on to which the pigment was originally applied, or from vaterite or calcite formation during burial. This reaction alters the original shade of blue to a faint green. The process leads to the development of highly friable and spongy pigment layers resulting in their disintegration, denudation and ultimately final destruction (Schiegl *et al*. 1989; 1992).

Lau *et al*. (2008) noted that in the literature it is suggested that Egyptian blue degrades to green by either of two mechanisms. In the first, the original blue colour may change to a faint green as copper ions are leached out and combine with chloride ions and calcium carbonate forming the basic copper chlorides atacamite and paratacamite. The second mechanism described instances where the organic binding medium around Egyptian blue had darkened or yellowed sufficiently altering the appearance of the blue to a green colour. Lau artificially aged Egyptian blue using HCl and then examined the degraded product by XRD and showed that atacamite, copper chloride hydroxide hydrate and eriochalcite formed. Baraldi *et al*. (2001) suggested that a weak Raman band at 222 cm^{-1} is attributable to $CuCl_2$. Other suggested minerals include lithiodionite, effenbergite and dioptase. Pavlidou *et al*. (2008) reported the formation at Abydos of calcium oxalate in Egyptian blue resulting from bio-oxidation.

Deterioration can also be influenced by lichen surface attack. As shown in Figures 4.20 and 4.23(d), weddellite (calcium oxalate dihydrate) and metastable hydrated calcium oxalate (whewellite) are present in Sample W4, Egyptian green decoration applied to the wall of the Main Temple, Kellis, D/2 Shrine 1 vault. The presence of calcium oxalate monohydrate is identified by its strong Raman bands as provided in Table 2.23, Appendix A2. The bands at 896 and 504 cm^{-1} are indicative of weddellite. Thus, an equilibrium exists between the stable and the metastable forms of calcium oxalate at this site. Furthermore, the presence of the hydrated calcium oxalate in the sample is attributable to lichen invasion, whose hyphae penetrate the calcareous substrates to form complexes with the oxalic acid secretions from the mycobiont. CH-stretching modes characterised by Raman bands in the region of 2935 cm^{-1} (and strongly visible in Figure 4.20) support the assignment of these features to a biological source (Giordani *et al*. 2003; Edwards and Farwell 2008: 990; Castro *et al*. 2008). Egyptian green, anhydrite, traces of feldspar, wollastonite, kinoite, calcium carbonate, traces of atacamite and amorphous carbon are present in the pigment. The presence of tin in the elemental analyses indicates the use of bronze material as the copper source.

Chapter 4
          Copper-based pigments
Egyptian blue and Egyptian green
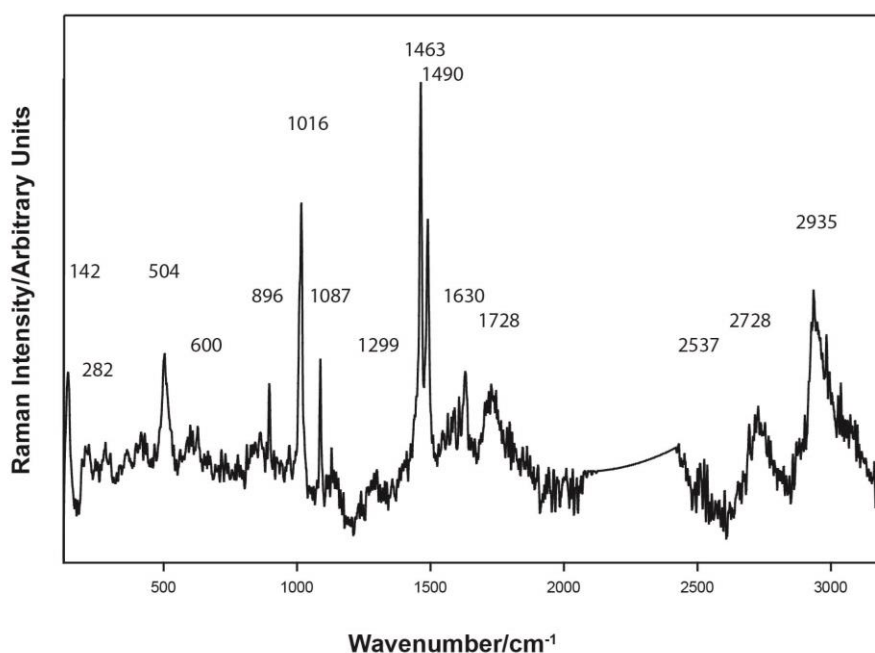
Figure 4.20. Raman spectrum, green pigment, wall decoration decomposition of sample W4 showing the presence of calcium oxalates ($\lambda = 514.5$ nm).

4.6.4   Egyptian green results and discussion

All supporting data in respect of this chapter is provided in Appendix A4. Only specific data which is considered necessary to assist in the understanding of the mineralogy and application of these green pigments to substrates is provided herein.

According to Pagès-Camagna *et al.* (1999), white grains are always associated with turquoise grains. This is evident in sample M1 as shown in Figures 4.19(a) and (b). However, the crystal size of the residual Egyptian green on sample M7 is too small to enable an objective comment to be made. These white grains were reported by Pagès-Camagna *et al.* (1999) to be present in seven cakes of Egyptian green excavated from an 18th Dynasty site in the village of the craftsmen who built the royal graves near Karnak. In studying these samples, Pagès-Camagna *et al.* (1999) observed that the hues of two samples varied from shades of blue to turquoise indicative that the raw materials may have been poorly blended.

Ambers (2004) and also Lau *et al.* (2008) reported that they were unable to obtain a satisfactory Raman signature for Egyptian green. Neither worker indicated the wavelength of monochromatic light source used in the particular spectrometer each of them employed. However, Pagès-Camagna *et al.* (1999) and as shown in the present work, successful spectra were obtained by employment of the 514.5 nm green laser.

Cristobalite was only detected by Pagès-Camagna *et al* (1999) in a few areas within the seven Egyptian green samples they analysed.   Cristobalite was not detected in the sherds under investigation, however, tridymite was normally present. This would indicate that the temperature was not the prime reason for the development of the green appearance. Rather, its colour was

developed from the octahedral structure formed at a lower temperature. However, the presence of the high sodium and calcium in these samples would have significantly lowered the melting point of the mix, making it difficult to predict the actual upper temperature reached.

It was proposed that <7% total flux leads to tridymite formation and 8% or more flux is required for cristobalite formation (Pagès-Camagna and Colinart 2003). These researchers also proposed that the copper content in this glass phase is influenced by both temperature and cooling time. Soda flux decomposes around 760°C and forms a eutectic with quartz. Ion diffusion is made easier and Cu(II) ions will diffuse into this phase and create the green colour. At about 950°C, Ca(II) ions form at the interface between the amorphous coatings. The crystallisation of parawollastonite through precipitation presents a higher nucleation rate than its growth rate which increases with time, the crystal size never exceeding 10 μm in width. Pagès-Camagna and Colinart (2003) explained this selective ionic diffusion to the relative ionic radii of the Cu^{2+} (0.63Å) and Ca^{2+} (1.0 Å) respectively.

Hatton *et al.* (2008) reported that the bulk copper to lime ratios in Egyptian green are greater than 1.8. The present research provided a CaO concentration of 18.3% and a CaO/CuO ratio of 1.6 for the turquoise-appearing Amarna sample A22/6/1966, closely matching the Hatton ratio for Egyptian green.   Hatton *et al*. (2008) also reported that two of the samples from Amarna which they examined (AM4 and AM9) were contaminated by lime (analyses of CaO of 16.7% and 14.0%) from the substrate and provided ratios of 1.5 and 1.8 respectively. Hatton *et al*. (2008) did not provide elemental analyses for phosphates or sulphates. Therefore, their assumption that the CaO contamination on the substrate was lime, is questionable and could have alternatively been from an insoluble mineral such as gypsum, hydroxyapatite or whitlockite. Without the elemental analyses for sulphates and phosphates or a mineralogical determination, it cannot be established if in fact bone ash, thénardite or gypsum was the cause for the reported contamination.

Hatton *et al*. (2008) reported that in their analyses of Egyptian green from Amarna that the CaO/CuO ratios were >1.8. In the present research, as provided in Table 4.11, similarly high CaO/CuO ratios were observed for the turquoise appearing Amarna sample A22/6/1966 and the two Malkata samples M73/K/5 and M73/K/1406.

Jaksch *et al*. (1983) examined pigments collected from the Amarna tombs. They eliminated the glass and the copper wollastonite particles from his analyses. Thus, without an actual percentage of each phase being given it is not possible to compare their results with those obtained in the present work. Suffice to say, Jaksch reported much higher calcium (average 45.2% CaO), lower copper (1.6% CuO), and silica (52.4% SiO$_2$) in the copper wollastonite fraction within their pigment sample analysis.

All of the samples examined by Pagès-Camagna and co-workers were heterogeneous with a mixture of amorphous and crystalline phases and in some instances several crystalline species are embedded in the amorphous matrix. Figure 4.19(c) demonstrates a similar occurrence with the Egyptian green applied to Malkata sherd M1. Blue crystalline phases are recognised in both samples M1 and M7 as shown by their Raman spectra in Figures 4.21 and 4.22. This conclusion is drawn from the Raman bands at 431 and 1086 cm^{-1}, indicative that at least some of these isolated blue crystals have the composition of cuprorivaite. Egyptian blue crystals were intermixed with

the predominantely Egyptian green pigments in Malkata samples M1 and M7. This is in agreement with the work of Ullrich (1987).

Pagès-Camagna *et al*. (1999) reported that the stoichiometry is the same for all microcrystals and is close to that of a calcium silicate (wollastonite) containing approximately 2% Cu. And, the Raman spectra for the pigments were consistent with the reference spectrum of β-wollastonite. Furthermore, Raman spectroscopy was unable to distinguish between β-wollastonite and cuprowollastonite. In the present study, low copper analyses were generally associated with either high sulphate or high iron particles as shown in the EDS-SEM spot analyses given in Appendix A4, Figure A4.M1.19, Spot 3 and Figure A4.M1.33, Area 1. Importantly, Figure A4.M1.19 indicated that some 30.2% As_2O_3 was associated with 46.3% SO_3 indicating that the particle is most likely orpiment, realgar or pararealgar, probably resulting from sample contamination.

In each sample examined by Pagès-Camagna *et al*. (1999) and which is included in a table by Hatton (2008: 164/5), the calcium concentration was greater than the copper concentration together with metallic elements including copper and tin. This is also demonstrated in Table 4.17.

Table 4.17. EDS analyses of the principal elements present (wt. %) in the various samples analysed.

Element	A22/6/1966	M1	M7	W4	Hatton (2008:164)
CaO	18.3	17.5	26.7	22.1	13.5
CuO	11.3	8.0	10.5	32.3	5.2
SiO_2	63.8	49.2	11.8	11.0	73.1
SO_3	0.6	3.0	9.9	13.6	
MgO	0.1	2.3	26.4	1.8	
SnO_2	-	tr	-	3.6	
As_2O_3	-	tr	variable 0-12	-	

The high MgO concentration can be directly attributed to the huntite substrate on which the Egyptian green had been applied (refer to the Raman spectroscopy results provided in Figure 4.22). And, the high SO_3 concentration would have been derived from the gypsum forming part of this slip coating.

Table 4.18. Element oxide ratios applicable to the samples analysed.

Ratio	A22/6/1966	M1	M7	W4	Hatton (2008: 164)
CaO/CuO	1.6	2.2	2.5	0.7	2.6
CaO/SiO_2	0.3	0.4	2.3	2.0	0.2
SiO_2/CuO	5.6	2.8	0.4	0.5	5.4
Na_2O+K_2O	3.3%	6.8%	2.4%	2.2%	1-11%
MgO	0.1%	2.3%	26.4%	1.8%	bld-6.1%

Other than for sample W4, the bulk copper oxide concentrations as provided in Table 4.17 are lower than the associated calcium oxide. This is reflected in the CaO/CuO ratios being >1.6. It is

understood that the wall decoration from which sample W4 was obtained is from the Roman period. However, the presence of lead was not detected in this sample, as might have been expected; tin bronze scrap having been employed. The high copper analysis combined with the high sulphate in W4 could suggest the presence of a copper sulphate mineral such as langite. A Raman signature for this mineral was not detected. Furthermore, the high chloride concentration, coupled with the detection of traces of atacamite would indicate that the reaction of the chlorine and copper described in Section 4.6.3 and its subsequent precipitation on the wall surface would have increased the apparent copper concentration. Note that the SEM-EDS analysis is obtained from the surface of the sample, an area in which the copper could be elevated by chemical reaction as described. The Raman spectra for the Egyptian green pigment W4 is provided as Figure 4.23. The element oxide ratios are provided in Table 4.18 and compared with the Hatton *et al.* (2008: 164) results; and the average analysis of Malkata Sample M1 is provided in Table 4.19.

Table 4.19. Average SEM-EDS elemental analyses (wt. %) of various green crystals obtained using the FIB electron microscope.

Element Sample	Elemental analysis													
	Na_2O	MgO	Al_2O_3	SiO_2	P_2O_5	SO_3	Cl	K_2O	CaO	TiO_2	MnO	FeO	CuO	SnO_2	As_2O_3
M1	6.7	0.9	2.6	31.1	0.2	1.9	1.9	0.7	21.2	0.2	tr	1.1	12.6	0.5	6.3

CaO/CuO = 1.73; SiO_2/CuO = 2.46

4.6.4.1 Alkali flux

As provided in the electron microscopy data in Appendix A4, Sample M1 and Sample M7, almost all of the flux has been derived from soda. Almost no potassium is present in the analyses conducted upon either sample M1 or M7 and much, if not all of the potash could potentially be accounted for in the analyses by the presence of various feldspars. The potential for potash to preferentially leach with respect to soda under burial conditions needs to be considered in this context. The evidence however, would strongly suggest that the flux has been derived primarily from trona (natron), probably as burkeite. However at the firing temperature between 900-950°C, the carbonate would have been lost.

Hatton *et al.* (2008) stated that in their analyses, the bulk soda contents of samples from Amarna are up to 6.5% Na_2O in Egyptian green. They reported that their samples AM5, AM6 and AM7 have been contaminated by the substrate as shown by their higher alumina concentration. And, according to Pagès-Camagna and Colinart (2003), Egyptian green pigment has a higher flux concentration (Na_2O + K_2O) of between 5.7% and 10% due to the presence of a silica-rich amorphous phase. In the present research, only Malkata M1 exhibited a high total alkali flux concentration, and supported this proposal, the remaining samples analysed contained between 2.2 and 3.3% total alkali as provided in Table 4.18. Furthermore, the bulk CaO/CuO ratio is always above 1.7 and the SiO_2/CuO is >4. Copper is thus much less abundant in Egyptian green than in Egyptian blue. Tite (1987) reported similar results for a material described as 'pale blue frit'. Raman spectroscopy detected tridymite in Malkata M1 but not in sample M7.

4.6.4.2 Silica polymorphs with respect to Egyptian green

Quartz sand, rather than crushed pebbles were considered to be the source of the silica. An increased amount of tridymite has been found in Egyptian green. And, at temperatures above 950°C tridymite appeared to be the most important crystalline phase; and in all samples fired to 950°C, quartz was the dominant crystalline phase. At temperatures of 1050°C, cuprorivaite transforms into Egyptian green. The heating procedure and mixture composition affect the appearance of wollastonite, a mineral always detected in Egyptian green. At 850°C, wollastonite was detected in mixtures containing a lower Cu/Ca ratio; at higher temperatures heating to 1050°C did not allow the formation of wollastonite. When hematite was present it acts as a catalyst and regardless of the copper concentration, wollastonite was formed.

The Raman bands for cristobalite and tridymite as provided by the RRUFF database are shown in Tables 2.22 and 2.23, Appendix A2. Bianchetti *et al*. (2000) indicated that at temperatures below 950°C, quartz was the dominant mineral, and above 950°C a greater concentration of tridymite was reported in Egyptian green in accordance with published phase diagrams. They also considered that the critical temperature was around 950°C, a temperature where impurities and kinetics could both play a decisive role. In the samples examined by Pagès-Camagna *et al*. (1999) the cristobalite is present in too small a concentration to be detected by XRD but was detected when using Raman spectroscopy. These researchers then stated that the presence of cristobalite is not a reliable temperature indicator because the high sodium and calcium present in Egyptian green will decrease its formation temperature. According to Pagès-Camagna and Colinart (2003), some samples showed the formation of gehlenite which would have formed at approximately 900°C and that cristobalite was much more prevalent than tridymite, generally co-existing with quartz.

4.6.4.4 Copper and tin with respect to Egyptian green

The tin concentration in Malkata sample M1 is reported as a trace, being <0.5% and which is in conformity with Amarna samples of <0.3% reported by Hatton *et al*. (2008: 172). The CaO/CuO ratio reported is >2.0 for Egyptian green. The present work indicates a ratio of 1.6 for sample E2 and 2.2 and 2.5 for samples M1 and M7 respectively. However, Hatton (2008: 172) reported that because of weathering and possible burial contamination the differences in the CaO/CuO ratios are less clear-cut.

Tenorite was observed in variable amounts when cuprite or malachite together with carbon black was used as the copper source. This would suggest that the carbon did not ensure reducing conditions. Thus, Bianchetti *et al.* (2000) showed that the same constitutive materials by control of temperature and fluxes, either Egyptian blue or green frit may be produced. And, the massive silica-rich areas are always α-quartz. The crystals lose their angular aspect and are surrounded by an amorphous zone around 50 μm thick, which becomes green. At higher temperatures, rounded quartz disappears, to be partially or totally replaced by acicular crystals which are about 20 μm long. Above 1050°C, and with slow cooling, new silica structures with a dendritic morphology are created. At 950°C, acicular crystals, either tridymite or α-cristobalite formed and which were able to be determined by micro-Raman spectroscopy; however, Pagès-Camagna and Colinart (2003) failed to provide Raman data to support this statement.

Table 4.20. Minerals located within Malkata samples M1 and M7.

Mineral	Formula	Wavenumber (cm⁻¹)	Sample M1 Raman signature (cm⁻¹)	Sample M7 Raman signature (cm⁻¹)
α-quartz	SiO_2	128, 357, 402, **464**, 1084, 1160	129, 359, 403, **464**, 1084	
tridymite	SiO_2	**209, 301, 351, 435**, 575, 790, 1071	356, **431, 572**, 790	
parawollastonite	$CaSiO_3$	322, 337, **637, 971**, 1045	322, 337, **638, 971, 1046**	**631, 977**
anhydrite	$CaSO_4$	**1018**, 1163	1017	**1017**
gypsum	$CaSO_4.2H_2O$	**1007**	**1006**	
aragonite	$CaCO_3$	**1084**	**1085**	**1087**
ferricopiapite	$Fe^{3+}_{2/3}Fe^{3+}_4(SO_4)_6(OH)_2.20H_2O$	268 301, 451, **479, 993, 1019**, 1147	480, 993, 1017	
langite	$Cu_4SO_4(OH)_6.2H_2O$	235, **431, 968/971**	234, **430**, 969/**971**	
jarosite	$KFe^{3+}3(SO_4)_2(OH)_6$	**223, 299, 434, 624, 1007,**1102	224, 298, **626**, 1103	420, 621`, 1002, 1106
cassiterite	SnO_2	**634**, 776	631	631, 776
malayaite	$CaSnO(SiO_4)$	**323, 465, 573**	322, **465, 572**	
graphitic carbon	C	**~1360, ~1600**	**1360, 1600**	**~1350, ~1590**
SLIP				
huntite	$CaMg_3(CO_3)_4$	**1125**	**1132**	**1122**
burkeite	$Na_4(SO_4)(CO_3)$	995, **1063**	**993, 1063**	
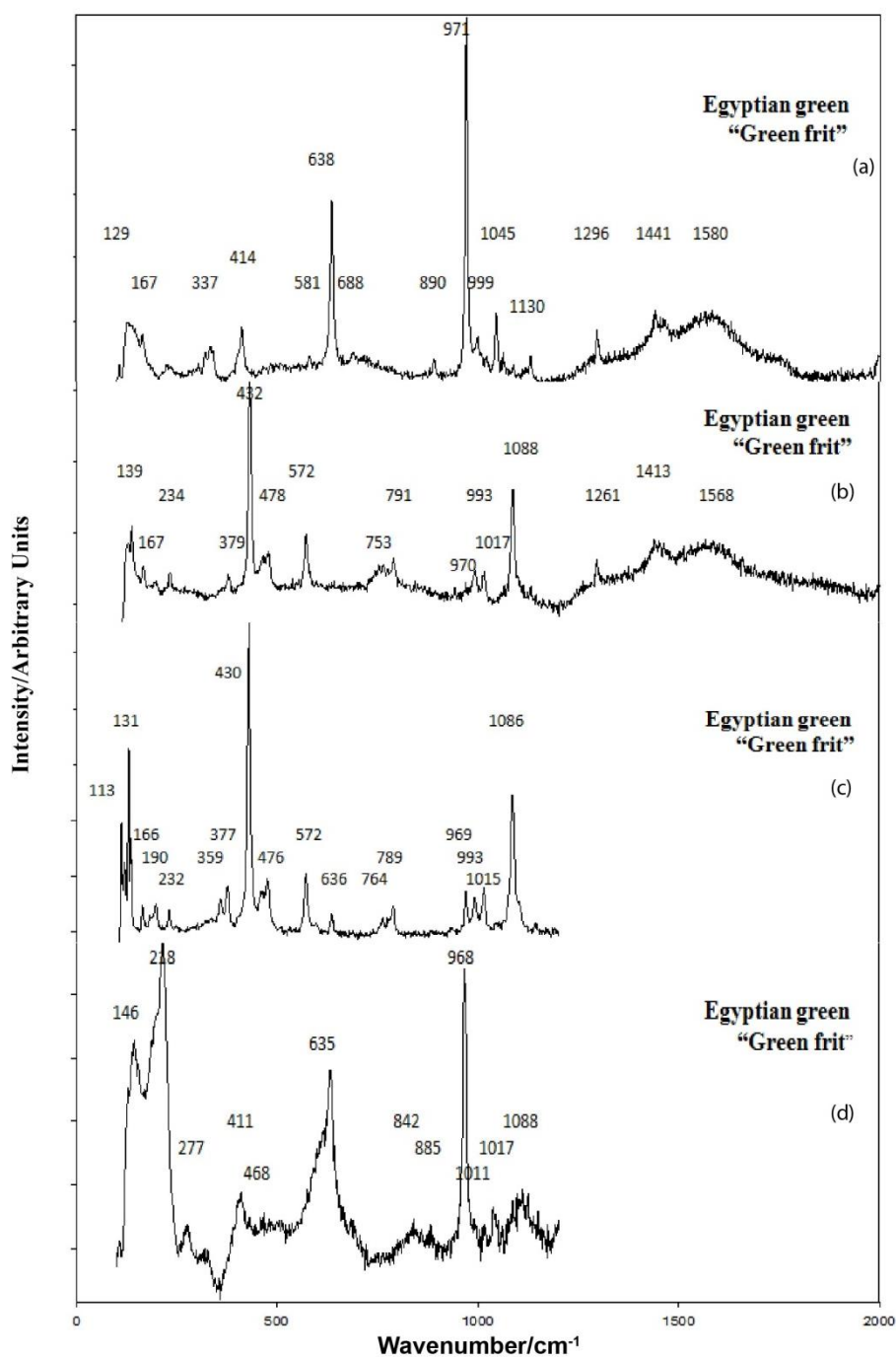
Figure 4.21. Raman spectra for Egyptian green pigment in Malkata sample M1 (λ = 514.5nm). The number of crystals all exhibiting various pigment shades are clearly evident in this and the accompanying two figures.
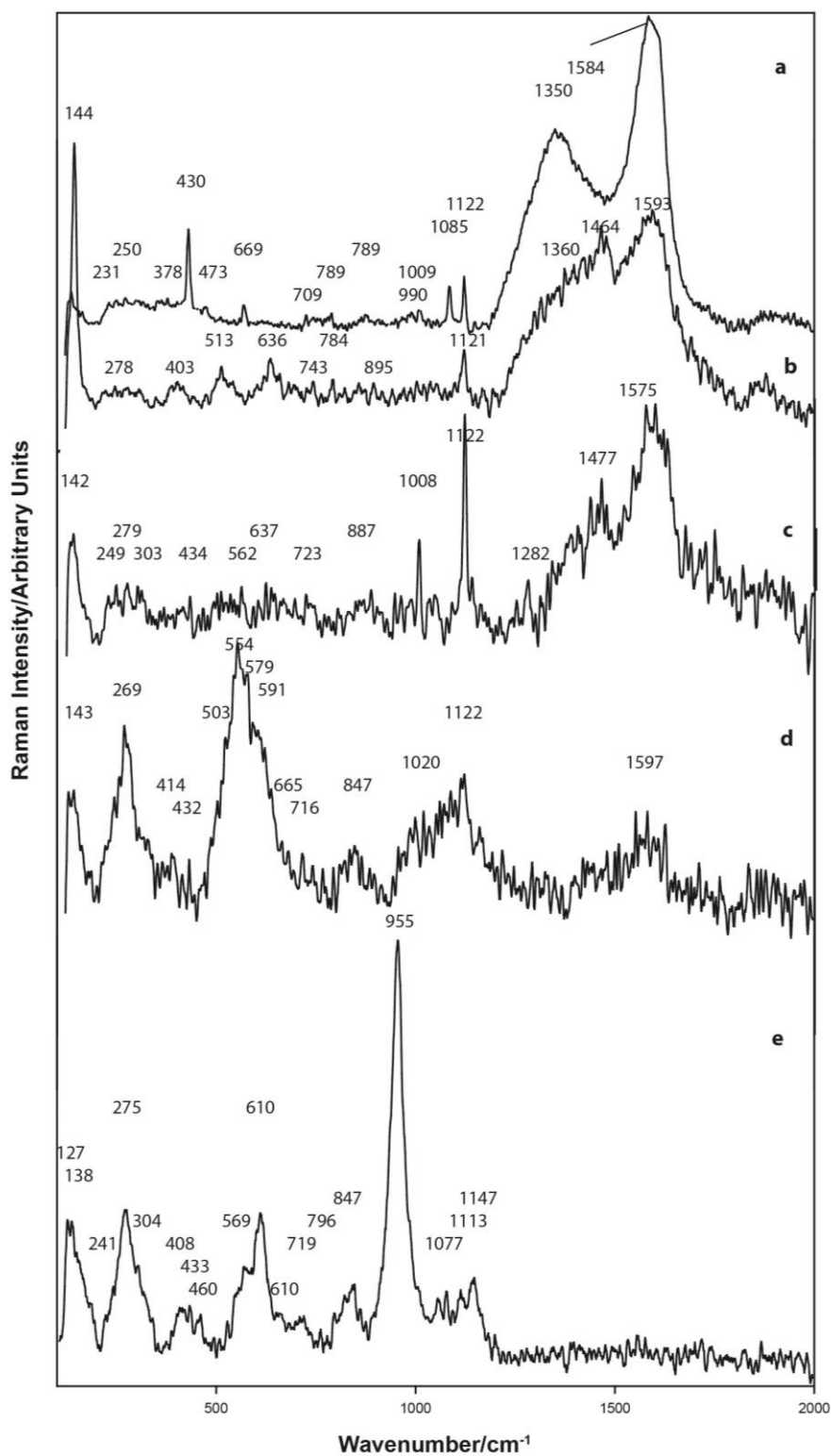
Figure 4.22. Raman spectra, residual Egyptian green pigment on the surface of Malkata sherd M7. (a) indicates the presence of traces of Egyptian blue within the green pigment. The band at 1122 cm^{-1} shows the presence of huntite. Gypsum, wollastonite, amorphous carbon and feldspars are detected. The strong band at 955 cm^{-1} is either an apatite or more likely, vivianite [$Fe^{2+}_3(PO_4)_2.8H_2O$] as indicated by their additional Raman bands.
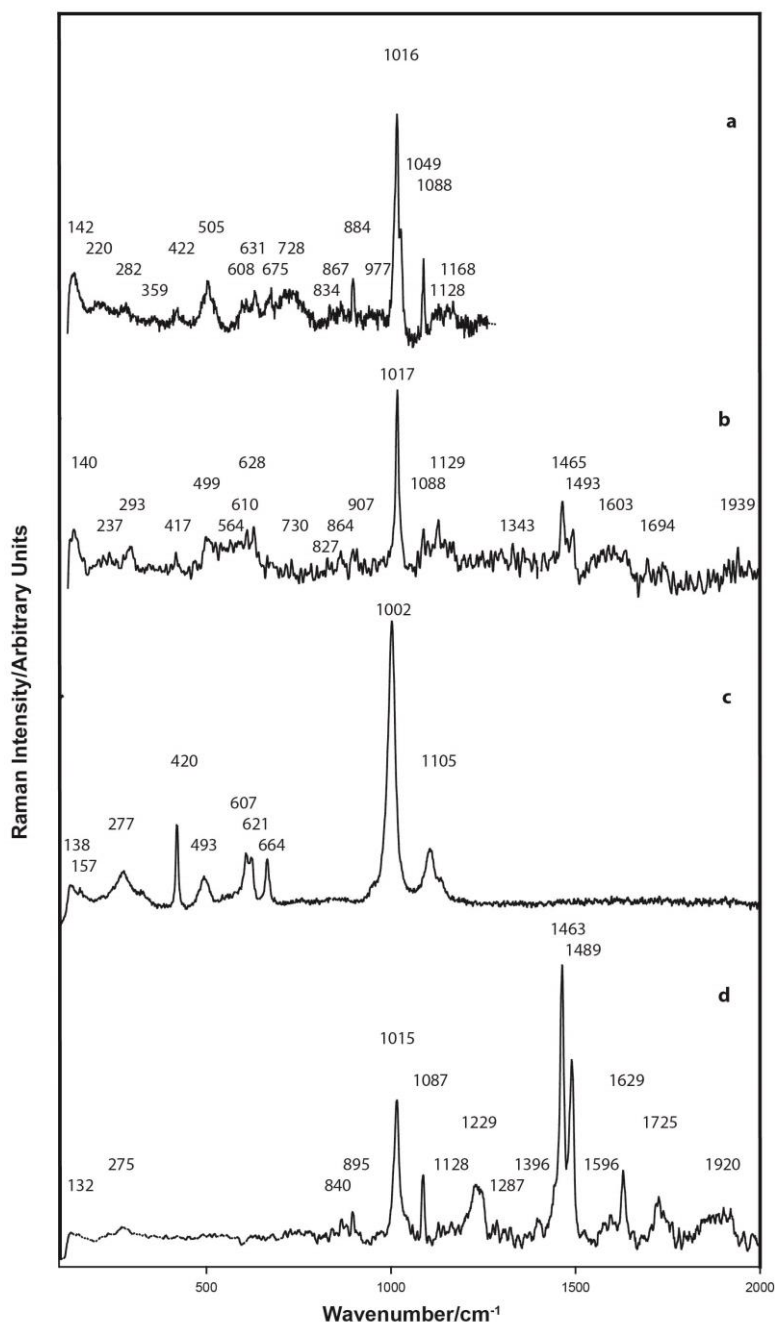
Figure 4.23. Raman spectra, green pigment on wall decoration, sample W4 (λ = 514.5 nm). The organic Raman bands at 1463 and 1489 cm^{-1} are discussed at Section 4.6.3.

4.6.4.5 Organic binder or coating

As provided in Figure 4.24, Table 2.22, Appendi8x A2 and Table A4.M1.1 in Appendix A4, beeswax has been clearly identified as the binder to fix the Egyptian green to the white slip applied to the surface of Malkata sample M1. Mackay (1920) discussed the use of wax and reported that its use as a fixative in tombs was limited to the 18th Dynasty from the time of Amenhotep I to Amenhotep II (c. 1525 -1400 BCE). He reported that the melting point of the wax was 64°C and as the MP of beeswax was 61 – 64°C he indicated that it was probable that beeswax was used.   The Raman spectrum precisely matches that of the spectrum

provided by Burgio and Clark (2001) indicating that the binder is certainly beeswax and therefore this Malkata sample, from the reign of Amenhotep III post-dates the time period suggested by Mackay (1920). The suggested source for the beeswax was by importation from the Sudan (Mackay 1920). As an addendum to the article by Mackay, the use of wax may be seen, mixed with a dark green colour as a filling of the hieroglyphs on the red granite coffin of Rameses III in the Louvre.
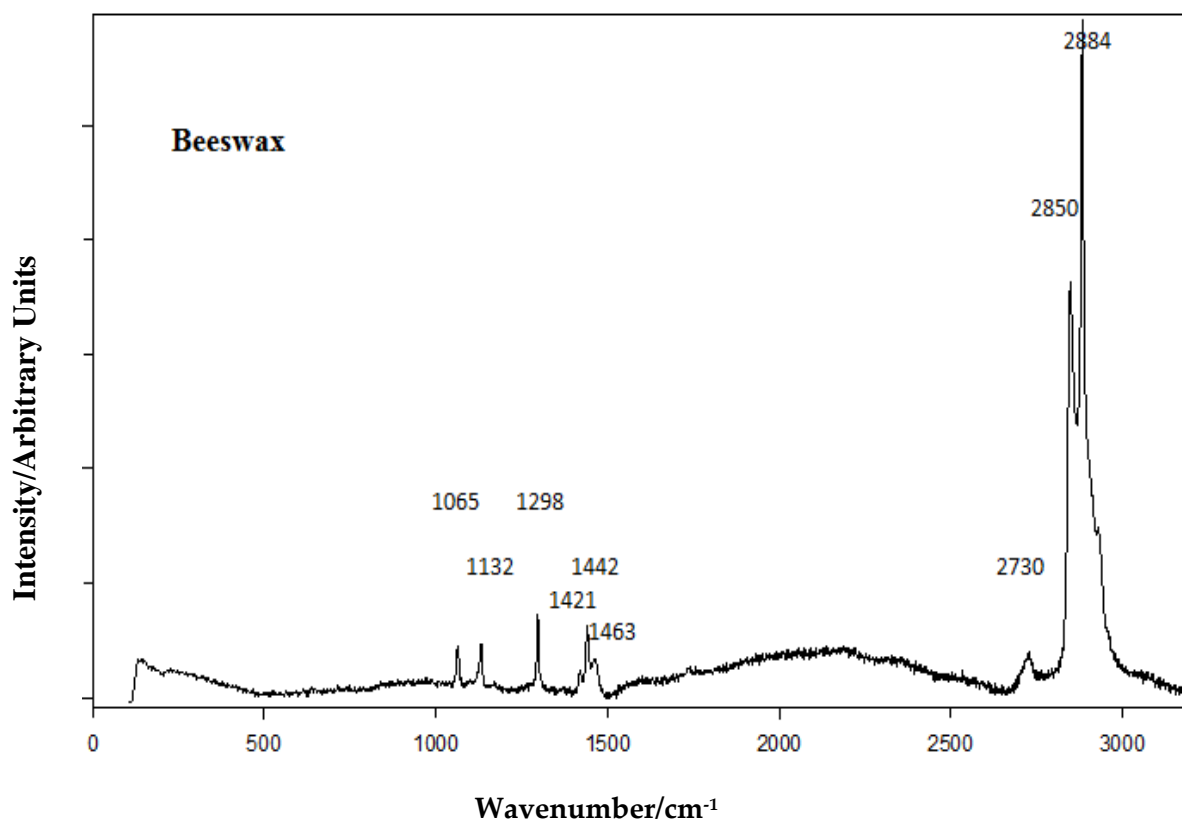
Figure 4.24. Raman spectrum for beeswax used to bind the Egyptian green to the Malkata M1 pottery surface. Refer to Table 2.5, Appendix A2 and Appendix A4.M1.1 for band assignment. (λ=514.5 nm)

4.6.4.5 Slip

The Raman spectra for the white slip provided in Figures 4.25 and 4.26 has been analysed and is shown to be huntite. It is likely that the Raman signature for burkeite, shown by the Raman band at 1129 cm^{-1} (another at 1132 cm^{-1} is not shown) together with possibly some bone ash is also present. The Raman band at 955 cm^{-1} is possibly that of tricalcium phosphate (bone ash) or alternatively the iron phosphate, vivianite. Whether the burkeite is from the alkali flux is unclear, however, its likely presence in the region of the white slip is strongly indicative of the use of this mineral as an alkali flux. Burkeite when heated to about 800°C would lose its carbonate anion but would retain its sulphate anion. However, one sample is insufficient to reliably advance any theory. What is evident is the failure of the post-firing applied huntite to act as a long-term binder to adhere the Egyptian green to the pottery surface. Huntite, being a carbonate ore is porous and crumbles when placed in water (Deer *et al*. 1992: 652).

Calcium, magnesium, and mixed carbonate ores, including huntite, are most likely to have formed by precipitation from solution by bacteria, including *Chromohalobacter marismortui* (Rivadeneyra *et al*. 2006).   The Egyptian green on Sherd M1 was applied to a white coating of huntite containing traces of gypsum.   The gypsum may well have been applied to the pottery surface and pre-fired then subsequently coated with the huntite.   This possible method of application cannot be determined without sectioning the sample, something that is now considered to be inappropriate.   The Egyptian green owes its long-term adhesion to the beeswax coating applied over the surface and which has prevented water ingress. Malkata Sample M7 (M/73/K/5) which has not been coated with beeswax or other organic binder, has lost most of its Egyptian green from the huntite surface, supporting the above observation.
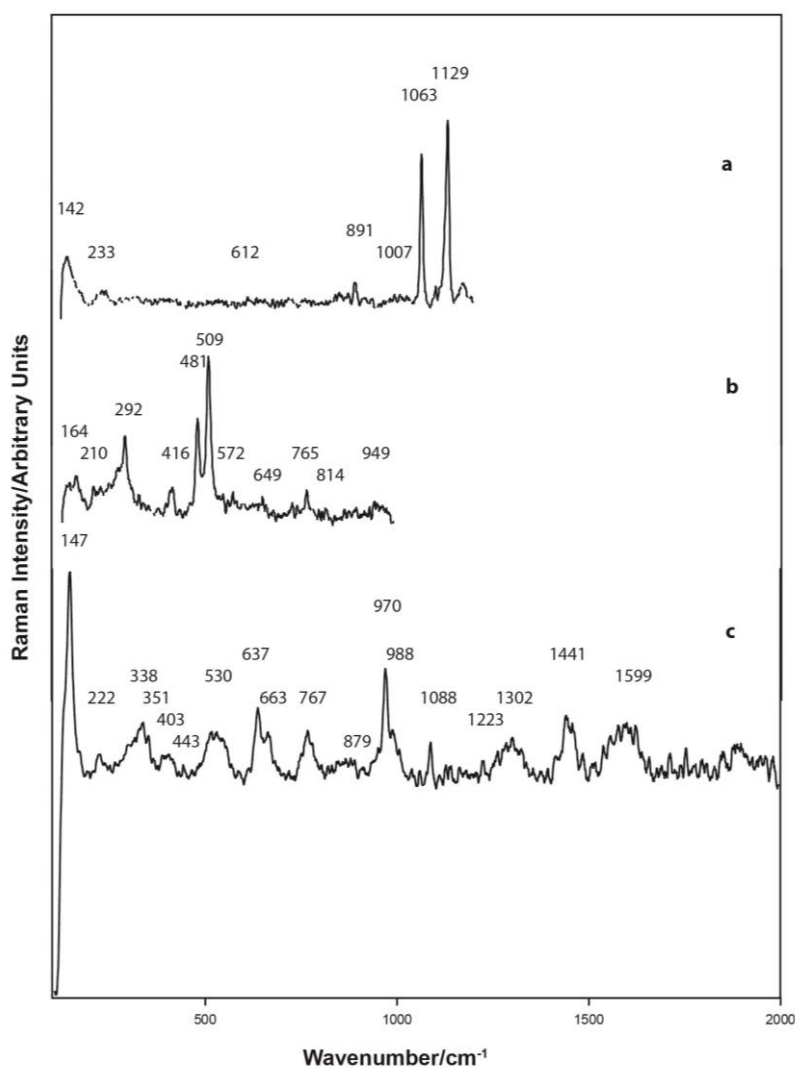
Figure 4.25. White slip coating on the surface of sherd M1. The coating is huntite together with calcite, wollastonite and possible gypsum. The presence of feldspar, as shown in (b), the more likely member being oligoclase rather than labradorite.
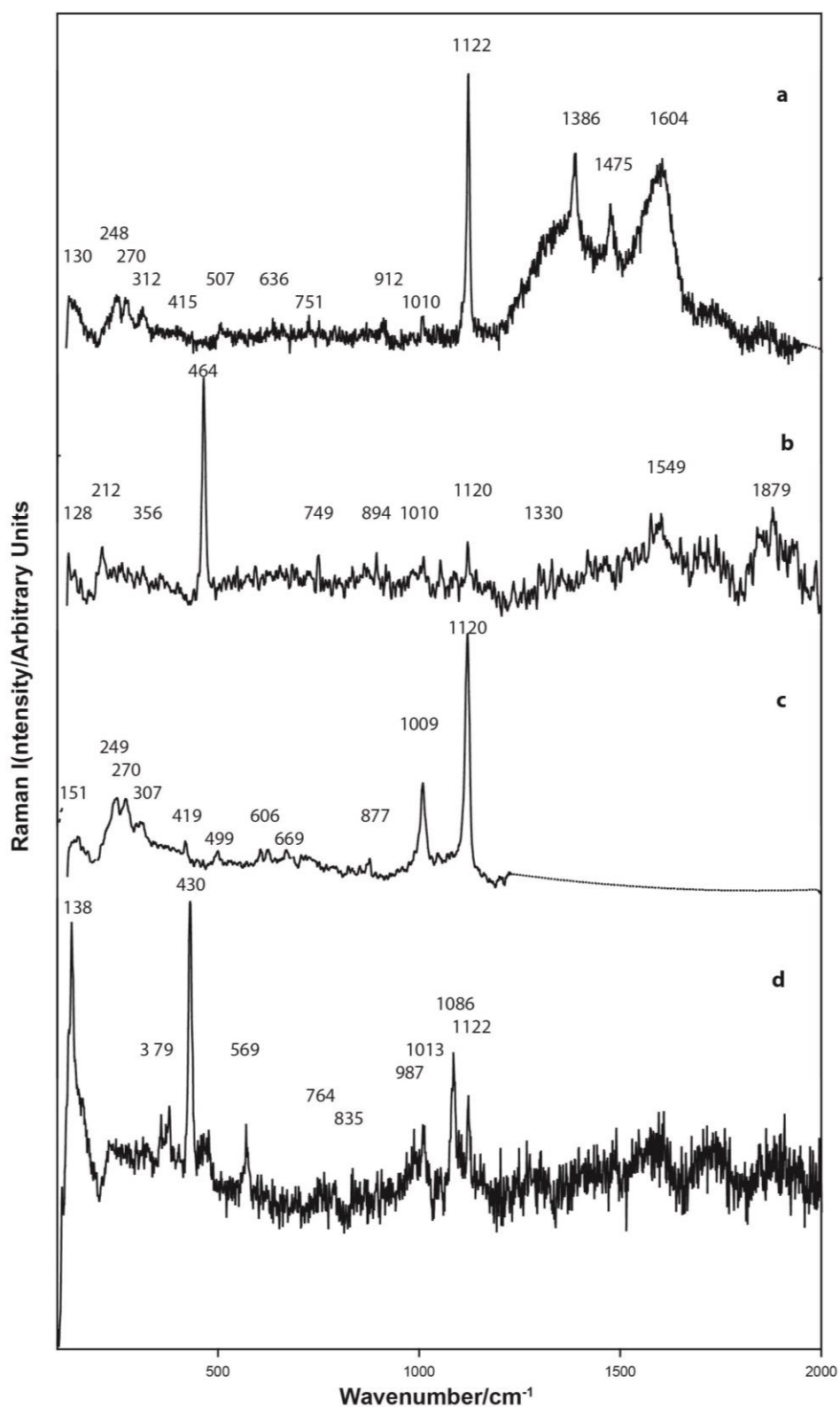
Figure 4.26.   Raman spectra, white areas on surface of sherd M7. The strong band at 1122 cm^{-1} is huntite together with traces of gypsum, indicated by the band at 1009 cm^{-1}. The peaks at 430 and 1086 cm^{-1} indicates the presence of minor Egyptian blue. Quartz, tridymite and traces of feldspar are also present.

4.7   Egyptian blue and Egyptian green reaction vessels

Turner (1954) was the first to report that the pots used at Amarna for glass manufacture appeared to have been wheel turned as shown by the shallow concentric circular grooves in their base. The pots have outwards tapering walls and have been pre-fired. The internal surfaces had then been lined with a slip varying in thickness from 0.5 to 0.7 mm consisting of two layers, a relatively thick one of light yellow covered with a film of grey or white material. He assumed that this slip lining was applied to protect the surface from corrosion by molten glass. By analysis, the slip layer contained 42.9% SiO_2, 26.8% CaO, 8.7% TiO_2, 6.88% Fe_2O_3, 4.1% Na_2O and 1.8% MgO indicative of a high lime and silica content. Weatherhead and Buckley (1989: 216) disagreed with Turner's interpretation (Turner 1954: 436-440) that the slip inside the vessel helped to prevent corrosion by the molten reactants. Rather, they considered that the "slip" is the corrosion product itself. Whilst the present samples only contain minor visible residual slip coating its likely composition can be deduced from the bone ash and gypsum particles analysed and it would appear to have a composition approaching 27% SiO_2, 32% CaO and 1% FeO.

Importantly, the interiors of most of the vessels in which glass was made at Amarna were found to be lined with a white slip. Shortland (2000) reported that after examination of vessels in various museum holdings that two differently shaped vessels were used for glass production, namely "cylindrical vessels" and "fritting pans". Of the 20 cylindrical vessels he examined, 16 were of a consistent shape and size and 11 of these contained a 1 mm thick layer of white slip as a lining, three had no lining and for two vessels no information was available. Vessel UC36458 in the Petrie Museum has glass on its external surface and Egyptian blue frit on its internal surface but is unlined. It does indicate that glass and Egyptian blue were likely to be fired using similarly made pottery vessels.

Nicholson (2007: 123) reported that at Amarna, the reaction between the raw materials, whether a single stage, or two-stage reaction, took place in these cylindrical vessels. And, according to Stocks (2003: 41) the crucibles used for copper or bronze production were similarly constructed from fine clay mixed with straw and shaped like a deep bowl.

Shortland (2000) determined that his synthetic pottery samples began to sag under their own weight at about 1150°C, and thus were on the verge of failure. He therefore concluded that it confirmed the Turner (1954) experiments, namely that the maximum working temperature for these vessels is 1100°C.

The crucibles used some 50 years later at Qantir-Piramesses were made from locally available Nile clay with a little added temper as chaff or other organic material. Little, if any sand was included into the mix. The vessels were of a different and more ovoid shape (Turner 1956; Rehren and Pusch 1997). Importantly these vessels were also lined internally with a white calcareous slip (refer Figure 4.1a in Appendix A4). Figure 4.1(b) in Appendix A4 shows the presence of Egyptian blue on the internal surface of the vessel.

4.7.1 *Vessel internal slip lining or parting layer*

As noted by Nicholson the white calcareous lining on the inside of the vessel should be seen as the defining feature of these vessels (Nicholson 2007: 123). This lining would protect the Egyptian blue or Egyptian green frit or glass from contamination from iron in the clay vessel and would assist as a parting agent.

Both Tite and Shortland (2003) and Turner (1954) reported that a lime-rich slip is often present between the frit and the ceramic vessel in which glass was fired. Tite and Shortland reported that the lime content of the glass frits (0.8-8.1% CaO) vary depending on their proximity to this lime-rich slip. They proposed that the CaO content of the frit is likely to have been in the order of only 1% in the glass phase.

At Qantir-Piramesses some 1100 fragments representing about 250-300 similar cylindrical vessels or glass-colouring vessels have been recovered (Rehren and Pusch 1997; 2005). Almost all vessels are said to have a thin layer of lime or a lime silicate on their internal surface, possibly applied as quicklime, which they considered to act as a parting agent by preventing liquid glass from contamination from the ferruginous clay vessel and from sticking to the ceramic vessel. This would then enable the glass ingot to be released from the vessel. Rehren and Pusch (1997) and Merkel and Rehren (2007) reported that the internal surface of many of these vessels was provided with a ceramic fabric coating, either white or grey, which they termed a parting layer. This coating, typically several millimetres thick, comprised a mixture of crushed lime and quartz sand together with clay to act as a binder, or Nile clay tempered with lime and chaff. This external layer tends to be somewhat fragile and is not strongly bonded to the pottery vessel. In hot firings this lime layer has reacted with the pottery to form a bottle-green interface glass layer. The fact that the inside "lime" slip layer failed to sinter, yet the outer "lime" layer did, would indicate that the "limes" used were in fact chemically different. This is consistent with bone ash or bone ash plus another calcium source forming the inner white slip layer and calcite or lime the outer layer. Calcite would react with iron oxides at about 450°C to form $Ca_2Fe_2O_5$ (Beuvier *et al*. 2013). The low Fe content of the Egyptian blue pigment examined would negate the probability that these particles were able to directly react with the ferruginous pottery body of the vessel in which they were prepared. Or, as previously stated, the decomposition of calcite at 860°C can form wollastonite. Wollastonite was present in most samples as shown in Table 4.5.

Rehren and Pusch (1997) reported that at Qantir this white layer comprised, a calcium silicate reaction zone next to the vessel, an intermediate layer of calcium carbonate and an outer layer rich in calcium silicate. Any residual lime would slowly re-carbonate to form $CaCO_3$. According to these workers, this white layer acted as a very effective barrier in separating the hot glass from the ceramic. On the vessel walls, traces of glass are usually absent; it is only at the bases that glass has sometimes penetrated through the white layer. Coincidentally, one of these spots where the white layer failed was at a "hotspot" at the base of the crucible.

Debris recovered at Memphis consisted of ceramic vessels which are lined with a white slip to which a layer of Egyptian blue adheres as discussed by Hatton *et al*. (2008). This report

supports the usage of similar vessels, similarly prepared, for either glass or Egyptian blue production. As discussed by Nicholson and Henderson (2000: 202) in the press moulding of glass a parting agent is required. Stern and Schlick-Nolte (1994: 23) proposed that bone ash would be a suitable choice.

The high calcium and sulphur elemental analysis provided in Table 4.8 for Sample E1 and in additional analyses contained in Appendix A4 and confirmed by a Raman band at 1007 cm^{-1} as provided in Table 4.4 for samples E4 (UC24684), E5 (UC24685) and E6 (UC24686a) and E8 (8979c), is attributed to gypsum or anhydrite. An approx. 85 μm long X 5 μm "diameter" fluoro-apatite associated with gypsum or anhydrite particle containing arsenic in sample UC24685 is shown as Spot 1 in Figure 4.13 and its EDS spectrum in Figure 4.14 and again as Spot 1 in Figure 4.27 where its analysis is given in the accompanying table; the Area analyses are provided in Appendix A4 and this analysis does not indicate the presence of phosphates.
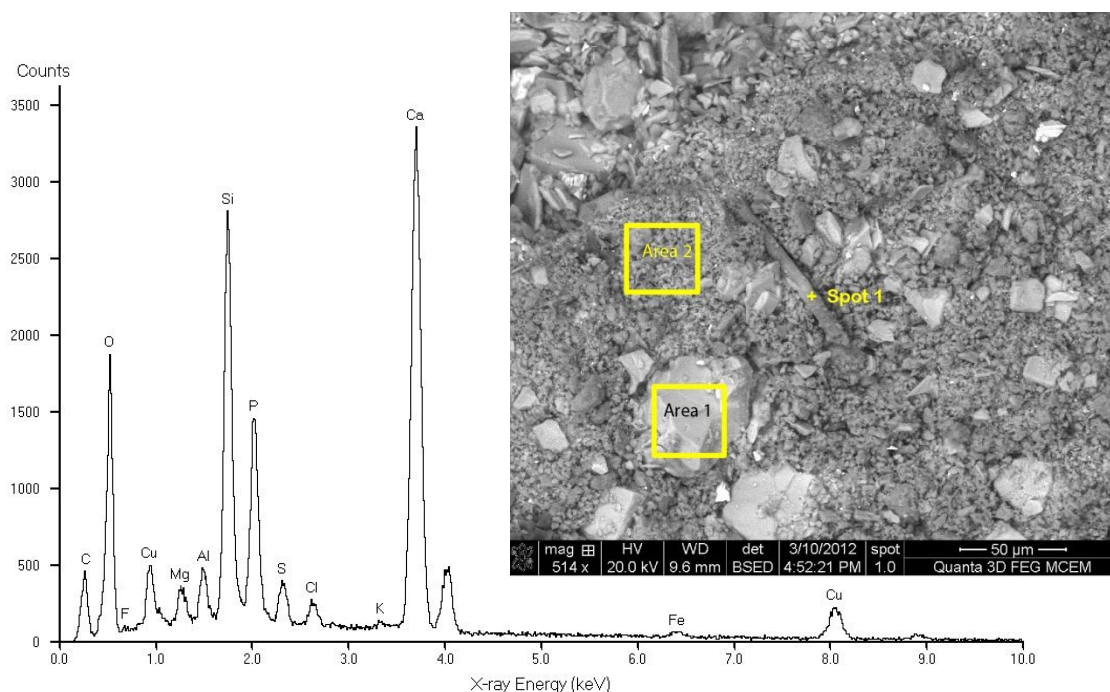
Figure 4.27. FIB-BSE image and EDS spectrum for the analysis of Spot 1 in sample E5 in Appendix A4 Figure A4.E5.28, being the analysis of the arsenical hydroxyapatite particle and which is provided below.

Elemental analysis, Egyptian blue, FIB-EDS Spot 1 analysis, Figure 4.27.

Na$_2$O	MgO	Al$_2$O$_3$	SiO$_2$	P$_2$O$_5$	SO$_3$	Cl	K$_2$O	CaO	TiO$_2$	MnO	FeO	CuO	F	As$_2$O$_3$	SnO$_2$
0.0	2.8	3.3	27.8	18.4	3.7	0.8	0.3	31.6	0.0	0.2	0.9	8.7	0.2	1.3	0.0

4.8 Egyptian blue and Egyptian green decoration

Table 4.21. Egyptian blue analyses on pottery, walls and cartonnage.

Egyptian blue on pottery:

Elemental analysis, Egyptian blue, FIB-EDS , Figure A4.M7 Malkata sherd M7

Na$_2$O	MgO	Al$_2$O$_3$	SiO$_2$	P$_2$O$_5$	SO$_3$	Cl	K$_2$O	CaO	TiO$_2$	MnO	FeO	CuO	PbO	As$_2$O$_3$	SnO$_2$
1.4	16.0	0.9	22.4	tr	2.9	0.5	0.3	8.5	0.3	0.0	0.9	46.0	0.0	0.0	0.0

Elemental analysis, Egyptian blue, FIB-EDS s, Figure A4.M8 Malkata sherd M8

0.8	0.8	1.9	68.5	tr	0.3	0.1	0.2	15.6	tr	0.0	0.3	12.6	0.0	0.0	0.0

Egyptian blue on wall:

Elemental analysis, Egyptian blue, FIB-EDS , Figure A4.16, Sample 16 Kellis

Na$_2$O	MgO	Al$_2$O$_3$	SiO$_2$	P$_2$O$_5$	SO$_3$	Cl	K$_2$O	CaO	TiO$_2$	MnO	FeO	CuO	PbO	As$_2$O$_3$	SnO$_2$
2.2	1.3	8.0	59.2	0.2	4.9	0.6	1.2	12.3	0.5	0.0	2.6	6.9	0.0	0.0	0.0

Elemental analysis, Egyptian blue, FIB-EDS, Figure A4.MUT25 Trench sample MUT25, Mut al-Kharab

2.3	2.0	1.5	63.9	tr	1.0	2.1	0.4	12	tr	0.0	0.6	13.8	0.0	0.0	0.2

Elemental analysis, Egyptian blue, FIB-EDS, Figure A4.MUT26, Trench sample MUT26, Mut al Kharab

2.6	3.4	2.5	55.9	0.6	2.0	0.1	0.6	14.9	0.2	0.0	2.0	15.1	0.0	0.0	0.0

Egyptian blue on cartonnage:

Elemental analysis, Egyptian blue, FIB-EDS , Figure A4.C2, Kellis 1 cemetery Tomb 22

Na$_2$O	MgO	Al$_2$O$_3$	SiO$_2$	P$_2$O$_5$	SO$_3$	Cl	K$_2$O	CaO	TiO$_2$	MnO	FeO	CuO	PbO	As$_2$O$_3$	SnO$_2$
3.6	0.7	5.3	40.2	tr	13.2	0.6	1.4	12.6	0.2	0.0	2.1	11.5	0.0	7.5	0.0

Elemental analysis, Egyptian blue, FIB-EDS s, Figure A4.C10, Kellis 1

4.0	1.3	5.0	56	0.0	6.1	2.3	1.0	17.5	0.2	0.0	0.2	4.5	0.0	0.0	tr

Elemental analysis, Egyptian blue, FIB-EDS, Figure A4.C17, North Tomb 2, Kellis

2.9	3.0	3.7	48.9	1.3	7.8	1.1	3.7	15.0	0.3	0.0	1.6	10.7	0.0	0.0	0.0

4.8.1 Egyptian blue and Egyptian green decoration on pottery

Egyptian blue is rarely used for decorating vessels. The two Malkata samples, M7 and M8, were obtained from a highly disturbed site and have previously been described by Hope *et al*. (1981) and the sherd from Anubieion has been described by French (2013: 343). Noll and Hangst (1975) observed that Egyptian blue is normally relatively coarse in particle size, namely 5-50 μm and therefore can only be applied in thick layers. Anubieion sample E11 (DAF 124) and both of the Malkata samples discussed below are highly variable in particle size approximating that described by Noll and Hangst.

Two Egyptian green samples from Malkata were also examined. Their analytical results are also provided below.

4.8.1.1 Malkata Egyptian blue samples

Only minor traces of the original Egyptian blue decoration remains on the surface of Malkata sherds M7 (M73/K/5) and M8 (M73/K/1406). The initial SEM analyses were conducted using the FIB microscope at an accelerating voltage of 20 kV, the results being provided in the tables provided in Appendix A4, at M7, M8 and DAF 124 (refer Table 4.22). The magnesium analysis provided for the Egyptian blue were considered to be unreliable, potentially caused by the electron beam generating an interaction volume which may have extended into the white huntite slip substrate coating. The analyses were then repeated at 15 kV accelerating voltage to decrease the interaction volume, thereby decreasing the depth of the electron beam penetration and using the Nova electron microscope. Some 24 residual surface particles were analysed, confirming the presence of a higher than expected magnesium concentration. However, some concern over the magnesia concentration is still expressed.

Raman signatures are provided in Appendix A4 at M7 and M8, and their mineral assignments are given in Appendix A4. The high MgO concentration in the Egyptian blue pigment on Malkata sherd M7 has led to the presence of diopside. Diopside was not observed in Malkata sherd M8. Both contained significant wollastonite and chalconatronite. There is a probability of hanksite being associated with M7.

4.8.1.2 Malkata Egyptian green samples

Egyptian green was observed on Malkata sherds M1 and M7. Both sherds are described in more detail in Appendix A4. The Raman spectra for Malkata Sample M1 is provided in Figure 4.21 and M7 in Figure 4.22. The Egyptian green pigment applied to both sherds was based upon arsenical copper (bronze). An anomalous average areal phosphate analysis of 1.6% was obtained for Sample M7. Potash analysis of <1% and sulphate analyses of up to 10% would support a natron-based flux, probably thénardite or burkeite; Raman spectroscopy would support this flux usage.   No cassiterite was observed in either sample. Thus, these results would again question the Schiegl *et al*. (1990; 1992) hypothesis that arsenical bronze was discontinued prior to the commencement of the 18th Dynasty.

4.8.1.3 Anubieion, Saqqara, Egyptian blue sample E 11 (DAF 124)

The Raman signatures generated by this pigment and the slip coating underlying it, is provided in Appendix A4.E11.34, and in Table 4.5. The SEM-EDS analyses are provided in Appendix A4.E11 and in Table 4.6. In sample E11, four copper-containing ores were identified by Raman spectroscopy, namely, pseudomalachite, malachite, connellite and chalconatronite.   Unfortunately, the Raman signature for the blue monoclinic mineral georgeite is not within the published literature. According to Pollard *et al*. (1991) synthetic and naturally occurring georgeite correspond to the stoichiometry of malachite, and whether this mineral is cryptocrystalline malachite or a separate amorphous phase of the same composition is unclear.   And, georgeite and chalconatronite can react to form malachite. Mineral samples have been noted with connellite crystals coating the masses of georgeite. Thus, it is likely that the copper minerals reported in this study can co-exist. As shown in

Figure 4.6, the high sodium analyses in E11 are attributed to residual, undissolved flux (natron-based) on the pigment surface.

Pagès-Camagna and Colinart (2003) reported that in the samples of Egyptian blue they examined the total flux concentration (Na_2O + K_2O) never exceeded 5%. And in turquoise samples the flux concentration varied between 5.7% and 10%. Sample E11 has a much higher flux content averaging 8.6% and which is principally provided by the sodium source. As will be shown, the high sodium surface deposit would have adversely modified the flux concentration. They reported that tridymite is only formed at flux concentrations of <7%, and that >8% flux is required for cristobalite crystallisation. The present results do not support this proposal as tridymite was present, not cristobalite.

Table 4.22. FIB SEM-EDS elemental analyses of the Egyptian blue pigment applied to the surface of Anubieion sherd DAF 124. Copper-tin (bronze) particles are shown in Figures A4.E11.1 (Spots 1 and 2) and A5.E11.5 (Spot 1) and the hydroxyapatite (bone ash) particle is shown in Figure 4.27 (Spot 1).

	Na2O	MgO	Al2O3	SiO2	P2O5	SO3	Cl	K2O	CaO	TiO2	FeO	CuO	SnO2
Hydroxyapatite*													
	2.0	1.8	0.4	5.9	29.9	0.0	0.7	0.1	53.5	0.0	0.2	2.5	0.0
Bronze particle													
	4.5	0.4	1.7	24.2	0.0	0.5	0.3	0.3	5.5	0.0	0.6	6.7	55.3
*F=2.9%													
	Na2O	MgO	Al2O3	SiO2	P2O5	SO3	Cl	K2O	CaO	TiO2	FeO	CuO	SnO2
DAF124-20keV	8.1	1.4	3.5	53.9	0.3	1.1	0.5	0.5	12.3	0.3	1.2	16.1	1.3
DAF124-15 kev	2.0	0.8	1.6	64.0	0.0	0.2	0.3	0.5	14.4	0.1	1.2	14.8	0.2

The reactivity profile given by Pagès-Camagna and Colinart (2003) is accepted and therefore sample E11 would have been produced at a temperature of between 900-950°C and probably close to 950°C as some tridymite and wollastonite had formed but residual colourless quartz crystals were also evident. Therefore, as shown in Table 4.22, the analysis of sample E11 is in accordance with the proposal of Pagès-Camagna *et al*. (1999) that all Egyptian blue samples contain a greater concentration of copper than calcium. According to Pagès-Camagna and Colinart (2003), the bulk CaO/CuO ratio is about 0.7 and the SiO_2/CuO is approximately 3. In the present sample the CaO/CuO ratio is 0.76 and SiO_2/CuO is 3.3, strongly supporting this proposition.

The low potassium content in DAF 124 is indicative that plant ash or kiln ash did not form part of the flux. It is therefore proposed that the presence of hanksite, gaylussite and natrite confirms that natron was the flux employed. Natron would melt at around 800°C at which temperature it will form a eutectic with quartz. Ion diffusion into the melt will then commence with Cu^{2+} ions diffusing into the melt followed by Ca^{2+} ions. The final operational temperature reached in the manufacture of E11 is postulated to be in the region of 950°C.

In Sample E11, bronze was observed from the presence of tin in metallic particles as shown in Figure 4.28 and in Figures A4.E11.1, A4.E11.5 and Table 4.22. However, the Raman signature for cassiterite was not found. Furthermore, the Raman signature for malayaite

[CaSnSiO5] was not observed by Pagès-Camagna *et al*. (1999) but they reported finding the Raman signature for cassiterite. In the present sample, neither malayaite nor cassiterite were observed. Pagès-Camagna *et al*. also reported cuprite [Cu2O] to be present in the product. The Raman signature for cuprite or tenorite was not found in the present sample.
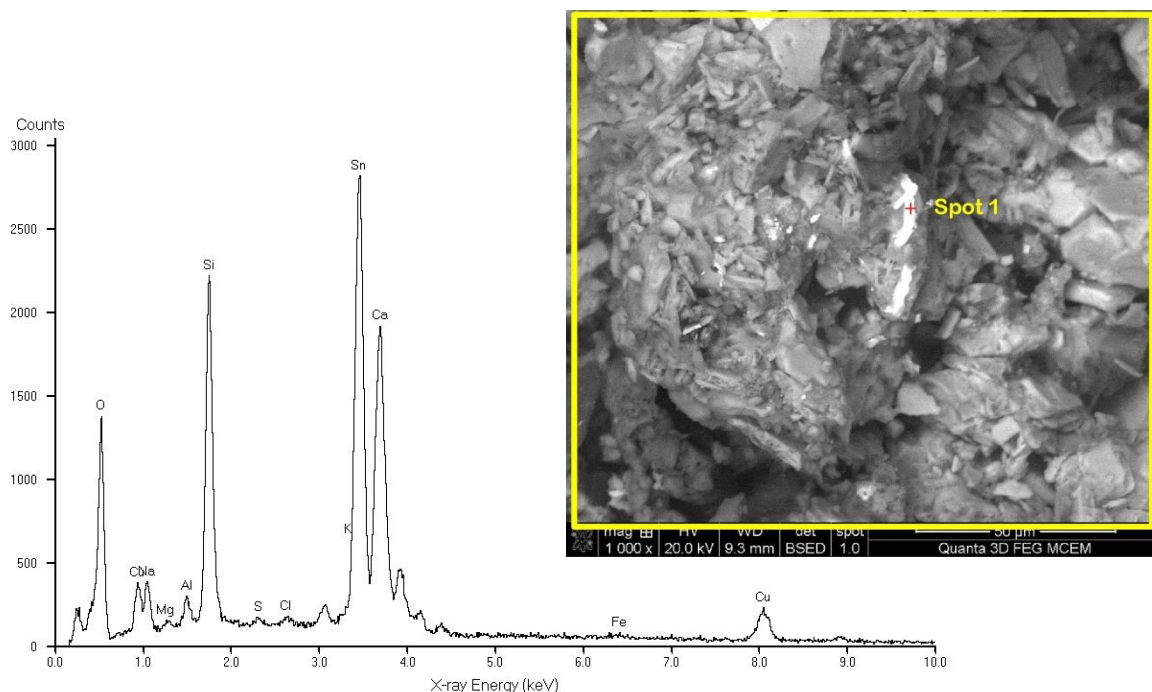
Figure 4.28. FIB BSE image of sample E11 (DAF124) showing the position of the Points of Interest for the analysis of Spot 1 and the EDS spectrum for the analysis of this location in Figure A4.E11.5.

Elemental analysis, Egyptian blue, FIB-EDS Spot 1 analysis, Figure 4.28 (also Figure A4.E11.5)

Na2O	MgO	Al2O3	SiO2	P2O5	SO3	Cl	K2O	CaO	TiO2	MnO	FeO	CuO	PbO	As2O3	SnO2
4.5	0.4	1.7	24.2	0.0	0.5	0.3	0.3	5.5	0.0	0.0	0.6	6.7	0.0	0.0	55.3

The phosphate would appear from the Raman signatures to have been derived from bone ash as indicated by the presence of the large particle of fluoro-apatite shown in Figure 4.29 (Appendix Figure A4E11.32) within the mineral assemblage. It contains 2.9% fluorine, and as such, the fluorine is confirmation of bone ash being the source of this particle. Naturally or artificially formed apatite would not be expected to contain fluorine. The presence of bone ash would be the source for the apatite Raman signature. Whether particles of bone ash entered into reaction with the copper minerals during production of the Egyptian blue to form pseudomalachite is uncertain. Both pseudomalachite and apatite will often be found in close mineralogical association. No arsenic mineralisation associated with the hydroxyl- or fluoro-apatite (bone ash) was observed in sample E11 as would have been expected from the results published by Schiegl *et al*. 1990; 1992). As previously discussed within this chapter, arsenic adsorbed on to calcium phosphate minerals has been observed in other samples. An alternative rationale to that proposed by Schiegl *et al*. (1990: 1992) for this observation is discussed in the present thesis at 4.5.2.6.
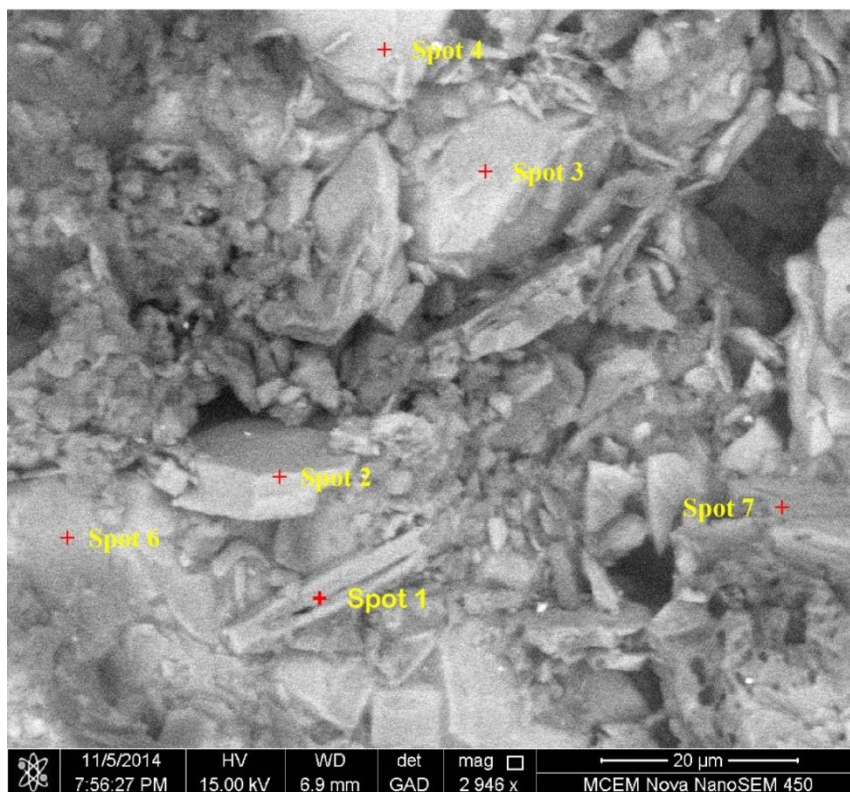
Figure 4.29. Nova low vacuum image showing Points of Interest analysed in Sample E11 (DAF 124) in Appendix A4 Figure A4.E11.32 Spot 1 is fluoro-hydroxyapatite, the analysis of which is provided in the accompanying table.

Elemental analysis, Egyptian blue, Nova-EDS Spot 1 analysis, Figure 4.29

Na_2O	MgO	Al_2O_3	SiO_2	P_2O_5	SO_3	Cl	K_2O	CaO	TiO_2	MnO	FeO	CuO	F	As_2O_3	SnO_2
2.0	1.8	0.4	5.9	29.9	0.0	0.7	0.1	53.5	0.0	0.0	0.2	2.5	2.9	0.0	0.0

Jaksch *et al.* (1983) observed that the melting temperature must have been conducted under reducing conditions and below 742°C as shown by the presence of pyrite in the cuprorivaite. (The conversion of pyrite to pyrrhotite occurs at 742°C.) Heating pyrite under oxidising conditions would have led to its oxidation at 400°C to hematite. Pyrite was observed in sample E11. However, as was shown by Jovanović (1989) when pyrite is heated in an inert atmosphere at 850°C, only 60 per cent of the pyrite had decomposed to pyrrhotite in three hours and furthermore, the reaction follows a straight line until decomposition commences at which a deflection point lowers the reactivity and slope is no longer temperature dependent. Thus, it is conceivable that under favourable conditions pyrite could have remained within the cuprorivaite at much higher temperatures than expected by Jaksch *et al*. (1983). It would support conceptually that Anubieion sample E11 was manufactured under strongly reducing thermal conditions at approximately 950°C. The phosphorus detected in the elemental analysis is attributed to pseudomalachite, apatite and fluoro-apatite (bone ash). Pseudomalachite and apatite enjoy a close relationship with each other in nature. The other major copper minerals present are cuprorivaite, malachite, connellite and chalconatronite.

4.8.1.4 Mut al-Kharab Egyptian blue

4.8.1.4.1 Sample D8 (also recorded as MUT 1), surface find.

Almost no Egyptian blue pigment remains on the surface of this sherd. The sherd is dated to Ptolemaic period and is a surface find. Only microscopic residual cuprorivaite crystals were located on the white slip in only one very small area. The Raman spectra for these crystals indicated the presence of hedenbergite, antlerite, chrysocolla, rutile, pseudowollastonite, diopside and amorphous carbon. It is more fully described in Appendix A4.

4.8.1.4.2 Sample MUT25, (context 32), Trench 38.

The blue pigment was identified as Egyptian blue. Its SEM-EDS analysis is provided in Table 4.21. Tridymite, rather than cristobalite is present indicating a firing temperature for the manufacture of this sample was in the order of $1000^{\circ}C$. The pigment sample also contains quartz and possibly a trace of ferrosilite. It is more fully described in Appendix A4.

4.8.1.4.3 Sample MUT26, (Context 22C), Trench 18.

The blue pigment has been identified as Egyptian blue. Its SEM-EDS analysis is provided in Table 4.21. The sample also contains amorphous carbon, gehlenite, fluoro-apatite, kinoite, gypsum and hanksite and traces of dioptase. It is more fully described in Appendix A4.

4.8.1.5 Surface slip on pottery vessel samples

The white slip mineral associated with the application of the Egyptian blue pigment to the surface of the vessel E11 (DAF 124) is proposed as being either calcite or aragonite. The Raman band for aragonite better fits the mineral spectral data. However, it is suggested by Edwards *et al*. (2004a) that calcite is more often found to have been used by Egyptian workers. It should be noted that calcite or aragonite are able to enter into the glass-forming reaction. Therefore its observance is likely to be from residual mineral used in the production of the cuprorivaite or more likely, it formed part of the slip composition applied to the vessel surface after firing and prior to its decoration.

A number of small red particles were attached to various Egyptian blue pigments observed in sample E11, potentially indicative of cuprite or of hematite. It is expected that this mineral assemblage would have formed part of the white slip material applied to the inner surface of the vessel in which the Egyptian blue was prepared. Riebeckite, reported in this study, is an amphibole closely associated with asbestiform habits. Therefore it offers good thermal resistance and may, together with hastingsite, a hornblende, have formed part of the slip lining the Egyptian blue reaction vessel. These two minerals were not present in the cuprorivaite Egyptian blue Raman spectrum. The presence of a related blue to black iron-containing amphibole, glaucophane has been reported at Knossos, Greece before 2100 BCE and at Thera before 1500 BCE (Filippakis *et al.* 1976; Profi *et al.* 1977). Feldspar in the form of

albite and devitrite has formed at the interface probably by a chemical reaction between the calcite, natron, and silica.

The analysis of the slip present on Malkata sherds M7 (M73/K/5) and M8 (M7/K/1406) is provided in Appendix A4. In both sherds, huntite and gypsum were blended together to provide the slip. Presumably, the two minerals were mixed with water and applied to the vessel, then the Egyptian blue and other pigments were subsequently applied. It is possible that the gypsum had been preheated to evolve its water of hydration (to form anhydrite). The anhydrite would slowly rehydrate, swelling and reducing the adhesion of the Egyptian blue to the surface. Huntite, a magnesium-calcium carbonate, would not offer any reasonable adhesion properties.

Hope (1980: 337) reported that, based upon the suggestion of Lucas, this white pigment would have likely to have been either calcium carbonate or gypsum. He indicated that gehlenite, quartz and gypsum were identified on these two Malkata sherds and that huntite had been identified by Riederer on C-Group pottery from Nubia. As noted above and in Appendix A4, gypsum and huntite are the two main minerals present together with minor quartz. Gehlenite or other members of the melilite group were not detected. However, gehlenite was detected in Mut al-Kharab trench sample MUT26. Therefore, this does not preclude their presence in very minor concentrations or on other sherds not examined.

4.8.2 Egyptian blue and Egyptian green on wall samples, Kellis.

4.8.2.1 Sample W4,Main Temple Complex, Area D, Shrine I

The Egyptian green pigment has been prepared using tin-bronze as shown from the presence of cassiterite. The pigment contains <1% K_2O, indicative for a natron-based flux having been employed. The pigment has undergone lichen attack as discussed in Section 4.6.3.

4.8.2.2 Sample W16, Main Temple, D/5 Shrine IV Room 1, south wall.

The blue pigment in this sample is Egyptian blue, manufactured using bronze scrap as shown by the presence of tin. It contains a number of contaminants including catapleite, which was confirmed by EDS analysis (refer Figure A4.W16.2, Spot 2), ilmenite, which was also confirmed by EDS analysis (refer Figure A4.W16.2, Spot 3), quartz, the feldspars oligoclase and albite and amorphous carbon.

4.8.3. Egyptian blue decoration on cartonnage

4.8.3.1 Sample C1. Kellis 1 cemetery, Tomb 20.

The pigment applied was possibly Egyptian green or malachite. It has seriously degraded to now consist of a mixture of malachite and carbonatotrichite, anatacamite and antlerite. Degradation is sufficient to render the determination of the original pigment applied to be uncertain.

4.8.3.2 Sample C2. Kellis 1 cemetery, Tomb 22.

The blue pigment as applied was most likely Egyptian blue. However, an organic material, presumably in the form of an oil, has been intermixed, or applied over the top of the pigment. This treatment has reduced the signal quality (caused by extreme fluorescence) and the broad carbonaceous band has exacerbated the problem. A red crystal of cuprite is provided in Appendix A4 (Figure A4.C2.1(e)). The presence of arsenic in the SEM-EDS analyses is indicative of either an arsenical copper ore being used to make the Egyptian blue or from arsenical bone ash. The lack of tin in the pigment would suggest that arsenical bronze scrap was not employed as a raw material, or it was below limits for detection. From the Raman peaks the alternative copper minerals are provided in Appendix A4.C2.

The pigment has been applied on to a gypsum plaster surface, and treated with an organic complex of unknown composition. A number of Raman bands would suggest that the organic material is likely to be a mixture of Gum Arabic and a diterpenoid resin probably from the resin collected from *Pinus pinea* or *P. haleopennsis.*

4.8.3.2 Sample C10, Kellis 1 Cemetery (C5.1), Tomb 16.

The blue pigment is identified as Egyptian blue. This pigment sample also contains quartz, diopside and one of the alkali feldspars (microcline, orthoclase, or sanidine) and a carbonaceous material. The higher concentration of sodium would have expected to favour a plagioclase feldspar, but this was not confirmed by the Raman spectrum (Figure A4.C10.1(c)). Bronze scrap as shown by the presence of tin in the EDS analysis; tin is also indicated by the Raman signature for cassiterite.

4.8.3.3 Sample C17, Kellis North Tomb 2.

The pigment is primarily Egyptian blue. Raman spectroscopy has indicated the presence of leightonite, syngenite and possibly aubertite together with traces of starkeyite and pseudowollastonite. The lead is present as cotunnite.   Two particles of calcium phosphate (Spots 3 and 4) indicate the presence of hydroxyapatite (bone ash).

4.9 Egyptian blue and Egyptian green summary

Egyptian blue and Egyptian green pigment production and application has been discussed in detail within this chapter. This has produced new evidence, particularly relating to the presence of arsenical hydroxyapatite (bone ash) particles and thénardite on the surface of these pigments providing an improved understanding of the production methods adopted. More detailed chapter conclusions are provided in Appendix A4.

CHAPTER 5. COBALT-BASED PIGMENTS

5.0 Introduction

Two different types of blue pigments were utilised during the New Kingdom, and into the Roman period. Namely, the coarser and darker Egyptian blue pigment based upon cuprorivaite discussed in Chapter 4, and the paler, finer grained blue pigment, based upon cobalt and which was employed to decorate a wide range of forms (Hope 1989: 56). This cobalt-based pigment is discussed in this chapter. All relevant supporting and experimental data is provided in the following link:
https://drive.google.com/drive/folders/0B1MXnIeNTO4icGV6dTFSaXhOQU0?usp=sharing

A significant body of research has been devoted to the cobalt blue pigment employed on ceramics found throughout Egypt during the New Kingdom, from the reign of Thutmose III (1479-1425 BCE) during the 18th Dynasty until manufacture ceased during the reign of Ramesses IV (1153-1147 BCE) in the 20th Dynasty (Hope 1989: 56; Arnold and Bourriau 1993 100; Shortland *et al*. 2006a; Aston 1998: 56). Whilst Shortland *et al.* (2006) indicated that the technology for using cobalt colourants in glass, glaze and ceramics was apparently discovered during the reign of Thutmose III, Hope (2011: 507) was less certain of this dating. He indicated that it is not impossible that blue-painted pottery was manufactured during the reign of Thutmose III because at that time post-firing decoration using Egyptian blue appears to have commenced; however far more material from carefully-controlled excavations is needed to clarify the date for its first use.

Understanding the chemistry and mineralogy of the cobalt blue pigment has provided evidence to support a new hypothesis for the particular method of production used in its preparation. Furthermore, Kaczmarczyk and Hedges (1983) hypothesised that as this pigment is used in glass and faience production, the blue decorated pottery may well have been produced in close proximity to, and perhaps in royal workshops. A limited study of glass sherds recovered within the Dakhleh Oasis provides support for the Kaczmarczyk hypothesis.

Following the initial work of Riederer (1974) and subsequent studies by Noll and Hangst (1975), Bachmann *et al*. (1980), Noll (1978), Noll (1981a, 1981b and Abe (2009) there has been some agreement that the cobalt is considered to be present as a cobalt spinel of the general form $(Co,Mn,Fe,Ni,Zn)Al_2O_4$ and that the source of the colorant was the alum deposits of the Dakhleh and Kharga Oases of the Western Desert, Egypt. In studying this pigment, Shortland *et al*. (2006) indicated that from a study of eight sherds, four from Malkata and four from Amarna, there are some slight differences between the composition of the pigment as found at each site, and that this might relate to the specific sources of alum exploited during the reigns of Amenhotep III and Akhenaten. In addition, there remains some difference in scholarly opinion over the exact way in which the pigment was produced and applied to vessels. It might also be noted that the composition of the cobalt colourant identified in contemporary glass possibly indicates a source with a different chemical profile from that identified upon the ceramics (Shortland 2006b).

In light of these issues, it was decided that further analyses should be undertaken of both samples of alum from the Western Desert and also of the blue pigment on sherds from various New Kingdom sites to seek corroboration of the suggested distinction proposed by Shortland and his co-workers and this research to include the mineralogy of the cobalt pigment. During the course of excavations at Mut al-Kharab in Dakhleh since 2000 a small selection of blue painted pottery has been discovered; such material has also been found at Ayn Asil in Dakhleh (Marchand and Tallet 1999: 323) and a few examples have also been found elsewhere in the Western Desert. Therefore investigation of this material is proposed as it has direct relevance to the present topic. The present research has provided an improved understanding for the method of extraction of the cobalt from the alum, its conversion into a blue pigment and its future possible surface degradation.

As discussed in Chapter 2, the combination of Raman spectroscopy, with either or both the synchrotron XFM beamline and high or low vacuum electron microscopy, is able to non-destructively determine both the mineralogy and chemical composition of the samples under examination. This has been supplemented by determining the iron phases present in a sample of kiln slag that contains cobalt from Mut al-Kharab using Mössbauer spectroscopy. These data have provided significant new evidence in respect of cobalt blue production. All data is provided in Appendix A5. Relevant parts of these results are reported upon in this chapter.

Raman spectroscopy has enabled the method for fixation of the cobalt pigment to pottery surfaces to be reinterpreted. This thesis now provides firm evidence to support a post-firing application.

The chapter has been divided into discrete sections as follows:
- the alum deposits within Dakhleh Oasis which provided the source of the cobalt and related transition elements;
- the mineralogy of a slag sample from Mut al Kharab indicative of a kiln associated with cobalt conversion;
- mineralogy of a range of cobalt pigments applied to sherds from various locations;
- method of fixation of the cobalt pigment to pottery surfaces;
- alternative hypothesis for the extraction of the cobalt and its related transition metals and its conversion into a solid pigment for its direct application on vessels or for its use as a source of cobalt in glass colouration.

5.1 Alum as the source of cobalt minerals

Lucas and Harris (1962: 260) maintained that the only known cobalt compounds found in Egypt were present as traces within the alums from Dakhleh and Kharga Oases and from nickel ore located on St. John's Island in the Red Sea. They considered that the extraction of the cobalt from the alums would have presented almost insuperable difficulties. Therefore, they hypothesised that any cobalt ore must have been imported into Egypt from Persia or from the Caucasus region.

Noll and Hangst (1975) noted that the slag material from hydrothermal copper deposits mined in the Eastern Desert contained cobalt, nickel and zinc, thus, they intimated that a mixed ore was the more likely source for the cobalt. They also reported that another possible cobalt source would include the Sinai Peninsula.

Alum deposits occur widely throughout the oases of Dakhleh and Kharga and there is ample evidence for their long-term exploitation throughout history to the current day (Christophe 1964; Picon *et al.* 2005). Richmond and Off (1892) collected and analysed cobalt-containing, iron-rich alum samples from Egypt, but they did not report the location for these alums. Subsequently, Beadnell (1899) provided analyses of iron-rich alums from Dakhleh but he was unable to determine the presence of cobalt. At Kharga, he observed alums that were often rose-tinted, and he therefore postulated the presence of cobalt.

Importantly, Kaczmarczyk (Kaczmarczyk and Hedges 1983: 151; Kaczmarczyk 1986) noted the use of cobalt colorant in glass and faience during the New Kingdom and reported that from the 12th to the 7th century BCE, cobalt was not employed as a colorant in Egypt. They provided an analysis for cobalt-containing alums from an unspecified Egyptian site of 10.6% Al_2O_3, 1.63% Fe_2O_3, 4.23% FeO, 2.56% MnO and 1.02% CoO but reserved their opinion on these oases as being the source of the cobalt until the presence of NiO and ZnO could be determined. Kaczmarczyk (1986) then made the connection between these oasis-derived cobalt-containing alums and their use in pigment and glass manufacture using samples derived from the Dakhleh Oasis. He used XRF analyses to draw a clear connection between the specific suite of transition metals present and their similar presence in Egyptian faience. Until this connection was made, it had been speculated that the cobalt used in Egypt had been derived from Iran or from mines in Central Europe (presumably the significant mines in Saxony that provided much of the cobalt used in China, Japan, Europe and England during and after the 17th century CE (Agricola 1556); Beckmann 1797: 353-371); Kerr and Wood 2004: 661-692). Kaczmarczyk (1986) disputed the suggestion of Dayton (1981) that during the New Kingdom cobalt was imported into Egypt from the Mycenaean world and this should be noted in relation to the similar suggestion by Lee and Quirke (2000: 111) that there might have been a trade route during the late 18th Dynasty directly or via Syria, "from the far side of the Balkans". Furthermore, Kaczmarczyk reported that it was highly unlikely that another cobalt deposit would be discovered with a similar sequential (except for copper) combination of five transition metals as found in the Dakhleh Oasis alums. Therefore, he considered that it was evident that if the New Kingdom colorants containing cobalt also contain similar transition metal constituents, then the cobalt source was from these cobalt-containing alums. Furthermore, he noted that Riederer (1974), Noll (1978; 1981), Bachmann *et al*. (1981) all reported elevated aluminium and as a consequence the pigment was tentatively labelled as a cobalt aluminate. The present work will establish additional and alternative forms of cobalt mineralisation. When the cobalt was employed again in the 7th century BCE (26th Dynasty) it was from a different type of mineral deposit (Kaczmarczyk 1986).

Alum samples from Bir al-Hurritiya within Mut, Dakhleh Oasis, were analysed by Segnit (1987). The results of his analyses were compared with alums from other Dakhleh sites, including Ain Asil, Qasr Dakheli and Hindaw by Shortland *et al*. (2006b). Shortland also

reanalysed alum samples obtained by Picon from a hill near Nadura, a few kilometres to the east of Kharga. These researchers also reported the presence of cobaltiferous alums close to Qasr Lebekha, a ruined Roman period fort in the vicinity of Ain Lebekha itself. They reported that these alums closely fitted the description for the cobalt alums reported by Beadnell (1901, 1909).

Kaczmarczyk proposed that if the alums are dissolved in water and made mildly alkaline using say natron, plant ash or ammonia, then the transition metals would precipitate as their hydroxides and oxides leaving the sulphate behind. Drying and heating the precipitate would then yield a blue mixture containing aluminates and oxides with a much higher cobalt content. Note that cobalt oxides vary in colour between dark green and black, the distinctive blue colour developing when the oxide is incorporated into a glassy structure and dissolves to form Co^{2+} ions or reacts to form a spinel, olivine or similar structure.

Samples of dark blue glass from the reign of Thutmose III from the tomb of his foreign wives were found to be coloured with cobalt (Lilyquist and Brill 1993: 33-36, 41-44) and others from Malkata and Amarna were analysed by Shortland and Tite (2000) who demonstrated that in addition to cobalt, these glasses contained significant amounts of aluminium, manganese, iron, nickel, zinc and sulphur and they concluded that these early glasses used a cobalt colorant from the Kharga Oasis and natron from the Wadi Natrun.

Abe *et al.* (2009, 2012) reported that an on-site analysis was conducted using a portable XRF and XRD combined instrument at Northwest Saqqara. They proposed that the cobalt was present as a spinel of the general formula MAl_2O_4 (where M = Mn, Fe, Co, Ni, Zn).

5.1.1 Alum samples examined in the present study

Six samples of alum were sourced by A/Prof. C. Hope from an artesian well located at Bir al-Hurritiya al-Gubli on the outskirts of modern Mut, the capital of Dakhleh Oasis and not too distant from the ancient site of Mut al-Kharab, and one sample from the extensive exploration conducted in the Kharga Oasis in 2002 by Shortland in collaboration with the Egyptian Geological Survey (Shortland *et al.* 2006b)[1]   The Dakhleh Oasis samples D1 to D4 were found to be clay/carbonate minerals and are briefly discussed in Section 5.1.4. Whilst single samples cannot be considered to be representative of the entire mineralisation at either site they do provide an indication of the likely composition of these minerals and the probable geographic spread of the cobalt-containing alums. Thus, the findings must be considered to be tentative until additional samples can be sourced.

5.1.2 Analysis

The elemental analyses of the alum samples were conducted using either a JEOL 840A electron microscope, or a Focussed Ion Beam Microscope (FIB) as described in Chapter 2. Raman spectroscopy was conducted using the 514.5 nm line of an inVia Renishaw Raman

---

[1]Andrew Shortland, now at Cranfield University is thanked for providing this sample; the well at Bir al Hurritiya al-Gubli has now been built over and so no new samples could be collected

spectrometer and in the examination of pigments which are sensitive to heat, such as iron minerals, the laser power at the sample was reduced to 0.8 mW, or less.
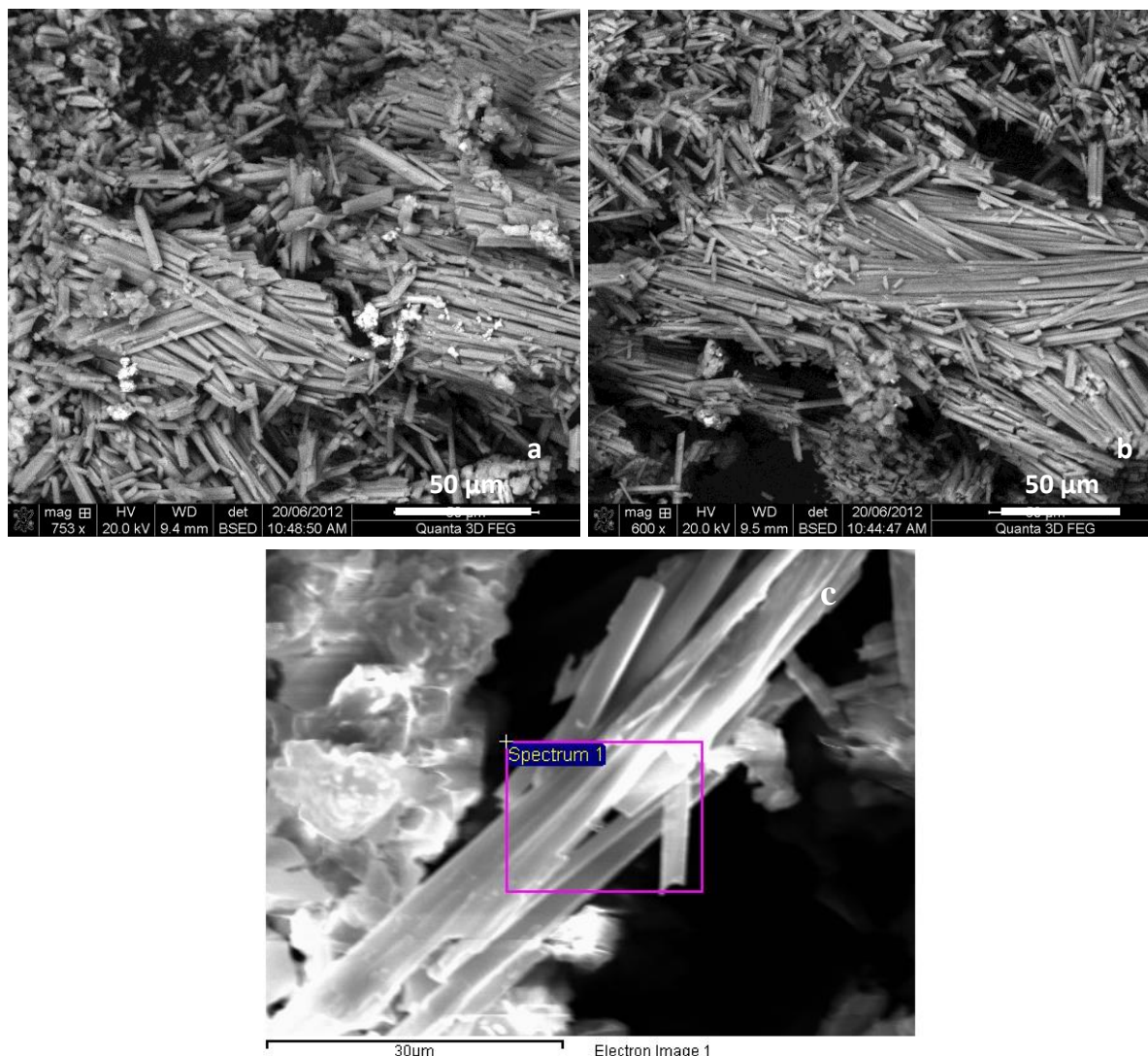
Figure 5.1. BSE images of Dakhleh Oasis alum sample D1A. (a) and (b) are low vacuum, FIB images, (c) is a high vacuum carbon-coated JEOL 840A BSE image.

5.1.3 Results

Back Scattered Electron (BSE) images of two alum samples are given in Figures 5.1 and 5.2. The Raman spectroscopy stacked plots for these alums are given in Figures 5.3 and 5.4 and the analyses of the Raman spectra are provided in Table 5.1. Table 5.1 also lists the Raman spectra for minerals that have been reported to be present in Western Oases alum analyses by other workers using XRD.   SEM-EDS analyses are provided in Table 5.2.   Raman spectroscopy has shown that for the samples examined in which alums are present, the transition element-based minerals are related to the trichite family.   Comparing the alum samples from Dakhleh and Kharga Oases shows some similarities in their chemical composition as given in Tables 5.1 and 5.2. Importantly, as provided in Table 5.2, Dakhleh

Oasis sample D1A is high in magnesium and sulphate, low in alumina and almost devoid of silica; D1A-2 has a high silica and iron concentration; whereas, the Kharga sample K18b is high in alumina and sulphate, variable but higher in silica and generally lower in magnesia. The Kharga sample also has a much higher concentration of manganese.

In Table 5.2, the elemental analysis marked 'w/p Spectrum 1' provides the analysis of the acicular minerals present in the Dakhleh alum D1A and marked Spectrum 1 in Figure 5.1. It is high in sulphate, alumina and in magnesia. Furthermore, the manganese mineral is concentrated within this mineral as shown by its analysis relative to the manganese analysis in D1A. In this sample, the weight percent for cobalt oxide, nickel oxide and zinc oxide are approximately equal one to the other and copper was in the order of approximately 50% of the concentration of each of the other transition metals. However, copper was not reported in w/p Spectrum 1, indicating that the copper present in D1A may not be directly related to the alum itself.
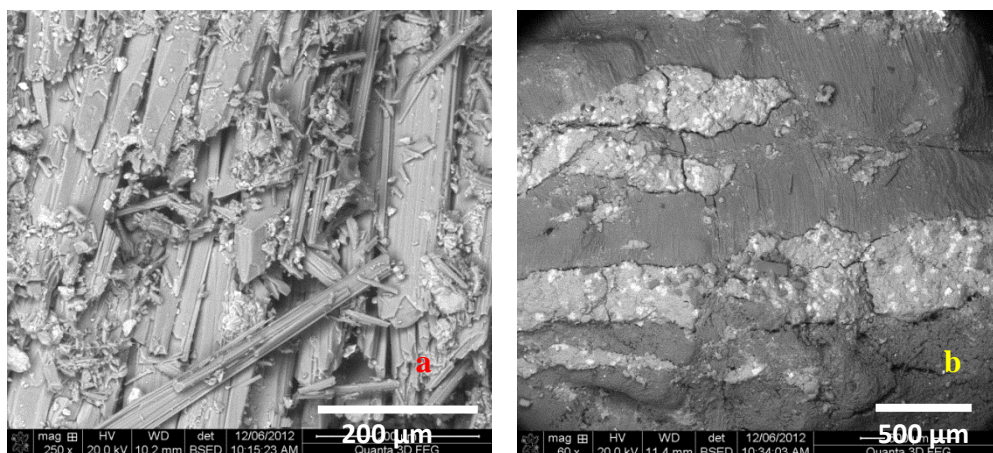
Figure 5.2 (a) and (b) are FIB BSE images of Kharga Oasis alum sample K18b.
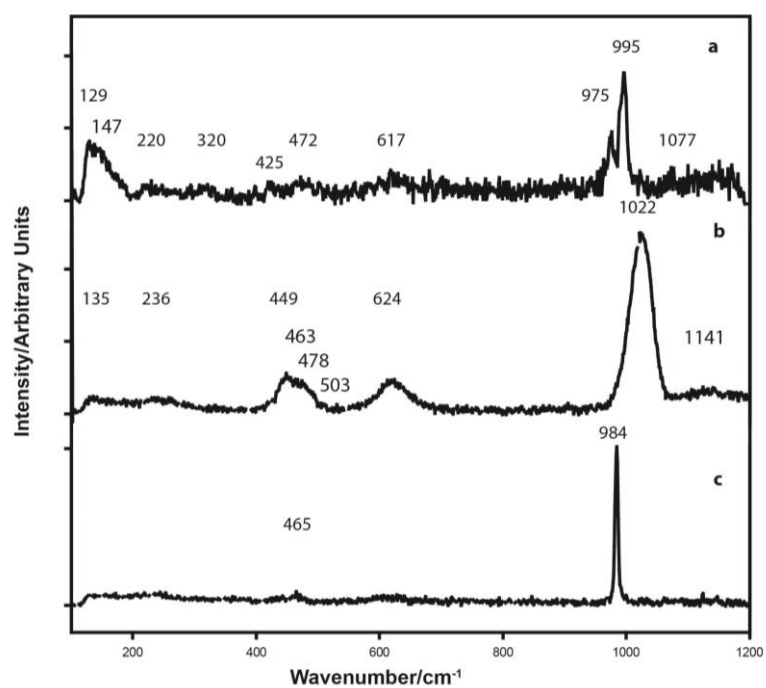
Figure 5.3.   Raman spectroscopy stacked plots for Dakhleh Oasis alum/clay sample D1A (λ=514.5nm).
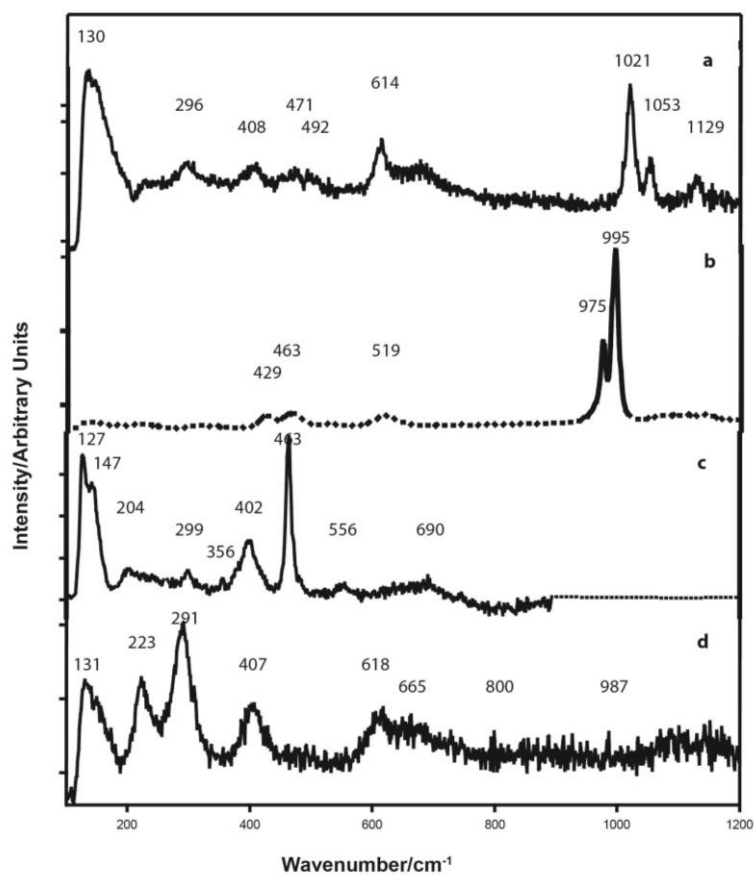
Figure 5.4.   Raman spectroscopy stacked plots for Kharga Oasis alum sample K18b (λ=514.5nm).

Table 5.1. Dakhleh and Kharga Oases cobalt-containing alum-based minerals. Raman spectroscopy band assignments are from the RRUFF database.

Sample / Mineral	Formula	Wavenumber/cm^{-1}	Dakhleh Oasis D1A	Kharga Oasis K18b
kieserite*	$MgSO_4.H_2O$	433, 499, **1042/1049**		
Starkeyite	$MgSO_4.4H_2O$	238, 464, 613, **1001**, 1047, 1155		
pentahydrite	$MgSO_4.5H_2O$	446, 597, **1005**		
hexahydrite	$MgSO_4.6H_2O$	485, 617, **998**		
epsomite	$MgSO_4.7H_2O$	227, 445, 467, 610, **983**, 1087, 1149	465, **984**	
apjohnite	$Mn^{2+}Al_2(SO_4)_4.22H_2O$	209, 309, 420, 454, 612, **974, 991**	425, 612, **975, 995**	423, 463, **975, 995**
boussingaultite	$(NH_4)_2Mg(SO_4)_2.6H_2O$	451, 622, 829, **983**		
dietrichite	$ZnAl_2(SO_4)_4.22H_2O$	321, 416, 465, 618, **973, 990**	320, 617, **975, 995**	463, 619, **975, 995**
halotrichite	$Fe^{2+}Al_2(SO_4)_4.22H_2O$	311, 421, 465, 613, **974, 994**	425, 617, **975, 995**	423, 463, 619, **975, 995**
pickeringite	$MgAl_2(SO_4)_4.22H_2O$	425, 460, 609, **975, 993**	425, **975, 995**	423, 463, **975, 995**
wupatkiite	$CoAl_2(SO_4)_4.22H_2O$	368, 428, 471, 619, **974, 994**, 1074	425, 472, 617, **975, 995**	423, **975, 995**
bieberite	$CoSO_4.7H_2O$	211, 275, 423, 504, 619, **984, 1025**	425, 617, **984**	
blödite	$Na_2Mg(SO_4)_2.4H_2O$	**992**		
geikietite	$MgTiO_3$	**209, 267, 334**, 386, 471, **699**		
ilmenite	$FeTiO_3$	223, 368, **678**		
rutile	TiO_2	233, 445, **608**		
brookite	TiO_2	**151,** 316, 407, 639		
wairakite	$Ca(Si_4Al_2)O_{12}.2H_2O$	**131, 146**, 326, 440, 912	**129, 147**	**130, 148**
muscovite	$KAl_2(Si_3Al)O_{10}(OH)_2$	**263,** 420, **703**		
dwornikite	$NiSO_4.H_2O$	**251,** 307, 353, 373, 447, **526**		
nickelhexahydrite	$NiSO_4.6H_2O$	**229, 377,** 462, 524, 682, **984,** 1043		
retgersite	$NiSO_4.6H_2O$	208, 369, 465, 611, **986**		
gunningite	$ZnSO_4.H_2O$	219, 275, 428, 503, 627, **1029,** 1083	503, 624, **1022**	
gypsum#	$CaSO_4.2H_2O$	420, 491, 623, **1008,** 1141		
γ-anhydrite#	$CaSO_4$	424, 490, 628, 668, **1026,** 1174		
α-anhydrite#	$CaSO_4$	490, 670, **1017**		
quartz	SiO_2	128, 205, **463**		129, 402, **463**
burkeite	$Na_4(SO_4)(CO_3)$	155, 452, 620, **993, 1063**		
alunogen	$Al_2(SO_4)_3(H_2O)_{12}.5H_2O$	300, 470, 607, **992**		
natroalunite	$NaAl_3(SO_4)_2(OH)_6$	**207,** 380, 458, 652, **1024,** 1048		**1021,** 1053
tamarugite	$NaAl(SO_4)_2.6H_2O$	460, 601, 624, **991,** 1066		
natrojarosite	$NaFe^{3+}_3(SO_4)_2(OH)_6$	**138, 224, 442,** 561, 622, **1010, 1108**		
ferricopiapite	$Fe^{3+}_{0.67}Fe^{3+}_4(SO_4)_6(OH)_2.20H_2O$	193, 268, 301, 451, **479,** 598, **993, 1019,** 1147		
coquimbite	$Fe^{3+}_2(SO_4)_3.9H_2O$	211, 284, 505, **1025,** 1202		
hematite	Fe_2O_3	226, **293, 411,** 613		223, **291, 407,** 618

*Wang *et al*. (2008) 39th Lunar and Planetary Conference, Houston, TX Abstract 2172.   # Prasad e*t al*. (2001)

Table 5.2. Average published analyses (or partial analyses) for alums recovered from Dakhleh and Kharga Oases by various researchers.

	Na2O	MgO	Al2O3	SiO2	P2O5	SO3	Cl	K2O	CaO	TiO2	MnO	FeO	CoO	NiO	CuO	ZnO	BaO	PbO
Dakhleh Oasis																		
Present research																		
D1A	1.2	8.1	22.9	0.3	0.0	61.1	0.1	0.0	0.0	0.1	2.6	1.2	0.8	0.3	0.9	0.7	0.0	0.0
D1A-2	5.3	4.9	14.7	23.6	0.0	33.4	0.0	1.1	0.2	0.4	0.0	12.1	1.2	1.6	0.6	1.1	0.0	0.0
w/p Spectrum 1	0.9	12.7	18.5	0.3	0.3	63.6	0.0	0.0	0.2	0.0	2.5	0.1	0.3	0.3	0.0	0.3	0.0	0.0
Kaczmarczyk (1986)																		
Dakhla alum 1		6.1	14.0			46.9					0.88	0.37	0.40	0.33		0.80		
Dakhla alum 2		8.5	10.7			47.7					0.93	0.25	0.43	0.58		0.99		
Dakhla alum 3		6.5	16.0								0.84	0.32	0.32	0.18		0.60		
Dakhla alum 4		6.0	16.1								1.13	0.35	0.31	0.16		0.62		
Shortland _et al_. (2006b)												Fe₂O₃	Co*	Ni*		Zn*		
K1	0.06	0.3	2.8						0.81	0.01	0.09	24.10	320	430		1400		
K3	0.01	3.5	9.9						0.01	0.78	0.52	0.40	1800	870		2600		
K5	0.02	0.3	3.3						0.78	0.09	0.17	22.60	480	690		2200		
K6		4.1	10.9						0.09		0.68	0.30	1800	1100		3300		
P3	0.01	2.3	12.4						1.49		2.99	0.30	920	520		220		
P4	1.31	3.8	12.1						0.09		0.66	0.20	960	870		650		
Kharga Oasis																		
Present research																		
K18b	0.0	3.7	24.9	31.2	0.2	31.4	0.0	0.3	0.2	1.3	1.6	5.0	0.2	<0.1	0.0	<0.1	0.0	0.0
Shortland _et al_. (2006b)												Fe₂O₃	Co*	Ni*		Zn*	*ppm	
Kharga P1	0.0	15.5	0.3						0.05		2.97	0.11	950	2500		15000		
Kharga KH6		20.5	0.1						0.03		0.00	0.08	1	3		2		
Kharga 17B	0.22	0.7	15.0						0.02		0.39	0.05	49	47		82		
Kharga 17CA		0.07	17.0						0.01		0.01	0.05	3	7		7		
Kharga 17F		3.5	11.6						0.02		1.82	0.03	260	220		390		

Table 5.3. SEM-EDS analyses of the slag sample marked MUT 31/405 G10 1/6 (104) S2002.58 10.1.02 at the external surface and at the conchoidal fractured surface. Refer also to Appendix A5.

MUT 31/405 G10 1/6 (104) S2002.58 10.1.02
FIB analyses external surface

	Na2O	MgO	Al2O3	SiO2	P2O5	SO3	Cl	K2O	CaO	TiO2	MnO	FeO	CoO	NiO	CuO	ZnO	BaO	PbO	SnO2	As2O3	Cr2O3	Sb2O5
G101_A	0.8	5.6	20.7	36.2	1.7	3.0	0.6	1.0	20.6	0.6	0.7	7.4	0.5	0.3	0.5	0.0	0.0	0.0	0.0	0.0	0.0	0.0
G101_A1	1.0	4.5	30.0	16.7	1.4	1.8	1.0	0.8	24.6	0.6	2.0	6.2	3.1	2.2	1.2	2.8	0.0	0.0	0.0	0.0	0.0	0.0
Average	**1.0**	**5.1**	**25.8**	**26.5**	**1.6**	**2.4**	**0.8**	**0.9**	**22.6**	**0.6**	**1.4**	**6.8**	**1.8**	**1.3**	**0.9**	**1.4**	**0.0**	**0.0**	**0.0**	**0.0**	**0.0**	**0.0**
G101_S2	10.0	3.9	25.8	7.1	1.3	2.2	21.2	0.7	8.3	0.7	2.2	4.3	3.8	3.1	1.5	3.7	0.0	0.0	0.0	0.0	0.0	0.0
G101_S4	1.8	8.6	48.8	12.6	2.1	1.6	1.2	0.6	8.0	0.0	2.0	3.9	3.2	2.4	0.0	3.1	0.0	0.0	0.0	0.0	0.0	0.0
G101_S5	26.0	3.6	20.2	7.2	1.1	1.9	27.2	0.5	5.2	0.0	0.8	1.7	1.3	1.1	0.9	1.4	0.0	0.0	0.0	0.0	0.0	0.0
G101_S6	1.2	9.7	19.9	34.0	0.3	4.3	0.5	4.8	6.9	1.6	0.7	14.3	0.6	0.7	0.0	0.0	0.0	0.0	0.0	0.0	0.3	0.0
G101_S7	0.9	5.5	24.6	32.7	2.1	1.7	0.5	0.9	18.9	0.7	1.1	6.6	1.3	1.2	1.2	0.0	0.0	0.0	0.0	0.0	0.2	0.0

MUT Slag
Nova analyses core

	Na2O	MgO	Al2O3	SiO2	P2O5	SO3	Cl	K2O	CaO	TiO2	MnO	FeO	CoO	NiO	CuO	ZnO	BaO	PbO	SnO2	As2O3	Cr2O3	F
Slag 1	0.2	0.5	30.8	39.7	0.2	0.3	0.0	2.9	0.0	0.5	0.1	12.6	0.0	0.1	0.7	0.3	0.0	11.2	0.0	0.0	0.0	0.0
Slag 2	1.4	0.7	23.4	45.9	1.3	5.7	0.0	3.0	1.0	0.3	0.0	7.1	0.0	0.4	1.4	0.3	0.0	8.0	0.0	0.0	0.1	0.0
Slag 3	0.8	0.0	0.5	2.9	0.0	0.4	0.3	0.2	0.4	0.2	5.2	87.5	1.3	0.0	0.3	0.0	0.0	0.0	0.0	0.0	0.0	0.0
Slag 4_rod	2.4	0.7	0.5	1.4	0.7	0.0	0.3	0.0	0.0	0.0	1.6	92.4	0.0	0.0	0.0	0.0	0.0	0.0	0.0	0.0	0.0	0.0
Slag 5	0.5	0.6	1.4	4.2	0.0	0.5	0.3	0.3	0.5	0.4	4.7	86.6	0.0	0.0	0.0	0.0	0.0	0.0	0.0	0.0	0.0	0.0
Slag 6	0.3	0.0	0.0	0.2	0.0	33.1	0.0	0.0	0.0	0.0	0.0	0.5	0.0	0.0	0.6	0.0	65.4	8.4	0.0	0.0	0.0	0.0

Table 5.3a. Elemental analyses of the clay/carbonate mineral samples.

Sample D1

	Na2O	MgO	Al2O3	SiO2	P2O5	SO3	Cl	K2O	CaO	TiO2	MnO	FeO	CoO	NiO	CuO	ZnO	BaO	PbO	SnO2	As2O3	Cr2O3	Sb2O5
D1_1	1.0	3.7	21.1	52.8	1.1	0.8	2.3	4.1	2.6	0.8	0.0	9.1	0.0	0.0	0.5	0.0	0.0	0.0	0.0	0.0	0.0	0.0
D1_2	0.1	2.1	11.5	77.4	0.4	0.8	0.9	1.9	1.3	0.0	0.0	3.5	0.1	0.0	0.1	0.0	0.0	0.0	0.0	0.0	0.0	0.0
Average	**0.6**	**2.9**	**16.3**	**65.1**	**0.8**	**0.8**	**1.6**	**3.0**	**2.0**	**0.4**	**0.0**	**6.3**	**tr**	**0.0**	**0.4**	**0.0**	**0.0**	**0.0**	**0.0**	**0.0**	**0.0**	**0.0**

Sample D2

	Na2O	MgO	Al2O3	SiO2	P2O5	SO3	Cl	K2O	CaO	TiO2	MnO	FeO	CoO	NiO	CuO	ZnO	BaO	PbO	SnO2	As2O3	Cr2O3	Sb2O5
D2_1	0.1	2.0	17.6	55.2	0.0	3.4	1.0	2.6	11.9	0.0	0.0	5.1	0.2	0.5	0.1	0.0	0.2	0.0	0.0	0.0	0.0	0.0
D2_2	0.2	2.2	19.5	47.9	0.4	6.0	0.8	2.8	11.0	1.4	0.6	6.6	0.4	0.2	0.0	0.0	0.0	0.0	0.0	0.0	0.0	0.0
Average	**0.2**	**2.1**	**18.6**	**51.6**	**0.2**	**4.7**	**0.9**	**2.7**	**11.5**	**0.7**	**0.3**	**5.9**	**0.3**	**0.4**	**tr**	**0.0**	**0.1**	**0.0**	**0.0**	**0.0**	**0.0**	**0.0**

Sample D3

	Na2O	MgO	Al2O3	SiO2	P2O5	SO3	Cl	K2O	CaO	TiO2	MnO	FeO	CoO	NiO	CuO	ZnO	BaO	PbO	SnO2	As2O3	Cr2O3	Sb2O5
D3_1	0.2	3.4	21.8	59.8	0.1	0.5	0.1	3.6	0.6	0.9	0.0	7.9	0.2	0.0	0.0	0.9	0.0	0.0	0.0	0.0	0.0	0.0
D3_2	0.4	3.6	16.7	62.5	0.6	0.0	0.0	4.2	0.9	0.0	0.0	9.8	0.2	0.2	0.6	0.0	0.2	0.0	0.0	0.0	0.0	0.0
Average	**0.3**	**3.5**	**19.3**	**61.2**	**0.4**	**0.3**	**tr**	**3.9**	**0.7**	**0.5**	**0.0**	**8.9**	**0.2**	**0.1**	**0.3**	**0.5**	**0.1**	**0.0**	**0.0**	**0.0**	**0.0**	**0.0**

Sample D4

	Na2O	MgO	Al2O3	SiO2	P2O5	SO3	Cl	K2O	CaO	TiO2	MnO	FeO	CoO	NiO	CuO	ZnO	BaO	PbO	SnO2	As2O3	Cr2O3	Sb2O5
D4_1	14.1	1.8	18.3	37.3	0.4	0.3	16.7	0.9	3.3	0.5	0.0	6.0	0.1	0.0	0.2	0.0	0.0	0.0	0.0	0.0	0.0	0.0
D4_2	9.5	1.1	19.6	42.4	0.4	0.0	9.0	1.6	2.8	1.8	0.0	9.9	0.7	0.1	1.1	0.2	0.0	0.0	0.0	0.0	0.0	0.0
Average	**11.8**	**1.5**	**19.0**	**39.9**	**0.4**	**0.2**	**12.9**	**1.2**	**3.1**	**1.2**	**0.0**	**8.0**	**0.4**	**tr**	**0.7**	**0.1**	**0.0**	**0.0**	**0.0**	**0.0**	**0.0**	**0.0**

A large sample of the Kharga K18b ore was placed directly into the FIB microscope and analysed under low vacuum conditions and, as shown in Table 5.2, no copper was able to be detected in any of the area or spot analyses conducted. In the report of Shortland *et al.* (2006b) the presence of copper was not reported. Shortland has confirmed[2] that copper was not detected above trace concentrations in any analysis. One spot analysis did indicate the presence of a titanium-based mineral such as anatase, brookite, rutile or more likely, ilmenite.

As shown by their respective Raman signatures in Table 5.1 for samples D1A and K18b the identification of pickeringite is favoured over halotrichite or other members of the trichite family. This is supported by their Raman signature for the position of bands at 423, 463, 975 and 995 cm^{-1} in the Kharga sample and at 425, 975 and 995 cm^{-1} for the Dakhleh sample. The presence of apjohnite (a Mn^{2+} trichite member), dietrichite (a Zn^{2+} trichite member), (and the zinc-containing mineral gunningite, halotrichite (Fe^{2+} trichite member) and wupatkiite (Co trichite member) epsomite (and possibly hexahydrite) are all indicated by their respective Raman signatures. Also present in both D1A and K18b is the mineral wairakite shown by its Raman signature. As shown in Table 5.1, the Kharga Oasis sample K18b also contained natroalunite, quartz, and hematite.

As indicated in Table 5.2, the transition metal concentrations in Dakhleh alum samples D1A, D1A-2 and Kharga K18b (Mn, Co, Ni, Zn) are generally of the same order of magnitude as those provided by Kaczmarczyk (1986: Table 34.3) and given here in Table 5.2. Manganese was not detected in sample D1A-2, a high iron, high silica alum. In the present study, copper was detected in all Dakhleh Oasis samples containing transition metals.

5.1.4 Clay/carbonate based samples

Dakhleh Oasis samples D1-D4 are described herein as being clay/carbonate-containing minerals. Their mineralogy is provided in Table 5.1 and their SEM-EDS analyses are given in Table 5.3a. As indicated, the iron mineralisation at approximately 6 to 9 wt.% and silica at 40-65% are significantly higher than that found in the alum sample D1A. However, magnesia at about 3% and almost no sulphate is present in any of the clay minerals. Traces of Co, Ni, Cu and Zn are variably present in these samples.

Raman spectroscopy indicated that the four clay-based samples varied widely one to the other in their mineralogy. Sample D1 was an alum containing quartz, anhydrite and both jarosite and natrojarosite. Sample D2 contained significant calcium and provided a Raman signature for calcite. Jarosite was also present in sample D2. Sample D3 contained significant alkali and plagioclase feldspars. And, sample D4 indicated a composition related to jarosite and burkeite.

---

[2]Shortland, Pers. comm. 24/01/2014

5.1.5 Discussion with respect to the alum mineralogy

The variability in composition of these samples would suggest that additional minerals may be detected if in the future a larger suite of minerals becomes available. Furthermore, long-term aging of these samples in the more humid Melbourne atmosphere could have modified, by hydrolysis, the composition of some of the alum samples.

The subterranean waters feeding the mineral springs at Dakhleh and Kharga are anaerobic, acidic and rich in both hydrogen sulphide and carbon dioxide (Clarke 1979). Furthermore, Clarke postulated that based on the carbon dioxide, iron, and calcium carbonate saturation values, the Dakhleh Oasis waters are more corrosive than those located at Kharga. Thus, these acidic and corrosive waters have the ability to dissolve iron, calcium and other components and re-precipitate them at the air/water table interface, thereby replenishing the various sulphate minerals within the oasis.

These alums have previously been described by Segnit (1987) and Shortland *et al*. (2006a, 2006b). Bachmann *et al*. (1980) reported that the alums were based on potash as alunite, which when heated to 800°C would form alumina.   This would then react with the cobalt oxides to form the spinel phase ($CoO.Al_2O_3$). As shown in Table 5.2, and by Rehren (2001: 484) potash was not present in the alum.   Furthermore, as shown by Weast (1978), aluminium sulphate decomposes at 770°C whilst magnesium sulphate decomposes at 1124°C. Magnesium sulphate will react with silica, particularly in the presence of an alkali flux at approximately 1000°C. Hope *et al*. (2009: 173) reported that the Dakhleh Oasis alums contained alunogen, together with apjohnite, wupatkiite and dietrichite. The presence of these minerals is confirmed by Raman spectroscopy as provided in Table 5.1. In their report, Shortland *et al.* (2006a) noted that a field study conducted in Dakhleh Oasis in September 2002 failed to detect cobalt in any of the samples analysed.

Shortland *et al*. (2006a) re-analysed the original samples obtained by Kaczmarczyk and by Picon. They proposed that from the XRD analyses of 6 samples from the Dakhleh Oasis, together with pickeringite, the samples variously contained coquimbite (aluminocopiapite), ferricopiapite, alunogen, starkeyite, tamarugite and gypsum. Segnit (1987) analysed a separate suite of samples from the Dakhleh Oasis and reported that an XRD analysis showed the presence of coquimbite, which would undergo gradual hydrolysis, together with copiapite, natrojarosite, pickeringite, hexahydrite and epsomite. As previously noted, these researchers did not detect copper other than at trace concentrations.

In examining six of the samples they recovered from Kharga Oasis using XRD, Shortland *et al.* (2006a) reported that the principal minerals determined were pickeringite, alunogen, halotrichite and pentahydrite (kieserite). The principal Raman signatures for these minerals are given in Table 5.1; the Kharga sample 18b which was not reported upon by Shortland *et al*. (2006a), does not support the presence of all of these minerals, rather, as provided in Table 5.1, a slightly different suite of minerals is present in this sample.   Traces of cobalt, nickel and zinc together with a higher manganese concentration were detected in Kharga Oasis sample K18b. As shown in Table 5.1, the Kharga Oasis sample K18b also contained natroalunite, anhydrite, quartz, and hematite.

Zinc is present in similar or greater concentrations than cobalt in the Dakhleh and Kharga Oases alums. It has been identified as dietrichite and as gunningite at Dakhleh Oasis, but not at Kharga Oasis. Cobalt when doped in zinc oxide matrices will produce various colours, particularly blue but also green (Lavat *et al*. 2008; Forés *et al*. 2000; de Souza *et al*. 2009; Bhargava *et al*. 2011) and, as demonstrated by Forés *et al*. (2000) the presence of very low concentrations of cobalt substituting for zinc in a willemite (Zn_2SiO_4) structure provides a lighter shade of blue. Noll (1981b: 136) stated that zinc stabilised the cobalt blue colour. The present results would support such a statement.

In the present study, copper was detected in all Dakhleh Oasis samples in which the transition metals were also present. Riederer (1974) also reported traces of both copper and beryllium; beryllium cannot be detected in the electron microscope used in the present study.

As shown in Table 5.2, the limited number of analyses available would suggest that the alum deposits at Dakhleh may have been richer in cobalt than the Kharga deposits. And, whilst the manganese concentrations are highly variable, the Kharga alums probably are higher in this element. Shortland *et al*. (2006a) suggested that the alums richest in cobalt seem to have come from Ain Asil in Dakhleh. But, the limited number of analyses and their variability suggest that it is possible, and indeed probable, that alums richer in cobalt exist in other sites in the Dakhleh Oasis and/or in the Kharga Oasis.

The extraction of the cobalt mineral from the alum and its conversion into a pigment will be discussed in Section 5.8.

5.2 Mut al-Kharab slag sample

5.2.1   *Sample analysis*

The elemental analyses were conducted using a Focussed Ion Beam Microscope (FIB) as described in Chapter 2. Raman spectroscopy was conducted using the 514.5 nm line of an inVia Renishaw Raman spectrometer and in the examination of pigments which are sensitive to heat, such as iron minerals, the laser power at the sample was reduced to 0.8 mW, or less. Mössbauer spectroscopy was conducted using [57]CoRh as the radiation source as previously described (Jay and Cashion 2013).

As discussed by Bouchard and Gambardella (2010), Raman spectroscopy is a perfect tool for studying the doping of various elements in the spinel lattice. They reported that at low concentrations of doping agents, XRD is unable to distinguish between doped and non-doped spinels and this has led to earlier studies being somewhat inconclusive with respect to the form of cobalt mineralisation.

5.2.2 *Results*

Pottery kilns have been excavated at a number of sites throughout the Dakhleh Oasis region. Many of these kilns appear to have been employed in the production of pottery vessels

intended for local use. Several kilns have been located in close proximity to each other, potentially suggesting the existence of one or more high temperature workshops (Eccleston 2006: 75). At site 31/405-F9-1 a large Roman period kiln has been excavated and based upon the clinker recovered, it would appear to have been employed for the burning of limestone, the lime then being used as wall plaster. To date, the kilns excavated have either been dated to Old Kingdom or to Ptolemaic or Roman periods.

An image is provided in Figure 5.5 of a stalactite-like sample (31/405-G10-1/6 S2002.58) showing a conchoidal fracture. The sample appears to have been broken away from a kiln wall when cold. It was recovered from a disturbed context (104) in an excavation below the floor of a shrine due west of the temple dedicated to Seth ("Lord of the Oasis") at Mut al-Kharab (Hope in press). A number of visually similar lumps of slag were excavated. However, to date, no kiln has been located and excavated within the immediate location of this sample although a magnetometer survey of the site indicates their possible existence in the vicinity. This sample is presently tentatively dated to 18th Dynasty production. As it was recovered from a highly disturbed site, this tentative dating may well be revised by further studies.

The term "slag" applied to this sample is in accordance with the discussion provided by Nicholson (2013: 72). If the stalactite-like runs illustrated of the internal structure of kiln HAC3, a late 2nd century kiln at Memphis (Nicholson 2013: 64) were to be broken away, their visual appearance would generally relate to the present sample.

Nicholson (2013: 78) noted that the slag recovered from kiln HAC3 at Kom Helul has not resulted from either metallurgical processes nor derived from the faience glaze raw materials. The present sample from Mut al-Kharab may indicate a slightly different kiln usage and therefore a slightly different slag formation. It does show the presence of transition elements, including cobalt, nickel and zinc and both magnesium and alumina. Within this chapter, alternative possible uses or requirements for this undiscovered kiln will be postulated.

The surface texture of the Mut al Kharab and the Kom Helul slags bear visual surface similarities. Nicholson suggested that the surface texture at Kom Helul was caused by the Halfa grass biomass used as the kiln fuel pressing against the molten slag, thereby imparting a surface texture to the slag. The high silica and alkali content in this biomass reacted with the kiln structure and this contributed significantly to the slag formation.

Figures 5.6 and 5.7 are BSE images of surface features. Figure 5.8 is the Raman spectrum obtained from the conchoidal fractured surface (core), and Figure 5.9 provides the Raman spectra from the external surfaces. The elemental analysis is given in Table 5.3 and the Raman spectra interpretations are provided in Table 5.4. Figures 5.10 and 5.11 are Mössbauer spectra of the iron phases present in respectively the core at the broken surface and at the external surface of the slag sample as described below.

Samples for [57]Fe Mössbauer spectroscopy[3] were prepared by scraping material from the curved outer surface of the slag (top surface in Figure 5.5) and from the fractured surface (left hand end in Figure 5.5) with a diamond tipped tool. The material from the curved surface came away both as powder and in the form of long needles, some up to 5 mm in length, which had formed in the flutes. Scraping the fracture surface produced fine powder as expected. Both samples were made up as absorbers to approximately 20 mg/cm² and mixed with boron nitride to ensure a uniform distribution. In contrast to usual practice, the material from the outer surface was not crushed, with the powder and needles used together. This allowed for the needles of various lengths to lie approximately flat in the absorber holder.

The room temperature spectrum of the core is shown in Figure 5.10. The majority of the spectrum shows strong magnetic ordering and this part has been fitted to four sextets using Voigtian lineshapes. The parameters are all given in the data accompanying Figures 5.10 and 5.11. From the similarity of the isomer shift and quadrupole splitting, it can concluded that they are all due to the same species with the parameters of the best formed one being very close to that of goethite, the literature values of which are also given accompanying Figure 5.11 together with the only other possibility, hematite.

Natural mineral samples of goethite very rarely have hyperfine fields of 38 T due to poor crystallinity or impurities such as Al^{3+}, other transition elements, vacancies or embodied OH^- or H_2O. These all have the effect of lowering both the Néel temperature from its usually accepted value of 400 K and the saturation hyperfine field. Consequently the spectra are commonly fitted with a distribution of hyperfine fields to account for the range of local environments of the iron ions. This provides rational and reproducible fits over a range of temperatures as reviewed, for example, by Murad and Cashion (2004: 77). In the present case, to minimize the number of parameters four sextets have been used to approximate this distribution to sufficient accuracy. The largest fitted hyperfine field in this spectrum is 97% of the maximum literature value, attesting to the purity of this best component of the iron phase.

There is one additional component in Figure 5.10 which is a doublet due to a paramagnetic ferric species. The quadrupole splitting of 0.74 mm/s is higher than that usually recorded for superparamagnetic goethite of approximately 0.5 mm/s, although the isomer shift value is correct. Consequently it is likely that the Fe^{3+} is in an aluminosilicate or other mineral approaching that of a high iron-containing oxide whose structure may possibly have been changed by firing in the kiln.

---

[3]Mössbauer spectroscopy was kindly conducted by Prof. J.D. Cashion, School of Physics and Astronomy, Monash University.

Figure 5.5. Slag sample recovered from excavation below the floor of a shrine at Mut al Kharab.

Figure 5.6. Image of high iron particle within the core of the Mut al Kharab slag sample.
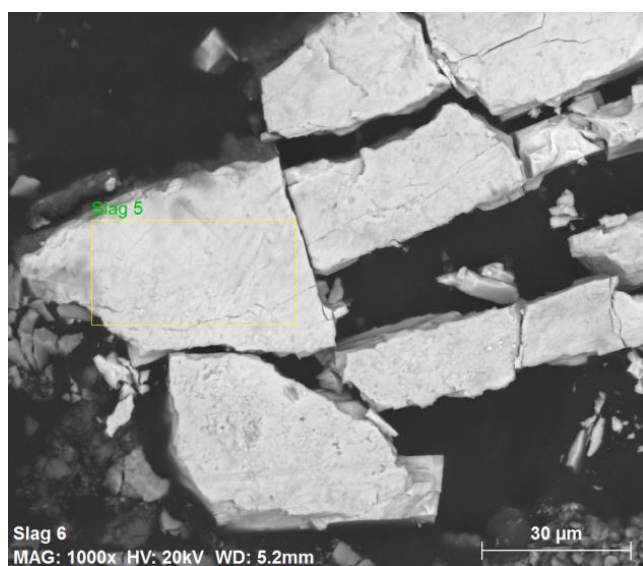

Figure 5.7. SEM image of a barium-based mineral within the core of the Mut al Kharab slag sample. Beadnell (1899: 103) reported barytes in sandstone and it is possible that they formed part of the raw materials selected for the construction of the kiln walls.

The room temperature spectrum of the scrapings from the outer surface is shown in Figure 5.11. It has been fitted to four magnetic sextets as for Figure 5.10, and is similarly an approximation to a relatively continuous distribution of hyperfine fields. The outer field of 36.0 T is again a remarkably high value for goethite which has been exposed to the atmosphere. It is noticeable that there is no paramagnetic doublet present in this spectrum suggesting that the material has been recrystallized on the outer surface in a process which was not available to the mineral responsible for the doublet. This conjecture is supported by the unusual intensity of the lines in the sextets. In a powder sample, the six lines in a magnetic sextet normally have the relative intensities 3:2:1:1:2:3 and this constraint was used in fitting Figure 5.10. However, in a single crystal, these intensities change to 3:4:1:1:4:3 if viewed parallel to the magnetization direction, or 3:0:1:1:0:3 if viewed perpendicular to the magnetization direction. The suspicion that the needles which flaked out of the flutes were single crystals is confirmed by the intensities of the lines in Figure 5.11 which are, on average, 3:2.9:1:1:2.9:3, a conclusive result given that no attempt was made to separate the needles from the powder, nor to orient the needles. Thus the outer surface has been modified by some process of dissolution and recrystallization during burial since the original firing as it is most unlikely that single crystals of many mm in length would be formed during the firing, even for an extended firing.

Fitted parameters to the Mössbauer spectra in Figures 5.10 and 5.11, together with the literature values for goethite and hematite. IS = isomer shift, QS = quadrupole splitting, ε = value of the QS associated with a sextet, Δ = QS of a doublet, HFF = magnetic hyperfine field, $\sigma(B)$ = the standard deviation of the hyperfine field distribution, A_2/A_3 = ratio of lines 2 and 3 in the sextet, * indicates that the value was fixed in the fitting. Values in brackets are the 90% uncertainty in the least significant digit.

Sample	IS (δ) mm/s	QS (ε or Δ) mm/s	HFF (B) T	$\sigma(B)$ T	A_2/A_3	Area %
Core	0.38(1)	-0.13(1)	36.9(1)	0.7	2*	10.2
	0.39(1)	-0.14(1)	34.5(4)	1.7	2*	11.1
	0.39(1)	-0.12(1)	30.3(10)	3.7	2*	23.8
	0.37(4)	-0.10(4)	18.8(11)	12.8	2*	22.8
	0.38(1)	0.74(1)	n/a	n/a	n/a	32.0
Surface	0.39(1)	-0.14(1)	36.0(1)	0.7	2.86(9)	36.0
	0.39(1)	-0.14(1)	34.0(8)	1.5	2.93(13)	32.0
	0.40(1)	-0.12(2)	29.5(13)	3.9	2.87(20)	24.7
	0.39*	-0.13(25)	10.1(42)	12	2*	8.1
Goethite	0.37	-0.13	38.0	n/a	2*	100.0
Hematite	0.37	-0.10	51.8	n/a	2*	100.0

The density of the sample was measured to be 3.3 g/cm^3. It should be noted that goethite has a density variously quoted in the range 3.4-4.4 g/cm^3 while diopside has a density of 3.39 g/cm^3 and wollastonite 2.8 g/cm^3 (Alizadeh and Murghussian 2000).
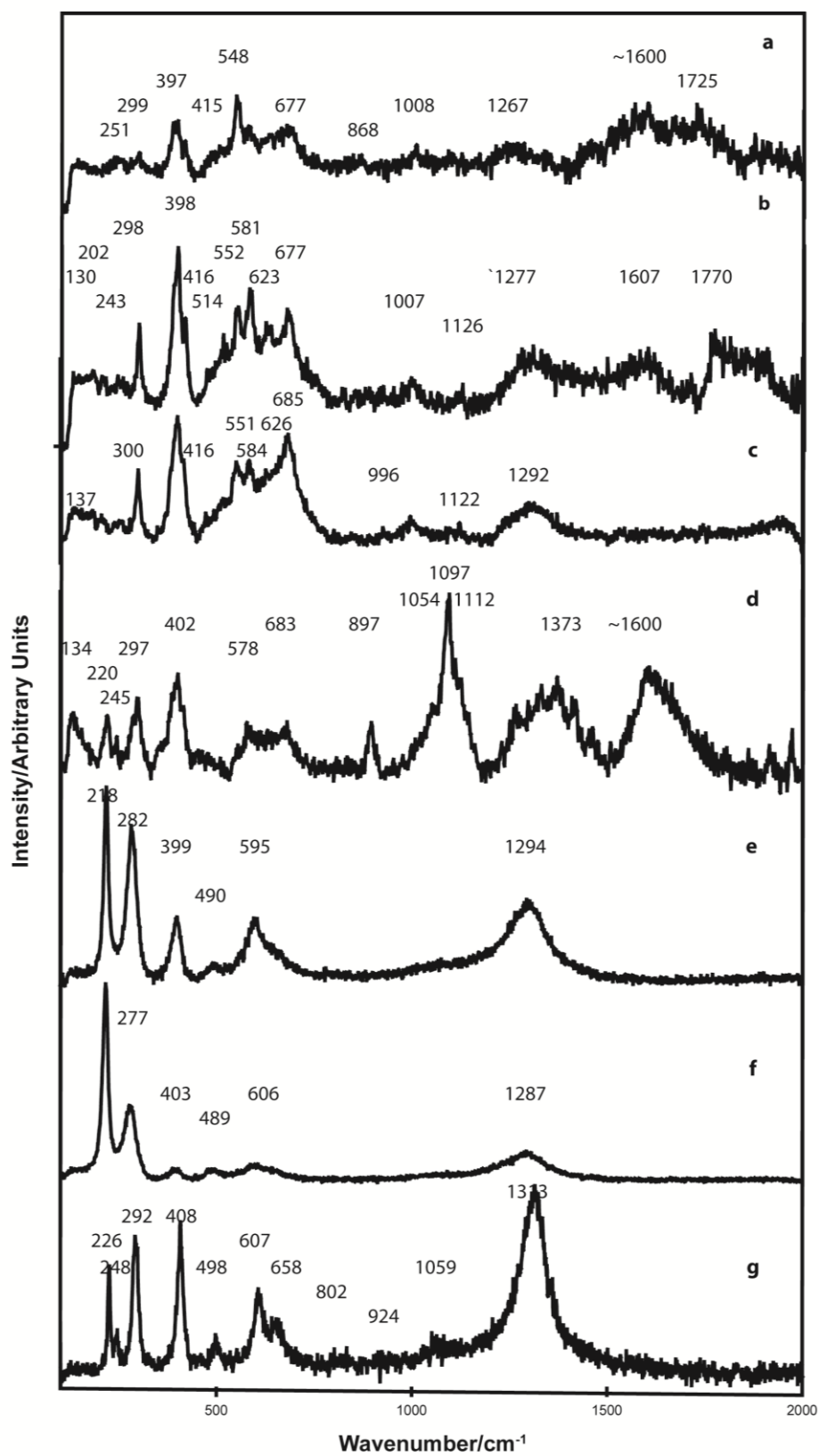
Figure 5.8.   Raman spectrum of Mut al Kharab slag core (λ=514.5 nm).
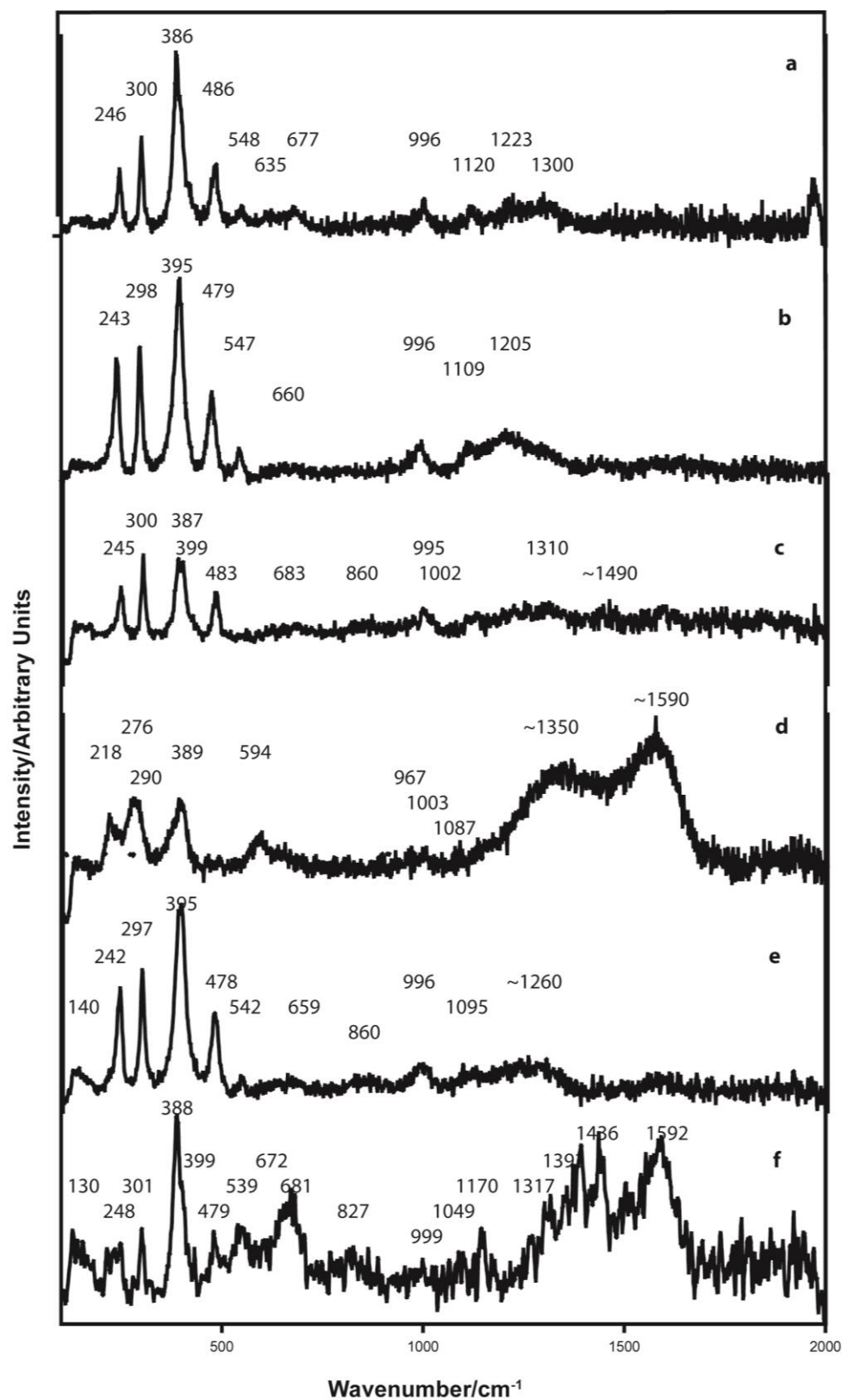
Figure 5.9. Raman spectrum of Mut al Kharab slag outer surface (λ=514.5 nm).
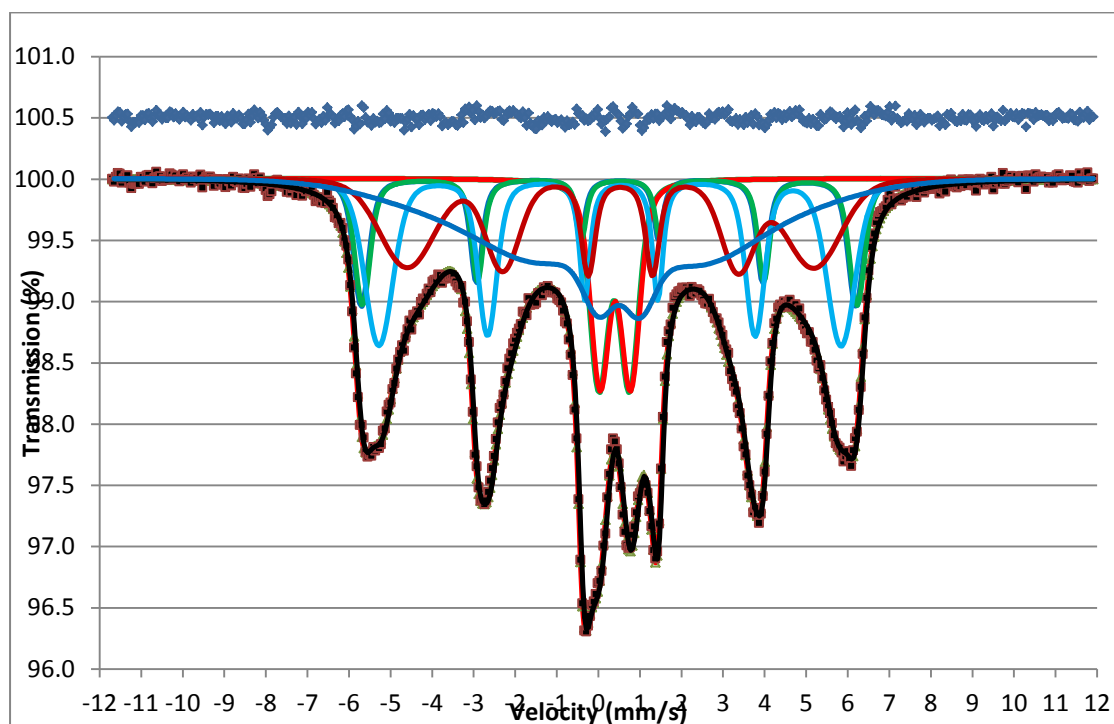
Figure 5.10. ^{57}Fe Mössbauer spectrum of powder scraped from the core. It has been fitted using Voigtians to four magnetically ordered sextets and one paramagnetic doublet. The blue line at the top is the difference between the data and the fit.
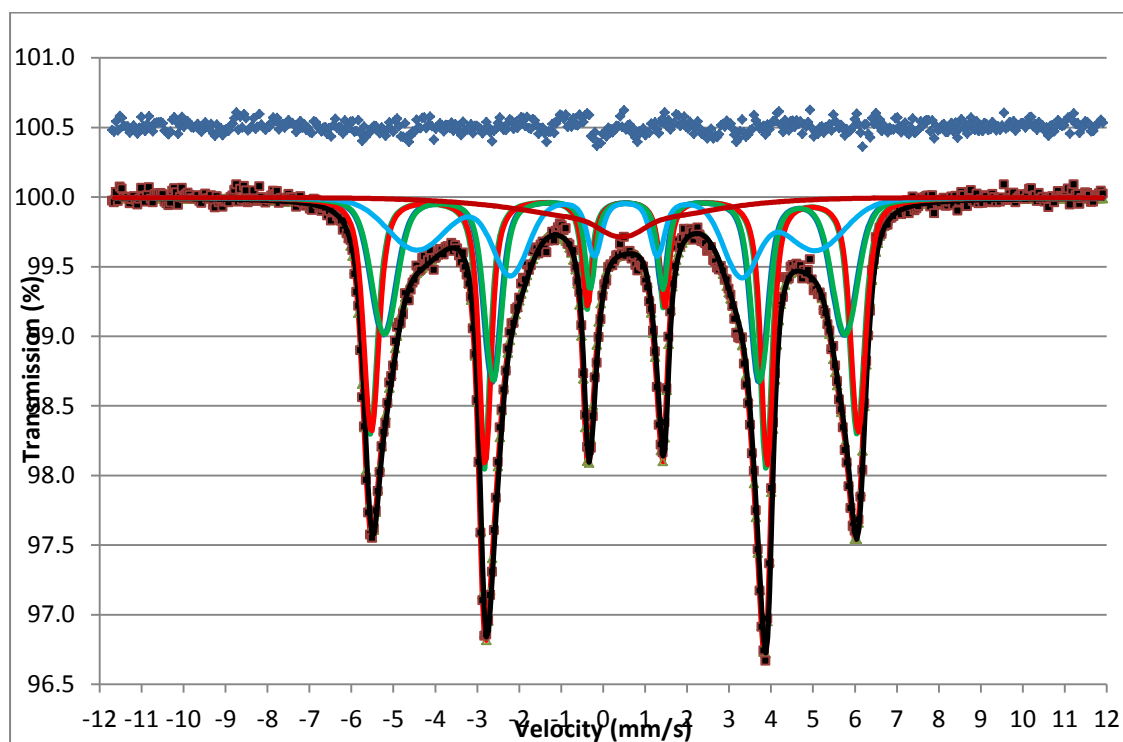
Figure 5.11. ^{57}Fe Mössbauer spectrum of mixed powder and needles scraped from the outer surface. It has been fitted using Voigtians to four magnetically ordered sextets. The blue line at the top is the difference between the data and the fit.

The slag sample can therefore be best described as high in alumina (clay), silica and iron and containing variable concentrations of magnesium together with low concentrations of transition elements. The variably high iron concentration is indicated in Table 5.3 and its Raman spectra provided in Figures 5.8 and 5.9 indicates the presence of goethite (α-FeOOH) and the spectrum shown in Figure 5.8(g) supports the presence of hematite. The surface also shows the Raman signature for diopside. As will be discussed within this report (for example at Section 5.3.1.3), these bands are slightly elevated from that of diopside itself due to the partial replacement of magnesium by transition elements. As shown in Figure 5.6, the core of the sample contains a particle of what would relate to bloomery iron; the elemental analysis of which provided an analysis of 60.4% Fe. Under extended burial, the particle has hydrated to goethite, retaining its original skeletal structure. Within the sample are several particles of baryte shown in Figure 5.7, the analysis of which is provided in Table 5.3. The external surface of the slag contained the transition elements Mn, Co, Ni, Zn in approximate equal proportions and therefore similar to the element ratios found in the Dakhleh Oasis alums. Variable concentrations of these transition elements exist within the slag particle. Lead oxide at an approximate concentration of 8-11% was found to be present in two core sample analyses. Tin was not detected. The core contained only minor calcium; however, the surface was variably high in CaO.

5.2.3 Discussion with respect to the Mut al Kharab kiln slag sample

This siliceous, aluminous, iron-containing lump of slag would have almost certainly been deliberately broken away from the internal surface of a kiln when cold. The kiln would have been operated under reducing conditions as shown by the presence of carbon in the Raman spectra; and at a sufficiently high temperature to volatilise various elements which have then condensed on the cooler wall surfaces of the kiln. As noted above, the biomass fuel used would have contributed significantly to slag formation. As shown in Figure 5.6, some of the iron oxide has been reduced to metal and the presence of this metallic rod indicates the redox firing conditions present in the kiln. Almost certainly, the aggressive siliceous slag has attacked the iron oxides and alumina present in the clay bricks forming the kiln walls. This would account for the high silica and alumina recorded in the slag; and, the alkali metals present in the biomass fuel would have lowered the melting point of the slag.

The surface of the sample as shown by its Raman signature contains goethite indicative of oxidative conditions resulting from the long burial period in a variably damp environment. Mössbauer spectroscopy confirms this, with the iron in the inner material distributed between goethite (68%) and a ferric aluminosilicate (32%), while the iron in the outer material is wholly goethite, much of which is composed of single crystals up to several mm in length. The ferric aluminosilicate is most likely diopside/hypersthene in which the iron is completely oxidised to ferric. Over the burial period, it would seem that the iron in the surface layers has exfoliated to form the single crystals of goethite, leaving the surface free of ferric aluminosilicate. Raman spectroscopy supports the presence of hypersthene as one such aluminosilicate and also the presence of ankerite, a calcium-iron carbonate. The presence of hematite as shown by its Raman signature (refer Figure 5.8(g)) obtained from well below the sample surface and within the core of the sample would suggest that at the time of formation of the slag, reducing conditions would have been present in the kiln.

The temperature within the kiln would have been in the order of 1000ºC as shown by the reaction of an iron source with magnesium to form hypersthene and the reaction of the transition elements also with magnesium to form the doped diopside as shown by their respective Raman signatures provided in Table 5.5. Several of the Raman spectra provided in Figures 5.8 and 5.9 show the presence of amorphous carbon indicating that the biofuel during combustion was generating some soot. The presence of this amorphous carbon supports the kiln being operated under reducing conditions.

Eccleston (2006: 182) reported that at the Roman period site C2/6 at Kellis, SEM analyses indicated the presence of Fe-Ca-Si and Al-Ca-Si phases containing some K, Na and Mg. Fuel ash slag containing high quantities of Ca, Mg and Al were recovered at Kellis. During the Roman period the biofuel used was reported to be acacia wood, palm fronds and straw (Eccleston 2006: 80). An analysis of such an ash type from Dakhleh Oasis is provided in Table 5.12.

Whilst this slag sample has many characteristics indicative of iron production, this is presently rejected. Firstly, the indicative age of the sample would preclude iron production. More importantly, the presence of cobalt and its accompanying transition elements in the sample would suggest that it has emanated from an alternative kiln use.

The cobalt and related transition metals found in the Dakhleh Oasis alums, together with magnesium oxides and found in this slag sample, suggest it could have resulted from the preparation of the cobalt-containing silica frit. The composition of the external surface material of the slag particle is remarkably similar to that of the cobalt used to decorate the vessels at Mut al Kharab and within the Nile valley. As will be discussed below, the final production step of the cobalt-based product involved a high temperature reaction.

A high calcium concentration was found on the surface of the Mut al Kharab slag sample but not within its core. Nicholson (2013: 76) reported that the Kom Helul HAC3 kiln slag visually contained small particles of lime on its surface. He suggested that handfuls of lime were presumably thrown into the Kom Helul kiln to help flux the slag by reducing the slag viscosity and thereby allowing it to run down the kiln walls. In Figure 5.9(d) the Raman band at 1087 cm^{-1} is indicative of the presence of calcite. At the kiln firing temperature, it would be expected that calcite would decompose to liberate carbon dioxide and form lime. Such lime would have been highly reactive and would have assisted in the formation of diopside. Therefore, the presence of residual calcite and the formation of ankerite would support the proposition of Nicholson (2013: 78) for the use of lime to flux the slag on the kiln wall surface to facilitate its later removal. The dissolution and recrystallization of these various iron phases present at the exposed surfaces of this slag sample would lead to further chemical modification of the surface of the sample during burial.

5.3 Cobalt blue pigment mineralogy and chemistry

This section is discussed in Appendix A5.
Raman spectral data is provided in Tables 2.25 and 2.25a, Appendix A2

5.4 Chemistry and Mineralogy of cobalt blue-decorated sherds

All of the supporting Raman spectroscopy data is provided in Chapter 2. This data is discussed in detail in Appendix A5.

5.4.1 Samples

The blue pigment upon 26 sherds has been analysed to determine its composition and particularly to attempt to identify any differences in the mineralogy of the pigments on sherds from different provenances. The sources of the sherds are: Amarna (8); Luxor – Malkata (9); Luxor - Karnak North (3); Luxor - Deir al-Medineh (1); Memphis (2); Dendera (1); North Sinai - Bir al-Abd (1) and Dakhleh Oasis - Mut al-Kharab (1). The sherds derive from surface collections except in the case of those from Mut al-Kharab and Bir al-Abd; the date range may be summarised as follows:

Malkata – late18[th] Dynasty, Amenhotep III to possibly Horemheb;
Amarna – late 18th Dynasty, probably Akhenaten;
Memphis - Ramesside period;
Deir al-Medineh - Ramesside
Dendera – New Kingdom
Karnak North – ?late 18th, possibly 19th Dynasty;
Bir al-Abd, North Sinai - late 18th Dynasty, uncertain find spot;
Mut al Kharab - from mid18[th] Dynasty, but more likely 19 to 20th Dynasties, or to the end of the Ramesside period (Hope *et al*. 2009).

Images of the sherds are provided in Figures 5.14(a) to 5.14(e).   Mineralogy was determined by Raman spectroscopy and is provided in Tables 5.4 to 5.6 and in detail for individual sherd samples in Appendix A5. The SEM-EDS elemental analyses were generally conducted using the FIB electron microscope and the results are provided in Table 5.7 and in detail in Appendix A5.

To date, no reported excavation conducted at any of the Nile valley or Western Oases sites has disclosed the presence of actual cobalt pigment production, although it was in widespread use for the decoration of a wide selection of vessels.

5.4.2 Analytical results

5.4.2.1 Cobalt

The EDS, Mössbauer, synchrotron and Raman data for each sample analysed is provided in Appendix A5 and provides part of the supporting evidence for the discussion within this chapter.

Figure 5.12(a). Images of Malkata sherd samples analysed. Some of the surfaces marked "burnished" may or may not have been burnished as the surface abrasion renders it difficult to necessarily reach a positive conclusion. Individual sherd results are provided in Appendix A5.

Malkata

Sample M3 (MA)	Sample M5 (MC)	Sample M6 (MD)	Sample M9 (Bachmann)	Sample M12 (M74/X ?G135) Tite (6)

MA:	Nile silt, cream burnished surface
MC:	Nile silt, white slip, pigment applied using beeswax
MD:	Nile silt, white slip, pigment applied using beeswax
Bachmann:	Nile silt, cream burnished surface
M74/X ? G135 Tite (6):	Nile silt, cream burnished surface

Sample M13 (M744/X G)	Sample M14 (M74/X G3989)	Sample M15 (M74/X G 3122)	Sample M16 (M74/X G138)

M74X/ G:	Nile silt, light cream, burnished surface.
M74/X G3989:	Nile silt, cream, burnished surface
M74/X G3122:	Nile silt, white, possible slip surface
M74/X G138:	Nile silt, cream, burnished surface

Figure 5.12(b). Images of Amarna sherd samples analysed. Individual sherd results are provided in Appendix A5.

Amarna			
Amarna 1 (Tite) (A1)	Amarna 2 (Tite) (A2)	Amarna 3 (Tite) (A3)	Amarna 4 (Tite) (A4)

Amarna 1 (Tite): Nile silt, burnished surface   Pigment applied using an unidentified wax
Amarna 2 (Tite): Nile silt, white slip
Amarna 3 (Tite): Nile silt, white slip
Amarna 4 (Tite): Nile silt, burnished surface

Amarna 362 (A5)	Amarna 423 (A6)	Amarna RH1 (A7)	Amarna RH2 (A8)

Amarna 362: Nile silt, cream slip
Amarna 423: marl, cream slip
Amarna RH1: Nile silt, burnished surface
Amarna RH2: Nile silt, burnished surface

Figure 5.12(c). Images of North Karnak sherd samples analysed. Individual sherd results are provided in Appendix A5.

Karnak		
PP100 (NK1)	PP449 (NK2)	PP473 (NK3)
PP100: Nile silt, cream burnished surface		
PP449: Nile silt, cream burnished surface		
PP473: Nile silt, cream burnished surface		
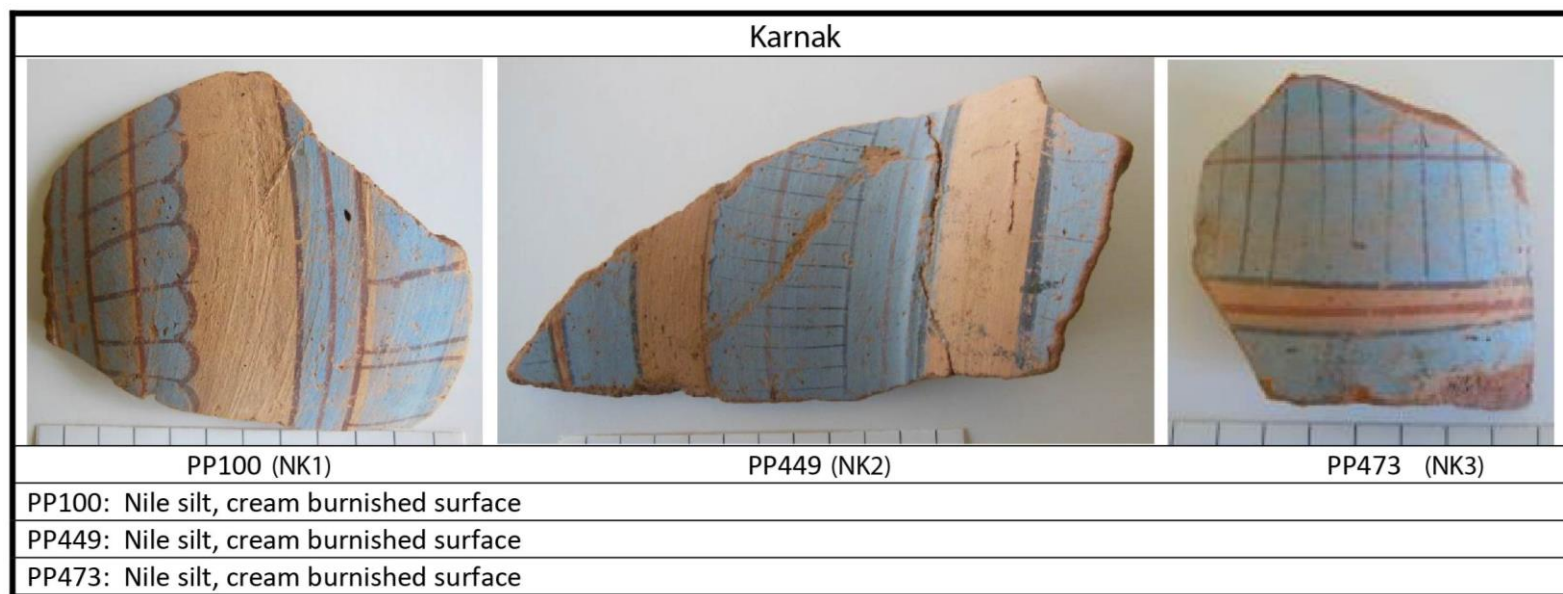
Figure 5.12(d). Images of sherd samples from various locations which have been analysed. Individual sherd results are provided in Appendix A5.

Memphis	Dendera	Deir el Medineh	Sinai
R1 R2	DE1	DM1	S1
	Nile silt, burnished surface	Nile silt, cream burnished surface	Nile silt, cream burnished surface

Figure 5.12(e). Image of a sherd sample from Mut el Kharab and of a sample of slag from the same region. Sherd results are provided in Appendix A5.

Mut al Kharab	Mut al Kharab Slag
Dakhlieh Oasis fabric, burnished surface	

Table 5.4. Raman spectra analyses for the cobalt-based pigments used to decorate a sherd from Mut al-Kharab and a slag from the same context. Refer also to Appendix A5.

Mineral	Formula	Wavenumber/cm^{-1}			
		RRUFF	**MUT D7 blue pigment**	**MUT slip**	**MUT slag**
quartz	SiO_2	266, 357, 402, **467**, 699, 810, 1162	464		
apatite	$Ca_5(PO_4)_3(OH,F,Cl)$	960, 1059			
diopside	$Ca(Mg,\square)Si_2O_6$	323, 356, 391, **666, 1012**, 1026	671, 1012		677, 1008
wollastonite	$CaSiO_3$	338, 412, 502, 581, **636, 972**			
anhydrite	$CaSO_4$	417, 499, 601, 676, **1017**, 1129			
gypsum	$CaSO_4.2H_2O$	414, 493, 670, **1007,** 1116		493, 1007, 1115	
aragonite	$CaCO_3$	155, 208, **1085/1088**			
calcite	$CaCO_3$	149, 276, 708, 1012, **1087**			
coquimbite	$Fe^{3+}_2(SO_4)_3.9H_2O$	211, **284**, 505, **1025**, 1202			
albite	$Na(Si_3Al)O_8$	290, 480, 508			
plagioclase feldspar	$Na_xCa_{1-x}Al_{1+x}Si_{3-x}O_8$	290, 486, **510**			
omphasite	$(Ca,Na)(Mg,Fe^{2+}Fe^{3+},Al(Si_2O_6)$	335, 377, 407, 556, **679**, 915, 1022			
heterogenite	$Co^{3+}O(OH)$	496, 621			
hypersthene	$(Mg,Fe^{2+})_2Si_2O_6$	656, 674, 1003			655, 677, 1007
mixed metal spinel	$(Mg,Zn,Mn,Fe)Al_2O_4$	~630	626		
cobalt aluminate	$CoAl_2O_4$	**~203, ~512**			
cobalt olivine	Co_2SiO_4	**824/826**			
magnesium olivine	Mg_2SiO_4	**820, 853**			
alunogen	$Al_2(SO_4)_3(H_2O)_{12}.5H_2O$	474, 607, **995**			
mooreite	$Mg_{15}(SO_4)_2(OH)_{26}.8H_2O$	437, 457, **982**			
amorphous carbon	C	~1350, ~1590			1350, 1590
anatase	TiO_2	**142/144**, 198, 392-398, 514-517, 637/			
ilmenite	$Fe^{2+}Ti^{4+})_3$	223, 368, **678**			677
actinolite	$Ca_2(Mg,Fe^{2+})_5Si_8O_{22}(OH)_2$	121, 178, 224, 393, **674**			178, 224, 388, 672
ankerite	$Ca_2Fe^{2+}(CO_3)_2$	287, **1094/1102**			290, 1087
copiapite	$Fe^{2+}Fe^{3+}_4(SO_4)_6(OH)_2.20H_2O$	242, 270, 302, **476, 985, 1027, 1114**			
goethite	$FeO(OH)$	245, **299, 396**, 478, 549			299, 395, 474, 554
hematite	$\alpha-Fe_2O_3$	225, 245, 292, 410, 496, 610, 1310			248, 292, 408, 498, 607, 1313
kôzulite	$NaNa_2[Mn^{2+}_4(Fe^{3+},Al)]Si_8O_{22}(OH)_2$	**386, 414**, 512, **597, 682, 904**, 1008,			388, 681, 900
mullite	$3Al_2O_32SiO_2$	480, 960, 1130, 1160			
Number of samples analysed			1	1	1

Table 5.5. Raman spectra analyses for the cobalt-based pigment decorated sherds from various locations and Dynasties. For individual sherd sample results, refer to Appendix A5.

Mineral	Formula	Wavenumber/cm^{-1}			
		Malkata	**Amarna**	**Karnak North**	**Memphis**
quartz	SiO_2	466	469	464	464
tridymite	SiO_2	293, 310, 354			
apatite	$Ca_5(PO_4)_3(OH,F,Cl)$	960, 1059	924, 966		
diopside	$Ca(Mg,\square)Si_2O_6$	324, 395, ~670, 1008, 1026	~670, 1009,	668, 1011	667, 1006
wollastonite	$CaSiO_3$		963, 1045		401, 506, 973
anhydrite	$CaSO_4$	420, 503, 1016, 1129	416, 1015, 1127	502, 609, 1015	1017
gypsum	$CaSO_4.2H_2O$	491, 673, 1134, 1007, 1143	414, 496, 626, 1009, 1131		
aragonite	$CaCO_3$	278, 713, 1085			
calcite	$CaCO_3$	1087			
coquimbite	$Fe^{3+}_2(SO_4)_3.9H_2O$			291, 496, 1025	281, 506, 1028
gunningite	$ZnSO_4.H_2O$				506, 621, 1028
albite	$Na(Si_3Al)O_8$	490, 510			
plagioclase feldspar	$Na_xCa_{1-x}Al_{1+x}Si_{3-x}O_8$		176, 287, 481, 510		
omphasite	$(Ca,Na)(Mg,Fe^{2+}Fe^{3+},Al(Si_2O_6))$	504, 905, 1015			
gunningite	$ZnSO_4.H_2O$				506, 621, 1028
$Zn_{1-x}Co_xO$ (x = 0.2)		490, 628	627, 717, 992		
heterogenite	$Co^{3+}O(OH)$	496, 621	495, 624	502, 628	506, 621
hypersthene	$(Mg,Fe^{2+})_2Si_2O_6$				392, 661, 871, 936, 1003
mixed metal spinel	$(Mg,Zn,Mn,Fe)Al_2O_4$	~630	~630	~630	287, 507, 643
cobalt aluminate	$CoAl_2O_4$	200, 512			
alunogen	$Al_2(SO_4)_3(H_2O)_{12}.5H_2O$		610, 996	992	
aluminite	$Al_2(SO_4)(OH)_4.7H_2O$			992	
mooreite	$Mg_{15}(SO_4)_2(OH)_{26}.8H_2O$		129, 457, 982		
anatase	TiO_2		143, 399, 514		
hematite	α-Fe_2O_3		222, 292, 412, 609	225, 294, 407, 502	
mullite	$3Al_2O_3 2SiO_2$		610, 1127, 1161		
Number of samples analysed		9	8	3	2

Table 5.6. Raman spectra analyses for the cobalt-based pigments used to decorate sherds from various locations and Dynasties. For individual sherd results, refer to Appendix A5.

Mineral	Formula	Wavenumber/cm^{-1}		
		Dendera	**Dier al-Medineh**	**Sinai**
quartz	SiO_2			
tridymite	SiO_2			
apatite	$Ca_5(PO_4)_3(OH,F,Cl)$			
diopside	$Ca(Mg,\square)Si_2O_6$	676, 1015	666, 1010	671, 1009
wollastonite	$CaSiO_3$			
anhydrite	$CaSO_4$	418, 500, 609, 1015	1017	
gypsum	$CaSO_4.2H_2O$			1136
aragonite	$CaCO_3$			
calcite	$CaCO_3$			
coquimbite	$Fe^{3+}_2(SO_4)_3.9H_2O$		281, 1024	1025
albite	$Na(Si_3Al)O_8$			
plagioclase feldspar	$Na_xCa_{1-x}Al_{1+x}Si_{3-x}O_8$			
omphasite	$(Ca,Na)(Mg,Fe^{2+}Fe^{3+},Al(Si_2O_6)$			556, 675, 1022
$Zn_{1-x}Co_xO$ (x = 0.2)				
heterogenite	$Co^{3+}O(OH)$	500, 628	493, 622	495, 622
hypersthene	$(Mg,Fe^{2+})_2Si_2O_6$			
mixed metal spinel	$(Mg,Zn,Mn,Fe)Al_2O_4$	~630	~630	
cobalt aluminate	$CoAl_2O_4$			
alunogen	$Al_2(SO_4)_3(H_2O)_{12}.5H_2O$			
aluminite	$Al_2(SO_4)(OH)_4.7H_2O$			
mooreite	$Mg_{15}(SO_4)_2(OH)_{26}.8H_2O$			
anatase	TiO_2	145		
hematite	$\alpha\text{-}Fe_2O_3$			
mullite	$3Al_2O_3 2SiO_2$	610, 1129, 1160	1161	
Number of samples analysed		1	1	1

A summary of the Raman spectra for the cobalt pigment applied to the surface of the various sherds is provided in Figures 5.15 to 5.20 and 5.22 to 5.35 and their interpretation is given in Tables 5.4 to 5.6. It should be noted that not every sherd provided bands indicating the presence of every mineral listed, indicative of the heterogeneous nature of the samples. The SEM-EDS elemental analyses accompany the Raman spectra. As shown in the Raman Tables, a variable range of minerals are present in individual sherds. Table 5.7 provides the average elemental analyses obtained for the various analysed sherd locations. Table 5.9 provides a summary of the minerals detected by Raman spectroscopy and detailed in Tables 5.4 to 5.6. The expected presence of cobalt aluminate as proposed by earlier workers was only rarely found. This can be explained by the ability of Raman spectroscopy to identify cobalt degradation minerals and is discussed in Section 5.8.3. The various analyses are provided below.

5.4.2.1.1 Cobalt pigment applied to Malkata sherds, late 18th Dynasty, probably Amenhotep III to possibly Horemheb

A pyroxene or clinopyroxene structure, directly related to diopside and in which part of the magnesium has been replaced by cobalt was observed in almost every instance. From the position of the Raman bands it is evident that in this mineral a partial replacement of magnesium by transition elements has occurred resulting in the diopside wavenumber at 666 cm^{-1} to move to slightly higher wavenumbers. The shift to higher wavenumbers is indicative of the ionic radius of these transition elements being less than that of the magnesium ion which is being replaced. Thus, this shift clearly indicates that at least one, if not all, of the cobalt, nickel and zinc ions are bound into this diopside structure. The pyroxene structure is not entirely stable under environmental conditions, enabling heterogenite, bieberite and/or cobalt hydroxide to form during burial or under surface hydrolysis conditions.

However, as shown in Appendix A5, sample M3, mapping of an area of cobalt pigmentation using the extreme high resolution Magellan 400 XHR FEGSEM electron microscope indicated a close relationship between phosphorus and aluminium but neither of the two aluminium phosphates berlinite or variscite were observed. Raman spectroscopy, as provided in Appendix A5, identified phosphosiderite. Whilst the phosphate was not uniformly spread over the surface of the alumina, it may be hypothesised that the adsorbent properties of alumina has led to phosphates being obtained from urine rather than the soil profile. And, a phosphorus-iron particle (P_2O_5 5.7%, 83.5% FeO) was observed in Egyptian blue sample E1 (Figure A4.E1.15).

5.4.2.1.2 Darker blue region, Malkata M3 area elemental analyses

Six small individual areas within the marked area 1 provided in Appendix A5, Figures A5.M3.37, A5.M3.38, A5.M3.44a and Figure 5.13 are of specific areas of interest which were analysed using the Magellan 400 XHR FEGSEM BSE-EDS. Their elemental results are provided below.

```
Spectrum: 1
Element       Series  unn. C norm. C Atom. C Error (3 Sigma)
                      [wt.%]  [wt.%]  [at.%]          [wt.%]
-----------------------------------------------------------
Oxygen     K-series  23.57   39.34   56.04            7.62
Aluminium  K-series  15.48   25.83   21.82            2.22
Calcium    K-series   4.05    6.75    3.84            0.44
Sodium     K-series   2.68    4.47    4.43            0.57
Magnesium  K-series   2.07    3.46    3.24            0.40
Sulfur     K-series   1.72    2.88    2.05            0.26
Silicon    K-series   1.89    3.15    2.55            0.31
Cobalt     K-series   1.99    3.32    1.28            0.26
Iron       K-series   1.61    2.68    1.09            0.22
Zinc       K-series   2.55    4.25    1.48            0.35
Phosphorus K-series   0.76    1.27    0.93            0.16
Chlorine   K-series   0.44    0.74    0.48            0.12
Manganese  K-series   0.18    0.31    0.13            0.10
Nickel     K-series   0.88    1.46    0.57            0.17
Potassium  K-series   0.06    0.10    0.06            0.08
-----------------------------------------------------------
           Total:  59.92  100.00  100.00


Spectrum: 2

El AN  Series     Net unn. C norm. C Atom. C Error (1 Sigma)
                      [wt.%]  [wt.%]  [at.%]          [wt.%]
-----------------------------------------------------------
O  8  K-series 443540  31.81   51.93   69.44           3.40
Ca 20 K-series 386622  11.10   18.11    9.67           0.35
S  16 K-series 482328   8.01   13.07    8.72           0.31
Al 13 K-series 209342   3.53    5.76    4.57           0.19
Si 14 K-series 168885   2.72    4.44    3.38           0.14
Na 11 K-series  45904   1.25    2.04    1.90           0.10
Fe 26 K-series  11182   0.97    1.58    0.60           0.06
Mg 12 K-series  32945   0.65    1.06    0.93           0.06
Zn 30 K-series   2220   0.56    0.91    0.30           0.05
Co 27 K-series   2178   0.25    0.40    0.15           0.03
Ni 28 K-series   1504   0.20    0.33    0.12           0.03
P  15 K-series   6600   0.11    0.18    0.12           0.03
K  19 K-series   4117   0.09    0.15    0.08           0.03
Cl 17 K-series   1379   0.03    0.04    0.03           0.03
Mn 25 K-series      0   0.00    0.00    0.00           0.00
-----------------------------------------------------------
           Total:  61.26  100.00  100.00
```

```
Spectrum: 3
```

El	AN	Series	Net	unn. C [wt.%]	norm. C [wt.%]	Atom. C [at.%]	Error (1 Sigma) [wt.%]
O	8	K-series	102772	27.99	43.55	61.90	3.17
Ca	20	K-series	96096	10.52	16.37	9.29	0.34
Al	13	K-series	151437	9.95	15.48	13.05	0.49
S	16	K-series	98161	6.46	10.06	7.13	0.25
Zn	30	K-series	1934	1.86	2.90	1.01	0.11
Co	27	K-series	3639	1.56	2.43	0.94	0.08
Mg	12	K-series	15952	1.21	1.88	1.76	0.09
Fe	26	K-series	3664	1.19	1.85	0.75	0.07
Si	14	K-series	17106	1.15	1.79	1.45	0.07
Na	11	K-series	10751	1.11	1.72	1.70	0.10
Ni	28	K-series	1150	0.58	0.90	0.35	0.05
P	15	K-series	5565	0.37	0.58	0.42	0.04
Mn	25	K-series	762	0.20	0.31	0.13	0.04
Cl	17	K-series	756	0.06	0.09	0.06	0.03
K	19	K-series	550	0.05	0.07	0.04	0.03
			Total:	64.26	100.00	100.00	

```
Spectrum: 4
```

El	AN	Series	Net	unn. C [wt.%]	norm. C [wt.%]	Atom. C [at.%]	Error (1 Sigma) [wt.%]
O	8	K-series	31228	27.12	46.15	63.66	3.35
Ca	20	K-series	19272	7.53	12.82	7.06	0.26
Al	13	K-series	30836	7.14	12.15	9.94	0.36
Si	14	K-series	26481	6.17	10.50	8.25	0.29
S	16	K-series	11764	2.85	4.84	3.33	0.13
Fe	26	K-series	1823	2.12	3.61	1.43	0.11
Na	11	K-series	3492	1.27	2.16	2.07	0.11
Mg	12	K-series	4173	1.11	1.90	1.72	0.09
Zn	30	K-series	324	1.11	1.89	0.64	0.10
Co	27	K-series	557	0.86	1.46	0.55	0.07
Ni	28	K-series	242	0.44	0.74	0.28	0.06
K	19	K-series	1336	0.42	0.71	0.40	0.04
P	15	K-series	1225	0.30	0.52	0.37	0.04
Cl	17	K-series	818	0.22	0.37	0.23	0.04
Mn	25	K-series	118	0.11	0.19	0.08	0.04
			Total:	58.76	100.00	100.00	

```
Spectrum: 5
El AN  Series      Net unn. C norm. C Atom. C Error (1 Sigma)
                       [wt.%]  [wt.%]  [at.%]          [wt.%]
-----------------------------------------------------------------
O  8  K-series 25869  33.14   46.61   64.05            4.16
Ca 20 K-series 23665  12.02   16.90    9.27            0.39
S  16 K-series 24020   7.15   10.05    6.89            0.28
Al 13 K-series 20578   6.12    8.60    7.01            0.31
Si 14 K-series 12139   3.53    4.96    3.88            0.18
Na 11 K-series  6302   2.92    4.10    3.92            0.22
Cl 17 K-series  5603   1.93    2.71    1.68            0.10
Fe 26 K-series   918   1.39    1.96    0.77            0.09
Mg 12 K-series  2830   0.98    1.37    1.24            0.08
Zn 30 K-series   132   0.58    0.82    0.28            0.08
P  15 K-series  1537   0.46    0.65    0.46            0.05
Co 27 K-series   204   0.41    0.57    0.21            0.06
K  19 K-series   554   0.22    0.31    0.18            0.04
Ni 28 K-series    74   0.17    0.24    0.09            0.05
Mn 25 K-series    78   0.10    0.14    0.05            0.04
Cu 29 K-series     0   0.00    0.00    0.00            0.00
-----------------------------------------------------------------
              Total:  71.11  100.00  100.00

Spectrum: 6
El AN  Series      Net unn. C norm. C Atom. C Error (1 Sigma)
                       [wt.%]  [wt.%]  [at.%]          [wt.%]
-----------------------------------------------------------------
O  8  K-series 100625  29.62   43.46   60.21           3.36
Al 13 K-series 173335  16.17   23.73   19.50           0.77
Ca 20 K-series  33855   5.22    7.66    4.24           0.18
Zn 30 K-series   1889   2.56    3.76    1.27           0.14
S  16 K-series  25123   2.46    3.61    2.50           0.11
Na 11 K-series  16645   2.30    3.37    3.25           0.17
Mg 12 K-series  21236   2.24    3.29    3.00           0.15
Si 14 K-series  21442   2.18    3.20    2.53           0.12
Co 27 K-series   3274   1.96    2.87    1.08           0.10
Fe 26 K-series   2953   1.33    1.95    0.77           0.07
Ni 28 K-series   1327   0.93    1.36    0.51           0.07
P  15 K-series   8918   0.90    1.32    0.94           0.06
Mn 25 K-series    532   0.19    0.28    0.11           0.04
Cl 17 K-series    422   0.05    0.07    0.04           0.03
K  19 K-series    356   0.04    0.06    0.04           0.03
-----------------------------------------------------------------
              Total:  68.15  100.00  100.00
```

Comment:
Spectrum 1 and Spectrum 6 are areas containing high Al and high Co, Ni and Zn, together with elevated Mn, Na (low chlorine), Mg and P. Si is similar in concentration to Co. Spectrum 4, is of a region containing similar concentrations of Ca, Al and Si and slightly elevated Na and K, and with lower, but still significant concentrations of Co, Ni, Zn and Mn. Spectrum 3 is rich in S as (gypsum) and Al but low in Si, but still retaining some Co, Ni and Zn. Whereas, Spectrum 2 and Spectrum 5 are both high in Ca and S (gypsum) with Spectrum 5 having 50% higher Al concentration than that in

Spectrum 2, but the Co, Ni and Zn concentrations, whilst low, are similar in both analyses; Si is similar in both analyses.
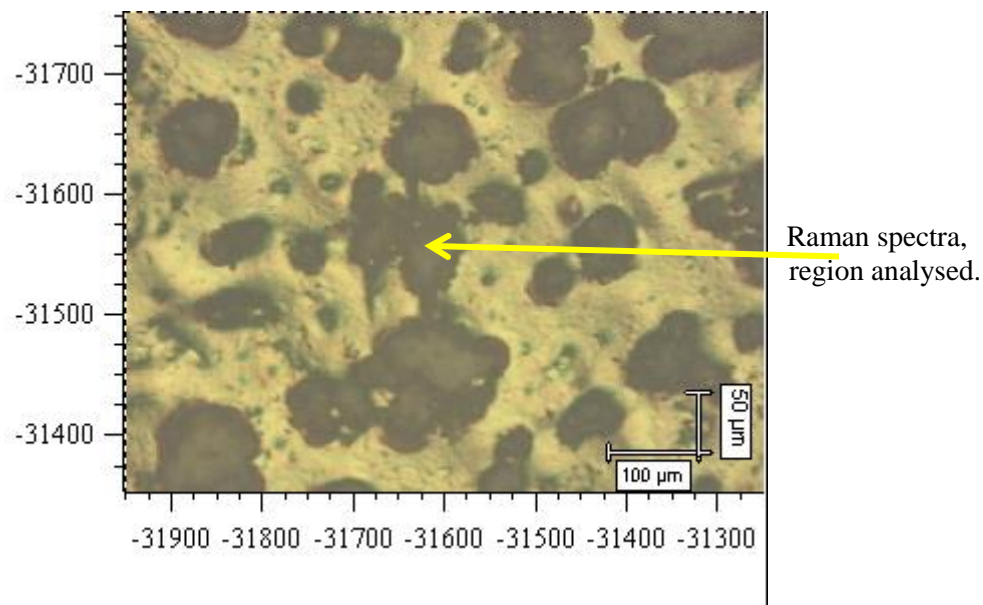

Figure 5.13. Raman microscope camera image showing the Point of Interest analysed in the spectra, Figure 5.14. Sample area analysed by Magellan, EDS results in Appendix A5 FiguresA5.M3.36 to A5.M3.44.
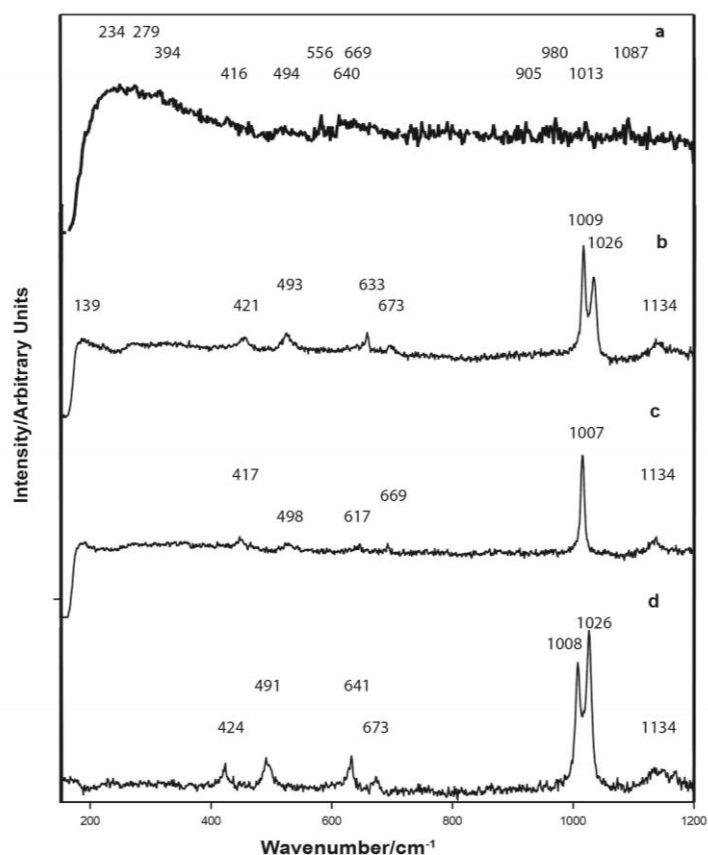

Figure 5.14. Raman spectra blue region, Malkata sherd M3 as shown in Figure 5.12(a) and Figure 5.13 ((a) is $\lambda = 413.2$ nm, (b) to (d) $\lambda = 514.5$ nm).

5.4.2.1.3 Mineralogy, Malkata M3 sherd:

Two shades of blue are evident on the surface of this sherd.

The lighter blue has been obtained by applying a lead oxide mineral (either massicot or plattnerite) over the cobalt blue pigment. A Raman band at 493 cm^{-1} could indicate the presence of lead silicate. This has had the effect of masking the Raman spectra. Unfortunately, as shown in Figure A5.M3.11, the Raman signature is dominated by the presence of orpiment as a contaminant. The EDS analysis indicated that the transition elements cobalt, nickel, copper and zinc are present in similar concentrations. The Raman signatures given in Figures A5.M3.27 and A5.M3.29 clearly indicate that the cobalt is present as a pyroxene, also as the spinel Co(II),Co(III)O$_4$ together with heterogenite, a Zn$_{1-x}$Co$_x$O (x = 0.2), possibly bieberite and spinel *sensu stricto* formation together with mullite, coquimbite, phosphosiderite and gunningite. The higher transition elements reported in Spectrum 1 and 6 in Figures A5.M3.37, A5.M3.38 and A5.M3.44a coupled with the higher aluminium would support alumina formation and probably (Co,Ni,Zn,Mn)Al$_2$O$_4$. A high temperature firing of the pigment is indicated by the formation of cristobalite. An unidentified K-feldspar is indicated from the EDS mapping and albite is indicated by Raman spectroscopy.

A single crystal of a tungsten mineral (ilmenite as shown by its Raman signature at 676 cm^{-1}) was also located by EDS mapping in the darker blue pigment.

Calcite is suggested as part of the slip binder as indicated from the high C shown in Figures A5.M3.23 and A5.M3.25. The presence of gypsum and possibly anhydrite together with probably traces of huntite is indicated from their respective Raman spectra.

An area, as defined in Figure A5.M3.44 and within the darker blue cobalt area was mapped using the Magellan electron microscope.   A selection of these maps is provided in Appendix A5 and these mineral assemblages show:

- Al + O maps show large areas of Al and oxygen indicating the formation of an aluminium oxide-based complex;
- Al-Co + O + Mg maps indicate no association between cobalt and aluminium but mineralisation is detected between Co and O, and mineralisation between Mg, O and Co;
- Al-Zn + O +Al-Co + Mg maps indicate an association between Zn, Al and O, and Zn and O, also Zn, Mg and O, and between Zn and Co + O;
- Al-Ni + O + Mg maps indicate an Al-Ni mineralisation, a Ni, Mg, O complexation, Co, Ni and Zn + O mineralisation;
- Al-Co-Ni-Zn map indicates that there is minor Ni-Zn-Al-O mineralisation, Ni-Al-O mineralisation and Co-Ni-Zn + O mineralisation;
- Mg map indicates a minor spinel formation;
- Mg-Al-P + O maps indicate the probable formation of an Mg-Al-P-O complex;
- Mg-Co-Ni-Zn + O + Ca maps indicate clinopyroxene formation;
- Mg-Al-Si-Fe-K + O + Ca maps indicate clinopyroxene formation, aluminosilicate formation such as mullite, feldspar formation, possibly Mg-Al-Si-O formation;

- Al-P-Fe + O maps indicate that the Fe is associated with Ti (from EDS analysis), there is no Fe-Al mineralisation however, the Al and P have formed an aluminophosphate, also there is an indication for the presence of an Fe-P or Fe-P-Al mineralisation;
- Al-Si + K maps indicate the formation of an aluminosilicate and an Al-P + K + O mineralisation (feldspar);
- Na + Cl show the presence of cubic sodium chloride crystals;
- S-Ca map indicates the presence of major gypsum formation;
- Si-Co map shows no association between these two elements;
- Ca-Si map suggests the presence of a calcium silicate mineral.

The brown line underlying the blue region as shown in Figure A5.M3.32 and its images in Figure A5 .M3 is composed of goethite and hematite. The movement and spread of the Raman peaks are directly related to the presence of titanium mineralisation. The presence of goethite under the blue pigment would confirm a post-firing decoration.

Similarly, brown lines underlying the cobalt blue decoration Malkata sherd M9 were reported by Bachmann *et al*. (1980).   However, they did not report the pigment mineralisation of the brown line or its elemental analysis. Thus, as provided in Figure A3.M9.2, the brown line in this sherd contains hematite together with goethite and hydroxyapatite again supporting a post-firing regime for the cobalt blue, rather than the pre-firing of the cobalt blue as proposed by Bachmann *et al*. (1980).

Anomalous phosphorus (~1% P_2O_5) was observed in the lead oxide coated lighter blue region of Malkata M3.
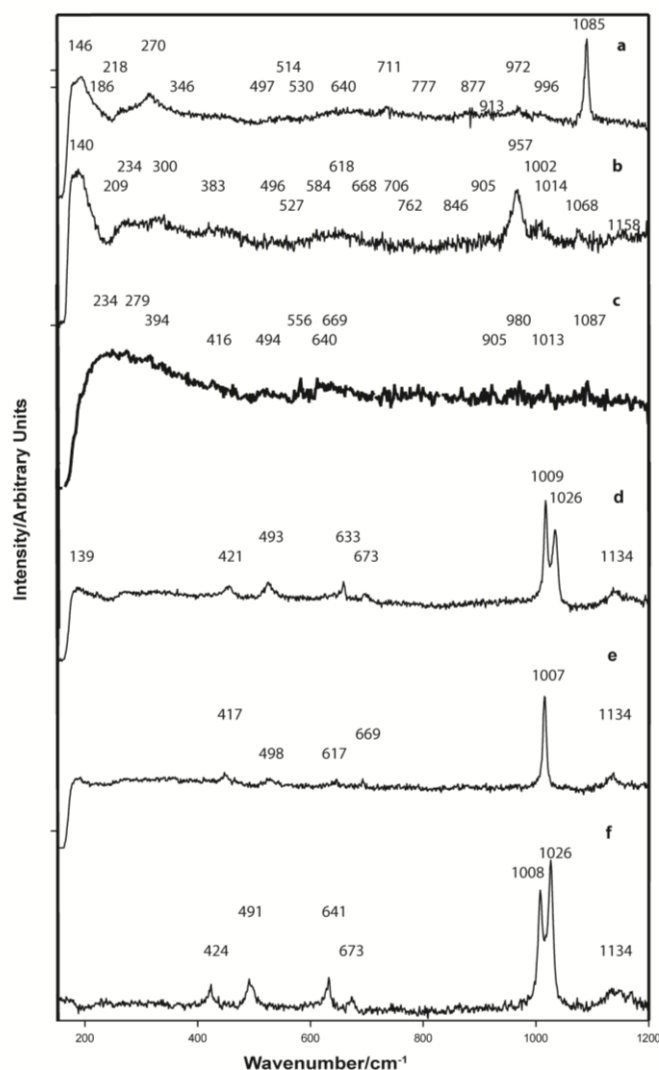
Figure 5.15. Raman spectra of the blue pigment applied to Malkata samples; (a) M9 (b) M9 (c) M9 (λ = 413.2 nm), (d) M3, (e) M5 and (f) M14 (λ = 514.5 nm). The mineralogy of the cobalt pigment has not been fully determined. The presence of a Co-Zn spinel and gahnite is observed (Raman bands at ~416 and 658 cm^{-1}) together with a cobalt pyroxene. However, the band at 514 cm^{-1}, indicative of a cobalt aluminate (spinel), could be assigned to anatase and also to the feldspars labradorite, microcline or orthoclase. The accompanying bands for both anatase and labradorite exist, but not for a cobalt spinel (lacking the expected band at ~202 cm^{-1}). Furthermore, the band at 504 cm^{-1} could be assigned to spinel, however, the expected major accompanying band at ~408 cm^{-1} is poorly resolved. The band at 618 cm^{-1} is assigned to magnesioferrite. Accompanying minerals include mullite, hydroxyapatite (bone ash), wollastonite, calcite, amorphous carbon, anatase and brookite, the feldspar (labradorite, orthoclase or oligoclase), wollastonite, natrite [Na_2CO_3], and possibly aluminite [$Al_2SO_4(OH)_4.7H_2O$]. And, the Raman band at 1022 cm^{-1} could be assigned to goslarite [$ZnSO_4.7H_2O$], bieberite [$CoSO_4.7H_2O$], hornblende (pargasite), coquimbite [$Fe^{3+}_2(SO_4)_3.9H_2O$] or natroalunite [$NaAl_3(SO_4)_2(OH)_6$; the band at 504 cm^{-1} supports the presence of coquimbite, although this suggested assignment is tentative. The presence of calcite could be related to post-depositional from burial. Calcite was not observed in the red or brown/black lines forming part of the decoration (refer Appendix A3, Figure A3.M9.1 and Figures 5.36 to 5.39) thereby supporting a post-manufacture contamination. As shown in Appendix A3, the presence of magnetite in the black line (together with amorphous carbon) which has been applied over the blue pigment does confirm that at least some, if not all, of the decoration was applied post firing of the vessel. Anomalous phosphorus (~1% P_2O_5) was observed from the EDS analyses. Sample M3 has been discussed above, and in which is included a significant body of information derived from a 12 hour mapping of the cobalt pigment using the Magellan 400, an extreme high resolution electron microscope. This has indicated a much more complex mineralogy than previously reported. It is discussed in Section 5.4.2.1.2 and the detailed element maps are provided in Appendix A5.

Lighter blue region Malkata M3 area elemental analyses

Na$_2$O	MgO	Al$_2$O$_3$	SiO$_2$	P$_2$O$_5$	SO$_3$	Cl	K$_2$O	CaO	TiO$_2$	MnO	FeO	CoO	NiO	CuO	ZnO
Elemental analysis, Blue, FIB-EDS Area 1 analysis, Figure A5.M3.1.															
6.9	3.8	37.2	14.2	0.8	3.7	7.9	0.7	7.6	0.6	0.0	4.5	3.7	2.0	1.8	4.4
Elemental analysis, Blue, FIB-EDS Area 2 analysis, FigureA57.M3.1.#															
1.9	3.3	21.8	37.4	0.8	4.9	2.3	1.7	13.7	1.7	0.0	5.2	1.1	0.0	1.6	0.0
Elemental analysis, Blue, FIB-EDS Area 1 analysis, Figure A5.M3.5.*															
1.6	2.6	20.0	35.5	0.7	6.3	2.7	1.6	14.3	2.0	0.6	5.4	1.6	0.0	1.5	0.0
Average analysis															
3.5	**3.2**	**26.3**	**29.0**	**0.8**	**5.0**	**4.3**	**1.3**	**11.9**	**1.4**	**0.2**	**5.0**	**2.1**	**0.7**	**1.6**	**1.5**

#+PbO = 2.6%,   *+PbO = 3.7%

As reported above, Malkata Sample M3 was subjected to detailed SEM-EDS elemental mapping, the results of which are provided in detail within Appendix A5. The discrete elemental regions are identified. This mapping indicates that much of the aluminium is present as an oxide and is not part of any cobalt aluminate structure. Rather, the cobalt and other transition elements are present as discrete particles, many of which are associated with calcium and magnesium, supporting the cobalt pyroxene hypothesis.
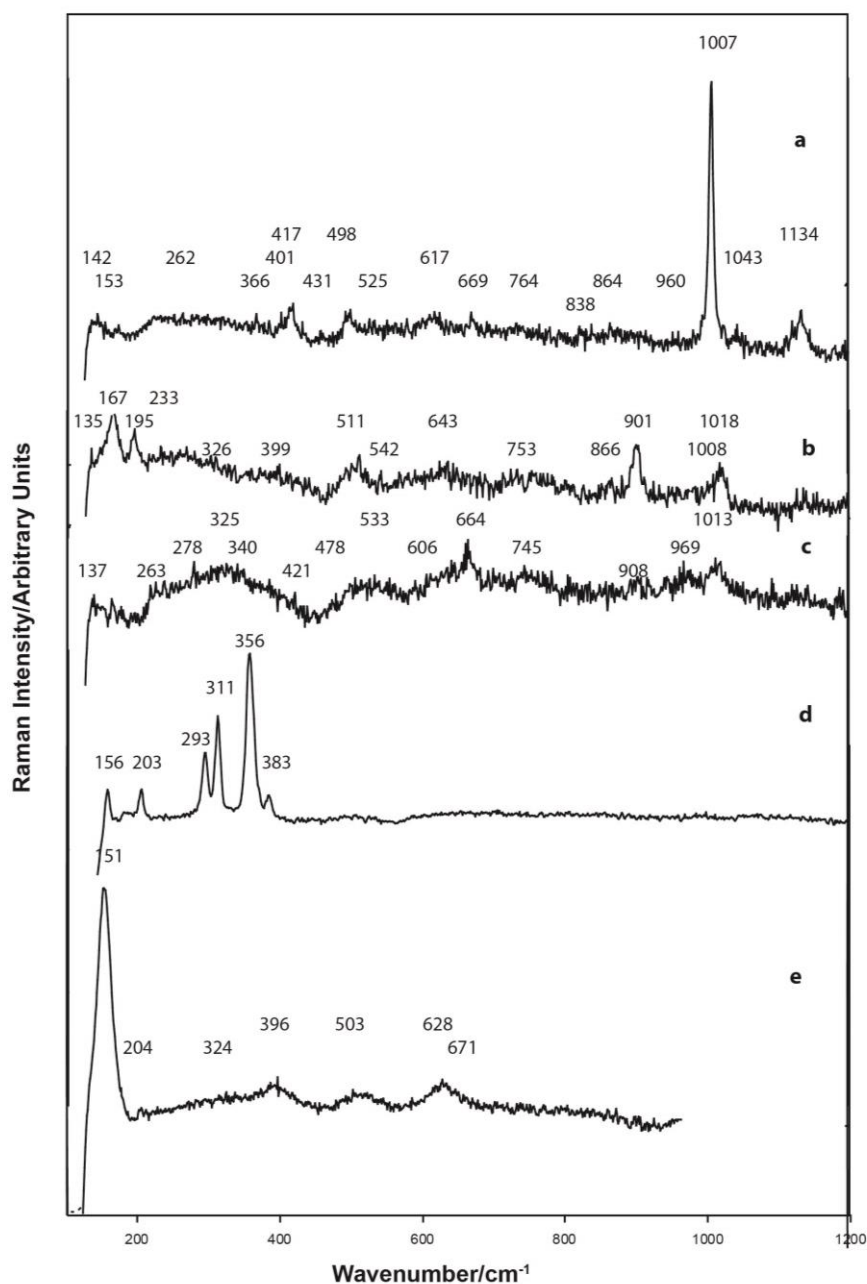
Figure 5.16. Raman spectra, blue regions, Malkata M5 λ = 514.5 nm). The cobalt mineralisation is shown by its Raman signatures to be cobalt pyroxene together with cobalt hydroxide (probably formed following the partial breakdown of the pyroxene structure), possibly cobalt aluminate and possibly spherocobaltite [$CoCO_3$]. Andalusite [Al_2OSiO_4], tridymite, feldspar (probably orthoclase) and mullite are present in the blue pigment. Barium was observed in one EDS analysis. The pigment has been applied on to a slip containing gypsum and anhydrite. In the absence of other data, the presence of anhydrite could support a high temperature firing of the cobalt pigment on to the vessel. Arsenic was detected by the synchrotron in a region visually low in calcium pigmentation and therefore it is not likely to be associated with the slip component. However, arsenic was not detected in any of the EDS analyses. Anomalous phosphorus (~2% P_2O_5) was observed to be present in the pigment.

Area elemental analyse Malkata M5

Elemental analysis, Blue, FIB-EDS Area 1 analysis, Figure A5.M5.1.

Na$_2$O	MgO	Al$_2$O$_3$	SiO$_2$	P$_2$O$_5$	SO$_3$	Cl	K$_2$O	CaO	TiO$_2$	MnO	FeO	CoO	NiO	CuO	ZnO
1.8	6.2	25.3	27.5	2.1	3.6	0.9	1.0	19.7	0.7	1.2	6.0	1.2	0.9	0.8	1.1
Elemental analysis, Blue, FIB-EDS Area 2 analysis, Figure A5.M5.1.															
1.7	6.7	28.5	23.6	2.0	5.4	0.8	0.9	16.8	0.7	1.7	5.1	1.6	1.6	1.3	1.8
Elemental analysis, Blue, FIB-EDS Area 3 analysis, Figure A5.M5.1.															
1.3	6.2	29.3	26.5	1.8	3.9	0.8	0.9	15.9	1.0	1.5	5.4	1.8	1.5	0.8	1.5
Elemental analysis, Blue, FIB-EDS Area 1 analysis, Figure A5.M5.8.															
1.1	6.1	23.9	29.1	1.9	2.6	0.5	1.1	18.1	0.7	1.5	7.7	1.6	1.2	1.3	1.7
Elemental analysis, Blue, FIB-EDS Area 1 analysis, Figure A5.M5.8.															
1.7	6.5	22.8	26.6	1.5	5.8	1.5	1.3	21.1	1.2	0.8	4.6	0.9	1.1	1.2	1.4
Elemental analysis, Blue, FIB-EDS Area 1 analysis, Figure A5.M5.15.															
2.2	7.3	31.6	24.1	2.5	4.5	1.1	0.8	14.7	0.1	1.0	4.2	1.6	1.3	1.0	2.0
Elemental analysis, Blue, FIB-EDS Area 1 analysis, Figure A5.M5.19.															
1.6	5.9	25.3	16.9	1.6	17.6	1.0	0.8	18.5	0.2	1.2	3.3	1.9	1.5	1.0	1.7
Average analysis															
1.6	**6.4**	**26.7**	**24.9**	**1.9**	**6.2**	**0.9**	**1.0**	**17.8**	**0.7**	**1.3**	**5.2**	**1.5**	**1.3**	**1.1**	**1.6**
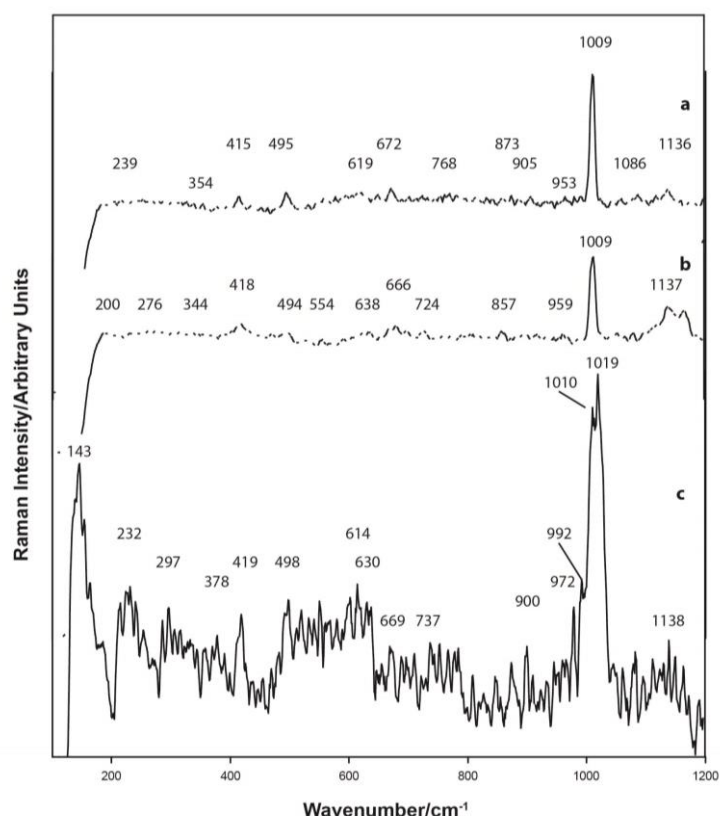
Figure 5.17.   Raman spectra, blue region, Malkata sherd M6 (a, b λ = 413.2 nm; c λ = 514.5 nm).   The mineralogy of this sherd is similar to that of the previous sherd (M5). The cobalt mineralisation is shown by its Raman signatures to be a cobalt pyroxene together with cobalt hydroxide, heterogenite and probably Co-ZnAl$_2$O$_4$, (both hydroxyl-containing minerals probably formed following the partial breakdown of the pyroxene structure).   Andalusite [Al$_2$OSiO$_4$] may be present, tridymite, possibly feldspar and mullite are present in the blue pigment. Barium was observed in the EDS analysis as was anomalous phosphorus (~2% P$_2$O$_5$). The

pigment has been applied on to a slip containing gypsum, anhydrite and minor calcite. Whilst the presence of anhydrite could support a high temperature firing of the cobalt pigment on to the vessel, the calcite would suggest otherwise. A gypsum-based slip was most likely fired with the vessel itself. It could be argued that the calcite could have been derived from the burial conditions, but in the present instance, no evidence has been supplied to confirm such a possibility.
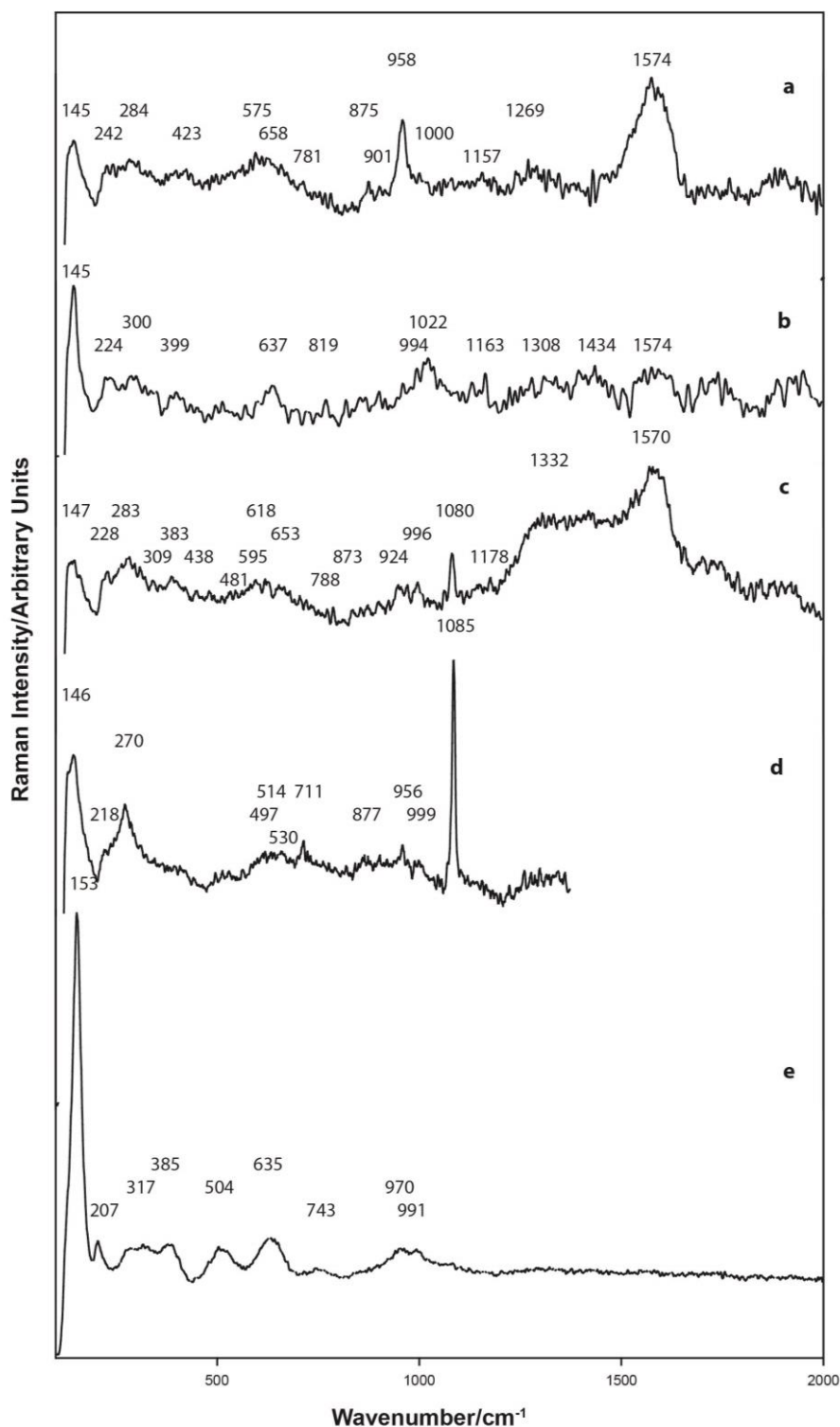
Figure 5.18. Raman spectra, blue region, Malkata sherd M9 (λ = 514.5 nm). Refer also to the Raman spectra provided for this sherd in Figure 5.15 and the mineralogy discussed therein.

Average SEM-EDS Elemental analysis, Malkata sherd M9 ("Bachmann")

Na$_2$O	MgO	Al$_2$O$_3$	SiO$_2$	P$_2$O$_5$	SO$_3$	Cl	K$_2$O	CaO	TiO$_2$	MnO	FeO	CoO	NiO	CuO	ZnO
Elemental analysis, Blue, FIB-EDS Area 1 analysis, Figure A5.M9.1.															
0.0	4.1	54.0	16.1	1.0	1.2	0.0	1.0	5.6	0.0	1.2	3.1	2.9	2.4	0.0	7.4
Elemental analysis, Blue, FIB-EDS Area 1, analysis, Figure A5.M9.3.															
1.0	1.9	27.2	17.4	1.1	1.0	0.1	1.3	4.5	0.0	1.0	41.3	0.0	0.5	0.0	1.8
Elemental analysis, Blue, FIB-EDS Area 2, analysis, Figure A5.M9.3															
3.0	4.7	50.5	18.0	1.4	1.1	0.0	0.9	4.6	0.0	1.0	6.7	2.4	0.0	0.0	5.7
Average analysis															
1.5	**4.4**	**52.2**	**17.0**	**1.2**	**1.2**	**0.1**	**1.0**	**5.1**	**0.0**	**1.1**	**4.9**	**2.7**	**1.2**	**0.0**	**6.6**

The cobalt mineralisation in sample M9 from Malkata, had previously been analysed by Bachmann *et al*. (1980) using XRF. Based upon the presence of aluminium, (the lowest element in the Periodic Table they were able to analyse with this instrument), they tentatively described the mineralogy to that of a spinel. Its image is provided in Figure 5.12(a) and both additional Raman spectra and EDS data are provided in Appendix A5. In discussing Malkata sherd M9, Bachmann *et al.* (1980) reported that the cubic crystals they observed were not sodium chloride as they had thoroughly washed the surface. They considered them to tentatively be interpreted as a zinc-cobalt-nickel-spinel with a crystal form they considered should be octahedral in shape, but that cubic crystals have been reported. In fact, the crystal structure for a normal AB$_2$O$_4$ spinel structure is cubic as shown by spinel *sensu stricto* and zinc aluminate (gahnite) and for the (Zn$_{1-x}$Co$_x$.Al$_2$O$_4$) complex (Fernández-Osorio *et al*. 2010). Caracas and Banigan (2009) confirmed that at room temperature and pressure, MgAl$_2$O$_4$ is crytallographically cubic and it is likely that this could alternatively account for the observed cubic crystals. As they were unable to detect magnesium, and the presence of silica was ignored as was the possibility of the cobalt oxide spinel structure, therefore their spinel with a general formula of (Zn,Co,Ni)Al$_2$O$_4$ as the sole cobalt mineral is open to question.

This sherd is also discussed in Section 5.4.4.
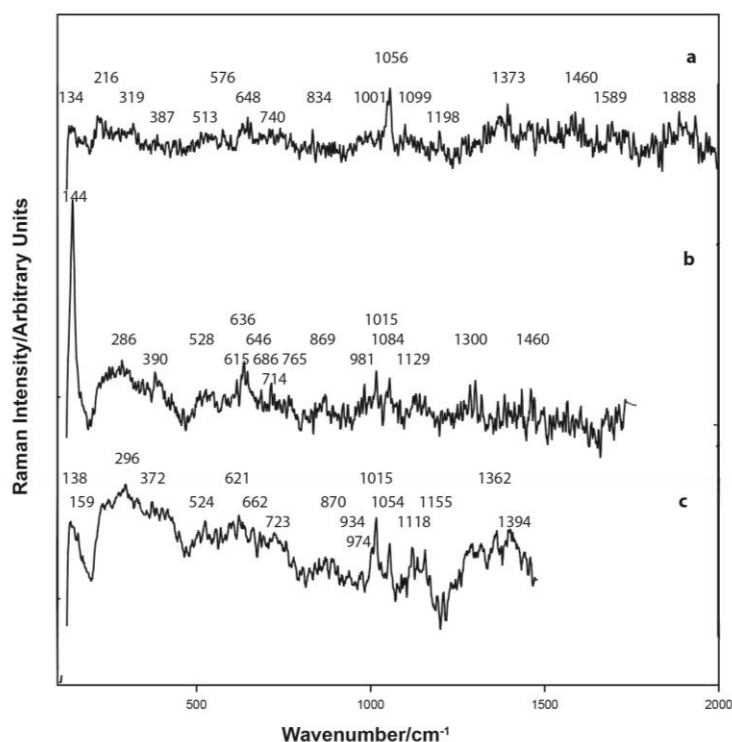
Figure 5.19.   Raman spectra, blue region, Malkata sherd M12 (λ = 514.5 nm). This sample is highly fluorescent as shown by the inability to obtain spectral information above about wavenumber 1500 cm^{-1}. The cobalt pigment was initially prepared as a cobalt pyroxene and possibly as cobalt aluminate. However, weathering of the mineral structure has produced cobalt hydroxide and heterogenite. Raman spectra, indicative of residual cobalt spinel (Figure A5.M12.26(b)) with Raman bands at 615 and 686 cm^{-1} but lacking the bands at ~201, 480 and ~519 cm^{-1}.   Nickel mineralisation as an aluminate is also confirmed.   Other minerals observed included ilmenite (EDS analysis), anatase, mullite, anhydrite, possibly dolomite and possibly magnesite, the manganese ferrite mineral jacobsite [$Mn^{2+}Fe^{3+}_2O_4$] and/or possibly hausmannite [$Mn^{2+}Mn^{3+}_2O_4$].

Area elemental analysis, Malkata sherd M12

Na$_2$O	MgO	Al$_2$O$_3$	SiO$_2$	P$_2$O$_5$	SO$_3$	Cl	K$_2$O	CaO	TiO$_2$	MnO	FeO	CoO	NiO	CuO	ZnO
Elemental analysis, Blue, FIB-EDS Area analysis, Figure A5.M12.1.															
0.8	2.8	13.1	26.2	0.7	15.8	0.8	2.3	23.4	1.0	0.7	7.8	1.2	0.7	1.2	1.4
Elemental analysis, Blue, FIB-EDS Area 1 analysis, Figure A5.M12.1.															
0.6	2.0	11.0	25.7	0.3	16.2	0.5	2.6	24.9	1.6	0.8	10.0	0.9	0.4	1.3	1.2
Elemental analysis, Blue, FIB-EDS Area 1 analysis, Figure A5.M12.6.															
0.9	3.7	36.7	5.4	o.2	12.7	3.0	1.0	19.0	0.0	1.4	2.8	5.1	1.8	0.0	6.1
Elemental analysis, Blue, FIB-EDS Area 1 analysis, Figure A5.M12.14.															
1.6	4.7	41.9	9.5	0.3	5.5	5.8	1.2	14.1	0.0	1.2	2.2	4.2	1.9	0.8	5.1
Elemental analysis, Blue, FIB-EDS Area 2 analysis, Figure A5.M12.14.															
1.3	3.8	33.5	6.3	0.4	14.6	4.1	1.0	19.0	0.0	1.3	2.6	4.6	1.4	0.8	5.4
Average analysis															
1.1	**3.4**	**27.3**	**14.6**	**0.4**	**13.0**	**2.8**	**1.6**	**20.1**	**0.5**	**1.1**	**5.1**	**3.2**	**1.2**	**0.8**	**3.9**
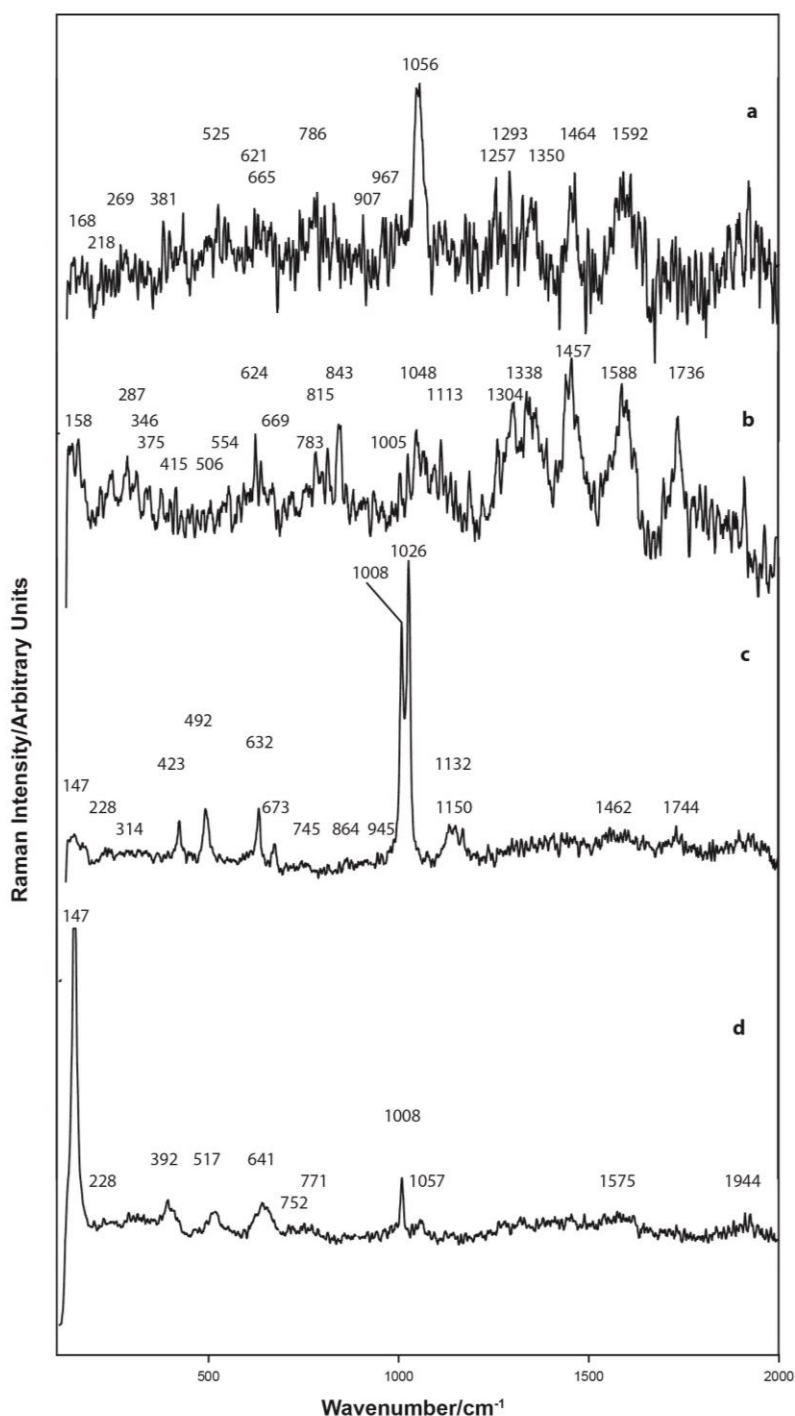
Figure 5.20. Raman spectra, blue region, Malkata sherd M14 (λ = 514.5 nm). The shape of the cobalt blue pigment crystals applied to the surface of this sherd is different to the crystal shape of all other Malkata sherds and in particular, the crystals in Figure A5.M14.13. This is evident from the phase change indicated by the splitting of the Raman bands at 1008/1026 cm^{-1}. And, the EDS analyses indicate a very high concentration of aluminium and iron, significantly higher than for the pigment on other sherds. The cobalt pigment is that of a spinel, a cobalt pyroxene together with gahnite. The only deterioration of the pyroxene as indicated by the Raman spectra is the formation of bieberite. As shown in the EDS analyses, the pigment is higher in cobalt, nickel, and particularly in zinc, manganese and iron than in other blue pigments. It is possible that the source of the cobalt mineralisation used in the manufacture of this cobalt blue is different to the source of the cobalt in the other Malkata sherds. Other pigments present include anatase, gypsum, mullite, coquimbite, probably wollastonite, and feldspar. Probably ferrite is the mineral indicated by the high alumina/iron complex, although

the Raman band at ~189 cm^{-1} is overlapped by the anatase band at 147 cm^{-1}. One EDS analysis indicated the presence of a significant concentration of chlorine and which is not compensated for by sodium. The mineral providing this chloride has not been identified. Barium was detected in several of the EDS analyses and the Raman band at 1056/7 cm^{-1} is indicative of the presence of witherite [$BaCO_3$]. As shown by the organic bands (refer also to Figure 5.59 (and A5.M16.19) the pigment has been applied to the pottery surface using egg protein as the fixative.
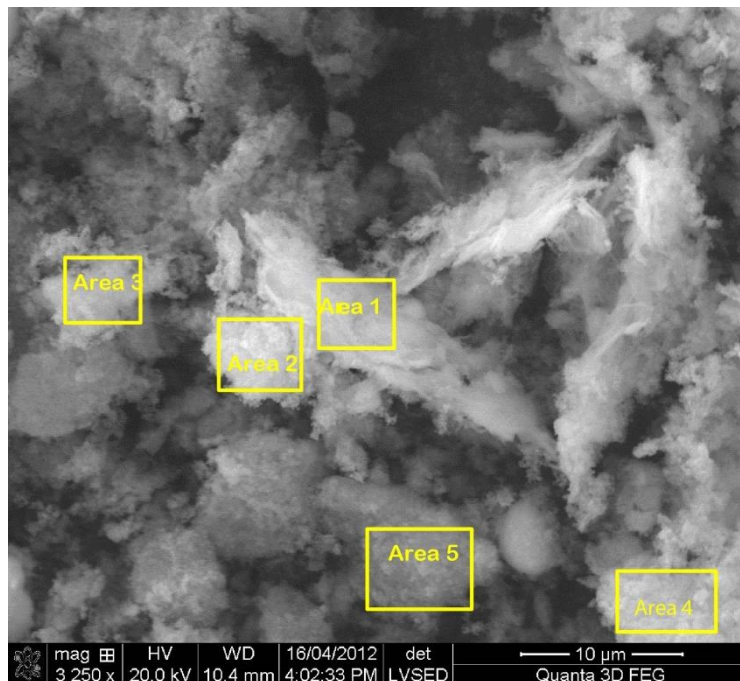
Figure 5.21. FIB BSE image, Points of Interest analysed as marked.

Area elemental analysis Malkata sherd M14:

Na₂O	MgO	Al₂O₃	SiO₂	P₂O₅	SO₃	Cl	K₂O	CaO	TiO₂	MnO	FeO	CoO	NiO	CuO	ZnO
Elemental analysis, Blue, FIB-EDS Area 1 analysis, Figure A5.M14.1.															
0.0	5.2	56.0	11.4	0.1	2.6	2.0	0.8	6.3	0.0	0.8	2.3	3.9	2.6	0.0	5.9
Elemental analysis, Blue, FIB-EDS Area 1 analysis, Figure A5.M14.13.*															
2.2	2.8	21.3	6.0	0.0	1.1	0.8	0.7	8.5	2.0	2.6	19.9	7.3	4.8	3.2	7.9
Elemental analysis, Blue, FIB-EDS Area 2 analysis, Figure A5.M14.13.**															
2.7	3.0	24.9	8.0	0.2	1.6	1.0	0.5	6.8	0.3	2.2	10.0	9.7	7.3	3.0	16.5
Elemental analysis, Blue, FIB-EDS Area 3 analysis, Figure A5.M14.13.#															
2.7	3.1	25.6	7.7	0.4	1.4	1.1	0.7	7.4	0.3	2.1	13.0	9.5	6.9	2.9	14.1
Elemental analysis, Blue, FIB-EDS Area 4 analysis, Figure A5.M14.13.															
3.0	2.9	24.3	6.9	0.2	1.3	0.9	0.5	5.9	0.7	1.7	8.1	11.9	9.0	2.8	20.0
Elemental analysis, Blue, FIB-EDS Area 5 analysis, Figure A5.M14.13.															
2.2	2.9	24.8	7.3	0.3	1.3	1.0	0.5	4.7	0.7	1.9	7.3	11.9	8.6	3.0	21.4
Average analysis															
2.1	**3.3**	**29.5**	**7.9**	**0.2**	**1.5**	**1.1**	**0.7**	**6.6**	**0.7**	**1.9**	**10.1**	**9.0**	**6.6**	**2.5**	**14.3**

*+BaO = 9.2%, **+BaO = 2.1%, #+BaO = 1.0%

5.4.2.1.2 Cobalt pigment applied to Amarna sherds, late 18th Dynasty, probably Akhenaten
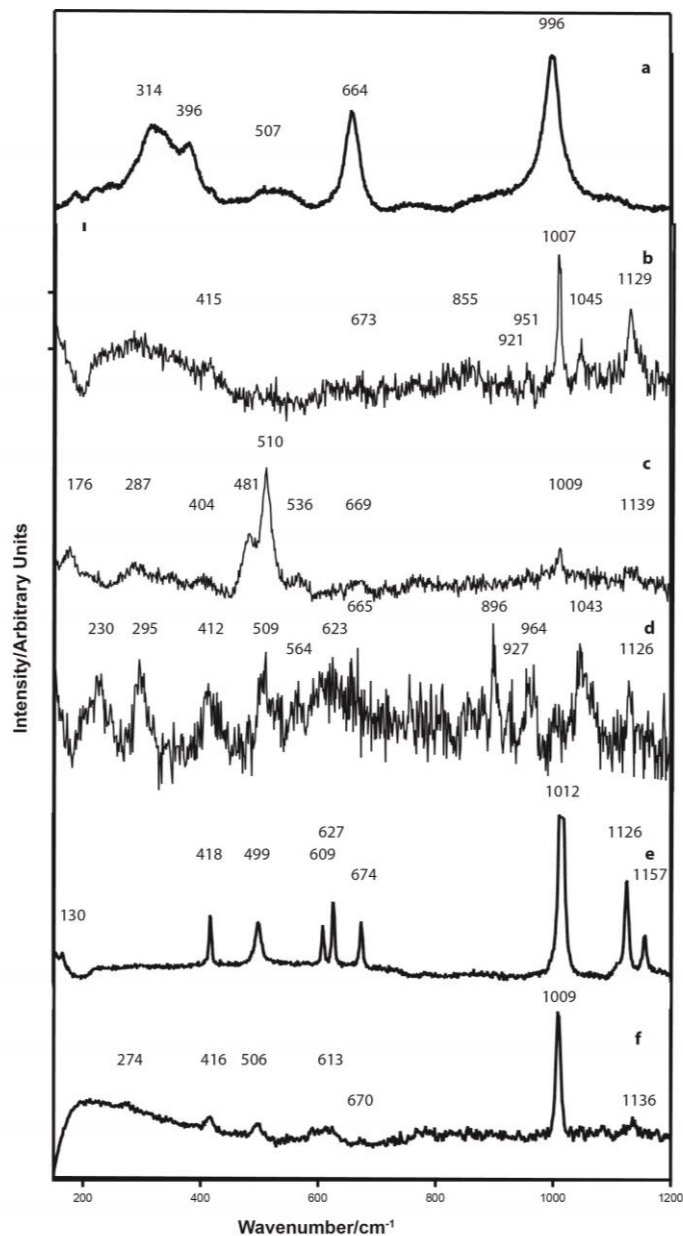
Figure 5.22.   Raman spectra for Amarna samples (a) A1, (b) is A1 (c) is A2, (d) is A4, (e) is A5, ($\lambda = 514.5$ nm) (f) is A6 ($\lambda = 413.2$ nm).   Cobalt, as a pyroxene, as heterogenite [Co(III)O(OH)] and possibly as the spinel (Co(II,III)$_3$O$_4$), feldspars (probably orthoclase), probably titanite [CaTiSiO$_5$], gypsum, amorphous carbon; sodium chloride crystals are randomly scattered over the surface.   The pigment contains anomalous phosphate (~1%), high in both alumina and magnesium.   The black line is a mixture of goethite and magnetite.

Elemental analysis, Amarna sherd A1

Elemental analysis, Blue, FIB-EDS Area analyses, Figure A5.A1.1, A5.A1.,4, A5.A1.24, A5.A1.26, and Nova EDS Area Figures A5.A1.33-36.

Na$_2$O	MgO	Al$_2$O$_3$	SiO$_2$	P$_2$O$_5$	SO$_3$	Cl	K$_2$O	CaO	TiO$_2$	MnO	FeO	CoO	NiO	CuO	ZnO
1.8	1.8	47.9	18.7	0.3	8.0	2.9	1.2	11.1	0.5	0.0	3.2	0.0	0.6	1.5	0.6
1.8	3.9	18.2	40.2	0.6	5.3	0.8	4.2	14.1	1.0	0.4	7.1	1.0	0.4	0.5	0.4
2.5	2.5	30.0	14.7	1.2	5.2	3.6	1.4	23.9	0.2	0.5	4.6	2.3	3.3	1.0	3.3
2.7	3.9	26.9	32.1	0.6	4.6	1.6	3.1	11.9	1.0	0.4	6.2	1.2	1.2	1.5	1.1
4.5	5.4	15.0	27.2	2.0	10.8	4.7	1.4	21.9	0.9	0.0	5.5	0.1	0.2	0.3	0.3
4.7	5.2	12.9	19.8	2.0	16.3	4.5	0.9	26.4	0.8	0.0	5.0	0.3	0.2	0.4	0.4
10.5	4.8	10.8	22.6	1.5	13.8	7.3	0.9	21.6	0.4	0.1	5.0	0.0	0.0	0.6	0.2
5.4	4.6	20.3	25.6	1.7	7.9	1.9	2.4	18.8	1.2	0.1	7.5	0.7	0.8	0.4	0.7
Average analysis															
4.2	**4.0**	**22.8**	**25.1**	**1.2**	**9.0**	**3.4**	**1.9**	**18.7**	**0.8**	**0.2**	**4.9**	**0.7**	**0.8**	**0.8**	**0.9**
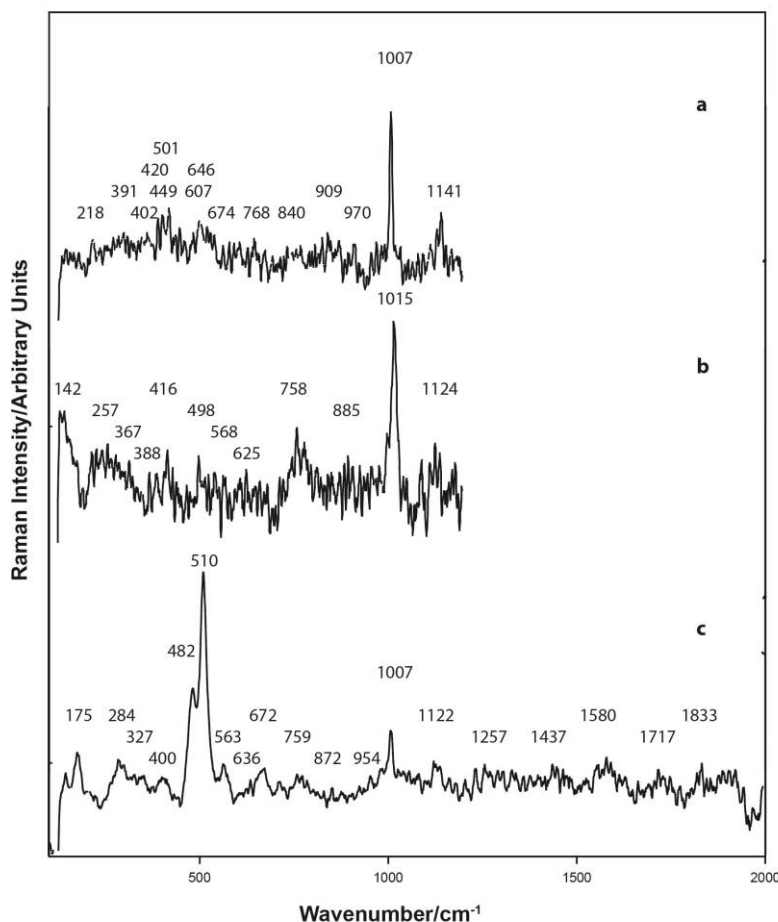
Figure 5.23.   Raman spectra, Amarna sherd A2, blue region ($\lambda = 514.5$ nm). Crystals of salt (NaCl) are present on the surface of the pigment together with feldspars (as probably orthoclase and possibly anorthite), gypsum, anhydrite, huntite and cobalt as a pyroxene and possibly as the Co(II,III)$_3$O$_4$ spinel together with Co(OH)$_2$. Anomalous phosphate is present together with high alumina and high magnesium. There is an indication from the Raman spectrum for the presence of an organic binder.

Area elemental analyses, Amarna sherd A2

Elemental analysis, Blue, FIB-EDS Area analyses, Figure A5.A2.1, A5.A2. 9, and A5.A2.15.

Na$_2$O	MgO	Al$_2$O$_3$	SiO$_2$	P$_2$O$_5$	SO$_3$	Cl	K$_2$O	CaO	TiO$_2$	MnO	FeO	CoO	NiO	CuO	ZnO
4.6	4.3	25.0	26.5	2.0	9.3	4.6	1.1	14.9	0.4	0.3	5.7	0.4	0.0	0.9	0.0
3.1	5.1	22.9	25.6	1.0	10.2	4.4	1.6	16.1	0.9	0.8	6.0	1.1	0.0	1.2	0.0
1.2	4.2	23.3	26.9	1.6	6.6	1.3	1.4	19.7	0.9	1.0	7.8	1.2	1.0	0.6	1.2
2.6	6.5	22.0	18.1	1.7	10.1	15.6	1.2	14.9	2.5	0.2	3.2	0.0	0.0	1.4	0.0
3.7	3.9	26.6	23.7	1.3	7.9	6.0	1.5	15.2	1.6	0.9	5.6	0.6	0.0	1.5	0.0
Average analysis															
3.0	**4.8**	**24.0**	**24.2**	**1.5**	**8.8**	**6.4**	**1.4**	**16.2**	**1.3**	**0.6**	**5.6**	**0.6**	**0.2**	**1.1**	**0.2**
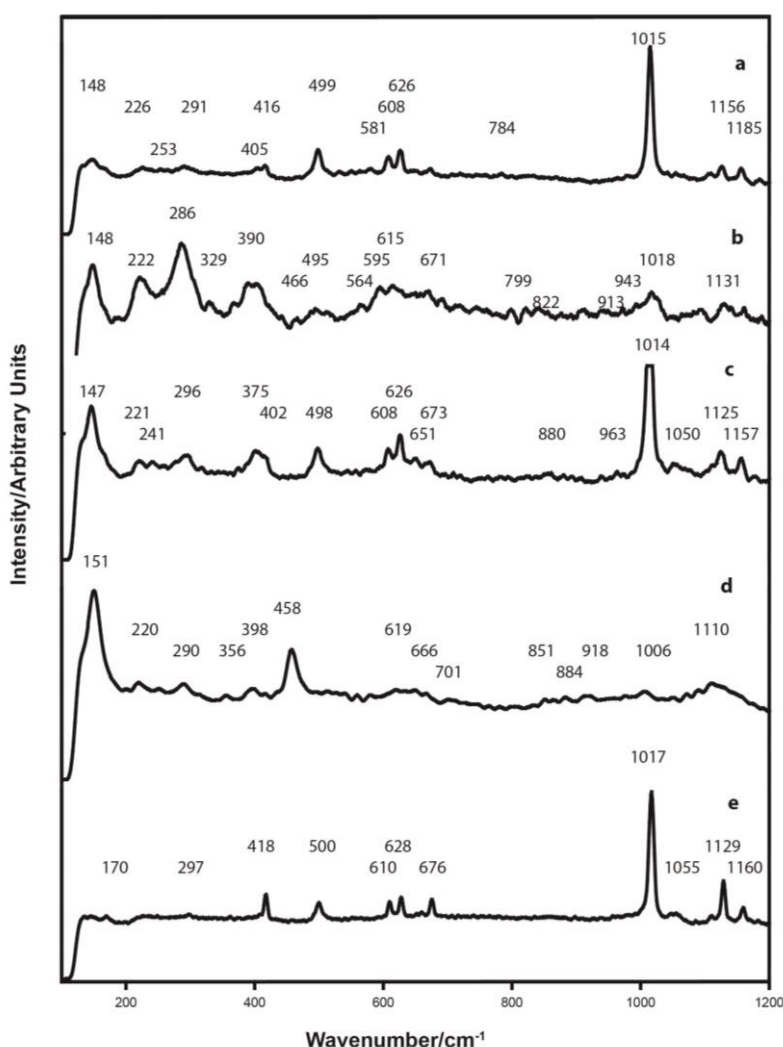
Figure 5.24. Raman spectra, Amarna sherd A5, blue region. (e) small area washed with distilled water to remove saline incrustation prior to analysis. The cobalt pigment is a pyroxene and also most likely as heterogenite [Co^{3+}O(OH)] and also Co$_3$O$_4$. In Appendix A5, Figure A5.A5.18 Spot 1 is rutile and in Figure A5.A5.18 Spot 2, is a small particle of bone ash. The surface of the sherd is coated with sodium chloride and gypsum. In this coating as shown in Figure A5.A5.2 are adsorbent materials which have adsorbed sodium

chloride and probably gypsum from the soil in which the sherd was buried. Washing of the surface with distilled water provided an opportunity to analyse the cobalt pigment. In association with the pyroxene was anhydrite and either huntite or more likely mullite. Up to 1% phosphate was detected (note Raman signature at 963 cm^{-1}) adsorbed on to the unwashed pigmented surface, but not in the washed pigmented surface area indicating that the phosphate was most probably derived from burial conditions. However, a particle of bone ash was analysed in the washed surface area. This could provide evidence for two forms of phosphate mineralisation.

Area elemental analyses, Amarna sherd A5, water washed area

Na_2O	MgO	Al_2O_3	SiO_2	P_2O_5	SO_3	Cl	K_2O	CaO	TiO_2	MnO	FeO	CoO	NiO	CuO	ZnO
Elemental analysis, Blue, FIB-EDS Area 1 analysis, Figure A5.A5.2.															
4.0	1.9	10.4	6.6	1.0	40.1	3.2	1.0	28.9	0.0	0.0	1.7	0.0	0.0	1.4	0.0
Elemental analysis, Blue, FIB-EDS Area 2 analysis, Figure A5.A5.8															
2.5	2.7	12.8	9.1	0.0	39.7	1.4	0.8	28.5	0.0	0.7	1.4	0.0	0.6	0.0	0.0
Surface washed with distilled water, Area 1, analysis, Figure A5.A5.16															
3.9	**2.8**	**15.9**	**6.1**	**0.0**	**35.7**	**3.1**	**0.7**	**26.2**	**0.0**	**0.6**	**1.3**	**0.9**	**0.8**	**1.0**	**1.1**

Area elemental analyses, Amarna sherd A6

Na_2O	MgO	Al_2O_3	SiO_2	P_2O_5	SO_3	Cl	K_2O	CaO	TiO_2	MnO	FeO	CoO	NiO	CuO	ZnO
Elemental analysis, Blue, FIB-EDS Area analysis, Figure A5.A6.1.															
5.2	4.2	57.0	8.9	0.2	1.1	0.5	0.7	7.4	0.3	0.8	1.7	3.4	0.0	0.0	8.6
Elemental analysis, Blue, FIB-EDS Area 1 analysis, Figure A5.A6.7															
0.4	3.9	43.1	21.4	0.5	1.6	0.9	1.2	10.5	0.6	0.9	4.7	2.3	1.4	1.0	5.6
Elemental analysis, Blue, FIB-EDS Area 1 analysis, Figure A5.A6.14															
0.7	4.0	44.3	19.3	1.1	1.6	0.5	1.1	9.9	0.0	1.0	3.8	3.0	1.9	1.4	6.3
Average Area analyses															
2.1	**4.0**	**48.1**	**16.5**	**0.6**	**1.4**	**0.6**	**1.0**	**9.3**	**0.3**	**0.9**	**3.4**	**2.9**	**1.1**	**0.8**	**6.8**
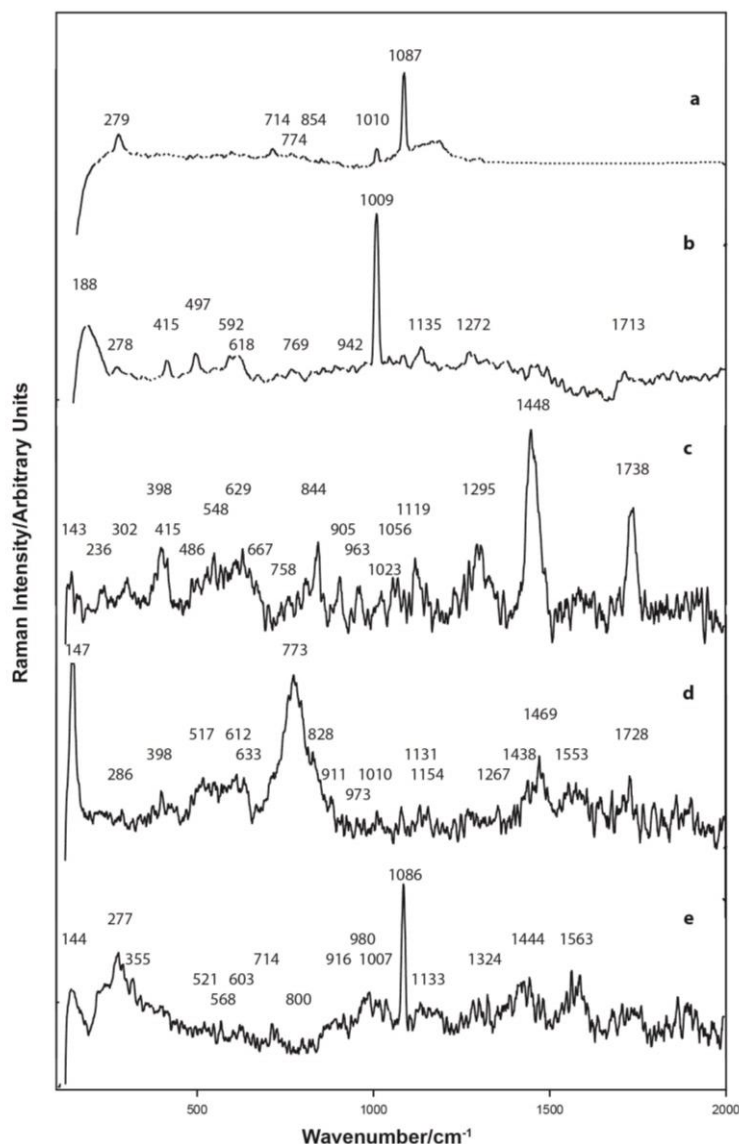
Figure 5.25.   Raman spectra, Amarna sherd A6, blue region ((a) and (b) (λ = 413.2 nm;) (c), (d) and (e), (λ = 514.5 nm). The cobalt is present as a pyroxene and possibly also as heterogenite together with bieberite. The cobalt mineralisation is present in association with calcite, gypsum, feldspar, mullite and barium. The presence of bone ash is evidenced in the EDS analysis and in the same analytical region, the rare earth elements cerium and neodymium were observed (total 5.5%). Anomalous phosphate is present (up to 1.1%) and probably unrelated to the bone ash. The strong bands at 1448 and 1738 cm^{-1} in Figure A5A6.18 is indicative of either beeswax or egg protein. Thus, these organic compounds and calcite (probably from post depositional adsorption and if fired which would have decomposed below the formation temperature of the cobalt mineral) confirm that the cobalt pigment and which has been applied over iron oxide compounds was decorated post-firing of the vessel. As provided in Appendix A3, the black region is magnetite.
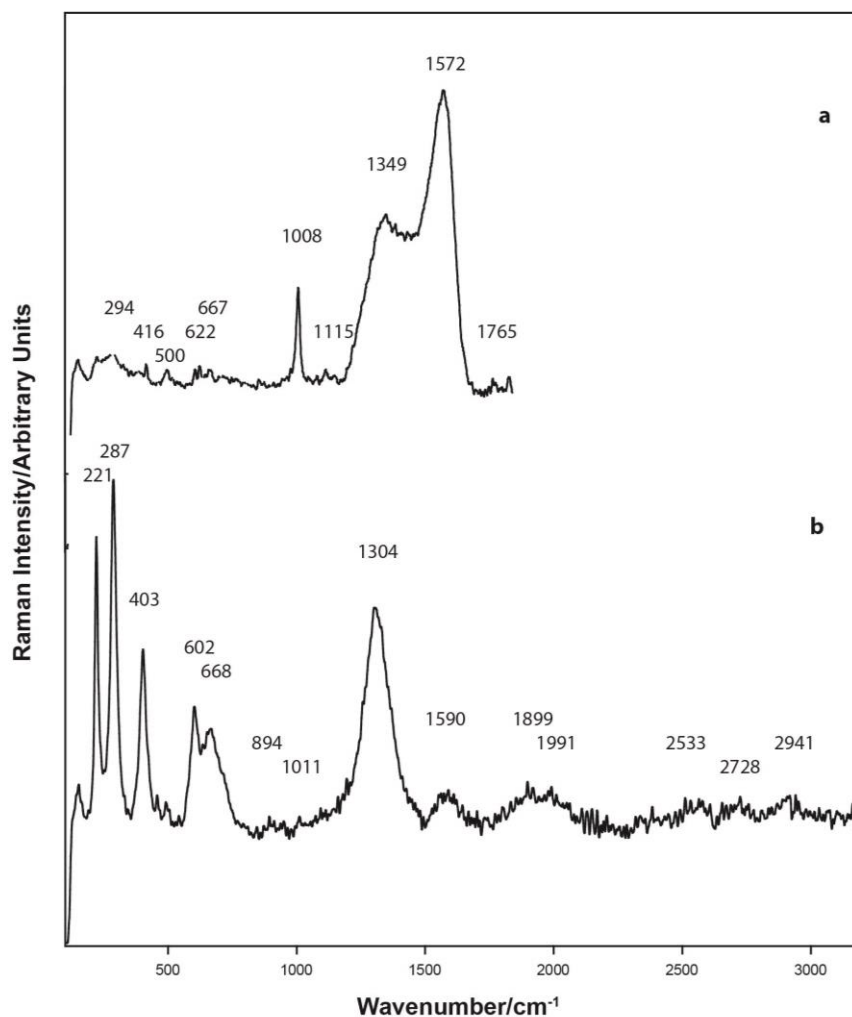
Figure 5.26. Amarna sherd A7, (a) Raman spectrum blue region, (b) Raman spectrum black line ($\lambda = 514.5$ nm). Cobalt, as a pyroxene, as heterogenite [Co(III)O(OH)] and possibly as the spinel (Co(II,III)$_3$O$_4$), feldspars (probably orthoclase), probably titanite [CaTiSiO$_5$], gypsum, amorphous carbon; sodium chloride crystals are randomly scattered over the surface. An unidentified sorbent material is coated with sodium chloride (refer Figure 5.49 (and A5.A4.3 and 4 spot 2) and another is encrusted with both gypsum and sodium chloride (refer Figure A5.A4.5 Spots 1 and 2). The pigment contains anomalous phosphate (~1%), high in both alumina and magnesium. The black line is a mixture of goethite and magnetite.

Area elemental analyses, Amarna sherd A7

Na$_2$O	MgO	Al$_2$O$_3$	SiO$_2$	P$_2$O$_5$	SO$_3$	Cl	K$_2$O	CaO	TiO$_2$	MnO	FeO	CoO	NiO	CuO	ZnO
Elemental analysis, Blue, FIB-EDS Area 1 analysis, Figure A5.A7.1.															
1.5	3.6	28.4	25.8	0.3	3.9	1.4	1.8	9.2	1.2	1.3	9.8	4.2	2.4	1.2	3.8
Elemental analysis, Blue, FIB-EDS Area 1, analysis, Figure A5.A7.8															
0.5	4.4	40.2	19.8	0.2	1.5	0.7	1.4	5.3	0.6	1.7	9.5	5.6	3.3	0.7	4.6
Elemental analysis, Blue, FIB-EDS Area 1, analysis, Figure A5.A7.12															
0.7	6.9	20.5	37.2	0.2	0.7	0.5	2.7	4.1	0.6	0.8	23.9	0.0	0.0	1.0	0.2
Elemental analysis, Blue, FIB-EDS Area 2, analysis, Figure A5.A7.12															
1.2	3.3	20.3	45.5	0.3	1.0	0.9	3.3	7.8	1.2	0.7	11.4	1.1	0.9	0.0	1.1
Average Area analyses															
1.0	**4.6**	**27.4**	**32.1**	**0.3**	**1.8**	**0.9**	**2.3**	**6.6**	**0.9**	**1.1**	**13.7**	**2.7**	**1.7**	**0.7**	**2.4**

5.4.2.1.3   North Karnak sherds, Luxor.   Either late 18th Dynasty, or possibly 19th Dynasty
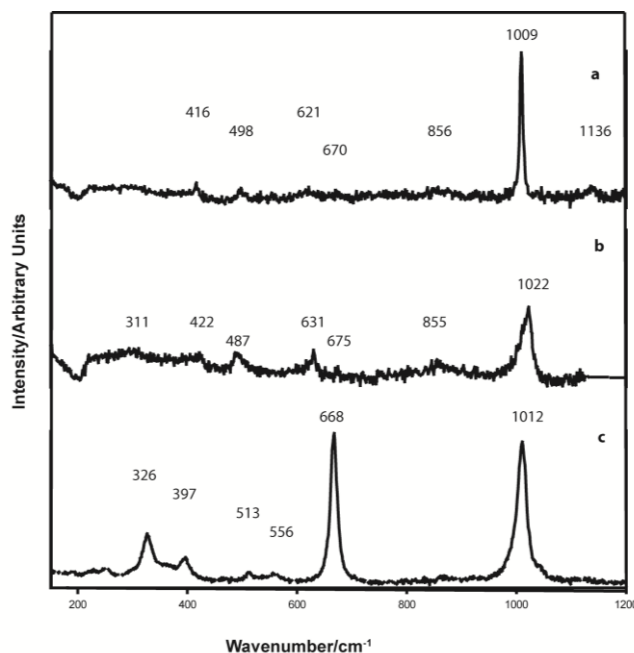
Figure 5.27.   Raman spectra of North Karnak sherds, (a) and (b) are NK1, (c) is NK3 ($\lambda = 514.5$ nm). Cobalt is present as cobalt pyroxene, Co-ZnAl$_2$O$_4$ and bieberite, probably as heterogenite and possibly as Co$_3$O$_4$. Other minerals present include quartz, amorphous carbon, tridymite, wollastonite, hydroxyapatite, ilmenite, rutile and/or anatase, gypsum, mullite, coquimbite, probably feldspar, gunningite, ferrite, manganite and jacobsite.

Area elemental analysis North Karnak NK1

Elemental analysis, Blue region, FIB EDS Area analyses.

Na$_2$O	MgO	Al$_2$O$_3$	SiO$_2$	P$_2$O$_5$	SO$_3$	Cl	K$_2$O	CaO	TiO$_2$	MnO	FeO	CoO	NiO	CuO	ZnO
1.3	4.0	26.5	32.6	0.4	1.3	0.0	5.6	3.2	1.2	2.0	16.3	1.9	1.3	1.7	0.0

Elemental analysis, North Karnak sherd NK2

Elemental analysis, Blue region, FIB-EDS Area analyses, refer Figure A5.NK2.1 and A5.NK2.6.

Na$_2$O	MgO	Al$_2$O$_3$	SiO$_2$	P$_2$O$_5$	SO$_3$	Cl	K$_2$O	CaO	TiO$_2$	MnO	FeO	CoO	NiO	CuO	ZnO
0.8	5.6	50.5	22.4	0.5	2.6	0.0	2.3	4.9	0.0	1.5	5.4	1.5	0.0	0.0	1.8
0.8	5.3	39.9	9.1	0.0	21.4	0.0	0.9	15.4	0.0	1.0	2.4	1.3	0.0	1.2	1.3
0.7	3.4	29.9	6.9	0.0	4.1	0.0	0.0	2.7	0.0	0.0	50.7	0.4	0.0	1.2	0.0
Average analysis															
0.8	4.8	40.1	12.8	0.2	9.4	0.0	1.1	7.7	0.0	0.8	19.5	1.1	0.0	0.8	1.0
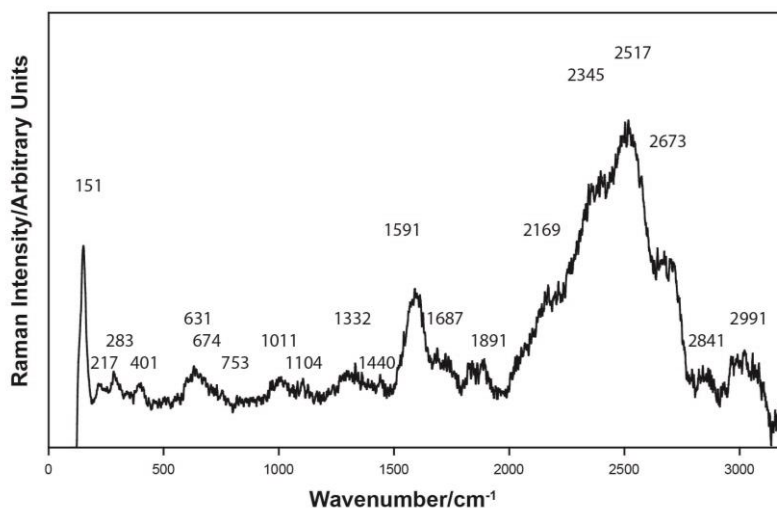
Figure 5.28.   Raman spectrum of a presently unrecognisable compound in the blue pigment of North Karnak sherd NK2 (λ = 514.5 m).   The cobalt mineralisation has been found to contain cobalt pyroxene, heterogenite, bieberite and cobalt hydroxide [Co(OH)$_2$] together with gahnite.   Other minerals present include goethite and hematite (probably from the pottery substrate), tridymite, quartz, mullite, spinel, either manganeseferrite or magnesioferrite, feldspar (probably labradorite), brookite and/or anatase, traces of gypsum, probably wollastonite, possibly fibroferrite, hornblende and prehnite.
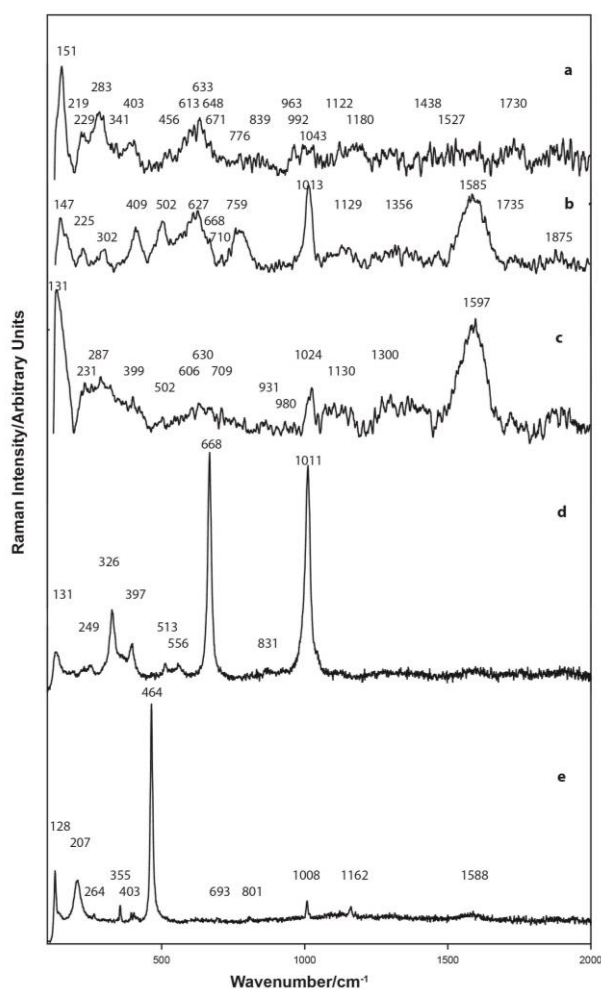
Figure 5.29. Raman spectra, North Karnak sherd NK3, blue region (λ = 514.5 nm).   The cobalt present in the blue pigment is cobalt pyroxene, bieberite and either as cobalt spinel or more likely as cobalt hydroxide.   Other

minerals present include quartz, tridymite, mullite, gypsum, diopside, spinel, goethite and hematite (probably from the pottery substrate), amorphous carbon, ilmenite (refer EDS spectrum Figure A5.NK3.10), alumina (refer EDS spectrum Figure A5.NK3.20), bismuth as indicated in the EDS analyses, possibly huntite and coquimbite.

Elemental analysis, North Karnak sherd NK3

Elemental analysis, Blue region, FIB-EDS Area analyses, refer Figure A5.NK3.1, A5.NK3.12, Figure A5.NK3.16.

Na$_2$O	MgO	Al$_2$O$_3$	SiO$_2$	P$_2$O$_5$	SO$_3$	Cl	K$_2$O	CaO	TiO$_2$	MnO	FeO	CoO	NiO	CuO	ZnO
1.1	3.3	33.1	37.4	1.2	1.7	0.1	2.8	6.5	1.4	0.7	7.9	0.6	0.6	1.6	0.0
0.7	2.8	29.4	41.1	0.7	0.1	0.1	3.9	4.4	1.4	0.9	12.4	0.5	0.0	1.4	0.4
1.7	2.8	27.2	42.8	0.9	1.1	0.1	4.5	4.4	2.4	0.7	10.5	0.2	0.0	0.9	0.0
0.9	2.7	27.7	39.6	0.4	1.1	0.4	2.5	12.5	1.8	0.4	8.7	0.3	0.0	1.2	0.0
0.3	1.1	18.9	71.4	0.6	0.7	0.0	1.2	1.9	0.3	0.2	2.2	0.2	0.0	1.1	0.0
1.8	3.3	22.8	50.4	0.8	0.2	0.0	3.5	4.4	1.3	0.5	9.3	0.2	0.4	0.9	0.0
1.6	4.6	49.0	9.5	2.1	9.9	0.0	0.8	9.8	0.3	1.0	2.6	2.7	2.1	1.3	2.8
Average analysis															
1.1	**2.9**	**29.7**	**41.7**	**0.9**	**2.1**	**0.1**	**2.7**	**6.3**	**1.3**	**0.6**	**7.7**	**0.7**	**0.4**	**1.2**	**0.5**

5.4.2.1.4 Deir al-Medineh, Luxor. Ramesside
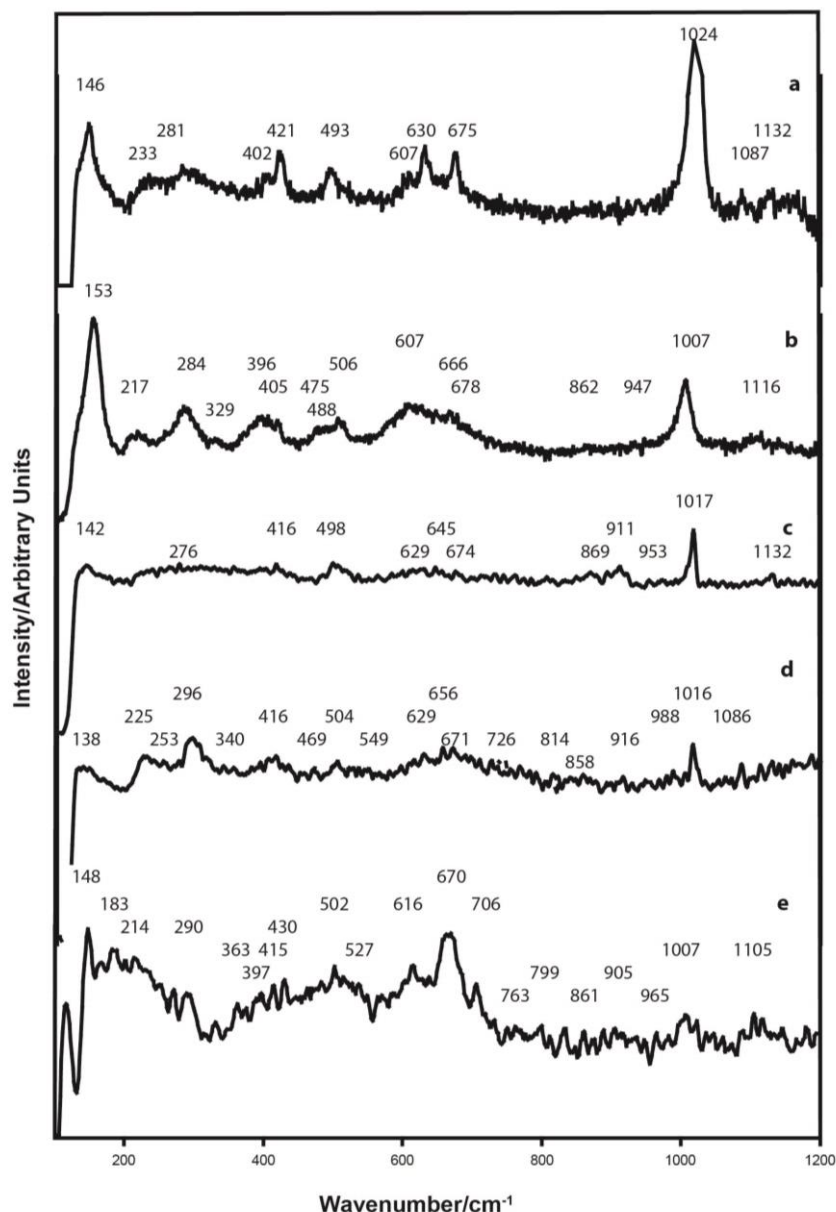
Figure 5.30.   Raman spectra, Deir al-Medineh blue pigment ($\lambda = 514.5$ nm). The cobalt blue consists of cobalt pyroxene, heterogenite, cobalt hydroxide, bieberite, and cobalt-zinc aluminate together with spinel. Anhydrite is indicated by the Raman band at 1017 cm^{-1} together with mullite, tridymite and the feldspar(s) labradorite, orthoclase and/or albite.   A particle of hydroxyapatite (bone ash) is indicated in the EDS analysis (refer Figure A5.DM1.8).   There is evidence for post-deposition of gypsum on the surface of the pigment; some calcite is also indicated from its Raman signature. Probably hematite and goethite from either the red/brown pigment decoration and possibly corundum are present. The anhydrite could indicate that gypsum formed part of the surface burnishing prior to the vessel being fired.   The over-decoration with black and red pigments does not enable any alternative decoration procedure to be advanced.

Elemental analysis, Deir al-Medineh sherd DM1

Elemental analysis, Blue region Nova Area analyses.

Na$_2$O	MgO	Al$_2$O$_3$	SiO$_2$	P$_2$O$_5$	SO$_3$	Cl	K$_2$O	CaO	TiO$_2$	MnO	FeO	CoO	NiO	CuO	ZnO
13.5	2.1	11.4	20.6	0.0	13.2	11.2	2.0	16.2	0.9	0.3	7.8	0.3	0.2	0.0	0.2
9.9	2.7	15.7	20.3	0.0	15.2	7.9	1.7	18.0	0.8	0.4	5.8	0.6	0.5	0.0	0.5
4.5	4.4	25.5	31.5	0.2	3.4	3.9	2.3	12.0	0.9	0.7	7.8	1.2	0.9	0.0	0.9
7.6	3.3	18.3	30.0	0.1	7.8	5.8	2.2	14.5	1.0	0.4	7.4	0.6	0.4	0.0	0.4
Average analysis															
8.9	**3.1**	**17.7**	**25.6**	**0.1**	**9.9**	**7.2**	**2.1**	**15.2**	**0.9**	**0.5**	**7.2**	**0.7**	**0.5**	**0.0**	**0.5**

5.4.2.1.5. Memphis, Ramesside
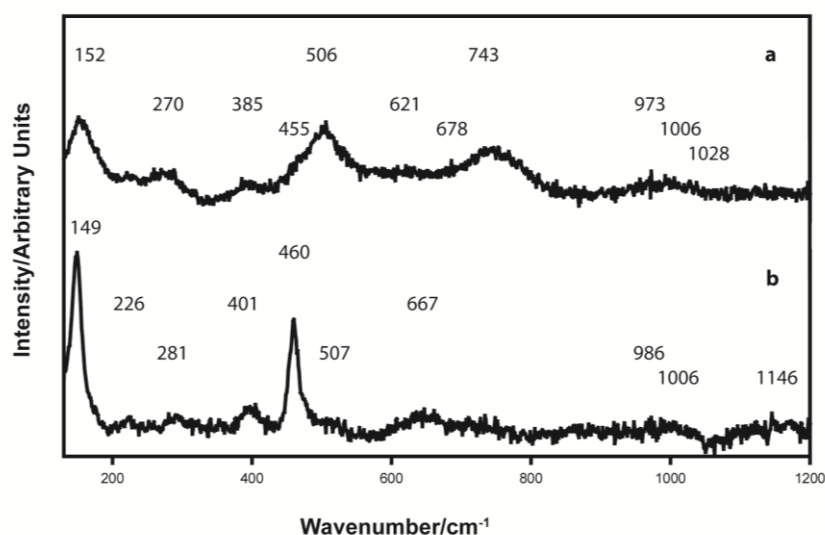
Figure 5.31.   Memphis Raman spectra, (a) is R1 (b) is R2 (λ = 514.5 nm). The cobalt in the blue pigment has been identified as cobalt pyroxene together with Co(OH)$_2$ and bieberite. Phosphate is widely disseminated throughout the sample. Hydroxyapatite (bone ash, refer Figures A5.R1.1 and A5.R1.5) is present as part of the phosphorus mineralisation. Barium is observed in the EDS analysis (refer Figure A5.R1.3) possibly as baryte. Quartz, tridymite, feldspar (probably labradorite); titanium as brookite, hematite and goethite, the latter three minerals are probably related to the pottery surface, together with probably pseudowollastonite.

Elemental analysis, Blue, FIB-EDS Area analysis, Figure A5.R1.10.

Na$_2$O	MgO	Al$_2$O$_3$	SiO$_2$	P$_2$O$_5$	SO$_3$	Cl	K$_2$O	CaO	TiO$_2$	MnO	FeO	CoO	NiO	CuO	ZnO
1.6	4.0	20.1	43.2	2.6	0.9	0.0	2.4	13.3	0.8	0.8	7.1	0.6	0.4	0.6	1.2

Elemental analysis, Memphis sherd R2

Elemental analysis, Blue, FIB-EDS Area analysis*, Figure A5.R2.1.														
Na₂O	MgO	Al₂O₃	SiO₂	P₂O₅	SO₃	Cl	K₂O	CaO	TiO₂	MnO	FeO	CoO	NiO	CuO	ZnO
3.3	5.3	41.9	25.1	0.6	0.9	0.1	1.2	7.3	0.4	1.5	4.3	2.0	1.8	0.7	3.5
Elemental analysis, Blue, FIB-EDS Area analysis Figure A5.R2.5															
3.6	5.3	40.6	27.7	0.6	0.6	0.0	1.2	7.0	0.5	1.3	4.3	2.2	1.6	0.4	3.4
Area Analysis															
3.5	**5.3**	**41.2**	**26.4**	**0.6**	**0.7**	**tr**	**1.2**	**7.2**	**0.5**	**1.4**	**4.3**	**2.1**	**1.7**	**0.6**	**3.5**
*+La = 0.4%.															

Note: the column headers row lists: Na₂O, MgO, Al₂O₃, SiO₂, P₂O₅, SO₃, Cl, K₂O, CaO, TiO₂, MnO, FeO, CoO, NiO, CuO, ZnO.
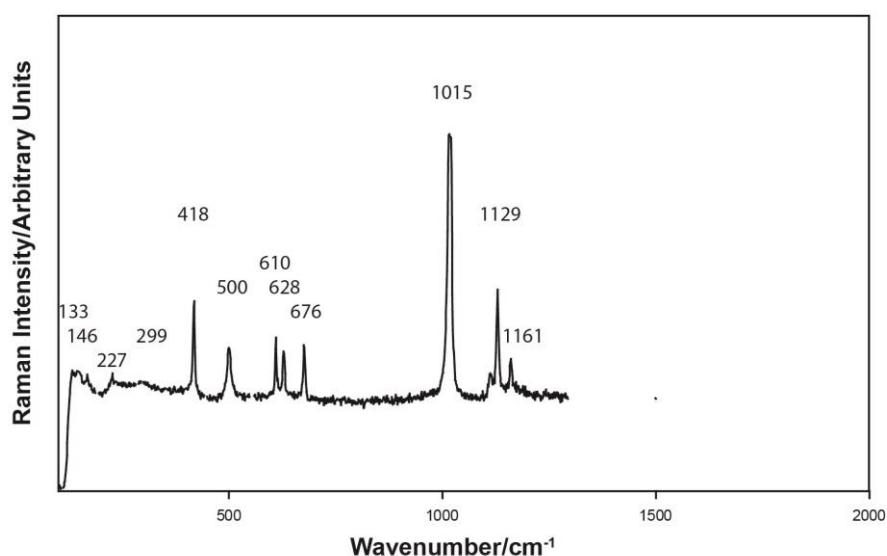
5.4.2.1.6. Dendera, New Kingdom

Figure 5.32. Raman spectrum, Dendera sherd, blue pigment (λ = 514.5 nm). The cobalt mineralisation in the blue pigment has been identified as cobalt pyroxene. This pyroxene has partially decomposed to form heterogenite, bieberite and the oxide $Co(OH)_2$. Calcite, gypsum and anhydrite together with rutile, tridymite, mullite, probably feldspar (either orthoclase or labradorite), possibly coquimibite and corundum. A number of 10 to ~90 μm long X ~2 to 10 μm in "diameter" particles are present in Figure 5.51 (and both Figures A5.DE.1 and A5.DE.1.2) all of which have adsorbed gypsum on to their surface. Whilst the adsorbent has not been determined, it is likely to be hydroxyapatite (bone ash) or possibly a piece of plant material. However, the carbon peak in the SEM-EDS image does not suggest a high organic loading.

Elemental area analyses, Dendera sherd DE1

Elemental analysis, Blue region Nova Area analyses.															
Na₂O	MgO	Al₂O₃	SiO₂	P₂O₅	SO₃	Cl	K₂O	CaO	TiO₂	MnO	FeO	CoO	NiO	CuO	ZnO
13.5	2.1	11.4	20.6	0.0	13.2	11.2	2.0	16.2	0.9	0.3	7.8	0.3	0.2	0.0	0.2
9.9	2.7	15.7	20.3	0.0	15.2	7.9	1.7	18.0	0.8	0.4	5.8	0.6	0.5	0.0	0.5
4.5	4.4	25.5	31.5	0.2	3.4	3.9	2.3	12.0	0.9	0.7	7.8	1.2	0.9	0.0	0.9
7.6	3.3	18.3	30.0	0.1	7.8	5.8	2.2	14.5	1.0	0.4	7.4	0.6	0.4	0.0	0.4
Average analysis															
8.9	**3.1**	**17.7**	**25.6**	**0.1**	**9.9**	**7.2**	**2.1**	**15.2**	**0.9**	**0.5**	**7.2**	**0.7**	**0.5**	**0.0**	**0.5**

Figure 5.33. Raman spectra. (a) is Dendera, D1, (b) is North Sinai NS1, (c) is Dier al-Medineh DM1 (λ = 514.5 nm).

5.4.2.1.7. Bir al-Abd, North Sinai, sherd S1, late 18th Dynasty
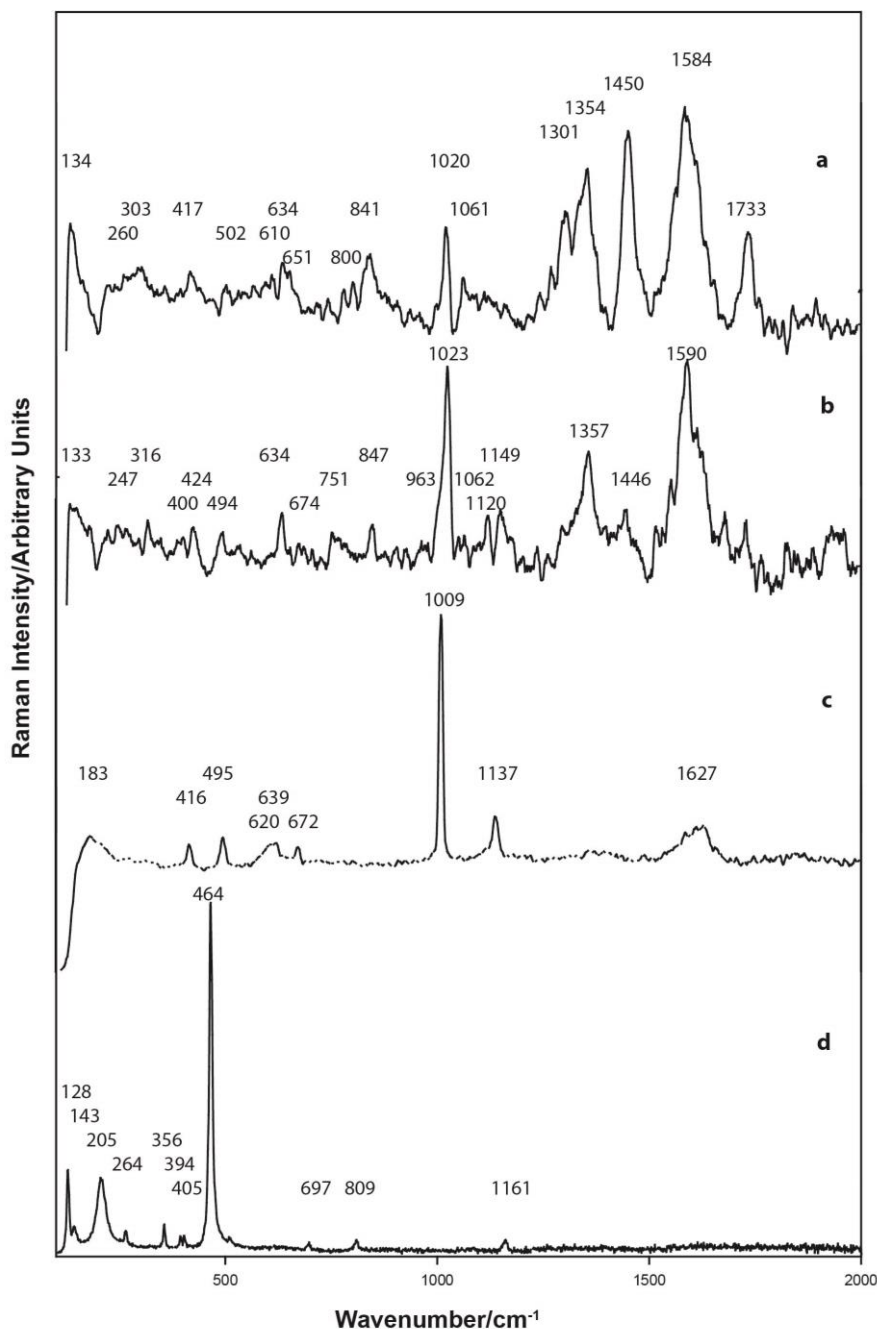
Figure 5.34. Raman spectra, blue pigment, North Sinai sherd S1. Spectrum (a) and spectrum (b) contains amorphous carbon from the black line. Spectrum (a) indicates that the pigments were applied using egg protein as the binder (for a more complete spectrum, refer to Figure A5.M16.19 (λ = 514.5 nm). The blue pigment is a cobalt-zinc spinel together with cobalt pyroxene; the cobalt pyroxene has degraded, enabling the formation of heterogenite, bieberite and cobalt hydroxide.. Other minerals present include quartz (refer to the spectrum at Figure A5.S1.11(d)), tridymite, mullite, calcite, goethite and hematite (the latter two most probably derived from the pottery surface or from the red/brown decoration. Both corundum and ferroactinolite could be present within the cobalt pigment. Interestingly, spectrum Figure A5.S1.11(c) is replicated in the Raman spectrum Figure A5.D7.43 for the Mut al-Kharab sherd. It does add weight to the proposition that the Dakhleh Oasis may well have been both the cobalt alum source and the site at which the cobalt was extracted from the alum and converted into the cobalt blue pigment. The pigment was applied using egg protein.

5.61

Elemental analysis North Sinai sherd S1

Na₂O	MgO	Al₂O₃	SiO₂	P₂O₅	SO₃	Cl	K₂O	CaO	TiO₂	MnO	FeO	CoO	NiO	CuO	ZnO
Elemental analysis, Blue, FIB-EDS Area analysis, Figure A5.S1.1.															
1.4	3.3	20.1	51.3	0.1	5.7	0.9	3.2	3.3	1.1	0.3	7.3	0.8	0.0	0.7	0.5
Elemental analysis, Blue, FIB-EDS Area 1 analysis Figure A5.S1.3															
0.1	7.1	57.2	18.3	0.2	3.1	0.2	1.9	2.0	0.2	1.1	2.6	1.8	1.5	0.4	2.2
Elemental analysis, Blue, FIB-EDS Area 1 analysis Figure A5.S1.9															
0.6	3.3	18.7	44.8	0.0	11.9	0.6	3.1	6.8	1.0	0.4	6.5	0.9	0.3	0.8	0.5
Area Analysis															
0.7	**4.6**	**32.0**	**38.1**	**0.1**	**6.9**	**0.6**	**2.7**	**4.0**	**0.8**	**0.6**	**5.5**	**1.2**	**0.6**	**0.6**	**1.1**

5.4.2.1.8.   Mut al Kharab, sherd D7, mid 18th Dynasty to more likely 19th or 20th Dynasties or the end of the Ramesside period.
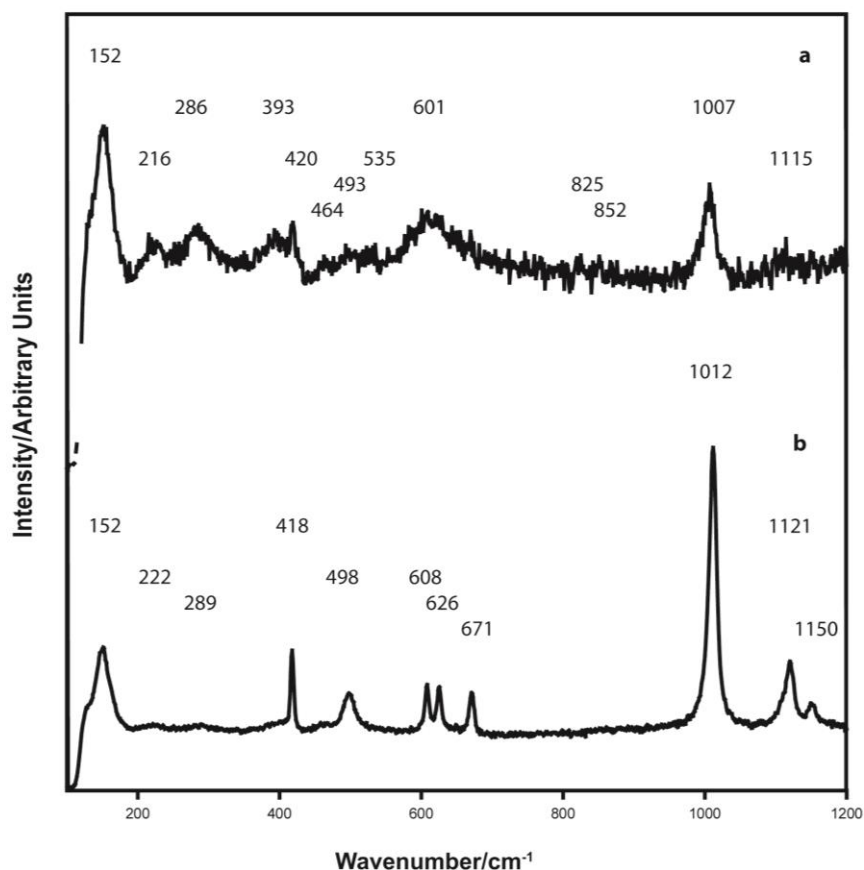
Figure 5.35. Raman spectra of the Mut al Kharab sherd D7 (MUT1)   (a) is the slip coating, (b) is the blue pigment (λ = 514.5 nm).   Cobalt blue mineralisation is primarily cobalt clinopyroxene together with heterogenite and the cobalt oxide (Co_2O_4). Tridymite possibly huntite or more likely mullite, and magnesium sulphate (either epsomite, starkeyite) or glauberite [$Na_2Ca(SO_4)_2$].   EDS analyses indicate the presence of quartz, gypsum, a titanium mineral, and a high iron-based mineral (refer Figure A5.D7.22). Several variable-sized particles of hydroxyapatite (bone ash) were observed (refer Figures A5.D7.4 (Spot 3), -.9 (Area 1), -.11 (Area 1), -.25 (Area 2), -.39 (Area 1), -.41 (Area 1). Anomalous phosphorus was noted from the EDS area analyses (1.4% P_2O_5).

Average elemental analysis, Mut al-Kharab sherd D7

Elemental analysis, Blue region, FIB-EDS Area analyses, refer Figures A5.D7.1, A5.D7.4, A5.D7.11, A5.D7.16, A5.D7.19, A5.D7.25, A5.D7.30, A5.D7.35, and A5.D7.39..

Na₂O	MgO	Al₂O₃	SiO₂	P₂O₅	SO₃	Cl	K₂O	CaO	TiO₂	MnO	FeO	CoO	NiO	CuO	ZnO
2.0	5.6	30.1	39.0	1.5	5.0	0.4	2.5	5.9	0.6	0.0	6.5	0.5	0.0	0.5	0.0
1.4	3.6	18.8	24.9	1.9	24.7	0.2	2.0	16.8	0.3	0.0	4.6	0.2	0.0	0.2	0.0
1.8	4.1	30.8	41.9	1.3	5.0	0.2	2.3	4.7	0.9	0.0	5.8	0.5	0.0	0.6	0.0
2.1	5.2	28.0	37.1	1.9	6.0	0.3	2.6	7.2	0.9	0.4	6.2	0.6	0.0	0.7	0.8
2.4	4.5	26.0	39.7	0.8	5.3	0.1	2.9	6.9	0.7	0.5	8.1	0.5	0.4	0.8	0.5
1.9	3.1	19.7	22.7	0.7	1.9	0.1	1.7	3.5	0.7	1.0	39.7	1.3	0.4	0.8	0.8
1.8	2.7	30.5	36.7	0.4	9.8	0.1	2.0	6.9	0.7	0.5	6.1	0.3	0.2	0.8	0.4
2.2	5.3	29.9	34.2	2.7	6.2	0.3	2.2	7.7	0.6	0.4	5.4	0.5	0.6	0.7	1.0
2.4	5.5	32.8	35.3	1.4	4.3	0.4	2.3	5.2	0.8	0.4	5.5	0.7	0.7	0.7	1.1
2.2	4.2	27.6	41.7	1.1	4.0	0.2	2.5	4.7	0.8	0.0	11.0	0.0	0.0	0.0	0.0
2.4	4.7	29.5	32.9	2.0	8.6	0.3	2.3	9.0	0.7	0.4	5.8	0.8	0.0	0.8	0.0
Average analysis															
2.1	**4.4**	**27.6**	**35.1**	**1.4**	**5.6**	**0.2**	**2.3**	**6.2**	**0.7**	**0.3**	**6.5**	**0.5**	**0.2**	**0.6**	**0.4**

Average elemental analysis, Mut al-Kharab sherd D7

5.4.2.1.9. Australian synchrotron XFM beamline elemental maps for various sherds examined from the Nile valley.

Relative Concentration Legend

Zero   Maximum

Figure 5.36. Synchrotron elemental maps generated using the XFM beamline, Australian synchrotron, for Malkata Bachmann sherd (M9). Note that the strong pattern labelled Rb is in fact likely to be due to Si.

Figure 5.37. Synchrotron elemental maps generated using the XFM beamline, Australian synchrotron, for sherds Amarna A2, Malkata M3 (MA) and Malkata M5 (MC).

Relative Concentration Legend

Zero   Maximum

Figure 5.38. Synchrotron elemental maps generated using the XFM beamline, Australian synchrotron, for North Karnak sherd NK3 (PP473). Note that the strong pattern labelled Rb is in fact more likely to be due to Si.

Relative Concentration Legend

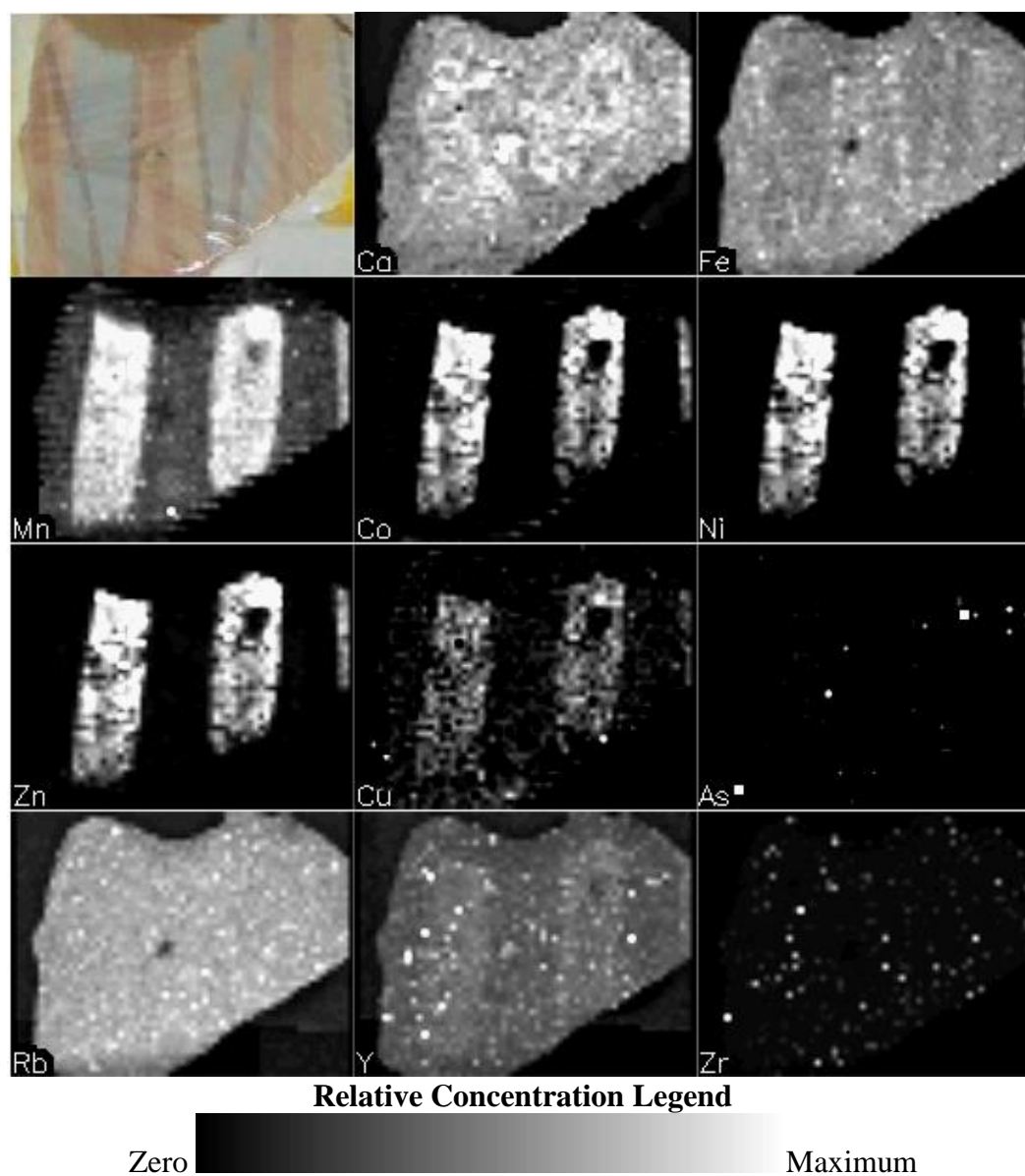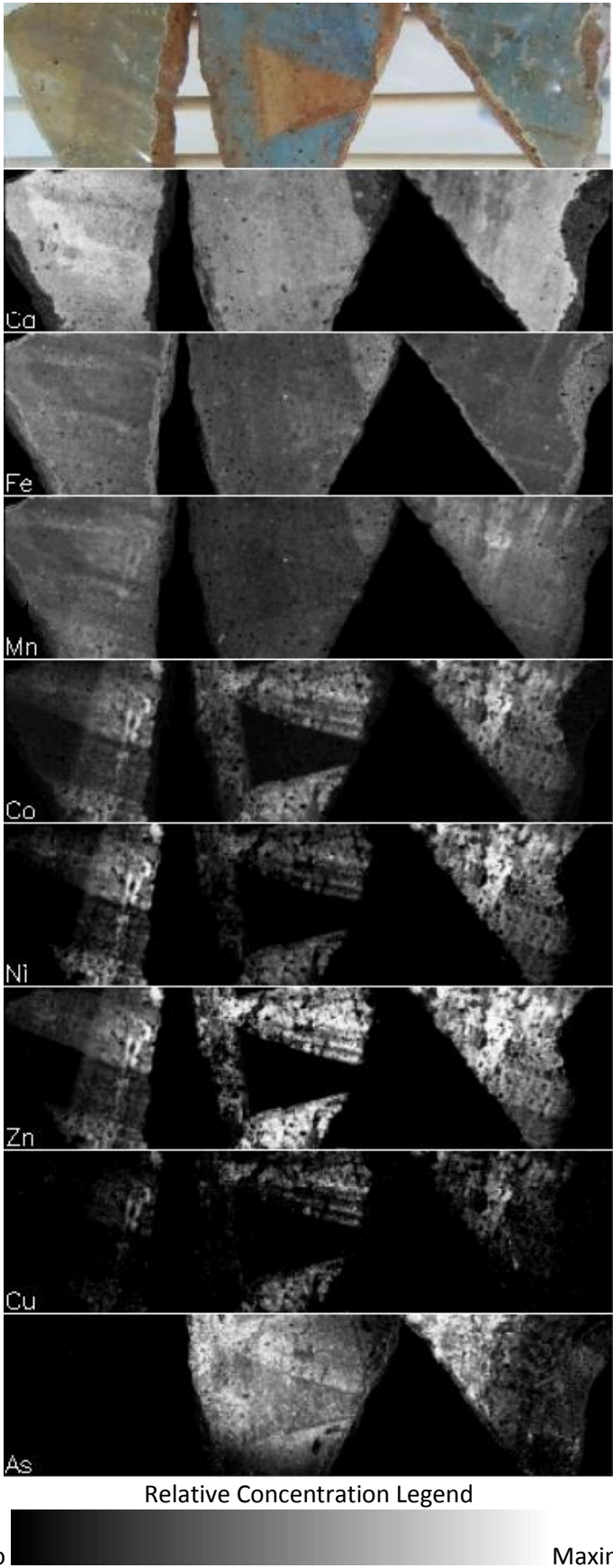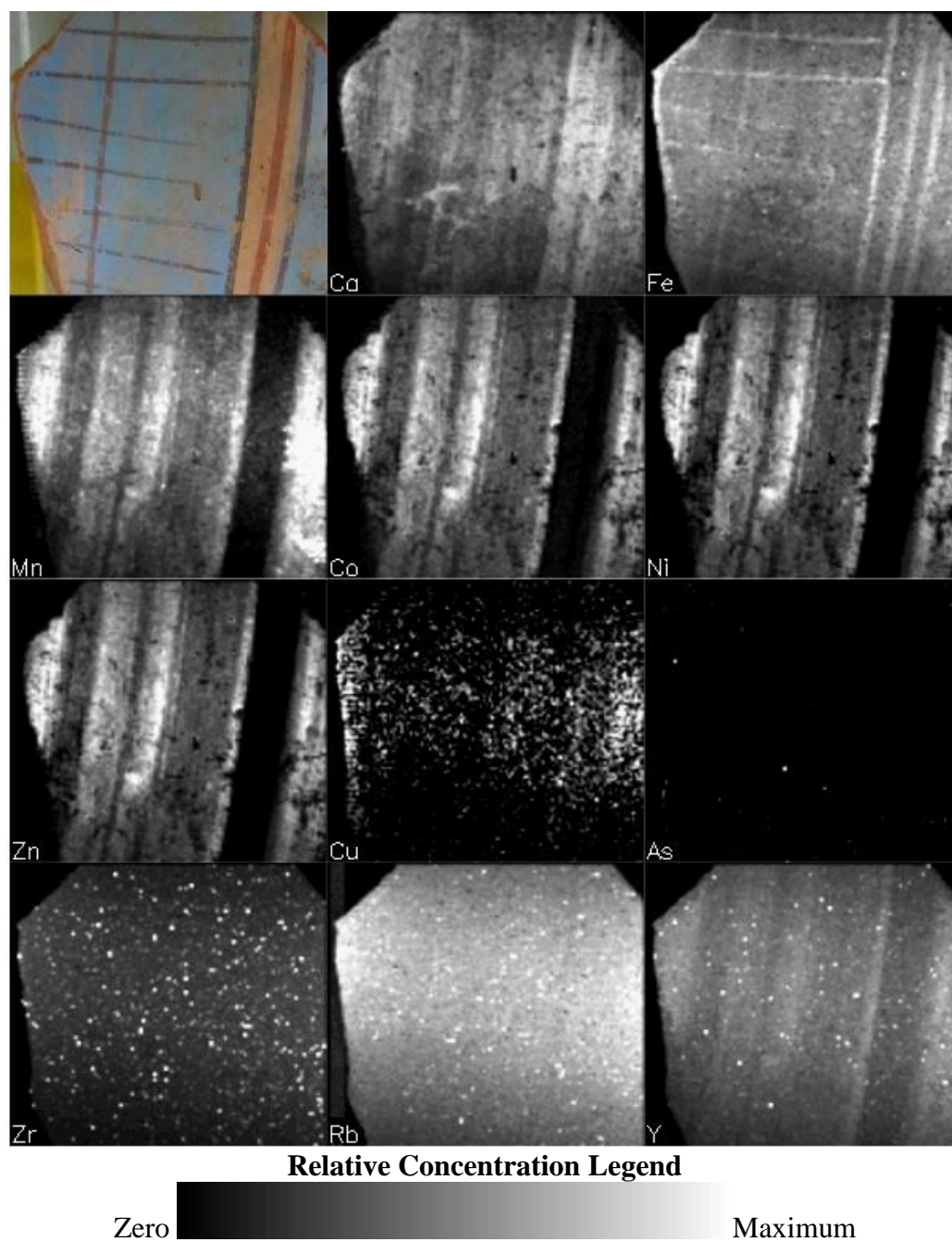Zero   Maximum
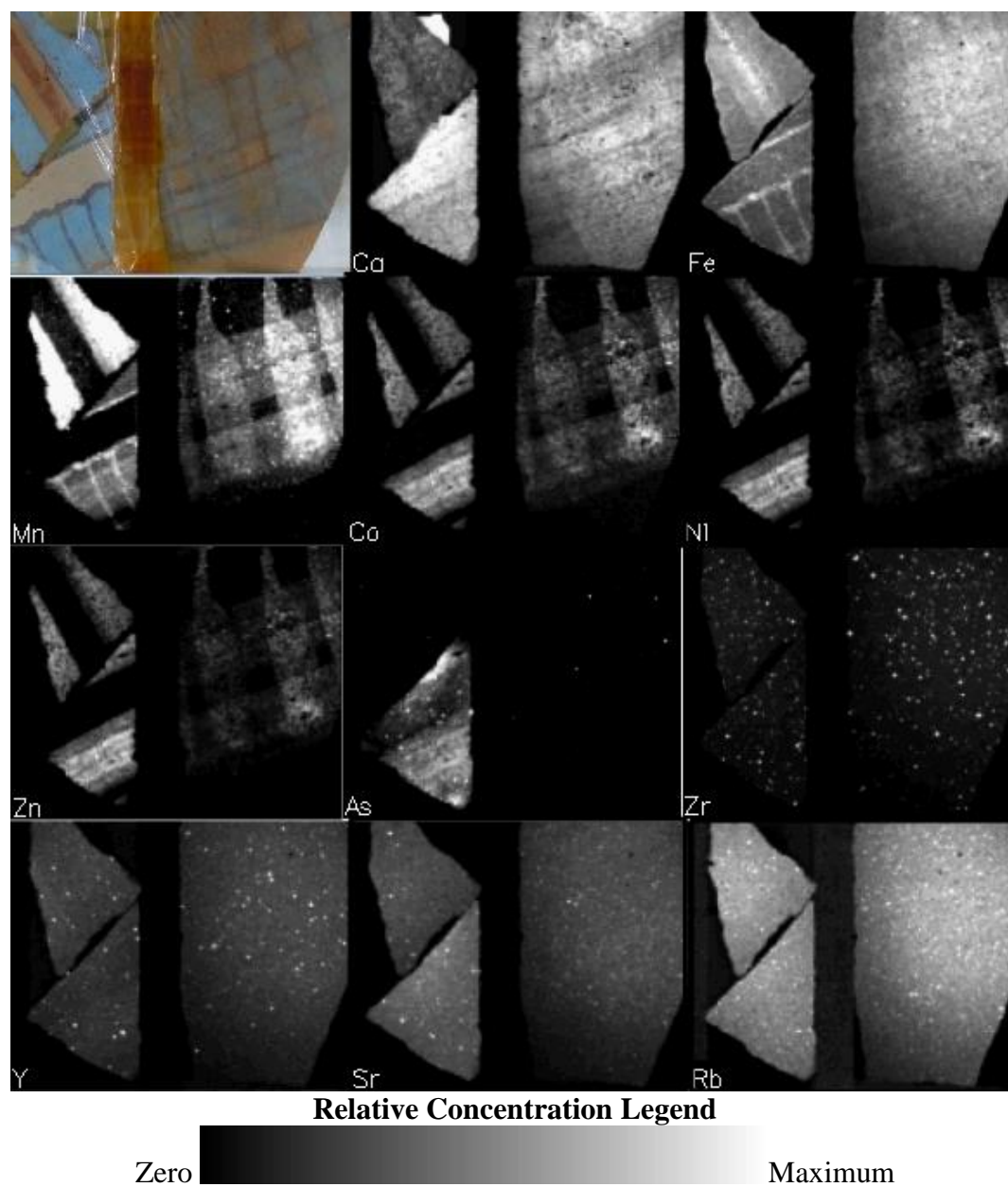
Figure 5.39. Synchrotron elemental maps generated using the XFM beamline, Australian synchrotron, for sherds North Sinai S1 (upper left), Deir al Medineh DM1 (lower left), Amarna A4 (right). Note that the strong pattern labelled Rb is in fact more likely due to Si.

Table 5.7. Average analyses of blue pigment applied to Egyptian pottery from various locations and sites. For individual sherd results, refer to Appendix A5.

	Na2O	MgO	Al2O3	SiO2	P2O5	SO3	Cl	K2O	CaO	TiO2	MnO	FeO	CoO	NiO	CuO	ZnO	BaO	PbO	SnO2	As2O3	Cr2O3	F
Malkata	1.8	4.3	29.5	21.4	0.8	7.8	1.4	1.4	15	0.6	0.9	5.1	2.8	1.7	1	3.8	0.0	0.3	0.0	0.0	0.0	0.0
Amarna	2.4	3.6	30.4	21.8	1.1	7.8	2.5	1.7	15.5	0.6	0.6	6	1.5	1	1.2	2.3	0.0	0.0	0.0	0.0	0.0	0.0
Karnak North	1.2	4	33.9	25.8	0.4	4.5	tr	2.1	5.6	0.9	1.3	13.9	1.8	1	1.3	1.6	0.0	0.0	0.0	0.0	0.0	0.0
Memphis	1.8	5.4	37.3	30	2.8	0.4	0.0	1.5	8.3	0.5	1.2	4.5	1.6	1.4	0.7	3.4	0.0	0.0	0.0	0.0	0.0	0.0
Dier al Medineh	1.8	2.6	42.3	18.8	0.9	6.1	0.0	1	12	0.0	0.7	3.5	2.7	2.4	0.0	5.2	0.0	0.0	0.0	0.0	0.0	0.0
North Sinai	0.4	5.3	39.4	30.1	0.2	6.3	0.4	2.5	3.9	0.6	0.8	5	1.5	1.1	0.7	1.7	0.0	0.0	0.0	0.0	0.0	0.0
Dendera	8.9	3.1	17.7	25.6	0.1	9.9	7.2	2.1	15.2	0.9	0.5	7.2	0.7	0.5	0.0	0.5	0.0	0.0	0.0	0.0	0.0	0.0
Mut al-Kharab	1.9	4.3	27.4	36.6	1.3	9.3	0.2	2.4	8.1	0.7	0.2	6.2	0.5	0.1	0.6	0.3	0.0	0.0	0.0	tr	0.0	0.0

Mut al-Kharab hydroxyapatite (bone ash) particle in Figure 5.44 (refer Appendix A5 analysis of area in Figure A5.D7.9).

	Na2O	MgO	Al2O3	SiO2	P2O5	SO3	Cl	K2O	CaO	TiO2	MnO	FeO	CoO	NiO	CuO	ZnO	BaO	PbO	SnO2	As2O3	Cr2O3	F
MUTB_3A1	1.8	2.2	17.9	9.7	20.8	9.0	0.5	1.0	31.5	0.4	0.3	2.6	0.3	0.0	0.7	0.0	0.0	0.0	0.0	0.0	0.0	1.2

Table 5.8. Average analyses of blue pigment applied to Egyptian pottery from various locations and sites and provided in Table 5.7. For individual sherd or site results, refer to Appendix A5.

	Na2O	MgO	Al2O3	SiO2	P2O5	SO3	Cl	K2O	CaO	TiO2	MnO	FeO	CoO	NiO	CuO	ZnO	BaO	PbO	SnO2	As2O3	Cr2O3	F
Average	2.5	4.1	32.3	26.3	1.0	6.5	0.6	1.8	8.7	0.6	0.8	6.4	1.6	1.2	0.7	2.4	0.0	0.0	0.0	0.0	0.0	0.0

Note that the high CaO and high SO$_3$ recorded in Table 5.8 above, most likely result from partial analysis of the underlying gypsum slip. This would be particularly evident where the remaining pigment is now thinly applied. This is evident in several of the images supplied in Figure 5.12 (a) to (e) and in Appendix A5.

Table 5.9. Cobalt pigment mineralisation determined by Raman spectroscopy and EDS elemental analysis.

Sample	MgAl spinel	CoAl spinel	(Co,Zn)Al spinel	ZnAl gahnite	CoSi olivine	#Co Pyroxene	CoO	CoOOH	*Co hydrox	CoSO$_4$ bieberite
Amarna										
A1	●		●	●		●				
A2					NiSi	●	●		●	
A3		?##	●			●	?	?		
A4						●	●	●		
A5						●	●	●		
A6						●		●		●
A7	●	●				●	●			
A8	●		●			●				●
Malkata										
M3	?	?	●			●		●		?
M5		?				●			●	**
M6		●				●		●	●	
M9		?		●		●			●	●
M12		?		NiAl		●		●	●	
M13					●/Ni	●	●	●		●
M14		●		●		●				●
M15	●					●	●			
M16		?			●	●	?			
Mut al-Kharab										
D7						●	●	●		
Karnak North										
NK1		?	●			●	●	●		●
NK2	●			●		●	●	●		●
NK3		?				●			?	●
Memphis										
R1						●			●	●
R2						●	●			●
Dendera										
DE1						●		●	●	●
Deir al Medineh										
DM1	●		●			●		●	●	●
Bir al-Abd, North Sinai										
S1			●			●		●	●	●

*Co hydrox is Co(OH)$_2$ **Possibly spherocobaltite [CoCO$_3$].   ? = probable presence
Co pyroxene in this context may be considered as Cobalt substituting for Mg in diopside.
? ## Indicates that additional bands to support the mineral assignment are missing and further, that the specific band identified is shared by other minerals.

Table 5.10. Element oxide/cobalt oxide based upon the analyses provided in Table 5.7 and compared with the results given by Shortland *et al*. (2006a).

Sample	MgO/CoO	MnO/CoO	FeO/CoO	NiO/CoO	ZnO/CoO	Al_2O_3/CoO
Malkata	1.5	0.3	1.8	0.6	1.4	10.5
Amarna	2.4	0.4	4.0	0.7	1.5	20.3
Karnak N	2.2	0.7	7.7	0.6	0.9	18.8
Memphis	3.4	0.8	2.8	0.9	2.1	23.3
Deir al-Medineh	0.7	0.3	1.3	0.9	1.9	15.7
Sinai	0.3	0.5	3.3	0.7	1.1	26.3
Mut al-Kharab	3.8	0.4	12.4	0.2	3.0	54.8
Shortland *et al*. (2006a) results						
Malkata average	1.0	0.2	0.5	0.6	3.2	14.7
Amarna average	2.4	0.4	1.3	0.8	3.3	17.5

5.4.2.2 *Alkali flux, natron or plant or vegetable ash.*

Tite and Shortland (2003) reappraised the chemical compositions and microstructures of the cobalt-blue frit at Amarna. They concluded that their evidence strongly supports natron being the flux used in the production of the cobalt-blue frits.

As reiterated by Rehren (2008), the identification of plant ash as the most likely flux in New Kingdom/Late Bronze Age Egyptian glassmaking by Brill (1970: 111) represented a major development in the understanding of the earliest glassmaking tradition. It is now proposed that this same plant ash technology formed the basis for cobalt pigment production, this technology occurring at about the same time as glass production was introduced into Egypt.

Thus, the translation of the Assyrian cuneiform glassmaking texts by Oppenheim has provided an opportunity for Brill (1970; 1972) to interpret this translation in the study of early glassmaking. He determined that the term *immanakku* is the source of the silica as pebbles, *aḫussu* as the plant ash and when they are reacted they formed a chemical intermediate, namely *zukû*. As described by Brill (1970) various species of the genera *salicornia* and *salsola* (amongst others) found in the marshy regions in Iraq, Iran, Syria and elsewhere within the general region are still gathered to this day, where they are burnt in pits to obtain hard, chunky, highly alkaline ashes. This ash can then be used in detergent (soap) manufacture, glass manufacture and as proposed in this thesis, for the production of cobalt pigments. Brill provided a number of plant ash analyses, including *Salicornia sp*. (Turkey), a desert bush (Egypt), seaweed (Israel) , a "soda plant" (Iran); tamarisk (Israel) the *chiăn* plant (Iraq), all of which indicate the wide range of minerals likely to be found in these various plant ashes. He reported that the high potash (1-4% K_2O) and high magnesia (MgO 3-7%) is indicative of their use in glass production. These alkali concentrations compare

favourably with the average analyses of the cobalt pigment on the sherds analysed and given in Table 5.8 of namely, 1.8% K_2O and 4.1% MgO. In glass manufacture, low potash and low magnesia are considered to indicate the use of natron, or a similar source of alkali.

Related to this study, is the work of Barkoudah and Henderson (2006) who studied plant ashes with high alkali contents and which were used in soap-making and glass-making throughout Syria and the Middle East. Interestingly, they observed that the mid-14th century Venetian glass makers were importing Levantine ashes from Aleppo, Sarmin, Beirut and elsewhere, with the greatest quantity being sought probably from Syria and to a lesser quantity from Egypt. These authors noted that a wide compositional variation exists within these ashes (and therefore glasses) even from the same species, the parts of the trees and the geological environment in which the plants were growing.

Colomban (2010/11) supported this information and he discussed the development of plant ash in glass manufacture within the Mediterranean world and the change from natron-based glasses to plant-based glasses at the end of the Roman period. The criteria for plant ash is the level of potassium, which he stated to be usually >1.5% in soda-based glass, the phosphorus concentration in wood and the magnesium in halophile plants. Colomban also noted that in the case of very alkaline or siliceous vegetable ashes from grasses, the ash was washed prior to use. He suggested that this washing step would remove some of the soluble ions and hence is a further method by which these ashes can vary in composition. He classified these ashes into two categories:

- acidic ashes, rich in silica and derived from grass, horsetails, ferns;
- alkaline ashes, rich in basic oxides which are modifiers and derived from wood.

Colomban also noted in this report that contrary to a common assertion, variability in phosphorus content is not proof that vegetable ashes were not used. Furthermore, these vegetable ashes are an important source of calcium. This observation is confirmed by the CaO concentration found to be present in the Dakhleh Oasis plant ash analysis provided in Table 5.12.

Rehren observed that the numerous analyses of Egyptian New Kingdom glass objects would suggest a relatively closely characterised 'profile' of the plant ash being used for most, if not all, Egyptian glass prior to c. 1000 BCE. He noted that glass from this period typically contains 18 ± 2 wt. % Na_2O, 12 wt.% K_2O, 5-10 wt.% CaO, and 3-5 wt.% MgO. As provided in Table 5.8, the cobalt pigment contains MgO and CaO in the same approximate concentration. However, the soda and potash concentrations are consistently lower than that in glass across all sites from which sherds were analysed. When coupled with the high MgO and CaO, this is clear evidence for the use of plant ash rather than natron.

Tite *et al.* (2006) reported that plant ashes from Syria, Iraq, Iran, Pakistan, Afghanistan, and Uzbekistan known to have been used for glass, glaze and soap production including *chinan*, *osnan*, *ghar* and *tezab* are all higher in soda than potash, the soda to potash ratio varying from 1.2 to 9.2 with the majority being in the range 4 to 8. They noted that in Pakistan, typically, some 400 kg of the shrub were burnt over a 24 hour period in pits some 1.6 to 3.0 m in

diameter and dug to a depth of about 1.6 m. The product of such combustion were friable lumps of ash of variable quality, the most friable, having the greatest porosity, highest Na_2O + K_2O of 46.7%, and the lowest fusibility exhibiting extensive flow by 700-750°C. The lowest grade contained significant charcoal, increasing lime and magnesia content of 16.1% CaO + MgO, and lower fusibility of 900-1000°C. The ashes they collected from Egypt were all soda rich with a soda/potash ratio between 2 to 11. A summary of a number of these plant ash analyses are provided in Table 5.11.

Table 5.11. Selected plant ash elemental analyses from various geological regions. (Blank analysis for individual elements indicate that the text failed to provide an analysis. This may be indicative of either not quoted or not analysed).

Syria, desert shrub, *(chinan)* (Tite *et al*. 2006)

Na₂O	MgO	Al₂O₃	SiO₂	P₂O₅	SO₃	Cl	K₂O	CaO	TiO₂	MnO	FeO	CoO	NiO	CuO	ZnO
31.3	6.0	0.7	0.5		8.1	15.0	5.2	9.5							

Pakistan, , shrub *(ghar)*, (Tite *et al.* 2006)

| 34.3 | 4.3 | 0.9 | | 0.7 | 4.0 | 10.2 | 14.1 | 3.0 | | | 0.3 | | | | |

Levant, herb, (*Salsola sodium*. (Tite *et al.* 2006)

| 43.0 | 1.8 | | | 0.9 | 3.0 | 6.8 | 3.6 | | | | | | | | |

Levant, (*Salsola kali*), (Tite *et al.* 2006)

| 14.3 | 9.0 | | | 5.5 | 1.4 | 15.5 | 14.4 | | | | | | | | |

Uzbekistan, (*Solsola crassi*), (Tite *et al.* 2006)

| 40.3 | 2.6 | 0.1 | 0.1 | 0.3 | 23.5 | 13.1 | 12.3 | 1.1 | | | 0.0 | | | | |

Egypt, Wadi Natrun, (Salsola), (Tite *et al.* 2006)

| 14.7 | 7.5 | 3.0 | 8.0 | 0.8 | 24.8 | 13.7 | 3.1 | 23.1 | | | 1.1 | | | | |

Egypt, Barnug, (*Suaeda*), (Tite *et al.* 2006)

| 43.4 | 3.9 | 1.5 | 5.1 | 5.3 | 8.2 | 20.0 | 6.5 | 5.2 | | | 0.9 | | | | |

Egypt, Barnug, (*Suaeda*) (woody), (Tite *et al.* 2006)

| 33.3 | 6.6 | 1.4 | 7.2 | 4.6 | 7.1 | 17.3 | 14.5 | 7.3 | | | 0.6 | | | | |

Egypt, Taposiris Magna *(Anabasis articulate)*, (Tite *et al.* 2006)

| 48.9 | 2.0 | 0.5 | 0.8 | 2.0 | 4.2 | 34.9 | 4.5 | 2.0 | | | 0.1 | | | | |

Egypt, Taposiris Magna (Suaeda), (Tite *et al.* 2006)

| 30.9 | 4.8 | 1.7 | 3.6 | 0.7 | 5.9 | 32.8 | 5.3 | 13.6 | | | 0.6 | | | | |

Egypt, twigs from a bush, Cairo-Alexandria Highway.(Brill 1970)

| 7.75 | 7.75 | 3.8 | ~8 | ~1 | 12.0 | 5.2 | 18.2 | 16.1 | | | 2.76 | | | | |

Naaman River, (Belus River) bush, (probably *Tamarix meyeri*), (Brill 1970)

| 21.7 | 6.28 | 1.06 | ~3 | ~1 | 28.8 | 13.9 | 5.18 | 13.0 | | | 0.97 | | | | |

Europe, Beech, (Tylecote 1986)

| 22.0 | 7.64 | 31.62 | 8.0 | 4.85 | Na₂O+ K₂O = Na₂O | | | 24.96 | | | tr | | | | |

England, Oak, (Tylecote 1986)

| 1.31 | 3.56 | | 55.3 | | | | 14.9 | 22.54 | | | 0.56 | | | | |

England, (Seaweed) Kelp, (Tite *et al.* 2006)

| **19.4** | **11.2** | **0.7** | | **0.3** | **31.0** | **5.1** | **16.4** | **11.6** | | | **0.4** | | | | |

5.4.2.2.1 D9, Dakhleh Oasis plant or vegetable ash.

A sample consisting of a combined mixture of *Acacia nilotica,* controversially known as *Vachellia nilotica* or gum Arabic tree and *Tamarix aphylla* (Tamarisk) was analysed providing the data in Table 5.12. Additional data is provided in Appendix A5.D9. The high chloride

and sulphate concentration would have negated its use in soap production as described by Tite *et al.* (2006). And, for glass production, it would have preferentially required washing in water to remove the chloride.
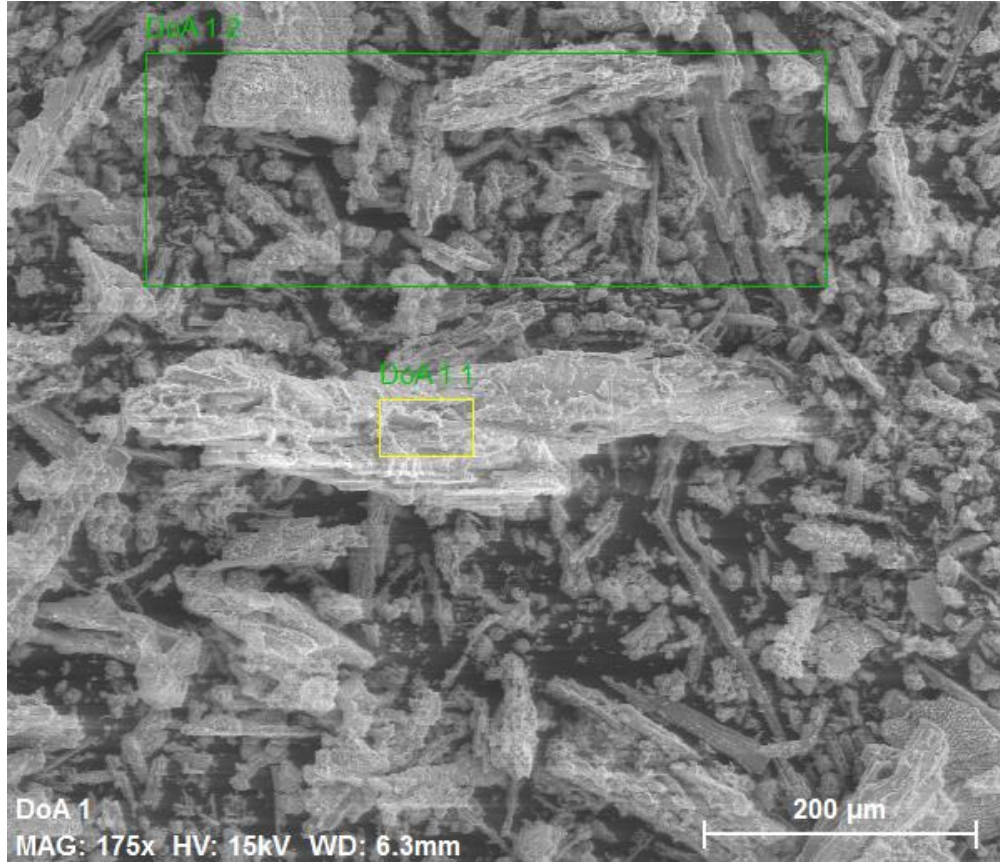

Figure 5.40. Nova, SE image of the plant ash showing the position for the analyses of plant ash from Dakhleh Oasis as indicated as Areas DoA 1.1 and DoA 1.2 in Appendix A5.D9 and forming part of the data in Table 5.12.

Table 5.12. Average elemental analysis plant ash sample, Dakhleh Oasis.

Elemental analysis, Blue region, FIB-EDS Area analyses, refer Figures A5.D9.4, A5.D9.5, A5.D9.6, A5.D9.7,

Na_2O	MgO	Al_2O_3	SiO_2	P_2O_5	SO_3	Cl	K_2O	CaO	TiO_2	MnO	FeO	CoO	NiO	CuO	ZnO
19.5	11.6	0.2	0.0	0.5	16.1	29.6	3.5	19.1	0.0	0.0	0.0	0.0	0.0	0.0	0.0
13.7	17.1	0.2	0.2	0.7	20.1	24.0	2.7	21.2	0.0	0.0	0.0	0.0	0.0	0.0	0.0
17.0	13.9	0.6	0.1	1.0	23.6	20.6	4.5	18.7	0.0	0.0	0.0	0.0	0.0	0.0	0.0
18.5	12.3	0.2	0.2	0.9	21.9	23.3	3.3	19.5	0.0	0.0	0.0	0.0	0.0	0.0	0.0
19.0	10.1	0.2	0.0	0.9	22.6	27.4	4.2	15.5	0.0	0.0	0.0	0.0	0.0	0.0	0.0
Average analysis															
17.5	**13.0**	**0.3**	**0.1**	**0.8**	**20.8**	**25.0**	**3.6**	**18.8**	**0.0**	**tr**	**0.0**	**0.0**	**0.0**	**0.0**	**0.0**

The ash sample is high in soda, magnesium and calcium, probably as chlorides or sulphates. It is therefore able to supply the alkalis in accordance with the requirements for Tables 5.7

and 5.8. The low phosphate analysis in Table 5.12 and the low phosphate concentration reported in Tables 5.7 and 5.8 provides evidence for the traces of phosphate when observed within the cobalt pigment to be generally from this alkali source or from urine. The large hydroxyapatite particles in Figures 5.44 to 5.47 are obviously from a different source.

5.4.2.2.2 Alkali flux, calcium, magnesium and potassium

Sedimentary limestone from biogenic marine sediments is composed mainly of the skeletal remains of marine organisms such as coral, foraminiferans such as nummulites and molluscs.   Other associated rock types include gypsum and anhydrite, both from evaporative marine sediments; sandstone, including siliceous (quartz-cemented) sandstone or quartzite (from continental sediments and, in part, shallow nearshore marine sediments); travertine and chert (both from secondary mineralization of limestone).

The analyses for the cobalt blue pigments given in Table 5.7 indicate the presence of magnesium in concentrations probably greater than that obtainable from natron thereby supporting the use of plant ash as the alkali flux. At least part of this magnesium would have been supplied from the alum precipitant. This establishes that a solution pH high enough to precipitate the magnesium from the aqueous alum solution was required. This would suggest the use of ammonia/urea as discussed in Section 5.8. Again, the low sodium concentration in the blue pigment, reported in Tables 5.7 and 5.8 would suggest that natron was not the preferred precipitant although it almost certainly would have formed part or all of the alkali added to the alum solution to precipitate the transition elements present therein.

And, as provided in Table 5.12, fuel ash of the type analysed and produced within the Oasis would provide the requisite alkalinity necessary for the production of the cobalt pigment. However, the glass structure into which the cobalt-containing precipitate may have been incorporated, could also have contained some natron (trona). Potassium, which is often in concentrations in the final pigment of about 1-2% K_2O would have been supplied by the ash (plant or biomass-based), or partially from urine as discussed in Section 5.4.2.7.3 below.   As shown in Table 5.10, the MgO/CoO ratios found at Malkata and at Amarna are comparable with those provided by Shortland *et al.* (2006a).

5.4.2.3 Silica

Silica and silicates have been previously discussed in some detail within AppendixA4. Analysis of a random sample of sand from Dakhleh Oasis has been analysed and its elemental analysis is provided in Appendix A5 as Dakhleh sample D10. The sample contained very minor calcium and sufficient alumina to suggest that some feldspar was present in the sample.   Additional lime or a calcium-containing plant ash would have been required to enable this sand sample to be used in glass or cobalt pigment production.   In the presence of a flux, such as potash or soda, silica will readily react with aluminium oxide to form complexes such as mullite.

Silica can form polymorphs such as tridymite and cristobalite, which are capable of formation at temperatures in excess of 1000ºC, and according to phase diagrams, again

discussed in Chapter 4, cristobalite requires a much higher temperature to form. Cristobalite has been reported to form in the literature in the production of Egyptian blue, but such formation is considered to be tenuous. As the cobalt pigment was presumably fired at temperatures corresponding to that of Egyptian blue, the more likely polymorph formed is tridymite. And, in the present study other than in one specific sherd, only tridymite formation was observed.

The presence of tridymite formation would however, preclude the direct firing of say a cobalt hydroxide precipitate on the vessel surface as proposed by Riederer. This would have required the vessel to reach a temperature close to, or above its point of thermal failure. This does not however, preclude the early Egyptian workers from attempting such a trial firing. Silica can also react with the MHP cobalt precipitate to form a cobalt olivine structure.

The application of the pigment to the pottery surface is discussed in Section 5.7.

5.4.2.3.1 Mullite formation [$3Al_2O_3.2SiO_2$]

Alumina can undergo a high temperature reaction with silica to form mullite. Such starting materials are present in the raw materials selected for the production of the cobalt pigment.

Mullite precursors can be grouped by two general pathways. Mullitisation from the amorphous phase occurs at around 1000°C and when from a spinel phase, mullitisation occurs at higher temperatures, in the order of 1200°C. In a study by Ban *et al*. (1996) they indicated that low temperature mullitisation is possible with the reaction commencing at 450°C and significantly more rapidly at 900°C. This reaction chemistry has been reviewed by Pask (1996). Mullite can also be formed by the reaction of kaolinite with alumina (Chen *et al*. 2000). Thus, in the formation of the cobalt pigment, the conditions exist for such a reaction to occur. The reaction has been observed and is reported within the text.

5.4.2.4 Nickel

Nickel was present in the cobalt-containing alum and in every sample of the cobalt pigment. A very high concentration of this element was located in North Karnak sherd NK2 as shown in Figure 5.41 and the accompanying element table.
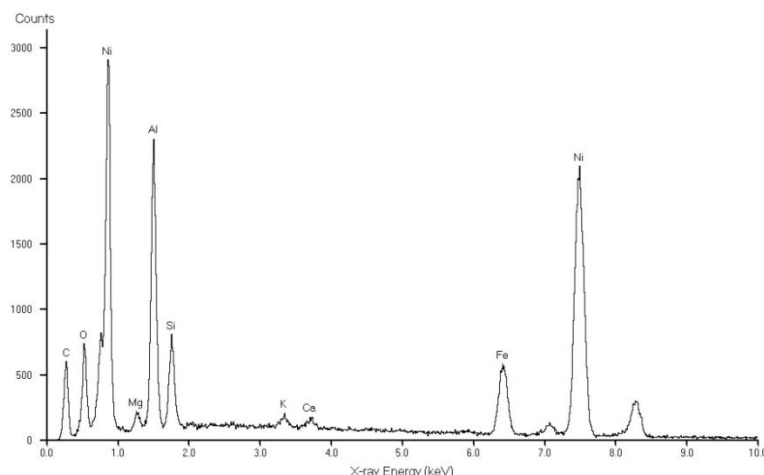
Figure 5.41. FIB SEM-EDS spectrum of the Bright Spot 1 in North Karnak sherd NK2 and its analysis is provided in the accompanying table and is discussed in Figure A5.NK2.1.

Elemental analysis, bright particle in North Karnak sherd NK2

Elemental analysis, Blue region, FIB-BSE Bright Spot analysis Figure A5.NK2.1

Na$_2$O	MgO	Al$_2$O$_3$	SiO$_2$	P$_2$O$_5$	SO$_3$	Cl	K$_2$O	CaO	TiO$_2$	MnO	FeO	CoO	NiO	CuO	ZnO
0.0	1.7	23.6	8.2	0.0	0.0	0.0	0.6	0.6	0.0	0.0	8.7	0.0	56.6	0.0	0.0

The presence of such a high nickel-containing particle is indicative of the variability in the various transition elements located in the Dakhleh Oasis alums.   The ratios of the various transition elements to cobalt for the sherds examined is provided in Table 5.10.   Shortland *et al.* (2006a) have provided results for Malkata and Amarna. There is general agreement in both sets of results. However, individual sherds from other locations are limited in number and this could potentially bias any decisions in their respect.

5.4.2.5 Lead

White lead was used in some instances to lighten the colour of the blue pigment. This is evident in Malkata sherd M3 shown in Figure 5.12(a) in which two shades of blue are evident. A spot analysis of the lead found in this sherd is provided in Figure 5.42.
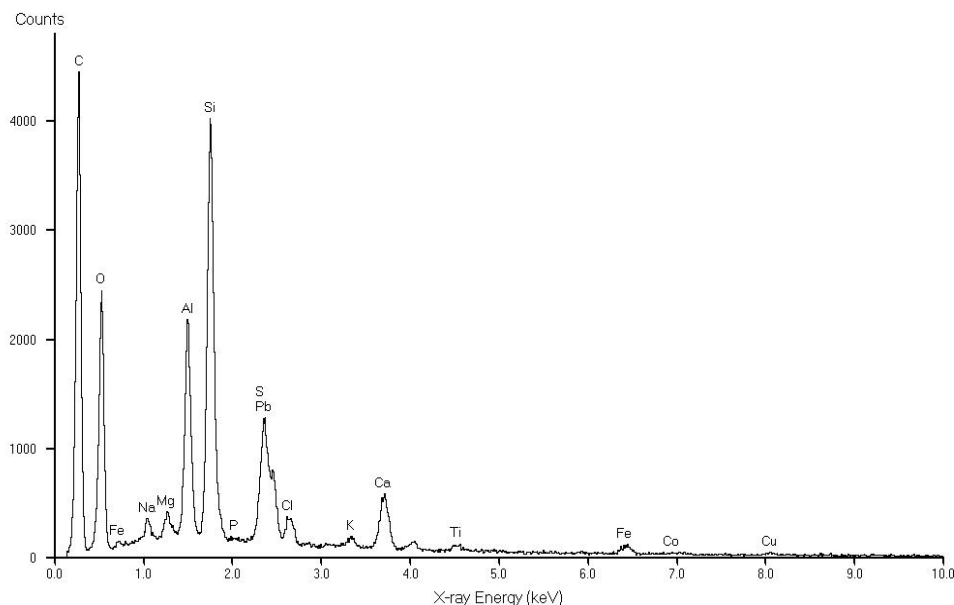
Figure 5.42. FIB SEM-EDS spectrum for the analysis of Spot 1 in Malkata sherd M3 and described more fully in Appendix A5, Figure A5.M3.1.

Elemental analysis, Malkata sherd M3 within a lighter blue area

Elemental analysis, Blue, FIB-EDS Spot 1 analysis, Figure A5.M3.1*.

Na$_2$O	MgO	Al$_2$O$_3$	SiO$_2$	P$_2$O$_5$	SO$_3$	Cl	K$_2$O	CaO	TiO$_2$	MnO	FeO	CoO	NiO	CuO	ZnO
1.2	1.6	15.9	39.6	0.1	3.1	1.6	1.2	7.5	1.3	0.0	2.9	0.8	0.0	1.5	0.0

*+PbO = 21.6%

5.4.2.6 Arsenic

Arsenic has been located as isolated spots in Malkata sherd M9 as shown in the XFM synchrotron map in Figure 5.36. It appears to correspond with spots also containing high iron, suggesting the possibility of it being present as ferric arsenate. Malkata sherd M13 also contains arsenic as provided in the area analysis given below and discussed more fully in Appendix A5.M13.

Area elemental analysis Malkata sherd M13, area analysis

Elemental analysis, Blue, FIB-EDS Area 1 analysis, Figure A5.M13.10*.

Na$_2$O	MgO	Al$_2$O$_3$	SiO$_2$	P$_2$O$_5$	SO$_3$	Cl	K$_2$O	CaO	TiO$_2$	MnO	FeO	CoO	NiO	CuO	ZnO
0.5	4.1	14.0	27.8	0.7	2.0	0.7	1.1	40.1	0.4	0.4	4.8	0.8	0.5	0.7	0.0

*+As$_2$O$_3$ = 1.2%

And, as shown in Figure 5.39, the XFM beamline mapping of Deir al Medineh sherd DM1, indicates that the cobalt pigment contains arsenic over its entire surface. There is no arsenic associated with the burnished surface, supporting the arsenic being introduced with the cobalt, possibly to modify its visual appearance. As such, it is probable that the arsenic was

present within an additive and not in the cobalt Mixed Hydroxide Precipitate (MHP) itself. The most likely source would therefore be as part of the flux or as a deliberate surface modifier as has been observed with the use of lead pigments.   Similarly, as shown in the synchrotron XFM beamline, Malkata sherds M3 and M5 in Figure 5.37 and Deir al-Medineh sherd DM1 in Figure 5.39 all show arsenic associated with the cobalt pigment.

5.4.2.7 Phosphorus

The presence of phosphorus in various Egyptian analyses is far more complex than the present literature would suggest. Phosphorus is essential for all life on earth. For example, phosphorus can be present in ground-waters; it can be available in both animal and fish bone; in plant material; in phosphate raw materials, including temper; or in urine. Thus, if as bone, the bone can be derived from ash from cooking or kiln fires; or it can be in the desert sands as relic bird, fish, or other crustacean material.

5.4.2.7.1 Egyptian phosphates

These analyses, particularly those of sherds recovered from within the region of the Dakhleh Oasis, would indicate that it is unlikely that fluorine or any of the heavy metals listed would be anticipated to register within any of the calcium phosphate analyses. If they do appear, then their presence would be from an alternative source. Thus, the trace elements present in Egyptian phosphates can provide an indication as to their potential for providing an influence on any calcium phosphate mineralisation detected in any of the samples under investigation.

There are a number of alternative or potential sources for the phosphate particles encountered during the examination of the pigments and pigmented sherds examined throughout this thesis. They include:

- soils and ground waters from burial;
- vegetable sources emanating from the use of plant ash;
- hydroxyapatite (or bone ash);
- use of urine as a gel-breaker in cobalt pigment production.

Each of these possible sources will be examined in some detail.

Phosphate mineralisation has been discussed in Chapter 4, Section 4.5.2.6 in respect of Egyptian blue. Similarly, anomalous phosphate mineralisation has been observed in respect of cobalt pigments as shown in Tables 5.7 and 5.8. The more likely sources are from the plant ash, from urine as proposed in the MHP hypothesis for cobalt extraction, or from vessel linings rather than from burial as is discussed below.

5.4.2.7.2 Phosphate deposition from ground waters

In a thought-provoking paper, Freestone *et al*. (1985) studied the adsorption of phosphorus on to pottery, slag and glass surfaces.   Analysis of cross sections through the pottery by

Freestone *et al*. (1985) indicated a U-shaped P_2O_5, CaO and FeO concentrations existed with the 1 mm closest to the external surface exhibiting the highest concentration of each of these three elements analysed. These workers were unable to locate discrete phosphate grains and presumed that if such discrete phosphate compounds are present in the sherds, their grain sizes were extremely fine and below 1 micron in size. And, XRD was similarly unable to detect crystalline phosphates. They concluded that the phosphate was present as either an amorphous coating on the silicate grains of the matrix, or as an extremely finely dispersed crystalline phase. Furthermore, their results supported the concept that phosphate deposition occurs so long as sufficient porosity exists to allow access for soil solutions. When firing temperatures are high enough to cause continuous vitrification and to thereby close interconnected pores present in the original clay structure, then phosphate is not adsorbed. The uptake of phosphate adsorption was highest when either the structurally disordered allophane or imogolite is fired to 600-800°C, and, whilst the pottery samples were considered to be non-calcareous, they agreed with the research of Franklin and Vitali (1985) that the presence of high calcium would result in a rapid precipitation of calcium phosphates occurring at the ceramic-solution interface. These workers concluded that whilst the mechanism is presently unknown, it has been demonstrated by other studies into geological apatite and archaeological bone that apatite is able to strongly adsorb many trace elements, including Cr, Sc, Ba and REE.

In their examination of a Mesopotamian opaque red glass dated to the 7th century BCE, the surface was shown to be depleted in alkalis and a strong enrichment of P, Pb, Ca and Cl was observed (Freestone *et al*. 1987). They were unable to obtain an accurate XRD analysis, but from the diffuse patterns obtained, they hypothesised that lead hydroxyapatite [$Pb_5(PO_4)_3OH$] and pyromorphite [$Pb_5(PO_4)_3Cl$] may have formed. Therefore they concluded that this work confirmed the findings of Duma (1972) and of Lemoine and Picon (1982) that the ceramics had adsorbed phosphate from burial; but they were unable to determine if the phosphate was adsorbed as anions on to the external surfaces of the ceramic or was precipitated from solution as a chemical compound. And, rather than the phosphate being present as apatite or brushite [$CaHPO_4.2H_2O$] it is more likely to be present as $Ca(H_2PO_4)_2.H_2O$.

Thus, according to the work of Freestone *et al*. (1985), phosphorus concentration, when derived from soil during burial, is anomalous above 0.2% P_2O_5. Freestone and co-workers had reported that there is a close relationship between the glass phases present in ceramic body composition and the increase in phosphorus up-take. Their work may be summarised as follows:

- X-ray mapping showed P_2O_5 to be homogeneously distributed on a scale of tens to hundreds of micrometres with very occasional enhanced levels around cracks and pores;
- under higher magnification, areas highly enriched in P_2O_5, CaO and FeO on a scale of a few micron but still associated with Al_2O_3 and SiO_2;
- discrete phosphate grains were not resolved;
- even very fine P_2O_5 areas were not observed;
- if discrete phosphate compounds are present in the sherds, their grain sizes are extremely fine, less than a micrometre or so;

- XRD failed to detect crystalline phosphates even after multiple sampling from the sherd exhibiting the highest phosphate content;
- at no stage was a single phosphate-bearing phase isolated;
- P_2O_5 is dispersed through the matrix until the transition between extensive continuous vitrification is reached;
- it appears that phosphate may be deposited in a ceramic as long as the porosity is sufficient to allow access for soil solutions;
- once interconnected pores close, then phosphate is not present;
- the phosphate was derived from the environment during burial;
- the high capacity of ceramics to retain phosphate is due to the amorphous silicate phases which are produced during firing. This accounts for their inability to isolate discrete grains of phosphate.

In the examination of glass and slag, the following observations were made:

- the glass surface is depleted in alkalis;
- there is an enrichment of phosphate, concentrated in finely spaced concentric Liesegang rings;
- mass balance calculations suggest that Ca, Pb and Cl in the P-enriched zone were derived from the depleted, weathered glass layer, while the phosphate was derived from an external source;
- XRD of the glass surface gave rather diffuse patterns, close to lead hydroxyapatite and pyromorphite;
- phosphate has precipitated within the silicate-glass matrix, rather than forming a coating on top of it;
- in spite of multiple sampling of the substantial areas of phosphate, XRD failed to detect crystalline phosphates.

They further reported that phosphate in the form of apatite, has a molar Ca/P ratio of 1.67, whereas in the sherds they studied, this ratio was around 0.5 indicating a marked deficiency in calcium. And, that it was difficult to determine if the phosphate was initially adsorbed as anions or was precipitated from solution as a chemical compound. Failure to detect the phosphate by XRD suggested to them that it is amorphous or poorly crystalline. Furthermore, the calcium was obtained from environmental contamination.

In ground-waters, Murray *et al*. (1983) reported that by experimentation, powdered calcite and gypsum were replaced at room temperature by apatite after treatment with 0.1 molar phosphate solutions as follows:

$$5CaCO_3 + 3K_3PO_4 + H_2O \rightarrow Ca_5(PO_4)_3(OH) + 4K_2CO_3 + KHCO_3$$
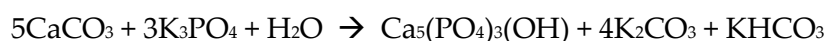
Apatite growth on barium sulphate was not observed, but a 50% replacement of calcite occurred in less than 30 days.

Clearly, the fluorine-containing hydroxyapatite particles encountered in the present research are significantly different to the phosphate encountered by Freestone and co-workers from burial conditions. These hydroxyapatite particles are discrete, able to be identified and analysed and the particles are not directly related to either silica or alumina. Importantly,

their molar Ca/P ratio is that of whitlockite, not that of a calcium-deficient mineral hypothesised by Freestone.

Whilst ground-waters cannot be dismissed, importantly, all of the Nile valley sherds were recovered from surface locations. Thus, they may never have been buried and have remained exposed to the annual rainfall events which have occurred subsequent to their disposal. Thus, the likelihood for burial or for phosphate deposition from ground-water, is not known, but it might have been fleeting or tenuous. The internal surface of the sherds examined only in one case contained an organic compound and this has been tentatively ascribed to palmatine.

To determine if the phosphate was from soil adsorption during burial, as indicated by Freestone *et al*. (1985) both the pottery core and the pottery external surfaces were analysed by SEM-EDS. The results are provided in Appendix A3 for all sherds, and their average analyses are summarised in Tables 5.13 to 5.19 below. It should be noted that the Freestone hypothesis was based upon four samples, widely different in type and find location. Whilst their work is not questioned, the present work would strongly support the proposition that not all pottery samples will necessarily adsorb phosphates under burial conditions. The analytical data indicates that there is no increase in phosphate concentration either on the surface, or within the core of the Malkata, Amarna and Dakhleh Oasis sherds analysed. There is a very slight increase on the surface of the three sherds from North Karnak, however, this is explained by the surface burnishing of the pottery vessels and this slight difference is within experimental error. Thus, the phosphate, when observed, is not derived from groundwater. When in significant concentration, as indicated in Figures 5.44 to 5.47 it is derived from bone ash.

Table 5.13. SEM-EDS analyses of the average concentration of elements on the outer surface of pottery sherds recovered at Amarna.

	Na2O	MgO	Al2O3	SiO2	P2O5	SO3	Cl	K2O	CaO	TiO2	MnO	FeO	CoO	NiO	CuO	ZnO	BaO	PbO	SnO2	Sb2O3	Cr2O3	F
O Edge																						
Amarna A1	2	3.3	17.5	56.4	1.4	0.5	0.4	2.2	5.2	1.9	tr	9.1	0	0	0.3	0	0	0	0	0	0	0
Amarna A2	3.4	4.1	17.2	48.8	1.9	1.5	0.6	3.5	6.9	1.6	0.2	10.2	0	0	0.3	0	0	0	0	0	0	0
Amarna A3	6	3.5	18.1	43.7	1.9	0.6	2.8	2.7	6.9	1.7	0.2	11.5	0	0	0.3	0	0	0	0	0	0	0
Amarna A4	3.1	4	18.9	47.8	1.9	1.3	0.8	3.6	7.4	1.8	0.1	10.3	0	0	0.3	0	0	0	0	0	0	0
Amarna A5	3	4.4	9.2	12.2	0.4	35.3	2.6	0.9	27.2	0.9	0.6	1.9	0	0	0.4	0	0	0	0	0	0	0
Amarna A7	1.8	3.6	17	55.8	0.6	0.5	0.5	2.6	3.4	1.7	0.3	11.2	0	0	0.5	0	0	0	0	0	0	0
Average	**3.2**	**3.8**	**16.3**	**44.2**	**1.4**	**6.6**	**1.3**	**2.6**	**9.5**	**1.6**	**0.2**	**9**	**0**	**0**	**0.4**	**0**	**0**	**0**	**0**	**0**	**0**	**0**

Table 5.14. SEM-EDS analyses of the average concentration of elements within the core of the pottery sherds from Amarna.

	Na2O	MgO	Al2O3	SiO2	P2O5	SO3	Cl	K2O	CaO	TiO2	MnO	FeO	CoO	NiO	CuO	ZnO	BaO	PbO	SnO2	Sb2O3	Cr2O3	F
Core																						
Amarna A1	2.7	2.8	17.4	63.2	1.2	0.8	0.7	2.2	6.9	2.1	0.2	9.6	0	0	0.3	0	0	0	0	0	0	0
Amarna A2	4.2	3.3	16.2	44.3	3.9	2	1.3	2.7	12	1.2	tr	8.4	0	0	0.5	0	0	0	0	0	0	0
Amarna A3	1.3	2	18	68.6	0.1	0.2	0.2	4.2	1	0.6		3.6	0	0	0.2	0	0	0	0	0	0	0
Amarna A4	2.6	3.5	20.9	52.3	0.9	0.4	0.4	2.6	4	1.9	0.1	10	0	0	0.2	0	0	0	0	0	0	0
Amarna A5	1.9	3	16.7	51.9	1.5	1.4	0.9	3.2	5.3	1.5	tr	12.1	0	0	0.3	0	0	0	0	0	0	0
Amarna A7	1.7	3	16.6	56.8	0.5	0.5	0.5	2.2	4.5	2.2	0.3	10.9	0	0	0.1	0.3	0	0	0	0	0	0
Average	**2.4**	**2.9**	**17.6**	**56.2**	**1.4**	**0.9**	**0.7**	**2.9**	**5.6**	**1.6**	**0.1**	**9.1**	**0**	**0**	**0.3**	**0**	**0**	**0**	**0**	**0**	**0**	**0**

Table 5.15.   SEM-EDS analyses of the average concentration of elements on the outer surface and from within the core of the pottery sherds from North Karnak.

	Na2O	MgO	Al2O3	SiO2	P2O5	SO3	Cl	K2O	CaO	TiO2	MnO	FeO	CoO	NiO	CuO	ZnO	BaO	PbO	SnO2	Sb2O3	Cr2O3	F
O Edge																						
North Karnak NK1cream	1.3	4.3	15.3	50.6	0.6	2.8	0.4	3.6	10.8	1.5	0.2	8.5	0	0	0	0	0	0	0	0	0	0
North Karnak NK2	1.4	2.8	14.5	58.8	1.4	0.4	0.1	3.5	3.7	1.6	tr	11.3	0	0.1	0.2	0	0	0	0	0	0	0
North Karnak NK3	1.3	2.4	13.3	58.4	1.8	0.4	0	2.2	4.1	2.3	0.3	12.1	0	0.5	0	0	0	0	0	0	0	0
Average	**1.3**	**3.2**	**14.4**	**56**	**1.3**	**1.2**	**0.2**	**3.1**	**6.2**	**1.8**	**0.2**	**10.6**	**0**	**0.2**	**0.1**	**0**	**0**	**0**	**0**	**0**	**0**	**0**
Core																						
North Karnak NK1	1.3	2.5	16.6	57.4	0.6	1	0.1	2.6	3.9	2.1	tr	11.3	0	0	0	0	0	0	0	0	0	0
North Karnak NK2	1.4	4.6	15.9	51.1	1.3	0.2	0.3	2.9	5.8	1.7	0.2	13.6	0	0	0.7	0.3	0	0	0	0	0	0
North Karnak NK3	1.6	2.1	18.3	52.8	0.8	0.4	o	3.8	4.4	1.4	0.2	12.7	0	tr	1	tr	0	0	0	0	0	0
Average	**1.4**	**3.1**	**16.9**	**53.7**	**0.9**	**0.5**	**0.1**	**3.1**	**4.7**	**1.7**	**0.1**	**12.5**	**0**	**0**	**0.6**	**0.1**	**0**	**0**	**0**	**0**	**0**	**0**

Table 5.16. SEM-EDS analyses of the average concentration of elements on the outer surface of pottery sherds recovered at Malkata.

	Na2O	MgO	Al2O3	SiO2	P2O5	SO3	Cl	K2O	CaO	TiO2	MnO	FeO	CoO	NiO	CuO	ZnO	BaO	PbO	SnO2	Sb2O3	Cr2O3	F
O Edge																						
Malkata M1	0.3	3.4	15.5	48.5	0.6	0.4	0	1.2	16.9	1	0.2	9.3	0	0	0.6	0	0	0	0	0	0	0
Malkata M2	0.7	2.2	13.6	41.7	0.3	0.4	0	2	25.4	1.1	0.2	9.9	0	0.4	1	0.2	0	0	0	0	0	0
Malkata M4	2.1	4.7	17.3	46	0	2.5	0.3	2.8	13.1	1.4	0	7.6	0	0	1.2	0	0	0	0	0	0	0
Malkata M5	1.9	3.1	18.5	54.3	0.9	0.5	0	3.3	5.2	1.8	0.4	10.1	0	0	0	0	0	0	0	0	0	0
Malkata M6	1.7	3.6	15.7	54.3	1	0.9	0.2	2.4	5.3	1.5	0.4	11.5	0.1	0.1	0.7	0.6	0	0	0	0	0	0
Malkata M7	0.4	3.6	14.2	52.5	0	0.5	0.3	1.4	18.9	0.9	0.1	7	0	0	0.8	0	0	0	0	0	0	0
Malkata M8_cm	1.8	3.8	12.7	41.6	1.7	1.5	0.3	3.1	23.1	1.3	0.5	8	0	0	0.2	0	0	0	0	0	0	0
Malkata M10_cm	1	3.1	14.8	40.8	0.7	1.7	tr	2.2	22.8	0.9	tr	9.2	0	0	1.8	0.2	0	0	0	0	0	0
Malkata M11_cm	2	4.9	18.2	44.4	tr	0.3	0.3	0.5	18.3	1.5	0	8.6	0.3	0.3	0.3	0.7	0	0	0	0	0	0
Malkata M12	2.4	3	15.6	49.8	0.9	1.4	0.5	3	5.7	1.9	0.2	14.2	0.3	0	1.1	0.1	0	0	0	0	0	0
Malkata M14	1.2	4.7	13.6	42.3	1.6	4.5	1.8	1.4	17.2	0.3	7.5	7.5	0.5	0.1	0.1	1.1	0	0	0	0	0	0
Average	**1.4**	**3.6**	**15.4**	**46.9**	**0.7**	**1.3**	**0.3**	**2.1**	**15.6**	**1.2**	**0.9**	**9.4**	**0.1**	**0.1**	**0.7**	**0.3**	**0**	**0**	**0**	**0**	**0**	**0**

Table 5.17. SEM-EDS analyses of the average concentration of elements within the core of the pottery sherds from Malkata.

	Na2O	MgO	Al2O3	SiO2	P2O5	SO3	Cl	K2O	CaO	TiO2	MnO	FeO	CoO	NiO	CuO	ZnO	BaO	PbO	SnO2	Sb2O3	Cr2O3	F
Core																						
Malkata M1	2	2.6	13	44.3	0	1.1	0	1.5	22.8	0.8	0.2	7.2	0	0	0.8	0.2	0	0	0	0	0	0
Malkata M2	0.8	3.2	14.1	44.1	0.4	0.2	0	1.3	22.6	1.4	0.1	8.9	0	0	0.5	0.3	0	0	0	0	0	0
Malkata M4	1.7	3.7	15.1	44.7	0.6	2.7	0.3	1.8	18.3	1.4	0	8.7	0	0	0.9	0	0	0	0	0	0	0
Malkata M5	1.8	2.9	19.6	48.2	0.7	0.8	0.6	2	6	1.7	0.6	12	0	0	1.2	0	0	0	0	0	0	0
Malkata M6	1.8	3.4	15	53.6	1.7	0.5	0.2	2.8	7.1	1.6	0.1	11.6	0	tr	0.5	tr	0	0	0	0	0	0
Malkata M7	0.6	3.9	14.7	47.3	0	0.4	0.2	1.4	22.8	0.9	0.1	6.7	0	0.2	1	0	0	0	0	0	0	0
Malkata M8	0.8	4.8	11.4	44.7	0.6	0.4	0.3	1.6	19.7	5.2	0.3	9.9	0	0	0.3	0	0	0	0	0	0	0
Malkata M10	0.6	3.6	12.7	56.2	0.2	0.4	0.1	1.4	17.2	0.7	0.2	5.5	0	0	0.7	0	0	0	0	0	0	0
Malkata M11	0.9	3.8	14.8	49.2	0.7	0.8	0.4	1.4	19.8	0.8	0.1	7	0	tr	0.3	tr	0	0	0	0	0	0
Malkata M14	1.3	4.1	11.8	45	0.8	0.8	0.7	1.8	24.4	1	0.1	7.7	0	0	0.6	0	0	0	0	0	0	0
Average	**1.1**	**3.3**	**12.9**	**43.4**	**0.5**	**0.7**	**0.3**	**1.5**	**16.5**	**1.4**	**0.2**	**7.7**	**0**	**tr**	**0.6**	**tr**	**0**	**0**	**0**	**0**	**0**	**0**

Table 5.18. SEM-EDS analyses of the average concentration of elements on the outer surface of pottery sherds recovered at Mut al Kharab and from Dakhleh Oasis.

	Na2O	MgO	Al2O3	SiO2	P2O5	SO3	Cl	K2O	CaO	TiO2	MnO	FeO	CoO	NiO	CuO	ZnO	BaO	PbO	SnO2	Sb2O3	Cr2O3	F
O Edge																						
Mut D7	2.2	4.8	14.9	33.7	1.8	2.1	0.3	2.4	30.6	0.8	0	6.1	0	0	0.3	0	0	0	0	0	0	0
Dakhleh D3	1.2	1.2	16.5	45.6	0.4	14.7	0.7	1.2	11.7	2	0	4.7	0	0.4	0	0	0	0	0	0	0	0
Dakhleh D4	1.7	2.4	22.3	61.5	0.2	0.6	0.3	2.3	1.5	1.4	0	4.9	0	0	0.9	0	0	0	0	0	0	0
Dakhleh D5_cm	1	1.9	28.5	50.5	0.2	1.7	0.6	1.5	2.8	1.5	0.5	8.6	0	0	0.9	0	0	0	0	0	0	0
Average	**1.3**	**1.8**	**22.4**	**52.7**	**0.3**	**5.7**	**0.5**	**1.7**	**5.3**	**1.6**	**0.2**	**6.1**	**0**	**0.1**	**0.6**	**0**	**0**	**0**	**0**	**0**	**0**	**0**

Table 5.19. SEM-EDS analyses of the average concentration of elements within the core of the pottery sherds from Mut al Kharab and from Dakhleh Oasis.

	Na2O	MgO	Al2O3	SiO2	P2O5	SO3	Cl	K2O	CaO	TiO2	MnO	FeO	CoO	NiO	CuO	ZnO	BaO	PbO	SnO2	Sb2O3	Cr2O3	F
Core																						
Mut D7	1.7	2.5	15.7	35.6	0.8	17.7	tr	1.7	16.5	0.8	0.2	6.1	0	0	0.6	0	0	0	0	0	0	0
Mut D8	0.9	3.1	20.2	55.3	0.3	0.9	0.6	2.4	7.2	1	0.2	6.9	0	0	0.8	0	0	0	0	0	0	0
Dakhleh_D1	1.2	1.4	28.9	56.9	0.2	0.5	0.6	1.3	1.7	1.8	0	4.7	0	0	0.5	0	0	0	0	0	0	0
Dakhleh_D2	0.5	1.7	24.2	60.6	0.9	1.1	0.4	1.9	1.9	1.2	0	5.5	0	0	0.4	0	0	0	0	0	0	0
Dakhleh_D3	0.5	1.1	24.1	62.6	0.3	1.2	0	1.5	1.2	2.3	0	4.5	0	0	0.7	0	0	0	0	0	0	0
Dakhleh_D4	1.8	2.5	21	62.9	0.3	0.6	0.3	2	2.1	1.3	0	4.4	0	0	0.7		0	0	0	0	0	0
Dakhleh_D5	0.7	2	20.8	59.7	0.3	2.9	0.2	1.7	4.5	1.2	0.2	5.3	0	0	0.9	0	0	0	0	0	0	0
Dakhleh D6	1.1	3.9	21.7	55.8	0.5	1.1	0.9	2.1	5.1	1	0	7.6	0	0	0.3	0	0	0	0	0	0	0
Average	**1**	**2.1**	**23.5**	**59.8**	**0.4**	**1.2**	**0.4**	**1.8**	**2.8**	**1.5**	**tr**	**5.3**	**0**	**0**	**0.6**	**0**	**0**	**0**	**0**	**0**	**0**	**0**

5.4.2.7.3 Phosphorus in urine

As reported in several of the sherds examined and, as shown from the elemental mapping of Malkata sherd M3, the phosphate is either in discre4te particles, or is sufficiently spread and apparently in close association with either aluminium or iron, indicative of it having been produced during its high temperature preparation rather than from burial, This is suggested from the Magellan 400 XHR FEGSEM electron microscope elemental maps provided in Appendix A5.M3 for this Malkata sherd.   The aluminium-phosphate association is evident and is spread over a finite area. A hypothesis is advanced within this thesis in Section 5.8 that urine was used to break the aluminate gel formed during the MHP process. Urine can contain significant phosphorus, and is therefore an additional potential source for phosphates.

This is supported from a NASA sponsored project, in which Putnam (1971) reported that in a study of 20 to 30 male subjects, the total dissolved solids (TDS) in their urine ranged from 24.8 g/kg to 37.1 g/kg. Of this, typical analyses indicated that the total inorganic salts comprised 14,157 mg/l of which NaCl represented 8000 mg/l, potassium chloride 1641 mg/l, potassium sulphate 2632 mg/l, magnesium sulphate and carbonate 926 mg/l, potassium phosphate 234 mg/l and calcium phosphate 62 mg/l. Urea represented an additional 13,400 mg/l with the balance being minor organic compounds.

Thus, if the MHP method was adopted, it is conceivable that some phosphate could have entered the cobalt precipitate by this method. Firing of the cobalt precipitate with silica containing some feldspar and alkali flux to make the glassy pigment would have provided an opportunity for some minor aluminium or other phosphate to form.

5.4.2.7.3 Phosphate in bone (hydroxyapatite)

As discussed in more detail in Chapter 4, Section 4.5.2.6.2 Chen and Miao (2005) studied the thermal treatment of hydroxyapatite and fluoroapatite [$Ca_{10}(PO_4)_6(OH)_{2-2x}F_{2x}$] and observed that the fluorinated product can increase its crystallinity and the strong ionic bonding within the crystal structures leads to increased density, and chemical and thermal stability.   This loss of visible structure is indicated in Figure 5.43 below and explains the failure to observe visible structure in Figures 5.44 to 5.46.
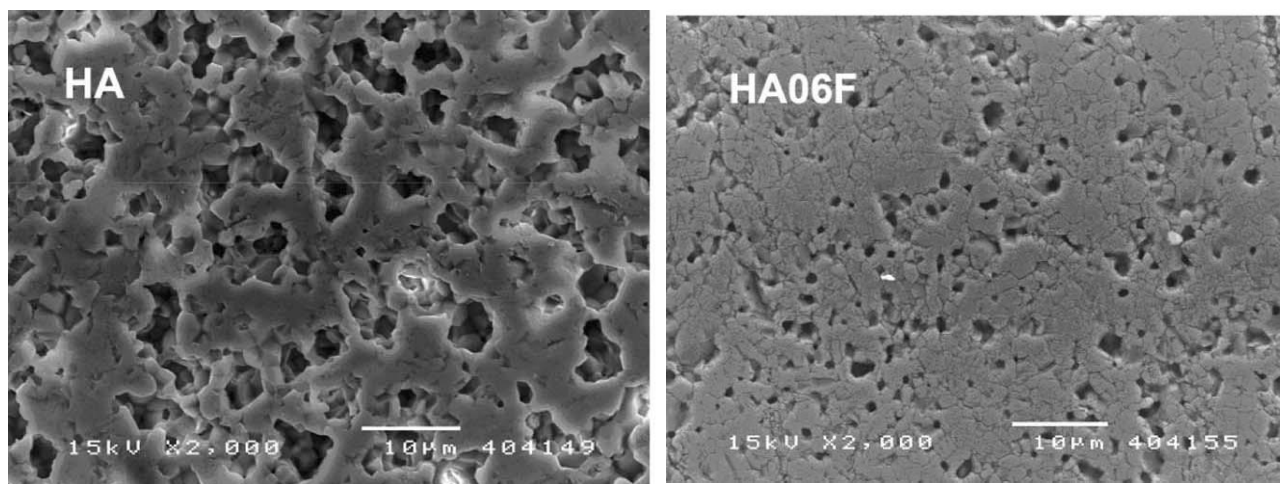
Figure 5.43. Surface morphologies of hydroxyapatite and fluoro-hydroxyapatite in which the F content was x = 0.6 in the above formula. Following sintering at 1300°C then polishing and etching for 10 minutes in a 2.5% solution of citric acid the above images were obtained. The scale bar is 10 μm. They clearly indicate the densification and loss of skeletal structure in fluoroapatite (Chen and Miao 2005).

When hydroxyapatite or fluoro-apatite are heated in air in the presence of aluminium oxide, as would potentially be the case in the production of cobalt aluminate blue, the aluminium-hydroxyapatite composites will decompose to tricalcium phosphate and the calcium oxide released. It would then be able to form various calcium aluminates including the spinel, $CaAl_2O_4$, at 1100°C and $CaAl_4O_7$ at 1200°C. As reported by Adolfsson *et al*. (1999) if the hydroxyapatite was intermixed with aluminium oxide, the reaction was initiated at 900°C and continues below 1000°C, significantly below that of the hydroxyapatite itself. These workers also reported that increased thermal stability was obtained by replacing some of the OH⁻ ions by F⁻ ions. Furthermore, they reported that the reaction with the oxide will not commence until sufficient vacancies created by the removal of water from the structure occurs. Thus, according to a reaction similar to that conducted at 800°C and which is discussed in Chapter 4, Section 4.5.2.6.2, the reaction will move to the right with increasing temperature; but if some of the OH⁻ is replaced by F⁻ the number of vacancies created by water leaving the structure is reduced. Thus, compounds with a lower concentration of F⁻ can sustain a larger number of vacancies before the reaction with aluminium oxide is initiated and therefore, the following reaction will not occur until a specific fraction of vacancies have been formed:

$$Ca_5(PO_4)_3(OH)_{1-x}O_{0.5x} + Al_2O_3 \rightarrow 3Ca_3(PO_4)_2 + CaAl_2O_4 + (1-x)H_2O$$
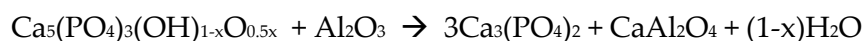
The phase diagram for the calcium phosphate at high temperature has been studied by Trömel (1943), Welch and Gutt (1961) and by Newesely (1977). Newesely (1977) confirmed at temperatures above 1000°C hydroxyapatites are not stable with the breakdown change not being a simple and homogeneous reaction, the reaction being strongly dependent on secondary conditions present during the formation of these crystals. The breakdown in releasing Ca^{2+} creates lattice imperfections or residual colloidal apatite adsorbed. Alternatively, fluoro-apatite is confirmed by Newesely to be thermally more stable than hydroxyapatite only losing fluorine slowly and can remain stable in temperatures as high as 1500°C.

The chemical conditions under which bone apatite can recrystallise into authigenic apatite are restricted within a narrow alkaline pH range. Thus, a small shift in pH of the environment determines bone preservation. And, as discussed by Berna *et al*. (2004), bone is best preserved only in sediments in which the pH of the pore solution is above 8.1, particularly those saturated with calcite. Thus, these workers identified a window between 7.6 and 8.1 which defines the conditions under which bone crystals dissolve and reprecipitate as a more insoluble form of carbonated hydroxyl apatite. When the pH of the sediment is below 7, fresh or recrystallised bone will rapidly dissolve.

In a study into the diffusion of phosphorus in a CaO-SiO_2-FeO_x slag, Wang *et al*. (2011) showed that due to the basicity of the slag, the phosphorus is concentrated in the dicalcium silicate and tricalcium phosphate phase and less in the glass phase. The reaction profile observed was one in which the phosphorus was concentrated from the surface of the $2CaO.SiO_2$ particles and then by diffusion into the core. Higher temperatures favour this diffusion process and for particles $<50\mu m$ in size, the reaction was completed within 300 seconds.

In the sherds examined, the low soda analyses would suggest the use of a "plant ash" or biomass-type ash rather than trona or other alkaline source as the flux. Some caution is extended in referring to the Na_2O/K_2O ratio quoted in Table 5.20 as surface deposition of sodium chloride has been regularly observed in many of the samples examined. This would bias the sodium elemental analysis reported. Thus, only limited reliance should be placed on this observation.

Table 5.20. Phosphate percentages obtained from large area SEM-EDS analyses.

Sample	Phosphate P_2O_5 Wt. %	CaO Wt.%	MgO Wt.%	Na_2O Wt.%	K_2O Wt.%	Ratio Na_2O/K_2O
A1	1.2	18.7	4.0	4.2	1.9	2.2
A2	1.5	16.2	4.8	3.0	1.4	2.1
A3	2.0	17.4	3.1	5.6	1.8	3.1
A4	0.9	18.8	4.2	0.9	0.8	1.1
A5	0.0	26.2	2.8	3.9	0.7	5.6
A6	0.6	9.3	4.0	2.1	1.0	2.1
A7	0.3	6.6	4.6	1.0	2.3	0.4
A8	0.4	20.3	2.2	1.1	1.5	0.7
M3	0.8	11.9	3.2	3.5	1.3	2.7
M5	1.9	17.8	6.4	1.6	1.0	1.6
M6	1.4	7.2	6.0	1.7	1.0	1.7
M9	1.2	5.1	4.4	1.5	1.0	1.5
M12	0.4	20.1	3.4	1.1	1.6	0.7
M13	0.7	26.4	6.5	1.1	1.0	1.1
M14	0.2	6.6	3.3	2.1	1.1	1.9
M15	0.3	9.7	5.1	1.6	3.4	0.5
M16	0.9	11.2	4.0	1.4	2.3	0.6
D7	1.4	6.2	4.4	2.1	2.3	0.9
NK1	0.4	3.2	4.0	1.3	5.6	0.2
NK2	0.2	7.7	4.8	0.8	1.1	0.7
NK3	0.9	6.3	2.9	1.1	2.7	0.4
R1	3.0	11.7	4.4	2.9	1.9	1.5
R2	0.6	7.2	5.3	3.5	1.2	2.9
DE1	0.1	15.2	3.1	8.9	2.1	4.2
DM1	0.5	11.8	2.5	1.2	0.9	1.3
S1	0.3	4.0	4.6	0.7	2.7	0.3

5.4.3. Hydroxyapatite (calcium phosphate) or bone ash mineralisation

The presence of the phosphate mineral hydroxyapatite, is clearly visible in Figure 5.44 within the cobalt blue pigment applied to the sherd sample D7 found at Mut al-Kharab. Its SEM analysis is provided in Table 5.7 and in the table accompanying Figure 5.44. This analysis indicates the presence of a bone ash structure containing 20.8% P_2O_5, 31.5% CaO and 1.2% F in an alumina-silicate-based mineralisation. As previously stated, fluorine is considered to be diagnostic for hydroxyapatite (bone ash).

Nicholson has shown that a kiln at site O45.1 at Amana and also kiln HAC3 at Kom Helul when excavated contained bone fragments (Nicholson 2007: 127; Nicholson 2013: 75). Bone ash (hydroxyapatite) has also been detected in several samples of Egyptian blue from

Amarna and in cobalt pigments applied to pottery from Amarna and Mut al-Kharab. Anomalous phosphorus (2% P_2O_5) was detected in Malkata sherds as provided in Table 5.20.

.
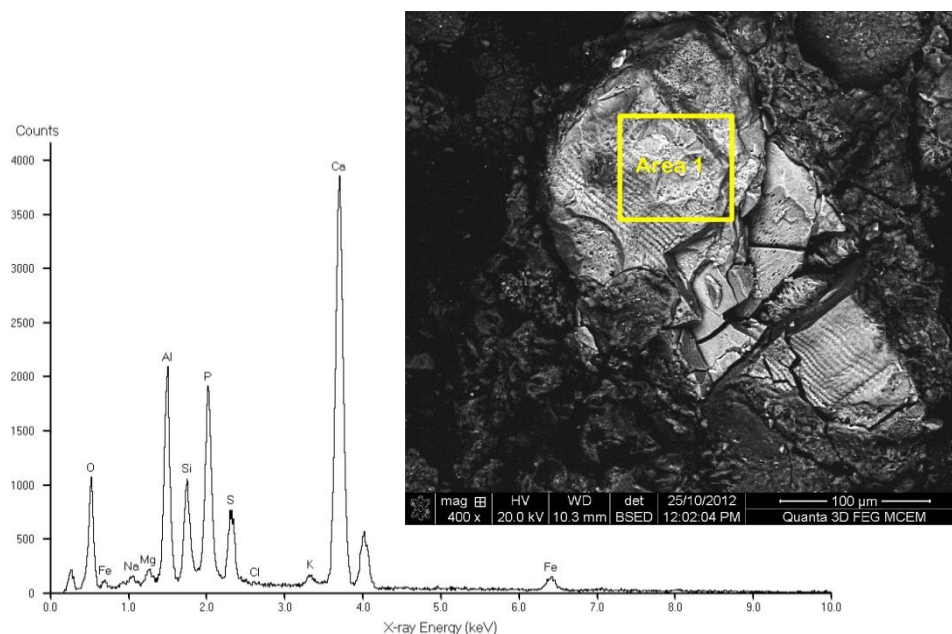
Figure 5.44. FIB-EDS spectrum and the BSE image for the analysis of Area 1 in Mut al Kharab sherd D7 (MUT 1). This sherd is discussed in more detail in Appendix A5, Figure A5.D7. Note the zoning within particle and the presence of fluorine. The presence of high alumina and high silica in this particle is further evidence for this hydroxyapatite ash particle is a high temperature reaction product formed within a kiln or cooking oven.

Elemental analysis, bone ash Mut al Kharab sherd D7 (MUT 1)

Elemental analysis, Blue, FIB-EDS Area1 analysis, Figure 5.44 (Figure A5.D7.9)*.

Na_2O	MgO	Al_2O_3	SiO_2	P_2O_5	SO_3	Cl	K_2O	CaO	TiO_2	MnO	FeO	CoO	NiO	CuO	ZnO
1.8	2.2	17.9	9.7	20.8	9.0	0.5	1.0	31.5	0.4	0.3	2.6	0.3	0.0	0.7	0.0

*+F = 1.2%

As proposed by Lucas and Harris (1962: 187) and by Lilyquist and Brill (1993: 41), the sand at Amarna when combined with natron produces a glass containing 15-20% Na_2O. The high potash concentration in this glass was considered by Lucas and Harris to result from contamination of the frit by fuel ash. Caley (1962: 81) however suggested that the ash from the fuel employed to melt the glass was often incorporated as one of the glass-making raw materials. Such an inclusion would provide the opportunity for phosphorus to be incorporated into the glass. Thus, as discussed in Section 5.4.2.7, it is feasible that the fuel ash or kiln ash containing calcined bone material, was used as part, or all of the alkali flux in the production of the cobalt blue pigment. To date, no site has been located which is considered to have been dedicated to the production, that is, preparation of plant ash or its storage (Nicholson 2007: 121). Furthermore, the bone material, confirmed by the fluorine analysis and shown in Figure 5.44 would suggest that kiln ash was therefore one probable

source for the flux. Analysis of a sample of plant ash from Dakhleh oasis is provided in Section 5.4.2.2.1 and Table 5.12
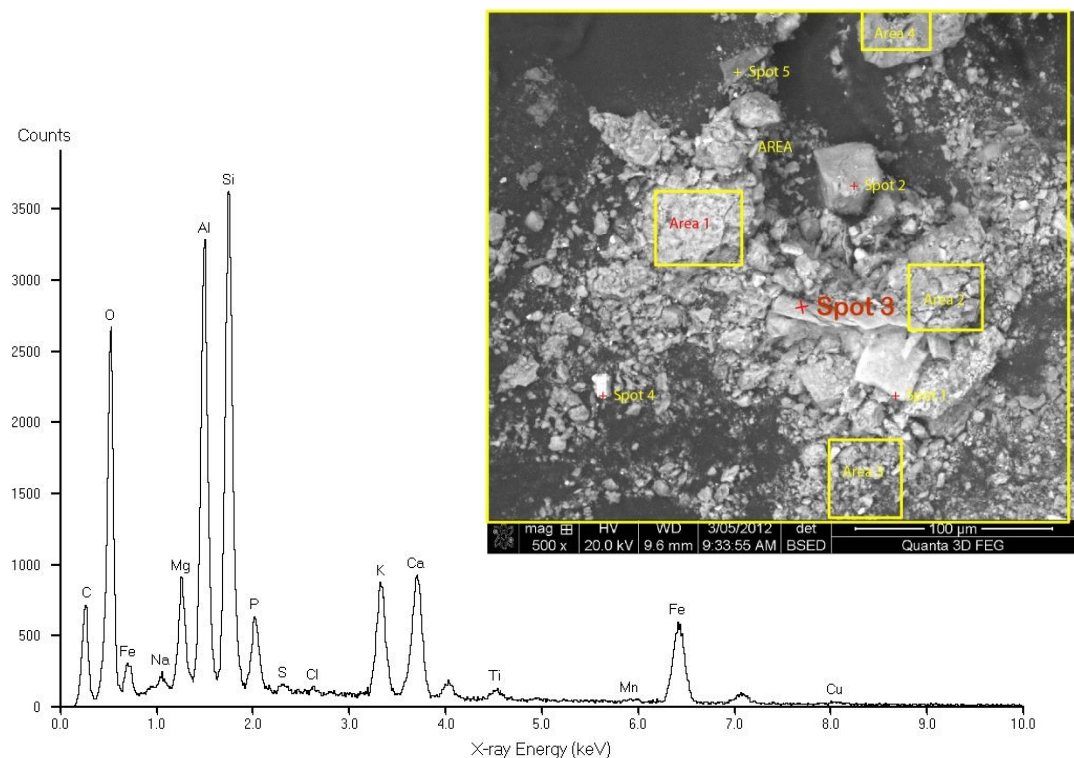
Figure 5.45. FIB SEM-EDS spectrum and BSE image for the analysis of Spot 3 in North Karnak sherd NK3. Refer also to Appendix A5, Figure A5.NK3.1. Significant phosphorus is evident in this sample.

Elemental analysis, Blue region, FIB-BSE Spot analyses Figure 5.45 (Figure A5.NK3.1)														
Na$_2$O	MgO	Al$_2$O$_3$	SiO$_2$	P$_2$O$_5$	SO$_3$	Cl	K$_2$O	CaO	TiO$_2$	MnO	FeO	CoO	NiO	CuO	ZnO
0.9	6.2	23.8	33.6	6.1	0.4	0.1	5.7	8.0	1.1	0.5	12.8	0.0	0.0	0.8	0.0
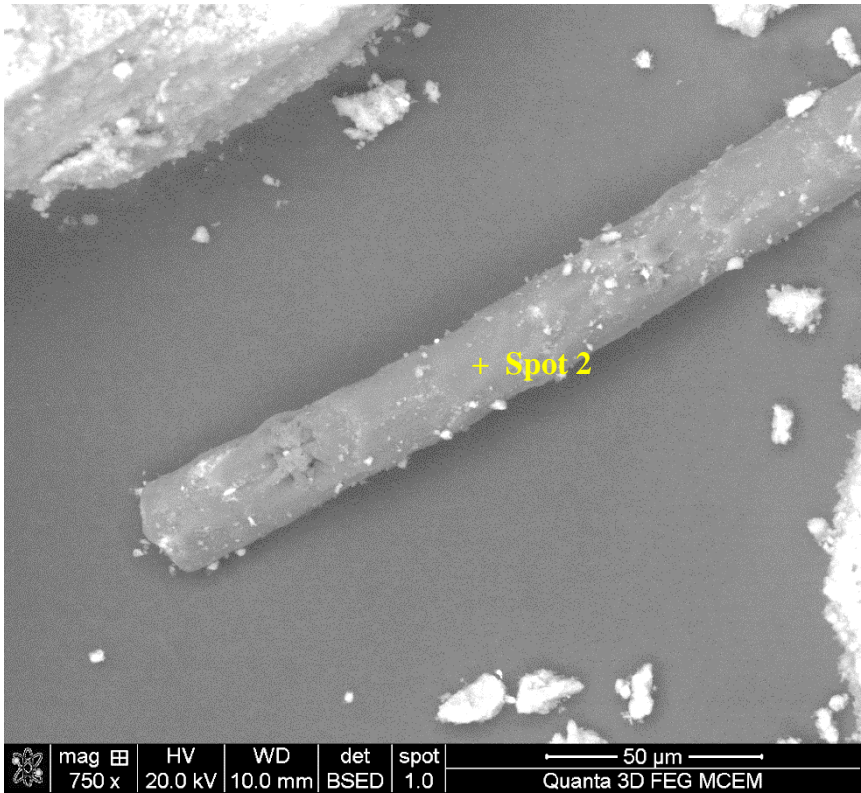
Figure 5.46. FIB BSE image of unusual rod-like particle of hydroxyapatite, being Spot 2 in Memphis sample R1 and discussed in Appendix A5 Figure A5.R1.1. The elemental analysis is provided in the accompanying table. Another spot analysis also contains anomalous phosphorus. This particle could not have been derived from the ashing of plant matter. However, it should be noted that Table 5.11 indicates that some plant material in Egypt does contain appreciable phosphorus.

Elemental analysis, Memphis sample R1

Na$_2$O	MgO	Al$_2$O$_3$	SiO$_2$	P$_2$O$_5$	SO$_3$	Cl	K$_2$O	CaO	TiO$_2$	MnO	FeO	CoO	NiO	CuO	ZnO
Elemental analysis, Blue, FIB-EDS Spot 1 analysis, Figure A5.R1.1*.															
0.0	3.9	26.4	15.8	2.4	5.3	0.0	1.0	3.7	0.0	0.5	1.9	0.6	0.7	0.5	1.7
Elemental analysis, Blue, FIB-EDS Spot 2 analysis, Figure A5.R1.1 and Figure 5.46 (Figure A5.R1.5)															
0.0	4.6	28.0	37.5	4.1	1.3	0.0	1.6	8.3	0.9	0.0	4.4	2.0	2.0	2.1	3.4
*+BaO = 35.6%															
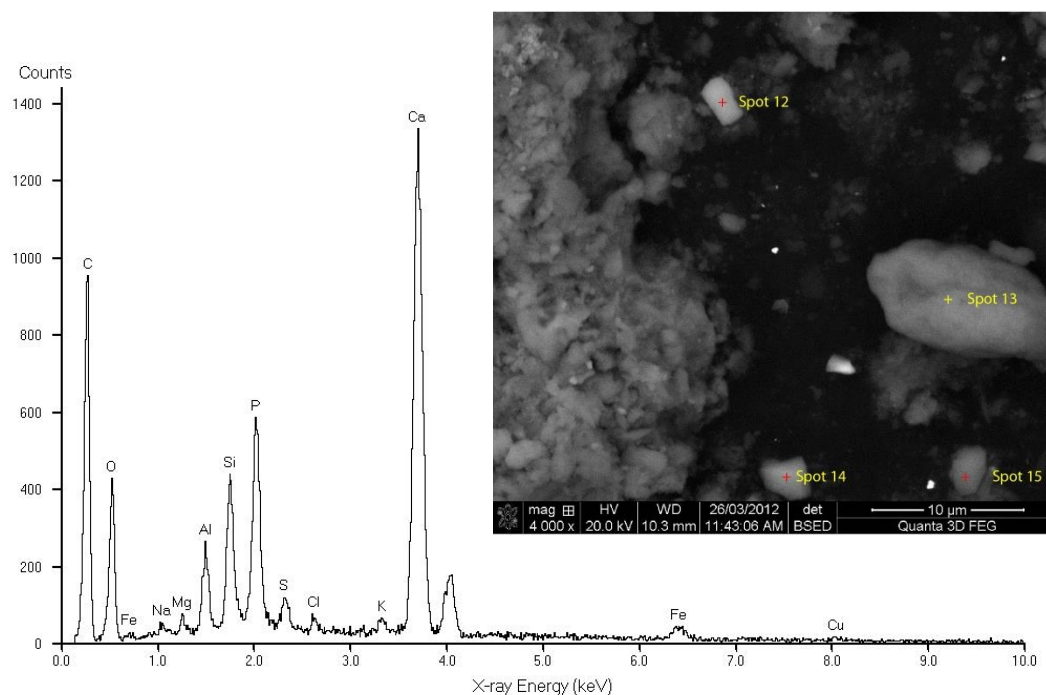
Figure 5.47. FIB SEM-EDS spectrum and BSE image for the analysis of Spot 14 in Amarna A3, a particle high in phosphorus, refer also Appendix A5, Figure A5.A3.15.

Elemental analysis Amarna sherd A3

Elemental analysis, Blue, FIB-EDS Spot 14 analysis, Figure 5.47 (Figure A5.A3.15).

Na$_2$O	MgO	Al$_2$O$_3$	SiO$_2$	P$_2$O$_5$	SO$_3$	Cl	K$_2$O	CaO	TiO$_2$	MnO	FeO	CoO	NiO	CuO	ZnO
1.0	1.2	6.2	13.1	22.4	3.9	0.7	1.0	45.3	0.0	0.0	3.6	0.0	0.0	1.7	0.0
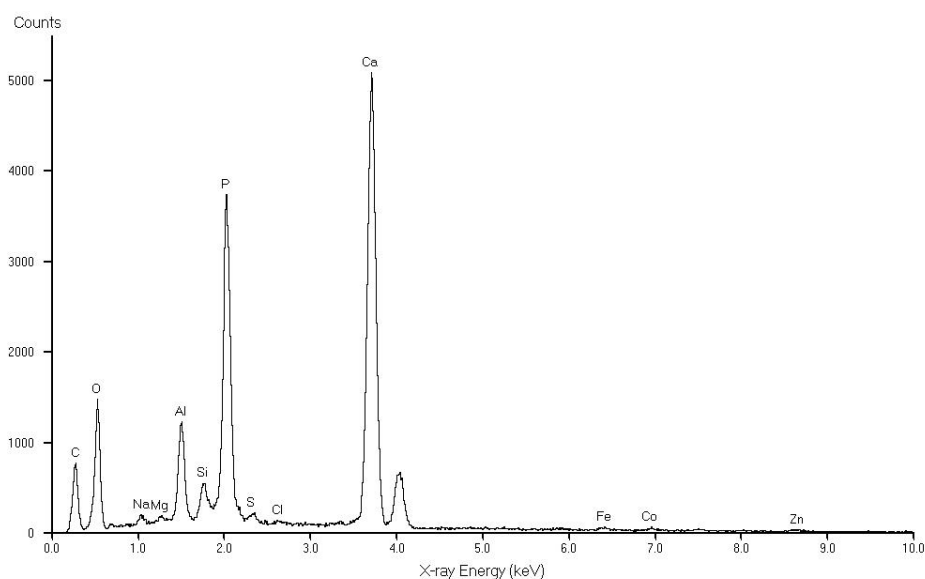
Figure 5.48. FIB SEM-EDS spectrum for the analysis of Spot 4 in Deir al-Medineh sherd DM1 as further discussed in Appendix A5, Figure A5.DM1.1, the analysis of the Spot is provided in the accompanying table.

Elemental analysis, high phosphorus analysis of a particle in Deir al-Medineh sherd DM1.

Elemental analysis, Blue, FIB-EDS Spot 4 analysis, Figure A5.DM1.1

Na$_2$O	MgO	Al$_2$O$_3$	SiO$_2$	P$_2$O$_5$	SO$_3$	Cl	K$_2$O	CaO	TiO$_2$	MnO	FeO	CoO	NiO	CuO	ZnO
1.5	1.4	9.3	9.3	33.2	1.9	0.3	0.0	45.8	0.0	0.0	0.6	0.5	0.0	0.0	1.0

5.4.3.1 Adsorbent particles, possibly bone ash with surface adsorption
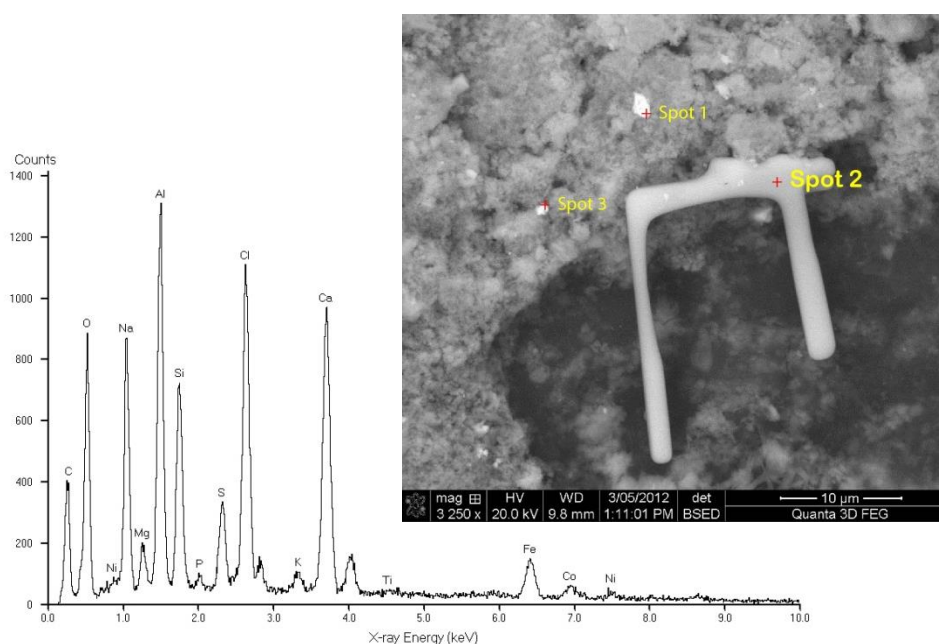
Figure 5.49. FIB-EDS spectrum and the BSE image of an adsorbent material, possibly phosphate as identified by the anomalous phosphorus analysis in Amarna sherd A4 and which is heavily encrusted with sodium chloride. The marked spots are all crystals of sodium chloride.   FIB SEM-EDS spectrum for the analysis of Spot 2 is provided in Figure 5.49 and in Appendix A5, Figure A5.A4.5 is provided in the accompanying table.

Elemental analysis, Amarna sherd A4.

Other particles were analysed in which the surface encrustation was gypsum. Refer Appendix A5, Amarna A4

Na$_2$O	MgO	Al$_2$O$_3$	SiO$_2$	P$_2$O$_5$	SO$_3$	Cl	K$_2$O	CaO	TiO$_2$	MnO	FeO	CoO	NiO	CuO	ZnO
Elemental analysis, Blue, FIB-EDS Spot 1 analysis, Figure A5.A4.5.															
10.9	3.2	21.2	10.8	1.6	6.5	24.3	0.9	10.2	0.7	0.0	3.4	1.7	1.3	1.3	1.9
Elemental analysis, Blue, FIB-EDS Spot 2, analysis, Figure A5.A4.5															
14.0	2.7	22.8	13.2	0.7	6.2	10.5	0.9	16.7	0.3	0.6	5.7	2.0	1.4	0.8	1.5
Elemental analysis, Blue, FIB-EDS Spot 3, analysis, Figure A5.A4.5															
7.5	2.7	22.9	26.1	0.6	10.6	6.7	0.7	15.2	0.0	0.0	4.8	0.8	0.4	0.2	0.7
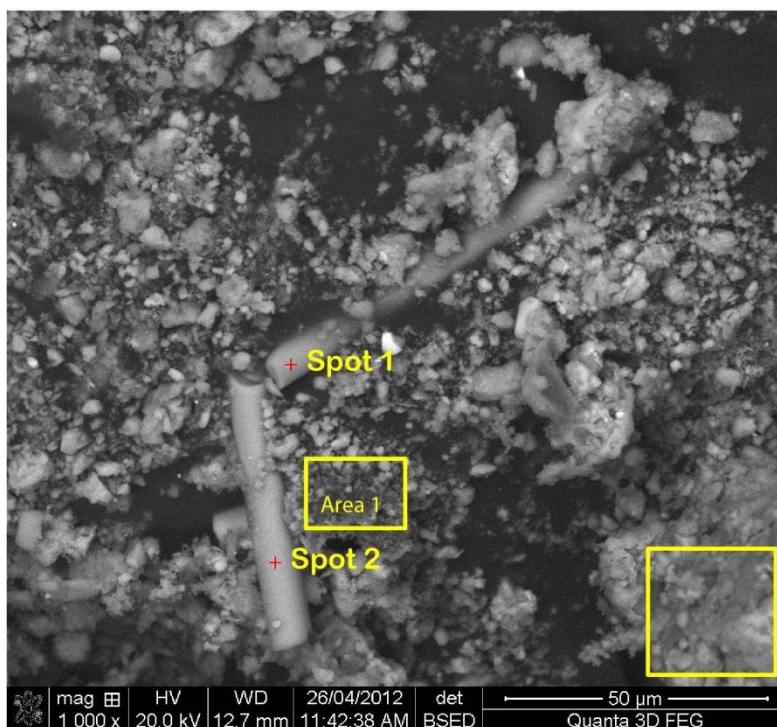
Figure 5.50. FIB BSE image, showing the Points of Interest analysed in Amarna sherd A8 as marked.

Elemental analysis particles within Amarna sherd A8

Na$_2$O	MgO	Al$_2$O$_3$	SiO$_2$	P$_2$O$_5$	SO$_3$	Cl	K$_2$O	CaO	TiO$_2$	MnO	FeO	CoO	NiO	CuO	ZnO
Elemental analysis, Blue, FIB-EDS Spot 1 analysis, Figure A5.A8.5.															
0.3	0.5	16.0	44.0	0.1	4.2	0.5	0.5	29.9	1.0	0.0	1.4	0.0	0.0	1.5	0.1
Elemental analysis, Blue, FIB-EDS Spot 2 analysis, Figure A5.A8.5.															
1.0	3.9	17.9	37.3	0.3	7.7	0.7	2.0	18.9	1.0	0.0	7.8	0.3	0.0	1.1	0.0

As provided in Appendix A5, the blue pigmented area in Amarna sherd A8 contains a cobalt pyroxene, spinel, Co-ZnAl$_2$O$_4$ and possibly bieberite, together with quartz, feldspar, wollastonite, anhydrite, ilmenite and rutile, and huntite.

A long, broken particle is shown in Figure 5.50 (Figure A5.A8.5) (Spots 1 and 2) of a sorbent material such as bone (hydroxyapatite) coated with either gypsum or calcite, (it is difficult to determine from the analysis); however Figures A5.A8.6 and A5.A8.7 indicate that there is a considerable percentage of elemental carbon present and the EDS analysis indicates that the SO$_3$ concentration is much lower than the CaO concentration potentially indicating that calcite could be the more likely mineral present. Such mineralisation would be anticipated to occur during burial of the sherd. Alternatively, if the particle was from a plant material, this would also provide a high carbon peak. And, as provided in Appendix A5, this could suppot the use of a plant-based ash as the alkali flux.

An organic compound is indicated by the Raman bands in Figure A5.A8.20 at wavenumbers 1441, 1615 and 1696 cm^{-1} which are indicative of either a wax or an egg protein material being used to fix the pigment to the substrate.

Figure 5.51.   Nova, BSE image showing the Points of Interest as marked, blue region within Dendera sherd DE 1. More of these long rod-like particles were observed spread widely over the entire blue pigmented region. Gypsum is both on the surface of these particles and crystals of gypsum were located. Again, the source of these particles is unknown, but it is likely to be from an organic source such as plant material.

Elemental analysis, Dendera sherd DE 1

Elemental analysis, Blue region, Spot analyses, Figure A5.DE1.1 (marked Dendera 2-7).

Na₂O	MgO	Al₂O₃	SiO₂	P₂O₅	SO₃	Cl	K₂O	CaO	TiO₂	MnO	FeO	CoO	NiO	CuO	ZnO
11.2	0.9	5.9	11.9	0.1	25.7	10.1	0.9	25.2	3.4	0.2	4.3	0.1	0.1	0.0	0.0
2.6	3.1	8.3	29.1	0.0	4.0	1.7	1.4	21.9	7.4	0.3	19.7	0.3	0.2	0.0	0.1
4.8	1.5	8.7	18.4	0.3	29.4	3.0	2.1	25.5	0.5	0.1	5.1	0.1	0.1	0.1	0.1
14.0	1.1	12.2	21.4	0.0	3.0	19.9	1.6	12.3	0.7	0.2	12.9	0.3	0.2	0.0	0.1
5.3	0.7	9.7	32.5	0.0	14.5	4.3	5.0	16.1	0.3	0.3	10.9	0.2	0.1	0.0	0.1
5.1	2.9	21.4	40.2	0.0	2.1	3.5	6.3	4.6	1.2	0.1	12.1	0.2	0.1	0.0	0.0
Average area analyses, blue region															
8.9	**3.1**	**17.7**	**25.6**	**0.1**	**9.9**	**7.2**	**2.1**	**15.2**	**0.9**	**0.5**	**7.2**	**0.7**	**0.5**	**0.0**	**0.5**

In summary, phosphorus can be introduced into the cobalt blue pigment from several sources. The phosphate which has been shown to be associated with aluminium can be attributed to adsorption from soils or from urine. Whereas, phosphorus, as calcium phosphate and particularly when containing fluorine, must indicate bone particles. In addition, it is likely that in the high temperature conversion of the MHP into the cobalt blue pigment was undertaken in vessels similar to those used for Egyptian blue production. Thus, the presence of gypsum and/or bone from the internal vessel lining would not be unexpected. This is an area for fruitful research, particularly within the Dakhleh Oasis.

5.4.4 Discussion with respect to cobalt mineralisation on sherds

The colouring performance of cobalt minerals is largely dependent on their excellent thermal stability, chemical reactivity towards glass and glaze components (silica-based mineralisation) and on the coordination of the Co^{2+} ions, the tetrahedral coordination being preferred to octahedral. de Waal (2004; 2009) has applied Raman spectroscopy to a range of ceramics and has demonstrated that the cobalt signature may be enhanced by focussing the microscope to below the actual mineral surface. However, when cobalt is dissolved and therefore in an ionic form, such as in a glass phase, it cannot provide a Raman signal because there is no consistent and well-defined Co-O distance because of the range of near neighbours perturbating it, so there is no single frequency vibration to detect. As will be seen, this fundamental condition is a limiting factor for the study of cobalt in glasses or glass-like structures by Raman spectroscopy.

Riederer (1974) examined the blue decoration on four vases using XRD and found all lines to support cobalt aluminate (Co-spinel) formation in amongst a considerable number of additional lines due to the presence of impurities, the balance of the spectrum was not reported. Importantly, he reported that copper, manganese, zinc and beryllium were present as trace elements. Furthermore, he postulated that aluminium hydrate may have been mixed with a cobalt mineral, applied to the vessel and then fired, forming the blue cobalt aluminate (a spinel) directly on the vessel surface. As reported by Shortland (2006a), the XRD spectra of spinels are all very similar making it difficult to separate various mineral forms. As will be shown below, the formation of cobalt aluminate was rarely detected in the 26 pigment samples analysed in this thesis. As previously discussed in Section 5.4.2.3, the presence of tridymite would negate such a direct firing of a cobalt hydroxide on to a pottery surface.

Cobalt spinel formation was also reported by Noll and Hangst (1975) and Noll (1981b) who disputed Riederer's earlier suggestion. These workers did not physically determine the presence of a cobalt spinel relying on the EDX elemental analysis for aluminium to propose the presence of the cobalt as an aluminate. Rather than a solid-state, direct firing of the pigment composition to form the colour on the vessel they proposed that the pigment must have been produced by precipitation from an aqueous alum solution of the cobalt salts contained therein, followed by pH adjustment using sodium or ammonium carbonate probably derived from natron or trona. The mixed hydroxide precipitate would then have been heated to between 800 and 1000°C to produce the Al-spinel. They also reported that a low cobalt concentration would facilitate the spinel formation; that the presence of chlorides accelerates the reaction and zinc stabilises the pigment.   Importantly, these researchers reported the presence of diopside in the body of the sherds examined and therefore this would indicate a firing temperature above 850°C if the cobalt pigment had been applied by pre-firing painting. Cobalt-zinc complexes are discussed in more detail in Appendix A5. Raman spectroscopy results provided in this thesis supports the Noll hypothesis, although, as shown, other cobalt compounds are also observed, probably from slight surface decomposition of the spinel and/or the cobalt-containing pyroxene.

Kaczmarczyk's analysis (1986 Table 34.3; reproduced herein in Table 5.2) of four samples of alum from the Mut al-Kharab region showed MgO varying from 6.0 – 8.5%, MnO 0.84 – 1.13%, Fe_2O_3 0.25 – 0.37%, CoO 0.31 – 0.43%, NiO 0.16 – 0.58%, ZnO 0.6 - 0.99% and in two samples 44.7% and 46.9% SO_3 was present. No silica was reported and therefore it is unclear if this mineral was found or ignored in the analyses. He supported the proposal of Noll that the cobalt and the associated oxides were precipitated from an aqueous solution by rendering the solution mildly alkaline using natron, plant ash or ammonia, leaving the sulphates behind. The precipitate was then dried and heated to produce the aluminates with a much higher transition element content in the pigment. As will be discussed in Section 5.8, this thesis supports such a hypothesis.

As discussed on page 5.44 and in Section 5.4.2.2, Bachmann *et al* (1980), tentatively proposed that he mineral form of the cobalt in the pigment was a spinel, although these researchers were unable to provide any firm evidence to support their hypothesis. They relied upon XRF to conduct the elemental analysis of one sherd and, it is evident from their published analysis that they were unable to detect the presence of any elements with Z< 13. Thus, they tentatively interpreted several cubic crystals to be a zinc-cobalt-nickel spinel of the general formula $(Zn,Co,Ni)Al_2O_4$. They then stated that these results were in conformity with the previous results published by Riederer(1974) in respect of Amarna sherds, and with Noll and Hangst (1975) particularly with regard to the cobalt/zinc ratio and the admixture of nickel. Unfortunately, they did not provide any analytical data to support this assertion. Nor did Bachmann and co-workers consider that the cobalt and the other transition elements could have been present in the form of a cobalt olivine or cobalt oxide ($Co^{2+}Co^{3+}_2O_4$), with a cubic spinel crystal structure (*Fd3m*) (Xu and Zeng 2003; Wang *et al*. 2009). They also ignored the likelihood for the aluminium to enter into chemical reactions with its nearest neighbours to form alumina, mullite, alumina-phosphate and related mineralisation.

Bachmann *et al*. (1980) considered that it would be possible that the cobalt blue could be fired "in situ" on to the vessel walls during its firing however, they agreed with Noll and Hangst (1975) and Hope (1977) that the pigment was prepared prior to its application to the vessel and suggested that the pigment may have been prepared by a solid state reaction between a cobalt-zinc ore and aluminium-based minerals (oxides, hydroxides, for example). Alternatively, they speculated that it could have been produced by direct calcination of the cobalt-containing alum (they incorrectly assumed it to be a potash alum) at above 800°C to transform the cobalt to its oxides and which would then simultaneously combine with alumina to form the blue cobalt spinel.

In discussing the method for the application of the cobalt pigment to the vessel, Bachmann *et al*. (1980) agreed with Hope (1977) that the pigment was applied before firing, noting that the cobalt blue pigment adheres as firmly to the pottery body as is achieved by the light and dark brown pigments (presuming that they were pre-fired on to the vessel). It should be noted that if the brown pigment was goethite, on firing it would convert to hematite, and change in colour to a bright red. Lucas stated that as far as he was aware, black was not introduced as a pigment before the 18th Dynasty, and then, it was applied after the firing of the pot. On the other hand, Hope (1977), based upon the suggestion of various potters,

disagreed with Lucas on the basis that if the pigment was applied after firing it would be very unstable and be easily rubbed off. The determination of egg or other binder was evidently not investigated or considered.

Carbon would not have been used as the black pigment as it would burn off. However, the XFM beamline synchrotron analyses provided in Figures 5.36 to 5.39 clearly indicate that the black lines are based upon iron and the Raman spectra provided in Appendix A5 and in selected spectra above has shown that the black pigment is the iron mineral, magnetite.

Shortland *et al*. (2006a) summarised the previously published data and again noted that the cobalt blue pigment was in the form of a cobalt spinel containing significant amounts of zinc and nickel and, that the pigment was applied over a thin slip containing gypsum. Eight sherds, four from Malkata and four from Amarna were sectioned and polished and examined by SEM-EDS analysis and XRD by Shortland *et al*. (2006a). They did not report the presence of sulphur, phosphorus or copper in their analytical tables, thus no conclusion can be reached as to whether or not these elements were present. Surprisingly, the actual concentrations of Co, Ni and Zn determined by SEM-EDS were significantly higher than those reported by all earlier workers, although this could be accounted for from the normalisation of a partial analysis. Shortland also reported that because only very small samples were available for XRD analysis, and because the XRD spectra for Al-spinels tend to be very similar, it was not possible to positively identify specific spinels. Therefore they conjectured, that on the basis of the bulk chemical analyses, it is possible that aluminium spinels incorporating cobalt, zinc, magnesium, iron and nickel were present. This conjecture is therefore open to question.

Shortland *et al*. (2006a) also postulated that the variation in the magnesium content may have resulted from incomplete precipitation of this element, it requiring the highest solution pH to proceed to completion. Unfortunately, this and all comparative studies have relied upon the four samples of alum from the Dakhleh Oasis analysed by Kaczmarczyk. Therefore, their attempt to compare ratios of one element with another is problematic and their discussion in respect of the Dakhleh and Kharga alums must be considered to be tentative.

Similarly, Wuttman (in Marchand and Tallet (1999: 323 note 68) relied upon XRF to analyse a blue painted sherd from Ayn Asil in Dakhleh Oasis. He was unable to report the presence of elements below calcium (Z<20). Importantly, the spectrum provided would suggest that he observed low manganese, cobalt and nickel in similar concentrations and a higher concentration of zinc. Minor copper was also present. This work is generally in conformity with the Dakhleh Oasis alums and the cobalt blue pigment applied to various vessels.

Uda *et al*. (2002) used PIXE, XRF and XRD to examine two pottery fragments excavated at Malkata. They concluded that "Amarna blue" might be a mixture of $CaSO_4$ and $Co(M)Al_2O_4$, at least in part, where M denotes Mn, Fe, Ni and Zn and the role of NaCl detected remained unresolved.

As stated in the Introduction to this chapter, because of the concern over the Bachmann work, and the degree of uncertainty expressed by other researchers, the specific sherd, "Bachmann" (sherd M9) and shown in Figure 5.12(a) along with a number of other sherds from the Nile valley, were examined by SEM-EDS, the XFM beamline of the Australian synchrotron and, using both the Raman blue and green laser lines to ensure that the maximum data could be ascertained. The detailed analyses are provided in Section 5.4.2.1 and in Appendix A5. The present research would strongly support a cobalt-diopside (a pyroxene or clinopyroxene) complex as shown by the Raman bands at 669-673 cm^{-1} and 1007-1013 cm^{-1} in conformity with the published work of Tribudino *et al.* (2012) and of Mantovani *et al.* (2014). Thus, the more likely cobalt mineral present in this and other 18th Dynasty pigments is based upon the pyroxene (diopside) structure and probably as $(Ca,Mg,Co,Fe,Ni,Zn)(Si,Al)_2O_6$. It is possible that a spinel did also form but its Raman signal is now being masked by the formation at the pigment surface of heterogenite, omphasite, or the cobalt hydroxide, oxidation to Co_3O_4, or by conversion to bieberite all or any of which could mask the cobalt aluminate mineralisation.

In respect of the Bachmann *et al* (1980) Malkata sample, (sherd M9) the presence of a cobalt aluminate spinel is suggested by its Raman signature at wavenumber 514 cm^{-1}, the Raman band at wavenumber 514 cm^{-1} could equally be assigned to the feldspars labradorite, microcline and orthoclase, to anatase, or to Co_3O_4 as provided in Appendix A5; both the feldspars, anatase and the cobalt oxide (spinel) have supporting Raman bands indicating their probable presence, whereas the cobalt aluminate is lacking in additional supporting wavenumber bands, particularly the band at 204 cm^{-1}. Other spinel-based minerals, including spinel *sensu stricto*, gahnite, Co_3O_4, and $Co-ZnAl_2O_4$ were present in various Malkata samples.

Having stated the potential for such a surface coating, Raman spectroscopy has indicated that various other spinels have been observed. Raman spectroscopy has shown that the most probable form of incorporation of cobalt into the pigment structure is by the partial replacement of magnesium ions by cobalt and other transition element ions in the pyroxene structure. This substitution reaction has been discussed in more detail together with cobalt chemistry and mineralogy in Appendix A5. Furthermore, there is significant evidence to suggest the pyroxene structure has undergone some decomposition leading to the formation of heterogenite, bieberite and cobalt hydroxide. Such decomposition, would add complexity to an XRD spectra as noted above.

As shown by Cultrone *et al.* (2001), calcium oxide will react with silica to form wollastonite at 800°C. Diopside will also commence to form in very low concentrations at this temperature. Noll (1981a) reported that the formation temperature for diopside is 850°C. Wollastonite was detected by its Raman signature in samples from both Amarna and from Memphis. The effect of mineralising additives on the synthesis of ceramic pigments in wollastonite has been discussed by Sedel'nikova and Pogrebenkov (2006). Unreacted quartz was detected by its Raman signature at ~467 cm^{-1} in most, but not all sherds as provided in Tables 5.4 to 5.6. Tridymite, a high temperature silica polymorph, was detected in sherds from Malkata. This presence would support the production of the cobalt pigment prior to its application to the vessel surface in a post-firing application. The other cobalt minerals

determined by their Raman signatures include omphasite, heterogenite, cobalt hydroxide and a cobalt doped zinc oxide which would have formed within the glass phase.

In several of the sherds the cobalt-based pigment is present only as a superficial remnant, enabling the minerals in the substrate to become visible. Thus, the feldspars and the calcium minerals may be related to the substrate on which the pigment has been applied. The fact that apatite has been detected indicates that at least some of the cobalt blue frit reaction vessels were probably lined with a hydroxyapatite (bone ash) gypsum composition, or that hydroxyapatite was part of the alkali flux generated from the use of kiln ash. These minerals could therefore also be present as contamination within the cobalt pigment. Similarly, as discussed in Chapter 4, hydroxyapatite was also observed in Egyptian blue samples, confirming the similarity in the thermal cycle.

Finally, as indicated in Table 5.9, whilst Raman spectroscopy revealed the presence of spinels, only rarely was the cobalt aluminate (spinel) observed. And, in the case of these samples, and all other samples examined, they indicated that the cobalt was bound into a diopside lattice by the partial replacement of a magnesium ion by a cobalt ion. This was true for the sample from Mut al-Kharab and for all sherds from sites examined from the Nile valley and North Sinai.

In summary, magnesium could have been derived from alum, from ground water, or from plant ash, therefore its concentration in the cobalt blue pigment is not considered to be diagnostic for the source of the flux. Phosphorus, as shown by the analyses in Table 5.7 is low in concentration (other than in the discrete hydroxyapatite particles), and therefore is not diagnostic for the flux. However, potash is significant in concentration and this is considered to be the only reliable marker for establishing that plant ash was the flux used in the production of the pigment.

5.5 Transition element data comparison

One of the great strengths of the synchrotron XFM beamline is its ability to scan and elementally map much larger areas of an object than is able to be achieved by other experimental methods. Unfortunately, it cannot map for light elements, particularly the important elements Na, Mg, Al, Si and P. As shown in Figure 5.52, the transition element weight percent ratios found in various Nile valley sherds manufactured during the period between the 18th and 20th Dynasties have been plotted. The results obtained clearly identify a very strong and direct relationship between the various transition elements mapped. Zinc appears to be normally in a higher concentration and manganese in a lower concentration when compared with cobalt; nickel closely matches the cobalt concentration. This finding is in accord with the alums analysed from the Dakhleh Oasis and support the proposition that the Western Desert oases provided the source for the cobalt-containing alums mined. Normal variation within various parts of the alum ore body, together with minor adjustment in production methods and normal batch-to-batch variation in production over this extended period would be expected. However, the results do show a very uniform quality of blue pigment produced over this significant time period, supporting the proposal that cobalt-blue frit production was conducted in very few locations using a constant source

of cobalt alum mineralisation. The very close relationship, particularly between NiO and CoO could have supported the mining of a single alum deposit and as such, this raw material could support a limited number of manufacturing sites. As discussed above, all of the necessary raw materials to produce the cobalt-blue pigment were available at Dakhleh oasis making it an ideal production site. And, if a biomass ash, similar to that analysed in Table 5.12 was utilised, this would have provided the requisite alkaline flux.
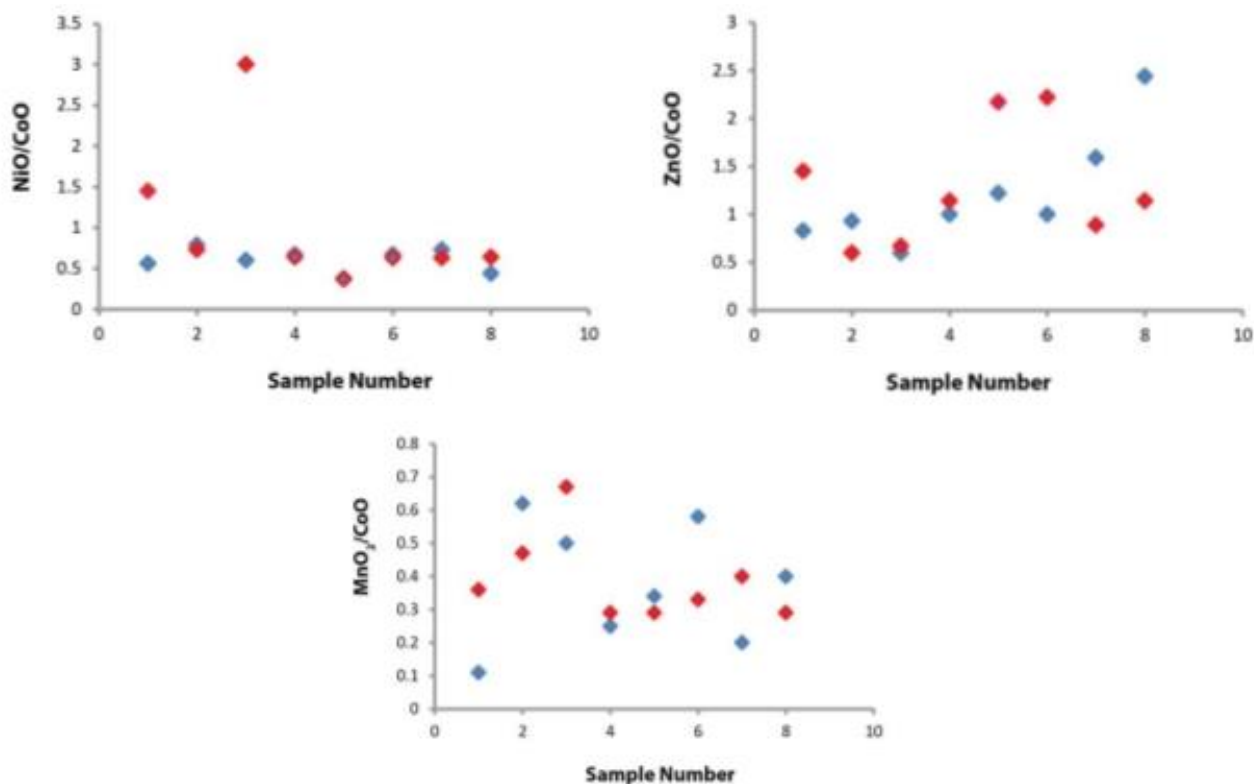
Amarna	
X Axis	**Sherd**
1	Amarna A1
2	Amarna A2
3	Amarna A3
4	Amarna A4
5	Amarna A5
6	Amarna A6
7	Amarna A7
8	Amarna A8

Malkata	
X Axis	**Sherd**
1	Malkata M1
2	Malkata M2
3	Malkata M6
4	Malkata M9
5	Malkata M5
6	Malkata M8
7	Malkata M7
8	Malkata M4

Figure 5.52. Plots of eight Amarna sherds and eight Malkata sherds providing the NiO to CoO, ZnO to CoO and MnO_2 to CoO ratios for the blue pigment applied to each of the sherds examined and listed in Figures 5.12(a) and 5.12(b). The blue data points are for the Malkata sherds and the red data points are for the Amarna sherds. Several points show an overlap of ratio data.

Shortland *et al*. (2006a) suggested that there were probable differences in the quality of the cobalt blue pigment used at Malkata and Amarna. In Figure 5.53, the EDS weight percent ratios of manganese dioxide, nickel oxide and zinc oxide to that of cobalt oxide are provided. Nickel and cobalt ratios show almost no differences for the various sherds analysed. There is slightly more variance in the zinc and cobalt results, but both of these elements also support the clear indication that both Malkata and Amarna obtained their cobalt-blue pigment frit from a similar specialist production site. It is now proposed that this site is located within the Dakhleh Oasis.

Shortland *et al*. (2006a) postulated that the ratios of Mg, Mn, Fe, Ni and Al to Co for the blue pigment found at Malkata tend to be lower than those for the same pigment ratios at Amarna. This data is considered to be somewhat tenuous. These element oxide ratios in the present study show rather similarly tenuous ratios as provided in Table 5.10. Figures 5.52 and 5.53 would suggest that no substantive changes in the ratios of the various transition elements to cobalt occurred either at Amana, Malkata, or more broadly throughout the Nile valley. The data generated by the Australian synchrotron provided in Figure 5.52 indicates that the cobalt blue pigment used between the 18th and 20th Dynasties did not substantially alter in its composition. Minimal variability is shown in Figure 5.52 for the ratios of MnO_2, NiO and ZnO to CoO for the eight sherds from Amarna and the eight sherds from Malkata shown in Figures 5.12(a) and 5.12(b). These results do not support the Shortland *et al*. (2006a) proposal.

Synchrotron images provided in Figures 5.36 to 5.39 show differences between Malkata and Amarna, particularly in respect of arsenic. Thus, this presence of arsenic, particularly within the cobalt blue pigment area, is evident at Malkata in samples M3 (MA) and M5 (MC) and also in the sherd from Deir al-Medineh. Arsenic is not found at Amarna in either sherds A2 or A4, nor in the North Karnak or North Sinai sherds. And, as shown in Figures 5.52 and 5.53, it is evident that slightly variable concentrations of manganese are present in Amarna sherd A2 and Malkata sherd M2 in comparison to the other samples analysed. The Deir al-Medineh sherd also contains a lower manganese concentration. This would support the suggestion that element oxide ratios may not provide a suitable method for differentiation of the actual sources of the cobalt-rich alums exploited.

In summary, the transition metal element concentrations support a common source for the cobalt-containing raw material used in their production. This source was the Dakhleh Oasis alums. The evidence would suggest that the cobalt blue pigment was produced within the Dakhleh oasis.
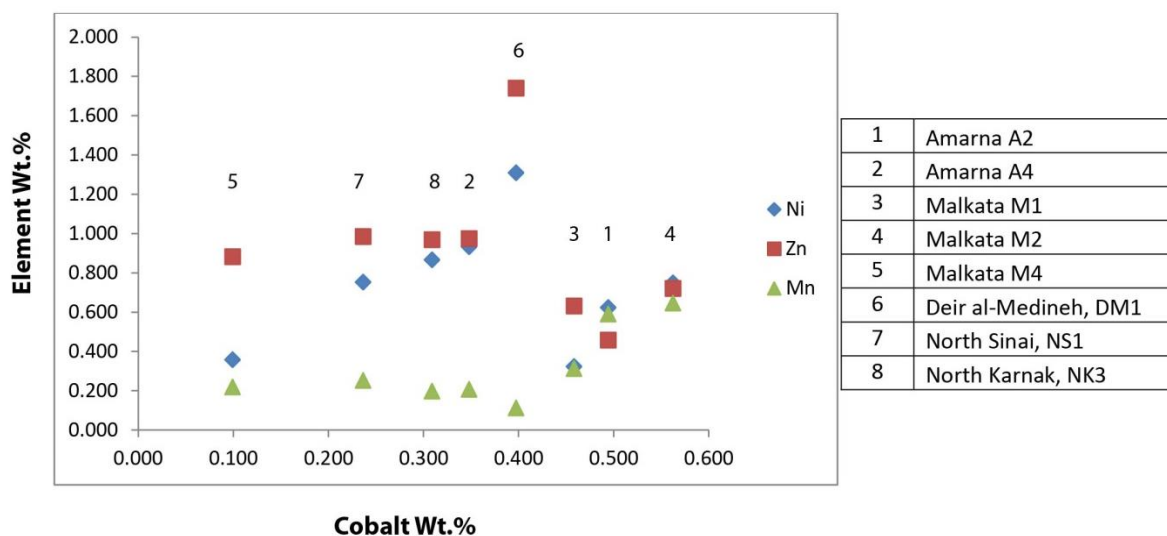
Figure 5.53. Synchrotron XFM beamline transition elements compared with cobalt, for various cobalt-blue pigment-decorated sherds recovered at sites located throughout the Nile valley and shown in Figure 5.12(a) to (e). All element results are expressed as weight percent, (♦ Ni, ■ Zn, ▲ Mn).

5.6 Cobalt pigment application to pottery surfaces

Malkata sherd M3 (MA) in Figure 5.12(a) has an area in which the blue had been rendered a paler shade. This was shown by EDS analysis to be achieved by overpainting with white lead, possibly as the mineral cerussite although the Raman signature for this mineral was not observed. Lead mineralisation was also detected in the blue pigment applied to Amarna sherd A1 and more particularly on Amarna sherd A5 where again white lead has been used to deliberately overcoat the blue to obtain a paler shade of blue. Alterations of the painted areas on pottery have also been observed at Amarna by Rose (2007: 26). In discussing overpainting, Rose described an additional form of alteration; namely the application of a slip coating over the blue decoration to obscure the original design. In one example, the uppermost slip coating was decorated in black and blue, below this is a middle layer decorated in blue, black and red again on a cream slip and under both of these there is, at least in some areas, a blue coating. How this could relate to the section heading "Pre-firing painted decoration" and thus whether this overpainting was again fired is not discussed. The application of the lead pigment is different in-so-far that it does not cover all of the blue decoration, but is intended to apparently change the shade of blue within various decorative areas.

Hope (1982; 1989) discussed the order in which the decorators applied the various pigments being used. In some instances black outlined patterns were in-filled with blue but generally coloured areas were later framed with black lines as shown in Figures 5.12(a) to 5.12(e). This latter sequence was proposed by Rose (2007: 19) in her study of the blue-painted material from Amarna and it has been confirmed by detailed analysis of photographs of the sherds analysed in this study. In Figures 5.12 (a) to (e), the pigment order of application on the sherds analysed is provided. Hope (2011: 508) also noted that the blue pigment was applied

before firing and thus presumably employing a cobalt base on Egyptian ceramics. The present results do not support this order of pigment application.

El Goresy (2000: 55) reported that the black pigment used for decoration requires scientific investigation and was generally soot or pyrolusite (MnO_2). However, Figures 5.36 to 5.39 identify the black pigment decoration to be the black iron oxide spinel, magnetite. Manganese is associated with only some of the iron-black lines.

5.6.1 Slip applied to the pottery surface

Tables 5.4 to 5.6 provide the Raman spectra and signatures for aragonite (which is metastable) and gypsum when present on the surface of various sherds, either within the pigment or as a slip coating applied directly to the pottery surface and under the pigment. Upon firing at temperatures above 800°C, aragonite would decompose (Cultrone *et al*. 2001) and the reactive calcium would potentially enter into a chemical reaction with the blue pigment if the cobalt had been applied pre-firing as suggested by Riederer (1974). As such a reaction is not indicated, the presence of calcite is likely to have occurred during burial, initially being deposited as the metastable vaterite. The failure to record a calcium reaction would support the blue pigment having been applied post-firing of the vessel.

Bachmann *et al*. (1980) considered that the possible presence of gypsum could have resulted from burial conditions rather than from the proposal of Noll and Hangst (1975) that the cobalt pigment was applied as a slip mixture containing gypsum on to the vessel. And, Shortland *et al.* (2006a) considered that gypsum was the most likely mineral used in any slip coating. Based upon the sulphate content, they suggested that a calcareous clay was also present. Gypsum, if present on the burnished surface, or as a slip coating, on firing would lose its water of hydration to form anhydrite. Thus, the presence of gypsum is also considered to have developed as either a surface deposit during burial by surface deposition from the surrounding soils or, more likely by the rehydration of the anhydrite slip. The addition of calcite or huntite with gypsum in preparing the slip was not considered.

The images provided in Figures 5.12(a) to (e), and a number of elemental analyses, supported by Raman spectroscopy, as provided in Figure 5.54, would suggest that gypsum formed part of the pottery surface burnishing process and was therefore on-fired with the vessel.

Raman spectral data for gypsum and anhydrite is given by Prasad (1999), Prasad *et al*. (2001) and by Bishop *et al*. (2013). The crystal structures of the various low temperature dehydration products of gypsum have been discussed by Lager *et al*. (1984). Gypsum dehydrates firstly to bassanite (hemihydrate) at approximately 70°C or below, and rapidly at 90°C. Heating above 200°C produces anhydrite, and this change is monotropic (Ramsdell and Partridge 1929; Deer *et al*. 1992: 614). The reaction kinetics of the dehydration and the effect of relative humidity on its stability have been discussed by Robertson and Bish (2007).

The rehydration of anhydrite to form gypsum is less understood. It has been investigated by Sievert *et al*. (2005) and by Ramsdell and Partridge (1929). According to Ramsdell and Partridge (1929) the reaction can proceed at temperatures as low as 11-15°C. Thus, it can be hypothesised that if anhydrite remains on the pottery surface then it is conceivable that the gypsum was fired on to the vessel surface. If the cobalt pigment has been applied over a brown goethite decoration, then this would again indicate that the vessel was post-firing decorated.
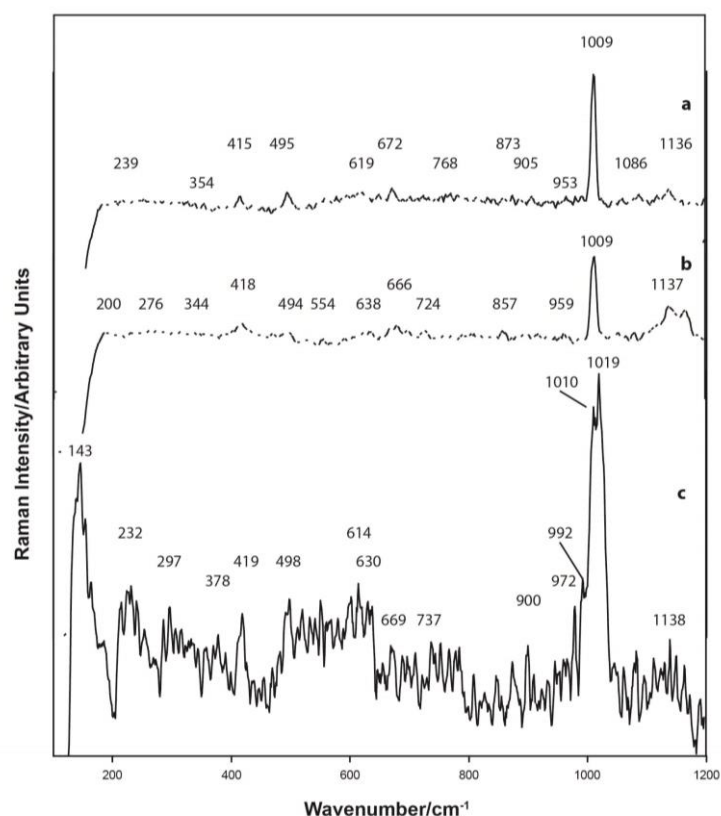
Figure 5.54. Raman spectra, blue region, Malkata sherd, M6 (a, b λ = 413.2 nm; c λ = 514.5 nm). The cobalt mineralisation is shown by its Raman signatures to be cobalt pyroxene together with cobalt hydroxide, heterogenite and probably $Co-ZnAl_2O_4$, (both hydroxyl-containing minerals probably formed following the partial breakdown of the pyroxene structure). Andalusite $[Al_2OSiO_4]$ may be present, tridymite, possibly feldspar and mullite are present in the blue pigment. Barium was observed in the EDS analysis as was anomalous phosphorus (~2% P_2O_5). The slip is identified as a slip containing gypsum, anhydrite and minor calcite. The presence of anhydrite could support a high temperature firing of the burnished surface during the firing of the vessel. The traces of calcite would suggest a post-depositional surface adsorption from the surrounding soils.

5.7 Pigment application to pottery surfaces, pigment binder

To date, the rationale provided in the literature to support the method of application of both the cobalt blue pigment and of the accompanying red, brown and black pigments is generally lacking in scientific rigour. It is an area of investigation which should become a study within itself and is only discussed in minor detail within this thesis. It is widely reported in the literature that the pigments were applied to the wares either using a binding medium such as gypsum applied as a white slip ("post-firing painting") or the pigment was applied to the unfired body and both were fired simultaneously ("pre-firing painting").

Bachmann *et al.* (1980), Hope (1989: 7) and Rose (2007: 18) all suggested that the pigment was applied before firing. Thus, depending upon the chemical composition of the pigment, the pottery surface and the firing temperature the potential for additional mineralogical changes both within the pigment and between the pigment and the vessel surface may exist.

In cases where the pigments were applied to the vessel surface post-firing and on to calcite or huntite surfaces they have been described by Hope (1987: 110; 2011: 496), Rose (2007: 31) as 'polychrome decoration' or by Arnold (1993: 101) as 'white background style' decoration. Thus, whether the application of the slip and the cobalt blue pigment was applied to the leather-dry vessel and then fired, or to the vessel surface post-firing has previously remained unresolved. Circumstantial evidence such as the loss of sharp edges to the pigment, or the presence of an anhydrite slip under the pigment in other cases, or the bloated sherds discussed below has suggested that the pigments may have been applied pre-firing.

Riederer (1974) alternatively proposed that an alkaline precipitated cobalt hydroxide product obtained from a cobalt-containing alum solution would have been directly applied to the pottery surface and then fired. However, as previously stated, the formation of tridymite in the cobalt complex is indicative of exposure to temperature, approximating, or above that at which the pottery vessel would fail. Noll and Hangst (1975) did consider that because of the cobalt pigment's excellent heat stability it could have alternatively been applied by direct firing on to a gypsum-containing slip. Noll (1981: 149) however, considered that the cobalt blue pigment was applied to the vessel after firing, El Goresy (2000: 62-3) disputed the Riederer (1974) claim that the pigment was fired on to the vessel. He unequivocally supported Noll and Hangst (1975) in that the presence of crystals of gypsum and anhydrite and the absence of any diffusion profile between the slip and the cobalt pigment supported a post-firing application. Lucas (1962: 384), Noll and Hangst (1975), Noll (1978: 227; 1981a: 149), el-Goresy (2000: 62), all concluded that the cobalt aluminate pigment was most likely applied by post-firing technology. Arnold (1993 :100) appears to suggest that sherds containing a gypsum-based slip were post-firing decorated.

Hope (1980: 329) considered that compositional differences in the chemistry of both Egyptian blue and cobalt aluminate would have precluded Egyptian blue from being applied pre-firing. This is unlikely to be the case as both pigments were found to contain tridymite, a silica polymorph which only forms at about 1000°C or above. Thus, whilst the evidence in support of a pre-firing regime is tenuous, the present evidence for both the blue-painted pottery and the polychrome decorated pottery now supports a post-firing decorating regime.

Hope (1980: 329) stated that Egyptian blue and the cobalt blue have different adhesion qualities and related this to Egyptian blue being applied post-firing and cobalt blue having significantly better long-term adhesion resulting from pre-firing application. The softness and porosity of calcite and huntite as a slip would also serve as a poor binder; huntite has been determined as the binder used for the Egyptian blue decorated sherds from Malkata examined (refer Chapter 4, Appendices A3 and A4 and samples M7 and M8). However, as

shown in Malkata sherd M1, when Egyptian green pigment was applied to a huntite slip and over-coated with beeswax it prevented water ingress and did not fail. It is now established that at least a significant number of the cobalt blue samples were applied using an organic binder and this has provided the improved adhesion.

Bachmann *et al*. (1980: 36) agreed with the report by Hope (1977) that he had been informed by local potters that if the pigment was applied post firing it would be unstable and easily rubbed off as was the case for amphorae of the period. Bachmann *et al*. (1980) reported the existence of a small number of blue-painted kiln wasters found during the excavation of Site J in the workmen's village at Malkata. These sherds had commenced to disintegrate due to exposure to excessive heat. They were all dark-grey to black in colour, with bloated and cracked surfaces and several were quite distorted. Rose (2007: 18) reported the recovery of a single badly vitrified waster in the Central City, Amarna. Thus, as no distorted vessels removed from a kiln in this condition would be decorated, it was reasonable to presume that they must have been decorated prior to firing. This suggestion however, fails to consider that alternative heat sources, including a subsequent exposure to extreme heat such as in a fire, may have led to blackening, distortion and bloating post decoration. Arnold (1993: 100) supported the pre-firing proposal as proposed by Hope (1982).

The justification provided by Rose (2007: 18) for presuming the cobalt blue pigment found at Amarna was applied pre-firing is presumably based upon the reports of Hope (1982: 88-100) and Bachmann *et al*. (1980) in respect of the bloated sherds excavated at Malkata. Thus, a theory for pre-firing decoration has been promoted based upon a small number of dark-grey to black sherds from Malkata. The source of this heat was not determined; the assumption being that it was during kiln firing. These bloated and distorted Malkata sherds were not available for analysis in the present work and therefore, no conclusions can be advanced in respect of the heat source. What is known is that the adhesion of the cobalt blue to the pottery surface as reported by Rose at Amarna is similar to the adhesion of the red, brown and black pigments. Hope[4] indicated that these Malkata sherds had been excavated prior to his first visit to the site and therefore he was unable to provide any additional information.

Another concept has been promulgated in support of pre-firing application and which requires further investigation. Namely, the pitting often observed within the blue pigment decoration. With Nile silt fabrics, the pottery surface was normally given a gypsum coating and/or surface smoothing, and this has produced a reasonably continuous slip coating suitable for application of the cobalt pigment. Whereas, in the case of marl clays the cobalt has normally been applied directly to the pottery surface (Shortland *et al.* 2006). Rose (2007: 19) reported that at Amarna, marl clays were very rare. The marl clays upon firing would, depending upon particle size, ensure that particles of limestone (calcium carbonate) would lead to lime spalling. Allegretta *et al*. (2016) positively correlated spalling to commence at 750°C and is triggered by coarse calcined grains directly related to the limestone temper size in the pottery fabric, Allegretta and co-workers concluded that the kaolinitic clays in the fabric decomposed at about 1000°C to form γ-Al$_2$O$_3$ with limited Si for Al substitution. Much unreacted lime in coarse grains survived firing and if open porosity was still present, formation of portlandite occurred after firing.

[4]Hope (Pers. Comm. 18 Feb. 2016)

As stated above, this could influence the pre-painted firing of the blue pigment. Bourriau *et al*. (2000: 129) reported that limestone will begin to decompose at temperatures of about 850°C. And, importantly, they supported their discussion by the observation that Marl A1 fabrics are distinguished by conspicuous fine to medium-sized angular particles of limestone added to the paste as filler. Thus, the presence of particles of limestone is indicative of a firing temperature below 800°C. (Note that limestone is a sedimentary rock composed of mainly calcite and aragonite.) Whereas Marl A3 seems to be consistently fired to temperatures of approximately 1000°C producing a characteristic pale green colour (Bourriau 2000: 131). Thus, both of these fabrics if employed in a pre-firing application would likely provide pitting within the blue painted decoration.

And, gypsum when added as temper to the clay, or if used as part of the burnishing process, would have led to the formation of anhydrite (conversion to anhydrite occurring at 200°C). On long standing, the anhydrite would, depending upon the environmental moisture present, alter to gypsum by hydration and this would be accompanied by an increase in volume and mechanical deformation. This transformation would be expected to rapidly occur slowly over time. Thus, any coating over large, calcium-based particles, would, given time, be expected to be dislodged. It would occur regardless of whether the cobalt pigment was applied before firing or post-firing.

In respect of the slip coating and its possible contribution to adhesion of the cobalt blue pigment, Cultrone *et al*. (2001) indicated that calcite will decompose between 700-800°C and Hollingbery and Hull (2010) has indicated that huntite will endothermally decompose over a temperature range of approximately 450°C to 800°C both with a loss of carbon dioxide. And, this would be accompanied by the loss of the Raman signature for the carbonate band. Traces of calcite and/or huntite were observed in most slips and these are considered to be related to burial conditions. Thus, if either mineral provided the slip composition, then failure of the surface adhesion of the pigment would occur in a pre-firing step subject to the potential for the CaO formed to react with the silica in the cobalt complex to form wollastonite at the cobalt pigment/slip interface. This reaction was not observed. However, the primary mineral found was gypsum and this is stable at the temperatures encountered.

Arnold (1993: 95-102) indicated that the 'white-background' style of decoration adopted from the First Intermediate period through to the Late period were decorated after firing with paints of various colours on to a white background. Similarly, the 'scenic' style of painting pottery is closely related to the 'white-background' style (Arnold 1993: 99); Rose 2007: 21) in which naturalistic motifs such as floral garlands, or scenes including plants, birds, fish and animals occur and was therefore presumably considered to have been applied after firing. And, whilst 'blue-painted' pottery was considered to be decorated prior to firing (Rose 2007: 18), Arnold (1993: 100) considered that a 19th Dynasty jar painted with a blue garland and described by Bell (1987) should preferably be classified under the 'white-background' style because a white gypsum background was used and thus, the decoration was applied after firing.

The suggestion by Rose (2007: 18, 26) that the black or red pigments were also applied before firing in the present instances has been shown to be incorrect. She assumed that as reported by Arnold (1993: 101-102) the red and black pigments were red ochres to which manganese has been added. In fact, as indicated in the synchrotron elemental maps provided in Figures 5.36 to 5.39 and in Appendix A3, the reds may be hematite and/or oxyhydroxides such as goethite; and the black, which may contain manganese and/or carbon, is principally magnetite. The oxyhydroxides will decompose below 300°C, however, hematite and magnetite would survive the firing temperature. Thus, the presence of goethite, which would convert to hematite if fired with the vessel and other related oxyhydroxide iron minerals, including lepidocrocite, must be applied post-firing. Thus, the presence of the oxide pigments should not be necessarily seen to provide an indication in respect of their time of application. As stated, goethite will convert to red hematite, lepidocrocite, the mineral most associated with brown ochres, will convert to the metastable maghemite and which on further heating to 700°C (or below) will convert to red hematite. Without a mineralogical determination of the form of the iron pigment, it is not prudent to presume that the presence of an iron oxide or oxyhydroxide pigment is indicative of a pre-firing application. Therefore, in the instances where the cobalt blue has been applied over goethite or lepidocrocite, this is a clear indication of post-firing decoration.

5.7.1 Determination of the organic binder used to fix the cobalt pigment

To resolve this, and similar questions, combined analytical and mineralogical studies are the most appropriate method to achieve the required answers particularly with respect to cobalt blue pre-firing or post-firing application. For this reason, a very brief but detailed study of the pottery has therefore been undertaken to enable any pottery body or slip and the decoration to be observed. This research is provided in Chapter 3 and more particularly in Appendix A3. As stated above, part of this research is relied upon in this chapter in discussing the cobalt question posed above. Additional data developed in Chapter 4 in respect of Egyptian blue and Egyptian green surface applications will similarly rely on an intimate knowledge of the substrate.

At both Malkata and Amarna, as indicated in Table 5.21, Figures 5.55 to 5.57 and Appendix A5, beeswax was certainly used to fix the pigments to the pottery surface of eight of the sherds examined (refer also Appendix A5 and Malkata sherds M3 (MA) and M5 (MC) and an Egyptian green decoration discussed in Chapter 4, and also Amarna sherd A1. In the case of the Amarna A1 sherd, the actual composition of the wax used has not been determined. And, the method of application of the beeswax as a binder or as an over-coating has not been determined. Was it applied to the hot surface of the vessel? Was beeswax applied to the surface of the pre-painted cobalt blue in a manner similar to that proposed to have been used to coat paintings in New Kingdom tombs (Serpico and White 2000: 411)? These questions represent subjects for future research.
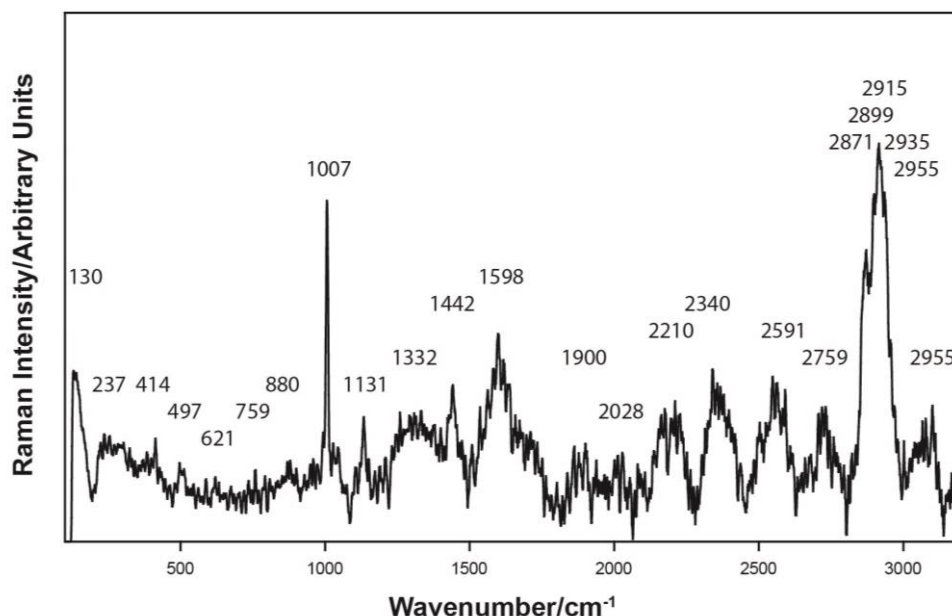
Figure 5.55. Raman spectra, of a wax mixture (such as beeswax) which may have contained some linseed oil present with the pigment applied to Amarna sherd A1. The Raman bands at wavenumber 2935 cm^{-1} is indicative of a mixed egg protein plus gypsum located within the cobalt blue pigment (λ = 514.5 nm). In this spectrum, and the related spectra provided in Appendix A3, the cobalt pigment contains gahnite [$ZnAl_2O_4$], and Co-Zn aluminate, gypsum, feldspar (probably either oligoclase or orthoclase), hexahydrate [$MgSO_4.6H_2O$] or possibly pickeringite $MgAl_2(SO_4)_4.22H_2O$ (presuming the band at 974 cm^{-1} is masked by the broad band at 998 cm^{-1}), cobalt pyroxene, spinel and amorphous carbon. Mullite [$3Al_2O_3.2SiO_2$] is indicated by the band at 1130 cm^{-1}. The pigment also contains anomalous phosphate (up to 2% P_2O_5) together with high alumina and high magnesium. The pigment has been applied to the surface using a wax composition (probably a mixture of beeswax and probably linseed oil) as is visually evident. The Raman spectrum is more closely linked to egg protein material. Therefore, wax would have prevented on-firing of the pigment; rather, it was applied post firing on to a gypsum-prepared surface or admixed with gypsum.

Egg protein, which is possibly a mixture of both the yolk and the egg white, has also been detected as the binder in nine samples as provided in Table 5.21 and in Figures 5.58 and 5.59. (It should be noted that modern eggs used to obtain the respective Raman signatures may vary very slightly from the eggs and the breed of the egg layers utilised in Egypt during and post New Kingdom period.) These organic compounds would decompose well below the firing temperature at which the vessels were fired. Therefore, in those instances in which the presence of these organic binders is established, this may be considered as proof of the pigment being post-firing decorated. It should be noted, that twelve samples still have not been examined at wavenumbers above 2000 cm^{-1} to assess whether or not an organic binder is present.
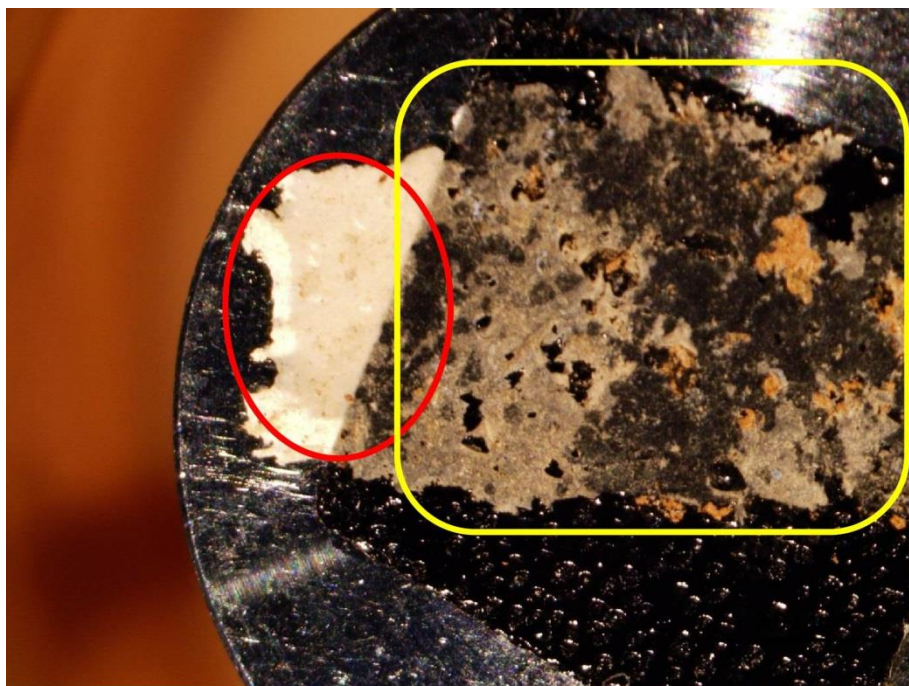
Figure 5.56. Area outlined in red is wax from the surface of the Malkata sherd M3 and which adhered to the carbon tape during sampling. The ares outlined in yellow is the cobalt blue pigment. As shown in Figure A5.M3.35, and Figure 5.57, the cobalt blue pigment was applied to the vessel surface using a wax-based compound, probably beeswax. Thus, together with the underlying brown line containing goethite would support the hypothesis that the cobalt pigment was applied post firing of the vessel.
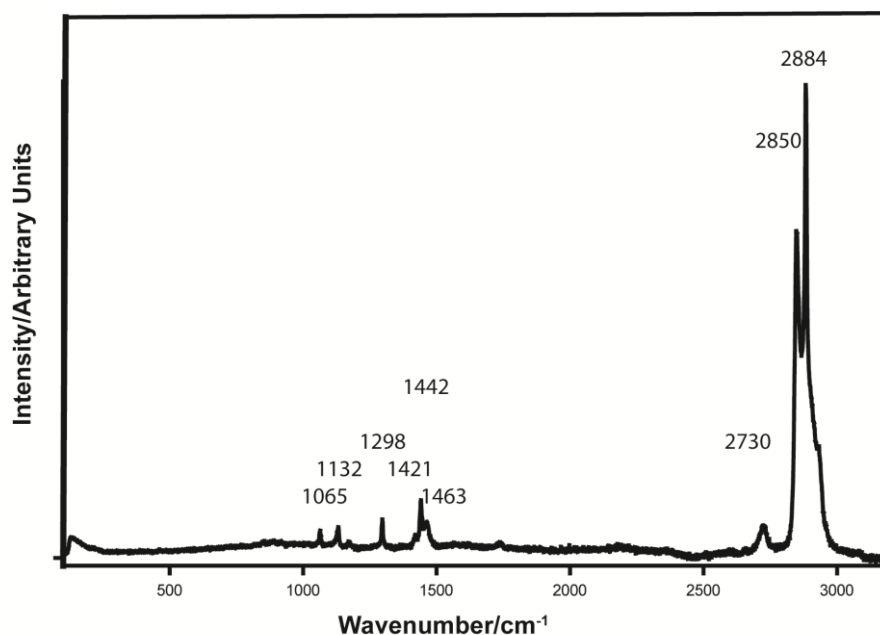
Figure 5.57. Raman spectrum of beeswax being used as a pigment fixative used at Malkata (sherd M3) (λ = 514.5 nm). This spectrum precisely matches the beeswax spectrum provided by Burgio and Clark (2001).
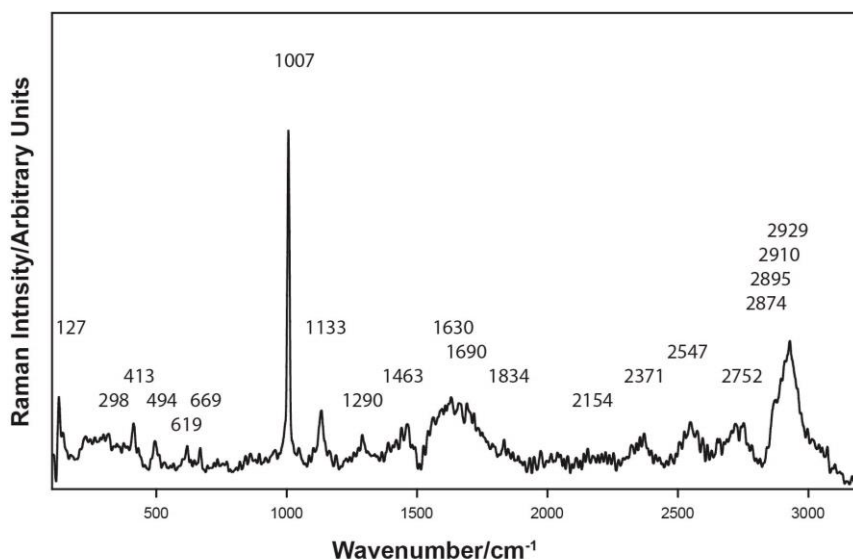
Figure 5.58.   Raman spectrum for the coating under the blue pigment on Malkata sherd M5 (λ = 514.5 nm). The Raman band at 1007 cm^{-1} is gypsum and the organic bands at 2920 cm^{-1} are gum Arabic together with probably egg protein (confirmed by the Raman bands at 1463, 1630 and 1690 cm^{-1}. Beeswax has probably been used as an additional binder (indicated by the Raman bands 133, 1290, and 2894 cm^{-1}.
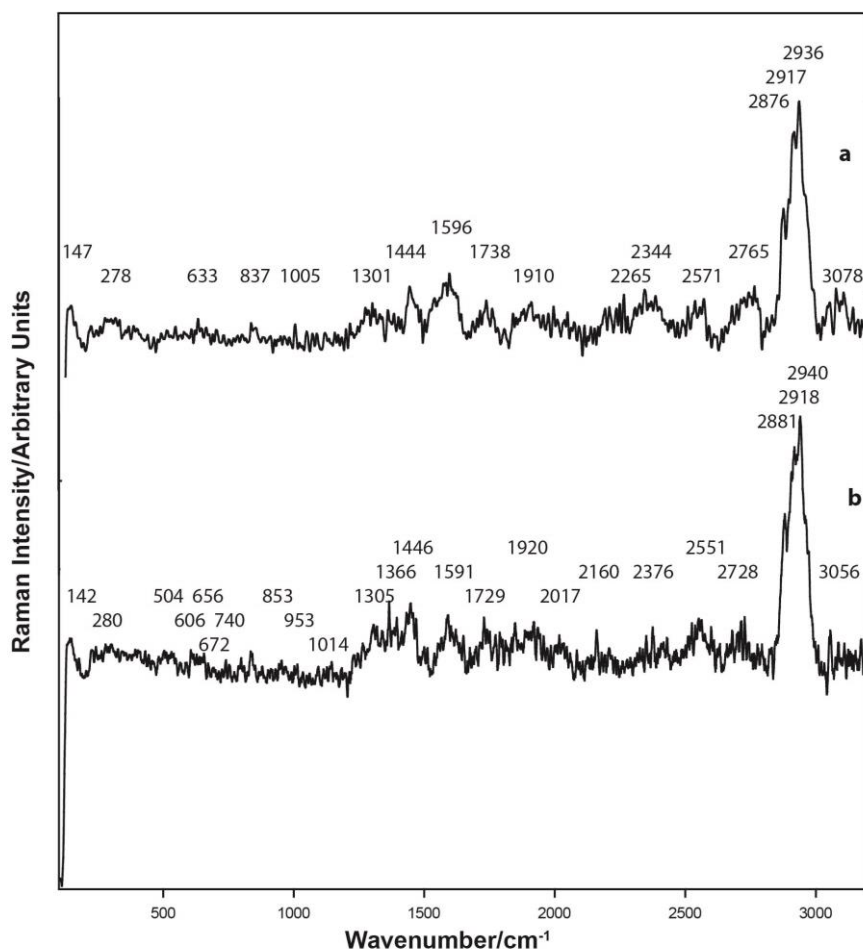
Figure 5.59. Raman spectra, egg white and/or egg yolk organic binder used as pigment fixative on Malkata sherd M16 (Refer A5.M16.19) (λ = 514.5 nm).   As discussed in the additional information provided in Appendix A5, The cobalt mineralisation is shown by its Raman signatures to be cobalt pyroxene together with cobalt hydroxide (probably formed following the partial breakdown of the pyroxene structure), possibly cobalt

aluminate and possibly spherocobaltite [$CoCO_3$].   Andalusite [Al_2OSiO_4], tridymite, feldspar (probably orthoclase) and mullite are present in the blue pigment. Barium was observed in one EDS analysis. Arsenic was detected by the synchrotron in a region visually low in calcium pigmentation and therefore it is not likely to be associated with the slip component. However, arsenic was not detected in any of the EDS analyses. Anomalous phosphorus (~2% P_2O_5) was observed to be present in the pigment. The pigment has been applied on to a slip containing gypsum and anhydrite. In the absence of other data, the presence of anhydrite could support a high temperature firing of the cobalt pigment on to the vessel. However, the organic binders would negate this possibility. Its presence can be therefore determined to be directly related to the slip coating or the pre-firing burnishing step. Organic binders including gum Arabic, egg protein and over-coating with beeswax have been applied to the gypsum or anhydrite slip.

Table 5.21. Binder chemistry as indicated by Raman spectroscopy.

Sample	Wax	Egg protein	Anhydrite/Gypsum	Calcite/Huntite
A1	●			
A2	◻	◻		●
A3			●	●
A4			●	●
A5			●	
A6	◻	◻	●	●
A7			●	
A8		●	●	●
M3	●		goethite ●	●
M5	●		●	
M6			●	
M9	◻	◻	●	●
M12			●	
M13		●		●
M14		●	●	
M15			●	●
M16		●	●	
D7				●
NK1	◻	◻	●	
NK2			●	
NK3			●	●
R1			●	
R2			●	
DE1			●	●
DM1			●	●
S1	◻	◻	●	

● indicates its positive determination.

◻ indicates either wax or egg protein, or a combination of either binder with gum Arabic or similar organic compound. It should be noted that because of fluorescence, not every sample has been examined by Raman spectroscopy at wavenumbers high enough to confirm the presence of organic binders and therefore, the lack of indication of the presence of wax or egg does not indicate the absence of such a binder composition having been used.

It is speculative, however, the question must be asked, if a cobalt blue was applied using a binder such as egg, beeswax or gum Arabic (as reported herein) to fix the decoration to the vessel surface, or wax was used to subsequently coat the applied decoration, then exposure of the decorated vessel to a high temperature such as in a fire, would the wax not melt or the gum Arabic or egg decompose, catch fire, burn and depending upon the redox conditions render the sherd surface dark-grey to black and bloat the pottery vessel? Could this be an alternative explanation for the few sherds found at the workman's village at Malkata and described by Bachmann *et al*. (1980), or for the single sherd from the Central City, Amarna as described by Rose (1987: 18)?

As provided in Table 5.21, Raman spectroscopy has definitely confirmed that beeswax, and/or egg has been used as the binder in about 50% of samples; fluorescence, if overcome by the use of an alternative wavelength, may increase this percentage. In some instances the wax has probably been modified by the addition of an oil or gum, such as gum Arabic. The adhesion of the pigment to the pottery surface using these organic binders has enabled them to survive burial and limited abrasion.

Due to possible changes in hydration under burial conditions, it is less likely that slip coatings containing gypsum or anhydrite in particular, will necessarily survive due to swelling and contraction. This could result in spalling of the slip and therefore loss of pigment adhesion.   And, as wall decoration applied using lime plaster has successfully survived, this is indicative that on-firing of the decoration is not a pre-requisite for a successful decoration. Calcite and particularly huntite being relatively porous are very likely to fail. Furthermore, the calcite could be a surface deposition from the ground-waters.

As reported in Chapter 4, in respect of the two Malkata sherds, M7 and M8, the pigment was applied to a huntite slip and which now only contains microscopic particles of residual Egyptian blue. Thus, it is now considered that cobalt blue survives because it was applied using an organic binder, whereas, Egyptian blue has failed because it has been directly applied on to an unstable slip.

Thus, whilst the presence of an organic binder would clearly indicate that the post firing application of the cobalt pigment was adopted, the presence of an undecomposed carbonate mineral may not absolutely prove post-pottery firing.

5.8 Cobalt extraction from Dakhleh and Kharga Oases alums and manufacture of the cobalt pigment: current understanding and a proposed alternative methodology

To date, two alternative methods have been proposed in an effort to explain the method adopted by Egyptian workers to extract the transition elements from alum and subsequently convert them into a blue pigment. The method most commonly proposed is a hydrometallurgical process preceding a pyrometallurgical process as proposed by Bachmann *et al*. (1980), Noll (1981a: 150), Kaczmarczyk (1986), Segnit (1988); the other, a direct pyrometallurgical process and considered by Rehren to be the "traditional" method. Arnold (in: Arnold and Bouriiau (1993: 102)) incorrectly interpreted the work of the above authors and stated that a source for cobalt aluminate had been identified in the oases.

Rehren (2001) carefully considered and summarised all of the published methods, both pyrometallurgical and combined hydrometallurgical and pyrometallurgical, to that date. And, whilst a quantitative precipitation using ammonia was not favoured, he proposed the application of natron as the alkali precipitant. As he noted, a hydroxide precipitate would have been an almost ideal colourant for plant ash-based glass.

The high temperature firing to produce the cobalt blue pigment, whether of the precipitate with glass, or more likely with silica, calcium and a flux, was therefore closely related to the production of Egyptian blue pigment. By the 18th Dynasty, when cobalt production first commenced, the production of Egyptian blue was a well-established process and able to be replicated in other processes.

These alternative processes, will be discussed in conjunction with the raw data provided within Appendix A5.

5.8.1 *Hydrometallurgy: Precipitation from aqueous solution*

The behaviour of sparingly soluble metal salts in aqueous solution and in their hydroxide precipitation has been almost certainly practiced in Egypt from about the 18th Dynasty. Riederer (1976) and Kaczmarczyk (1986) proposed that if the alums were dissolved in water and made mildly alkaline using say natron, plant ash or ammonia, then the transition metals would precipitate as their hydroxides and oxides leaving the sulphate behind (refer to Section 5.7). Drying and heating the precipitate would then yield a blue mixture containing aluminates and oxides with a much higher cobalt content. It should be noted that cobalt oxides vary in colour between dark green and black, the distinctive blue colour developing when the oxide is incorporated into a glassy structure and dissolves to form Co^{2+} ions or such as when it reacts to form a spinel, olivine or pyroxene structure.

Nicholson and Henderson (2000: 198) suggested that the alum was mixed with water and natron, plant ash or ammonia were added to make it slightly alkaline. The precipitate so formed, was then heated at between 800-1000°C to produce the blue pigment. This proposal does not explain the high silica content found in all pigment analyses as provided in Tables 5.7 and 5.8, nor the source of the ammonia as the alkali precipitant.

Shortland *et al*. (2006b) reported that when aqueous solutions of the alums are rendered alkaline using sodium carbonate that precipitation proceeds in the order as suggested by Rehren (2001) namely, aluminium hydroxide, followed by cobalt and manganese hydroxides and finally magnesium hydroxide to form the Mixed Hydroxide Precipitate (MHP). This would be in accordance with the chemistry provided by Monhemius (1977) as shown in Figure 5.60 or the Pourbaix Diagrams (Eh-pH diagrams) provided in Figures 5.61 to 5.65. Shortland *et al*. (2006b) did not report the solution pHs at which precipitation proceeded. Nor did they consider the varying solubility between sodium, ammonium and potassium double alums as provided in Table 5.22 or the effect of temperature on solubility or the addition of urine in the precipitation process to act as a water- or gel-breaker, or of the aging of the hydroxide precipitate changing its crystal form.

As stated by Nicholson and Henderson (2000) and by Shortland *et al*. (2006b) natron, or trona, or similar carbonates are readily available either from the Wadi Natrun, or from evaporite mineral deposits within the Dakhleh Oasis. Such evaporites at Wadi Natrun have been found to comprise sodium carbonate, sodium bicarbonate and chloride and sulphate impurities (Edwards *et al*. 2007) as discussed in Section 5.1.4. The addition of these salts would readily raise the solution pH of the dissolved alums. As reported by Eggeman (2001) the pH of a 1% solution of sodium carbonate is 11.37. As such, as shown in the hydroxide precipitation diagram provided by Monhemius (1977) and reproduced as Figure 5.60 all of the transition metals would have formed a precipitate.
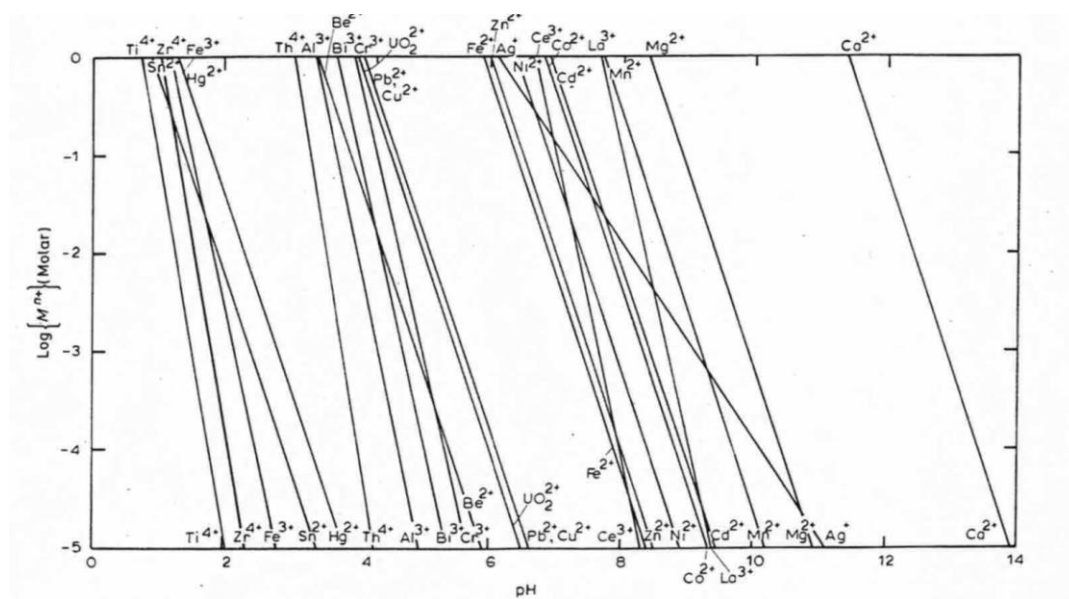
Figure 5.60. Hydroxide precipitation diagram, 25°C (Monhemius 1977).

Whilst the reaction chemistry occurring in these precipitation processes is complex, a brief explanation is provided in an attempt to simplify the process probably undertaken by the Egyptian workers at that time.

The chemical reaction for the carbonate precipitation can be written as:

$$M^{2+} + CO_3^{2-} \rightarrow MCO_3$$
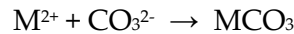
where the carbonate may for example be $CaCO_3$, Na_2CO_3, $MgCO_3$. This is an oversimplification of the reaction chemistry with mixed hydroxide-carbonates being formed.

Alternatively, if lime water [$Ca(OH)_2$], or magnesium hydroxide was used as the alkali, then the mixed hydroxide reaction would occur:

$$M^{2+} + 2\ OH^- \rightarrow M(OH)_2$$

Or more generally,

$$MSO_4 + 2H_2O \rightarrow M(OH)_2 + H_2SO_4$$
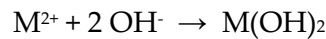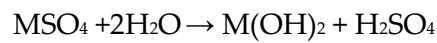
Therefore in this case, a mixed hydroxide precipitate would form as shown in the accompanying Eh-pH diagrams (Pourbaix Diagrams) provided in Figures 5.61 to 5.65. Plant ash, if used as the   alkali precipitant, would proceed in a similar manner. This could enable the very small particles of hydroxyapatite (bone ash) to be incorporated within the alkali precipitant and report with the MHP. This is discussed in Section 5.8.2.
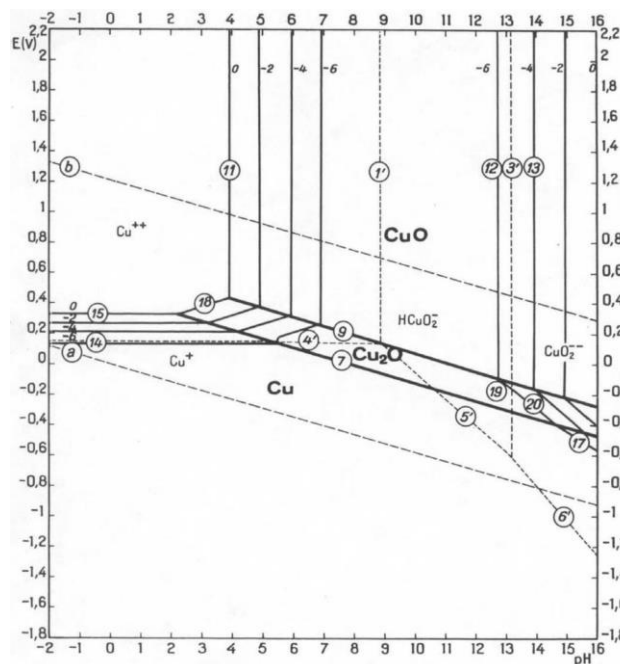
Figure 5.61. Potential-pH equilibrium diagram for the system copper-water, at 25°C. (Considering the solid substances Cu, Cu_2O and Cu). $Cu(OH)_2$ is not considered.)
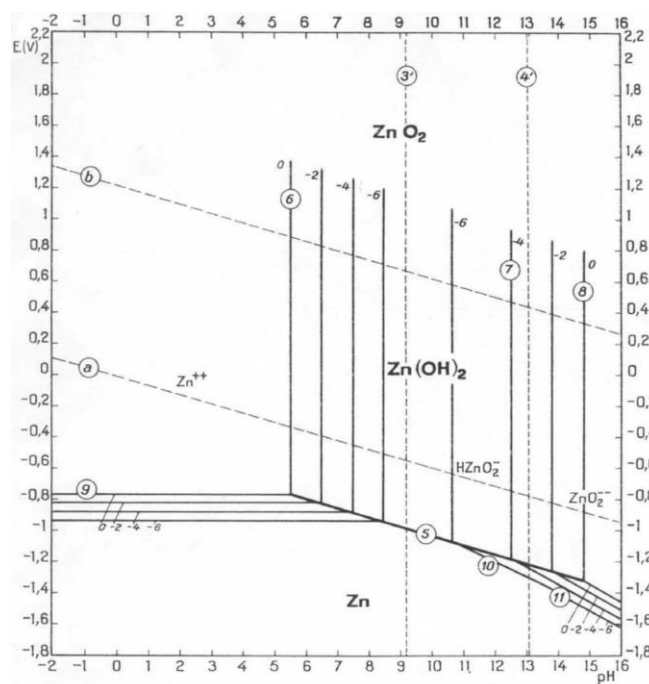
Figure 5.62. Potential-pH equilibrium diagram for the system zinc-water, at 25°C.
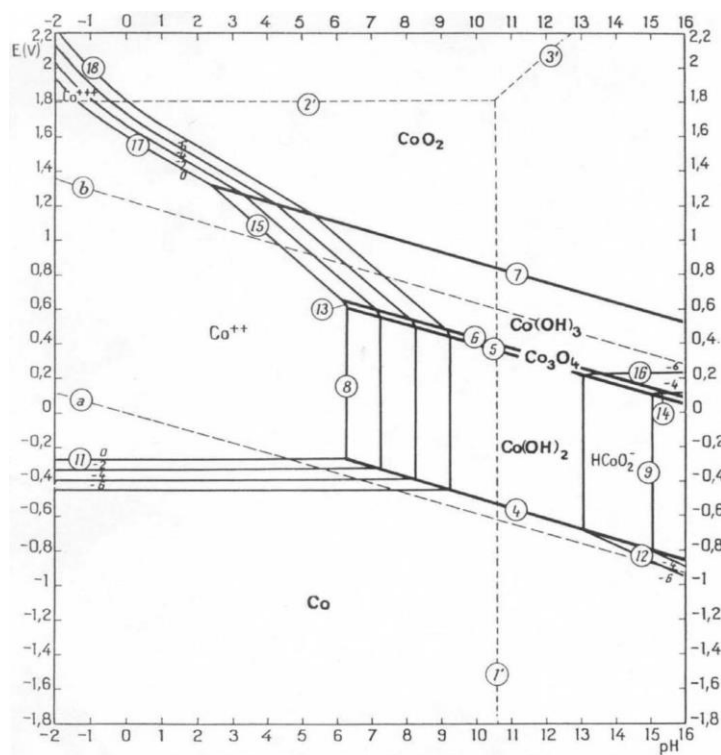
Figure 5.63. Potential-pH equilibrium diagram for the system cobalt-water, at 25°C

5.120
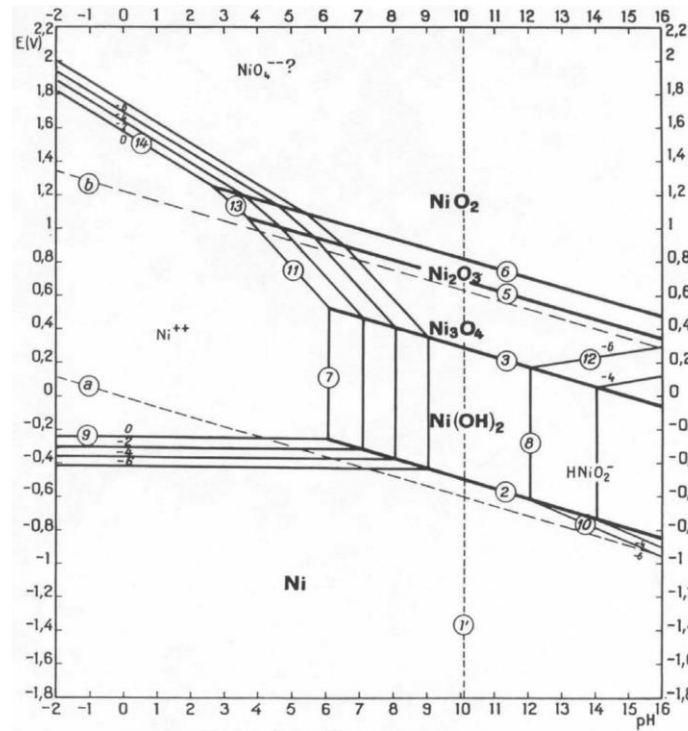
Figure 5.64. Potential-pH diagram for the system nickel-water at 25°C.
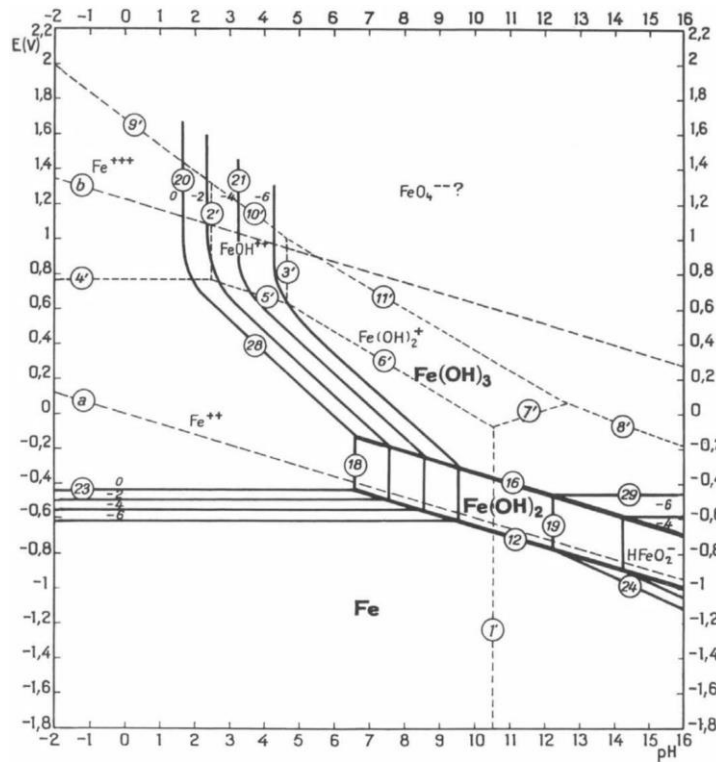
FIG. 5. Potential–pH equilibrium diagram for the system iron–water, at 25°C
[considering as solid substances only Fe, Fe(OH)₂ and Fe(OH)₃].

Figure 5.65. Potential-pH diagram for the system iron-water at 25°C. (considering as solid substances only Fe, Fe(OH)₂ and Fe(OH)₃).

Table 5.22. Solubilities of various alums in water (R.H. Perry and D. Green, "Perry's Chemical Engineers' Handbook", 6th Edition (1984), McGraw-Hill International.

Alum	Formula	Melting Point °C	Solubility in cold water/ 100 parts	Solubility in hot water/ 100 parts
Ammonium	$Al_2(SO_4)_3.(NH_4)_2SO_4.24H_2O$	93.5	3.9 (0°C)	∞ (100°C)
ammonium iron	$Fe_2(SO_4)_3.(NH_4)_2(SO_4).24H_2O$	40	124 (25°C)	
Potassium	$Al_2(SO_4)_3.K_2SO_4.24H_2O$	92	5.7 (0°C)	∞ (93°C)
Sodium	$Al_2(SO_4)_3.Na_2SO_4.24H_2O$	61	106.4 (0°C)	121.7 (45°C)

Table 5.23.   The solubility of metal hydroxides at 25°C (Fischer and Peters 1968); Garrels 1965).

Metal Hydroxide	K_{SP} (25°C)
$Al(OH)_2$	2×10^{-32}
$Ca(OH)_2$	5.5×10^{-6}
$Co(OH)_2$	2×10^{-16}
$Co(OH)_3$	1×10^{-43}
$Fe(OH)_2$	8×10^{-16}
$Fe(OH)_3$	4×10^{-38}
$Mg(OH)_2$	1.2×10^{-11}
$Mn(OH)_2$	1.9×10^{-13}
$Ni(OH)_2$	6.5×10^{-18}
$Zn(OH)_2$	1.2×10^{-17}
$Cu(OH)_2$	3.7×10^{-43}

Whilst Table 5.23 indicates a significant solubility difference between various hydroxides such as the relatively insoluble $Co(OH)_3$ and $Cu(OH)_2$ and the more soluble $Ni(OH)_2$, from a thermodynamic viewpoint, there is little difference between the solubility of the cobalt (II), Zinc (II), nickel (II) and manganese (II) hydroxides.

Thus, under laboratory conditions, when various cobalt salts were added to a 0.5M ammonia solution only poorly ordered α-$Co(OH)_2$ formed. And, when $CoSO_4$ reacts with soda, again a blue α-$Co(OH)_2$ forms, but which spontaneously transforms into a pink β-$Co(OH)_2$ precipitate of higher stability.

Nickel behaves slightly differently. When precipitated from an ammonia solution it formed a disordered α-$Ni(OH)_2$ precipitate into which water and carbonates were incorporated. And, β-$Ni(OH)_2$ formed when sodium hydroxide was used as the precipitant. Furthermore, the substitution of aluminium for nickel in the $Ni(OH)_2$ lattice leads to a hydrotalcite-like compound $[(Ni_6Al_2(OH)_{10}).(CO_3..4H_2O)]$ being formed.

The presence of magnesium oxide, because of its slow release of hydroxyl ions is said to favour higher recovery of the transition elements and improved crystallinity of the precipitate.

Urea, when added to an alkaline system, has been shown to lead to a significant inclusion of intercalated ions and was poorly crystalline. Whereas samples prepared using sodium hydroxide and ammonia showed a high nickel content, low degree of hydration and much less intercalated ions. An IR study has indicated that magnesium-nickel hydroxide precipitates form $Mg(OH)_2$ and β-$Ni(OH)_2$. These mixed hydroxide precipitates are discussed in detail by Harvey *et al*. (2011).

Aluminium oxide is amphoteric, and as such, can neutralise either acids or bases. Because of the oxide ion O^{2-}, which is a powerful proton-accepting base, Al_2O_3 can react with acids as follows:

$$Al_2O_3 + 6H^+ \text{ (aq)} + 9\,H_2O \;\rightarrow\; 2[Al(H_2O_6]^{3+}\text{(aq)}$$
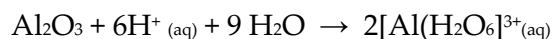
And, whilst the O^{2-} ion has the properties of a base, so the Al^{3+} ion has the properties of an acid, a strong Lewis acid or electron-pair acceptor. Thus, the high concentration of a positive charge on the small Al^{3+} ion makes it able to attract species with ion-pairs, such as OH^- or H_2O. Because both the hydroxyl ion and the water molecule are both Lewis bases, Al^{3+} ions react with the hydroxyl ions and dissolve, thus:

$$Al_2O_3 \text{ (s)} + 2\,OH^- \text{ (aq)} + 7H_2O \;\rightarrow\; 2[Al(H_2O)_2(OH)_4]^{2-} \text{ (aq)}$$
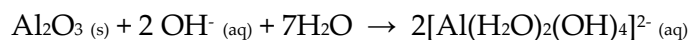
Importantly, the significant contribution to the solution from the aluminium hydroxide or other insoluble anionic species would result in a gel formation. Such aluminium hydroxides and mixed hydroxides and carbonates have been studied (Pacewska *et al*. 2006; Jones 2013; Harvey *et al*. 2011; Steemson 1999). Gelatinous aluminium hydroxide precipitates in the presence of chloride, nitrate or sulphate anions. Hydroxide precipitation commences to form at about pH 4.0 in the presence of sulphate ions and around pH 7.0 in the presence of chloride or nitrates (Sato *et al*. 1980). Based upon the analysis of the single sample of plant ash from Dakhleh Oasis which is provided in Table 5.12, both high sulphates and high chlorides are present strongly supporting aluminium hydroxide gel formation if this plant ash is used as the alkali source.

Separation by crystallisation of the hydroxide gels has been achieved using urea (Van Dijk 1976; Sato *et al*. 1980; Ramesh *et al*. 2003; Yang *et al*. 2010; Yang *et al*. 2012; Ibupoto *et al*. 2014; Ibrahim 2012; al-Sobay *et al*. 2013; Xu and Zeng 2003; Dixit *et al*. 1996). Urea is a non-electrolyte and hydrophilic water structure breaker (Ramakrishna and Rao 2007; Whitney and Tanford 1962; Levine *et al*. 1963; Palma and Morel 1981). The coordination mode of the urea is monodentate through the oxygen atom forming C=O…M angle considerably smaller than 180°, in accordance with the sp2 hybridisation of the O atom (Keuleers *et al*. 2000; Ibrahim 2012).

And, the effect of urea on the speciation of cobalt(II) has been examined by Ramakrishna and Rao (2007) and nickel (II) complexes by Rao and Ramakrishna (2005). And, cobalt and zinc carbonates have been obtained at ~90°C by the reaction of some metal ions in aqueous solution with urea (al-Sobay *et al*. 2013). When precipitated at elevated temperature by

hydrolysis of urea, novel NH_3 intercalated α-type hydroxide can be formed, including α-cobalt hydroxide.

As explained by Yang *et al*. (2012), the formation mechanism for an aluminium-magnesium-urea precipitation from a magnesium-aluminium precursor salt solution, the first stage in the synthesis process involves the formation of an amorphous colloidal aluminium hydroxide gel. Then, the amorphous hydroxides are transformed into the crystallites of oxide-hydroxide aluminium boehmite (γ-AlOOH), accompanied by the continuous incorporation of Mg^{2+} ions into the lamellar sheet structure creating a charge imbalance. This charge imbalance of the sheet destroys the hydrogen bonds existing between the sheets and subsequently carbonate ions in the solution are intercalated into the interlayer galleries by an electrostatic interaction to balance the electron charge. These layered double hydroxide, hydrotalcite-like compounds, have as a general chemical composition $[M^{2+}_{1-x}M^{3+}_x(OH)_2]-(A^{n-})_{x/n}.mH_2O$, where A^{n-} is an interlayer anion with a charge n, and x is the $(M^{3+})/(M^{2+}+M^{3+})$ molar fraction. Thus, the layered double hydroxide structure is related therefore to brucite, $Mg(OH)_2$, which consists of infinite sheets of edge-sharing MgO_6 octahedra.

Whilst the Egyptian workers did not have the chemical controls over their chemical syntheses, neither did the workers discussed by Agricola (1556) or in England in the 1600s. However, they had a readily available source of urea, namely human urine. Putnam (1971) analysed human urine and concluded that its pH ranged from 6.3 to 8.3, Total Dissolved Solids (TDS) was 37 g/Kg, with urea representing some 13.5 g/Kg and ammonia concentration ranging from 200-730 mg/l. Ibrahim (2012) reported that the average human excretes about 30 g/day of urea in urine.

5.8.1.1 *Urine (urea/ammonia) precipitation: research hypothesis*

Urine did have known uses in Egypt in the 18th Dynasty, particularly in gold purification (Ogden 2000: 165) and in the tanning of animal skins (Van Driel-Murray 2000: 303, 316) and it provided an excellent source of urea. Alum was also widely used in medicines, mummification, etc. Therefore, it is conceivable that the use of urine to form a metal-urea-hydroxide (via ammonia) or a metal-urea-carbonate precipitate was a likely method for its concentration, crystallisation and effective purification of cobalt in Egypt during the 18th Dynasty. Urine (urea) would have acted as a hydrophilic aluminium hydroxide gel- or water-breaker thereby enabling crystallisation to proceed more rapidly. Thus, as suggested by Warachim *et al*. (1985), ammonia precipitation would enable aluminium, magnesium and the transition metals to be recovered effectively as a mixed metal–urea-hydroxide. As explained above, magnesium would have assisted in the formation of the precipitate. And, as shown in Table 5.22, ammonium and potash alums offer much lower solubility in cold water and therefore more readily crystallise from solution.

The work of Sato *et al*. (1980) is instructive. These workers investigated heating an aluminium sulphate (i.e., alum) solution at 95°C with urea for a given period of time and compared the results with those obtained by heating aluminium chloride and aluminium nitrate solutions under the same conditions. They reported that the pH value of the solution

gradually increases, rises steeply at pH 4.0-7.5 and finally approaches a constant value. The effect of the anionic species provided different outcomes. The pH of the aluminium sulphate solution is independent of the salt concentration and on heating the pH value increase gradually up to 3.5-4.0; precipitation commenced at pH 4.0. The precipitate formed was reported to be granular and filterable, not the more gelatinous precipitate obtained with the chloride and nitrate solutions. They noted that Vermeulen *et al*. (1978) had suggested that the presence of the sulphate ion had acted as a catalyst in the formation of the precipitate. Furthermore, they reported that there is no evidence for the presence of basic aluminium sulphate, i.e., the concentration of sulphate ions in the precipitate is <1% and decreases with extended heating time.

It is well-known that cobalt hydroxide has two polymorphs, α- and β-Co(OH)$_2$. These two phases are hexagonal layered structures, the α-hydroxide being metastable and age rapidly to the β-hydroxide on aging or in alkaline solutions. The β form is isostructural with brucite-like compounds and consist of a hexagonal packing of hydroxyl ions with Co^{2+} occupying alternate rows of octahedral sites. And, the α-Co(OH)$_2$ is isostructural with hydrotalcite-like compounds that consist of stacked Co(OH)$_{2-x}$ layers intercalated with various anions, such as carbonate in the interlayer space to restore charge neutrality (Liu *et al*. 2008). Dixit *et al*. (1996) examined the precipitation of cobalt and nickel hydroxides by hydrolysis of urea to form novel hydroxide phases and fine particle materials. They reported the presence of intercalated anions and particularly among urea hydrolysis reactions including ammonia. The thermal decomposition of these hydroxide compounds led to the formation of NiO and Co$_3$O$_4$.

Importantly, this "quantitative" precipitation would have approximated the composition of the magnesia, alumina and transition metals found in the cobalt-based pigments as indicated in Tables 5.7 and 5.8. The mixed hydroxide precipitate (MHP) containing the co-precipitated transition metals would have been decanted, removing almost all of the sulphate ions. Then dried and combined with desert sand, (with any contained calcium) and plant ash (probably as kiln or oven ash and which can contain sufficient calcium as indicated in Tables 5.11 and 5.12) or less likely, trona as the alkali flux and then heated to about 1000°C to form a cobalt- nickel- zinc-based glassy structure as a frit with a composition similar to the cobalt pigment analysis provided in Tables 5.7 and 5.8. It is alternatively possible that the MHP could have been mixed with powdered raw glass and then calcined to form the mixed cobalt pigment frit. However, the low soda concentration found in the cobalt complex would suggest that this methodology was not adopted.

The results provided herein, support the precipitation route as confirmed by the presence of all of the precipitated transition elements together with aluminium and magnesium. The process would therefore have emulated the process for the production of Egyptian blue with the copper being replaced by the cobalt mixed hydroxide precipitate and the trona flux by plant ash as the flux. The use of desert sand together with an alkali flux was well established technology for Egyptian blue production. Thus, the similar use of desert sand, an alkali flux (plant, biomass or kiln ash) and the cobalt precipitate when fired would, in a similar manner, have produced the cobalt blue pigment in a fritted form.

The use of kiln ash, as indicated by the significant number of bone ash particles observed and shown in Appendix A5 (images and analyses) and in Figures 5.44 to 5.47 above, would have provided the source for the potassium derived from combustion of the plant biomass used to fire the kilns or cooking ovens (refer to Tables 5.11 and 5.12) (Henderson 1989). Halfa grass was evidently used to fire the kilns at Kom Helul, Memphis, during the Roman period for faience production (Nicholson 2013: 59); and the salt-resistant halophytic plants of the genus *Salsola* (Tite *et al*. 2006) and *Salicornia* Henderson 1989) have also been proposed as a suitable source for plant ash. Nicholson and Henderson (2000: 214) also noted the use of plant ash at Amarna. A range of plant-based ash material from various regions throughout the Mediterranean region is provided in Table 5.11. The analysis of plant ash from vegetation growing within the Dakhleh Oasis is provided in Table 5.12, Section 5.4.2.2.1.. In respect of the use of these plant ashes, consideration must be given to their method of application. Namely, were they added without modification (other than possible sieving), or were they dissolved in water and the soluble salts separated and then evaporated to dryness and used? Or, was the plant ash washed before use? Caley (1962: 81), on the basis of previous work conducted by Turner, suggested that possibly the fuel ash employed to melt the glass was directly incorporated into successive batches as one of the raw materials. The presence of bone ash particles containing fluorine as demonstrated in Figure 5.44 supports the direct application of the kiln ash.

Thus, the coarse cobalt glassy frit would then have been powdered and directly applied to the surface of the vessel using a suitable binder as discussed in Section 5.7. The vessel itself may have had a slip coating applied directly to its surface to improve adhesion or to provide a visually brighter undercoat.

5.8.1.2 *Thermal conversion of MHP into a cobalt frit*

The thermal decomposition of aluminium sulphate (Truex *et al*. 1977; Chou and Soong 1984; Apte *et al*. 1988), of aluminium carbonate (Morinaga *et al*. 2000), of the aluminium and magnesium hydroxide (Chen *et al*. 1989; Sato 1985; Zeng *et al*. 1997), sodium aluminium sulphate (Pelovski *et al*. 1995) and of nickel-aluminium mixed hydrotalcite-type precursors (Clause *et al*. 1992) have been studied.

In the thermal decomposition of aluminium sulphate at temperatures between $500 - 700 °C$ with, or without oxygen, results in the formation of sulphur trioxide:

$$Al_2(SO_4)_3 \;\leftrightarrow\; Al_2O_3 + 3SO_3$$
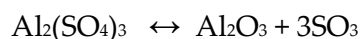
The movement of the reactant-product interface in a decomposition reaction is controlled by heat and mass transfer, rather than by the chemical bond-breaking reaction. The heat is transported by conduction from the surface through the product layer to the reaction interface, and the gaseous product then moves counter-currently by outward diffusion.

Bretsznajder and Pysick (1965) demonstrated that ammonium aluminium sulphate undergoes a step-wise decomposition in which water, ammonia and sulphur trioxide are sequentially evolved with increasing temperature. Evolution of residual water and

ammonia commenced at 400-470°C and is diffusion controlled. Above 470°C the reaction increases rapidly and above 860°C decomposition of anhydrous $3Al_2O_3.4SO_3$ commences. Below 860°C, the reaction is retarded by the diffusion of gaseous decomposition products through the grains of the solid Al_2O_3 produced. It has been reported by Apte *et al*. (1988) that the activation energies for sulphate decomposition starting with ammonium alum is about 10% higher than for aluminium sulphate. And they reported that at 900°C, the final weight loss values observed were 82% for aluminium sulphate, 87% for ammonium alum, 69% for potash alum and 48% for the mineral, alunite $[KAl_3(SO_4)_2(OH)_6]$.

Ingo *et al*. (1998) have shown that the thermal decomposition of calcium sulphate commenced at 1240°C. However, in the presence of silica, thermal decomposition commenced at about 990°C and is practically complete at 1260°C. Therefore, as these temperatures are at the thermal limit of the Egyptian pottery reaction vessels in use at that time could sustain, calcium sulphate if present, is unlikely to enter into any significant reaction with any of the other raw materials and unvolatilised sulphate would remain as unreacted calcium sulphate surface dross.

Pelovski *et al*. (1995) studied the thermal decomposition of sodium aluminium sulphate. They reported that heating in air up to a temperature of 631 K about 11 moles of water per mole of sulphate were evolved. The desulphurisation reaction commenced above 873 K, with the maximum decomposition rate occurring at 1025 K. The overall mass loss is 64.5% which corresponds to a desulphurisation of 97.6% to form Na_2SO_4 and Al_2O_3. Then, in the temperature range 983-1113 K sodium sulphate decomposes. Although, Perry and Greene (1984: 3.10-3.22) suggest 1100°C and Tite *et a*l. (2006) quote ~1200°C.

In heating ammonium aluminium carbonate hydroxide, various transformations were observed by Morinaga *et al*. (2000); namely the formation of amorphous alumina, crystallisation of γ-Al_2O_3 (if the powder is annealed for 6 hours at 1073 K (800°C)), and to finally α-Al_2O_3 at 1423 K.

Thermal decomposition of gelatinous aluminium hydroxides at 110°C indicated that the loss of adhesive water molecules led to observable peak losses in the IR spectrum. At about 130°C the DTA curve exhibits a very strong endothermic peak due to the release of adhesive water and a very broad endothermic reaction centred around 250-300°C resulting from the thermal decomposition of aluminium hydroxide to amorphous alumina. Then, depending upon the time/temperature, various intermediates can form and which can then convert to α-Al_2O_3 at temperatures ranging from 1100-1140°C (Sato 1985). Chen *et al*. (1989) reported that with a mixed aluminium hydroxide-magnesium hydroxide that the thermal decomposition from hydroxides to oxides occurred between 623-823 K for aluminium hydroxide and 736-1006 K for magnesium hydroxide, and above the respective thermal maxima, no further reaction was observed.

In studying mixed nickel-aluminium hydroxides, Clause *et a*l. (1992) concluded that after calcining, the formation of nickel oxide and Ni-doped alumina phases in strong interaction with partially decomposed precursor layers or with a spinel-type phase occurred at the NiO-Al_2O_3 interface. The latter phase was considered to be responsible for the thermal

stabilisation of the nickel oxide phase. Such an observation is important, in-so-far that as reported in Table 5.9, such complexes are suggested to have formed in isolated instances. As such, this reaction, together with that of cobalt under similar conditions, and with, or without zinc should be carefully examined.

Smirniou and Rehren (2011) stated that it is still uncertain whether the colourant was mixed with the initial raw materials or added to the crushed semi-finished glass during a second stage, or whether a third stage heating was required in which the colourant was added. To further elucidate the likelihood for the use during the 18th Dynasty of a high temperature approach Rehren and co-workers have investigated glass production at temperatures of up to 1050°C, this being the maximum temperature that the pottery vessels used for glass manufacture during the 18th Dynasty could withstand. Aspects such as the alkali metal and alkaline earth partitioning and the transfer of these fluxes into the glass were investigated (Rehren 2008; Tanimoto and Rehren 2008; Smirniou and Rehren 2011). Rehren (2008) concluded that more work is required before the various factors involved in glass and faience production and therefore, by extension, cobalt pigment production can be fully understood.

5.8.2 *Pyrometallurgy, alternative formation of the cobalt pigment*

In examining the chemistry of the various coloured glasses produced in Near Eastern Late Bronze Age, Rehren (2001) observed that the cobalt glasses were unique in their composition. These cobalt glasses are characterised by significantly higher concentrations of Al_2O_3 and lower concentrations of K_2O when compared with other glasses. As shown in Table 5.2, both the Dakhleh Oasis sample D1A and the Kharga Oasis sample K18b contain little to no K_2O but in the order of 20% alumina. Rehren also observed that the glasses containing this cobalt colorant were higher in aluminium but with a greatly reduced potash content. He therefore questioned how the addition of the cobalt colourant could have reduced the potash content in the glass.

This perceived inconsistency led him to further investigate the methods by which the cobalt might have been extracted from the alum or if the alum was used as a direct source of cobalt. He suggested that the methods proposed up to the year 2001 fail to explain how the colorant was actually added to the glass and in particular, to address the nature of the raw materials used, and the problems of salt melt and glass melt interaction if the cobalt-containing alum was directly added to the glass. With a direct addition of alum, then the partitioning of the pigments between the two phases created would require further investigation.

The diagnostic criteria for the separation of glasses based upon plant ash and soda-based glasses is the approximate 2-3% higher content of K_2O and MgO in the plant ash glasses. Shugar and Rehren (2002) reported that in considering soda-lime-silica glass production over a period of some 2000 years that two compositional groups prevailed. The first type of glass was high in magnesium and potash, plant ash based, and described as Late Bronze Age (LBA) Egyptian and Mesopotamian glass. The second type of glass identified was low in magnesium and potash, and described as natron-based Hellenistic and Roman glass. To further understand the various relationships, these workers investigated a smelting model

that included the formation of a cotectic glass melt in the presence of a considerable quantity of crystalline material to act as a buffer. In their investigation of chlorine they determined that it did not act as a thermometer as the concentration of calcium oxide controls the chlorine uptake and not temperature or the soda content.

Thus, Rehren (2001) reported that from his perspective, the various alternative models are all lacking in essential detail. In particular, the thermal process lacks an explanation for the lower potash content in these glasses when compared with their counter-parts coloured using alternative colouring agents. He considered the Shortland and Tite (2000) proposal that the consistency in the ratios of cobalt to the other transition metal elements present in the alums and in the cobalt glass itself would suggest that the cobalt was not concentrated with respect to the accompanying transition metal elements, but that alum from Kharga was added with minimal processing, to the glass. As the alum contained low potash, it was therefore seen by Rehren to overcome the perceived potash "problem". However, Rehren suggested that a number of other issues remained unresolved or were not addressed by this direct addition process.

The suggestion by Shortland and Tite (2000) that by starting with natron-based glass, poor in potash and magnesia, that the final glass composition could have its magnesia and alumina concentrations raised through the addition of the cobalt-bearing alum. Rehren stated that the direct addition of cobalt-containing alum directly with a glass would require an approximate 50:50 mixture of alum and glass and he saw partioning problems between the glass and the sulphur and chlorine. And, as the magnesium sulphate would only decompose at 1124°C or the sodium sulphate at >1100°C as discussed in Chapter 4, Section 4.5.2.5.2, this would create an additional problem which was not addressed by Shortland and Tite. And, furthermore, this concept fails to explain why this natron-based glass production remained restricted to one colour only. It required the addition of unprocessed salt in order to adjust the ratio of MgO to CoO; and it does not discuss the implications of mixing these sulphate salts and glass at melting temperatures. The subsequent decomposition of such salts at glass melting temperatures, and the different ratios of MgO to Al_2O_3 in the alum and the glass respectively also requires explanation.

Tite and Shortland (2003) discussed the work of Rehren (2001) and reported that based upon the variation in the decomposition temperatures of aluminium sulphate and magnesium sulphate, there would be a preferential partitioning of alumina over the magnesia depending upon whether or not the two sulphates decomposed separately or at the same temperature. To date, no residual slag from the resultant salt phase has been reported in the literature and as stated by Rehren, too little is known about the relevant pyrometallurgical systems. He therefore considered the concept to be purely speculative and as such, he could not take this proposal further.

As reported by Rehren (2001), the precipitate, or concentrate method originally proposed by Noll (1981) and later adopted by Kaczmarczyk (1986) was favoured, but he still considered that the potash issue had not been addressed. He suggested that the concentrate was therefore related to the dark blue cobalt aluminium spinel to have been found on the blue painted pottery during the New Kingdom and as such, would have been an almost ideal

colorant for plant ash based glass. Rehren favoured the use of natron as the precipitant as did Noll (1981a) as this would decrease the final solution pH at which precipitation would occur, allowing the transition elements and some of the aluminium but probably none of the magnesium to precipitate. Whereas, based upon the data provided by Eggeman (2001), a 1% solution of sodium carbonate would have resulted in a total precipitation of all of the contained metals. This is confirmed by the Monhemius hydroxide precipitation diagram provided in Figure 5.60 and the Pourbaix Diagrams provided in Figures 5.61 to 5.65.

The analyses for the cobalt blue pigments given in Table 5.7 and 5.8 require the presence of magnesium in concentrations greater than that directly obtainable from plant ash. And, as shown above, at the solution pH developed by trona or natron, all of the magnesium and transition elements would have been present in the alumina-based mixed hydroxide precipitate (MHP). Therefore, as previously stated, the present work would suggest that natron (trona) alone would not have been the sole precipitant as it does not contain either high potash or magnesia (or calcium if the local sand is low in calcium and therefore a supply of this element is required). However, the glass into which the pigment-based cobalt-containing frit may have been incorporated would have contained soda.

Thus, the dissolution, and subsequent mixed hydroxide-urea precipitate outlined in 5.8.1 and for which the average elemental analysis is provided in Table 5.8 when incorporated into either an uncoloured glass, or a silica plus plant ash composition, would have provided the low potash glass frit as required by Rehren (2000). An addition of <20% of the cobalt blue pigment to the glass would have been sufficient to achieve the Amana blue glass formulae given in Table 5.24. This frit, used to decorate vessels throughout Egypt would therefore now appear to be the ideal starting material for the production of cobalt-based glass in Egypt during, and particularly subsequent to, the 18th Dynasty. It would be infinitely miscible in a bulk glass composition and could be readily melted and blended into the molten base glass.

5.8.3 Cobalt pigment deterioration

Raman spectroscopy has demonstrated, particularly in Section 5.4 and in Table 5.9, that the chemistry of the cobalt pigments is far more complex than the simple cobalt aluminate hypothesised by Riederer (1974), Noll and Hangst (1975), Bachmann *et al.* (1980), Noll (1981b), Shortland *et al.* (2006a), Abe (2009) and which were hypothesised based upon either limited elemental analyses or XRD analyses. XRD analyses, as discussed by Shortland (2006a), had difficulty in separating the cobalt aluminate from competing minerals. Furthermore, Srisawad *et al.* (2012) and Ji *et al.* (2000) reported that XRD peaks assigned to $CoAl_2O_4$ could be alternatively assigned to Co_3O_4 because their respective peak positions are almost identical. Both minerals have the same spinel cubic crystallographic structure with slight differences in the lattice constant ($a = 8.111$ for $CoAl_2O_4$ and $a = 8.0885$ for Co_3O_4). This alternative spinel was not considered by any of the earlier researchers. And, Fernandez-Osorio *et al.* (2010) reported that nano-sized $Zn_{1-x}Co_xAl_2O_4$ formed a normal spinel with Co^{2+} situated at the tetrahedral site, however, the optical spectra of the nano-sized particles are coherent with a hexa-coordinated Co^{2+} ion. Whereas, the bulk system exhibited the expected intense bonds attributable to the transition of Co^{2+} in a 4-fold coordination.

The system is complex as both a number of different cobalt minerals which may have been produced in the original manufacturing process, or, subsequent atmospheric or burial conditions may have further modified the mineral surfaces. As previously noted, the cobalt hydroxide present in the MHP on heating to an elevated temperature may have entered into reactions with accompanying minerals to form aluminates, olivines, spinels, pyroxenes, Zn-Co spinels or other mineral forms.

In considering the potential reactions capable of occurring during the initial production of the cobalt blue pigment, the role of the spinel formation, the partial replacement of magnesium in the crystal structure by cobalt and the transition metal elements present in the alum to form a pyroxene, the non-stoichiometric ratio of cobalt and the additional transition metal elements with alumina or silica, the role of zinc in the MHP, the flux added, the cobalt valency state(s), the kiln redox conditions, kiln temperature, kiln atmosphere, and time are all variables which can impact upon the product formed.

The decomposition of the cobalt mineralisation is complex. Its deterioration within the atmosphere or under burial conditions to which the sherds may have undergone over the past 2000 to 3500 years is equally complex and would be a significant study in itself. It will only be discussed briefly herein.

In the final stage sintering of magnesium aluminate (spinel, *sensu stricto*) Ting and Lu (2000) have demonstrated that the ratio of MgO-excess, stoichiometric and Al_2O_3-excess when heated in air or under low oxygen partial pressure that densification enhancement of the surface caused by MgO evaporation, generate oxygen vacancies in the host crystal lattice. Air sintering, as would have occurred in Egyptian production at that time, consistently gave a higher MgO loss. These researchers considered that cation vacancies were thought to be the principal charge-compensating defects rather than oxygen vacancies.

The structure defects and stability of different terminations of the surface of cobalt spinel under various redox conditions imposed by different oxygen partial pressures and temperature were studied by Zasada *et al*. (2015). Under reducing conditions the surface is readily reduced by the formation of oxygen vacancies; whereas, under oxidising conditions co-existence of stoichiometric and over-stoichiometric were observed. Formation of the oxygen vacancies involves reduction of the octahedral trivalent cobalt and is accompanied by the divalent tetrahedral cobalt into empty interstitial octahedral positions. In the case of cobalt-depleted surfaces, the octahedral vacancies are thermodynamically unfavourable with respect to the tetrahedral ones in the whole range of temperature and oxygen pressures examined. The perturbation of the normal Co_3O_4 structure by partial inversion is favoured at higher temperatures and involves the transfer of electrons from divalent cobalt cations to trivalent cobalt cations giving rise to the appearance of a fraction of the Co^{3+} ions in the A sites and Co^{2+} in B sites. The off-stoichiometric spinels in turn form a cation vacancy. This complex reactivity is explained in more detail by Zasada *et al*. (2015) and it provides the evidence for the future mineral surface instability.

In the firing of these MHP complexes in the presence of aluminium hydroxide to form a spinel the rate follows the sequence $FeAl_2O_4 < NiAl_2O_4 < CoAl_2O_4 < CuAl_2O_4$. Penetration of

transition metal ions into the γ-Al_2O_3 is noted to occur at considerably lower temperatures than with α-Al_2O_4 substrates mainly due to grain boundary diffusion (Bolt *et al*. 1998). They reported that annealing of the Co_3O_4/α-Al_2O_3 at 1000°C for 20 hours, the reaction had almost gone to completion. And with γ-Al_2O_3 in air at 900°C that the γ-Al_2O_3 is much more highly reactive. Using XRD to monitor the reaction proved to be difficult due to the fact that $CoAl_2O_4$ diffraction peaks have almost the same position as the broad γ-Al_2O_3 peaks. Formation of α-Al_2O_3 was not observed after annealing at temperatures up to 900°C. They did observe that after 5 hours at 900°C, the transformation of γ-Al_2O_3 to θ-Al_2O_3 is accelerated by cobalt ions. With nickel oxide on alumina, longer reaction times were required, but pale blue $NiAl_2O_4$ did form.

Other spinels are known to form inverse spinels in which the octahedral sites are occupied by B cations, while the octahedral sites are occupied by equal numbers of A and B atoms. Intermediate phases with the formula $(A_{1-x}B_x)[A_xB_{2-x}]O_4$ also exist. Here the cation in () brackets occupy tetrahedral sites and the cations in [] brackets occupy the octahedral sites (Wei 2000).

Beale and Sankar (2006) used a combined QEXAFS/XRD to study the surface reactions of cobalt on zeolites. They indicated that the cobalt will preferentially ion-exchange on to Al^{3+} rather than Si^{4+} tetrahedra. After heating to above 860°C $CoAl_2O_4$ spinel formed together with minor amounts of the secondary phase Co_2SiO_4. Because the cobalt environment in both the amorphous state and the final $CoAl_2O_4$ is tetrahedral, it is difficult to know what proportion of this is in the final crystalline material and what remains as part of the amorphous state. It is also possible to interpret this amorphous portion as a poorly crystalline spinel phase. This would suggest that cobalt aluminate would have been preferentially prepared, but some olivine would have also been produced.

The decomposition of ferrous, cobalt (II) and nickel (II) hydroxides has been studied by Hazell and Irving (1966) and they expected that these brucite structures would all decompose according to the equation:

$$M(OH)_2 \rightarrow MO + H_2O$$
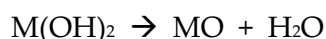
where M = Fe, Co, Ni

In the case of iron, ferrous hydroxide is unstable and reacts with water to form magnetite. Heating magnetite in air at 180°C, it will undergo further decomposition to form maghemite and finally hematite. These researchers reported that nickel formed a more crystalline hydroxide product. And, in the production of cobalt hydroxide, oxidation led to cobalt preferring to form an oxidation product. Furthermore, for cobalt and nickel , the M(III) state is less stable than the M(II) state and the crystal field and other effects associated with the spinel structure are not great enough to stabilise the trivalent state. As provided in Table 5.7, all pigments contained >5% FeO and therefore this element needs to be considered as it is capable of modifying the pigment colour.

In a study by Swaddle and Oltmann (1980), they reported that the presence of water is necessary for the oxidation of magnetite to maghemite, probably because the cation

vacancies in the pseudo-spinel lattice can be stabilised by the occupation of some, or all, of the vacant octahedral sites by H^+ up to a limiting composition HFe_5O_8 and indeed, virtually all maghemite samples appear to contain some bound water.   The presence of water is suggested to facilitate the conversion of maghemite to hematite.

The rate of hydrothermal decomposition of maghemite is strongly retarded by silica. The conversion of magnetite to maghemite occurred in the "dry" state in air after 15 minutes at 180°C, whereas, under hydrothermal conditions at 180°C in air the reaction was incomplete with the conversion to hematite being 99% complete in 12 hours in a silica free environment. And, coarsely-crystalline magnetite underwent "dry" oxidation in moist air directly to hematite, whereas, fine-particulate $Fe_{3-x}O_{4-x}$ oxidised rapidly to maghemite. With well-crystallised magnetite only a 2% conversion to hematite occurred at 260°C after 24 hours, and maghemite decomposed only to the extent of 5% at 400°C, with 50% resulting after 24 hours and 95% after 4 days. The iron is also capable of forming a ferrite. The Fe, Ni and Mn ferrite spinel-type structure have been investigated by Graves *et al*. (1980) using Raman spectroscopy.

The presence of cobalt oxyhydroxide (CoOOH) is considered as a non-stoichiometric oxyhydroxide and has a higher oxidation state (Co^{3+}) than Co_3O_4 and blue cobalt hydroxide [$Co(OH)_2$]. Both were determined by Raman spectroscopy. These minerals have also been studied by Yang *et al.* (2011) where synthesis was achieved using urea in a sodium phosphate solution. Such a reaction could have occurred if the urine precipitation route proposed in Section 5.8.2 had been employed. These minerals, such as cobalt oxyhydroxy carbonate [$Co_2CO_3(OH)_2$] belong to the rosasite mineral group with the general formula $A_2(CO_3)(OH)_2$ or $AB(CO_3)(OH)_2$ where A and B is cobalt. copper, magnesium nickel and zinc.

Cobalt oxide hydroxide [$HCoO_2$] is a hexagonal layered structure whose stacking unit is composed of two dimensionally connected [CoO_6]$^{9-}$ planes bonded to each other by H-bonds. This compound has been shown by Kittaka *et al*. (1989) to decompose over the temperature range 244-312°C regardless of whether in air or under nitrogen.

Amongst the cobaltites, Klissurski and Uzunova (1993) reported that zinc cobaltite has the highest thermal stability.   They reported its synthesis by the thermal decomposition of a hydroxide-carbonate precursor obtained by co-precipitation at pH 9 and its decomposition at 300°C. They also reported a second endothermal transition that corresponded to the transformation spinel to give a rock-salt structure:

$$Zn_xCo_{3-x}O_4 \rightarrow (Zn,Co)O + ZnO + O_2$$
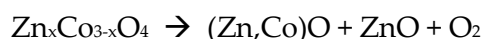
Such a reaction could explain the presence of the zinc oxide in the cobalt pigment as reported in Table 5.9.

According to Liotta *et al.* (2003) the presence of Co^{2+} species tetrahedrally and octahedrally coordinated appears strongly influenced by the nature of the alumina support and the cobalt concentration. They were prepared by the wet impregnation of a solution of a cobalt salt at

room temperature on alumina and calcined at 500°C for 5 hours forming Co_3O_4 particles. A successive thermal treatment at 800°C promotes the dispersion of Co_3O_4 clusters in the network of alumina with formation of $CoAl_2O_4$ spinels. And, as demonstrated by Srisawad *et al.* (2012) the relative amount of Co^{2+} ions in octahedral sites was found to increase with increasing temperature.

Wang *et al.* (2006) reported that cobalt spinels always agglomerate regardless of the calcination temperature . They observed that cobalt spinel formation commenced at 200°C and XRD indicated the presence of both Co_3O_4 and CoO and at temperatures above 500°C only Co_3O_4 remains.

Markov *et al.* (1986) and Petrov *et al.* (1988) have shown that the composition $Zn_{0.33}Co_{0.67}(OH)_2$ this brucite-like structure shows bands characteristic of octahedrally coordinated Co^{2+} ions only. Thermal decomposition leads to the formation of a partially invers spinel with the cationic distribution $(Zn_{0.56}Co_{0.44})\{Zn_{0.44}Co_{0.56}\}O_4$.

5.9 Cobalt glass and/or frit usage

Comparisons have been made by Shortland *et al.* (2006; 2006a) with respect to the similarities and differences between the blue pigment applied to decorate vessels and the contemporaneously produced cobalt-containing glasses. Their results for glass recovered at Amarna are provided in Table 5.24.

Based upon the mineralogy and the elemental analysis of these cobalt pigments it is feasible that their admixture with a glass and subsequent melting could have provided the conditions discussed by Shugar and Rehren (2002) for cobalt glass production. More work will be required to confirm such a hypothesis.

Table 5.24. Elemental analyses of glass from Amarna (Tite and Shortland 2003).

Na₂O	MgO	Al₂O₃	SiO₂	P₂O₅	SO₃	Cl	K₂O	CaO	TiO₂	MnO₂	FeO	CoO	NiO	CuO	ZnO
Average elemental analysis, cobalt blue glass, Amarna frits.
12.2	2.0	4.6	78.0	#	#	#	0.6	1.0	0.2	0.4	0.7	0.3	#	0.0	#
Corrected average elemental analysis, copper-coloured glass, Amarna frits.
13.9	0.8	1.5	73.9	#	#	#	1.5	1.0	0.1	0.1	0.8	0.01	#	6.3	#
Average elemental analysis, cobalt faience, Amarna.
9.9	1.9	6.3	77.1	#	#	#	1.9	1.2	#	0.5	0.7	0.5	#	0.1	#

#Analysis not provided. Results stated as normalised to 100%.

5.9.1 Cobalt pigment in glass coloration

Shortland and Tite (2000) undertook a study into copper- and cobalt-blue frit, glass and faience from the 18th Dynasty New Kingdom site at Amarna. In discussing the glass samples they found at Amarna, they suggested that different alkali raw materials were used for the production of the cobalt-containing glass and the copper-containing glass. They noted that

in the copper- and the cobalt-blue vitreous materials the copper-blue is significantly lower in magnesium and alumina than that found in the cobalt blue glasses. Furthermore, Kaczmarczyk (1986) had reported that the cobalt glass was also associated with nickel, zinc, and manganese and the presence of these metals could serve as a tentative provenance for the colourant source. These authors suggested that the copper-containing glass was manufactured using plant ash and the cobalt-containing glass used natron. They did not comment upon the method for concentrating the cobalt and/or its conversion into an olivine, pyroxene or an Al- or Mg-spinel. Furthermore, Shortland and Tite (2000) proposed that the cobalt-bearing alum was directly added to a raw glass of a unique composition, different to that used for all other coloured glasses. The alkali source for Egyptian glasses is generally considered to be plant ash-based and which introduces a few per cent of elements such as K and Mg into the glass. By way of contrast, Shortland and Tite noted that soda-rich glass with less than 1% of K and Mg is generally considered to have been derived using the mineral natron as the alkali source (Henderson 1985; Freestone 1987; Freestone and Gorin-Rosen 1999).

The diagnostic criteria for the separation of glasses based upon plant ash and soda-based glasses is the approximate 2-3% higher content of each of K_2O and MgO in the plant ash glasses. Shugar and Rehren (2002) reported that in considering soda-lime-silica glass production over a period of some 2000 years that two compositional groups prevailed. The first type of glass was high in magnesium and potash, plant ash based and described as Late Bronze Age (LBA) Egyptian and Mesopotamian glass. The second type of glass identified was low in magnesium and potash, natron-based Hellenistic and Roman glass. To further understand the various relationships, these workers investigated a smelting model that included the formation of a cotectic glass melt in the presence of a considerable quantity of crystalline material to act as a buffer. They investigated chlorine and determined that it did not act as a thermometer as the concentration of calcium oxide controls the chlorine uptake and not temperature or the soda content.

Tite and Shortland (2003) considered the various proposed technologies, namely;
- direct high temperature addition as discussed by Rehren;
- an alternative hydroxide precipitation process;
- and finally a two stage process as proposed by Turner (1956) in which a cobalt frit was formed and that this was added to the glass.

They concluded that probably four different plant ashes were employed for the production of copper- and cobalt-blue glasses at Amarna. Furthermore, that natron was the more likely alkali used to precipitate the cobalt and therefore that natron would have also been used in the production of a cobalt-containing frit. These workers stated that depending upon whether the supernatant liquid was decanted or allowed to evaporate, that this would have influenced the concentration of magnesium hydroxide in the precipitate and also the incorporation of natron into the frit. The solution pH employed was not stated; however, as discussed above, at the solution pH probably employed, all of the magnesium would have precipitated, leaving no magnesium in solution to be decanted. This frit would have then been formed into a glass using additional plant ash and quartz. These researchers then proposed that further work should be conducted in an effort to increase the understanding of the raw materials used and the production techniques adopted. The present research

hypothesis is that the cobalt blue frit was prepared at Dakhleh Oasis and not at Amarna. It is probable that this cobalt blue frit would have been incorporated as a colourant into local glass production.

5.9.1.1 *Dakhleh Oasis blue glass samples*

Glass sherds from Kellis, listed in Chapter 1 and presently dated to 3-4th century CE have been examined. The results are provided in Appendix A5.

5.9.1.1.1 Glass, results and discussion.

The average analytical results are reported below. All Raman spectroscopy and SEM-EDS results are provided in Appendix A5.

Table 5.25. Average elemental analysis in various blue glass samples from Kellis.:

Average elemental analysis, A/6/93/393 blue glass, Kellis, Sample 2, FIB EDS analysis															
Na$_2$O	**MgO**	**Al$_2$O$_3$**	**SiO$_2$**	**P$_2$O$_5$**	**SO$_3$**	**Cl**	**K$_2$O**	**CaO**	**TiO$_2$**	**MnO$_2$**	**FeO**	**CoO**	**NiO**	**CuO**	**ZnO**
2.9	1.4	3.8	79.2	0.3	0.3	0.5	1.7	6.1	0.2	0.0	2.1	0.3	0.0	0.4	0.0
Average elemental analysis, A/6/93/514 blue glass, Kellis, Sample 1, FIB EDS analysis															
2.6	1.2	4.6	76.7	0.0	0.8	1.4	1.9	5.8	0.0	0.1	0.9	0.2	0.2	3.6	0.3
Average elemental analysis, Dayr Abu Matta, DAM [12] Trench 13 JM. 8/1/11-S11.008 blue glass[5], FIB EDS analysis.															
3.4	0.9	3.4	78.7	tr	1.3	1.6	1.5	8.0	0.1	tr	0.8	0.1	tr	0.2	0.0
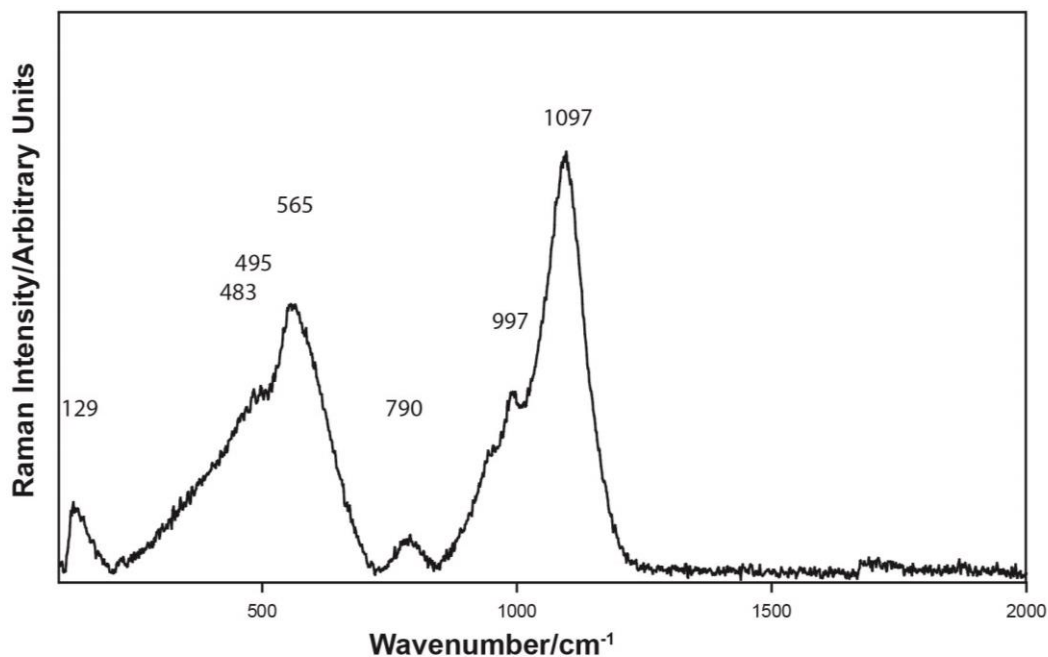
Figure 5.66. Raman spectrum, blue glass sample A/6/93.393 Room 4 (3) ($\lambda = 514.5$ nm).

---

[5]Dr. Bowen indicated that the sample was recovered from Dayr Abu Matta, Dakhleh Oasis (Pers. Comm. 06/05/2013). She is thanked for providing the sample.
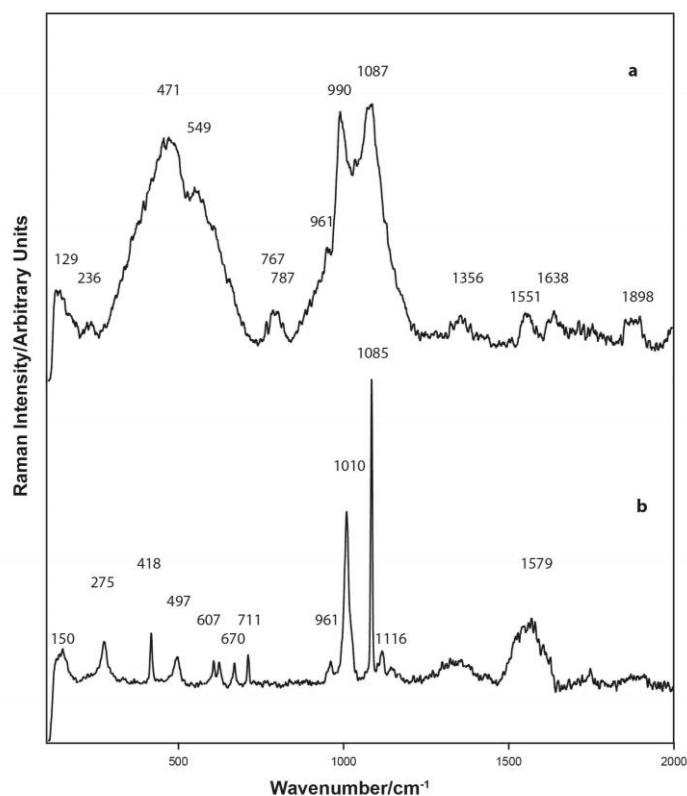
Figure 5.67. Raman spectra, (a) blue glass sample, Dayr Abu Matta, (b) post manufacture calcite deposit on surface of sample ($\lambda = 514.5$ nm).

The analyses of the cobalt blue glass samples are provided in Table 5.25 and in Appendix A5. These samples are low in soda (<4.0% Na_2O possibly related to surface leaching) and low in magnesia (<1.5% MgO), although, the likely surface leaching of alkalis would compromise the analyses. Consideration was given to sectioning the glass and epoxy mounting samples to enable the core of the glass to be analysed. This was dismissed as it would have destroyed the integrity of the glass sherds. The Raman spectrum for Kellis Sample 2 (A/6/93.393) is provided in Figure 5.66 and Dayr Abu Matta, Sample 13, in Figure 5.67.

Shortland and Tite (2000) indicated that glass from 1500-800 BCE in the Eastern Mediterranean, Egypt and Mesopotamia was of the high magnesia (3-7%), high potash (1-4%) type, whilst in the following period up to the latter part of the first millennium CE low magnesia (0.5-1.5%), low potash (0.1-1.0%) glass predominates. The Kellis samples are low magnesia but high potash, indicating another slightly modified base glass was being used at Kellis before the 4th century CE and into which the coloured glass was added. Furthermore, the likelihood is that preferential leaching of sodium over potassium from the glass surface has almost certainly limited the data comparison. The moisture content of the soil and its variation over a period of two millennia is unknown. And, the possibility for recycling of earlier glass production at Kellis cannot be excluded from any discussion in respect of the cobalt source present in these blue glass sherds.

Lilyquist and Brill (1993) proposed that glass production commenced in Egypt at around the same time as glass production commenced in Mesopotamia. Lucas and Harris

(1989: 183), Freestone (2006) and Nicholson and Henderson (2000) all suggest that the first significant production of glass occurred during the 18th Dynasty. All of the analyses produced by these various workers relate to the period from about the 18th Dynasty through to the Roman period. These glasses can be characterised as being low melting soda-lime-silica glasses and all contain a soda content (Na_2O) of >10% and generally in the order of 20%. Rehren (2000) stated that the knowledge in respect of glass manufacture during the Late Bronze Age (LBA) is limited. He indicated that the present knowledge is limited to the use of a plant ash-type soda and some form of quartz. He further suggested that there is no indication of a fritting step, nor is there any certainty about the furnaces or installations used. Sayre and Smith (1961) suggested that these soda-based glasses can be subdivided into two groups, high K_2O + high MgO in which each mineral oxide is >1.5% and low K_2O, low MgO with <1.5% of each oxide although some exceptions and intermediate compositions are now reported. This is discussed in Section 5.4.2.2, including the reporting by Barkoudah and Henderson (2006) and by Colomban (2010/11).

The cobalt blue glasses recovered at Kellis and Dayr Abu Matta were coloured with cobalt pigment and their respective analyses are provided in Table 5.25. Glass Sample 1, find location House 4, Room 6 (Context 6) contains manganese, nickel and zinc mineralisation in accordance with the alums located within this oasis and the glass can be classified as being low in iron. The presence of significantly elevated copper does suggest that the sherd could be related to the CoCu or Co+Cu glasses as discussed by Shortland and Eremin (2006), Walton *et al*. (2009), Smirniou *et al*. (2009), Polikreti *et al*. (2011), Walton *et al*. (2012), Smirniou and Rehren (2013) although again, the dating of these Co-Cu glasses still requires further investigation. Whilst the analyses given in Table 5.25 indicate that the cobalt colouration used in Samples 1 (A/6/93.514), and Dayr Abu Matta Sample 13 (DAM [12]) could have been derived from the cobalt blue pigment now proposed as having been made at Dakhleh, Sample 13 appears to be lacking in zinc. However, because the concentrations of the respective transition elements are low, the lack of zinc could be related to the percentage of zinc in the added cobalt pigment, or to orientation of the crystal being examined under the electron microscope.

Whereas, blue glass Sample 2, find location House 4, Room 4 (Context 3) is different. It does not indicate the presence of manganese, nickel or zinc and is high in iron, indicative of the use of an alternative source of cobalt, probably from Persia (Iran).

Cobalt ore-bodies are generally complex, thus to attribute the cobalt source to a specific site is not straightforward. However, as Sample 2 is manganese-free and high in iron, this is probably indicative of a Persian (Iranian) deposit. Kaczmarczyk (1986: 373-4) stated that Egyptian sources of cobalt were only in use from the 16th to 17th century BCE and after that date, all cobalt was sourced elsewhere, probably Iran. Sample 1, being dated to 4th century CE and Dayr Abu Matta Sample 13 dated to 5th to 6th century CE, and both contain Egyptian-sourced cobalt would now question this Kaczmarczyk assertion.   However, according to Hope *et al*. (2009), the mining of alum may have continued into the early Late Period or the Roman period. And, this could account for a continuing supply of cobalt. Alternatively, recycling of glass could possibly provide the cobalt glass with the unique Dakhleh/Kharga Oases cobalt mineralisation.

The cobalt blue Dayr Abu Matta Sample DAM [12] – S11.008 provided by Dr. G. Bowen is dated to 5th to 6th century CE. It is probably a boss broken off a glass vessel and shows considerable deposition of calcite on to its surface. This clearly evidences the presence of moisture over an extended period in the soil profile from which the sherd was recovered. One analysis of a spot within this sample indicated an anomalous concentration of P_2O_5 (0.3%), As_2O_3 (0.1%) and CuO (0.2%), Whilst no tin in any form was detected within this sample, its composition may indicate that bronze formed part of the raw mineral used, in a manner similar to that discussed in Chapter 4 in respect of Egyptian blue manufacture. Phosphorus, as bone ash (tricalcium phosphate) will readily adsorb arsenic and could carry this element into glass production. Arsenic could also be present in the copper or cobalt raw material selected. It would be somewhat tenuous to connect this observation to the earlier discussion on bone ash, never-the-less it does provide evidence for further research in this field. As indicated from its analysis provided in Appendix A5, Table A5.13.1 (DAM12.9A) and Figure A5.7.13, Spot 1 a particle of tin and lead was analysed (37.2% SnO_2 plus 2.1% PbO). In Appendix A5, Figure A5.7.13 Spot 1, tin was certainly present in the copper blue Sample 7 (A/6/93.692). It does assist in supporting the possible use of bronze in DAM [12] or contamination of the glass from another source of blue glass.

Images in Appendix A5 indicate crystal growth on the surface of glass Sample 13 (DAM [12]). The presence of what appears to be patches of gypsum and of calcite would negatively impact upon the EDS analyses as they would mask the surface undergoing elemental analysis. Under burial conditions, potash would be expected to be preferentially leached, as discussed by Jay *et al.* (2013); 2015).

The respective I_P results for Samples 1 and 2 would indicate a melting point of ~1000°C and for Sample 13, the I_P is suggestive of a melting point in the region of 800-900°C.

The above preliminary results potentially support glass colouring, if not actual glass manufacture within the Dakhleh Oasis.

5.10 Cobalt blue summary

The source of the cobalt minerals being located at Dakhleh Oasis has been confirmed. A slag sample, indicative of the kiln firing of a cobalt complex has been identified, providing preliminary evidence for the production of the cobalt pigment at Dakhleh Oasis. A new hypothesis for the extraction and co9nversion of a mixed hydroxide precipitate into the blue pigment is advanced. The mineralogy of the cobalt blue pigment has been identified in detail. Its fixation to pottery surfaces using egg protein, beeswax and probably gum Arabic has been determined. The use of the cobalt blue pigment as a raw material for the production of cobalt blue glass is proposed. More detailed chapter conclusions are provided in Appendix A5.

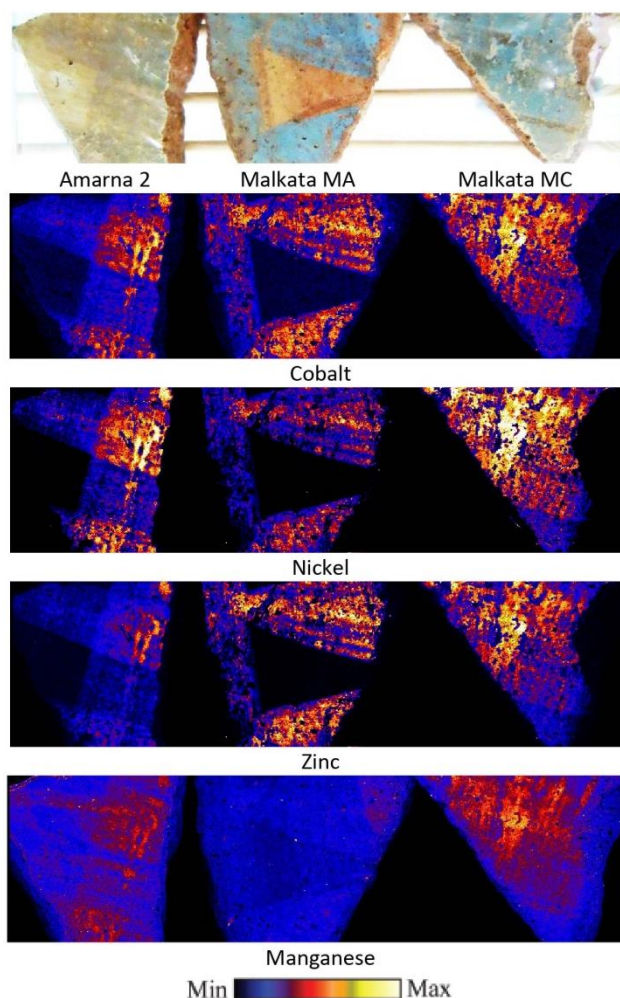**CHAPTER 6.   CONCLUSIONS AND RECOMENDATIONS**

Figure 6.1 Australian synchrotron images of cobalt, nickel, zinc and manganese concentrations present in the decoration applied to Nile Valley sherds from Amarna and Malkata.

This thesis has applied modern analytical instruments to non-destructively examine a range of New Kingdom to Roman period pigments. The samples analysed were recovered within the Dakhleh Oasis at ancient Kellis (Ismant al-Kharab), Mut al-Kharab, Dayr Abu Matta and Qasr al-Dakhleh, or from the Nile Valley at Amarna, Malkata, Dendera, Dier el-Medineh, Karnak North, and Memphis, and one sample from North Sinai. The instruments used include optical microscopy, electron microscopy under low or high vacuum, Focussed Ion Beam (FIB) electron microscope (with gallium ion milling capacity), the synchrotron XFM beamline for elemental analyses, Raman spectroscopy and Mössbauer spectroscopy for mineralogy determination. This research, which has adopted a non-destructive multi-instrumental analytical procedure, has produced a more detailed understanding into a number of aspects of Egyptian pigments and their decorative applications. A 'forensic' or micro-sampling and analysis regime has also been demonstrated.

Earlier investigations using techniques such as petrology or XRD, require the removal of material of significant volume for examination. The combination of elemental and mineralogical analytical methods used in the present research offers a substantial developmental tool for the non-destructive examination of Egyptian artefacts and cultural

heritage wares more generally. XRD, with its well-developed database does however offer an excellent alternative instrument, particularly if the removal of sufficient material is permissible. The supporting mineralogy information non-destructively conducted using a range of Raman spectrometers evidences the suitability of this instrument for the examination of pigments, pottery, cartonnage and other related materials. As has been demonstrated, even microscopic samples or sherds in which most of the pigment has been lost, when examined by Raman spectroscopy, can still provide significant data, something which cannot be achieved by XRD. The ability of Raman spectrometers to examine areas as small as 2 μm^2 (microscope lens dependent) has enabled pigment particles to be analysed in greater detail than that obtainable from XRD instruments. A number of pigments on wall decorations which have become dislodged were micro-sampled 'forensically'. Additional samples, pin-head in size, were similarly obtained from pigments located in trench excavations and these samples were also able to be analysed by SEM-EDS and by Raman.

The great advantage of using more than one instrument and to not damage the specimen surface in the examination process is demonstrated by the detection in the elemental analysis of the arsenical hydroxyapatite particles found initially in Egyptian blue using the XFM beamline of the synchrotron. It is now established the these particles were not Ca-P-As particles emanating from bronze, but rather, bone ash particles (confirmed by the presence of F) on to which arsenic had been adsorbed. The presence of hydroxyapatite particles has also been detected in cobalt blue pigments.

Individual instrumental analyses may not provide sufficient data to enable the composition of the material under examination to be fully determined. For example, the potential for the leaching of alkali metals from the surface of glass sherds, or the deposition of calcium-based minerals or phosphates on to sherd surfaces must also be considered mineralogically, particularly if no pre-surface preparation is able to be undertaken. As has been demonstrated within this thesis, phosphorus can be introduced into the system via ground-waters, from urine, through the use of kiln ash as part of the alkali flux, or as part of the internal lining material of pottery reaction vessels. The aluminium phosphate, probably vivianite, detected in a cobalt blue pigment from Malkata (M3), in the residual green pigment on Malkata sherd M7 and in a brown/black line on sherd S1 from North Sinai illustrates the additional complexity of this system. It does support the much greater understanding of various aspects of pigment technology which has now been demonstrated.

The recent development of electron microscopes capable of directly inserting larger specimens into the sample chamber and examining them under low vacuum without the requirement for pre-coating with a conducting film has been used for much of the present research. And, the ability to mill a sample using a Ga^+ ion beam in a FIB and then analyse the milled surface has provided new and relevant data, in respect of phosphates.

Depending upon the power setting, electron beams and laser beams can thermally modify heat-sensitive minerals and alter their mineralogy. This is particularly important in the case of the iron oxide pigments when studied using Raman spectroscopy. These considerations are discussed within Chapter 2 of this thesis. Steps were taken throughout the thesis to prevent any mineralogical changes during the examination process.

The XFM beamline on the synchrotron can examine a much wider sample area than is possible in an electron microscope and therefore, the synchrotron has been used as a large area identification scanning tool. Subsequently other analytical methods such as electron microscopy with a much narrower field of view and with higher resolution, were then applied. This method has been advantageously adopted in this thesis and will be discussed in reference to arsenical particles located in Egyptian blue.

Thus, in this thesis, Raman spectroscopy has been applied to obtain information in respect of the mineralogy of inorganic minerals, organic binders including waxes, egg protein, casein, animal glue, gum Arabic, sugars and a range of oils and molecular biological degradation in the one spectrum. Gum Arabic and a diterpenoid resin, probably *Pinus pinea* or *P. haleopennsis* some, or all of which have been detected in several cartonnage samples from Kellis. Organic binders, particularly egg and gum Arabic have been used to fix cobalt blue pigments to the pottery surfaces. According to Newman and Serpico (2000: 485), the use of egg yolk, egg white and gum (unidentified type) were used to apply pigments to wall tombs. However, in the limited number of wall samples examined, Raman spectroscopy failed to provide a signature for an organic binder on any of the pigments examined. The identification of key Raman spectral biomarkers of lichen, algal or cyanobacterial biodegradation attack on exposed decorated Egyptian blue surfaces as discussed in Chapter 4 was achieved non-destructively.

The images provided in Figures 5.12(a) to (e), and a number of elemental analyses, supported by Raman spectroscopy, as provided in Figure 5.54, and by electron microscopy in Chapter 3 and Appendix A3 would suggest that gypsum or anhydrite is present on many burnished pottery surfaces indicating that this mineral formed part of the vessel preparation process. The presence of anhydrite in some sherd surfaces as shown by its Raman signature, would suggest that the burnishing and gypsum slip coating application would have occurred prior to the firing of the vessel. SEM-BSE imaging and analysis of the 4th century Roman pottery from Dakhleh Oasis indicates the presence of straw, chaff or similar matter as temper in the pottery fabric.

As shown in Chapter 4 and Appendix A4, the plaster applied to the decorated walls at Kellis similarly contained coarse, rounded quartz pebbles together with straw or chaff as a reinforcing aid. The inclusion of egg-based and/or carbohydrate-based additives including malt, sugar, molasses, gum Arabic have been studied by Rampazzi *et al*. (2016) in wall plaster. They reported that the lime and the sugar derivatives rapidly reacted to form calcium saccharate which would strengthen the cohesion properties of the mortars. Such possible usage within the painted walls at Kellis and elsewhere within the Dakhleh Oasis should be investigated *in situ* by Raman spectroscopy.

The plaster used on walls is different to that applied to bandages as part of the mummification process. The wall samples have used a mixture comprising calcite, feldspars, quartz and gypsum and are discussed in Appendix A3. When only traces of gypsum are reported, this may indicate a surface reaction with the calcite reacting with atmospheric sulphur dioxide (particularly from cooking ovens) in the presence of moisture. Gypsum has been used as the sole plaster binder for the cartonnage samples.

The results presented in this thesis represent a significant advancement in the fundamental understanding of the various pigments examined. For example, contrary to published data, Raman spectroscopy and the synchrotron XFM beamline have shown in Chapters 3 and 5 and Appendices A3 and A5 that the black pigment applied to Egyptian New Kingdom period pottery from the Nile Valley and produced during the Ptolemaic Period at Dakhleh Oasis, is normally derived from magnetite together with amorphous carbon obtained from plant material rather than from ivory, bone, or other phosphorus-containing source. However, at Karnak North, each of the three sherds contained hydroxyapatite (bone ash) in the black carbonaceous pigment potentially indicating the use of ivory or bone ash. The Ptolemaic sherd D8 from Mut al-Kharab contained phosphorus in the elemental analysis, and Raman spectroscopy provided a signature for phosphate indicating that the likely source of the carbon was from an animal-based source.

The red pigments, whether applied to pottery, walls or cartonnage, are hematite-based and of variable quality. These hematite-based dull red and brown pigments were shown by Raman spectroscopy and SEM-EDS, to be often indurated with titanium or aluminium. Whereas, the bright red pigment colours were likely to have been from specially selected hematite deposits. They may well have been prepared by heating goethite to >300°C. Raman spectroscopy has also detected various iron oxyhydroxide-based minerals being used, including goethite, lepidocrocite and maghemite and their presence would indicate a post-firing application.

More detailed theoretical studies using synthetic minerals is required to fully develop a Raman database to understand the changes introduced by the adsorption of hydroxyl groups on to the iron surface rather than being incorporated into the mineral structure. The presence of the oxyhydroxides, goethite, akaganéite and lepidocrocite and/or with OH$^-$ surface adsorption and thus their differentiation by Raman spectroscopy still requires further elucidation. However, goethite can be determined with reasonable certainty. And goethite was the preferred brown pigment used on each of the sherds decorated. On cartonnage, both hematite red and also pink pigments formed by a mixture of hematite, feldspar and starkeyite and the carbonate minerals dolomite and ankerite were used. The pink on the wall of the Main Temple D/2 Shrine I, Kellis is an unusual mixture of natrojarosite, goethite, calcite, amorphous carbon and possibly augite.

The yellow pigments were obtained from the use of either orpiment as detected on Nile Valley sherds or from jarosite and natrojarosite observed in samples from Kellis; the yellow pigment on a cartonnage sample was jarosite. The orpiment analyses were found to contain ~50% silica and this is considered to have been added as a grinding aid. On a wall sample from Shrine I, Main Temple, Kellis the yellow is a mixture of the iron oxides lepidocrocite and goethite and on the north wall of North Tomb 1, Kellis it is a mixture of hematite and goethite. The yellow pigment, natrojarosite was determined in Shrine I, Main Temple D/2, Kellis and natrojarosite plus goethite on its floor. Ambers (2004) reported that natrojarosite pigment was present on Old Kingdom objects held in the British Museum collection. Jarosite and natrojarosite pigment samples found at Kellis, indicate that these Egyptians had access to either iron or copper mines containing pyrite and which were undergoing oxidation in an aqueous environment. The production of these two iron-based pigments is

an indication of acid mine drainage. Thus, locating such areas would provide potential evidence for trade or supply routes. It is an additional area for future research.

Malachite and carbonatecyanotrichite has been observed in green pigments on cartonnage from Kellis 1 cemetery and this has been shown to have partially deteriorated to form atacamite and antlerite. Green earths (glauconite) were also selected for wall decoration in the main Temple, Shrine IV and on the south wall of North Tomb 1, Kellis. The copper mineral, brochantite was blended with hematite to prepare a green pigment and this, together with spinel *sensu stricto* and calcite was found in the wall decoration in the painted villa, B/3/1 in Area B, Kellis. As shown by Raman spectroscopy, 'Green earth' pigments were also employed to decorate walls at Kellis. Egyptian green containing tin, indicative of the use of bronze as the copper source and a different green pigment, containing copper and zinc, indicative of the use of brass were both observed on Kellis wall decorations.

As demonstrated, Raman is readily able to non-destructively differentiate between silica and its polymorphs, tridymite, cristobalite and moganite, each of which has been found to be present in various pigment samples examined. Importantly, a white pigment decoration on a 4th century sherd from Mut al-Kharab has been confirmed by Raman spectroscopy and by electron microscopy, to be silica. Raman spectroscopy has identified the presence of moganite and tridymite in this pigment, indicating that the source of the silica was flint or chert and which had had been heated to about $1000°C$ to form this white siliceous pigment. Heating above $600°C$ would have caused silanol present in the chert to rapidly expand significantly aiding in pulverising the material. BSE electron images confirmed that plant ash present in the pigment had formed residual hollow silica shell structures, supporting a high temperature preparation. This unexpected result, warrants further investigation in an effort to determine the extent of usage of silica as a white pigment within the Dakhleh Oasis and elsewhere.

Huntite, a white pigment, has been found to have been used at Malkata and at Mut al-Kharab on pottery sherds as a slip coating prior to the application of Egyptian blue in a post-firing surface coating. As a soft, unprotected carbonate, it was unstable and failed to adequately fix any of the red, blue, green or yellow pigments applied to its surface. The pigment adhesion failure, particularly in the case of Egyptian blue, is exacerbated by its coarse, plate-like crystal shape as shown in the many SEM-BSE images provided in Chapter 5 and Appendix A5. This has created a limited surface area to bind the pigment to the substrate exacerbating the problem. When coated with beeswax as the case for Malkata sherd M1, the huntite slip has survived without loss of the Egyptian green decoration.

Egyptian blue decoration was found on both a wall sample from North Tomb 2, Kellis, the south wall Shrine IV Main Temple, Kellis and on a cartonnage sample from Tomb 16, Kellis 1 cemetery. It is clearly evident that Egyptian blue and Egyptian green are different pigments. However, both pigments can be obtained by heating a mixture of silica, calcium carbonate copper and a flux to temperatures between 870 and $1100°C$ for $15 – 72$ hours under either oxidising or reducing conditions. The present research has confirmed that Egyptian blue (cuprorivaite) was produced preferably under oxidising conditions and at a temperature of approximately $1000°C$ as confirmed by the Raman signature for tridymite. Although Pradell *et al*. (2006) using XRD proposed that at a measured temperature of $1000°C$

in their experiments, cristobalite formed. Furthermore, the colour of the synthesised product was influenced by temperature and the added flux and the CuO/CaO ratio. Raman spectroscopy has proved to be a beneficial tool for examining Egyptian blue and Egyptian green.

A white mineralisation has been observed on the surface of several Egyptian blue samples and Raman spectroscopy has indicated that this white surface coating is a variable mixture of hanksite, gaylussite, natrite or thénardite thereby confirming the use of trona (or natron) as the major fluxing mineral until a probable change occurred at, or slightly before the 2nd century CE, when plant ash, as shown by the much higher K_2O concentration, is now seen to be the more likely flux. Thus, the use of trona (natron) and later plant ash from earlier than the 2nd century CE as alkaline fluxes in Egypt in the production of Egyptian blue has been confirmed.

Colomban *et al.* (2010/11) suggested that with the end of the Roman domination the availability of natron became very limited and this led to the introduction of plant ash as the flux for European and Middle Eastern glass production. Barkoudah and Henderson (2006) alternatively suggested that halophytic plant ashes were used from about 2500 BCE to about 800 BCE and between 800 BCE and 800 CE that natron was the mineral alkali flux source. Brill (1993: 41) suggested that Egyptian glass, such as that from Nuzi was made with high-soda plant ash and siliceous pebbles, although he stated that he based this plant ash presumption on the high levels of magnesium found in plant ash and further, the low potash analyses might argue against this hypothesis. The evidence within the literature therefore indicates that a change in the composition of the alkali flux used in glass production and thus, Egyptian blue production in Egypt may have undergone a similar change in flux selection at around the same period in time.

In the case of Egyptian green, the green colour results from the formation of a copper-containing wollastonite, the copper ion being in an octahedral environment in a silica-rich glass phase. This pigment would have been prepared by reducing the copper concentration in the composition and increasing the flux to form a copper-wollastonite mineral. Wollastonite can also form by heating the Egyptian blue pigment itself to >1050°C. In the Egyptian green samples examined, the presence of tridymite confirms that the reaction would have been conducted at approximately 1000°C. Natron would most likely have been used as the alkali flux. The potash concentration in the samples examined is low and possibly was derived from the K-feldspar. This establishes that copper can produce different colours even when in the same oxidation state. Furthermore, divalent copper ions and not divalent iron ions create the green colour.

Both Egyptian blue and green pigments have generally been applied to walls and cartonnage. Noll and Hangst (1975, 1975a) proposed a post-firing of the Egyptian blue on to pottery surfaces. Amphora, such as exemplified by Malkata sherd M73/K/5 has been decorated with Egyptian blue and termed by Hope as polychrome decorated (Hope 1980: 333; 1987: 110; 2011: 495) or by Rose (2007: 31) as post-fired polychrome decorated, the pigment determination in both cases being by XRD. Malkata sherd M73/K/5 was stated to be decorated in blue, green and red on a white ground (Hope *et al*. 1981: 145). Raman spectroscopy has non-destructively confirmed that on this sherd the blue is Egyptian blue,

the green is Egyptian green, the red is a highly crystalline form of hematite and, the white ground is huntite.   Similarly, Egyptian blue and Egyptian green, orpiment, red oxide and black pigments have been determined by SEM-EDS and by Raman spectroscopy to be present on the huntite slip applied to the surface of Malkata sherd M73/K/1406.   The Egyptian blue decoration on both sherds was recognised as being Egyptian blue and applied post-firing (Hope 1987: 110).   And, a microscopic trace of Egyptian blue (invisible to the human eye) was detected on sherd D8 from Mut al-Kharab as provided in Appendix A5. Again, the Egyptian blue had been applied over huntite.

Weddellite (calcium oxalate dihydrate) and metastable calcium oxalate (whewellite) are present in an Egyptian green pigment from the Main Temple Site D/2, Kellis and in which bronze formed part of the copper source. As discussed in Chapter 4, the presence of calcium oxalate monohydrate and dihydrate are identified by their strong Raman bands at 1463, 1474 and 1492 cm^{-1} respectively, indicative of equilibrium between the stable and the metastable forms of calcium oxalate. Furthermore, the presence of the hydrated calcium oxalate in the sample is attributable to lichen invasion, whose hyphae penetrate the calcareous substrates to form complexes with the oxalic acid secretions from the mycobiont. CH-stretching modes characterised by Raman bands in the region of 2935 cm^{-1} support the assignment of these features to a biological source.

As proposed in this thesis, kiln ash, or what may alternatively be described as fuel ash or cooking ash was also used as a flux in various other high temperature processes. A sample of plant ash derived from a combined mixture of *Acacia nilotica*, (also known as *Vachellia nilotica* or gum Arabic tree) and *Tamarix aphylla* (Tamarisk) was analysed providing the data in Table 5.12. The ash is high in sodium, magnesium, and calcium, contains substantial potash and is high in both chlorine and sulphates. It is very low in aluminium, silica and phosphorus.   This plant ash concept was subsequently adopted in Europe with the substitution of Beech ash (forest ash) in northern Europe and later in England by the substitution of kelp ash as the preferred alkali flux in porcelain glazes.   More regional studies into the fuel sources used for kilns, bread ovens, and other similar thermal processes should be undertaken in an effort to better understand the possible variability within regions of the likely mineral assemblage in the ash produced. This study could assist in determining the variability in various glass analyses already highlighted in previous analytical studies.

Schiegl *et al*. (1990) correctly identified an arsenic phase present in polished samples of Egyptian blue, and attributed the presence of the arsenic to the use of an arsenical bronze. These researchers therefore suggested that this might serve as a method for dating the pigment samples to before the 18th Dynasty, tin (bronze) being introduced into the production cycle during the 18th Dynasty. However, the combination of the XFM beamline of a synchrotron with the gallium ion milling capacity of a FIB has now provided new information in respect of these Ca-P-As surface particles by the direct examination of unpolished samples of Egyptian blue. As stated, the presence of many arsenic-containing particles were detected at the surface of an Egyptian blue sample in the synchrotron analyses; the same sample was then examined in the FIB, the arsenical particles were located, milled using the gallium ion facility of the FIB, rotated and the milled area analysed by SEM-EDS. This work established the arsenical particles to be calcium phosphate-based.

The presence of fluorine in the analyses confirmed the particles to be hydroxyapatite (bone ash) on to which arsenic had preferentially adsorbed. Thus, this analysis supports an animal source for the bone material and not a chemical reaction synthesis or surface deposition from ground waters.   Furthermore, without the multi-instrument approach adopted, these arsenical hydroxyapatite particles would not have been observed as their shape blends into the platelet structure of the Egyptian blue.

Similar bone ash particles have been found in cobalt blue and in one black pigment from Mut al-Kharab; however, in both cases no arsenic was associated with the bone ash. The presence of these bone ash particles which have also been observed in pottery fabrics as reported herein, identifies the disposal of bones and probably animal dung in cooking ovens and kilns and the subsequent use of this readily obtainable ash as a flux. These results would therefore suggest that a possible reason for the failure to discover plant ash production sites is that plant ash flux was not specially prepared at specific locations. This hypothesis of local kiln ash usage would include its use in the production of Egyptian blue, Egyptian green (Green frit), cobalt-based blue production, and probably glass and faience. It is supported by the observation by Nicholson (2007) that bone material was present in ash at Amarna site O45.1 or wood and cattle dung in cooking installations (Gur-Arieh *et al*. 2014) or cattle dung as the alkali flux in Egyptian faience (Matin and Matin 2014). Rehren 1997) examined the phosphorus concentration in crucible fragments used for glass production and for bronze melting; he attributed the higher concentration of phosphorus in the glass vessels to contamination by the fuel ash during the firing of the vessels.

Surface deposition of phosphate from ground-waters on to the surface of the sherds under examination has been dismissed.   No actual difference in the phosphate concentration on the internal or external sherd surfaces and its core were observed for the eight Amarna sherds and the eight Malkata sherds analysed. As stated, the phosphate particles generally contained fluorine, indicative of hydroxyapatite and provided analyses similar to the phosphate particles observed in Egyptian blue.

This thesis does not support the proposal that during the New Kingdom period, Egypt also obtained cobalt from an external source such as Isphahan, Persia (Riederer 1974), or "the far side of the Balkans" (Lee and Quirke 2000: 111), or by Mycenaean traders with access to the silver-cobalt deposits from the Baltic across Central Europe (particularly from a silver smelting area such as Schemnitz in Hungary) (Dayton 1981) or Asia or Bohemia (Kozloff 1997).   Detailed chemical and mineralogical analyses conducted using a combination of instruments as part of the research into the cobalt pigments applied to wares in the Western Desert and in the Nile Valley support a unique Western Desert source for the cobalt-transition element complex ore present in alum as stated by Bachmann *et al*. (1980) and Kaczmarczyk (1986).

As shown in Figure 1, the synchrotron XFM beamline has been used to scan and elementally map much larger areas of an object than is able to be achieved by other experimental methods. *T*he transition element weight percent ratios found in various Nile Valley sherds manufactured during the period between the 18th and 20th Dynasties has been plotted and is provided in Chapter 5.   The results obtained clearly identify a very strong and direct relationship between the various elements mapped. Zinc appears to be normally in a higher

concentration and manganese in a lower concentration when compared with cobalt; nickel closely matches the cobalt concentration. This finding is in accord with the alums analysed from the Dakhleh Oasis and support the proposition that the Western Desert oases provided the source of the cobalt-containing alums mined. The results do show a very uniform quality of blue pigment produced, supporting the proposal that cobalt-blue frit production was conducted in very few locations using a constant source of cobalt alum mineralisation. The very close relationship, particularly between NiO and CoO could have supported the mining of a single alum deposit and as such, this raw material could support a limited number of manufacturing sites. All of the necessary raw materials to produce the cobalt-blue pigment were available at Dakhleh oasis making it an ideal production site. And, if a biomass ash, similar to that analysed in Table 5.12 was utilised, this would have provided the requisite alkaline flux.

A sample of a high iron-containing slag obtained from Mut al-Kharab was examined by Raman spectroscopy, electron microscopy and Mössbauer spectroscopy. The core of the slag is high in hematite and calcium, and the external surface is composed of goethite. The slag also contains the various transition elements thereby supporting the proposition that it has been derived from the internal lining of an as-yet, undiscovered kiln used in the firing of cobalt blue-containing pigments. Furthermore, it supports the proposal of Nicholson (2007) that lime was thrown into the kiln to assist in surface slag viscosity reduction and draining of any slag build-up from off of the kiln walls. Furthermore, it supports the proposition that this cobalt blue pigment was produced at Dakhleh Oasis. And, as shown by the analysis of a random sample of Dakhleh Oasis sand, this would have been suitable for producing the cobalt glass frit.

The surface of the slag sample as shown by its Raman signature contains goethite indicative of oxidative conditions resulting from the long burial period in a variably damp environment. Mössbauer spectroscopy confirms this, with the iron in the inner material distributed between goethite (68%) and a ferric aluminosilicate (32%), while the iron in the outer material is wholly goethite, much of which is composed of single crystals up to several mm in length. The ferric aluminosilicate is most likely diopside/hypersthene in which the iron is completely oxidised to ferric. Over the burial period, it would seem that the iron in the surface layers has exfoliated to form the single crystals of goethite, leaving the surface free of ferric aluminosilicate. Raman spectroscopy supports the presence of hypersthene as one such aluminosilicate and also the presence of ankerite, a calcium-iron carbonate.

In the case of blue-painted pottery, the cobalt blue BSE images provided in Chapter 5 and Appendix A5 indicate a much finer particle size than Egyptian blue providing a greater surface area for bonding. The use of egg protein and particularly over-coating with beeswax has provided improved adhesion to the pottery surface. Furthermore, the use of huntite slips was not encountered in any of the cobalt-decorated sherds.

The two general forms of blue decorated pottery can be grouped into two categories as described by Hope (1987: 110), (2011: 496) and by Rose (2007: 18, 31); namely blue-painted pottery using a cobalt-based pigment, often highlighted in red/brown and/or black and more rarely, yellow, and polychrome-decorated pottery (Hope 1987: 110; 2011: 496, Rose 2007: 31. Rose 2007: 21) also used the word 'scenic' to describe some of the naturalistic cobalt blue

motifs such as floral garlands, or scenes including plants, birds, fish and animals in a distinct band or decoration around the upper body of closed forms. Or, as described by Arnold (1993: 101) as 'white background style', in which Egyptian blue, often together with a range of colours including green, red and yellow was applied particularly on to white or cream slip coated amphorae vessels.

The usual order of pigment application on to the Nile Valley vessel surface was cobalt blue, followed by reds and brown and finally black, but this was not necessarily absolute. An example of goethite applied to pottery surfaces prior to application of the cobalt blue pigment has been observed in Malkata sample M3.   However, the limited number of sherds available does not allow this order to be considered in detail.

The application of cobalt pigments on to pottery surfaces (blue painted pottery) remains controversial.   Riederer (1974) proposed that a hydrometallurgical process was adopted in which the alum was dissolved in water, made alkaline with natron, to precipitate the metal hydroxide. Then, direct firing of this cobalt hydroxide precipitate on to the prepared pottery surface.   Subsequently, most researchers have suggested that the cobalt mineral was extracted from the alum by aqueous dissolution, precipitated as a mixed hydroxide by alkali addition, converted into a frit and then applied to the pottery vessel surface.   A number of experts consider that its decoration on to the pottery was prior to the firing of the pottery vessel itself (Bachmann 1981; Hope 1987: 110; Rose 2007: 18) Hope 2011: 495); whereas, Noll (1978: 227); 1981a: 149) and el-Goresy (2000: 62) favoured a post-fired regime because no reaction profile between the gypsum pottery surface and the cobalt blue pigment could be detected.

The conclusion that the cobalt pigment was applied pre-firing was based upon an isolated number (two or three) of black or grey, bloated blue-decorated pottery samples recovered in an excavation at the workman's village (site J) at Malkata and another badly vitrified surface find located in the Central City, Amarna.   The suggestion of a pre-firing application has evidently been supported by modern potters.   It is noteworthy that present-day potters would not be using the cobalt-based pigment employed during the New Kingdom period and who would now be producing pottery for an alternative market and therefore may have developed alternative production techniques, particularly in respect of decoration.   This suggestion is therefore considered to be of limited value.

Alternatively, post firing of the decoration to the vessel was proposed by Noll (1978: 227), (1981a: 149) and el-Goresy (2000: 62). Noll (1981: 148) considered that the presence of hydrated calcium sulphate (gypsum) was evidence for its use as a binder in a post firing application of the pigment; the suggestion being that the gypsum slip being under the cobalt had acted as a binder to fix the pigment to the pottery surface. Noll also considered that if residues of organic binders were detected then this would provide further evidence for a post-firing application.   As discussed in this thesis, such an organic binder has been confirmed. Whereas Bachmann *et al*. (1980) considered that the possible presence of gypsum could have resulted from burial conditions rather than from the proposal of Noll and Hangst (1975) that the cobalt blue pigment was applied as a slip mixture containing gypsum on to the vessel. And, Shortland *et al*. (2006a) considered that gypsum was the most likely mineral used in any slip coating. Based upon the sulphate content, they suggested that a

calcareous clay was also present. The addition of calcite or huntite with gypsum in preparing the slip was not considered.

This thesis has produced evidence using Raman spectroscopy to positively identify in a number of sherds an egg-based protein binder possibly containing gum Arabic, or similar resin or organic compound as the binder used to fix the cobalt blue pigment to the pottery surface. Furthermore, the Raman signature for beeswax has demonstrated that the pigmented surface was, on occasions, subsequently over-coated with this material and may possibly have been used directly as the binder. This wax coating has assisted in partially protecting the blue painted pottery substrate from removal by abrasion. As such, this would support a post-firing application of the cobalt blue pigment.

The method for the application of the beeswax to the pottery surface remains unresolved. Lucas and Harris (1989: 352) suggested that beeswax has been mixed with the pigment and the applied to New Kingdom tomb walls and cartonnage and in other instances applied to the surface of a finished painting as a protective layer. In the case of the beeswax used as a protective coating was it applied by warming and then either its direct application to the surface, or was it applied by dilution in an organic solvent, such as linseed oil, myrrh, or other oil and then brush applied? This is an important area for future research, particularly in respect of the wall paintings at Kellis and elsewhere in the Dakhleh Oasis.

The analysis by Raman spectroscopy of goethite as a brown pigment below the cobalt blue decoration on a sherd from Malkata (M3) would, in that instance also negate the pre-firing decoration proposal. Goethite would convert to hematite in the vessel firing process at 290-385°C. Thus, whether pre-fired, or post-fired, application of the cobalt pigment to the pottery surface is an important aspect for future research. This should preferably combine the XFM beamline with electron microscopy and Raman spectroscopy to extend the significant understanding developed within this thesis.

This thesis would not support the suggestion for the use of egg, wax, or other binder to be used to apply the cobalt pigment to the vessel surface and then to on-fire the decorated pottery. If such a pre-decorated step was contemplated, then firing the vessel at a kiln temperature of ca. 800°C, the waxes or egg would initially convert to carbon and then to carbon dioxide depending upon the kiln redox conditions. Carbon would offer no structural or adhesive integrity. As such, adhesion failure would be expected. Hope (1980: 334) conducted an experiment in an effort to further elucidate the adhesion failure of Egyptian blue to a pottery surface. He applied the ground Egyptian blue pigment to a pottery surface using an aqueous mixture of egg white and then fired the pottery. As anticipated, he established that adhesion did not occur, demonstrating as stated above, that at a firing temperature of 850°C, the egg white would decompose.

Bachmann *et al* (1980) used XRF for the analysis of the cobalt blue pigment on a blue-painted pottery sherd from Malkata and as these researchers advised, they were unable to identify elements below aluminium in the Periodic Table. Therefore, they tentatively came to the conclusion, based upon the limited elemental analysis available to them, that the cobalt was present together with nickel and zinc as a spinel [(Co, Ni, Zn)Al$_2$O$_4$]; spinel, *sensu stricto* is magnesium aluminate and magnesium is too light an element to be seen by the XRF

analytical instrument utilised. This was a reasonable conclusion based upon the limited experimental data then available. Shortland *et al*. (2006), reported that spinels tend to provide very similar XRD spectra. In their work they had only very small samples available to them for analysis, therefore they were unable to positively identify individual spinels with any certainty. As reported by Srisawad *et al*. (2012), ($CoAl_2O_4$) and Co_3O_4 cannot be separated by XRD. Shortland and co-workers also presumed from the bulk elemental compositions of the pigment layers analysed that spinels incorporating cobalt, zinc, magnesium, iron and nickel were present. Thus, on the basis of elemental analyses it has been proposed by a number of earlier researchers that the cobalt was a simple (Co,Ni,Zn) aluminate (spinel) and generally had been directly applied over either a calcareous marl clay pottery body, although, Rose (2007: 24) considered that marl clay vessels with blue-painted designs are rare. Or, in the case of Nile Valley silt fabrics, the pigment was applied onto a calcareous clay slip, containing gypsum (or anhydrite) (Shortland *et al*. (2006: 98) and then fired. This is now considered to be unlikely.

Present research, including a combination of the XFM beamline of a synchrotron, the high end (Magellan 400) electron microscope mapping ability, FIB microscopes and Raman spectrometers, a range of minerals present within the cobalt blue painted pottery pigment were identified. This confirmed that a much more complex series of cobalt-based minerals were either prepared or subsequently formed from long term exposure to the environment. Spinel, *sensu stricto* was certainly identified together with cobalt in a pyroxene, as heterogenite, cobalt hydroxide, cobalt oxide ($Co(II,III)O_4$), ($Zn_{1-x}Co_x$)Al_2O_4, spherocobaltite and bieberite. In isolated instances the cobalt aluminate (cobalt spinel) was observed. This thesis has established that the formation of a pyroxene in which the partial replacement of the magnesium by elements with a similar ionic radius is one major form of cobalt mineralisation found present. Portion of the aluminium has formed an aluminium oxide, including corundum and also evidence exists for the possible formation of an aluminium phosphate and a separate zinc complex. Significantly, hydroxyapatite (bone ash) particles were observed within the pigment. This would add additional support for the use of kiln ash rather than a specifically prepared plant ash as part, or all of the flux.

Synchrotron images provided in Figures 5.36 to 5.39 show differences between Malkata and Amarna, particularly in respect of arsenic although some concern is expressed that this might represent silica, silica being at the limits of detection for the XFM beamline. This presence of arsenic, particularly within the cobalt blue pigment area, is evident at Malkata in samples M3 and M5 and also in the sherd from Deir el-Medineh. Arsenic is not found at Amarna in either sherds A2 or A4 nor in the North Karnak or North Sinai sherds. If present, it has probably been applied as a colourant modifier. And, as shown in Figures 5.52 and 5.53, it is evident that different concentrations of manganese are present in Malkata sherds A2 and A4. The Deir al-Medineh sherd also contains a lower manganese concentration. This would support the suggestion that element oxide ratios may not provide a suitable method for differentiation of the actual sources of the cobalt-rich alums exploited.

A new hypothesis for the production of cobalt blue pigments, based upon the cobalt-containing alums from Dakhleh Oasis, is advanced within this thesis. The minerals in the alums detected by Raman spectroscopy include wupaktite (Co-containing), apjohnite (Mn-containing), dietrichite (Zn-containing) and halotrichite (Fe-containing). These cobalt-

containing pigments all contain manganese, iron, nickel, zinc, found in the Dakhleh Oasis alums and confirmed by SEM-EDS all are present in the final cobalt pigment. Zinc, is normally in a higher concentration than the other transition elements.

As discussed in Section 5.8.1, a modified precipitation (MHP) and firing regime has now been proposed for the extraction of the cobalt from the alum and its subsequent conversion into the cobalt blue pigment. The cobalt extraction from the alum was probably conducted by either the direct addition of plant ash or alternatively and more likely, with additional natron. Urine, supplying urea would have been added to the aqueous alum solution containing its extracted soluble magnesium, aluminium and transition elements to restrict aluminium hydroxide gel formation and assist crystallinity. Precipitation and crystallisation on aging of these mixed magnesium/aluminium hydroxides together with the precipitated transition metal hydroxides present in the alum would have been favoured by lower temperatures. The MHP product obtained would then have been combined with desert sand and a flux such as kiln ash and then fired to approximately 1000°C to form the final cobalt blue pigment frit. It is possible, but discounted, for the MHP to be mixed with powdered raw glass and then fritted. This would have introduced a soda concentration much greater than the analyses provided in Tables 5.7 and 5.8 for the cobalt blue pigment.

Compositionally, the blue cobalt pigment applied to the Mut al-Kharab sherd and to all of the Nile Valley sherds is relatively similar as demonstrated in Figures 5.52 and 5.53. Thus, it is now proposed that all of the production would have been conducted within the Oasis, close to the alum source and the source of all other required raw materials.

The strong likelihood is that specialist manufacturers prepared the cobalt pigment as a frit using techniques directly related to those employed in the production of Egyptian blue but within the Dakhleh Oasis. This is strongly indicated by the presence of calcium phosphate (as bone ash) having been detected in both Egyptian blue and in the cobalt pigment indicating a commonality of production methods. It would then only require transportation of small volumes of this precious colorant from the Oasis to the Nile Valley workshops. This provides support for the proposal that the desert dwellers were the instigators of at least part of the technological, political and societal interchange between themselves and the peoples within the Nile Valley with both groups being under the same governmental controls.

As indicated in Chapter 5, traces of copper were detected by EDS analyses in the alum but not in the acicular, crystalline cobalt-containing transition element complex itself. The presence of copper is attributed to the use of bronze tools employed in mining the alum. Similarly, the trace of copper observed in most pottery analyses was also considered to have been derived from similar tool usage to mine or extract the clays and the various other raw materials. Copper mineralisation is not considered to be ubiquitous throughout Egypt.

Glass sherds examined from Kellis and reported in this thesis show that a variety of glass types were present. And the run of a copper-coloured glass bead on clear glass would support glass-working. The much lower surface concentration of soda (<10% Na_2O) when compared with LBA glass at ~ 20% Na_2O is interesting, and whether this points to glass production at Kellis remains unresolved. Tentatively, the low sodium analyses suggest

leaching from the surface of the glass sherds and will require permission to remove surface glass in order to better understand these analyses. These low potash and soda concentrations at the surface of some of the glass samples suggests a future requirement for moisture and pH readings to be obtained by the archaeologist at the point of detection of the sherd. However, it would only reveal the present conditions and not necessarily the conditions which may have prevailed for the past two millennia. A sample would need to be microtomed from the glass sherd and the removed particle then reanalysed to possibly eliminate or confirm the alkali leaching effect and which alkali element was more prone to leaching. There is evidence that the larger ionic radius of the potassium ion will enable it to leach more rapidly than sodium if both ions are directly related to non-bridging oxygens. However, the level of aluminium observed in the EDS analyses and the Raman spectra support a potash-based alkali feldspar as the potash source. As such, in these glasses, the potassium is less likely to leach. And, this would support the results provided by Smets and Lommen (1982) who indicated a lower leaching of sodium when compared with potassium from aluminosilicate glasses.

The glass samples analysed from 4th century CE and 5th to 6th century CE from Kellis indicate a significant variation in the selection of the blue colouring element. However, these two cobalt pigments, produced from Dakhleh Oasis alums as indicated by the presence of the accompanying transition elements Mn, Ni and Zn, is shown to form the blue colour in glass. As such, this is a much later date for the change in cobalt source previously proposed by Kaczmarczyk (1986). In Kellis glass Sample 1, these elements are accompanied by elevated copper (3.6%) which, is in accordance with the suggestion by Shortland and Eremin (2006: 591) and Smirniou and Rehren (2013) of CoCu (or Co+Cu) glass being traded by the Egyptians with Greece and throughout the Mediterranean. Thus, this glass may have been involved in trading between Egypt and the Mycenaean world. Glass Sample 2 does not contain manganese, nickel or zinc and is high in iron, indicative of the usage of a cobalt raw material from Persia (Iran). The limited number of samples available for analyses obtained to date does not answer this question. It may well indicate recycling of glass from much earlier production but this must be considered to be unlikely.

Modern Raman spectrometers have been developed which are portable and can be used within museums and private holdings where removal of artefacts for laboratory analysis is not possible. For example, Edwards (2005) used portable Raman spectrometers to examine prehistoric rock art sites; Bruni et al. (2006: 143) to study 16th century Italian polychrome frescoes; Burgio (2006: 180) in museum collections; Colomban (2004: 2008: 2013), Colomban et al. (2006), Bouchard et al. (2007) have all demonstrated the use of portable Raman spectroscopy instruments for on-site analysis of stained glass. Presently, there is no other individual analytical instrument available which combines these capability features with portability for on-site mineralogical analyses. Thus, the Raman spectroscopy results in this thesis indicate that non-destructive analyses of extant wares held in museum collections can be conducted in situ.

The need for improved portable XRF (p-XRF) instruments to enable on-site elemental analyses to be conducted remains a challenge. The requirement for the analysis of elements, including sodium is required. Abe et al. (2009) operated a portable XRF instrument in Egypt which reputedly is close to achieving this outcome. However, Tantrakarn et al. (2012)

reported that a similar instrument when used by Nakai *et a*l. (2006) in Egypt failed under the high desert climatic conditions encountered. In a detailed study of p-XRF, the practical limitations of these instruments was carefully investigated by Hunt and Speakman (2015). They reported that phosphorus in archaeological ceramics and non-anthropogenic sediments cannot be accurately determined. They stated that this is also true for sodium as these X-rays are extremely low energy and so, to an even greater extent than other low-Z elements are reabsorbed into the sample matrix and/or detector and scattered as bremsstrahlung radiation. Furthermore, the low/mid-Z trace elements (Z = 21-30), (thus including the transition elements cobalt and nickel) can only be measured semi-quantitatively due to spectral overlay interference. In this respect, the cautionary recommendations made by Shugar (2013) need to be carefully considered. If a portable XRF instrument can be developed, then when combined with a portable Raman spectrometer, the necessity to remove samples from their find location is probably negated. Therefore, the ability of researchers to more closely analyse the vast array of Egyptian wares held in museums and on-site, both in Egypt and elsewhere, using the principles enunciated in this thesis is a future likelihood.

As detailed in this thesis, a continuum of knowledge, commencing with pottery production, metal working and other high temperature processes for production of Egyptian blue and green pigments, the introduction of bronze scrap or shavings from metalworking into Egyptian blue pigment production; the development of extraction and subsequent conversion of cobalt alum deposits located at Dakhleh Oasis into cobalt blue frits; glass production or glass working in Egypt; the production of faience and the subsequent development of this technology into glazed pottery have all contributed to the knowledge-base which, with various modifications, then spread throughout the Roman Empire and subsequently throughout Europe.

In summary, the combination of electron microscopy, the synchrotron XFM beamline, Raman spectroscopy and Mössbauer spectroscopy has been able to determine the major processes used, as follows:
- gypsum was generally used during the burnishing process and was therefore fired on to the vessel;
- the presence of anhydrite would confirm such a high temperature step;
- tridymite formation in lime plaster suggests a limestone calcination at 1000°C;
- huntite, being a carbonate mineral, has been applied, post firing;
- huntite has been shown to fail as a long-term binder particularly for the coarser pigments such as Egyptian blue or green, hematite red or orpiment yellow;
- Egyptian green was over-coated with beeswax at Malkata;
- beeswax, egg protein, albumen, casein, animal glue, gum Arabic, sugars or similar binder was used in conjunction with the cobalt blue application step and this has generally effectively stabilised the finer cobalt blue pigment particles;
- normally, the cobalt blue was applied in the first post-firing decorating step;
- a number of cobalt complexes have been identified, including spinel, *sensu stricto*, as an aluminate, together with cobalt in a pyroxene, as heterogenite, cobalt hydroxide, cobalt oxide ($Co(II,III)O_4$), $(Zn_{1-x}Co_x)Al_2O_4$, spherocobaltite and bieberite
- calcite has been either used as a post-firing pigment, or as a surface deposit formed during burial;

- the red and brown pigments used at Dakhleh Oasis normally only contain traces of manganese-based minerals;
- the minimal size of the sherds has rendered it difficult to determine in most instances if the hematite red pigments have been applied pre-firing, their colour development would support pre-firing application;
- black pigments are a mixture of magnetite and carbon black;
- brown pigments based upon goethite would support a post-firing application. Goethite would thermally decompose below 350°C;
- white pigments were calcite, huntite or gypsum as slips; and,
- the white pigment on one sherd from Dakhleh Oasis was decorated using silica which had undergone a thermal treatment. It contained a residual silica skeleton of straw or chaff;
- moganite has been detected in a white silica. Its presence indicates the potential use of chert (flint) as a white siliceous pigment;
- two yellow sherds, both from Malkata were based upon orpiment with silica present at 45 and 46%. Whether the silica was from a grinding process or deliberately added was not able to be determined;
- the oxide yellow pigments applied to walls were iron oxyhydroxides;
- green pigments used included 'green earths', green pigments (including malachite) and synthetically prepared Egyptian green;
- Egyptian blue, Egyptian green, and cobalt-based pigments have been reported on in detail;
- an alternative hypothesis is proposed for the extraction of the cobalt and accompanying transition metal complexes from the Dakhleh Oasis alums as Mixed Hydroxide Precipitates and their subsequent conversion into pigments;
- kiln ash as a flux;
- the possible use of hydroxyapatite (bone ash) as a high temperature pottery vessel lining;
- confirmation of cold applied (post-firing) decoration of blue painted pottery;
- detection of lichen attack on wall pigments;
- colour modification caused by copper deterioration to atacamite and paratacamite.

Bibliography

Abd-Allah, R., (2012), "Damage assessment and chemical characterisation of glass objects excavated from Gadara, Northern Jordan", in: Progress in Cultural Heritage Preservation, *EUROMEXD 2012*, (Eds., Ioannides, D. Fritsch, J. Leissner, R. Davies, F. Remondino, R. Caffo,), Limassol, Cyprus, 277-282.

Abd El-Rahman, Y., Surour, A.A., El Manawi, A.H.W., Rifai, M., Motelib, A.A., Ali, W.K., El Dougdoug, A.M., (2012), "Ancient Mining and Smelting Activities in the Wadi Abu Gerida Area, Central Eastern Desert, Egypt,: Preliminary Report", *Archaeometry*; **55**, (2013), 1067-1087, (DOI 10.1111/j 1475-1754.2012.000728x).

Abdul-Nasr, R.A., Thunell, R.C., (1987), "Eocene eustatic sea-level changes, evidence from the Western Sinai, Egypt, *Palaeogeography, Paleoclimatology, Paleoecology*, **58**, 1-9.

Abe, Y., Harimoto, R., Kikugawa, T., Yazawa, K., Nishisaka, A., Kawai, N., Yoshimura, S., Nakai, I., (2012), "Transition in the use of cobalt-blue colorant in the New Kingdom of Egypt:, *J. Archaeol. Sci.* **39**, 1793-1808.

Abe, Y., Nakai, I., Takahashi, K., Kawai, N., Yoshimura, S., (2009), "On-site analysis of archaeological artifacts excavated from the site on the outcrop at Northwest Saqqara, Egypt, by using a newly developed portable fluorescence spectrometer and diffractometer", *Anal. Bioanal. Chem*. **395**, 1987-1996.

Abouzeid, A-Z, M., (2008), "Physical and thermal treatment of phosphate ores – An overview", *Int. J. Miner. Process*, **85**, 59-84.

Accorsi, G., Verri, G., Bolognesi, M., *et al*. (2009), "The exceptional near-infrared luminescence properties of cuprorivaite (Egyptian blue)", *Chem. Commun.*, 3392-3394.

Adamson, D.A., Gasse, F., Street, F.A., Williams, M.A.J., (1980), "Late Quaternary History of the Nile", *Nature* **288**, 5055.

Adelsberger, K.A. and Smith, J.R., (2010), "Paleolandscape and paleoenvironmental interpretation of spring-deposited sediments in Dakhleh Oasis, Western Desert of Egypt", *Catena*, **83**, 7-22.

Aerts, A., Velde, B., Janssens, K., Dijkman, W., (2003), "Change in silica sources in Roman and post-Roman glass", *Spectrochim. Acta B* **58**, 659-667.

Afifi, H.A.M., (2011), "Analytical investigation of pigments, ground layer and media of cartonnage fragments from Greek Roman period", *Mediterranean Archaeology and Archaeometry* **11**, 91-98.

Agricola, G., (1556) *"De Re Metallica"*. Translated by H.C. Hoover and L.H. Hoover, Pub. by The Mining Magazine, London, 1912.

Allan, J.W. (1973), "Abu'l –Qasim's Treatise on Ceramics", *Iran*, **11**, 111-120.

Allegretta, I., Pinto, D., Eramo, G., (2016), "Effects of grain size on the reactivity of limestone temper in a kaolinitic clay", *Appl. Clay Science*, **126**, 223-234.

Aliatis, I., Bersani, D., Campani, E., Casoli, A., Paolo Lottici, P. Mantovan, S., Marino, I-G, (2010), "Pigments used in Roman wall paintings in the Vesuvian area", *J. Raman Spectrosc*. **41**, 537-1542.

Alizadeh, P. and Murghussian, V.K., (2000), "The effect of compositional changes on the crystallisation behaviour and mechanical properties of diopside-wollastonite glass ceramics in the SiO_2-CaO-MgO(Na_2O) system", J. *Eur. Ceram. Soc*. **20**, 765-773.

al-Saad, Z., (2002), "Chemical Composition and Manufacturing Technology of a Collection of Various Types of Islamic Glazes Excavated from Jordan", *J. Archaeol. Sci*., **29**, 803-810.

al-Sobay, M.M.H., El-Megharbel, S.M, Refat, M.S., (2013), "Simple Chemical Reactions for the Preparation of Metal Carbonates to be Used as a Nucleus for the Preparation of Nanometer Oxides: Infrared Spectral Studies", *Intl. J. of Innovative Research in Science, Engineering and Technology*, **2**, 7127-7132.

Ambers, J., (2004), "Raman analysis of pigments from the Egyptian Old Kingdom", *J. Raman Spectrosc.*, **35**, 768-773.

Anon., *Encyclopedia Iranica*, Vol. 1, London.

Anon., Final Report – Arsenic Stabilization Research Project. Mine Waste Technology Program Activity IV, Project 5, *U.S. Dept. of Energy*, **1998**.

Anzelmo, J.A., and Lindsay, J.R., (1987), "X-ray fluorescence spectrometric analysis of geologic materials" *Topics in Chemical Instrumentation*, **64**: A181-A185

Apte, N.G., Kiran, E., Chermovsky, J.V., (1988), "Thermal decomposition of aluminium-bearing compounds", *J. of Thermal Analysis*, **34**, 975-981.

Arcolao, C., (1998), *Le ricette del restauro: malte, intonaci, stucchi dal XV al XIX secvolo*, Marsilio, Venezia.

Arnold, D., (1972), "Weiteres zur Keramik von el Târif", *Mitteilungen des Deutchen Archäologischen Instituts, Abteilung Kairo* **28** 33-46.

Arnold, D., (1993), "Techniques and Traditions of Manufacture in the Pottery of Ancient Egypt", in: *An Introduction to Ancient Egyptian Pottery*", (Eds. D. Arnold and J. Bourriau), Phillip von Zabern, Mainz am Rhein.

Arnold, D., and Bourriau, J., (1993), "*An Introduction to Ancient Egyptian Pottery*", Phillip von Zabern, Mainz am Rhein.

Arnold, D.E., Neff, H.A., Bishop, R.L., Glascock, M.D., (1999), "Testing Interpretative Assumptions of Neutron Activation Analysis", in: *Material Meanings: Critical Approaches to the Interpretation of the Material Culture* (Ed. E.S. Chilton) Univ. Utah Press, Salt Lake City, USA.

Aston, D.A., (1996), "*Egyptian Pottery of the Late New Kingdom and Third Intermediate Period (Twelfth – Seventh Centuries BC*", Studien Zur Archāologie und Geschichte Altagyptens Band 13, Heidelberger Orientverlag, Heidelberg.

Aston, D.A., (1998), "*Die Keramik des Grabungsplatzes Q1, Tiel 1:Corpus of Wares and Shapes*". Phillip von Zabern, Mainz am Rhein.

Aston, D.A., (2003), "Reviews", *J. Egyptian Archaeol*. **89**, 264-268.

Aston, D.A., (2004), "Amphorae in New Kingdom Egypt", *Egypt and the Levant*, **14**, 175-213.

Aston, B.G., Harrell, J.A., Shaw, I., (2000), "Stone", in: *Ancient Egyptian Materials and Technology*, (Eds. P.T. Nicholson and I. Shaw), Cambridge University Press, Cambridge, pp. 5-77.

Bachmann, H.G., Everts, H., Hope, C., (1980), "Cobalt-Blue pigment on 18th Dynasty Egyptian Pottery", in: *Mitteilungen des Deutschen Archäologischen Instituts Abeilung Kairo*, Band 36, Pub. Verlag, Mainz/Rhein, 33-38.

Bagnall, R.S., (2001), "Archaeological Work on Helenistic and Roman Egypt, 1995-2000", *American Journal of Archaeology* **105**, 227-243.

Baines, J., (1985), "Color Terminology and Color Classifications: Ancient Egyptian Color Terminology and polychromy", *Am. Anthropologist*, **87**, 282-297.

Baioumy, H.M. and Boulis, S.N., (2012), "Glauconites from the Bahariya Oasis: An evidence for Centomanian marine transgression in Egypt", *J. African Earth Sciences* **70**, 1-7.

Ban, T., Hayashi, S., Yasumori, A., Okada, K., (1996), "Characterisation of Low Temperature Mullitization", *J. Eur. Ceram. Soc.*, **16**, 127-132.

Baraldi, P., F. Bondioli, C. Fagnano, A.M. Ferrari, A. Tinti, M. Vinella, (2001), "Study of the vibrational spectrum of cuprorivaite", *Ann. Chim.*, **91**, 679-692.

Bard, K.A., (1999), "*Encyclopaedia of the Archaeology of Ancient Egypt*", Routledge, London.

Barkoudah, Y. and Henderson, J., (2006), "Plant Ashes from Syria and the manufacture of Ancient Glass: Ethnographic and Scientific Aspects", *J. Glass Studies* **48**, 297-321.

Barrett, G.T., (2013), "Rehydroxylation dating of fired clays: an improved *time-offset* model account for the effect of cooling on post-reheating mass gain", *J. Archaeol. Sci.*, **40**, 3596-3603.

Barrios, A., (1932), "The Mines of Sinai", *The Harvard Theological Review* **25:**101-121.

Bass, G.F., (1986), "A Bronze Age Shipwreck at Ulu Burum (Kaş)", *Amer. J. Archaeol.*, **90**, 269-296.

Bass, G.E., Pilak, C, Collon, D., Weinstein, J., (1989), "The Bronze Age Shipwreck at Ulu Burun", *Amer. J. Archaeol.*, **93**, 1-29.

Batonneau, Y., Brémard, C., Laureyns, J., Merlin, J.C., (2000), "Microscopic and imaging Raman scattering study of PbS and its photo-oxidation products", *J. Raman Spectrosc.*, **31**, 1113-1119.

Bayer, G. and Wiedemann, H.G., (1976), "Agyptisch blau: ein synthetisches Farbenpigment des Altertums, wissenschaftlich betrachter", *Sandoz Bull.*; **40**, 20.

Beadnell, H.J.L., (1899), "*Dakhla Oasis: Its Topography and Geology*", Geological Survey Report 1899, Part IV, National Printing Department, Cairo, 1901.

Beadnell, H.J.L., (1901), "*Dakhla Oasis: its topography and geology*", Egyptian Geological Survey Report 1899, Part IV, National Printing Department, Cairo.

Beadnell, H.J.L., (1909), *"An Egyptian Oasis, An account of the Kharga Oasis in the Libyan Desert, with special reference to its history, physical geography and water supply"*, J. Murray, London.

Beck, H.C., (1934), "Glass before 1500 BC", *Ancient Egypt*, **XIX,** 7-21.

Beckmann, J. (1797), "*A History of Inventions and Discoveries*", Vol. 2. Translated by W. Johnston, Pub. J. Bell, London.

Bell, I.M., Clark, R.J.H., Gibbs, P.J. (1997), "Raman spectroscopic library of natural and synthetic pigments (pre- ~1850 AD)", *Spectrochim. Acta A***:53**, 2159-2179.

Bell, M., (1985), "Gurob Tomb 605 and Mycenaean Chronology", in: *Mélanges Eddin Mokhtar* **1**, 61-86.

Bell, M.R., (1987), "Regional variation in polychrome pottery of the 19th Dynasty", *Cahiers de la Ceramique Egyptienne*, **1**, 49-76.

Berke, H., (2007), "The invention of blue and purple pigments in ancient times", *J. Roy. Soc. Chem.*, **36**, 15-30.

Berlin, B. and Kay, P., (1969), "*Basic Color Terms: Their Universality and Evolution*" Berkeley: University of California Press.

Berna, F., Matthews, A., Weiner, S., (2004), "Solubilities of bone material from archaeological sites: the recrystallization window", *J. Archaeol. Sci.*, **31**, 867-882.

Bernal, J.L.P. and Bello, M.A., (2003), "Modelling Sulphur Dioxide Deposition on Calcium Carbonate", *Ind. Eng. Chem. Res*. **42**, 1028-1034.

Bersani, D., Lottici, P.P., Montenero, A., (1999), "Micro-Raman Investigation of Iron Oxide Films and Powders Produced by Sol-Gel Syntheses", *J. Raman Spectrosc*. **30**, 355-360.

Bersani, D., Lottici, P.P., (2016), "Raman spectroscopy of minerals and mineral pigments in archaeometry", *J. Raman Spectrosc.*, wileyonlinelibrary.com, DOI 10.1002/jrs.4914.

Bertoncello, R., Milanese, L., Russo, U., Pedron, D., Guerriero, P., Barison, S., (2002), "Chemistry of cultural glasses: the early Medieval glasses of Monselice's Hill (Padova, Italy)", *J. Non- Crystalline Solids* **306**, 249-262.

Beuvier, T., J.-F. Bardeau, B. Calvignac, G. Corbel, F. Hindré, J.-M Grenèche, F. Boury, A. Gibaud, (2013), "Phase transformations in the $CaCO_3$/iron oxide composite induced by thermal treatment and laser irradiation", *J. Raman Spectrosc*. **44,** 489-495.

Bhargava, R., Sharma, P.K., Kumar, S., Pandey, A.C., Kumar, N., (2011), "Raman investigations of $Zn_{1-x}Co_xO$ nanocrystal: role of starting precursors on vibrational properties", *J. Raman Spectrosc*. **42**, 1802-1807.

Bianchetti, P., Talarico, F., Vigliano, M.G., Ali, M.F., (2000), "Production and characterization of Egyptian blue and Egyptian green frit", *J. Cultural Heritage* **1**, 179-188.

Bikiaris, D., Sister Daniilia, Sotiropoulou, S., *et al.* (1999), "Ochre-differentiation through micro-Raman and micro-FTIR spectroscopies: application on wall paintings at Meteora and Mount Athos, Greece", *Spectrochim. Acta* **A 56**, 3-18.

Birrell, M., (1999), "Excavations in the Cemeteries of Ismant el-Kharab", in: *Dakhleh Oasis Project: Preliminary Reports on the 1992-1993 and 1993-1994 Field Seasons*, (Eds. C.A. Hope and A.J. Mills), Oxbow Books, Oxford, 29-41.

Bishop, J., Lane, M.D., Darby Dyer, M., King, S.J., Brown, A.J., Swayze, G., (2013), "Spectral Properties of Ca-sulfates: Gypsum, Bassanite and Anhydrite", *Am. Mineral.* Submitted September 25, 2013, Pub. (2014), **99**, 2105-2115.

Blom-Böer, I., (1994), "Zusammensetzung altägyptischer Farbpigmente und ihre Herkunftslagerstätten in Zeit und Raum", OMRO, **74**: 55-107.

Bollong, C.A., Vogel, J.C., Jacobson, L., van der Westhuizen, W.A., Sampson, C.G., (1993), "Direct-dating and identity of fibre temper in Pre-Contact Bushman (Basarwa) Pottery", *J. Archaeol. Sci.*, **20**, 41-55.

Bonizzoni, L., Bruni, S., Guglielmi, V., Milazzo, M., Neri, O., (2011), "Field and laboratory multi-technique analysis of pigments and organic painting media from an Egyptian coffin (26th Dynasty)", *Archaeometry*, **53**, 1212-1230 (doi:10.1111/j.1475-4754.2011.00592.x)

Bordignon, F., P. Postorino, P. Dore, G. Trojsi, G., (1997), "Raman identification of green and blue pigments in Etruscan polychromes on architectural terracotta tiles", *J. Raman Spectrosc.*, **38**, 255-259.

Bouchard, M., Gambardella, A., (2010), "Raman microscopy study of synthetic cobalt blue spinels used in the field of art", *J. Raman Spectrosc.*, **41**, 1187-1195.

Bouchard, M., Smith, D.C., Carabatos-Nédelecv, C., (2007), "An investigation of the feasibility of applying Raman microscopy for exploring stained glass", *Spectrochim. Acta A* **68,** 1101-1113.

Boucherit, N., Delicher, P., Joiret, S., Hugot-Le Goff, A., (1989), "Passivity of iron alloys studied by voltammetry and Raman Spectroscopy", *Materials Science Forum* **44-45**, 51.

Bourriau, J.D. and Nicholson, P.T., (1992), "Marl clay pottery fabrics of the New Kingdom from Memphis, Saqqara and Amarna", *J. Egyptian Archaeology*, **78**, 29-91.

Bourriau, J.D., Nicholson, P.T., Rose, P.J., (2000), "Pottery", in: "*Ancient Egyptian Materials and Technology*", (Eds. P.T. Nicholson and I. Shaw), Pub. Cambridge University Press, Cambridge, UK.

Bourriau, J.D, Smith M.V., Nicholson, P.T. (2000a), "*New Kingdom Pottery Fabrics*", 14th Occasional Publication (Ed. P. Spencer), Egypt Exploration Society, London.

Bowen, G.E., (2002), "The Fourth-Century Churches at Ismant el-Kharab", in: *Dakhleh Oasis Project Preliminary Reports on the 1994-1995 to 1998-1999 Field Season*, (Eds. G.E. Bowen and C.A. Hope), Oxbow Books, Oxford, 65-85.

Bowen, G.E., (2003), "The Small East Church at Ismant el-Kharab", in: *The Oasis Papers 3* (Eds. G.E. Bowen and C.A. Hope), Oxbow Books, Oxford, 153-165.

Bowen, G. E., (2003a), "Some Observations on Christian Burial practices", in: *The Oasis Papers 3* (Eds. G.E. Bowen and C.A. Hope), Oxbow Books, Oxford, 167-182.

Bowen, G.E., (2008), "Report to the Supreme Council of Antiquities on the Survey and Testing at Deir Abu Metta and a Christian cemetery at Muzawwaqa in 2008",

Bowen, G.E., (2013), "The Church of Dayr Abu Matta and its Associated Structures: an overview of four seasons of excavations", in: *The Oasis Papers 6,* (Eds. R.J. Bagnall, P. Davoli, and C.A. Hope) Monograph 15, Pub. Oxbow Books, 429-450.

Bowen, G.E., Dolling, W., Hope, C.A., Kucera, P., "Brief Report on the 2007 Excavations at Ismant el-Kharab", *BACE* **18**, 21-52.

Bretsznajder, S. and Pysiak, J., (1965), "Thermal dissociation of basic ammonium aluminium sulphate II. Measurements of the decomposition rate and attempt to explain the reaction mechanism", *NASA Technical Translations TT F-11,479* (Feb.), pp 1-15.

Brill, R.H., (1970), "The chemical interpretation of the texts", in: *Glass and glassmaking in Ancient Mesopotamia*, (Eds., A.L. Oppenheim, R.H. Brill, D. Barag, and A von Saldern), Corning Museum of Glass, NY, pp 105-130.

Brill, R.H., Barnes, I.L., Adams, B., (1974), "Lead isotopes in some ancient Egyptian objects", in: *Recent Advances in Science and Technology of materials*, Vol. 3 (Ed. A. Bishay), Plennum, London, 9-27.

Brindley, G.W. and Nakahira, M., (1959), "The kaolinite-mullite series: I, A survey of outstanding problems", *J. Amer. Ceram. Soc.*, **42**, 311-314.

Brindley, G.W. and Nakahira, M., (1959a), "The kaolinite-mullite series: II, Metakaolin", *J. Amer. Ceram. Soc.*, **42**, 314-318.

Brindley, G.W. and Nakahira, M., (1959b), "The kaolinite-mullite series: III, The high temperature phases", *J. Amer. Ceram. Soc.*, **42**, 319-324.

Brody, R.H., Edwards, H.G.M., Pollard, A.M., (2002,), "Fourier Transform-Raman Spectroscopic study of natural resins of archaeological interest", *Biopolymers*, **67**, 129-141.

Bronk, H., and Freestone, I.C., (2001), "A quasi non-destructive microsampling technique for the analysis of intact glass objects by SEM/EDXA", *Archaeometry*, **43**, 517-527.

Bruni, S., Cariati, F., Casadio, F., Toniolo, L., (1999), "Spectrochemical characterisation of micro-FTIR spectroscopy of blue pigments in different works of art", *Vibrational Spectrosc.*, **20**, 15-25.

Burgio, L., Clark, R.J.H., (2001), "Library of FT-Raman spectra of pigments, minerals, pigment media and varnishes, and supplement to existing library of Raman spectra of pigments with visible excitation", *Spectrochim. Acta* **A57**, 1491-1521.

Burlet, C., Vanbrabant, Y., Goethals, H., Thys, T., Dupin, L., (2011), "Raman spectroscopy as a tool to characterize heterogenite (CoO.OH) (Katanga Province, Democratic Republic of Congo", *Spectrochim. Acta* **A80** 138-147.

Burns, R.G., (1969,1970), "Site preferences of transition metal ions in silicate crystal structures", *Chem. Geol.*, **5**, 275-283.

Burns, R.G., (1973), "The partitioning of trace transition elements in crystal structures: a provocative review with application to mantle geochemistry", *Geochim. Cosmochim. Acta* **37**, 2395-2403.

Burns, R.G., (1993), "*Mineralogical applications of crystal field theory*", Cambridge University Press, Cambridge, UK..

Butzer, K.W. and Hansen, C.L., (1968), *"Desert and River in Nubia"*, Univ. Wisconsin Press, Madison, Wisconsin, USA.

Buzatu, A., Buzgar, N., (2010), "The Raman study of single-chain silicates", *Analele Ştiinţifice Ale Universităţii,,Al. I. Cuza'' Iaşi Geologie Tomul* **LVI**, nr.1

Buzon, M.R., Simonetti, A., Creaser, R.A., (2007), "Migration in the Nile Valley during the New Kingdom period: a preliminary strontium isotope study", *J. Archaeol. Sci.*, **34**, 1391-1401.

Caggiani, M.C., Colomban, Ph., (2011), "Raman identification of strongly absorbing phases: the ceramic black pigments", *J. Raman Spectrosc.*, **42**, 839-843.

Cagno, S., Cosyns, P., Izmer, A., Vanhaecke, E., Nys, K., Janssens, K., (2014), "Deeply coloured and black-appearing Roman glass: a continued research", *J. Archaeol. Sci.* **42**, 128-139.

Cagno, S., Cosyns, P., Van der Linden, V., Schelm, O., *et al*. (2013), "Composition data of a large collection of black-appearing Roman glass", *Open J. Archaeom.* **1e22**, 104-108.

Cagno, S., Cosyns, P., Izmer, A., Vanhaeke, F., Nys, K., Janssens, K., (2014), "Deeply coloured and black-appearing Roman glass: a continued research", *J. Archaeol. Sci.*, **42**, 128-139.

Caley, E.R., (1962), *Analyses of Ancient Glasses 1790-1957*. Corning: Corning Museum of Glass.

Calley, E.R., Richards, J.F.C., (1956), "Theophrastus on Stones", *Contributions in Physical Science No. 1,* Pub. Columbus Ohio Univ., 183-184.

Cameron, M.A.S., Jones, R.E., Filippakis, S.E., (1977), "Scientific Analysis of Minoan Fresco Samples from Knosos", *Annual of the British School in Archaeology in Athens,* **72**, 121-184.

Caracas, R. and Banigan, E.J. (2009), Elasticity and Raman and Infrared spectroscopy of MgAl$_2$O$_4$ spinel from density functional perturbation theory", *Phys. of the Earth and Planetary Interiors* **174**, 113-121.

Carbonara, G., (2007), *Traitato di restauro architettonico, Vols I and II*, UTET, Rome.

Cashion, J.D. and Murad, E., (2004), "*Mössbauer Spectroscopy of environmental Materials and their Industrial Utilisation*", Kluwer Academic Publishers, Dordrecht.

Castro, K., Sarmiento, A., Martinex-Arkanazo, I., Madariaga, J.M., Fernández, L.A., (2008), "Green Copper Pigments Biodegradation in Cultural Heritage: From Malachite to Moolooite, Thermodynamic Modelling, X-ray Fluorescence, and Raman Evidence", *Anal. Chem.*, **80**, 4103-4110.

Catuneanu, O., (2006), "*Principles of Sequence Stratigraphy*" Elsevier, 375 pp.

Catuneanu, O., Abreu, V., Bhattacharya, J.P., Blum, M.D., Dalrymple, R.W., (2006a), "Towards the Standardisation of sequence stratigraphy", *Earth Science Reviews,* **92,** 1-33.

Cavalheri, A.S., Balan, A.M.O.A., Künzli, R., Constantino, C.J.L., (2010), " Vibrational spectroscopy applied to the study of archaeological ceramic artifacts from Guarani, Brazil", *Vibrational Spectroscopy* **54**, 164-168

Chandramohan, P., Srinivasan, M.P., Velmurugan, S., Narasimhan, S.V., (2011), "Cation distribution and particle size effect on Raman spectrum of CoFe$_2$O$_4$", *J. Solid State Chem.* **184**, 89-96.

Chaplin, T.D., Clark, R.J.H., Scott, D.A., (2006), "Study by Raqman microscopy of nine variants of the green-blue pigment verdigris", *J. Raman Spectrosc.*, **37**, 223-229.

Chaptal, J., (1809), "Sur quelques couleurs trouvées à Pompeia", *Annales de chimie*, **70**, 22-31.

Chase, W.T., (1968), in: *Science and Archaeology* (Ed. R.H. Brill), Cambridge (Mass.), pp. 80-90.

Chen, C.Y., Lan, G.S., Tuan, W.H. (2000), "Preparation of mullite by the reaction sintering of kaolinite and alumina", *J. European Ceram. Soc.*, **20**, 2519-2526.

Chen, C.Y., Lan, G.S., Tuan, W.H. (2000a), "Microstructural evolution of mullite during the sintering of kaolin powder", *Ceramics International*, **26**, 715-720.

Chen, I., Hwang, S-k., Chen, S., (1989), "Chemical Kinetics and Reaction Mechanism of Thermal Decomposition of Aluminium Hydroxide and Magnesium Hydroxide at High Temperatures (973-1123 K), *Ind. Eng. Chem. Res.*, **28**, 738-742.

Chen, Y and Miao, X, (2005), "Thermal and Chemical stability of fluoro-hydroxyapatite ceramics with different fluorine contents", *Biomaterials*, **26**, 1205-1210.

Chiriu, D., Carlo Ricci, P., Polcaro, A., Braconi, P, Lanzi, D., Nadali, D., (2014), "Raman Study on Pompeii Potteries: The Role of Calcium Hydroxide on the Surface Treatment", *J. of Spectroscopy*, **Article ID 435026**, pp 10.

Chou, K-S and Soong, C-S., (1984), "Kinetics of the thermal decomposition of aluminium sulphate", *Thermochim. Acta*, **78**, 285-295.

Christophe, L-A., (1964), L'Alun Egiptien – Introduction Historique, *Bulletin de la Societe de Geographie d'Egypte* XXXVII, 75-91.

Chu, V., Regev, L., Weiner, S., Boaretto, E., (2008), "Differentiating between anthropogenic calcite in plaster, ash and natural calcite using infrared spectroscopy: implications in archaeology" *J. Archaeol. Sci.*, **35**, 905-911.

Churcher, C.S., and Mills, A.J., (1999), "*Reports from the survey of the Dakhleh Oasis Western Desert of Egypt 1977-1987"*, Oxbow Monograph 99, London.

Churcher, C.S., Kleindienst, M.R., Schwarcz, H.P., (1999), "Faunal remains from a Middle Pleistocene lacustrine marl in Dakhleh Oasis, Egypt: palaeoenvironmental reconstructions", *Palaeogeography, Palaeoclimatology, Palaeoecology*, **154**, 301-312.

Ciobotă, V., Salma, W., Tarcea, N., Rösch, P., El Aref, M., Gaupp, R., Popp, J., (2012), "Identification of minerals and organic materials in Middle Eocene ironstones from the Bahariya Depression in the Western Desert of Egypt by means of micro-Raman spectroscopy", *J. Raman Spectrosc*. **43**, 405-410.

Clarke, F.E., (1979), "The Corrosive Well Waters of Egypt's Western Desert", *Geological Survey Water-supply Paper 1757-O*, Pub. U.S.A, Govt. Printing Office, Washington.

Clark, R.J.H., (2007), "Raman microscopy as a structural and analytical tool in the fields of art and archaeology", *J. Molecular Structure*, **834-836**, 74-80.

Clark, R.J.H., Cridland, L., Kariuki, B.M., Harris, K.D.M., Withnall, R., (1995), "Synthesis, Structural Characterisation and Raman Spectroscopy of the Inorganic Pigments Lead Tin Yellow Types I and II and Lead Antimonate Yellow: Their identification on Medieval Paintings and manuscripts", *J. Chem Soc. Dalton Trans.*, 2577-2582.

Clark, R.J.H. and Curri, M.L., (1998), "The identification by Raman microscopy and X-ray diffraction of iron-oxide pigments and of the red pigments found on Italian pottery fragments", *J. Molecular Structure* **440**, 105-111.

Clark, J.R.H., and Gibbs, P.J., (1997), "Non-Destructive In Situ Study of Ancient Egyptian Faience by Raman Microscopy" *J. Raman Spectrosc.*, **28**, 99-103.

Clarke, F.E., (1979), "The Corrosive Well Waters of Egypt's Western Desert", *Geological Survey Water-supply Paper 1757-O*, Pub. U.S.A, Govt. Printing Office, Washington.

Clauβen, O., Gerlach, S., Rüssel, C., (1999), "Self-diffusivity of polyvalent ions in silicate liquids", *J. Non-Crystalline Solids*, **253**, 76-83.

Clause, O., Rebours, B., Merlin, E., Trifiro, F., Vaccari, A., (1992), "Preparation and Characterization of Nickel-Aluminium Mixed Oxides Obtained by Thermal Decomposition of Hydrotalcite-Type Precursors", *J. of Catalysis*, **133**, 231-246.

Cole, S.S., (1935), "The conversion of quartz into cristobalite below 1000°C, and some properties of the cristobalite formed", *J. Am. Ceram. Soc.*, 18(1-12), 149-154.

Colomban, Ph., (2003), "Polymerisation degree and Raman identification of ancient glasses used for jewellery, ceramic enamels and mosaics", *J. Non-Crystalline Solids*, **323**, 180-187.

Colomban, Ph., (2004), "Raman spectrometry, a unique tool to analyse and classify ancient ceramics", *Appl. Phys. A*:**79**, 1x67-170.

Colomban, Ph., (2008), "On-site Raman identification and dating of ancient glasses: A review of procedures and tools", *J. Cultural Heritage*, **9**, e355-e60.

Colomban, Ph., (2013), "Non-Destructive Raman Analysis of ancient Glasses and Glazes", in: *Modern Methods for Analysing Archaeological and Historical Glasses*, (Ed. K. Janssens), Pub. John Wiley & Sons Ltd.

Colomban, Ph., (2013a), "Rocks as blue, green and black pigments/dyes of glazed pottery and enamelled glass artefacts – A review", *Eur. J. Mineral*. **25**, 863-879.

Colomban, Ph., Etcheverry, M-P, Asquier, M., Bounichou, M., Tournié, A., (2006), "Raman identification of ancient stained glasses and their degree of deterioration", *J. Raman Spectrosc.*, **37**, 614-626.

Colomban, Ph., Sagon, G., Faurel, X., (2001), "Differentiation of antique ceramics from the Raman spectra of their coloured glazes and paintings", *J. Raman Spectrosc.*, **32**, 351-360.

Colomban, Ph. and Schreiber, H.D., (2005), "Raman signature modification induced by copper nanoparticles in silicate glass", *J. Raman Spectrosc.*, **36**, 884-890.

Colomban, Ph., Tournié, A., Bellot-Gurlet, L., (2006), "Raman identification of glassy silicates used in ceramics, glass and jewellery: a tentative differentiation guide", *J. Raman Spectrosc.*, **37,** 841-852.

Cooper, E., and Lewenstien, E., (1988), "*Clays and Glazes – the Ceramic Review Book of Clay Bodies and Glaze Recipes*" Pub. Ceramic Review, London.

Cornell, R.M. and Schwertmann, U., (1996), "*The Iron Oxides: Structure, Properties, Reactions, Occurrence and Uses*", Pub. VCH, Weinheim, New York.

Coutellier, V. and Stanley D.J., (1987), "Late Quaternary stratigraphy and palaeogeography of the eastern Nile Delta", *Egypt. Mar. Geol.* **77**, 257-275.

Coupry, C., Lautie, A. Revault, M., Dufilho, J., (1994), "Contribution of Raman spectroscopy to art and history", *J. Raman Spectrosc.*, **25,** 89-94

Cox, G.A. and Ford, B.A., (1993), "The long-term corrosion of glass by groundwater", *J. Matl. Sci.* **28**, 5637-5647.

Cristini, O., Kinowski, C., Turrell, S., (2010), "A detailed micro-Raman spectroscopic study of wall paintings of the period AD 100-200: effect of atmospheric conditions on the alteration of samples", *J. Raman Spectrosc.*, **41**, 1120-1127.

Crupi, V., Majolino, D., Venuti, V., Barone, G., Mazzoleni, P., Pezzino, A., La Russa, M.F., Ruffolo, S.A., Bardelli, F., (2010) "Non-destructive identification of green and yellow pigments: the case of some Silician Renaissance glazed pottery", *Applied phys. A.* **100**: 845-853.

Cultrone, G., Rodriguez-Navaro, C., Sebastian, E., Cazalla, O., de La Torre, M.J., (2001), "Carbonate and silicate phase reactions during ceramic firing", *Eur. J. Mineral.* **13,** 621-634.

D'Angelo, P., Boratti, E., Festa, M.R., Notling, H-F., Pavel, N.V., (1997), *J. Chem. Phys.* **107:**2807.

Daniilia, S., Biklaris , D., Burgio, L., Gavala, P., Clark, R.J.H., Chryssoulakis, Y., (2002), "An extensive non-destructive and micro-spectroscopic study of two post-Byzantine overpainted icons of the 16th century", *J. Raman Spectrosc.*, **33**, 807-814.

David, A.R., Edwards, H.G.M., Farwell, D.W., De Faria, D.L.A., (2001), "Raman spectroscopic analysis of ancient Egyptian pigments", *Archaeometry*,**43,** 461-473.

Davies, W.V., (2001), "*Colour and Painting in Ancient Egypt*", Brit. Museum Press, London.

Davy, H., (1815), "Some Experiments and Observation on the Colours Used in Painting by the Ancients", *Philos. Trans. of the Roy. Soc. London,* **105**, 97-104.

Dayton, J.O., (1981), "Cobalt, silver and nickel in late Bronze Age glazes, pigments and bronzes, and the identification of silver sources for the Aegean and Near East by lead isotope and trace element analyses", in: *Scientific Studies in Ancient Ceramics* (Ed. M.J. Hughes), British Museum Occasional Paper No. 19, 129-142.

Debb, C., Walter, P., Castaing, J., Penhoud,P., Veyssiere, P., (2004), "Transmission Electron Microscopy investigations of ancient Egyptian cosmetic powders. *Applied Physics A* **79,**393-396.

De Benedetto, G.E., Catalano, F., Sabbatini, L., Zambonin, P.G., (1998), "Analytical characterisation of pigments on pre-Roman pottery by means of spectroscopic techniques: Part I: white coloured shards", *Fresenius J. Anal. Chem*. **362**, 170-175.

De Benedetto, G.E., Nicoli, S., Pennetta, A., Rizzo, D., Sabbatini, L. Mangone, A., (2011), "An integrated spectroscopic approach to investigate pigments and engobes on pre-Roman pottery", *J. Raman Spectrosc.,* **42**, 1317-1323.

Deer, W.A., R.A. Howie, J. Zussman, (1992), *Rock Forming Minerals*, Pub. Pearson, Prentice Hall, London.

de Faria, D.L.A. and Lopes, F.N., (2007), "Heated goethite and natural hematite: Can Raman spectroscopy be used to differentiate them?", *Vibrational Spectroscopy* **45**, 117-121.

de Faria, D.L.A., Venâncio Silva, S., de Oliveira, M.T., (1997), "Raman Microspectroscopy of some Iron Oxides and Oxyhydroxides", *J. Raman Spectrosc*. **28**, 873-878.

de Fontenoy, H., (1874), "Note sur le bleu égyptien", *Annales de Chimie* 2, ser. 5, 193-199.

De Francesco, A.M., Scarpelli, R., Del Vecchio, F., Giampaola, D., (2013), "Analysis of early medieval glass from excavations at 'Piazza Bovio', Naples, Italy", *Archaeometry*, doi: 10.1111/arcm.12070, Pub. (2014), **31**, 137-147.

de Souza, L.K.C, Zamian, da Rocha Filo, G.N., Soledade, L.E.B., dos Santos, I.M.G., Souza, A.G., Scheller, T., Angélica, R.S., da Costa, C.E.F., (2009), "Blue pigments based on $Co_xZn_{1-x}Al_2O_4$ spinels synthesised by the polymeric precursor method", *Dyes and Pigments* **81**, 187-192.

de Waal, D., (2004), "Raman investigation of ceramics from 16th and 17th Century Portuguese shipwrecks", *J. Raman Spectrosc.,* **35**, 646-649.

de Waal, D., (2009), "Micro-Raman and portable Raman spectroscopic investigation of blue pigments in selected Delft plates (17th-20th Century)", *J. Raman Spectrosc*., 4**0**, 2162-2170.

Delamare, F., (1984), "Analyse des couches picturales", *Histoire et Archéologie*, **89**, 90-92.

Delamare, F., (1998), "*De la composition du Bleu Egiptien utilisè en Peinture Murale Gallo-romaine"*, in: *La Couleur dans la Peinture et l'Émaillage de l'Égypte ancienne*, (Eds. S. Colinart, M. Menu), Actes de la Table Ronde Ravello, 20-22 Mars, 1997, Edipuglia, Bari, 177-193.

Delaplane, R.G., Ibers, J.A., Ferraro, J.R., Rush, J.J., (1969), "Diffraction and Spectroscopic Studies of the Cobaltic Acid System $HCoO_2$-$DCoO_2$", *J. Chem. Phys*. **50**, 1920-1927.

Diamandopoulos, A.A., (1996), "Organic and Inorganic Cosmetics in the Preclassical Eastern Mediterranean", *International Journal of Dermatology* **35:**751-756.

Dill, H.G., Pöllmann, H., Techner, A., (2013), "500 Million years of rift- and unconformity-related Mn mineralisation in the Middle East: a geodynamic and sequence stratigraphical approach to the recycling of Mn", *Ore Geology Reviews*, **53**, 112-133.

Dill, H.G., (2016), "Kaolin: Soil rock and ore. From the mineral to the magmatic, sedimentary and metamorphic environments", *Earth-Science Reviews* **161**, 16-129.

D'Ippolito, V., Andreozzi, G.B., Bersani, D., Lottici, P.P., (2015), "Raman fingerprint of chromite, aluminate and ferrite spinels, *J. Raman Spectrosc.*, **45**, 1255-1264.

Dixit, M., Subbanna, G.N., Karmath, P.V., (1996), "Homogeneous precipitation from solution by urea hydrolysis: a novel chemical route to the α-hydroxides of nickel and cobalt", *J. Mater. Chem.* **6**, 1429-1432.

Drits, V.A., Derkowski, A, McCarty, D.K., (2011), "Kinetics of thermal transformation of partially dehydroxylated pyrophyllite", *Amer. Mineral.*, **96**, 1054-1069.

Duma, G. (1972), "Phosphate content of ancient pots as indication of use", *Current Anthropology*, **13** 127-130.

Dungworth, D., (2009), "Innovations in the 17th-century glass industry: the introduction of kelp (seaweed) ash in Britain", *Intl. Colloquium Innovations in compositions and in production processes*, 26-28 Mar., Nancy, France, p 301.

Dunnwald, J. and Otto, A., (1989), "An investigation of phase transitions in rust layers using Raman spectroscopy", *Corrosion Science* **29**, 1167-1176.

Dyer, J., Ambers, J., (2009), Identification of a red substance on the surface of a fourteenth century iron 'kettle hat' (Prehistory and Europe 1856,0701.2243), *CSR Report No. AR2009/72*, Department of Conservation and Scientific Research, British Museum, London pp 4.

Ead, H.A., (2006), "Cosmetics in Ancient Egypt", *Ambix***: 1-4.

Eccleston, M.A.J., (2002), "Metalworking at Kellis: A Preliminary Report", in: *Dakhleh Oasis Project: Preliminary Reports on the 1994-1995 to 1998-1999 Field Seasons*, (Eds. C.A. Hope and G.E. Bowen), Oxbow, Oxford, 143-149.

Eccleston, M., (2006), "Technological and Social aspects of High-Temperature Industries in the Dakhleh Oasis, Egypt, During the Ptolemaic and Raman Periods", *PhD Thesis*, Monash University.

Edwards, H.G.M., (2005), "Case Study: Prehistoric Art", In: *Raman Spectroscopy in Archaeology and Art History*, Eds. H.G.M. Edwards and J.M. Chalmers, Pub. *Roy. Soc. Chem.*, Cambridge, UK, pp. 84-96.

Edwards, H.G.M., and Ali, E.M.A., (2011), "Raman spectroscopy of archaeological and ancient resins: Problems with database construction for applications in conservation", *Spectrochim. Acta PartA:***80**, 49-54

Edwards, H.G.M., and Chalmers, J.M., (2005), "Raman Spectroscopy in Archaeology and Art History", *RSC Analytical Spectroscopy Monographs*, Pub. Roy. Soc. Chemistry, Cambridge, UK.

Edwards, H.G.M., Currie, K.J., Hassan, R.H.A., Jorge Villar, S.E., David, A.R., Denton, J., (2007), "Raman spectroscopy of *natron*: shedding light on ancient Egyptian mummification", *Anal. Bioanal. Chem*. 388:683-689.

Edwards, H.G.M., and Falk, M.J., (1997), "Fourier Transform Raman Spectroscopic study of Frankincense and Myrrh", *Spectrochim. Acta A***53**, 2393-2401.

Edwards, H.G.M. and Farwell, D.W., (2008), "The conservational heritage of wall paintings and buildings: an FT-Raman spectroscopic study of prehistoric, Roman, mediaeval and Renaissance lime substrates and mortars", *J. Raman Spectrosc.*, **39**, 985-992.

Edwards, H.G.M., Farwell, D.W., Quye, A., (1997), "'Dragons Blood' 1-Characterisation of an Ancient Resin using Raman Spectroscopy", *J. Raman Spectrosc*. **28**, 243-349.

Edwards, H.G.M., Farwell, D.W., Rozenberg, S., (1999), "Raman Spectroscopic Study of Red pigment and Fresco Fragments from King Herod's Palace at Jericho", *J. Raman Spectrosc*. **30**, 361-366.

Edwards, H.G.M., Jorge Villar, S.E., David, A.R., de Faria, D.L.A., (2004), "Non-destructive analysis of Ancient Egyptian funerary relics by Raman spectroscopic techniques", *Anal. Chim. Acta* **503,** 223-233.

Edwards, H.G.M., Jorge Villar, S.E., Eremin, K.A., (2004a), "Raman spectroscopic analysis of pigments from dynastic Egyptian funerary artefacts", *J. Raman Spectrosc.*, **35**, 786-795.

Egerton R.F., (2005), "*Physical Principles of Electron Microscopy*", Springer, USA.

Eggeman, T., (2001), "Ammonia", in: *Kirk-Othmer Encyclopedia of Chemical Technology*, John Wiley and Sons, New York.

El-Asmar, H.M., Wood, P., (2000), "Quaternary shoreline development: the Northwestern coast of Egypt", *Quaternary Science Reviews* **19**, 1137-1149.

El Goresy, A., (2000), "Polychromatic Wall Painting Decoration in Monuments of Pharaonic Egypt: Composition, Chronology and Painting Technology", in: Proc. Of the First International Symp., *The Wall paintings of Thera*, (Ed. S. Sherratt), Thera Foundation, Piraeus, pp. 49-70.

El Goresy, A., Jaksch, h., Abdel Razek, M., Weiner, K.L., (1986), "Ancient pigments in wall paintings of Egyptian tombs and temples: an archaeometric project", In: *Interdisziplinäres Gespräch: Geistesweisenschaft-Naturwissenschaft-Technik anhand konkreter Projekte*, (Eds. H. Trenkwalder, F. Purtscheller, W. Lukas, H. Seidl), 1-57, Sonderheft des Bunddesministerium für Weissenschaft und Forschung, Wien.

El Maghraby, A., (2012), "Phosphate Mining Waste at Abu Tartur Mine Area, Western Desert of Egypt", *Australian J. of Basic and Appl. Sci.*, **6**, 231-248.

El-Mottaleb, M.A., Cheira, M.F., Gouda, G.A.H., Ahmed, A.S.A., (2016), "Leaching of Rare Earth elements from Egyptian Western Desert Phosphate Rocks using HCl", *Chemistry of Advanced Materials*, **1**, 33-40.

El-Rahman, Y.A., A.A. Surour, A.H.W. El Manawi, M. Rifai, A.A. Motelib, W.K. Ali, A.M. El Dougdoug, (2012), "Ancient Mining and Smelting Activities in the Wadi Abu Gerida Area, Central Eastern Desert, Egypt,: Preliminary Report", *Archaeometry*, **55**, (2012), 1067-1087 (DOI 10.1111/j 1475-1754.2012.000728x).

Eliyahu-Behar, A., Shai, I., Regev, L., Ben-Shlomo, D., Albaz, S., maeir, A.M., Greenfield, H.J., (2016), "Early Bronze Age Pottery Covered with Lime-Plaster: Technological Observations", *Tel Aviv University* **43**, 27-42.

Elmaadawy, Kh.G., el Din, E., Khalid, A.M., Abouzeid, A.-Z.M., (2015), "Mineral Industry in Egypt – Part II Non-Metallic Commodities – Phosphate Rocks", *J. Mining World Express* (MWE), **4**, 1-18.

El Salam, S.A., (2004), "Scientific study of Graeco/Roman wall plasters & pigments in Alexandria, Egypt", in:*34th Intl. Symp. on Archaeometry*, Zaragoza, Spain, 253-259.

Etchepare, J., Merian, M., Kaplan, P., (1978), "Vibrational normal modes of SiO_2, II. Cristobalite and tridymite", *J. Chem. Phys*. **68(4),** 1531-1537.

Falgayrac, G., Sobanska, S., Brémard, C., (2014), "Raman diagnosis of the reactivity between $ZnSO_4$ and $CaCO_3$ particles in humid air relevant to heterogeneous zinc chemistry in atmosphere", *Atmospheric Environment* **85**, 83-91.

Farnsworth, M. and Ritchie, P.D., (1938), "Spectrographic studies on ancient glass", *Technical Studies VI* (3).

Fernández, A.L., de Pablo, L., (2002), "Formation and the colour development in cobalt spinel pigments", *Pigment & Resin Technol.*, **31**, 350-356.

Fernández-Osorio, A., Vázquez-Olmos, A., Sato-Berru, R., Escudero, R., (2009), "Hydrothermal synthesis of Co_3O_4 octahedra and their magnetic properties", *Rev. Adv. Mater. Sci.*, **22,** 60-66.

Filippakis, S.E., Perdikatsis, B., Paradellis, T., (1976), "An Analysis of the Blue Pigments from the Greek Bronze Age", *Studies in Conservation* **21**, 143-153.

Fischer, R.B. and Peters, D.G., (1968), "*Quantitative Chemical Analysis*", W.B. Saunders Co., 3rd Edit.

Forés, A., Llusar, M., Badenes, J.A., Calbo, J., Tena, M.A., Monrós, G., (2000) "Cobalt minimisation in willemite ($Co_xZn_{1-x}SiO_4$) ceramic", *Green Chemistry* **2**, 93-100.

Foucault A., and Stanley, D.J., (1989), "Late Quaternary paleoclimatic oscillations in East Africa recorded by heavy minerals in the Nile delta", *Nature* **339**, 44-46.

Fouqué, F., (1884), "Sue le bleu égyptien ou vestorien", *Compres Rendus hebdomaire des Séances*, **108**, 325-327, and *Bull. Soc. De Mines de France*, **12**, 36-38.

Franklin, C.E.L., and Forrester, A.J., (1975), "The Development of Bone China", *Trans. Brit. Ceram. Soc.*, **74**, 141-145.

Freeman, J.J., Wang, A., Kuebler, K.A., Jolliff, B.L., Haskin, L.A., (2008), "Characterisation of natural feldspars by Raman spectroscopy for future planetary exploration", *The Canad. Mineralogist* **46**, 1477-1500.

Freestone, I.C., (1987), "Composition and microstructure of early opaque red glasses", in: *Early vitreous material* (Eds. M. Bimson and I. Freestone), *Brit. Museum Occasional Pap.* **56**, London, 173-191.

Freestone, I.C., (1993), " A Technical Study of Limehouse Ware*", in: *Limehouse Ware Revealed*, (Ed. D. Drakard), English Ceramic Circle, **68-73.**

Freestone, I.C., (2006), "Glass production in Late Antiquity and the Early Islamic Period: a geochemical perspective", in: *Geomaterials in Cultural Heritage* (Eds. M. Maggetti, B. Messiga), Geological Soc., London, Special Publications **257**, 201-216.

Freestone, I., and Gorin-Rosen, Y., (1999), "The great glass slab from Bet She'arim, Israel: an early Islamic glassmaking experiment?", *J. Glass Studies*, **41**, 105-116.

Freestone, I., Meeks, N., Middleton, A., (1985), "Retention of phosphate in buried ceramics: an electron microbeam approach", *Archaeometry*, **27**, 161-177.

Freestone, I., Middleton, A., Meeks, N., (1994), "Significance of Phosphate in Ceramic Bodies: discussion of paper by Bollong *et al*." *J. Archaeol. Sci*. **21**, 425-426.

Freestone, I.C., Price, J., Cartwright, C.R., (2006) "The batch: its recognition and significance", in: *Annales du 17e Congrès de l'Association Internationale pour l'Histoire du Verre*, (Eds. K. Janssens, P. Degryse, P. Cosyns, J. Caen, L. Van't dack), Antwerp.

Freeth, S.J., (1967), "A chemical study of some bronze age pottery sherds", *Archaeometry*, **10**, 104-119.

French, P., (2013), "*The Anubieion at Saqqara III*", (Ed. D. Aston), Egypt Exploration Society, London.

Froment, F., Tournié, A., Colomban, Ph., (2008), "Raman identification of natural red to yellow pigments: ochre and iron-containing ores", *J. Raman Spectrosc.*, **39**, 560-568.

Frommold, C., (2004), "An Archaeometric Application of External Beam PIXE: Colour Reconstruction of an Egyptian Temple Relief", *10th Intl. Conf. Particle Induced X-ray Emission and its Analytical Applications, PIXE 2004*, Portorož, Slovenia.

Garland, H., and Bannister, C.O., (1927), "*Ancient Egyptian Metallurgy*", Chas. Griffin & Co. Ltd., London.

Garrels, C., (1965), "*Solutions, Minerals and Equilibria*", Freemen, Cooper & Co., San Francisco.

Garrett, D.E., (2001), "*Chemistry – Sodium Sulfate Handbook of Deposits: Processing and Use*", Academic Press, San Diego.

Garcia-Vallès, M., Gimeno-Torrente, D., Martínez-Manent, S., Fernández-Turiel, J.L., (2003), "Medieval stained glass in a Mediterranean climate: Typology, weathering and glass decay, and associated biomineralisation processes and products", *Am. Mineralogist*, **88**, 1996-2006.

Genedi, A., (1998), "Formation of the Upper Cretaceous cherts in northeastern Sinai", *J. African Earth Sciences*, **28**, 297-311.

Gerlach S., Clauβen, O., Rüssel, C., (1998), "Self-diffusivity of iron in alkali-lime-aluminosilicate glass melts", *J. Non-Crystalline Solids*, **240**, 110-117.

Gerlach S., Clauβen, O., Rüssel, C., (1998), "Self-diffusivity of iron in alkali-magnesia-silica glass melts", *J. Non-Crystalline Solids*, **240**, 11-18.

Gettens, R.J., and Stout, G.L., (1966), "*Painting materials, A Short Encyclopaedia*", Dover, N.Y. pp 134.

Giannakas, A.E., Ladavos, A.K., Armatas, G.S., Pomonis, P.J., (2007), "Surface properties, structural features and catalytic performance for NO + CO abatement of spinels MAl_2O_4 (M= Mg, Co and Zn) developed by reverse and bicontinuous microemulsion method", *Appl. Surface Sci.*, **253**, 6969-6972.

Giddy, L.L., (1987), "*Egyptian Oases: Bahariya, Dakhla, Farafra and Kharga during Pharaonic Times*", Warminster, Aris and Phillips.

Gill, M.S. and Rehren, Th., (2014), "The intentional use of lead-tin orange in Indian Islamic glazes and its preliminary characterisation", *Archaeometry*, **56**, 1009-1023.

Gingerich, P.D., (2008), "Early Evolution of Whales: A Century of Research", in: "*Elwyn Simons: A Search for Origins*", (Eds., J.G. Fleagle, C.C. Gilbert), Univ. Chicago, Chicago, Ill p107-124.

Giordani, P., Modenesi, P., Tretiach, M., (2003), "Determinant factors for the formation of the calcium oxalate minerals, weddellite and whewellite, on the surface of foliose lichens", *The Lichenologist*, **35**, 255-270.

Glebycheva, A.I., Kazakova, N.N., Vizir, L.A., Bystrikov, A.S., Gorbachev, V.V., (1983), "Ceramic pigments based on cobalt-containing forsterite", *Steklo I Keramika*, **2**, p24, UDC 666.295, Plenum Publishing Corp. 105-106.

Glenn, C.R., (1990), "Depositional sequences of the Duwi, Sibâîya and Phosphate formations, Egypt": phosphogenesis and glauconitization in a Late Cretaceous epiric sea", *Geol. Soc. Special Pub. No 52*, 205-222.

Gliozzo, E., Cavari, F., Damiani, D., Memmi, I., (2012), Pigments and plasters from the Roman settlement of *Thamusida* (Rabat, Morocco), *Archaeometry*, **54**, 278-293.

Goldstein, J.I., Lyman, C.E., Newbury, D.E., Lifshin, E., Echlin, P., Sawyer, L., Joy, D.C., Michael, J.R., (2003), "*Scanning Electron Microscopy and X-Ray Microanalysis, 3rd Edit.*, Springer, USA.

Goodgame, M., and Cotton, F.A., (1961), "Magnetic investigations of spin-free cobaltous complexes. IV. Magnetic properties and spectrum of cobalt(II) orthosilicate", *J. Phys. Chem.* **65**, 791-792.

Green, L., (2001), "Colour transformation of ancient Egyptian pigments", in: Colour and Painting in Ancient Egypt, (Ed. W.V. Davies), *The British Museum Press*, 43-47.

Groat, L.A., Kek, S., Bismayer, U., Schmidt, C., *et al.,* (1996), "A synchrotron radiation, HRTEM, -ray powder diffraction, and Raman spectroscopic study of malayaite, $CaSnSiO_5$", *Am. Mineralogist*, **81**, 595-602.

Guido, M., Henderson, J., Cable, M., Bayley, J., Biek, L., (1984), "A Bronze Age Glass Bead from Wilsford, Wiltshire: Barrow G.42 in the Lake group", *Proc. of the Prehistoric Soc.* **50**, 245-254.

Gur-Arieh, S., Shahack-Gross, R., Maeir, A.M., Lehmann, G., Hitchcock, L.A., Boaretto, E., (2014), "The taphonomy and preservation of wood and dung ashes found in archaeological cooking installations: case studies from Iron Age Israel", *J. Archaeol. Sci.* **46**, 50-67.

Hadjeiv, V.G., Iliev, M.N., Vergilov, I.V., (1988), "The Raman spectra of Co_3O_4", *J. Phys. C:Solid State Phys.* **21**, L.199-L.201.

Hagen A., and Östby, J., (2006), "Oxidation States of Mn, Cr, and Co in *Mixed Spinels Studied by XANES*", Pub. Risø National Laboratory, Denmark, 130.226.56.153, 1-10.

Hall, C., Hamilton, A., Wilson, M.A., (2013), "The influence of temperature on rehydroxylation [RHX] kinetics in archaeological pottery", *J. Archaeol. Sci.*, **40**, 305-312.

Hamdan, M.A., Martinez, S.M., Garcia Vallès, Nogués, J.M., Hassan, F.A., Flower, R.J., Aly, M.H., Ebrahim, E.S., (2013), "Ancient Egyptian pottery from the subsurface floodplain of the Saqqara-Memphis area: Its mineralogical and geochemical implications", *Archaeometry* (2014), **56**, 987-1008. (doi:10.1111/ arcm.12075).

Hancock, R.G.V., Millet, N.B., Mills, A.J. (1986), "A Rapid INAA Method to Characterise Egyptian Ceramics", *J. Archaeol. Sci.*, **13**, 107-117.

Hanesch, M., (2009), "Raman spectroscopy of iron oxides and (oxy)hydroxides at low laser power and possible applications in environmental magnetic studies", *Geophys. J. Intl.* **177**, 941-948.

Harris, J.R., (1961), "Lexicographical studies in ancient Egyptian minerals*", Institut für Orientforschung Veröffentlichung* **54.1**, Berlin.

Harvey, R., Hannah, R., Vaughan, J., (2011), "Selective precipitation of mixed nickel-cobalt hydroxide", *Hydrometallurgy*, **105**, 222-228.

Hassan, N.M., Mansour, N.A., Fayez-Hassan, M., Sedqy, E., (2013), "Elemental analysis of Egyptian phosphate4 fertiliser components samples by TGA, DTA and IR methods", *ISOR J. Environmental Sci, Toxicology and Food Technology* **7**, 98-106

Hatton, G.D., (2008), "Production of Egyptian blue and green frits", in: *Monograph 72*, (Eds. M.S. Tite and A.J. Shortland), *Oxford University School of Archaeology*, p 147-185.

Hatton, G.D., A.J. Shortland, M.S. Tite, (2001), "Egyptian blue: Where, When and How?" in: *Current Research in Egyptology III*, (Eds. R. Ives, D. Lines, C. Naunton, N. Wahlberg) BAR International Series **1192**.

Hatton, G.D., A.J. Shortland, M.S. Tite, (2008), "The production technology of Egyptian blue and green frits from second millennium BC Egypt and Mesopotamia", *J. Archaeological Science*, **35**, 1591-1604.

Hayes, W.C., (1951a), "Inscriptions from the palace of Amenhotep III", *J. Near Eastern Studies*, **10**, 35-56.

Hayes, W.C., (1951b), "Inscriptions from the palace of Amenhotep III", *J. Near Eastern Studies*, **10**, 82-112.

Hayes, W.C., (1951c), "Inscriptions from the palace of Amenhotep III", *J. Near Eastern Studies*, **10**, 156-183.

Hayes, W.C., (1951d), "Inscriptions from the palace of Amenhotep III", *J. Near Eastern Studies*, **10**, 231-242.

He, X., Xu, M., Zhang, H., Zhang, B., Su, B., (2014), "An exploratory study of the deterioration mechanisms of ancient wall-paintings based on thermal and moisture expansion property analysis", *J. Archaeol. Sci.*, **42**, 194-200.

Heinrich, C., (2015), "Ancient life helped form Earth's largest gold hoard", *New Scientist*, 5 Feb. p11

Henderson, J., (1985), "The raw materials of early glass production", *Oxford J. Archaeology* **4**, 267-291.

Henderson, J., (1989), "The scientific analysis of ancient glass and its archaeological interpretation" in: *Scientific Analysis in Archaeology* (Ed. J. Henderson), Oxford: Oxford University Committee for Archaeology, *Monograph* **19**, pp 30-62.

Henderson, J., (2003), "Glass" in: *The Science and Archaeology of Materials: An Investigation of Inorganic Materials*, Pub. Taylor and Francis, Florence, Italy.

Hernanz, A., Ruiz-López, J.F., Gavira-Vallejo, J.M., Martin, S., Gavrilenko, E., (2010), "Raman microscopy of prehistoric rock paintings from the Hoz de Vicente, Minglanilla, Cuenca, Spain", *J. Raman Spectrosc.*, **41**, 1104-1109.

Hey, M.H., (1962), "Cobaltic oxide in nature", *Mineralogical Mag*. **33:258**, 253-259.

Hickson, K., (2002), "Excavations in Area C at Ismant el-Kharab in 1996-1997", in: *Dakhleh Oasis Project: Preliminary Reports on the 1994-1995 to 1998-1999 Field Seasons*, (Eds. C.A. Hope and G.E. Bowen), Oxbow, Oxford, 157-166.

Hill, W.L., Faust, G.T., Reynolds, D.S., (1944), "The Binary System P_2O_5-$2CaO.P_2O_5$ Part I", *Am. J. Sci*. **242**, 457-477.

Hill, W.L., Faust, G.T., Reynolds, D.S., (1944a), "The Binary System P_2O_5-$2CaO.P_2O_5$ Part II", *Am. J. Sci*. **242**, 542-562.

Hingston, F.J., Posner, A.M., Quirk, J.P., (1971), "Competitive adsorption of negatively charged ligands on oxide surfaces", *Discuss. Faraday Soc*. **52**, 334-342.

Hodges, H., (1976), "*Artifacts: An Introduction to Early Materials and Technology*", Pub. John Baker, London.

Holdridge, D.A., Vaughan, F., *"The Kaolin Minerals (kandites)"* in: *The Differential Thermal Investigation of Clays*, (Ed. R.C. Mackenzie), Mineralogical Soc. London, UK, **1957**, 98.

Hollingbery, L.A., Hull, T.R., (2010), "The Thermal Decomposition of Huntite and Hydromagnetite – a Review", *Thermochim. Acta* **509**:1-11.

Hope, C.A., (1977), "Two Examples of Egyptian Blue-painted Pottery in the Medelhavsmuseet". *Medelhavsmuseet. Bulletin*. **12**.1977

Hope, C.A. (1980), "Blue Painted Pottery of the XVIIIth Dynasty". *PhD thesis*, University College London.

Hope, C.A., (1980a), "Dakhleh Oasis Project – Report on the study of the pottery and kilns", *Journal of the Society for the Study of Egyptian Antiquities*, **11**:233-241.

Hope, C.A., (1982), "Blue Painted Pottery", in: *Egypt's Golden Age; The Art of Living in the New Kingdom 1558-1085 BC.*, Exhibition Catalogue, Boston.

Hope, C.A., (1987), "Innovation in the decoration of ceramics in the mid-18th Dynasty", *Cahiers de la Céramique Égyptienne*, **1**. 97-122

Hope, C.A., (1989), *"Pottery of the Egyptian New Kingdom: Three Studies"*, *Occasional Paper No. 2*, Victoria College, Melbourne.

Hope, C.A., (1991), "Blue-painted and polychrome decorated pottery from Amarna: a preliminary corpus", *Cahiers de la Céramique Égyptienne* **2**, 17-92.

Hope, C.A., (1993), Pottery kilns from the Oasis of el-Dakhla", in: *An Introduction to Ancient Egyptian Pottery*, (Eds. D. Arnold and J. Bourriau), Verlag Philipp Von Zabern, Mainz Am Rhein.

Hope, C.A., (1999), "Pottery manufacture in the Dakhleh Oasis", in: "*Reports from the Survey of the Dakhleh Oasis Western Desert Egypt 1977-1987"*, Eds. C.S. Churcher and A.J. Mills, Oxbow Monograph 99, Oxford, pp 215-250.

Hope, C.A., (2001), "Egypt and Libya: The excavations at Mut el-Kharab in Egypt's Dakhleh Oasis", *The Artefact*, **24**, 29-46.

Hope, C.A.., (2001a), "Observations on the Dating of the Occupation at Ismant el-Kharab", in: *The Oasis Papers: Proc. Of the First International Symp. of the Dakhleh Oasis Project*, (Eds. C.A. Marlow and A.J. Mills), Oxbow Books, Oxford, 43-59.

Hope, C.A., (2001b), "Excavations at Ismant el-Kharab and Mut el-Kharab in 2001", *Bulletin of the Australian Centre for Egyptolog*y **12**, 35-64.

Hope, C.A., (2002), "Early and Mid-Holocene Ceramics from the Dakhleh Oasis: Traditions and Influences", In: *Egypt and Nubia – Gifts of the Desert*, Ed. R. Friedman, pub. The British Museum Press, 39-61.

Hope, C.A., (2004), "A note on Some Ceramics from Mut, Dakhleh Oasis", *Cahiers de la Céramique Égyptienne* **7**, 99-110.

Hope, C.A.., (2004a), "Excavations at Ismant el-Kharab and Mut el-Kharab in 2004", *BACE* **15**, 19 - 49.

Hope, C.A., (2011), "Possible Mid-18th Dynasty examples of blue-painted pottery from the Egypt Exploration Society's excavations at Memphis", in: "*Under the Potter's Tree*", (Eds. D. Aston, B. Bader, C. Gallorini, P. Nicholson, and S. Buckingham), Peeters Publishers, 495-512.

Hope, C.A., (2014), "The Kellis 1 Cemetery: Roman Period Burial Practices in Dakhleh Oasis", in: *Le myrte & la rose, (Eds.* G. Tattet and C. Zivie-Coche), Montpellier, 325 – 348.

Hope, C.A., (2015), "The Roman-Period Houses of Kellis in Egypt's Dakhleh Oasis", in: *Housing and Habitat in the Ancient Mediterranean: Cultural and Environmental Responses*, (Eds. A.A. Di Castro and C.A. Hope), Pub. Peeters, Leuven 199-229.

Hope, C.A., Blauer, M., Riederer, J., (1981), "Recent Analyses of 18th Dynasty Pottery", in: *Studien zur altägyptischen Keramik*, (Ed. D. Arnold) Verlag Philipp Von Zabern, Mainz am Rhein, 139-166.

Hope, C.A., Bowen, G.E., Cox, J., Dolling, W., Milner, J., Pettman, A., (2009), "Report on the 2009 Season of Excavations at Mut el-Kharab, Dakhleh Oasis", *Bull. The Australian Centre for Egyptology*, **20**, 47-86.

Hope, C.A., Jones, D., Falvey, L., Petkov, J., Whitehouse, H., Worp, K., (2010), "Report of the 2010 season of excavations at Ismant el-Kharab, Dakhleh Oasis", in: *The Bulletin of the Australian Centre for Egyptology*, **21**, 21-54.

Hope, C.A., Kucera, P., Smith, J., (2009), "Alum exploitation at Qasr el-Dakhleh in the Dakhleh Oasis", In: *Beyond the Horizon* Vol. 1, (Eds., S. Ikram and A. Dodson), Pub. Supreme Council of Antiquities Press, Cairo, 165-179.

Hope, C.A. and McKenzie, J., (1999), "Intrim Report on the West Tombs", in: *Dakhleh Oasis Project: Preliminary Reports on the 1992 - 1993 and 1993 - 1994 Field Seasons*, (Eds. C.A. Hope and A.J. Mills), Oxbow Books, Oxford, 53 - 68.

Hope, C.A., and Pettman, A.J., (2012), "Egyptian Connections with Dakhleh Oasis in the Early Dynasticf period to Dynasty IV: new data from Mut al-Kharab", in: *The Oasis papers 6, Proc. Of the Siuxth Intl. Conf. of the Dakhleh Oasis Project*, (Eds. R.S. Bagnall, P. Davoli, C.A. Hope), Dakhleh Oasis Project 15, Oxbow Books, Oxford.

Hope, C.A., and Whitehouse, H., (2004), "The Gladiator Jug from Ismant el-Kharab", in: *The Oasis Papers, 3, Proc. Third Intl. Conference of the Dakhleh Oasis Project* (Eds. C.A. Hope and G.E. Bowen), Oxbow Books, Oxford, 291-310

Hope, C.A., and Whitehouse, H., (2006), "A painted residence at Ismant el-Kharab (at Kellis) in the Dakhleh Oasis", *J. Roman Archaeology*, **19**, 313-328.

Horgnies, M., Bayle, M., Gueit, E., Darque-Ceretti and Aucouturier, M., (2015), "Microstructure and surface properties of frescoes based on lime and cement: The influence of the artist's technique", *Archaeometry*, **57**, 344-361.

Houben, A.J.P., van Mourik, C.A., Montanari, A., (2012), "The Eocene-Oligocene transition: Changes in sea level, temperature or both?", *Palaeogeography, Paleoclimatology, Paleoecology*, **335-336**, 75-83.

Hradil, D., Grygar, T., Hruškova, M., (2004), "Green earth pigment from the Kadaň region, Czech Republic: Use of rare Fe-rich smectite:, *Clays and Clay Minerals*, **52**, 767-778.

Huang, E., Chen, C.H., Huang, T., Lin, E.H., Xu, J.-A., (2000), "Raman spectroscopic characteristics of Mg-Fe-Ca pyroxenes", *Am. Mineralogis*t **85**, 473-479.

Hubschmann, C., (2012), "Searching for an Oasis Identity: Dakhleh Oasis in the Third Intermediate Period", in; *Egyptology in Australia and New Zealand*, (Eds. C.M. Knoblauch and J.C. Gill), Proc. Conf. Melbourne, BAR Intl. Ser. 2355, pp 61-70.

Huheey, J.E., (1978), "*Inorganic Chemistry: Principles of Structure and Reactivity*", Harper and Row, New York.

Huijgen, W.J.J. and Comans, R.N.J., (2006), "Mechanisms of aqueous wollastonite carbonation as a possible CO_2 sequestration process", *Report ECN-RX-06-056*, Pub. Energy Research Centre of the Netherlands, Petten, The Netherlands.

Hunt, A.M.W., Speakman, R.J., (2015), "Portable XRF analysis of archaeological sediments and ceramics", *J. Archaeol. Sci.*, **53**, 626-638.

Huyge, D., (2002), "Cosmology, Ideology and Personal Religious Practice in Ancient Egyptian Rock Art", In: "*Egypt and Nubia, Gifts of the Desert*", (Ed. R. Fiedman), The British Museum Press, London, pp 192-206.

Ibrahim, O.B., (2012), "Complexes of urea with Mn(II), Fe(III), Co(II) and Cu(II) metal ions", *Advances in Applied Science Research*, **3**, 3522-3539.

Ibupotto, Z.H., Elhag, S. Al-Salhi, M.S., Nur, O., Willander, M., (2014), "Effect of Urea on the Morphology of Co_3O_4 Nanostructures and their Application for potentiometric Glucose Biosensor", *Electroanalysis*, **26**, 1773-1781.

Iqbal, Y., Messer, P.F., Lee, W.E., (2000), "Microstructural evolution in bone china", *Brit. Ceram. Trans*. **99**, 193-199.

Iqbal, Y., Messer, P.F., Lee, W.E., (2000a), "Non-equilibrium microstructure of bone china", *Brit. Ceramic Trans*. **99**, 110-116)

Ikram, S., (2000), "Meat processing", in: "*Ancient Egyptian Materials and Technology*", (Eds. P.T. Nicholson, I. Shaw, Pub. Cambridge University Press, Cambridge, UK., 656-672.

Ingo, G.M., Chiozzini, G., Faccenda, V., Bemporad, E., Riccucci, C., (1998), "Thermal Microchemical Characterisations of $CaSO_4$-SiO_2 Investment Materials for Casting Jewellery Alloys", *Thermochimica Acta* **321**:175-183.

Ingo, G.M., Çilingiroğlu, A., Di Carlo, G., Batmaz, A., De Caro, T., Riccucci, C., Parisi, E.I., Faraldi, F., (2013), "Egyptian blue cakes from the Ayanis Fortress (Eastern Anatolia, Turkey): micro-chemical and –structural investigations for the identification of manufacturing process and provenance", *J. Archaeol. Sci.*, **40**, 4283-4290.

Ismail, A.A., Hussein-Kamel, Y., Boukhary, M., Ghandour, A.A.A., (2007), "Campanian-Early Eocene Stratigraphy of the Southern Galala Plateau, Eastern Desert, Egypt", *Geologica Croatica* **60(2)**, 119-127.

Iversen, E., (1955), "*Some ancient Egyptian paints and pigments: A lexicographical study*", Pub. København E Munksgaard.

Jackson, C.M., Greenfield, D., Howie, L.A., (2012), "An assessment of compositional and morphological changes in model archaeological glasses in an acid environment", *Archaeometry*, **54**, 489-507.

Jackson, C.M., Nicholson, P.T., Gneisinger, W., (1988), "Glass making at Tell el-Amarna: an integrated approach", *J. Glass Studies*, **40**, 11-23.

Jaksch, H., (1985), *PhD thesis*, Universität Heidelberg.

Jaksch, H., W. Scipel, K.L. Weiner, A. El-Goresy, (1983), *Die Naturwissenschaften*, **70,** 525.

Jay, W.H., Cashion, J.D., (2013), "Raman spectroscopy of Limehouse porcelain sherds supported by Mössbauer spectroscopy and electron microscopy", *J. Raman Spectrosc*. **44**, 1718-1732.

Jay, W.H., Cashion, J.D., Blenkinship, B. (2015), "Lancaster delftware: a Raman spectroscopy, electron microscopy and Mössbauer spectroscopy compositional study", *J. Raman Spectrosc.*, **46**, 1265-1282.

Jay, W.H., Hope, C.A., Cashion, J.D., D. L. Howard, D.L.,K. M. Spiers, K.M., (forthcoming), "Blue-Painted Pottery of the New Kingdom: A New Study of Pigment Sourcing and Production", *Cahiers de la Ceramique Egyptienne* **11**.

Jeffreys, D., (2006), "Survey of Memphis V. Kom Rabia: The New Kingdom Settlement (Levels II-V), *Egypt Exploration Society*, London, 142.

Jenkins, R., (1995), "*X-ray Fluorescence Spectroscop*y", John Wiley& Sons, NJ., USA.

Jones, A., (2013), "Enhanced metal recovery from a modified caron leach of mixed nickel-cobalt hydroxide", *PhD. Thesis*, Murdoch University, W.A.

Jongsomjit, B., Panpranot, J., Goodwin Jr. J.G., (2001), "Co-Support Compound Formation in Alumina-Supported Cobalt Catalysts", *J. Catalysis* **204**, 98-109.

Jonynaite, D., Senvaitiene, J., Beganskiene, A., Karieva, A., (2010), "Spectroscopic analysis of blue cobalt smalt pigment", *Vibrational Spectroscopy* **52**, 158-162.

Johnson-McDanielo, D., Barrett, C.A., Sharafi, A., Salguero, T.T., (2013), "*Nanoscience of an Ancient Pigment*", *J. Am. Chem. Soc.*, **135**, 1677-1679.

Jope, E.M., Huse, G., (1940), "Examination of Egyptian blue by X-ray powder photography", *Nature*, **146**, 26.

Jovanović, Dj., (1989), "Kinetics of thermal decomposition of pyrite in an inert atmosphere", *J. Thermal analysis*, **35**, 1483-1492.

Kaczmarczyk, A., (1986), "The Source of Cobalt in Ancient Egyptian Pigments", In: *Proc. of the 24th Intl. Archaeometry Symp..* (Eds: J.S. Olin and M.J. Blackman), Smithsonian Institution Press, Washington D.C, 369-376.

Kaczmarczyk, A., Hedges, R.E.M., (1983), "*Ancient Egyptian Faience: an analytical survey of Egyptian Faience from Predynastic to Roman times*", Aris and Phillips, Warminster, England.

Kahlenberg, V., Girtler, D., Arroyabe, E., Kaindl, R., Többens, D.M., (2010), "Devitrite ($Na_2Ca_3Si_6O_{16}$) – structural, spectroscopic and computational investigations on a crystalline impurity phase in industrial soda-lime glasses", *Miner. Petrol.* **100**, 1-9.

Kamino, T., Yaguchi, T., Ohnishi, T., Ishitoni, T., (2007), "In-situ sample manipulation and imaging", in: *Focused Ion Beam Systems* (Ed. N. Yao), Cambridge University Press, Cambridge, UK.

Katsaros, T., Liritzis, I., Laskaris, N., (2009), "Identification of Theophrastus' pigments *egyptios kyanos* and *psimythion* from archaeological excavations: A case study", *revue d'archaéométrie*, **34**, 69-79.

Kaufmann, J., and Rüssel, C, (2010), "Diffusion of copper-silicate and soda-lime-silicate melts", *J. Non-Crystalline Solids*, **356**, 1158-1162.

Kerr, R., and N. Wood (2004), in: "*Science and Civilisation in China*", Vol. 5, Chemistry and Chemical Technology, Part XII: Ceramic Technology (Ed. R. Kerr), Pub. Cambridge University Press, Cambridge.

Keuleers, R., Papaefstathiou, G.S., Raptopoulou, G.S., Raptopoulou, C.P., Perlepes, S.P., Desseyn, H.O., (2000), "Comparative study of the metal-ligand bond strength in $Mn^{II}/X/U$ complexes (X = Cl, Br, I, U = urea)", *J. of Molecular Structure*, **525**, 173-183.

Khater, A.E.M., Higgy, R.H., Pimpl, M., (2001), "Radiological impacts of natural radioactivity in Abu-Tarto9r phosphate deposits, Egypt", *J. Environmental Radioactivity* **55**, 255-267.

Kingery W.D., Vandiver, P.B., (1986), "*Ceramic Masterpieces*", Collier Macmillan Publishers, London.

Kirmizi,B., Colomban, Ph., Blanc, M., (2010), "On-site analysis of *Limoges* enamels from sixteenth to nineteenth centuries: an attempt to differentiate between genuine artefacts and copies", *J. Raman Spectrosc.*, **41**, 1240-1247.

Kissin, S.A., (1992), "Five-element (Ni-Co-As-Ag-Bi) Veins", *Geoscience Canada*, **19**, 113-124.

Kleindienst, M.R., Churcher, C.S., McDonald, M.M.A., Schwarcz, H.P., (1999), "Geography, Geology, Geochronology and Geoarchaeology of the Dakhleh Oasis Region: An Interim Report", in: *Reports from the survey of the Dakhleh Oasis Western Desert of Egypt 1977-1987,* (Eds. C.S. Churcher and A.J. Mills), Oxbow Monograph **99**, 1-54.

Knudstad, J.E. and Frey, R.A., (1999), "Kellis: The architectural survey of the Romano Byzantine town at Ismant el-Kharab", in: *Reports from the Survey of the Dakhleh Oasis Western Desert of Egypt, 1977-1987*", (Eds. C.S. Churcher and A.J. Mills) Oxbow Monograph **99**, 189-214.

Koch, L.D., and de Waal, D., (2007), "Raman studies of the underglaze blue pigment on ceramic artefacts of the Ming Dynasty and of unknown origins", *J. Raman Spectrosc.*, **38**, 1480-1487.

Kont, J., (1995), "Clay and man: Clay raw materials in the service of man", *Applied Clay Science* **10,** 275-335.

Košařová, V., Hradil, D., Němec, I., Bezdička, P., Kanický, V., (2013), "Microanalysis of clay-based pigments in painted artworks by means of Raman spectroscopy", *J. Raman Spectrosc.*, **44**, 1570-1577.

Kozloff, A., (1997), "The Malqata/El-Amarna Blues: Favourite Colours of Kings and Gods", in: "*Chief of Seers: Egyptian Studies in Memory of Cyril Aldred*" Ed. E. Goring, N. Reeves, J. Ruffle, Pub. Keegan Paul Intl. London in assoc. with Natl. Museums of Scotland, Edinburgh, 178-191.

Kracek, F.C., (1932), "The Ternary System K_2SiO_3-Na_2SiO_3-SiO_2", *J. Phys. Chem*. **36**, 2529-2542.

Krzemnicki, M.S., (1999), "Diopside Needles as Inclusions in Demantoid Garnet from Russia: A Raman Microspectrometric Study", *Gems and Gemology*, **Winter** , 192-195.

Kucera, P., (2012)," al-Qasr: the Roman *Castrum* of Dakhleh Oasis", in *The Oasis Papers 6: Proceedings of the Sixth International Conference of the Dakhleh Oasis Project,* (Eds. R.S. Bagnall, P. Davoli and C.A. Hope), Oxbow Books, Oxford, 305 - 316.

Kuehni, R.G., (1980), "Color and Colorants in Ancient Egypt", *Color Research and Application. * **5(3**), 169-172.

Kühne, K., (1969), "Äegyptische Fayencen, Part I", in: Grabungen der Deutschen Orient-Gesellschaft, (Ed. S. Wenig).

Lager, G.A., Armbruster, Th., Rotella, F.J., (1984), "A crystallographic study of the low-temperature dehydration products of gypsum, $CaSO_4.2H_2O$; hemihydrate $CaSO_4.0.5H_2O$ and γ-$CaSO_4$", *Am. Mineral*. **69**, 910-918.

Laguna-Bercero, M.A., Sanjuán, M.L., merino, R.I., (2007), "Raman spectroscopic study of cation disorder in poly- and single crystals of the nickel aluminate spinel", *J. Phys: Condens. Matter* **19**, 186217 (10pp).

Landgráfová, R., (2006), "*Faience inlays from the funerary temple of King Raneferef*", ABUSIR XIV, Pub. Czech Institute of Egyptology, Prague.

Lau, D., Kappen, P. Strohschneidr, M., Brack, N., Pigram, P.J., "Characterisation of green copper phase pigments in Egyptian artifacts with X-ray absorption spectroscopy and principal component analysis", *Spectrochim. Acta B* **63**, 1283-1289.

Laurie, A.P., McLintock, W.F.P., Miles, F.D., (1914), "Egyptian blue", *Proc. Roy. Soc. London*, **89**, 418-429.

Lavat, A.E., Wagner, C.C., Tasca, J.E., (2008), "Interaction of Co-ZnO pigments with ceramic frits: A combined study by XRD, FTIR and UV-visible", *Ceramics International * **34**, 2147-2153.

Lawrence, R.M., Mays, T.J., Rigby, S.P., Walker, P, D'Ayala, D., (2007), "Effects of carbonation on the pore structure of non-hydraulic lime mortars", *Cement and Concrete Research* **37**, 1059-1069.

Lee, L., and S. Quirke (2000), "Painting materials", in: *Ancient Egyptian Materials and Technology*, (Eds. P.T. Nicholson, I. Shaw), Cambridge University Press, Cambridge, UK.

Le Fer, D., (1994), "La Conversation des Peintures Murales des Temples de Karnak. Recherches sur les Civilisations", *CNRS Erec*: Paris.

Legler, B., Johnson, H.D., Jackson, M.D., Hamson, G.J., Jackson, A-L., El-Barkooky, A., Ravnas, R., Alsop, D., Le Varlet, X., (2009), "Characterisation of tide-dominated heterolithic reservoir analogies: Eocene Qasr El Sagha Formation, Western Desert Egypt", in: *Sediment Body Geometry and Heterogeneity*, Geol. Soc. Conf., London.

Leichmann, J., (2006), in: Appendix to "Faience inlays from the Funerary Temple of King Raneferef", *ABUSIR XIV* (Ed. R. Landgráfová), Czech Institute of Egyptology, Prague.

Leite, A., Costa, G., Hajjaji, W., Ribeiro, M.J., Seabra, M.P., Labrincha, J.A., (2009), "Blue cobalt doped-hibonite pigments prepared from industrial sludges: Formation and characterisation", *Dyes & Pigments* **81**, 211-217.

Lemoine, C., Meille, E., Poupet, P., Barrandon, J.N., Bouderie, B., (1981), "Etude de quelques alterations de composition chimique des céramiques en milieu marin et terrestre", *Actes XX Symp. d'Archéom., Paris, Rev. d'Archéom. Suppl. 349-353.*

Leon, Y., Lofrumento, C., Zoppi, A., Carles, R., Castellucci, E.M., Sciau, Ph., (2010), "Micro-Raman investigation of terra sigillata slips: a comparative study of central Italian and southern Gaul productions", *J. Raman Spectrosc.*, **41**, 1550-1555.

Levine, L., Gordon, J.A., and Jenks, W.P., "The relationship of structure to the effectiveness of denaturing a deoxyribonucleic acid", *Biochemistry* **2**, 168-175.

Liang, H., Sax, M., Tite, M., (2012), "Optical Coherence Tomography for the non-invasive investigation of the microstructure of ancient Egyptian faience", *J. Archaeol. Sci.*, **39**, 3683-3690

Lilyquist, C., and Brill, R.H., (1993), "*Studies in ancient Egyptian glass*", Pub. Metropolitan Museum of Art, New York.

Lin, C-C., (2001), "Vibrational Spectroscopic Study of the System α-Co_2SiO_4-α-Ni_2SiO_4", *J. Solid State Chemistry* **157**, 102-109.

Liu, H., Chen, T., Zou, X., Qing, C., Frost, R.L., (2013), "Effect of Al content on the structure of Al-substituted goethite: a micro-Raman spectroscopic study", *J. Raman Spectrosc.* **44**, 1609-1614.

Liu, W-x, Coveney, R.M., Tang, H-x, (2003), "Spectrographic study on variation in illite surface properties after acid-base titration", *J. Environmental Sciences*, **15**, 456-463.

Llusar, M., Forés, A., Badenes, J.A., Calbo, J., Tena, M.A., Monrós, G., (2001), "Colour analysis of some cobalt-based blue pigments", *J. Eur. Ceramic Soc.,* **21**, 1121-1130.

Long, R.J., (2012), "Administrative Control of Egypt's Western Oases during the New Kingdom: A tale of two cities", in: *Egyptology in Australia and New Zealand*, (Eds. C.M. Knoblauch and J.C. Gill), Proc. Conf. Melbourne, BAR Intl. Ser. 2355, 105-113.

Loyson, P., (2011), "Chemistry in the Time of the Pharaohs", *J. Chem. Edu*. 88(2), 146-150.

Lucas, A., (1927), "Copper in Ancient Egypt", *The Journal of Egyptian Archaeology* **13:**162-170.

Lucas, A., (1989), *Ancient Egyptian Materials and Industries* 4th Edit. (Revised, J.R. Harris), Histories & Mysteries of Man Ltd, London.

Luo, W., Li, T., Wang, C., Huang, F., (2012), "Discovery of Beeswax as binding agent on a 6th-century BC Chinese Turquoise-inlaid Bronze Sword", *J. Archaeol. Sci*., **39**, 1227-1237

Maas, J.L., Wypski, M.T., Stone, R.E., (2002), "Malkata and Lisht glassmaking technologies: Towards a specific link between Second Millennium BC metallurgists and glassmakers", *Archaeometry* **44**, 67-82.

McBride, E.F., Abdel-Wahab, A., El-Younsy, A.R.M., (1999), *Sedimentology*, **46**, 733-755.

Mackay, E., (1920), "On the use of beeswax and resin as varnishes in Theban Tombs", in: *Ancient Egypt 1920,* (Ed. F. Petrie), Pub. Macmillan and Co., London.

McCarthy, B., Vandiver, P.B., Gibson, M., (1995), " Innovation and continuity of Southwest Asian monochrome blue glazes", in: *The Ceramics Cultural Heritage Academy of Ceramics, Proc. Intl. Symp.: The Ceramic Heritage of the 8th CIMTEC-World Ceramic Congress and Forum on New Materials* (Ed. P. Vincenzini,) Florence, Italy. Pp. 207-218.

McKelvey, V.E., (1967), "Phosphate Deposits", U.S. Geological Survey Bull. 1252-D, D1-D21.

MacKenzie, D.A., (1922), "Colour Symbolism", *Folklore* **33:**136-169.

McMillan, P., (1984), "Structural studies of silicate glasses and melts – applications and limitations of Raman spectroscopy", *Am. Mineralogist*, **69,** 622-644.

Mahmoud, M.H.M.H., (2009), "Examination of some inorganic pigments and plaster layers from excavations at Saqqara area, Egypt", *e-Conservation Magazine*, **12**, 39-46.

Mahmoud, M., (2011), "A preliminary investigation of ancient pigments from the mortuary temple of Seti I, El-Querna (Luxor, Egypt)", *Mediterranean Archaeology and Archaeometry*, **11,** 99-106.

Mahmoud, H.H.M., (2014), "Investigation by Raman microscopy, ESEM, and FTIR-ATR of wall paintings from Qasr el-Ghuieta temple, Kharga Oasis, Egypt", *Heritage Science*, **2**, 18.

Mahmoud, M., Kantrianis, N., Ali, M., Stratis, J., (2011), "Characterisation of ancient Egyptian wall paintings, the excavations of Cairo University at Saqqara", *Intl. J. of Conservation Sci.*, **2**, 145-154.

Maltoni, S., Silvestri, A., Marcante, A., Molin, G., (2016), "The transition from Roman to Late Antique glass: new insights from the *Domus of Tito Macro* in Aquileia (Italy), *J. Archaeol. Sci.*, **73**, 1-16.

Maniatis, Y. and Tite, M.S. (1981), "Technological Examination of Neolithic-Bronze Age Pottery from Central and Southeast Europe and from the Near East", *J. Archaeological Sci.* **8**, 59-76.

Mantovani, L., (2013), "Synthesis and characterisation of $CaCoSi_2O_6 - Co_2Si_2O_6$ pyroxenes", *PhD Thesis*, University of Parma, Italy.

Mantovani, L., Tribaudino, M., Aliatis, I., Lambruschi, E., Lottici, P.P., Bersani, D., (2015), "Raman spectroscopy of $CaCoSi_2O_6 - Co_2Si_2O_6$ clinopyroxenes", *Phys. Chem. Minerals* **42,** 179-189.

Marchand, S., Tallet, P., (1999), "Ayn Asil et I'oasis de Dakhleh au Nouvel Empire", *Bulletin de L'Institut Français d'Archéologie Orientale*, **99**, 307-352.

Marciuš, M., Ristić, M., Ivanda, M., Musić, S., (2012), "Formation of Iron Oxides by Surface Oxidation of Iron Plate", *Croat. Chem. Acta*, **85**, 117-124.

Masse, S., Boch, P., Vaissière, N., (1999), "Trapping of Nickel and Cobalt in $CaNiSi_2O_6$ and $CaCoSi_2O_6$ Diopside-Like Phases in Heat-Treated Cement", *J. of the European Ceram. Soc.*, **19**, 93-98.

Matin, M. (2013), "An experimental investigation into the accidental invention of ceramic glazes", *Archaeometry*, doi: 10.1111/arcm.12039.

Matin, M., and Matin, M., (2012), "Egyptian faience glazing by the cementation method part I: an investigation of the glazing powder composition and glazing mechanism", *J. Archaeol Sci.*, **39**, 763-776.

Mazzetti, L., and Thistlethwaite, P.J., (2002), "Raman spectra and thermal transformations of ferrihydrite and schwertmannite", *J. Raman Spectrosc.*, **33**, 104-111.

Mazzi, F., Pabst, A., (1962), "Reexamination of Cuprorivaite" *Am. Mineral.,* **47**, 409-411.

Mazzocchin, G.A., Orsega, E.F., Baraldi, P., Zannini, P., (2006), "Aragonite in Roman wall paintings of the *VIIIᵃ Regio Aemilia* and *Xᵃ Regio, Venetia et Histria*", *Annali, di Chimica* **96**, 377-387

Mazzocchin, G.A., Rudello, D., Bragato, F.A., (2004), "A Short Note on Egyptian blue", *J. Cultural Heritage*, **5**, 129-133.

Melcher, M. and Schreiner, M., (2005), "Evaluation procedure for leaching studies on naturally weathered potash-lime-silica glasses with medieval composition by scanning electron microscopy", *J. Non-Crystalline Solids*, **351**, 1210-1225.

Merkel S., and Rehren, Th., (2007), "Parting Layers, Ash Trays, and Rameside3 Glassmaking: An Experimental Study", in: "*Hochtemperatur-Technologie in der Ramses-Stadt,* (Eds. E.B. Pusch, and Th. Rehren, Verlag Gebrüder Gerstenberg, Hildesheim, Germany.

Mernagh, T.P., (1991), "Use of Laser Raman Microprobe for Discrimination Amongst Feldspar Minerals", *J. Raman Spectrosc.,* **22**, 453-457.

Mernagh, T.P. and Hoatson, D.M., (1997), "Raman spectroscopic study of pyroxene structures from the Munni Munni", *J. Raman Spectrosc.,* **28**, 647-658.

Meseguer, S., Tena, M.A. Gargori, C. Badenes, J.A., Llusar, M., Monrós, G., (2007), "Structure and colour of cobalt ceramic pigments from phosphates", *Ceram. Intl*. **33**, 843-849.

Meseguer, S., Tena, M.A. Gargori, C. Badenes, J.A., Llusar, M., Monrós, G., (2007), "Development of blue ceramic dyes from cobalt phosphates", *Ceram. Intl*. **34**, 1431-1438.

Miller, B.F., (1986), "Blue Pigment in the Inscription on an Alabaster Jar: Technical Appendix", *Bulletin of the Cleveland Museum of Art* **73**, 342-347.

Mills, A.J., (1999), "Pharaonic Egyptians in the Dakhleh Oasis", in: *"Reports from the Survey of the Dakhleh Oasis Western Desert in Egypt 1977-1987"*, (Eds. C.S. Churcher and A.J. Mills) Oxbow Monograph 99, Oxbow Books, Oxford, 171-178.

Mills, A.J., (2002), "Another Old Kingdom Site in the Dakhleh Oasis", In: *Egypt and Nubia – Gifts of the Desert*, Ed. R. Friedman, pub. The British Museum Press, 74-78.

Minguzzi, C., (1938) "Cuprorivaite un nuovo minerale", *Periodic Mineral*. **8**, 333-345.

Mirti, P., Appolonia, L. Casoli, A., Ferrari, R.P., Laurenti, E., Canesi, A.A., Chiari, G., (1995), "Spectrochemical and Structural Studies on a Roman sample of Egyptian blue" *Spectrochim. Acta* **A51**: 437-446.

Molina, G., Odin, G.P., Pradell, T., Shortland, A.J., Tite, M.S., (2014), "Production technology and replication of lead-antimonate yellow glass from New Kingdom Egypt and the Roman Empire", *J. Archaeol. Sci.*, **41**, 171-184.

Monari, G., and Manfredini, T., (1996), "Colouring effects of synthetic inorganic cobalt pigments in fast-fired porcelainized tiles", *Ceram. Eng. Sci. Proc.*, **17**, 167-172.

Möncke, D., Papageorgiou, M., Winterstein-Beckmann, A., Zacharias, N., (2014), "Roman glasses coloured by dissolved transition metal ions: redox-reactions, optical spectroscopy and ligand field theory", *J. Archaeol. Sci.*, **46**, 23-36.

Monhemius, A.J., (1977), "Precipitation diagrams for metal hydroxides, sulphides, arsenates and phosphates", Trans. IMMC, 86, C202-C206.

Moorey, P.R.S., (1985), "*Materials and Manufacture in Ancient Mesopotamia: The evidence of Archaeology and Art Metals and Metalwork, Glazed Materials and Glass* ", BAR international Series 237, Oxford , UK.

Morey, G.W., (1930), "The devitrification of soda-lime-silica glasses" *J. Am. Ceram. Soc*. **13,** 683-713.

Morey, G.W., and N.L. Bowen, (1925), "The Melting Relation of the Soda-Lime-silica Glasses", *J. Soc. Glass Technol*., **9**, 226-264.

Morton, G.R., and Wingrove, J., (1969), "Constitution of Bloomery Slags: Part i: Roman. *Journal of the Iron and Steel Institute* **207**, 1556-1564.

Mouri, T., Enami, M., (2008), "Raman spectroscopic study of olivine-group minerals", *J. Mineralogical and Petrological Sci.*, **103**, 100-104.

Morinaga, K., Torikai, T., Nakagawa, K., Fujino, S., (2000), "Fabrication of fine α-alumina powders by thermal decomposition of ammonium aluminium carbonate hydroxide (AACH)", *Acta mate*r. **48**, 4735-4741.

Mukhopadhyay, T.K., Ghosh, S., Ghutak, S., (20110, "Phase analysis and microstructure evolution of a bone china body modified with scrap addition", *Ceramics International* **37**, 1615-1623.

Murad, E., (2003), "Raman and x-ray diffraction data on anatase in fired kaolins", *Clays Clay Miner*., **51(6)**, 689-692.

Murad, E., (2014), *Mössbauer Effect Reference and Data Journal*, **37**, 13-25.

Murad, E. and Cashion, J. (2004), "*Mössbauer Spectroscopy of Environmental Materials and their Industrial Utilisation*", Kluwer Academic publishers, Boston.

Murray, M.A., (2000), "Viticulture and wine production", in: "*Ancient Egyptian Materials and Technology*", (Eds. P.T. Nicholson, I. Shaw, Pub. Cambridge University Press, Cambridge, UK., 577-608.

Mutke, M., Kreye, M., Shi, J., Becker, K.D., (2008), "Kinetics of cation distribution in cobalt-containing olivine, $(Co_{0.6}Mg_{0.4})_2SiO_4$, *Phys. Chem. Chem. Phys.*, **10**, 3895-3902.

Mwenesongole, E., (2008), "A Raman- and XRD study of the crystal chemistry of cobalt blue", *MsC.*, Univ. Pretoria, S. Afr.

Nakai, I., Numako, C., Hosono, H., Yamasaki, K., (1999), "Origin of the Red Colour of Satsuma Copper-Ruby Glass as Determined by EXAFS and Optical Absorption Spectroscopy", *J. Am. Ceram. Soc.*, **82**:689-695.

Newesely, H., (1977), "High temperaturebehaviour of hydroxyl- and fluorapatite", *J. of oral Rehabilitation*, **4**, 97-104.

Nicholson, P.T., (1993), "The firing of pottery", in: *An Introduction to Ancient Egyptian Pottery*, (Eds., D. Arnold and J. Bourriau), Verlag Philipp Von Zabern, Mainz Am Rhein.

Nicholson, P.T., (2007), *Brilliant Things for Akhenaten*, "The Production of Glass, Vitreous materials and Pottery at Amarna Site O45.1", *Excavation Memoir* **80**, Egypt Exploration Society, London.

Nicholson, P.T., (2013), "Working in Memphis: The Production of Faience at Roman Period Kom Helu*l*", *Excavation Memoir* **105**, Egypt Exploration Society, London.

Nicholson, P.T. and Henderson, J., (2000), "Glass", in: *"Ancient Egyptian Materials and Technology"*, 195-226, Pub. Cambridge University Press, Cambridge, UK.

Nicholson, P.T., Peltenburg, E., (2000), "Egyptian Faience", in: "*Ancient Egyptian Materials and Technology*", (Eds. P.T. Nicholson and I. Shaw), 177-194, Pub. Cambridge University Press, Cambridge, UK.

Nicholson, P.T., Shaw, I., (2000), "*Ancient Egyptian Materials and Technology*", Pub. Cambridge University Press, Cambridge, UK.

Nicolini, L and Porter, P., (1970), "Preparation, X-ray and magnetic investigations of some silicates containing transition metal ions", *Gazz. Chim. Ital*. **100**, 923-930.

Noble, J.V., (1969), "The technique of Egyptian faience:, *American Journal of Archaeology*, **73**, 435-439

Noll, V.W., (1978), "Mineralogie und Technik der bemalten Keramiken Altägyptens", *N. Jb. Miner. Mh.*, **133**, 227-290.

Noll, W., (1981a), "Mineralogy and Technology of the Painted Ceramics of Ancient Egypt", in: *Scientific Studies in Ancient Ceramics* (Ed. M.J. Hughes), Occasional Paper No. 19, Brit. Museum, 143-154.

Noll, W., (1981b), "Bemalte Keramiken Altägyptens: Material, Rohstoffe und Herstellungstechnik", in: *Studien zur altägyptischen Keramik*, (Ed. D. Arnold) Philipp von Zabern, Mainz am Rhein, 103-138.

Noll, W., Hangst, K., (1975), "Grün- und Blaupigmente der Antike", *N. Jb. Miner. Mh., H.* **12**, 529-540.

Noll, W., Hangst, K., (1975a), "Zuz Kenntnis der altägyptischen Blaupigmente", *N. Jb. Miner. Mh., H*. **12**, 309-314.

Nordström, H-Å., and Bourriau, J., (1993), "Clays of the Nile Valley", in: *"An Introduction to Ancient Egyptian Pottery"*, (Eds. D. Arnold and J. Bourriau), Fascicle 2, Ceramic Technology: Clays and Fabrics, Verlag Philipp von Zabern, Mainz, Germany.

Nriagu, J.O., (1985), "Cupellation: The Oldest Quantitative Chemical Process", *J. Chem. Edu.* **62,** 668-674.

Ogden, J., (2000), "Metals", in: "*Ancient Egyptian Materials and Technology*", (Eds. P.T. Nicholson, I. Shaw, Pub. Cambridge University Press, Cambridge, UK., 148-176.

Oh, S.J., Cook, D.C., Townsend, H.E., (1998), "Characterisation of iron oxides commonly formed as corrosion products on steel", *Hyperfine Interactions* **112**, 59-65.

Ohtsuka, T., (1996), "Raman Spectra of Passive Films of Iron in Neutral Borate Solution", *Materials Transactions, JIM* , **37**, 67-69.

Ohtsuka, T., Kubo, K., Sato, N., (1986), "Raman Spectroscopy of Thin Corrosion Films on Iron at 100-150C in Air", *Corrosion* **42**, 476-481.

O'Neill, H., and Navrotsky, A., (1983), "Simple spinels: crystallographic parameters, cation radii, lattice energies, and cation distribution", *Am. Mineral.* **68**, 181.

Oppenheim, A.L. (1970), "The cuniform tablets with instructions for glassmakers", in: *Glass and Glassmaking in Ancient Mesopotamia* , (Eds. Oppenheim, A.L., Brill, R.H., Barag, D., von Saldern, A.), Corning Museum of Glass, Corning, New York, 22-53.

Oppenheim, A.L., Brill, R.H., Barag, D., von Saldern, A. (1988), *"Glass and Glassmaking in Mesopotamia:"*, Corning , New York.

Orlovskii, V.P., Komlev, V.S., Barinov, S.M. (2002), "Hydroxyapatite and Hydroxyapatite-Based Ceramics", *Inorganic materials* **38**, 973-984.

Ospitali, F.M, Bersani, D., Di Lonardo, G., Lottici, P.P., (2008), 'Green earths': vibrational and elemental characterisation of glauconites, celadonites and historical pigments", *J. Raman Spectrosc.*, **39**, 1066-1073.

Owen, J.V., Adams, B., Stephenson, R., (2000), "Nicholas Crisp's "Porcellien". A petrological comparison of shereds from the Vauxhall (London 1757-1774) factory sites", *Geoarchaeology*, **15**, 43.

Owen, J.V., Hillis, M., (2003), "From London to Liverpool: Evidence for a Limehouse-Reid porcelain connection based on analysis of sherds from the Brownlow Hill (ca. 1755-1767) factory site", *Geoarchaeology*, **18**, 851-882.

Pabst, A., (1959), "Structures of some Tetragonal Sheet Silicates", *Acta Crystallogr.*, **12**, 733.

Pacewska, B., Kluk-Ploskońska, O., Szychowski, D., ((2006), "Influence of aluminium precursor on physico-chemical properties of aluminium hydroxides and oxides Part II", J. *Thermal Anal. and Colorimetry*, **86**, 751-760.

Pachur, H.J., and Kröpelin, S., (1987), "Wadi Howar: paleoclimatic evidence from an extinct river system in the south-eastern Sahara", *Science*, **237**, 298-300.

Pagès-Camagna, S., (1998), "Bleu et vert égyptiens en question: vocabulaire et analyses", in: *La couleur dans la peinture et la céraqmique de l'Egypte Ancienne,* 1997, (Eds. S. Colinart and M. Menu), Edipuglia, Ravello.

Pagès-Camagna, S., Colinart, S., (2003), "The Egyptian green pigment: its manufacturing process and links to Egyptian blue", *Archaeometry*, **45**, 637-658.

Pagès-Camagna, S., Colinart, S., (2006), Authors' Reply, *Archaeometry* **48**, 707-713.

Pagès-Camagna, S., Colinart, S., Coupry, C., (1999), "Fabrication Processes of Archaeological Egyptian Blue and Green Pigments enlightened by Raman Microscopy and Scanning Electron Microscopy", *J. Raman Spectrosc.,* **30**, 313-317.

Pagès-Camagna, S., and Guichard, H., (2007), "Egyptian colours and pigments" *in*: *French collections: 30 years of physicochemical analyses on 300 objects*", In *Decorated Surfaces on Ancient Egyptian Objects: Technology, Decoration and Conservation,* (Eds. J. Dawson, C. Rozeik, M.M. Wright), Proc. Conf. Cambridge, UK, 7-8 Sept.

Pages-Camagna, S., Laval, E., Vigears, D., Duran, A., (2010), "Non-destructive and in situ analysis of Egyptian wall paintings by X-ray diffraction and X-ray fluorescence portable systems", *Appl. Phys A* **100**, 671-681.

Pagès-Camagna, S., Reiche, C., Brouder, C., Cabaret, D., Rossana, S., Kanngieβer, B., Erke, A., (2006), *"*New insights into the colour origin of archaeological Egyptian blue and green by XAFS at the Cu K-edge*", X-ray Spectrosc.*, **35**, 141-145.

Pailhé, N., Wattaiux, A., Gaudon, M., Demourgues, A., (2008), "Impact of structural features on pigment properties of α-Fe_2O_3 hematite", *J. Solid State Chem.* **181**, 2697-2704.

Palma, M. and Morel, J.P., (1981), "Viscosity of ternary mixtures, IV. Urea-tert.-butyl alcohol-water, *Can. J. Chem*. **59**, 3248-3251.

Parras, D., Vandenabeele, Sanchez, A., Montejo, M., Moens, I., Ramos, N., (2010), "Micro-Raman spectroscopy of decorated pottery from the Iberian archaeological site of Puerto Tablas (Jaén, Spain, 7th-4th century B.C.)", *J. Raman Spectrosc.*, **42**, 68-73.

Pask, J.A., (1996), "Importance of Starting materials on Reactions and Phase Equilibria in the Al_2O_3-SiO_2 System", *J. Eur. Ceram. Soc.*, **16**, 101-108.

Paterson, D., de Jong, M.D., Howard, D.L., Lewis, W., McKinlay, J., Starritt, S., Kusel, M., Ryan, C.G., Kirkham, R., Moorhead, G., Siddons, D.P., (2011), "The X-ray Fluorescence Microscopy Beamline at the Australian Synchrotron*", AIP Conf., Proc. 1365*, pp. 219-222.

Pavlidou, E., Mahmoud, M., Roumeli, E., Zorba, F., Paraskevopoulos, K.M., (2008), "Identifying pigments in the temple of Seti I in Abydos (Egypt)", In: *EMC 2008, 14th European Microscopy Congress*, Aachen, Germany, Vol 2: Materials Sci. (Eds. S. Richter, A. Schwedt), 829-830.

Pecchioni, E., Fratini, F., Cantisani, E., (2008), *Le malte antiche e modern tra tradizione e innovazione*, Patron Editore, Bologne.

Pelovski, Y., Tsankov, M., Petkova, V., Gruncharov, I., (1995), "Thermal decomposition of sodium aluminium sulphate crystallohydrate", *J. of Thermal Analysis*, **43**, 351-357.

Peltenburg, E.J., (1992), "Early faience: recent studies, origins and relations with glass", in: *Early Vitreous Materials, British Museum Occasional Paper* **56** (Eds. M. Bimson and I.C. Freestone), 5-30.

Pérez-Ramírez, J., Mul, G., Moulijn, J.A., (2001), "In situ Fourier transform infrared and laser Raman spectroscopic study of the thermal decomposition of Co-Al and Ni-Al hydrotalcites", *Vibrational Spectroscopy* **27**, 75-88.

Pérez-Robles, F., Garcia-Rodriguez, F.J., Jiménez-Sandoval, S., González-Hernández, J., (2009), "Raman study of Copper and Iron Oxide Particles Embedded in an SiO_2 Matrix", *J. Raman Spectrosc.*, **30**, 1099-1104.

Perry, R.H. and Green, D., (1984), *Perry's Chemical Engineers Handbook*, 6th Edition, McGraw Hill, New York.

Petrie, W.M.F., (1894), *Tell-el-Amarna*, Methuen & Co., London.

Petrie, W.M.F., (1924-25), *Trans. Newcomen Soc.*, **5**, 72.

Phillips, A. and Muan, A., (1959), "Phase Equilibria in the System CaO-Iron Oxide-SiO$_2$ in air", *J. Am. Ceram. Soc.*, **42(9),** 413-423.

Picon, M., Vichy, M., Ballet, P., (2005), "L'alun des oasis occidentales d'Egypte. Recherches sur le terrain et recherche en laboratoire", in: *L'alun de Mediterrannée,* (Eds. P. Borgard, J-P Brun, and M. Picon), Naples/Aix-en-Provence, 43-57.

Pinch, G., (2001), "Red things: the symbolism of colour in magic", in: *Colour and Painting in Ancient Egypt,* (Ed. W.V. Davies), The British Museum Press, 182-185.

Plinius, G. Secundus (23-79), *Historia naturalis,* Translated by Cristoforo Landino (1424-1492), Pub. Venice: Nicolaus Jensen, 1476.

Pliny the Elder, (1983), *Naturalis historiae,* transl. H. Zehnacker, Les Belles Lettres, CUF, Paris.

Polikreti, K., Murphy, J.M.A., Kantarelou, V., Karydas, A.G., (2011), "XRF analysis of glass beads from Mycenaean palace of Nestor at Pylos, Peloponnesus, Greece: new insight into the LBA glass trade", *J. Archaeol. Sci.*, **38**, 2889-2896.

Pollard, A.M., Heron, C., (2008), "The Development of Archaeological Chemistry", in: *Archaeological Chemistry*, 2nd Edit., Pub. The Royal Society of Chemistry.

Powell, C.J., (1990), "Inner-shell Ionisation Cross-Sections", in: *Microbeam Analysis* (Eds. J.R. Michael and P. Ingram), San Francisco Press, San Francisco.

Pradell, T., Salvado, N., Hatton, G.D., Tite, M.S., (2006), "*Physical Processes Involved in Production of the Ancient Pigment, Egyptian blue*", *J. Am. Ceram. Soc.* **89**, 1426-1431.

Prasad, P.S.R., (1999), "Raman intensities near gypsum-bassanite transition in natural gypsum", *J. Raman Spectrosc.*, **30**, 693-696.

Prasad, P.S.R., Pradham, A., Gowd, T.N., (2001), "*In situ* micro-Raman investigation of dehydration mechanism in natural gypsum", *Current Science*, **80**, 1202-1207.

Prencipe, M., Mantovani,L., Tribaudino, M., Bersani, D., Lottici, P.P., (2012), "The Raman spectrum of diopside: a comparison between *ab initio* calculated and experimentally measured frequencies", *Eur. J. Mineral.* **24**, 457-464.

Profi, S., Perdikatsis, B., Filippakis, S.E., (1977), "X-ray Analysis of Greek Bronze Age Pigments from Rhera (Santorini)", *Studies in Conservation* **22**, 107-115.

Prothero, D.R., Berggren, W.A., Bjork, P.R., (1990), "Late Eocene-Oligocene climatic and biotic evolution", *GSA News and Information*, March 74-75.

Pujalte, V., Schmitz, B., Baceta, J.I., (2014), "Sea-level changes across the Palaeocene-Eocene interval in the Spanish Pyrenees, and their possible relationship with North Atlantic magmatism", *Palaeogeography, Paleoclimatology, Paleoecology*, **393**, 45-60.

Pusch, E.B and Rehren, Th., (2007), "*Hochtemperatur-Technologie in der Ramses-Stadt,* Verlag Gebrüder Gerstenberg, Hildesheim, Germany.

Putnam, D.F., (1971), "Concentration and concentrative properties of human urine", *NASA Contract No. CR-1802*, Washington D.C., USA.

Ragai, J., (1986), "Colour: its significance and production in Ancient Egypt", *Endeavour,* **10**, 74-79.

Rahman, A., Charoo, M.S., Jayaganthan, R., (2015), Structural, optical and photocatalytic properties of zinc aluminate spinel nanoparticles", *Materials Technology: Advanced Performance Materials* **30**, 168-176.

Ramakrishna, A., and Rao, N., (2007), "Effect of urea on speciation of cobalt(II) complexes of L-gluttamine and succinic acid", *Chemical Speciation and Bioavailability*, **19**, 103-108.

Ramesh, T.N., Rajamathi, M., Kamath, P.V, (2003), "Ammonia induced precipitation of cobalt hydroxide: observation of turbostratic disorder", *Solid State Sciences* **5**, 751-756.

Rampazzi, L., Campo, L., Cariati, F., Tanda, G., Colombini, M.P., (2007), "Prehistoric wall paintings: The case of *Domus De Janus* necropolis (Sardinia, Italy)", *Archaeometry*, **49**, 559-569.

Rampazzi, L., Colombini, M.P., Conti, C., Corti, C., A. Lluveras-Tenorio, A., Sansonetti, A., Zanaboni, M., (2016) "Technology of Medieval Mortars: An investigation into the use of organic additives", *Archaeometry*, **58**, 115-130.

Ramsdell, L.S., Partridge, E.P., (1929), "The crystal forms of calcium sulphate", A*m. Mineral.* **14**, 59-74.

Ransom Williams, C., (1932), "*The Decoration of the Tomb Per-Neb: "The Technique and The Color Conventions*", Vol. 3, Metropolitan Museum of Art, Department of Egyptian Art, New York.

Rao, G.N. and Ramakrishna, A., (2005), "Speciation of Ni(II) complexes of L-glutamine and succinic acid in urea-water mixtures", *Proc. Nat. Acad. Sci. India*, **75A, IV**, 245-248.

Rashad, M., Rüsing, M., Berth, G., Lischka, K., Pawlis, A., (2013), "CuO and Co_3O_4 Nanoparticles: Synthesis, Characterisations, and Raman Spectroscopy", J. Nanomaterials, Article IDS 714853, 6 pages.

Rehren, Th., (1997), "Rammeside glass-colouring crucibles", *Archaeometry*, **39,** 355-368.

Rehren, Th., (2000), "Rationales in Old World base glass compositions", *J. Archaeological Sci*. **27**, 1225-1234.

Rehren, Th., (2000a), "New aspects of ancient Egyptian Glassmaking", *J. of Glass Studies*, **42**, 13-24.

Rehren, Th., (2001), "Aspects of the production of cobalt-blue glass in Egypt", *Archaeometry* **43**, 483-489.

Rehren, Th., (2008), "A review of the factors affecting the composition of early Egyptian glasses and faience: alkali and alkaline earth oxides", *J. Archaeol. Sci.* **35**, 1345-1354.

Rehren, T., and E.B. Pusch, (1997), "New Kingdom Glass-Making Crucibles from Qantir-Piramesses", *J. Egyptian Archaeology*, **83**, 127-141.

Rehren, T., and E.B. Pusch, (2005), "Late Bronze Age Glass Production at Qantir-Piramesses, Egypt", *Science*, **308**, 1756-1758.

Ricciadi, P., (2006-2007), "Raman spectroscopy for the non destructive characterization of ancient pottery, porcelains and mosaic glasses", *PhD thesis Universita dogli Studi di Firenze*.

Rice, P.M., (1987), "*Pottery Analysis: A Source Book* ", The University of Chicago Press.

Richmond, H.D., and Off, H. (1892), "Indications of a possible new element in an Egyptian mineral", *J. of the Chem. Soc*. *Trans*. **61**, 491-495.

Riederer, J., (1974), "Recently identified Egyptian pigments", *Archaeometry* **16**, 102-109.

Riederer, J., (2012), "Egyptian blue" in: *Artists' Pigments: A Handbook of their History and Characteristics* (Ed. E.W. FitzHugh), **Vol. 3**, Archetype Publications, London.

Rivadeneyra, M.A., Martin-Algarra, A., Sánchez-Navas, A., Martin-Ramos, M., (2006), "Carbonate and Phosphate Precipitation by *Chromohalobacter marismortui*", *Geomicrobiology Journal*, **23** 89-101.

Robertson, K. and Bish, D., (2007), ":The dehydration kinetics of gypsum: The effect of relative humidity on its stability and implications in the Martian environment", *Lunar and Planetary Science* XXXVIII, 1432.pdf

Rodriguez-Navarro, C., Ruiz-Agudo, E., Luque, A., Rodriguez-Navarro, A.B., Ortega-Huertas, M., (2009), "Thermal decomposition of calcite: Mechanisms of formation and textural evolution of CaO nanocrystals", *Am. Mineralogist*, **94,** 578-593.

Rose, P.J., (2007), *The Eighteenth Dynasty Pottery Corpus from Amarna*, 83rd Excavation Memoir, (Ed. J. Bourriau), Egypt Exploration Society, London.

Rosi, F., Miliani, C., Borgia, I., Brunetti, B., Sgamellotti, A., (2004), "Identification of nineteenth century blue and green pigments by *in situ* x-ray fluorescence and micro-Raman spectroscopy", *J. Raman Spectrosc.*, **35**, 610-615.

Rosi, F., Manuali, V., Miliani, C., Brunetti, B.G., Sgameliotti, A., (2009), "Raman scattering features of lead pyroantimonate compounds. Part I:XRD and Raman characterisation of $Pb_2Sb_2O_7$ doped with tin and zinc", *J. Raman Spectrosc.*, **40**, 107-111.

Rothenberg, B., (1972), "Timna : Valley of the Biblical Copper Mines", Pub. Thomas and Hudson, London.

Rouchon, O., Fabre, J., Etcheverry, M.P., Schvoerer, M., (1990), "Pigments d'Egypte. Étude physique de matieres colorantes: blue, rouge, blanche, verte et jaune provenante de Karnak", *Rev.* Archeometrie, **14**, 87-97.

Roy, J., Bandyopadhuyay, N., Das, S., Maitra, S., "Effect of CoO on the Formation of Mullite Ceramics from Diphasic Al_2O_3-SiO_2 Gel", *J. Eng. Sci. and Technol. Rev.*, **2010**, 3(1), 136-141.

Roy, D.M. and Roy, R., (1964), "Tridymite-cristobalite relations and stable solid solutions", *The Am. Mineral.*; **40**, 952-962.

Ryan, C.G., Kirkham, R., Hough, R.M., Moorhead, G., Siddons, D.P., de Jong, M.D., Paterson, D.L., De Geronimo, G., Howard, D.L., Cleverley, J.S., (2010), "Elemental X-ray imaging using the Maia detector array: The benefits and challenges of large solid-angle", *Nucl. Instrum. Methods Phys. Res., A*, **619**, 37-43.

Ryan, C.G., Cousens, D.R., Sie, S.H., Griffin, W.L. Suter, G.F., Clayton, E., (1990), "Quantitative PIXE microanalysis of geological material using the CSIRO proton microprobe", *Nucl. Instrum. Methods Phys. Res., B* **47**, 55-71.

St. Pierre, P.D.S., (1955), "Constitution of bone china II: Reactions in bone china bodies", *J. Am. Chem. Soc.*, **38**, 217-223.

Sabbatini, L., Tarantino, M.G., Zambonin, P.G., De Benedetto, G.E., (2000), "Analytical characterization of paintings on pre-Roman pottery by means of spectroscopic techniques. Part II: Red, brown and black colored shards", *Fresenius J. Anal. Chem.* **366**, 116-124.

Said, R., (1962), "*The Geology of Egypt*", Amsterdam, New York.

Said, R. (1982), "The geological evolution of the River Nile in Egypt", *Zeitschrift für Geomorphologie*, **26**, 305-314.

Saleh, S.A., Iskander, Z., El-Masry, A.A., Helmi, F.M.,(1974), in: *Recent Advances in Sciences and Technology of Materials 3*, Plenum Press, New York, pp. 141-155.

Salem, S., (2014), "Effect of calcination temperature on colorant behaviour of cobalt-aluminate nano-particles synthesised by combustion technique", *J. Industrial and Engineering Chemistry* **20**, 818-823.

Samanian, K., (2014), "Identification of green pigment used in Persian wall paintings (AD 1501-1736) using PLM, FT-IR, SEM-EDX and GC-MS techniques", *Archaeometry* (2015), 41, 740-758 (doi: 0.1111/arcm 12102).

San Andrés, M. de la Roja, J.M., Baonza, V.G., Sancho, N., (2010), "Verdigris pigment: a mixture of compounds. Input from Raman spectroscopy", *J. Raman Spectroac.*, **41**, 1178-1186.

Sapsford M., (2009), "The use of sodium salt deposits in medical and medically associated industries in Ancient Egypt", *PhD Thesis*, Department of Applied Science, Security and Resilience, Cranfield University.

Sato, T., (1985), "Thermal decomposition of aluminium hydroxides to aluminas", *Thermochim. Acta*, **88**, 69-84.

Sato, T., Ikoma, S., Ozawa, F., (1980), "Preparation of Gelatinous Aluminium Hydroxide by Urea from Aqueous Solutions Containing Chloride, Nitrate and Sulphate of Ammonia", *J. Chem. Tech. Biotechnol.*, **30**, 225-232.

Sayre, E.V. and Smith, R.W., (1961), "Compositional categories of ancient glass", *Science,* **133**, 1824-1826.

Sayre, E.V. and Smith, R.W., (1973), "*Analytical Studies in Ancient Egyptian Glass*", Pub. Brookhaven National Laboratory, Upton, N.Y. USA.

Sayre, E.V., and Smith R.W., (1974), "Analytical Studies in ancient Egyptian glass", in: *Recent Advances in the Science and Technology of Materials*, (Ed. A. Bishay) Plenum Press, NY, pp 47-70.

Schairer, J.F., Bowen, N.L., (1938), "The system Leucite-Diopside-Silica", *Am. J. Sci.*, **35-A,** 289-309.

Schenkel, W., (1963), "Die Farben in ägyptischer Kunst und Sprache", *Zeitchrift für ägyptische Sprache und Altertumskunde* **88**, 13-147.

Schiegl, S., and El Goresy, A., (2006), "Comments on S. Pagès-Camagna and S. Colinart, 'The Egyptian green pigment: its manufacturing process and links to Egyptian blue', Archaeometry, 45(4) (2003), 637-58*", *Archaeometry* , **48**, 707-713.

Schiegl, S., Weiner, K.L., El-Goresy, A., (1989) "*Discovery of copper chloride cancer in ancient Egyptian polychromic wall paintings and faience: A developing archaeological disaster*", Pub. Max-Planck-Institut Für Kernphysik, Heidelberg, Germany, pp 15 plus appendices.

Schiegl, S., Weiner, K.L., El-Goresy, A., (1990), "Zusammensetzung und Provenienz von Blau- und Grünpigmenten in Altägyptischen Wandmalereien: Ein Beitrag zur exakten Chronologie der Bronzetechnologie in Altägypten", *Erzmetall* **43**, 265-272.

Schiegl, S., Weiner, K.L., El-Goresy, A., (1992), "The diversity of newly discovered deterioration patterns in ancient Egyptian pigments: consequences to entirely new restoration strategies and to the Egyptological symbolism", *Mat. Res. Soc. Symp. Proc.* **267**, 831-858.

Schoer, B. and Rehren, Th., (2007), "The Composition of Glass and Associated Ceramics from Qantir", in: "*Hochtemperatur-Technologie in der Ramses-Stadt,* (Eds. E.B. Pusch, and Th. Rehren), Verlag Gebrüder Gerstenberg, Hildesheim, Germany.

Sedel'nikova, M.B., and Pogrebenkov, V.M., (2006), "The effect of mineralising additives on synthesis of ceramic pigments based on natural wollastonite", *Glass and Ceramics*, **63**, 22-225.

Segnit, E.R., (1987), "Evaporite minerals from the Dakhleh Oasis", In: *Ceramics from the Dakhleh Oasis* (Eds. W.I. Edwards, C.A. Hope, E.RT. Segnit), Victoria College Press, Burwood, Victoria, Australia, *Occasional Paper* **1**, 97-102.

Segnit, E.R. and Holland, A.E., (1965), "The System $MgO-ZnO-SiO_2$", *J. Am. Ceram. Soc*. **48**, 412.

Sepelak, V. and Becker, K.D., (2004), "Comparison of the cation inversion parameter of the nanoscale milled spinel ferrites with that of the quenched bulk materials", *Materials Sci. and Eng. A*, 375-377:861-864.

Serpico, M., and White, R., (2000), "Oil, fat and wax", in: "*Ancient Egyptian Materials and Technology*", (Eds. P.T. Nicholson, I. Shaw), Pub. Cambridge University Press, Cambridge, UK.

Shackleton, N.J., (1986), "Paleogene stable events", *Paleogeography, Paleoclimatology, Paleoecology*, **57**, 91-102.

Sharkey, J.B., and Lewin, S.Z., (1971) "Conditions governing the formation of atacamite and paratacamite", *Am. Mineralogist*, **56**, 179-192.

Shaw, I., (1997), "Review", *The Journal of Egyptian Archaeology* **83**, 231-233.

Shaw, I., (2012), "*Ancient Egyptian Technology and Innovation*", Bristol Classical Press, UK.

Shebanova, O.N., and Lazor, P., (2003), "Raman study of magnetite (Fe₃O₄): laser-induced thermal effects and oxidation", *J. Raman Spectrosc.*, **34**, 845-852.

Shirai, H., Morioka, Y., Nakagawa, I., (1982), "Infrared and Raman Spectra and Lattice Vibrations of Some Oxide Spinels", *J. Phys. Soc. Jpn.* **51**, 592-597.

Shortland, A.J., (2000), "Vitreous Materials at Amarna. The production of glass and faience in 18th Dynasty, Egypt", *BAR Intl. Series* **827**, Archaeopress, Oxford, UK.

Shortland, A.J., (2002), "The use and origin of antimonate colourants in early Egyptian glass", *Archaeometry*, **44**, 517-530.

Shortland, A.J., Degryse, P. Walton, M. Geer, V. Lauwers, L. Salou, (2011), "The evaporite deposits of Lake Fazda (Wadi Natrun, Egypt) and their use in Roman glass production", *Archaeometry*, **53**, 916-929.

Shortland, A.J., and Eremin, K., (2006), "An analysis of second millennium glass from Egypt and Mesopotamia, Part 1: New WDS analyses", *Archaeometry*, **48**, 581-603.

Shortland, A.J., Hope, C.A., and Tite, M.S., (2006) "Cobalt blue painted pottery from the 18th Dynasty Egypt", In: *Geomaterials in Cultural Heritage* (Eds. M. Maggetti, & B. Messiga) Geological Soc., London, Special Publications, **257**, 91-99.

Shortland, A.J., Nicholson, P.T., Jackson, C.M., (2000), "Lead isotopic analysis of eighteenth-dynasty Egyptian eyepaints and lead antimonite colourants", *Archaeometry* **42**, 153-157.

Shortland, A.J., Rogers, N., Eremin, K., (2007), "Trace element discrimination between Egyptian and Mesopotamian Late Bronze Age glasses", *J. Archaeol. Sci.*, **34**, 781-789.

Shortland, A.J., Schachner, L., Freestone, I., Tite, M., (2006b), "Natron as a flux in the early vitreous materials industry: sources, beginnings and reasons for decline", *J. Archaeol. Sci.*, **33**, 521-530.

Shortland, A.J., and Tite, M.S., (2000), "Raw materials of glass from Amarna and implications for the origins of Egyptian glass", *Archaeometry*, **42**, 141-151.

Shortland, A.J., Tite, M.S., Ewart, I., (2006a), "Ancient exploitation and use of cobalt alums from the Western Oases of Egypt", *Archaeometry*, **48(1),** 153-168.

Shoval, S. Boudeulle, M., Panczer, G., (2011), "Identification of the thermal phases in firing of kaolinite to mullite", *Optical Materials*, **34**, 404-409.

Shugar, A., Rehren, Th., (2002), "Formation and composition of glass as a function of firing temperature", *Glass Technol.* **43C**, 145-150.

Shugar, A., (2013), "Portable X-ray Fluorescence and Archaeology: Limitations of the Instrument and Suggested Methods to Achieve Desired Results" in: *Archaeological Chemistry VIII*, (Eds Armitage and Burton), Am. Chem. Soc., 173-193.

Sickafus, K.E., and Wills, J.M., (1999), "Structure of spinel", *J. Am. Ceram. Soc.*, **82**, 3279-3292.

Sickels, L.-B., (1981), "Organics vs synthetics: their use as additives in mortars", in: *Mortars, cements and grouts used in the conservation of historic buildings, Symp., Rome, 3-6 November, 25-52*, ICCROM, Rome.

Sieffert, E.R., Bown, T.M., Clyde, W.C., Simons, E., (2008), "Geology, Paleoenvironment, and Age of Birtket Qarum Locality 2 (BQ-2), Fayum Depression, Egypt", in: "*Elwyn Simons: A Search for Origins*", (Eds., J.G. Fleagle, C.C. Gilbert), Univ. Chicago, Chicago, Ill p71-86.

Sievert, T., Wolter, A., Singh, N.B., (2005), "Hydration of anhydrite of gypsum (CaSO$_4$.II) in a ball mill", *Cement and Concrete Research* **35**, 623-630.

Sinha, M.M. and Kim, J-S., (2003), "Analysis of Vibrational Modes and Phonon Density of States of Aluminate Spinels", *J. Korean Phys. Soc.*, **43**, 237-241.

Smeddley, J.W., Jackson, C.M., Booth, C.A., (1997), "Back to the roots: the raw materials, glass recipes and glassmaking practices of Theophilus", In: *The Prehistory & History of Glassmaking Technology*, (Eds. P. McCray, W.D. Kingery), Pub. Am. Ceram. Soc., 145-165.

Smets, B.M.J., and Lommen, T.P.A., (1982), "The leaching of sodium containing glasses: ion exchange or diffusion of molecular water?", *Journal dePhysique Colloque C9*, supplément au n° 12, Tome **43**, pages C9-649-C9652.

Smirniou, M., and Rehren, Th., (2011), "Direct evidence of primary glass production in late Bronze Age Amarna, Egypt", *Archaeometry* **53**, 58-80.

Smirniou, M., and Rehren, Th., (2013), "Shades of blue – cobalt-copper coloured blue glass from New Kingdom Egypt and the Mycenaean world: a matter of production or colourant source?" *J. Archaeol. Sci.*, **40**, 4731-4743.

Smirniou, M,, Rehren, Th., Sismani, A., Asderaki, E., Gratuze, B.,)2009), "Mycenaean beads from KAZANAKI, Volos: A further node in the LBA glass network", in: *Annales du 18e Congrès de l'Association Internationale pour L'Histoire du Verre*, (Eds. D. Ignatiadou and A. Antonaras), Thesaloniki.

Smith, G.D. and Clark, R.J.H., (2004), "Raman microscopy in archaeological science", *J. Archaeological Sci.*, **31**, 1137-1160.

Smith, H.S. and Jeffreys, D.G., (1979), "The "Anubieion" North Saqqara, Preliminary Report", *J. Egyptian Archaeology* **66**, 17-27.

Snoeck, C., Schulting, R.J., Lee-Thorpe, J.A., Lebon, M., (2016), "Impact of heating conditions on the carbon and oxygen isotope composition of calcined bone", *J. Archaeol. Sci.*, **65**, 32-43.

Soukiassian. G., Wuttmann, M., Pantalacci, I., Ballet, P., Picon, M., (1990), *Balat III. Les Ateliers de Potiers d'Ayn-Asil*, Cairo, Institut Français d'Archéologie Orientale.

Spaer, M., (1988), "The pre-Islamic glass bracelets of Palestine", *J. of Glass Studies*, **30**, 51-61.

Spaer, M., (1992), "The Islamic glass bracelets of Palestine: Preliminary findings", *J. of Glass Studies"*, **34**, 44-62.

Spataro, M., Meeks, N., Bimson, M., Dawson, A., Ambers, J., (2009), "Early porcelain in seventeenth century England: non-destructive examination of the two jars from Burghley House", *British Museum Technical Research Bulletin* **3**, 37-46.

Spring, M., Higgitt, C., Saunders, D., (2005), "Investigation of Pigment-Medium Interaction Processes in Oil Paint containing degraded Smalt", National Gallery (UK) *Tech. Bull.* **26**, London.

Spurrell, F.C.J., (1895), "Notes on Egyptian Colours", *Archaeological Journal*, **52**, 222-239.

Stalder, R., Kronz, A., Schmidt, B.C., (2009), "Raman spectroscopy of synthetic $(Mg,Fe)SiO_3$ crystals. An analytical tool for natural orthopyroxenes", *Eur. J. Mineral*. **21**, 27-32.

Stanley, D.J. and Maldonado, A., (1977), "Nile Cone: Late Quaternary stratigraphy and sediment dispersal", *Nature*, **266**, 129-135.

Stanley, D.J., Sheng, H., Pan, Y., (1988), "Heavy minerals and provenance of Late Quaternary sand, Eastern Nile delta", *J. African Earth Sci.*, **7(4)**, 735-741.

Stapleton, C.P. and Swanson, S.S., (2002), "Batch Material Processing and Glassmaking Technology of the 9th Century B.C. Artifacts Excavated from the site of Hasanlu, Northwest Iran", in: *MRS Proceedings* Vol. **712** (Eds: P.B. Vandiver, M. Goodway, J.R., Druzik, J.l. Mass), 2001 MRS Fall Meeting, USA.

Steemson, M.L., (1999), "The selection of a hydroxide precipitation/ammoniacal releach circuit for metal recovery from acid pressure leach liquors", *ALTA Conference*, Perth, W.A.

Stern, E.M., and Schlick-Nolte, B., (1994), "*Early glass of the Ancient World 1600 BC-AD 50"*, Ostfildern: Verlag Gerd Hatje.

Stevenson, C.M. and Gurnick, M., (2016), "Structural collapse in kaolinite, montmorillonite, and illite clay and its role in the ceramic rehydroxylation dating of low-fired earthenware" *J. Archaeol. Sci.*, **69**, 54-63.

Stocks, D.A., (2003), "*Experiments in Egyptian Archaeology: Stoneworking technology in Ancient Egypt*" Pub. Routledge, London.

Stoch, H.G., "Sc, Cr, Co, and Ni Partitioning Between Minerals from Spinel Peridotite Xenoliths", *Contrib. Mineral Petrol.* **78**, 166-174

Stola, M., Stefanescu, M., Dippong, T., Stefanescu, O., Barvinschi, P., (2010), "Low temperature synthesis of Co_2SiO_4/SiO_2 nanocomposite using a modified sol-gel method", *J. Sol Gel Technol*. **54**:49-56.

Strobel, R., Pratsinis, S.E., (2009), "Direct synthesis of maghemite, magnetite and wustite nanoparticles", *Advanced Powder Technology* **20**, 190-194.

Strung, H., (1957), "*Mineralogische Tabellen*" Akad. Verlag. Leipzig.

Stuart, B., (2007), "*Analytical Techniques in Materials Conservation*", John Wiley & Sons Ltd., UK.

Swartz Dood, L., Scott, D.A., Nikias, G.A., Au, J., Ramos, A., (2009), "The ritual significance of colour: Specialised pigments in a wooden Egyptian funerary statuette from the New Kingdom", *J. Egyptian Archaeology* **95**, 83-104.

Symons, A., (2008), "A search for origins", (Eds. J.G. Fleagle and C.C. Gilbert), Springer.

Tang, C-W., Wang, C-B., Chien, S-H., (2008), "Characterisation of cobalt oxides studied by FT-IR, Raman, TPR, and TG-MS", *Thermochim. Acta* **473**, 68-73.

Tanimoto, S., (2007), "Experimental study of Late Bronze Age glass-making practice", *PhD Thesis*, UCL Institute of Archaeology, University of London.

Tanimoto, S., Rehren, Th., (2008), "Interactions between silicate and salt melts in LBA glassmaking", *J. Archaeol. Sci.* **35**, 2566-2573.

Tantrakarn, K., Kato, N., Nakai, I., Shindo, Y., Chaisuwan, B., (2012), "The application of a portable X-ray fluorescence spectrometer to the on-site analysis of glass vessel fragments from Southern Thailand", *Archaeometry*, **54,** 508-527.

Taylor, J.B., (1977), "The origin and use of cobalt compounds as blue pigments", *Science and Archaeology*, **19**, 3-15.

Thér, R., (2014) "Identification of pottery firing structures using the thermal characteristics of firing", *Archaeometry* **56(S1)**, 78-99.

Thibeau, R.J., Brown, C.W., Heidersbach, R.H., (1978), "Raman Spectra of Possible Corrosion Products of Iron", *Applied Spectroscopy* **32,** 532-535.

Thys, T., Burlet, C., De putter, Th., Dupin, L., Goethals, H., Vanbrabant, Y., (undated), "Characterisation of heterogenite (CoOOH) from oxidised copper-cobalt deposits in the Katanga Copperbelt", *www.geoproject.org/pdf/characterisation_heterogenite.pdf*

Tite, M.S., (1987), "Characterisation of early vitreous materials", *Archaeometry*, **56**, 39.

Tite, M.S., (2998), "Ceramic production, provenance and use – A review", *Archaeometry*, **50,** 216-231.

Tite, M.S., (2009), "The production technology of Italian maiolica: a reassessment", *J. Archaeol. Sci.*, **36**, 2065-2080.

Tite, M.S., and Bimson, M., (1986), "Faience: An investigation of the microstructures associated with the different methods of glazing", *Archaeometry*, **28**, 69-78.

Tite, M.S., Bimson, M., Cowell, M.R., (1984), "Technical Examination of Egyptian Blue", in; *Archaeological Chemistry* (Ed. J. Lambert), *Advances in Chemistry*, Pub. American Chemical Society, Chapter 11, 215-242.

Tite, M.S., Bimson, M., Cowell, M.R., (1987), "The Technology of Egyptian Blue", in: *Early Vitreous Materials* (Eds. M. Bimson and I.C. Freestone), British Museum occasional paper 56, British Museum, London.

Tite, M.S., Bimson, M., Meeks, N.D., (1980), "*Technological Characterisation of Egyptian blue*", Revue d'Archemetrie, Actes du XX Symp. Intl. d'Archéométrie Symp. For Archaeometry, Paris, 26-29 March 1980, Vol III, 297-301.

Tite, M.S., Pradell, T., Shortland, A., (2008), "Discovery, production and use of tin-based opacifiers in glasses, enamels and glazes from Late Iron Age onwards: a reassessment", *Archaeometry*, **50**, 67-84.

Tite, M.S., Manti, P., Shortland, A.J., (2007), "A technological study of ancient faience from Egypt", *J. Archaeol. Sci.*, **34**, 1568-1583.

Tite, M.S., and Shortland, A.J., (2003), "Production technology for copper- and cobalt-blue vitreous materials from the New Kingdom site of Amarna – a reappraisal", *Archaeometry* **45**, 285-312.

Tite, M.S., Shortland, A. Maniatis, Y., Kavoussanaki, D., Harris, S.A., (2006), "The composition of the soda-rich and mixed alkali plant ashes used in the production of glass", *J. Archaeol. Sci.,***33**, 1284-1292.

Tite, M.S., Shortland, A.J., Nicholson, P.T., Jackson, C.M., (1998), *"The use of copper and cobalt colourants in vitreous materials in ancient Egypt"*, in: La Couleur dans la Peinture et l'Émaillage de l'Égypte ancienne, (Eds. S. Colinart, M. Menu), Actes de la Table Ronde Ravello, 20-22 mars, 1997, Edipuglia, Bari, 111-120.

Tobia, S.K. and Sayre, E.V., (1974), "The geological evolution of the River Nile in Egypt", in: *Recent Advances in Science and Technology of Materials III*, (Ed. A. Bishay) Plenum Press, New York, 99-128.

Toffolo, M.B., Klein, E., Elbaum, R., Aja, A.J., Master, D.M., Boaretto, E., (2013), "An early Iron Age assemblage of faience beads from Ashkelon, Israel: chemical composition and manufacturing process", *J. Archaeol. Sc*i., **40**, 3626-3635.

Tribaudino, M., (2011), "Raman Investigation on Pigeonite in Ureilite", *Spectroscopy Letters*, **44**, 480-485.

Tribaudino, M., Mantovani, L., Bersani, D., Lottice, P.P., (2011), "Raman investigation on pigeonite in ureilite", *Spectrosc. Letters* **44**, 480-485.

Tribaudino, M., Mantovani, L., Bersani, D., Lottice, P.P., (2012), "Raman spectroscopy of $(Ca,Mg)MgSi_2O_6$ clinopyroxenes", *Am. Mineralogist* **97**, 1339-1347.

Trömel, G., (1943), "Investigation of the ternary system $CaO-P_2O_5-SiO_2$ and their importance in the production of Bessemer slags", Stahl und Eisen, **63**, 21.

Truex, T.J., Hammerle, R.H., Armstrong, R.A., (1977), "The thermal decomposition of aluminium sulphate", *Thermochim. Acta* **19**, 301-304.

Turner, W.E.S., (1954), "Studies of ancient glass and glassmaking processes, Part I. Crucibles and melting temperatures employed in ancient Egypt at about 1370 BC", *J. of the Society of Glass Technology*, **38:183**, 436-44T.

Turner, W.E.S., (1956), "Studies of ancient glass and glassmaking processes, Part V. Raw materials and Melting Processes", *J. of the Society of Glass Technology*, **40**, 277-300.

Tylecote, R.F., (1986), *"The Prehistory of Metallurgy in the British Isles"*, Pub. Institute of Metals, London.

Uda, M., (2004), "In situ characterisation of ancient plaster and pigments on tomb walls in Egypt using energy dispersive X-ray diffraction and fluorescence", *Nuclear Instruments and Methods in Physics Research B* **226**, 75-82.

Uda, M., Sassa, S, Yoshimura, S., Kondo, J., Nakamura, M., Ban, Y., Adachi, H., (2000), "Yellow, red and blue pigments from ancient Egyptian palace painted walls", *Nuclear Instruments and Methods in Physics Research* B 161-163, 758-761.

Uda, M., Nakamura, M ., Yoshimura, S., Kondo, J., *et al..*, (2002), "'Amarna Blue' painted on ancient Egyptian pottery", *Nuclear Instruments and Methods in Physics Research* B **189**, 382-386.

Ullrich, D. (1979), "Agyptisch Blau", Unpublished MSc thesis, *Diplomarbeit* FU Berlin.

Ullrich, D. (1987), "*Egyptian blue and Green Frit*" Pact 17 II.3.1, 323-332.

Uvarov, V., Popov, I., Rozenberg, S., (2014), "X-ray diffraction and SEM investigation of wall paintings found in the Roman temple complex at Horvat Omrit, Israel", *Archaeometry* (2015), 57, 773-787 (doi:10.1111/arcm.12124)

Vandenberghe, R.E. and De Grave, E., (1989), "Mössbauer Effect Studies of Oxidic Spinels", In: *Mössbauer Spectroscopy Applied to Inorganic Chemistry"*, Vol. 3 Eds. G.J. Long and F. Grandjean, Plenum Press, N.Y. Ser. Title: Modern Inorganic Chemistry, Ed. J.P. Fackler, Jr., 59-182.

Van der Linden, V., Cosyns, P. Schalm, O., Cagno, S., Nys, K., Janssens, K., Nowak, A., Wagner, B., Bulkska, E., (2009), "Deeply coloured and black glass in the northern provinces of the Roman Empire: Differences and similarities in chemical composition before and after AD 150", *Archaeometry* **51**, 822-844.

Van Dijk, J., (1976), The formation and thermal decomposition of aluminium hydroxide doped with Fe(III) and Cr(III), *PhD thesis*, Der Technische Hogeschool, Delft, Holland.

Vandiver, P.B., (2008), "Raw materials and fabrication methods used in the production of faience", in: in: *Monograph* **72**, (Eds. M.S. Tite and A.J. Shortland), *Oxford University School of Archaeology*, p 37-55.

Vandiver, P.B. and Kingery, W.D., (1987), "Egyptian Faience, the First High-Tech Ceramic", *Ceramics and Civilisation*, **III**, 23.

Van Driel-Murray, C., (2000), Leatherwork and skin products", in: "*Ancient Egyptian Materials and Technology*", (Eds. P.T. Nicholson, I. Shaw), Pub. Cambridge University Press, Cambridge, UK., 299-319.

Van Minh, N. and Yang, I.S., (2004), "A Raman study of cation-disorder transition temperature of natural $MgAl_2O_4$ spinel", *Vibrational Spectrosc.*, **35**, 93-96.

Vauquelin , L.N., (1826),"Lettre à M. Passalacqua" in: *Catalogue raisonné et historique des antiquities décvouvertes en Egypte* (Ed. M. Passalacqua), Paris, 129.

Vermeulen, A.C., Geus, J.W., Stol, R.J., De Bruyn, P.L., (1975), *J. Colloid Interface Sci.*, **51**, 449.

Verney-Carron, A., Gin, S., Libourel, G., (2008), "A fractured Roman glass block altered for 1800 years in seawater: Analogy with nuclear waste glass in a deep geological repository", *Geochim. et. Cosmochim. Acta* **72**, 5372-5385.

Vieira Ferreira, L.F., Casimiro, T.M., Colomban, Ph., (2013), "Portuguese tin-glazed earthenware from the 17th century, Part 1: Pigments and glazes characterisation", *Spectrochim. Acta* **A:104**, 437-444.

Vitruvius, M., (1912), Pollio, *de Architectura*, Libri Decem. Pub. F. Krohn.

Vitruvius, P. (1999) *The Ten Books on Architecture*, transl. I.D. Rowland, Cambridge University Press, Cambridge, UK.

Vogelsang-Eastwood, G., (2000), "Textiles" in: "*Ancient Egyptian Materials and Technology*", (Eds. P.T. Nicholson, I. Shaw, Pub. Cambridge University Press, Cambridge, UK., 268-299.

von der Gönna, G., Rüssel, C., (2000), "Diffusivity of various polyvalent elements in a $Na_2O.2SiO_2$ glass melt", *J. Non-Crystalline Solids*, **261**, 204-210.

Wagner, G. (1987), "Les oasis d'Egypte à l'époque grecque, romaine et byzantine d'après les documents grecs", *IFAO, Bibliothèque d'Étude 100*, Cairo:IFAO, 142-143.

Walton, M., Eremin, K., Shortland, A., Degryse, P. Kirk, S., (2012), "Analysis of Late Bronze Age glass axes from Nippur – a new cobalt colourant", *Archaeometry*, **54**, 835-862.

Walton, M., Shortland, A., Kirk, S., Degryse, P., (2009), "Evidence for the trade of Mesopotamian and Egyptian glass to Mycenaean Greece", *J. Archaeol. Sci.*, **36**, 1496-1503.

Walton, M.S., Tite, M.S., (2010), "Production technology of Roman lead-glazed p0ottery and its continuance into late antiquity", *Archaeometry*, **52**, 733-759.

Wang, A., Haskin, L.A., Jolliff, B.L. (1998), "Characterisation of mineral products of oxidation and hydration by Laserraman spectroscopy – implications for *in situ* petrologic investigation of the surface of Mars", *XXIX Lunar and Planetary Science Conference,* 16-20 March, Houston, TX., USA.

Wang, A., Jolliff, B.L., Haskin, L.A., Kuebler, K.E., Viskupic, K.M., (2000), "Characterisation and comparison of structural and compositional features of planetary quadrilateral pyroxenes by Raman spectroscopy", *Am. Mineralogist* **86**, 790-806.

Wang, G., Shen, X., Horvat, J., Wang, B., Lin, H., Wexler, D., Yao, J., (2009), "Hydrothermal Synthesis and Optical, Magnetic and Supercapacitance Properties of Nanoporous Cobaltic Oxide Nanorods", *J. Phys. Chem.*, **113**, 4357-4361.

Wang, N., Shen, Y., Chen, M., (2011), "Enrichment Behaviour of Phosphorus in CaO-SiO$_2$-FeO$_x$-P$_2$O$_5$ Based slag", *2nd Intl. Symp. on High Temperature Metallurgical Processing*, TMS, 397-402.

Warachim, H., Rzechula, J., Pilak, A., (1985), "Magnesium-cobalt-aluminium spinels for pigments", *Ceramics International*, **11**, 103-106

Warner, T.E. (2011), "Artificial Cuprorivaite CaCuSi$_4$O$_{10}$ (Egyptian Blue) by a Salt-Flux Method", in: *Synthesis, Properties and Mineralogy of Important Inorganic Materials*, Pub. John Wiley & Sons Ltd., Chichester, UK. doi: 10.1002/9780470976012.ch3

Weast, R., (1978), *RC Handbook of Chemistry and Physics*", CRC Press, Boca Raton, Florida, USA.

Weatherhead, F., A. Buckley, (1989), "Artists Pigments from Amarna", in: *Amarna Reports V* (Ed. B. Kemp), Pub. Egypt Exploration Society, London.

Wedepohl, K.H., Simon, K., Kronz, A., (2011), "Data on 61 chemical elements for the characterisation of three major glass compositions in late antiquity and the Middle Ages", *Archaeometry*, **53**, 81-102.

Wegener, A., (1912), "Die Herausbildung der Grossformen der Erdrinde4 (Kontinente und Ozeane) auf geophisikalischer Grundlage", *Petermanns Geographische Miteilungen* **63**, 185-195, 253-256, 305-309.

Weidenroth, A. and Rüssel, C., (2004), "The effect of MgO on the diffusivity of iron and incorporation of iron in soda-magnesia-aluminosilicate melts", *J. Non-Crystalline Solids*, **347**, 180-186.

Welch, J.H., W. Gutt (1961), "High-temperature studies of the system calcium oxide-phosphorus pentoxide", *J. Chem. Soc.* **874**, 4442-4444.

Wendorf, F., Said, R., Schild, R., (1970), "Egyptian prehistory: some new concepts", *Science*, **169**, 1161-1171.

Wendorf, F., and Schild, R., (2002), "Implications of Incipient Social Complexity in the Late Neolithic in the Egyptian Sahara", in: *Egypt and Nubia, Gifts of the Desert,* (Ed. R. Friedman), The British Museum Press, London.

West, G.D., Birosca, S., Higginson, R.L., (2005), "Phase determination and microstructure of oxide scales formed on steel at high temperature", *J. of Microscopy*, **217 Part II**, 122-129.

Whitney, P.L. and Tanford, C. (1962), "Solubility of amino acids in aqueous urea solutions and its implications for the denaturation of proteins", *J. Biol. Chem.* **237**, 1735-1737.

Wiedemann, H-G., Arpagaus, E., Müller, D., Marcolli, C., Weigl, S., Reller, A., (2002), "Pigments of the bust of Nefertete compared with those of the Karnak Talatats", *Thermochimica Acta*, **382**, 239-247.

Wiedemann, H.G., G. Bayer, A. Reller (1998), "Egyptian blue and Chinese blue. Production technologies and applications of two historically important blue pigments", in: *La Couleur, Dans La Peinture et l'emaillage de l'Égypte Ancienne*" (Eds. S. Colinart, M. Menu), Pub. Edipuglia, Bari-S. Spitito.

Wiedenroth, A. and Rüssel, C., (2004), "The effect of MgO on the diffusivity of iron and incorporation of iron in soda-magnesia-aluminosilicate melts", *J. Non-Crystalline Solids*, **347**, 180-186.

Wilkinson, G. (1843), "Some Accounts of the Natron Lakes of Egypt"; in a letter to W.R. Hamilton, Esq. 1842. *Journal of the Royal Geographical Society of London* **13:**113-118.

Wilson, I.R., *Cerâmica*, **1998**, 44, 287.

Wilson, M.A., Clelland, S., Carter, M.A., Ince, C., Hall, C., Hamilton, A., Batt, C.M., (2013), "Rehydroxylation of fired-clay ceramics: Factors affecting early-stage mass gain in dating experiments", *Archaeometry*, **56**, 689-702.

Wilson-Yang, K.M., and Burns, G., (1988), "Electron microprobe studies of chemical reactions in ancient painted murals: The Beni Hasan Tombs, Egypt", *Can. J. Chem.*, **66**, 2348-2361.

Worobiec, A., Darchuk, L., Brooker, A., Potgieter, H., Van Grieken, (2011), "Damage and molecular changes under a laser beam in SEM-EDX/MRS interface: a case study on iron-rich particles", *J. Raman Spectrosc.*, **42**, 808-814.

Wulff, H.E., Wulff, H.S., Koch, L., (1968), "Egyptian faience, a possible survival in Iran", *Archaeology* **21**, 98-107.

Wypyski, M.T., (1998), in "*Gifts of the Nile, Ancient Egyptian Faience*", Pub. Thames and Hudson, London.

Xu, R and Zeng, H.C., (2003), "Dimensional control of Cobalt-hydroxide-carbonate Nanorods and Their Thermal Conversion to One-Dimension Arrays of Co_3O_4 Nanoparticles", *J. Phys. Chem B* **107**, 12643-12649.

Yang, J., Liu, H., Martens, W.N., Frost, R.L. (2010), ":Synthesis and Characterisation of Cobalt Hydroxide, Cobalt Oxyydroxide, and Cobalt Oxide Nanoparticles", *J. Phys. Chem.* **114**, 111-119.

Yang, Y., Zhao, X., Zhu, Y., Zhang, F., (2012), "Transformation Mechanism of Magnesium and Aluminium Precursor Solution into Crystallites of Layered Double Hydroxide, *Chem. Mater*. **24**, 81-87.

Zakaria, R.K.M., Atta, E.R., Ibrahim, M.S., (2016), "Assessment of the Heavy Metals and Natural Radioactivity in Phosphate Mines and Occupational Health Effects at some Egyptian Regions", *J. Environ. & Anal. Toxicology*, **6**, 1-6.

Zeng, W., Chen, N., Chen, Q., (1997), "Thermodynamics of thermal decomposition of aluminium hydroxide", *Trans. Nonferrous Met. Soc. China*, **7**, 132-134.

Zoppi, A. Lofrumento, C., Castellucci, E.M., Dejoi, C., Sciau, Ph., (2006), "Micro-Raman study of aluminium-bearing hematite from the slip of Gaul *sigillata* wares", *J. Raman Spectrosc.*, **37,** 1131-1138.